Cranfield University

R. Backhouse

Multiaxial Non-Crimp Fabrics: Characterisation Of Manufacturing Capability For Composite Aircraft Primary Structure Applications

School of Industrial and Manufacturing Science

Eng.D Thesis

Cranfield University

School of Industrial and Manufacturing Science

Eng.D Thesis

Academic Year 1993-1997

R. Backhouse

Multiaxial Non-Crimp Fabrics: Characterisation Of Manufacturing Capability For Composite Aircraft Primary Structure Applications

Supervisor: Professor P.E.Irving

March 1998

Abstract

Carbon composite reinforcement fabrics aimed at flight critical aircraft structure application were designed and the capability of the process used to manufacture them examined. Studies of the LIBA multiaxial non-crimp fabric manufacturing process focused on the effect of changes to four manufacturing parameters using an experimental design process to design the fabrics and analyse the results. The composite properties measured included microstructural features of the fibre tows and resin distribution, and mechanical performance both in-plane and their damage resistance and tolerance characteristics.

Nine pairs of Toray T300 carbon based LIBA multiaxial non-crimp fabrics were manufactured and converted to composite laminates. Processing was accomplished using the interleaved Resin Film Infusion processing route with commercial Fiberdux 914 matrix resin. All the fabrics were of the same reinforcement type, consisting of 816 g/m² of fibre; 376 g/m² oriented along the fabric length (0°) and 220 g/m² oriented in each of the ±45° directions. Differences between the nine pairs of fabrics were restricted to the settings of four manufacturing parameters; stitch course (needle penetrations/cm); stitch tension, 0° tension and 0° coverage (amount of constraint on the 0° material provided by the stitch). Three settings were used for each of the parameters; each representing the upper and lower limits, and standard setting.

Microstructural characterisation of the laminates indicated large differences in both resin distribution and levels of 0° fibre crimp caused by the changes in manufacturing parameter settings. In-plane and damage resistance and tolerance tests on their composites allowed relationships between manufacturing settings, microstructure and engineering properties to be deduced. It was found that selected in-plane properties could be increased by as much as 17% relative to standard production materials, although a wide range of influence was observed. For damage resistance and tolerance characteristics, reductions in impact damage area (C-scan) of between 13-50% are expected across a range of energies. Manufacturing settings to maximise the impact force for delamination initiation were found to minimise the impact damage areas. Similarly the same settings maximised both the Mode I propagation strain energy release rate and the Compression After Impact strength of the materials. It was found that polyester knitting yarn was largely responsible for the control of the damage resistance and tolerance characteristics together with the mean size of the resin areas and layers within the composite.

The manufacturing/microstructure/property relationships identified provide those wishing to exploit these materials with design guidelines to tailor fabric structure and performance characteristics for the intended application. Above all else the results highlight the need for precision in specifying and controlling the manufacturing process in order to repeatably produce the desired performance. Further work on the same materials could be used to provide a link to processing characteristics such as permeability for liquid resin moulding processes and ability to conform to complex curved surfaces.

Acknowledgements

My thanks and gratitude to all those who have helped guide this study; all my colleagues and friends in the Aerospace Composites Group and especially: Andrew Mills, Dave Cahill, Denis Turmel and Lee Bateup.

Professor Phil Irving for his interest, support and guidance.

Bob Heath, British Aerospace Airbus Ltd, and John Clark for their interest and direction in the early stages of the project.

Engineering and Physical Science Research Council (EPSRC) for the Engineering Doctorate Grant and continued funding of the work through the EPSRC IMI funded 'Innovative Fabrics and Preforms for Aircraft Composite Structures' (INFACS) program.

British Aerospace Airbus Ltd for the supply of materials and provision of funding through the DTI CARAD supported 'Affordable Manufacture of Composite Aircraft Primary Structures' (AMCAPS I) program

All the staff at Brunswick Technologies Europe Ltd (Formerly TTIL) for their hospitality and use of the LIBA machine during the manufacture of the fabrics.

Hexcel Composites for the supply of matrix resin films and for access to their ultrasonic C-scan equipment.

British Aerospace Defence Ltd, at Warton for the provision of test facilities and personnel and all the other INFACS project partners for their support and encouragement.

Ron James for proof reading the text.

Tracy for her continuing support in the face of adversity...!

Table Of Contents

Table Of Figures

List Of Tables

Chapter 1

Introduction And Background

1.1 Introduction

Carbon fibre/epoxy composites, with their high specific stiffness, strength and excellent corrosion and fatigue resistance[1] have become accepted as the preferred material for structural aircraft component manufacturing. However, aluminium alloys still dominate civil aircraft primary structure components, owing to their relatively low material cost and a long period of experience in design and manufacture.

The development of composite materials and structures was initiated in military fighter airframes and has been dominated since then by either the highly skilled craft of hand lay-up of unidirectional pre-impregnated tapes or the application of automated lamination equipment to replicate this dexterity. Laminated composites suffer from well-documented interlaminar weakness resulting in low damage resistance and tolerance. Because of the thin layers of fibres required to minimise interlaminar stresses both material and fabrication costs are high. For military airframes material and fabrication costs have been largely tolerated as they form a relatively small proportion, around 25%, of total cost. Much of the remainder is attributable to avionics and propulsion. For large civil transport structures the amount of material required and the attendant need for automated technology makes aircraft designs based upon unidirectional pre-impregnated (UD prepreg) tapes unattractive from a cost viewpoint.

The performance of a component in service is determined by the ability of the designer to understand the loading required to be sustained by a structure and the ability to create a design, select a material and manufacturing process to align the correct amount of reinforcement to transmit or react these loads. When appropriate this includes a provision for undetected damage and repairs to damaged structure. The process of matching material and manufacturing processes to the demands of aircraft loading and design has lead to the development of machines and intermediate materials to automate or simplify the fibre alignment process. Figure 1 illustrates the two main options; the conversion of fibres and matrix into a stable intermediate product and its assembly to create final part; the direct assembly of fibre tow into the structural shape. With Direct methods the creation of the composite material happens simultaneously with the creation of the part itself. (M) symbols indicate options of where matrix resin may be introduced in the process.

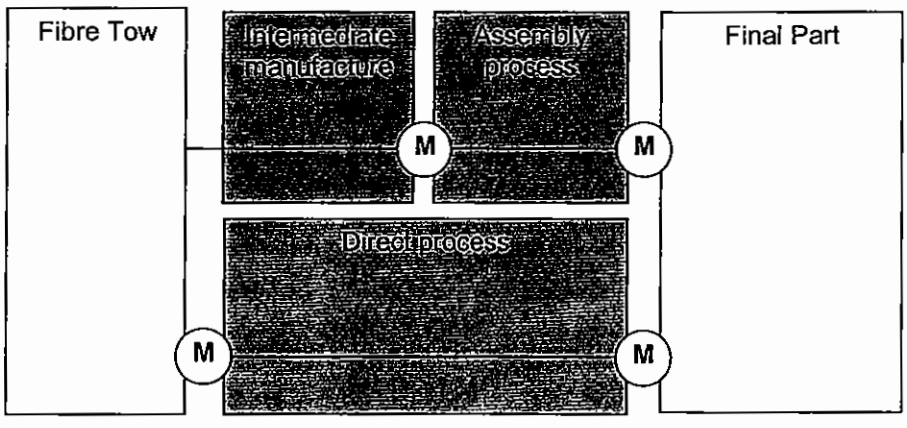

Figure 1: Process steps in creating a composite structure

Control surfaces, exterior panels and fairings of most large commercial transport aircraft are now routinely manufactured from woven pre-impregnated composites using the autoclave processing route. The advancement of composites into large primary structure components has been to apply composites to the tail-fin and tail-plane, using experience gained from secondary and tertiary structures. Current civil aircraft research and development programmes, experience from military airframes and smaller civil aircraft, indicate that the

next and last remaining structures to be developed for civil aircraft production are wing-box and fuselage structures.

In section 1.4 the basic functions and structural configuration of a civil transport wing are described. This provides general information on the types of loads applied to the wing; its geometric shape requirements and the types of metallic structures adopted to meet these requirements. Composite materials since their introduction have been applied in place of metals. In section 1.5 a summary of the history of composite applications to aircraft wing structures is recorded so as to illustrate how materials, manufacturing techniques and designs have evolved.

In order to simplify the matching of aircraft geometric and structural requirements to the capability of materials and manufacturing systems, proprietary design rules were developed. These were largely empirically derived and provide a knowledge base which is performance, rather than cost driven. Refinements to the design rules are made as requirements placed on, and the capabilities of materials and manufacturing systems change. Presented at the end of the chapter is a detailed overview of the materials and manufacturing system options that are, or appear capable of, being successfully applied to composite aircraft structures.

The remainder of the thesis is dedicated to one intermediate manufacturing technique, a textile process called multiaxial warp-knitting, which is finding increasing favour with aircraft structure manufacturers. Multiaxial warp-knit 'non-crimp' fabrics potentially combine the benefits of straight fibres found in unidirectional tape materials with the ability to conform to curved and doubly curved surfaces found in woven fabrics. Fibre orientations and areal weights may also be specified over a wide range as can the number of layers in a single fabric.

1.2 Project Scope

The project scope was set by the development activities being carried out under the DTI CARAD funded AMCAPS I programme. After reviewing developed and emerging composite manufacturing technologies for civil transport wing structures, carbon multi-axial warp knit non-crimp fabric and interleaved epoxy Resin Film Infusion were selected. Structural weight and cost reduction targets of 20% and 30% respectively over current (1991) aluminium structures were set, as was the target airframe and loading.

Few constraints were placed upon the design of the initial wing structure as there was suspicion concerning the applicability of the design rules for thin skinned military airframe structures to large, thick section, civil transport aircraft. Materials used were required to match or better current composite design allowables for the same fibre/matrix resin combination. The proportion of axial 0° to ±45° fibres was set at 50% with no requirement at this stage for the inclusion of general 90° (chord-wise) reinforcement. This was decided as the structure was to be fully bonded without mechanical fasteners which would make the inclusion of 90° material desirable to improve bolt-bearing performance.

Multiaxial warp-knit non-crimp fabrics were developed in the mid 1980's primarily as an industrial reinforcement textile. They have been widely applied in boat construction and industrial applications because of their improved performance over woven fabrics, ability to include a range of fibre orientations and low cost. Early studies suggested that multiaxial warp knit non-crimp fabrics were potentially viable as an alternative to unidirectional prepreg or woven fabrics. However a large number of questions remained as to the capability of the manufacturing technique to meet aircraft design requirements, both in terms of performance, quality and design flexibility. The LIBA manufacturing process had not been subject to assessment of its ability to provide materials capable of application in flight critical structures. There was also little published information on the performance and mechanisms of failure for

carbon reinforcing fabrics at the high fibre volume fractions required for weight critical structure.

1.3 Project Objectives

A work plan was developed to asses the suitability of this class of material for structural application with plans instigated to improve the capability of the process when deficits, considered recoverable though machine development, were identified.

The main tasks were as follows:

1. Compare multi-axial warp-knit composite performance with equivalent unidirectional prepreg tape laminates.

2. Measure the influence of selected manufacturing control parameters on composite performance and where possible identify the mechanisms responsible for the differences.

3. Provide guidelines for the optimisation of machine settings to best match aircraft design requirements using current fabric manufacturing technology.

An analysis of the forces acting within the competitive environment of the multi-axial warp knit non-crimp fabric industry was also undertaken and submitted here as the 'non-technical' chapter.

1.4 Civil Aircraft Wing-box Structural Features

A civil aircraft wing is a long slender surface that creates aerodynamic lift, due to movement of air around its external profile. At the heart of the wing is a box structure, the wing-box, onto and into which other structures are attached. The wing-box contains a majority of the aircraft fuel load and often supports the engines that add additional local loads, due to engine weight, reaction to thrust, vibration, rotational inertia and gyroscopic forces. These are applied to the wing skin via an engine pylon attached usually to the skin, rib and spar. Undercarriage and control surfaces are also attached and apply loads to the wing-box. Ailerons to turn the aircraft and large retractable surfaces called flaps provide additional lift during low speed manoeuvres during take off and landing; both located at the back of the wing-box. The tail plane and fin are generally of similar construction to the wing and also have control surfaces attached to their trailing edges.

The basic structure of a metallic civil transport wing is shown in Figure 2. Upper and lower wing skins create the external aerodynamic profile and carry a majority of the wing bending loads as tension in the lower skin and compression in the upper skin. This situation being reversed when the aircraft is stationary due to self weight. The skins are obviously thickest at the root end and taper to the tip each cross-section being sufficient to support the rest of the outboard wing and its aerodynamic load. The outer surface of the wing has both chord-wise and span-wise curvatures and may also be slightly twisted along the span. The two skins are separated by two types of structures: (a) Spars, which close the wing box at its front and rear and serve to transfer shear loads due to wing, (b) Ribs, which run at regular intervals broadly perpendicular to the spars and attached to them by cleats. Their function is to support the aerodynamic profile of the skins; to prevent them from buckling and providing torsional stiffness, transferring shear loads across the chord between top and bottom skins. They also act as baffles for the fuel contents of the wing; restricting flow along the span particularly in the crash case. In this situation the fuel contents must not burst from the wing-box, although the box may be irrevocably damaged. The ribs alone however are insufficient to prevent buckling of the skins and so stiffeners or stringers run the length of the wing box bonded, riveted to, or machined directly from the skins. The ribs are usually profiled so as to allow the stiffeners to run continuously between rib bays.

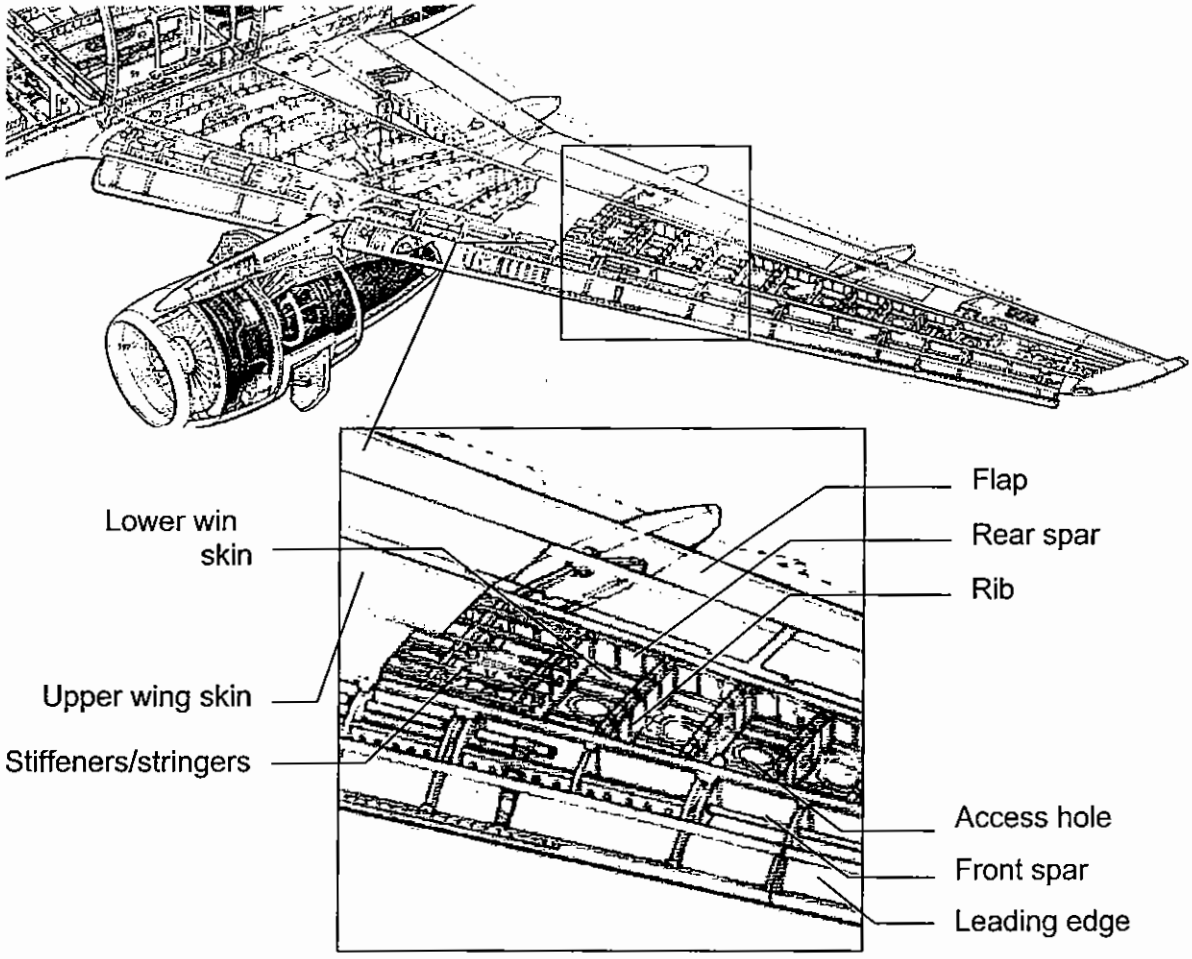

Figure 2: Wing structure configuration (A320-200)[2]

The most highly loaded inner section of the wing is milled from a solid billet of aluminium alloy. The spars, ribs and stiffeners are bolted onto the skins after each have been machined, heat treated, chromate primed and all mating surfaces and fasteners sealed to be fuel and pressure proof. More lightly loaded outer wing sections may be manufactured from formed sheet metal, milled or chemically machined to the desired thickness and the stiffeners bonded or riveted in place.

In the transition to composite structures this basic configuration of tapering thickness skins, spars, ribs and skin stiffeners is often replicated, replacing the skin milling operation with tape laying using automated equipment. The use of closed section stiffeners or honeycomb cored skins have not been widely used because of encroachment on the potential fuel volume of the wing. Difficulties repairing wet or fuel soaked honeycomb cored panels, resulting from impact damage or manufacturing defects followed by fluid ingress have been widely experienced, both in military and civil aircraft components. Measuring the cell damage growth from freeze-thaw cycling of wet cores and difficulties in cleaning fuel ingress to a level suitable for bonding are examples of these problems. Such experiences have led to the replacement or phasing out of these structures as parts are replaced or new models are introduced[3]. The loads on the wing skin are principally in the plane of the material, with large through thickness loads only at major joints; engine pylon and undercarriage attachment, control surface fittings, spar-to-skin and rib-to-skin joints. Through thickness loads induced by operational impact damage lead to particular concerns of delamination beneath stiffener elements and at ply drop-off locations.

In comparison with a metal wing a composite wing provides optimum performance at a higher aspect ratio[4] (length/width). Reduced drag is achieved because the stiffness characteristics of composite allow an increased aspect ratio without attendant weight penalties[5]. This suggests that re-engineering a current metallic wing design in composites and maintaining the geometric envelope is unlikely to yield the most efficient design. This may also pose problems for future large aircraft, whose wing spans may as a result have to extend beyond limits considered manageable by current airport terminals.

1.5 The history of composite wing structure development

A comprehensive chronology of advanced composite applications for military, civil and general aviation aircraft is presented by Hadcock and Vorsteen[3]. Aircraft structures from this list (Table 1 and Table 2), notable for their application of new material or manufacturing techniques are described in more detail together details of relevant research programmes. With the lessons learned from these programmes it is possible to build up a picture of the reasons for the observed evolution of composite structures

Many of the applications, both military and civil, have been heavily funded by national governments with the aim of gaining both performance benefits and technological superiority over rival manufacturers. Figure 4 however suggests that the use of 'state-of-the-art' materials and manufacturing, meaning the hand lay-up and automated tape-laying of prepreg tapes as is widely used in military aircraft programs, produces civil aircraft structures that are approximately twice the cost of equivalent aluminium airframes. 50% increases in manufacturing cost to achieve 25% weight reductions over equivalent aluminium structures have been reported[5].

The impact of new-technology and other factors on the economics of an aircraft in service is generally measured using the Direct Operation Cost (DOC) per seat mile. The factors and their typical percentage contribution to the DOC are given in Figure 3 for two different fuel prices.

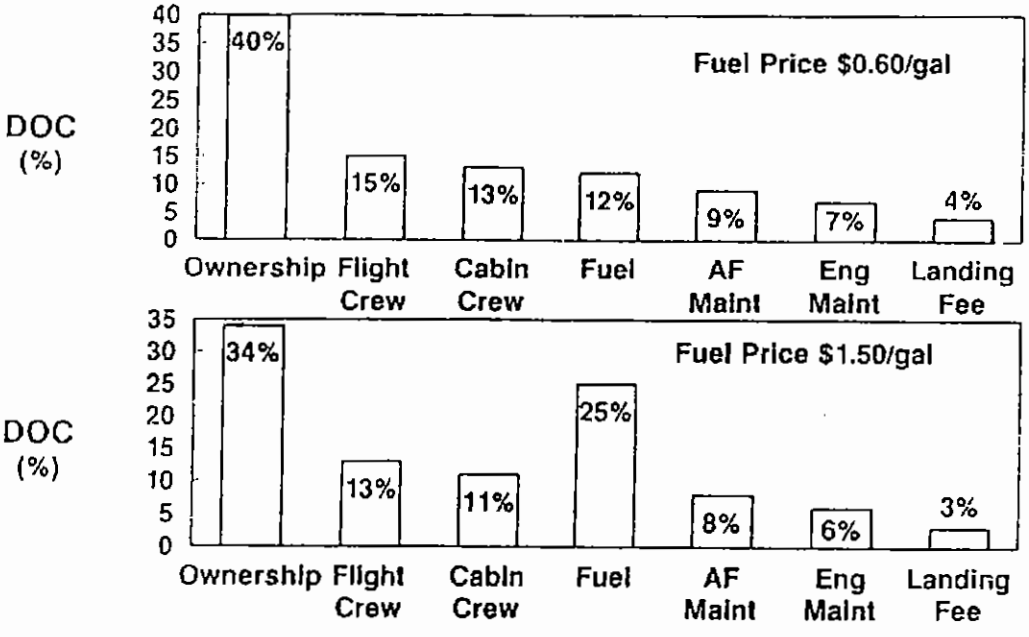

Figure 3: Factors contributing to direct operating cost[5]

In the mid 1970's when 'state-of-the-art' materials began to be introduced into civil aircraft development programmes it was on the prediction that aviation fuel prices would continue to rise dramatically as they had throughout the 1970's. This was expected to result in large direct operating cost (DOC) savings for lighter weight composite airframes; benefits that

would outweigh some manufacturing cost penalty. However with fuel prices effectively dropping from $1.50/gallon in 1980 to around $0.60/gallon currently in constant dollar terms[5], programmes have been increasingly directed towards reducing manufacturing costs. This consequently affects the cost of ownership (purchase or lease) which forms by far the greatest contribution to DOC. The NASA/Department of Defence (DoD) funded Advanced Composite Technology (ACT) is the largest of the many research programmes now moving attention towards affordable composite structures. The programme, over a period of around 15 years, aims to reduce manufacturing costs for civil aircraft wing structure by 25% over current aluminium designs (Figure 4).

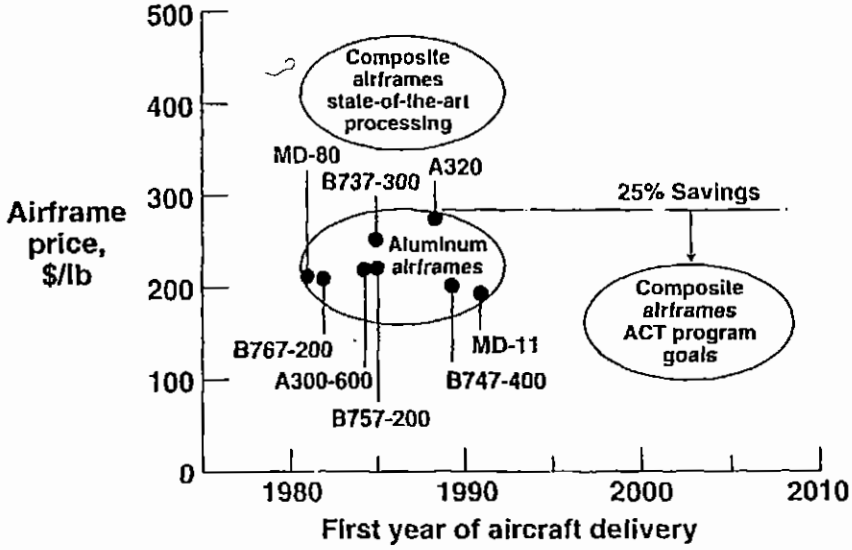

Figure 4: Estimated price of airframe structures[6]

There is evidence that with the end of the 'Cold War' and the subsequent defence cutbacks, military aircraft now have manufacturing and supportability cost considerations, figuring much more prominently than during the period 1980-86 when the B2, V22 and F-22 programmes were instigated. Technology transfer during the 1970 and 80's was a 'push' from military to commercial programs. This is now being reversed, with some of the technologies from the civil transport directed NASA ACT programme being 'pulled' into military aircraft development[7].

1.5.1 Military Aircraft Chronology

The first structural production application of advanced composites was in 1960 with the manufacture of glass fibre composite fins and rudders for the Grumman E-2A aircraft.

Boron filaments were developed as a use for large quantities of boron trichloride from an abandoned rocket fuel programme and became available in 1965, a year after the Royal Aircraft Establishment (RAE) filed a patent for high-strength, high modulus PAN based carbon fibres. Both boron and carbon fibre based composites possessed sufficiently high specific strength and stiffness to be considered as alternatives to aluminium structure.

Between 1965 and 1973 boron filaments were less expensive and had higher specific properties than the carbon fibres available at that time. This was primarily due to the large diameter of boron fibres providing superior fibre straightness and compression buckling stability compared to carbon fibre materials. For these reasons they became the preferred material for the development and production of control surfaces on the McDonnell F-4 (1969), the tail-plane and later a wing-box extension for the General Dynamics F-111. With

experience gained from the F-111 and F-4, the first safety-of-flight critical component to go forward to production was a tail-plane for the Grumman F-14 (1970). Similarly the McDonnell F-15 tail-plane, fin and rudders made extensive production use of boron/epoxy prepreg. A boron/epoxy wing was also manufactured but never flown. The first composite wing components to enter military service was on the Vought A-7D, again using boron/epoxy for wing skins with carbon/epoxy internal structure (1973).

Table 1: Military aircraft composite applications[3]

		WING BOX		FUSELAGE				STAB.		CONTROL SURFACES						
AIRCRAFT	YEAR	COVERS	SUBSTRUCT	FORWARD	MID	REAR	INTERNAL	HORIZONT'L	VERTICAL	ELEVATOR	RUDDER	AILERON	FLAP	SLAT	SPOILERS	AIR BRAKE
Grumman E-2	1960								P		P					
MD F-4E	1969										L					
Douglas A-4	1959/70							D					D			
Northrop F-5	1970				D			D								
GD F-111/FB-111	1970/73	D	D			D		D								
Lockheed C-5A	1970													D		
NA F-100	1970	D	D													
Grumman F-14A/D	1970/88							P								
HS Vulcan	1971															D
MD F-15	1972	D	D					P	P							P
Vought A-7D	1973	L	L													P
Lockheed S-3	1973														L	
HS Harrier	1975	D														
Northrop YF-17	1975							D	D		D	D	D			D
Lockheed C-130	1974	L														
GD YF/F-16	1974/6							P	P		P					
Dassault Mirage III	1975										D					
Dassault Mirage F1	1976							D				P				
Rockwell B-1A	1976						P	D	D							
MiG-29	1977							P	P		P	P	P			P
MD F/A-18	1978	P						P	P		P					P
SAAB Viggen	1978							D	D	D						
Panavia Tornado	1978							D								
Dassault Mirage 2000	1978								P		P	P				
SEPECAT Jaguar	1979	D	D	D												
Mitsubishi T-2	1979										D					
Dassault Mirage 4000	1979							P	P		P	P				P
Alphajet	1980	D	D					D								D
Vought VSTOL A	1980					D										
Fuji MT-X	1981								D				D			
Grumman VSTOL A	1981				D											
MD AV-8B	1981	P	P	P				P			P					
Lockheed C-141	1981					D										
GD F-16XL	1982	D	D						D			D	D			
Antonov An-124	1982						P									
Northrop F-20	1983							D								
Grumman X-29	1984	D														
Dassault Rafale A	1986	D	D	D	D			D	D		D	D	D			D
BAe EAP	1986	D	D					D								
IAI Lavi	1987	D	D					D	D		D	D	D			D
Grumman A6-E	1988	P	P													
SAAB Gripen	1988	P	P					P	P			P		P		P
Bell/Boeing V-22	1989	P	P	P	P	P	P	P	P	P	P	P	P			
Northrop B-2A	1989	P	P	P	P	P	P						P		P	
Lockheed F-117	1990								P							
Northrop YF-23	1990	D	D	D	D	D	D	D			D	D	D	D		D
Lockheed YF-22	1990	D	D	D	D	D	D	D	D		D	D	D	D		D
MD C-17A	1991									P	P	P			P	
Rockwell/MBB X-31	1991	D		D								D	D			
Dassault Rafale C/M	1991	P	P	P	P				P		P	P	P			P
Eurofighter EFA	1992	P	P	P					P		P	P	P			P
GD/MD A-12	1992	D	D	D	D	D	D									
MD F-18E/F	1995	P			P	P		P	P		P					P
Mitsubishi FSX	1995	P	P					P	P		P	P	P			
Lockheed F-22	1995	P	P	P	P	P	D	P	P		P	P	P	P		

P = Production L = Limited Production D = Development

The last development boron/epoxy structures were two centre-wing boxes built by Lockheed for the C-130 'Hercules' which have been in service since 1974[8,3]. A half scale centre wing-box for the C-130 was build and tested by Lockheed during the first phase of the NASA ACT programme to develop understanding of weight and manufacturing cost trade-offs for heavily

loaded wing structure. Manufacturing used prepreg tape and the 'best' composite fabrication technology available[13].

Between 1968 and 1971 carbon fibre components were test-flown on Hawker Siddeley (HS) Harrier AV-8A, British Aircraft Company (BAC) Vulcan Bombers and BAC Jet Provost trainers. In around 1974 the wing and forward fuselage of the Jaguar ground attack aircraft were demonstrated in carbon/epoxy composite. This was followed by a development of a carbon/epoxy taileron, primarily with honeycomb internal structure, for the BAC Tornado in conjunction with Messerschmitt-Bolkow-Blohm (MBB) now Daimler Benz.

By 1974 improvements in carbon fibres and their matrices led to their inclusion in aircraft competing in the US Air Force Light Weight Fighter Program from which the General Dynamics F-16 was the victor. The design of the Northrop YF-17 that had competed with the F-16 was in 1978 adopted my McDonnell Douglas and modified for US Navy use where it became known as the F/A-18.

The F/A-18 was the first military aircraft with a composite wing designed from the out-set. Carbon/epoxy (AS4/3501-6) wing skins are mechanically fastened to aluminium sub-structure. Tail-plane and fin skin panels and centre fuselage panels are similarly of carbon/epoxy construction. Carbon/epoxy comprised 9.5% of structural weight and this is set to rise to 19% in the F-18 E/F (1995) with 25% larger wing and 36% large tail-plane and fin surface areas. During these changes the matrix resin was changed from 'first-generation' relatively low toughness 3501-5 to improved toughness 977-3 and from AS4 fibres to higher stiffness IM7. The 977-3 matrix as well as offering improved delamination resistance is compatible with both prepreg and RTM process routes[9], allowing a wider range of manufacturing techniques to be employed. The use of high temperature thermosetting matrices such as bismaleimide in contact with aluminium and particularly in sea water environments has, in the experience of the US Navy, led to severe stiffness and strength degradation. The problems have been so severe that they are now considered unacceptable for use in future aircraft in these environments. The problem contributed to the cancellation in 1991 of the stealthy A-12 Navy attack bomber, of which a majority of the 26% composite weight was to have been carbon/bismaleimide. Problems with the face-sheet de-bonding and moisture up-take of honeycomb cored structures has similarly led to their virtual exclusion from all new and up-graded US Navy aircraft[3].

In 1978, co-operation between McDonnell Douglas and Hawker Siddeley (now British Aerospace - BAe) on the Harrier AV-8A led to the complete re-design of the aluminium wing to an enlarged 'all composite' design (1980). This was followed in 1984 with a production forward fuselage taking the proportion of structural weight in composites for the AV-8B to 26%[3]. These changes resulted in a doubling of the range-payload capability of the aircraft.

Interest from the US navy in V/STOL aircraft led to the development and demonstration of post-buckled damage tolerant carbon/epoxy fuselage test articles incorporating for the first time, glass/epoxy crack-arrestment strips in the lay-up.

The first thermoplastic composite wing was of carbon/polyamide construction and applied to the F-16XL of which two were constructed. The cover panels were made using the patented 'Therm-X' iso-static pressing process and employed moulded inner and outer wing skin surfaces to simplify attachment to the internal wing structure which was of aluminium construction. The Japanese F-2 (formerly FS-X) is a 'all composite' derivative of the F-16 fighter. It is still in pre-production development at Mitsubishi Heavy Industries.

Design studies for the Northrop B2 Stealth bomber started in 1979 and development in 1981. First flight took place in 1989. Almost all of the skin and much of the substructure are carbon composite manufactured by a combination of automated tape-laying and hand lay-

up. The cost of the composite structure is quoted as $4000/lb making it the most expensive aircraft ever built at around $1bn each.

The British Aerospace Experimental Aircraft Program (EAP) initially included the input of Germany and Italy. The German partners MBB and Dornier withdrew support in 1983 leaving BAe and Aeritalia to complete the programme. The aircraft was primarily a technology demonstrator for the European Fighter Aircraft (EFA) and is now considered a cost effective wing structure in military terms. A multi-spar design (Figure 5) in which the sub-structure spar elements are co-bonded to the lower wing skin whilst, at the same time, the upper flanges are cured in place to the upper skin, thus eliminating an expensive shimming operation. This was the first time that important load carrying joints relied on adhesive bonding[10]. The small triangular region created where the spar web separates into two flanges and is co-bonded to the lower skin was found to act as potential site for crack initiation and subject to optimisation using finite element analysis. The region was filled with a adhesive 'noodle' having low shear modulus, high 'plasticity' and good resistance to moisture and temperature. The first Eurofighter (EFA) flew in 1992 with a similarly constructed wing.

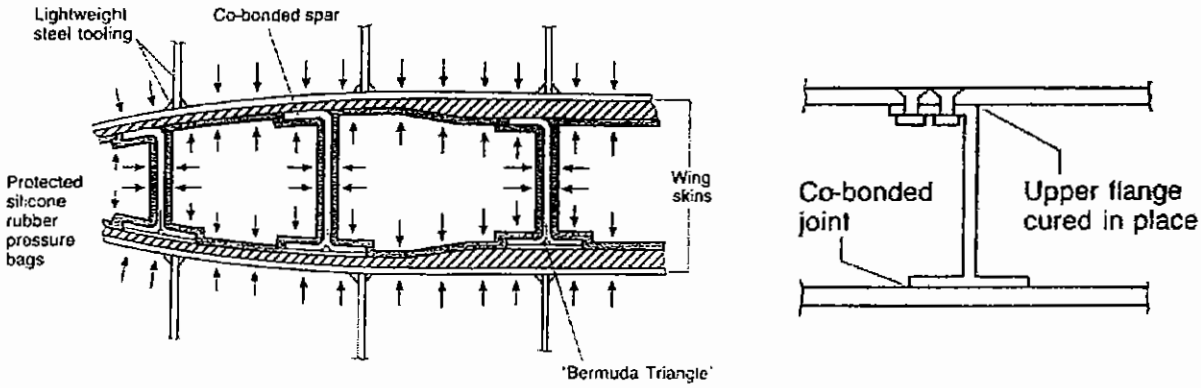

Figure 5: EAP skin to spar co-curing approach[8]

The SAAB Grippen has 30% of structural weight in composites. The vertical fin, canards and control surfaces are manufactured by SAAB and the un-swept wings by British Aerospace.

Dassault Aviation have a long history of carbon composite applications dating from the 1970's. These include a rudder (1970), horizontal (1976) and vertical stabilisers (1978) and other control surfaces for the Mirage range of fighters. Sponsored by the French government Dassault and Aerospatiale designed, flew and certified a composite wing for the Dassault Falcon 10 business jet providing Aerospatiale the know-how to build the first commercial aircraft primary structure wing for the ATR-72 and Dassault the confidence to develop the carbon composite wing for the Rafael fighter. The Rafael first flew in 1986 and 35% of structural weight is carbon composite manufactured with both thermosetting and thermoplastic matrices.

The American V-22 VSTOL tilt-rotor aircraft comprises between 50-70% of aircraft weight in carbon/epoxy composite. The wings use pultruded carbon/epoxy rods in the base and crowns of hat stiffeners and 'soft', predominantly ±45°, damage tolerant wing skins[11]. Current design efforts are focused on achieving 50% manufacturing and 25% supportability cost reduction for the wing, mainly though the use of a highly integrated wing structure design which will be of fully bonded construction. Both tape lay-up and RTM stitched preforms are being evaluated with the aim of developing design/build technology for future fully bonded wing and fuselage programmes[12]. The rear fuselage is manufactured by the Tow Placement process on a large rotating mandrel. The rotor grip is also manufactured by the Tow

Placement process. Since first flight in 1989 the V-22 has been subject to many design, engineering and manufacturing changes to reduce its cost and weight.

The McDonnell Douglas (Now Boeing) C-17 military transport, in the same way as commercial aircraft, has a majority of control surfaces and fairings manufactured in composites. As with commercial aircraft a majority of these components are manufactured by sub-contractor companies although some have been manufactured using a Kevlar stitched Resin Film Infusion manufacturing route by McDonnell Douglas, a process developed in the NASA ACT programme.

The structure of the F-22 low-observable fighter is 26% composite of which 4% is thermoplastic based. Around 200 components are manufactured using the Resin Transfer Moulding process including most wing spars, panel close-outs and internal fuel tanks. Tail-plane skins and control spline are manufactured using the Tow Placement process.

The American Joint Strike Fighter (JSF) program is likely to see the further development of manufacturing concepts first put into production on the F-22 and V-22 aircraft. However to ensure the 'affordability' requirements are met a number of supporting programmes have been instigated. The Composites Affordability Initiative (CAI) was set up by the US Department of Defence (DoD) as a vehicle for developing and demonstrating affordable technologies primarily for the JSF application. Participants co-operating in the initiative are Boeing, Lockheed Martin and Northrop Grumman. The programme includes the input of Burt Rutan of Scaled Composites who designed the first 'all composite' aircraft in 1974[14]. The Affordable Lightweight Aircraft Fuselage Structures (ALAFS) programme is similarly developing structural concepts to create a more integrated and cost efficient airframe using the F/A-18 as a testbed but aimed ultimately at JSF application[15]. Of the two contenders for the final JSF contract, Lockheed Martin is likely to be more ambitious than Boeing with the use of textile composites. Lockheed Martin managed a bulk of the textile composite work in the NASA funded, civil transport aircraft directed, Advanced Composite Technology programme. Boeing however are known to favour thermoplastic composites for a majority of the external surface of the aircraft. This is despite the only known production thermoplastic component in active service being the stabiliser (V-tail) on the Lockheed F-117A stealth fighter and some small components on the F-22.

1.5.2 Civil Transport Aircraft Chronology

Table 2: Civil aircraft composite applications[3]

		WING BOX		FUSELAGE				STAB.		CONTROL SURFACES					
AIRCRAFT	YEAR	COVERS	SUBSTRUCT	FORWARD	MID	REAR	INTERNAL	HORIZONT'L	VERTICAL	ELEVATOR	RUDDER	AILERON	FLAP	SPOILERS	AIR BRAKE
AIRLINERS															
Boeing 707	1970							L					D		
Boeing 737-200	1973/84								L		L			L	
MD DC-10	1975-78														
Boeing 727	1980									L					
Boeing 767	1981									P	P	P		P	
Lockheed L-1011	1982								D			L			
Boeing 757	1882									P	P	P	P	P	
Airbus A300-600	1983													P	
Boeing 737-300	1984									P	P				
Airbus A310	1985								P	P	P			P	
Airbus A320/A321	1987							P	P	P	P	P	P	P	
Ilyushin Il-96	1988						P						P		
Tupolev Tu-204	1989									P	P			P	P
MD MD-11	1990						P			P	P	P	P	P	
Airbus A330/A340	1993/91							P	P	P	P	P	P	P	
Boeing 777	1995						P	P	P	P	P	P	P	P	
REGIONAL TRANSPORTS															
Embraer Brasilia	1983					P							P		
SAAB 340							P						P		
ATR 42	1984									P	P	P	P		
Fokker 100	1986											P	P		P
ATR 72	1988	P	P							P	P	P	P		
Dornier 328	1991					P	P	P	P	P	P	P	P		

P = Production
L = Limited Production
D = Development

Aircraft designer Burt Rutan in May 1975 flew the first all non-wooden composite light aircraft, the aptly named 'Vari-eze'. It was a 'home-built' aircraft manufactured from a low density core, covered on both sides by fibre-glass composite[16].

In December 1975 the Lear Fan business jet, conceived by Bill Lear in 1954, flew for the first time. This was to be the first commercially manufactured all composite aircraft with production commencing in 1977. The fuselage was manufactured from four glass fibre composite panels; upper, lower and two sides, and the wing manufactured with four continuous carbon fibre composite spars running tip-to-tip. The project was abandoned in 1985 due to the discovery of fatigue fractures in areas of unexpectedly high stress during rig tests. This was blamed on incorrect stress analysis during the earlier design phase.

The first all carbon composite commercial aircraft was the Beech Starship which entered production in 1988. The fuselage was intended as a filament wound structure and a

prototype was manufactured by this technique, later abandoned in favour of prepreg skinned honeycomb panels. The wing is a 'fail safe' designed bonded box structure with three spars and Nomex honeycomb cored skin panels. Spar and rib attachment was facilitated by a paste adhesive/slotted joint arrangement made possible using routed slots in the skins into which are placed and spliced pre-cured 3D woven π inserts (Figure 6). Despite the use of three spars and bonded joints it was found necessary, in order to satisfy airworthiness authorities, to include 'chicken fasteners' on some joints to negate the risk of joints being in-completely bonded or contaminated during manufacture and subsequently failing in service. Owing to a heavier than anticipated structure and relatively poor aerodynamic efficiency only fifty aircraft were produced.

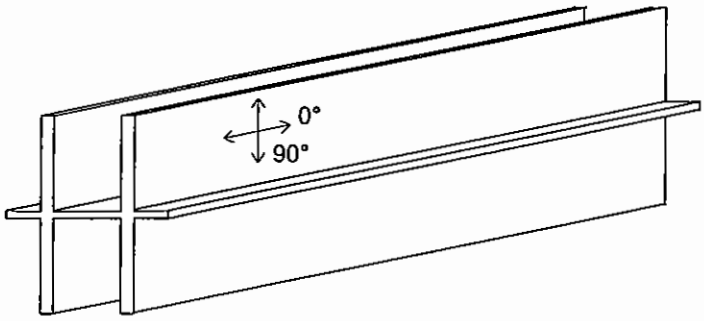

Figure 6: 3D woven π insert schematic for Beech Starship bonded joints

The application of composite materials to large commercial aircraft took place under two major NASA funded programs; the Flight Service Evaluation Programme and Aircraft Energy Efficiency (ACEE) scheme. With a budget of $450 million[17,8] the programmes were aimed at developing materials and manufacturing technology for initially secondary, non flight critical, and later primary structures commercial transport aircraft already in production. Through the Flight Service Evaluation Programme graphite/epoxy spoilers for the Boeing 737 entered flight testing in 1973 and series production in 1980. With funding from the ACEE programme contacts were awarded in 1975 to Lockheed, Boeing and Douglas to fund the development of three secondary and three primary structures[18] (Table 3). Detailed descriptions of the manufacture and assembly of the Douglas DC-10 rudder and Lockheed L-1011 (Tri-star) aileron and fin can be found in reference [8]. The DC-10 rudder approach was and still remains innovative, relying on the use of thermal expansion internal tooling and oven curing, rather than an autoclave, reducing manufacturing cost. The rudder was also a post-buckled design which saves weight by allowing the thin tri-axial skins (0° along span and ±45°) limited buckling between ribs, thus using the material more efficiently and saving weight. A similar approach is used for thin-skin co-cured assemblies on the Harrier AV8-B and for the ailerons of the more recent McDonnell Douglas MD-11. The Lockheed L-1011 fin box is one of very few composite structures for which both weight savings (25%) and cost savings (12%) over metallic structure were claimed. However the structure failed prematurely in rig tests, a lack of experienced design personnel being blamed for the failure caused by unexpectedly high interlaminar through thickness stresses and fatigue damage at the spar to skin joint[3,19].

Table 3: Composite structures developed through ACEE[18]

Secondary Structures	Primary Structures
Boeing 727 Elevator	737 Horizontal Stabiliser
Douglas DC10-Rudder	DC-10 Vertical Fin
Lockheed L-1011 Inboard aileron	L-1011 Vertical Fin

Composite fin-box units were certified and fitted to five commercially operational Boeing 737 aircraft in 1984, one year ahead of Airbus Industrie. Each tail-fin skin panel was fully co-

cured with woven fabric I beam stiffeners[8]. This fin-box never entered series production but paved the way for the design of composite primary structures for a new aircraft from 'scratch'. This allowed the weight savings achieved in the composite to be passed on to re-designing the whole structure which in turn reduces take off weight in what is known as the 'benign cycle'. This aircraft was to be the Boeing 777 whose empennage (tail-plane and fin) was designed and manufactured primarily from unidirectional prepreg tape by tape-laying and was the first production civil aircraft primary structure in composites for Boeing. A detailed description of the manufacture of this structure is presented by Iden and Pham[20].

Following the Flight Service Evaluation and ACEE programmes the NASA/DoD Advanced Composites Technology (ACT) programme was instigated by NASA as a $130m three phase programme running from 1989-2002. The informally stated impetus for the programme was the perceived threat of technological dominance posed by the Airbus consortium. The broad contents of the programmes three phases are shown in Figure 7.

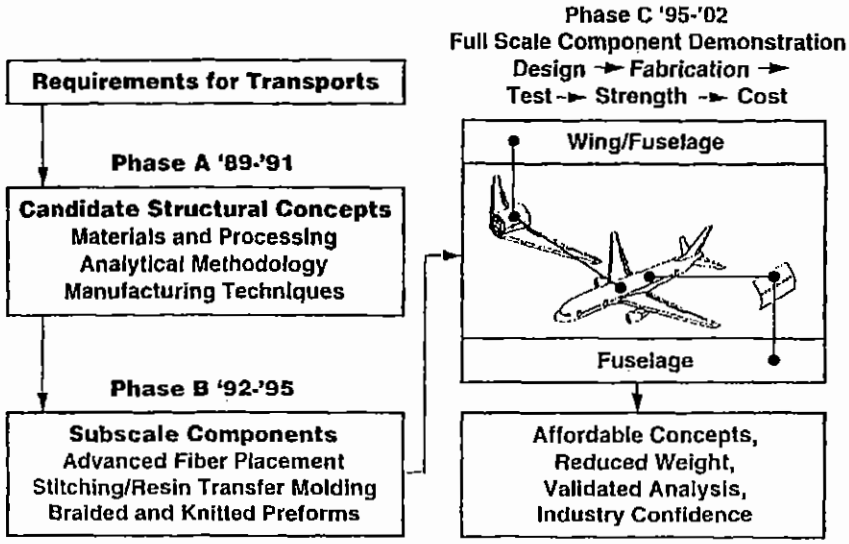

Figure 7: Advanced Composites Technology (ACT) programme[6]

Prime Contractors involved in the programme are Boeing, McDonnell Douglas (now incorporated in Boeing), Northrop Grumman and Lockheed Martin. Each contractor has focused on a different aspect of composite material and structure development, supported by NASA and a large number of sub-contractor companies and university research departments.

Within the textile part of the programme, five main structural sub-components were developed; fuselage keel beam, circumferential fuselage frames, fuselage window belt and various stiffened skin fuselage panels, and a dry stitched wing-box structure. Of these, the stitched multiaxial non-crimp fabric wing-box and triaxial braided fuselage frames are considered most likely to go forward to civil aircraft production. Automated fibre/tow placement was the other major, non-textile technology to be demonstrated as potentially cost effective and as now entered production for engine cowlings on the Boeing 777. As part of the final phase of this programme a large multihead stitching machine built by Ingersol and Pathe was commissioned (Figure 8). Capable of production size wing skin manufacture it has been used to manufacture demonstration civil aircraft wing boxes for test, as well as manufacturing demonstration wing skins for the F/A-18 fighter and flight control surfaces for the C-17 military transport aircraft. The machine is capable of stitching a one piece 12.5 metre span, 2.4 metre width and up to 38mm thick curved wing skin panel encompassing both braided blade stiffeners and spar caps. The wing skin lay-up is carried out using automated ply cutting followed by location using laser projection. In the subsequent

modified lock stitching process, access is required to the underside (outer wing surface) of the preform, which is achieved by lowering one of the 50 lift tables that support the curved profile of the preform and replacing it with the lower stitching mechanism. Stitching of each wing panel takes two shifts (approximately 14 hours).

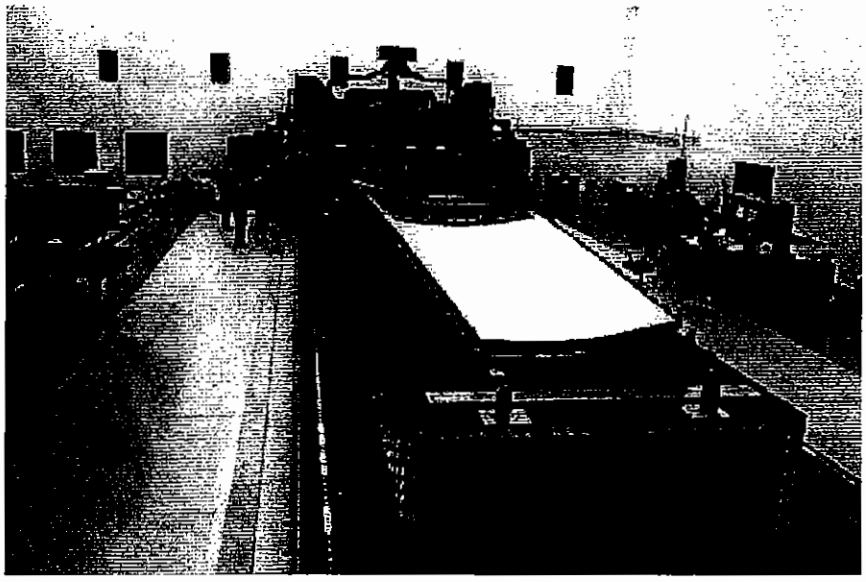

Figure 8: Boeing Advanced Stitching Machine (ASM)

Cost analyses indicate a reduction of 20% in cost can be achieved over equivalent wings built from aluminium and 50% cost savings over combined automated tape lay-up and hand lay-up. This saving compared to prepreg lay-up can be attributed principally to the high cost of manufacturing complex parts by hand in prepreg tape (rib caps and cleats), where automated tape laying cannot be applied. The breakdown of the costs of a stitched multi-axial warp knit route compared with prepreg technology is summarised in Table 4. This technology was originally aimed at the MD-XX aircraft[5] which, following McDonnell Douglas acquisition by Boeing in 1997 is considered unlikely to enter production.

Table 4: McDonnell Douglas stitched wing cost versus prepreg tape[21]

Stitched non crimp fabric + Thick film RFI		Automated tape lay-up and Hand lay-up			
Task	Hours	Task	Skin (Hours)	Stringers (Hours)	Rib Caps and Cleats (Hours)
Preform fabrication	58	Tape laying	14	7	
Trim preform	2	Hand lay-up (cut/collate/debulk)	4	40	100
Tool clean and prepare	16	Tool preparation	16		
Assemble tool	12	Assemble tool	12		
Bag part	4	Bag part	5		
Cure	9	Cure	4		
Unbag	4	Unbag	1		
Trim part	4	Trim part	4		
			60	47	100
TOTAL HOURS	109	TOTAL HOURS	207		

In 1972 the Airbus A300 fin leading edge and various non-structural panels were manufactured from glass fibre composite and in 1983 a single piece carbon-epoxy rudder was applied to all A300 and A310 aircraft with a weight saving of some 22% and at a comparable price to the previous metallic structure[22]. In 1985 the A310-300 entered service with a carbon/epoxy fin-box manufactured by Messerschmitt-Bolkow-Blohm (Now Deutsche

Airbus) at its Stade Plant. By 1987 an A320 was manufactured with both the fin and the tail plane in composite and entered series production the following year with composites comprising 16% of structural weight. The virtually unchanged A310 tail fin has been applied to all but the most recent A330 and A340 aircraft.

Both the fin, manufactured by Deutsche Airbus and tail plane manufactured by CASA, Airbus' Spanish partner, utilise a co-curing manufacturing process. The autoclave process used is additionally reliant on thermal expansion of aluminium blocks to consolidate a grid of blade stiffeners. These are formed by wrapping the blocks with pre-impregnated woven cloth oriented at ±45° (Figure 9). This array of tape wrapped blocks is compacted as a whole and loaded onto a woven fabric (fin), or tape-laid tail plane skin and subsequently co-cured. The fittings which allow the bolted attachment of the fin-box to the horizontal stabiliser are RTM carbon-epoxy, pre-cured and integrated into the lay-up prior to cure. Weight savings in the order of 20% have been achieved for the A320, 330 and 340 aircraft and they are said to be delivering excellent performance in service.

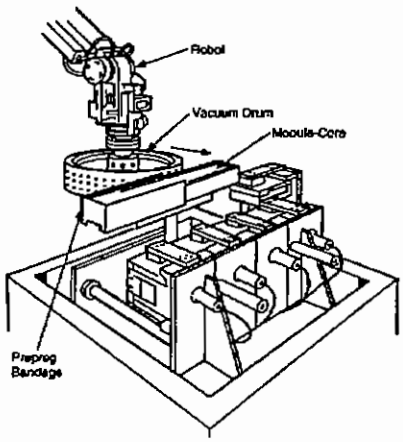

Figure 9: Airbus Fin woven prepreg tape wrapping and pre-compaction schematic[23]

However, after more than ten years of production the modular aluminium block co-curing approach used in the fin-box has lost favour, primarily due to the cost of making design changes when new aircraft and model variants are introduced. New A330-600 and A340 variants are expected to utilise the secondary bonding of blade stiffener elements manufactured by a continuous RTM/pultrusion process, giving more design flexibility whilst reducing tooling complexity and process risk[22,24].

The ATR-72, an aircraft built by a consortium of Aerospatiale and Alenia, is the first European production aircraft with carbon-epoxy composite outer wing sections. Measuring some 8x1.2 metres it is manufactured with carbon/epoxy integrally stiffened skins, two spars and aluminium ribs. These structures have been in full commercial service since 1987[25].

Aerospatiale, having gained significant experience on the Falcon 10 with Dassault Aviation and ATR-72 composite wing, have developed a highly loaded composite wing box for an 80-120 seat jet airliner. Targets are 20% weight savings at equal manufacturing cost to a metal wing. Started in 1991 and due to last 6 years the programme included the fabrication of a full scale wing-box incorporating RTM components, improved toughness resins, improved strength and modulus fibres. Skin stresses are believed to be three times higher than those in the ATR-72[22]

Deutsche Airbus completed the manufacture and test of a flat skinned (non-aerodynamic) box in 1994[26]. Additional boxes were subsequently built to test engine and undercarriage attachment schemes, and lightning strike and fuel sealing approaches. A fourth box incorporating secondary bonded continuous RTM stringers, Resin Film Infused multiaxial

non-crimp fabric ribs, some multiaxial non-crimp RTM spar elements as well as 24k based prepreg tape-laid spars and wing skins is to be completed in early 1998 followed by full structural testing.

The Airbus A318/AE100 development programme, a partnership between Aerospatiale and Aircraft Industries of China (AVIC) has developed a composite wing box for a 80-100 seat regional airliner. The wing-box is of unidirectional prepreg construction with continuous RTM/pultruded stiffeners. The status of the programme at present is unknown particularly in the light of Boeing entering this market with the re-badging of the MD-90 as a Boeing 717.

As with American and other European commercial aircraft manufacturers the Russian Illushin Il-86 and Il-96 has some secondary structures and panels in carbon/epoxy composite. The Tupolev Tu-204, the Russian equivalent of the Boeing 757, is about 18% by weight in composites, including most control surfaces and part of the wing skin[3].

1.6 Design allowables and guidelines for composite design and manufacturing

1.6.1 Design Allowable Stresses/Strains

The cost of qualifying a new material and determining its design allowables is quoted as being $3-5m. It is advised that material qualification should be performed separately from aircraft structure design and development as co-development poses too greater a risk[3].

The translation of in-plane material property 'coupon' data into the allowable stresses or strains in a structure is complex. It is dominated by the requirement for bolted repairs and damage tolerance requirements. These generally require the structure be able to sustain design ultimate loads, in the worst case temperature/humidity environment, in the presence of repaired structure and barely visible damage (below the threshold for detection). The nature of these are as follows:

1. Repairs; drilled holes (filled and un-filled) created in the bolted repair of detected damage or out-outs created in the preparation of patch repairs.
2. Undetectable damage caused by 'in-service' usually low velocity impact
3. Un-detected manufacturing defects.

Furthermore the structure must be able to sustain a proportion of the allowable design stress with levels of detectable or discrete damage sustained in-service, in order to allow the aircraft to operate with restrictions until a repair can be carried out, or as a minimum to land safely. These requirements are summarised in Figure 10.

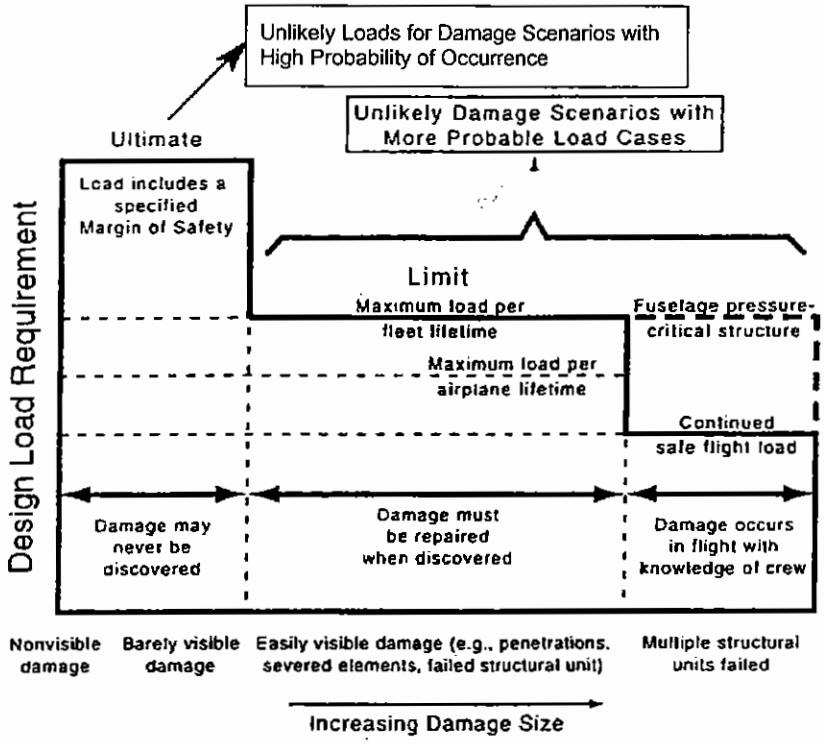

Figure 10: Damage tolerance design requirements[3]

In most cases it is Barely Visible Impact Damage (BVID) that restricts design allowable stresses in compression areas (upper wing skins) and open hole tension in tension areas (lower wing skins). For civil aircraft wings which are long and slender, deflection levels resulting from high design strains adversely affect the aerodynamic profile of the wing and this places an upper ceiling on the allowable design strain irrespective of the allowable stress[27]. Similarly because wing skins are optimised between strength and buckling a large proportion of the outer wing, where the stress due to wing bending is lower, might be working to design strains much lower than those at the root. These can be as low as 0.2-0.25% strain[28]. Because of the aerodynamic profile of the wing, the tensile and compressive stress/strain in the skin due to wing bending is not evenly distributed over the chord, with a maximum stress expected at the point of inflection.

In military aircraft allowable strains of -0.39% strain in compression and 0.42% strain in tension were used in early wing designs. This was increased to -0.42% and 0.475% strain for toughened epoxy systems and as high as ±0.55% strain for high modulus fibre, high toughness resin combinations such as 5245/T800 as used for a majority of the Eurofighter 2000 airframe[29]. However as strain levels are increased the allowable in the compression skin becomes governed by ply-dropoff and damage tolerance (rather than resistance) strength requirements[28,4].

To account for the variability in mechanical test data used to generate design allowables, confidence limits are assigned to the test data; Statistically based 'A-basis' design allowables and later 'B-basis' allowables are used for design purposes as performance confidence increases. These calculations take into account performance degradation due to moisture and humidity and highlight the importance of both absolute performance and its variability in material and manufacturing process selection.

In summary, the allowable stresses in a structure will be determined by; (1) constituent properties of the composite system; (2) component and lay-up design and structural configuration; (3) strength/stiffness translation efficiency in the fibre architecture of the reinforcement when subject to holes; filled and un-filled, detectable damage, undetectable

damage (impact or manufacturing defects); (4) the density of the component (fibre volume fraction). The weight efficiency of a material can be measured by considering only the allowable working stress divided by the laminate density; for the same fibres and resin, this is proportional to the fibre volume fraction.

1.6.2 Design Guidelines

Damage tolerance improvements have been demonstrated by through thickness reinforcement techniques such as stitching and pinning, as described in section 1.7.6.1 and 1.7.6.2, and potentially through the use of integrated 3-Dimensional preforms which are manufactured with reinforcing fibres passing through the entire thickness of the structure. Other design approaches used to improve the damage tolerance of aircraft structure are based upon reducing the probability or effect of hitting critical structure. 'Soft skin' approaches, where the primary load bearing reinforcement is moved away from the vulnerable skin surface and into wing spars or stiffener elements has been employed in the V-22 Osprey tilt-rotor aircraft[3,11], and the BAe Jaguar wing demonstrator[28].

As these techniques move away from reliance on constituent properties of the laminate and towards structural configuration or a tailored reinforcement architecture, so the design guidelines that have largely been derived empirically from prepreg tape military aircraft programmes[28] become less relevant. and can restrict the development and application of more cost effective and damage tolerant designs. This leads to the generation of design allowables from test elements representative of the final structure rather than coupon tests.

Prepreg design guidelines advise on material thickness, fibre orientations, lay-up, thickness tapering and joint schemes so as to optimise the performance of the structure and simplify the design process. A summary of design advice as considered likely to impinge on the application of new materials and manufacturing processes as alternatives to unidirectional prepreg tapes is given below.

1. Although the ability to tailor the directions of fibre reinforcement is generally regarded as one of the principal benefits of composite materials, the use of basic ply families of 0°/90°/±45° has been used successfully for most applications, with the proportions in each orientation being proportional to the stress or strain requirement in that direction. Limits are placed upon the maximum and minimum proportion of plies in any one orientation. A minimum of 10% of the total number of plies in each of the four directions (0°, 90°, ±45°) is widely applied[4,30] and is used to allow for 'unexpected local stresses'. For load bearing skin structures a maximum of 50%[3,27] or 67%[28] in any one orientation have been suggested. At points of load introduction or geometric discontinuity the number of plies in the principal load direction can be reduced to 'soften' the structure and reduce the stress concentration factors[3]. The fibre steering capability of the latest tape-layers and tow placement machine has generally been restricted to coping with laying prepreg tape onto double curved surfaces whilst avoiding wrinkles and gaps.

2. Thin (0.125mm) prepreg tapes are used for most structures, with no more than four plies of the same orientation placed together (0.5mm or 525g/m² of carbon fibre at 60% V_f). This rule is justified due to observations of transverse thermal cracking in the resin matrix, leading to poor interlaminar shear strength. Thick 0.25mm prepreg tapes are not widely used in military airframes as they produced poor interlaminar shear results during testing, said to be due to transverse thermal cracks[28] although it may be due to the reduced number of interlaminar planes for a given thickness and the consequently higher interlaminar stress.

3. Laminate stacking sequences which minimise the angular mismatch between adjacent plies are preferred as this minimises differential interlaminar stresses between the

layers[30]. This is typically achieved using repeating balanced ply families such as [0°,+45,0°,-45°,90°,-45°,0°,+45°,0°]^4

4. Laminates should be balanced about the mid-plane to minimise distortion due primarily to resin matrix shrinkage during curing and cool down from curing temperature. Hybrid laminates contain a mixture of two or more reinforcing fibre types can cause additional difficulties. It is suggested that the combination of carbon and aramid fibres should be generally avoided due to their different coefficients of thermal expansion which can lead to matrix cracking[3].

5. To satisfy strength and damage tolerance requirements plies should be dropped-off symmetrically within the stack allowing plies to continue on the top and bottom surface of the laminate. The exception to this may be in the application of composites to cored structures where plies may be dropped against the core surface. Ply-dropoff rates should be such that they give a maximum gradient of 1 in 20

6. Whiteside[28] suggests that external plies should be perpendicular to the main load bearing fibres to assist in the resistance to external (impact) damage. However other guidelines suggest that external plies should not be transverse to the major load axis as this encourages transverse matrix cracking. In another study it is implied that external plies should not be the primarily load bearing plies as they may be easily damaged by scratches or impact leading to a lack of fibre continuity. Consequently most external surfaces use woven plies typically oriented at ±45°.

7. In co-cured (joined parts both un-cured), co-bonded (one part on-cured) or secondary bonded structures (both parts cured), the stress concentration where details, such as longitudinal stiffeners attach to skins, make tapered flanges necessary. Taper angles shallower than 30° are preferred, as is the interleaving of the flange under some skin plies or the use of a covering ply to reduce the effect of peel stresses[28].

The high level of performance optimisation of military aircraft structures and their relatively small size means that commonality of parts and design is not large within the structure. This favours materials and manufacturing processes that are able to create generally thin structures with large amounts of thickness tailoring. There is therefore little benefit from the use of processes which are only economic when manufacturing large quantities of a single part or have long set-up times. Damage resistance/tolerance issues relate primarily to ballistic high velocity impact and their effects degrade the strength of the joints rather than skins, which are expected to be perforated. These risks have been dealt with through the use of mechanical fasteners for joints or the removal of bending strength critical structure behind the skins in stringers or multi-spar constructions .

For commercial aircraft the wing structure is long and slender with a surface area and material thickness that is much greater than that of a military fighter wing. The internal structure is also simpler and consequently there is more scope for the use of continuous section stiffeners throughout a large proportion of the wing.

From a cost efficiency viewpoint, materials and fabrication costs form the largest part of the overall production cost, 25% and 55% respectively are suggested by Horsting et al[31]. Thus because the weight of structure increases dramatically when moving from a military fighter airframe to a large civil aircraft, so material cost increases proportionately. If prepreg tapes of the same thickness as typically applied in military programmes are used for civil aircraft, because the deposition of prepreg tapes is area rather than volume based, fabrication times and hence costs using the same manufacturing techniques are likely to be prohibitive unless automated manufacturing technology can operate extremely fast. This suggests a greater scope for the use of new materials and processes particularly for complex components

which cannot be manufactured economically by either hand lay-up or automated equipment in the volumes required for civil aircraft production.

The Materials and Manufacturing Technology Options described in the following section are presented as technologies considered as substitutes, in full or in part, for current aluminium primary structure manufacturing and alternatives to laminated prepreg tape structures.

1.7 Materials and Manufacturing Technology Options

The manufacture of structures from carbon fibres is, in most cases, a two stage process, firstly conversion of the fibres and matrix resin into a stable intermediate product and secondly the assembly of the intermediate into the final part shape (Figure 11). This is particularly true of the aerospace composites industry where thin skinned components are most suited to a laminated composite approach. However there are also processes capable of creating the final part geometry directly from fibre tow and matrix resin avoiding the need for an intermediate stage.

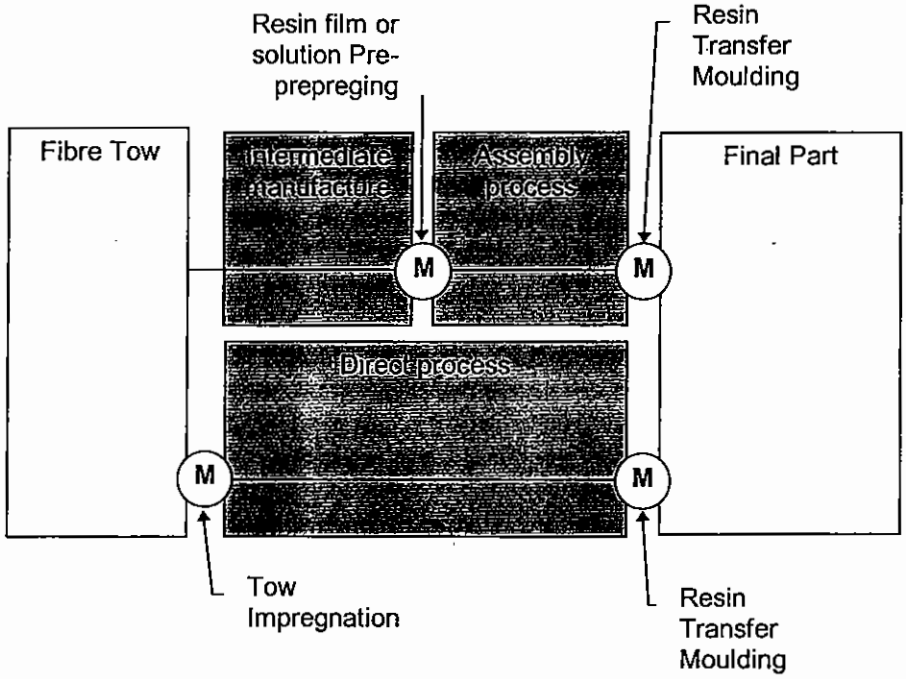

Figure 11: Process steps from raw materials to final part

In this chapter, methods used to classify composite reinforcements are discussed. This is important as it allows the materials and manufacturing processes available to be grouped according to their capability to meet certain design requirements. Raw materials are very briefly discussed primarily to consider how materials have changed and the implications of this on aircraft design. Intermediate materials and methods of assembling them into complete parts are then briefly described in general terms focusing on the manufacturing hardware used for different types of parts. Included in this section are techniques used to impart discrete areas of through thickness reinforcement or to attach layers of material together as an aid to assembly. Finally manufacturing technologies that create the net shape of the component in a single operation avoiding the need to manufacture an intermediate product are presented.

1.7.1 Classification of Structural Composites

By consideration of structural integrity, fibre linearity and continuity, Ko[32] classifies textile preforms into four categories; discrete, continuous, planar interlaced (2D) and fully

integrated (3D) structures. These different levels of fibre architecture are summarised in Table 5 and described below according to Scardino[33].

Table 5: Classification system for fibrous reinforcements[33]

Level	Reinforcement System	Textile Construction	Fibre Length	Fibre Orientation	Fibre Entanglement
I	Discrete	Chopped Fibre	Discontinuous	Uncontrolled	None
II	Linear	Filament Yarn	Continuous	Linear	None
III	Laminar	Simple Fabric	Continuous	Planar	Planar
IV	Integrated	Advanced Fabric	Continuous	3D	3D

The first category of textile preforms is the discrete-fibre system. A discrete fibre system such as a whisker or fibre mat has no material continuity; the orientation of the fibres is difficult to control precisely, although aligned discrete fibre systems have been produced and used commercially. The structural integrity of the fibrous preform is derived from inter-fibre friction and often additionally from the application of heat fusing thermoplastic or thermosetting binders. The strength translation efficiency, or the function of fibre strength translated to the fibrous assembly of the reinforcement system is quite low.

The second category of preform is the continuous filament or unidirectional (0°) system. This architecture has the highest level of fibre continuity and linearity, and therefore has the highest level of property translation efficiency and is very suitable for filament wound and angle ply tape lay-up structures. The drawback of this architecture is its intra and interlaminar weakness due to the lack of in plane and out of plane interlacing.

The third category of fibre reinforcement is the planar interlaced and interlooped system. Although the intralaminar failure problem associated with the continuous filament system is addressed with this form, the interlaminar strength is limited by the matrix strength due to the lack of through thickness fibre reinforcement.

The fully integrated system forms the fourth category of textile preform wherein the fibres are oriented in various in plane and out of plane directions. With a continuous filament yarn, a three dimensional network of yarn bundles is formed in an integral manner. The most attractive feature of the integrated structure is the additional reinforcement in the through thickness direction which makes the composite both delamination resistant and tolerant. Another interesting aspect of many of the fully integrated shapes is their ability to assume complex structural shapes.

Cox and Flanagan[34] categorise groups of textile reinforcements as either 'quasi-laminar' or 'nonlaminar'. Quasi-laminar textiles include all 2D and many 3D reinforcements where high in-plane stiffness and strength are demanded and consequently a majority of the reinforcing fibres lie in-plane and relatively few are dedicated to through thickness reinforcement. In structures where substantial triaxial stresses exist, the optimal reinforcement will be arranged by some process capable of orienting fibres along all three axes of a Cartesian system. Such non-laminar textiles are often manufactured to correspond to complex part geometry such a the joint of a skin and a wing spar or stiffener element. The secondary stitching of textile preforms is categorised as quasi-laminar unless the through thickness tensile forces are such that so much through thickness reinforcement is needed to suppress delamination whereby the part may be considered non-laminar.

Dickinson[35] in this matter categorises stitching as either 'Selective'; where it is applied locally for joining applications as a means of 'handling' the interlaminar stresses near a free edge, or 'Comprehensive' where it is applied across the entirety of a part or panel primarily with the

aim of improving material properties and more specifically damage resistance and tolerance. In this situation we can categorise 'selective' stitching as creating a 3D textile preform, and 'comprehensive' as creating a 'quasi-laminar' system in which damage resistance and tolerance properties have been enhanced.

1.7.2 Raw Materials Choice

The first decision is that of fibre and matrix systems. This is not solely an issue of cost constraints and performance requirements but also ease of conversion to an intermediate or direct arrangement into the final component. For carbon fibre based structures this is dictated by the strength/stiffness of the fibre which is primarily dictated by the thermal treatment during manufacture and also its precursor. Most important from a handling viewpoint is the tow filament count, tow bundle shape and sizing; that is the pre-treatment type and amount added to modify the interfacial properties and handling behaviour.

On the most fundamental level structures may be created by arranging fibres directly into a mould tool, but this tends to be difficult and slow for anything but tubular structures, where processes such as filament winding and braiding are effective. Fibres without a means of constraint are unlikely to stay where they are placed and will retain their 'as manufactured' bundle shape leading to low packing efficiency as layers cannot sit as closely together as if the layers were uniformly flat. Stable intermediate arrangements of fibres or application of all (pre-impregnation) or some of the resin (binders) are therefore generally used.

1.7.2.1 Fibres

Consolidation of carbon fibre manufacturing businesses since the late 1980's has left only three companies producing significant quantities of aerospace qualified materials world-wide; Tenax, Toray and Hexcel (formerly Hercules). The inclusion of this information is important as they have a very strong strategic position within the aerospace composite structures business environment. At present and for the foreseeable future, demand outstrips supply, particularly from the recreational goods industry where a higher price per kilo can often be obtained for a lower performance product. This is despite the two European based manufacturers Toray and Tenax putting new plant on line by the end of 1998 dedicated to the production of 12 and 24k tow. Additionally, qualification of components once in-place constrains the choice of material usually to two specified materials, creating sizeable barriers to the entry of other fibre manufacturers and allowing those selected to maintain a very healthy margin on their product. However despite this the movement in fibre prices is downward, to encourage more composite usage in the long term and due to the economies of scale benefits of larger filament count tows and the increased capacity being brought on-line.

Continuous fibres are generally available in the following filament counts ½k, 1k, 3k, 6k, 12k, 24k. Of these 3, 6 and 12k are the most widely used, ½ and 1k finding use in specialist applications such as the production of fine pultruded rods or as a high performance stitching yarn. 24k tow is becoming increasingly important as it offers significant cost benefits to fibre producers; almost doubling the throughput of manufacturing plant. 24k has been difficult to produce with uniform properties until recently, as process control in fibre manufacture could not sufficiently control the exothermic carbonisation of such large bundles during the carbonisation of the precursor. The costs of high strength aerospace qualified carbon tow (Tenax HTA) of different filament counts is shown in Table 6.

Table 6: Relative costs of different tow sizes (Carbon HTA)[36]

Filament Count	Price/kg
1k	137

3k	37
6k	27
12k	20
24k	17

Costs of 3k and 6k tow can be expected to increase or at least remain static as recreational and industrial applications, that make up a majority of world-wide carbon fibre applications, move to use lower cost 12 and 24k (and higher) tow. A majority of 3k and 6k capacity will be used for current production aircraft and particularly for woven reinforcements and there is not thought to be sufficient demand to increase capacity for filament counts less than 12k.

In the traditional textile industry, yarns are twisted to provide structural integrity and the ability to hold shape. In forming structural composites, in contrast, 'softer' yarns are desirable, since this allows compaction to maximise the total volume fraction or flattening to maximise coverage. Furthermore, twist would reduce the axial stiffness and strength of the yarns, which is paramount in airframe applications. Therefore, yarns with minimal (rovings) or nominally zero-twist (tows) are preferred[34]. As well as zero-twist tows, some grades of material are also available in tape form, providing a wide, flat band of fibres effectively pre-spread to an areal weight suitable for the manufacture of either tow-preg for tow placement machines or for the manufacture of high quality prepreg tapes.

1.7.2.2 Matrix Resins

Consolidation of epoxy matrix manufacturing companies has been more extreme than that in the fibre manufacturing business with Hexcel dominating the prepreg resin market having acquired Ciba Composites and Hercules' resin matrix business. Cytec, who now owns Fiberite, and 3M are significant competitors, 3M particularly in the Resin Transfer Moulding market. Unsurprisingly therefore matrix costs have not fallen and cost premiums with the introduction of matrices with enhanced toughness are higher still.

A majority of military aircraft were designed and are still built with 6k tow based unidirectional pre-preg tapes and/or five-harness satin fabrics based on 3k tow using relatively low toughness epoxy based matrices such as Hexcel 914 or Hercules 3501-6 and standard high strength fibres such as Hercules AS4 or Toray T300. As new aircraft and aircraft upgrades are introduced these are now using more modern fibres and tougher matrices such as Hercules IM7 or Toray T800 fibres and 977-2/3 or 8552 matrices to allow either higher working stresses or to reduce weight. Some matrices such as Cytec 977 series are available in 'grades' for use in the pre-impregnation of tapes or woven fabrics (977-2) and also for resin transfer moulding process (977-3)[9].

With the new found interest in textile techniques and stitching with their increased damage tolerance it was anticipated that there would be a move away from high cost toughened matrix systems such as that used in the Boeing 777 tail-plane, to low toughness and low cost epoxies[27]. The argument in this case being that the damage tolerance afforded by the stitching process negates the need for any additional toughness from the resin. In practice the reductions in the propensity for microcracking and improved consistency of mechanical properties offered by more modern tougher matrices has meant that they are still used despite the cost penalty.

1.7.3 Intermediates

Intermediate products are pre-arrangements of fibres, often with matrix resin, in a material form which in some way simplifies the creation of the composite part. In most cases the materials are laminar or quasi-laminar, that is they are suitable for sheet or skin applications and behave as laminates although some of the reinforcing material may pass through the thickness of the material. Intermediates are used in assembly processes such as hand lay-

up, automated pick and place systems or tape-laying to create the final structural shape. They range from at the lowest performance level, chopped strand mat to high performance unidirectional prepreg tapes. In this section only materials in which the fibres are primarily aligned are considered.

1.7.3.1 Unidirectional Tapes

Unidirectional pre-impregnated tape, 'prepreg', consists of bundles of continuous fibre tow spread, by pulling over a series of rollers, to a prescribed thickness/areal weight and uniformly impregnated with usually the net volume of matrix resin to create a nominal fibre volume fraction of around 60% in the final cured structure. Dry, non woven unidirectional tapes, manufactured principally as unidirectional reinforcements for the RTM process, include sheets of unidirectional fibre spread and subsequently stabilised by powder binders, resin beads or by resin coated or melted thermoplastic webs or threads.

For prepreg tapes the impregnation process may be solvent based. The matrix resin is dissolved in solution to create a 'lacquer' which with its reduced viscosity, and with the help of rollers, wets out and coats the fibres. Subsequent drying evaporates off the solvent leaving the desired net volume of matrix resin. The second process, Resin Film Prepregging, requires the creation of usually two resin films cast off-line onto silicon coated backing papers, which together provide the net resin volume needed. These are rolled at elevated temperature and under pressure onto each side of the spread fibre sheet causing the matrix to soften and impregnate the fibres. The backing papers are then removed and discarded and new thicker papers and or plastic films applied prior to slitting to the desired width and spooling onto drums. Typically a width of 300mm is used although 'broadgoods' of more than one metre width are common, as are narrow slit tapes of around 150mm for use in automated tape laying equipment. Most materials used in aerospace applications have been 0.125mm thick and manufactured from 6k tow, 0.25mm thick material from lower cost 24k tow is only now being qualified as an acceptable alternative.

The use of a one-part pre-mixed epoxy matrix makes storage below -18°C necessary in most cases and restricts life at even this temperature to between 6 months and one year and significantly less at room temperature. In terms of fabrication the most important feature of a prepreg tape is its level of tack, that is its level of adhesion and ability to be repositioned with respect to adjacent plies. The level of tack is generally controlled by either the state of pre-advancement of cure (degree of cross-linking) or by the addition of secondary lower viscosity epoxy groups which modify the level of tack.

The manufacture of impregnated tow (towpreg) initially as a low cost alternative to slit prepreg tape for filament winding has been further refined as a feedstock for automated tow-placement machines. Resin deposition is usually accomplished using a resin bath method or electrostatic or gravity fed powder deposition of the resin followed by a fusing and rolling stage, the latter being applied to both thermoplastic and thermosetting matrices where the matrix viscosity is considered to be too high for a resin bath method. The use of impregnated tow in Automated Tow Placement is quoted as offering a 20% raw material cost benefit over slit prepreg tape and without any performance penalty[37,38]. Difficulties in producing a consistent width, void free tow often make it more reliable, if more expensive, to use prepreg tape slit to the desired width.

The costs of producing prepreg tapes are high and highly dependant on the cost of the resin constituents, its ability be pre-mixed in economically large batches without the risk of uncontrolled exothermic reaction, and on the amount of consumable materials used in its production. There is also a significant cost premium for high toughness systems which may offer considerable performance benefit to the customer.

A number of unidirectional dry tape systems have been developed aimed primarily at RTM components as a replacement for unidirectional materials. Among these are fibre tapes stabilised by resin threads, thermoplastic yarns and webs coated in resin, powder binders and those stabilised by fine weft yarns (dealt with in 2D weaving). A majority of these have found applications in the recreational goods industry but have also been considered by aerospace companies and their part suppliers. The main concern with these materials is compatibility of the stabilising threads or resins and the risk of fibre wash during RTM impregnation.

The principal limitation of prepreg tape materials is its low thickness, a requirement based upon reducing interlaminar stresses, at ply drops and free-edges and due to thermal stresses. This leads to very low lay-down rates of around 0.5kg per hour for hand-lay up, unavoidable for small detailed parts and around 3-5kg per hour for state-of-the-art tape laying equipment for the lay-up of flat or gently curved tapering thickness parts.

1.7.3.2 2D Woven Fabrics

2D weaving prearranges the reinforcing fibres usually in the 0°/90° orientations and usually in the same proportion. This is done on a relatively conventional weaving loom; with a large creel supplying the axial 'ends' or 'warp' fibres and a rapier (connected by rod or belt) or more unusually a shuttle inserting the weft fibres. The raising and lowering of alternate warp yarns creates a 'plain' weave and different combinations of raising and lowering creates different weave patterns common among which are satin and twill weaves. In a twill weave each warp and weft end passes over two and sometimes four crossing yarns and produces a fabric identical on both faces. A satin weave is produced when each warp and weft passes over usually five or eight and under one crossing yarn (Figure 12) This reduces the amount of crimp in the fibres and because the fabric now has a warp and weft face it is preferable to place like layers together to minimise resin rich areas.

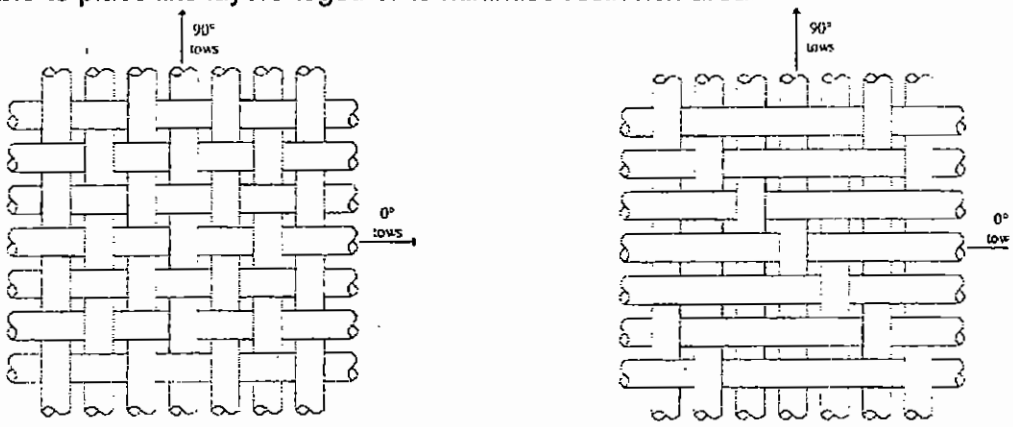

(a) plain weave (b) 5-harness satin weave

Figure 12: Common woven reinforcement styles[39]

Woven fabrics tend to be made from low filament count tows, usually 3 or 6k. This is because the nature of the weaving process does not readily allow spread tows to be used and so in doubling the tow filament count the fabric weight is approximately doubled. Similarly the larger the filament count the coarser the weave and the greater the level of out-of-plane tow crimp.

Out-of-plane tow crimp lowers both the in-plane strength and modulus of the woven composite. Tensile strength and modulus reductions of 15% have been reported comparing woven carbon with unidirectional tape composite[40]

The microcracking which occurs between the transverse fibres during tensile loading can be modified by manufacturing the fabric with highly twisted roving. This prevents microcracks

from moving between transverse tows through matrix rich regions. Instead cracks grow around or into the twisted roving and result in a higher residual tensile stiffness compared with woven fabric composite manufactured from untwisted tows for a given applied strain[41].

Woven materials are sold 'dry' or 'prepregged' but usually with a reduced fibre volume fraction of around 55% to allow for the resin pockets created by the interweaving of warp and weft yarns. Material widths are typically the same as those for other woven textiles at 1.27m as the machines are usually built by the same companies.

Woven fabrics with more than 95% warp yarns are known as Uniweaves and have the remainder of the total weight as glass fill or weft yarns. They are generally used as a replacement for unidirectional prepreg tape in liquid moulding processes where dry 'unidirectional' fibres are required.

A small number of companies including Hexcel are able to manufacture bias woven reinforcements, where the fabric is manufactured with the weave in the ±45° direction relative to the length of the fabric as opposed to the more normal 0/90° arrangement. The Barber-Coleman Company and Nissho Iwai Corporation are also able to manufacture multi-axial woven materials with as many as three orientations present, typically 0° warp with ±45° or ±60°. However, in order to obtain acceptably small 'windows' around where the yarns intersect, very small filament counts (1k) are used (Figure 13)[42].

Figure 13: Triaxial weave indicating large 'windows' resulting from yarn cross-over points

Radial weaves are a special case of the 2D weave still consisting of warp and weft yarns, this time with warps arranged circumferentially with radial weft yarns weaving in between them. They are produced on a relatively simple modification of a standard loom using two adjacent cones which form the weave into a spiral 'racetrack' as it is comes off the loom. Their major application has been in the manufacture of silicon carbide fibre preforms for metal and ceramic matrix composite turbine engine parts, although they could equally be applied to the reinforcement of holes and an cut-outs in polymer matrix composites. Dow-UT and Lydell Manning (formerly Textile Technologies Industries Inc.) produce such reinforcements commercially.

Dow-United Technologies (Dow-UT), a joint venture between Dow Chemicals and the United Technologies corporation, have since the early 1980's been manufacturing high quality and high cost RTM components principally aiming at high value military components and particularly parts traditionally manufactured in titanium. With the exception of a few partially braided components, all parts are manufactured from 2D woven fabrics stabilised by compatible 3M PT500 epoxy or Cytec bismaleimide powder binder and preformed to shape prior to loading into mould tool and resin transfer moulding.

Despite the property limitations of woven reinforcements due to fibre crimp and of volume fractions limited to 55%, the extreme repeatability of the manufacturing process is reliant on the stable woven reinforcement, both in its forming to shape and its resistance to 'fibre-wash' during RTM. Parts of consistent performance and shape allow reliable interchangability of parts, critical in military airframes and provide a direct composite replacement for metal structures but with reduced weight.

'Pre-plied' uni-weave fabrics, stitched together in multiaxial stacks of nine plies using Kevlar yarn, were extensively developed and characterised for aircraft wing manufacture by McDonnell Douglas. Preplied families were passed through a multineedle quilting machine (Figure 14) manufactured especially by American stitching equipment manufacturer Pathe.

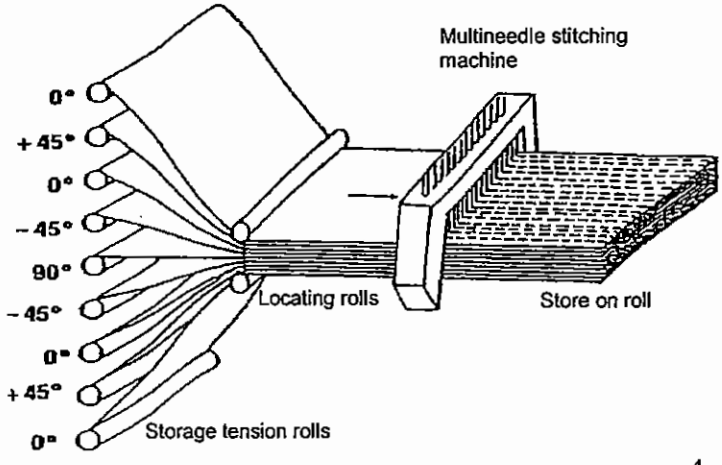

Figure 14: Multi-needle stitching machine schematic[4]

However problems of material stability and handleability led to the consideration of multiaxial warp knit fabrics as an alternative in around 1992. The results of comparative tests are reported in Dexter and Hasko[43] and indicate equivalent performance of uniweaves and LIBA multiaxial warp knit fabric composites.

The range of Airbus aircraft from the A320 onwards have all been manufactured with the tail fin-box manufactured from woven pre-impregnated cloth for both skins and internal structure, much of which is manufactured by a modular interlocking aluminium block approach relying on thermal expansion to consolidate the blade stiffener webs during co-curing. Automated woven cloth tape wrapping is employed to lay web material around the aluminium formers prior to loading onto the skin.

1.7.3.3 Multi-axial Warp Knitted Non-crimp Fabrics

From the structural geometry point of view a multiaxial non-crimp fabric system consists of warp (0°), weft (90°) and bias (±θ°) fibres held together by a chain or tricot stitch through the thickness of the fabric (Figure 15). Combining the desired fibre orientations and layer weights in a single fabric creates a 'preform' having the multidirectional reinforcement similar to laminate ply lay-up but produced in a single step process.

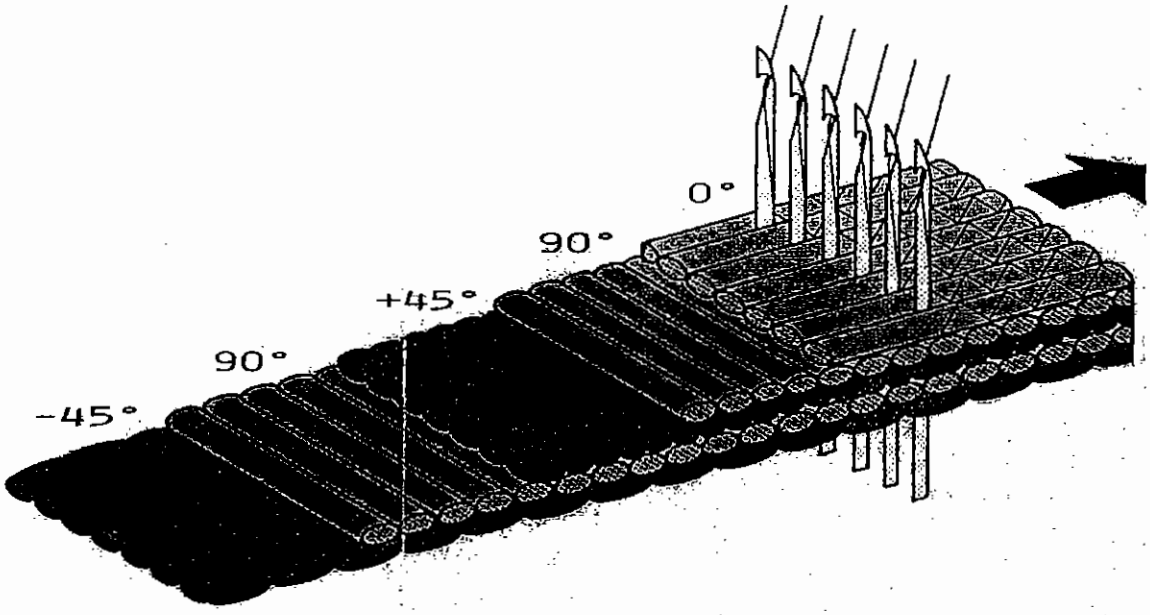

Figure 15: Multi-axial fabric schematic

Pastore[44] classifies multiaxial non-crimp fabrics by four parameters; linearity of bias yarns, number of axes, stitching geometry and stitching mechanism. These are shown in Table 7 along with the possible levels for each of these parameters.

Table 7: Manufacturing parameters for multi-axial fabrics[44,33]

Variables	**Level**
Linearity of Bias Yarn	Linear, Non-linear
Number of Layers Possible	1,2,3,4,...7
Stitching Geometry	Chain, Tricot
Stitching Mechanism	Impalement, Non-impalement

The selection of these parameters depends both on the flexibility of the machine type used and on the requirements of the final application. Three machine types are used to manufacture multiaxial non-crimp fabrics; LIBA, Malimo and Mayer. Machines manufactured by Malimo are able to manufacture only impaled non-linear fabrics, whereas a Mayer machine can produce only non-impaled linear fabrics but with a limitation of four layers of fibres.

Commercial applications using multiaxial non-crimp fabrics can be divided into three categories according to Kaufman[45] and are shown in Table 8. In the marine industry because of the isotropic properties of the multiaxial non-crimp fabric structure, boat designers are finding that they can use less multiaxial non-crimp fabric in the boat structure and maintain or enhance the structural integrity and torsional stiffness of the boat. The most advanced production use of multi-axial warp knits in the marine industry is in the Norwegian navy with its fleet of predominantly carbon multiaxial non-crimp structured fast vessels. In the aerospace industry light aircraft and particularly home-built craft have utilised glass fibre multiaxial non-crimp fabric composites for some years. Most current applications centre around the skin components of the aircraft; tail plane and fins, fuselage panels, control surfaces and fairings.

Table 8: Multi-axial fabric applications by sector[45]

Industry	Marine	Aerospace	Other
Estimated % of multiaxial non-crimp fabric composite market	65%	20%	15%
Applications	• hulls • deck superstructure and substructure • support beams • motor bays • sails • racing shells	• aircraft skin • tail plane and fins • fuselage panels • leading edges • engine cowlings • rotor blades • ballistic protection	• flooring • geotextiles • wall panels • automotive applications • protective helmets • industrial belting • inflatables

The most publicised application of multiaxial non-crimp fabrics has been in the NASA ACT funded ICAPS programme at McDonnell Douglas (Boeing). Through this programme carbon/epoxy composite wing structures have been developed based upon quadraxial LIBA multiaxial non-crimp fabrics.

Testing showed that the in-plane properties of two types of multiaxial non-crimp fabric composites, those manufactured using Mayer RS2DS and 1st generation LIBA, were poor compared with unidirectional prepreg tape. Reductions of up to 25% in compression strength were observed for the LIBA fabric composite. The poor results were attributed to poor fibre straightness caused both by the stitching process and by gaps between fibre tows into which adjacent fibres were displaced causing wrinkles. Open hole tension and compression however showed little reduction and CAI strength was as much as 50% higher[43,46,47].

After problems of stability of uniweave fabrics, LIBA fabrics from European supplier Saertex were used as an alternative. The tension, compression, OHT, OHC and compression after impact performance of quadriaxial carbon fibre LIBA multi-axial fabric were shown to be equivalent to uniweave fabrics of equivalent lay-up. As a result, emphasis was switched away from the pre-plying of uniweave reinforcements to the assembly and secondary stitching of LIBA fabrics. The material was used both for wing skins and the use of cut and folded multiaxial non-crimp fabric for stringers and other internal structures[21]. The construction of the fabric used was 44% 0°, 44% ±45° and 12% 90° (from 12, 6 and 3k fibre respectively) with a total weight of 1305 g/m² and manufactured from Hercules (now Hexcel) AS4 fibres by Saertex in Germany. Laminates were impregnated by RTM with 3M PR500 resin matrix. The use of LIBA multi-axial fabrics was estimated to save 35% in material cost and 40% in fabrication cost compared with the use of the 3k uniweave fabric. More recent developments included the hybridisation of fibre type; applying AS4 fibres to the axial 0° material and intermediate modulus IM7 fibres to the ±45° and 90° layers. this reduced the thickness and hence weight of the structure for the same torsional and chordwise stiffness. Machine modifications have also allowed the manufacture of balanced seven layer fabrics with 0° fibres contained internally within the fabric.

Bi-axial and multiaxial non-crimp fabrics were also considered as a cost effective alternative to woven broadgoods and were used in the manufacture of sine-wave spars elements. Fabrics were stabilised using powder binder and post-formed into the structural shape[48]. The same process as used by Dow-UT in the manufacture of sine-wave spar elements for the F-22 fighter.

Carbon multiaxial non-crimp ribs and rear spar sections are being applied in the latest Deutsche Airbus wing box demonstrator. LIBA fabrics manufactured by Saertex are used and the ribs impregnated by a liquid resin infusion process and the spars by RTM.[24]

Hexcel (Dublin CA, USA) manufactured multi-axial preforms for RTM with each layer of the fabric chain stitched with Kevlar yarns to enhance damage resistance. In extensive tests Hexcel demonstrated no degradation of in-plane or damage tolerance properties[49]. What appears to be the same material was tested as part of the NASA ACT programme and showed lower tension and compression strengths than equivalent prepreg tape samples but the same modulus, OHC and enhanced compression after impact strength[43]. The Hexcel chain knitted laminate exhibited more out of plane crimp than was expected. This was attributed to the gaps in the fabric allowing adjacent tows to displace out-of-plane and fill the gaps during panel consolidation. Similar observations were made for triaxial 0°, ±45° fabrics by Godbehere[50].

A thorough review of the materials and processes used in the NASA ACT programme is presented by Dexter and Hasko[43] who conclude that the results of the investigation indicate that multi-axial knitting is a viable process for producing high quality fabrics and that to achieve aerospace quality fabrics, the knitting process must incorporate stringent on-line process controls that will control fibre tension, alignment and gaps between tows.

The defining features of the reinforcing structure of multiaxial non-crimp fabrics and descriptions of their manufacture are presented in Chapter 2. Chapter 3 reviews material characterisation techniques with particular reference to multi-axial fabrics.

1.7.3.4 Braids

Braiding, like filament winding, is a process best suited to the manufacture of long slender components and particularly those of hollow cross-section. Mandrels are often over-braided to create the final part shape and control the fibre orientation. Because of the interlacing of fibres they have a higher level of structural integrity than filament wound components; beneficial for handling, joining and damage resistance. Fibre volume fractions are lower than for filament winding but braids are able to conform to sharper curvatures and can include axial (0°) fibres when triaxial braiding is employed.

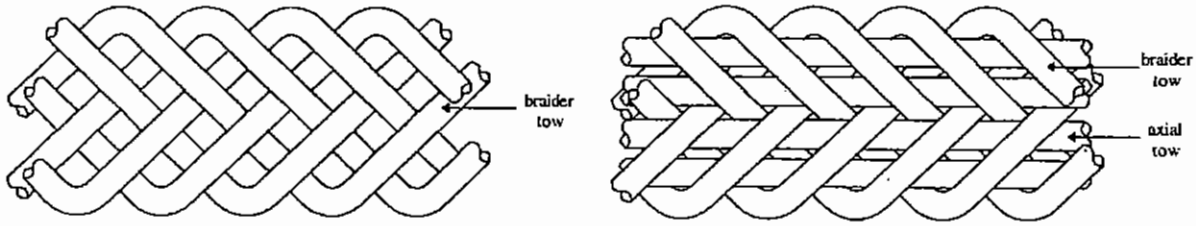

(a) ±45° biaxial braid (b) 0°, ±45° triaxial braid

Figure 16: Biaxial and triaxial braid schematics[39]

A typical braiding machine consists of a track plate, yarn carriers, a mandrel or former and a take-up device. In its most basic form, biaxial circular braiding, the yarn carriers are arranged in a circle around the central mandrel and rotate around one another and in so doing interlace the reinforcing fibres (Figure 17). The resulting braid is defined by the braiding angle, θ, which is half the angle of interlacing between the yarn systems with respect to the braiding direction. The 'tightness' of the braid is determined by the frequency of interlacing (analogous to the fineness of a weave). The interlacing of the fibres is usually achieved by horn-gears which hold the yarn carriers and travel 'maypole' fashion around the track. The number of carriers and rate at which the mandrel is pulled trough the braider can be used to control the braiding angle (θ) and the diameter (d) of the braid. The introduction

of axial 0° material creates a triaxial braid and is achieved by inserting yarns between the braiding yarns to produce a triaxial braid with 0° ±θ° fibre orientation (Figure 16b).

As well as for cylindrical components where axial strength is required, triaxial braids are used for skin stiffening applications, collapsed or cut and folded into the desired profile. Although the fibres are not as straight as would be found in unidirectional or warp-knitted materials and the un-notched in-plane properties suffer as a result, the ability to efficiently lay shear-load carrying off-axis fibres and manufacture the material in long or continuous lengths of a desired profile and width can make the process more cost effective. This has led to stitched braids being used to stiffen the lower wing skin (tension skin) of the most recent NASA-ACT stitched wing-box structure[6].

Overbraiding, by passing the mandrel again through the braider, can be used to achieve multilayer structures of the required thickness although the interlacing benefits will not be seen between braided layers. Stitching typically with Kevlar has been used to impart shape stability and some through thickness reinforcement to stiffener elements prior to RTM moulding.

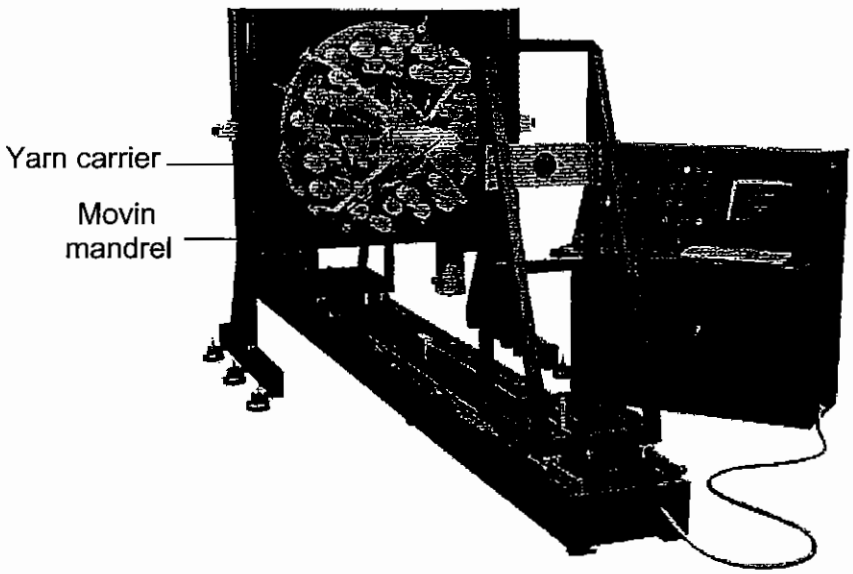

Figure 17: Biaxial circular braiding machine (courtesy Wardwell Braiding Company)

For higher levels of through thickness reinforcement or to create net shape preforms of complex 3D geometry with integrated structures, multiple track or Cartesian braiding can be used. These are considered here has direct preforming methods and are described in the direct methods section.

Circular braiders have a relatively large throughput but are limited both by the number of yarns required to create large diameter parts and by the crimping of yarns inherent in the process. Although fibre angles can be controlled braiding is best suited to the 30°-60° range and the need to change if cross sectional differences are encountered and windowing, that is gaps were there is in-sufficient material to completely cover the surface, is to be avoided. In modern computer controlled braiders these changes can be made automatically to produce parts with consistent fibre orientations or coverage.

In the manufacture of stiffener elements or other long details, the braiding process is unable to apply 90° material relative to the direction of manufacture. To account for this, the shear carrying bias layers (±45°) have been successfully changed to ±60°.[51]

1.7.4 Direct Methods

These take fibre tow, and maybe matrix resin, and assemble the component directly in one operation, thus eliminating the requirement for an intermediate product to be manufactured. This may be for reasons of cost or waste reduction or for the ability to create part shapes or reinforcing architectures not possible using intermediate materials.

1.7.4.1 Automated Fibre/Tow Placement

Tow placement evolved from the filament winding process to overcome the latter's limitations of fibre orientation, inability to add or terminate tows or to lay into concave surfaces. The material feed-stock for the process is impregnated tow at a tow width typically of 2.5mm. Multiple tows are used, individually controlled and cut, allowing tapering, curved fibre paths and thickness build-ups during one head pass. The tows are fed from individual spools behind the head and may need to be cooled to prevent resin deposition within the head itself. The matrix resin is heated as the tows are applied to the surface and all the component compaction is provided by the head itself. Curing 'on-the-fly' has been claimed although it is more common to subsequently vacuum bag and autoclave or oven cure the component. Thermoplastic matrices are also used although the heat input to sufficiently melt the polymer is very high and achieved using heated nitrogen gas locally on each tow. The differential heating rates which result tend to induce stresses which lead to component distortion. The typical configuration of the machine is as shown in Figure 18 and Figure 19.

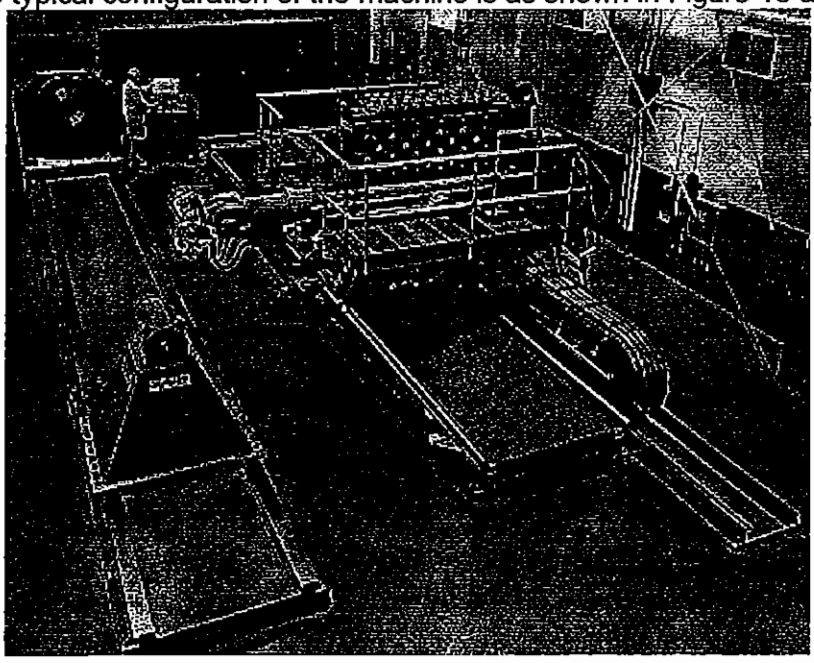

Figure 18: Cincinnati Milacron 'Viper' tow placement machine

The original technology was developed by Hercules in 1980 and the first machine built in 1983. The most recent machines utilise Band Cut and Add (BCA) actuators to achieve component tapering using 32 tows in a 114mm (4½") band. It is claimed that the cost of impregnated tow is 20% lower than the equivalent prepreg tape and has equivalent performance[37,38]. Hercules sold the technology to Alliant Techsystems in 1994 who are manufacturing tail skins for the Lockheed Martin F-22 Raptor, The technology has similarly been applied to tail-plane and low-observable engine inlet duct of the F-18 E/F in a US Navy MANTECH sponsored programme and the Bell Boeing V-22 Osprey rear fuselage, probably the largest component constructed using this technology.

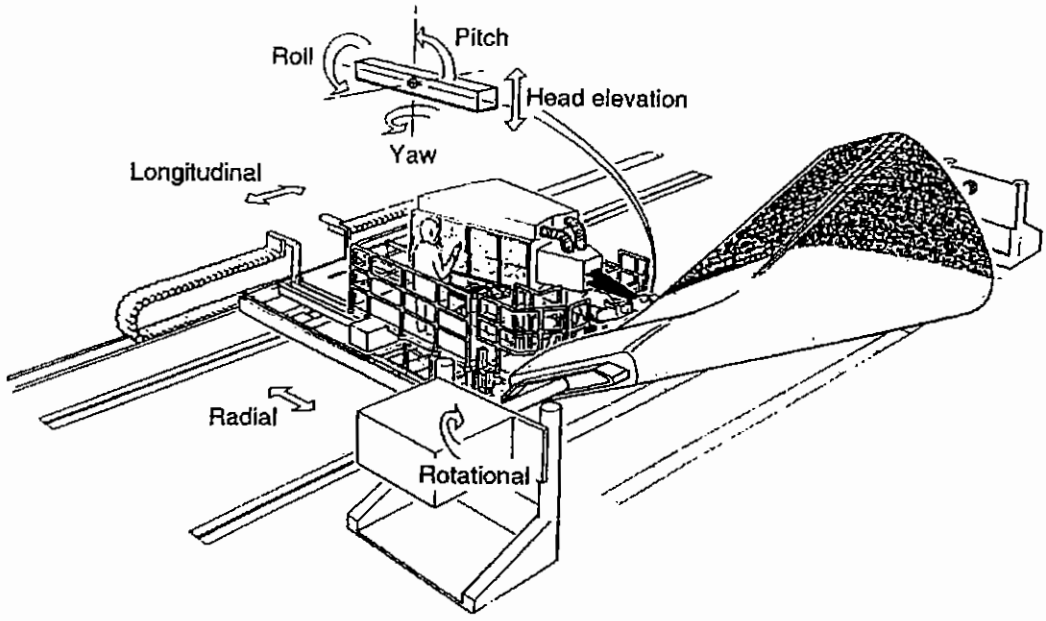

Figure 19: Alliant Techsystems seven-axis fiber placement machine

The design refinement made possible by the ability to steer the application of fibres and terminate and re-start individual fibre bundles are considered not to have been fully realised[52], even in current 'state-of-the-art' military airframes that use this manufacturing technique. It is anticipated that the amount of material required to fabricate some composite components could be reduced by approximately 30% if the fibre steering and thickness tailoring capability were used to their fullest extent[53].

1.7.4.2 Directed Fibre Preforming

Directed fibre preforming was developed as a logical progression from the use of glass fibre continuous fibre mat (CFM) in roll form, a material used for low fibre volume fraction automotive and industrial components. The directed fibre preforming process works by feeding, at a prescribed rate, continuous glass fibre and usually a binder directly into the mould tooling. This eliminates the scrap otherwise created in cutting of CFM blanks before placing in the mould tool and forming to shape.

The directed fibre preforming process uses either a gantry or multiaxis robot device with air-blown or roller driven glass yarn. The swirled yarn is held to the tool surface using a combination of the binder and porous tooling through which air is drawn (Figure 20). The system may be used to lay unidirectional material although the control needed to keep the fibres straight and under tension, particularly when following curves makes lay-down rates low and the porous tooling tends to become ineffective after only a few layers of material, the air flow having become blocked. The technique was originally developed by Owens-Corning for net shape preforms for the automotive industry and is known as the '4-P' process (Powder Preform Production Process). Similar development machines have been built by Nottingham University on Government funded research programmes (PLMP I, DTI LINK) where the device was used to manufacture oil sump guards for Ford and a propeller form for Dowty Propellers. The driving force for the machines development was to eliminate the waste generated in cutting swirl mat materials. The Owens-Corning 4-P machine in 1997 attracted an $8million US government grant to investigate its possible application to aircraft structure manufacturing.

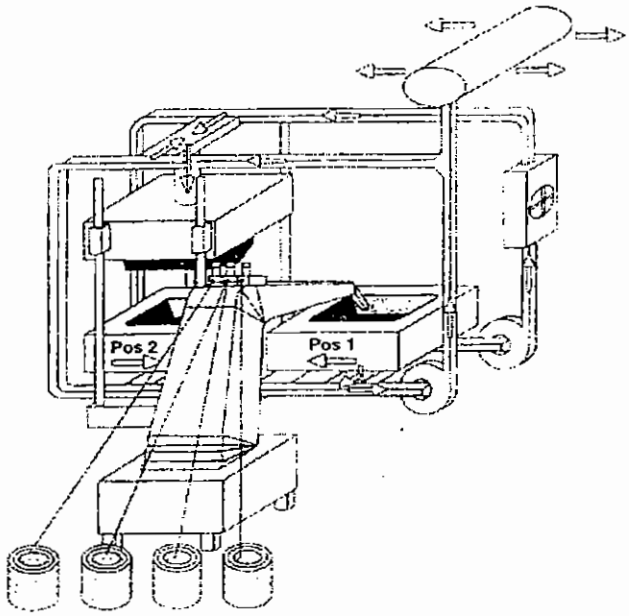

Figure 20: Owens-Corning '4-P' directed fibre preforming cell schematic

1.7.4.3 Filament Winding

Although the parts produced by this process are almost always long slender shells of revolution, the process forms the basis for automated tow/fibre placement and has been applied directly to some very adventurous structures, the most notable of which was a demonstrator fuselage for the Beech Starship all composite business jet.

The process involves pulling usually multiple fibre tows through a hot melt resin bath, squeezing off the excess, passing them through a delivery eye or from a delivery roller across an air space and onto the rotating mandrel. During laying the mandrel or the laying head traverses so as to lay the band of impregnated fibres in a helical path. The coverage and lay-down angle are determined by the relative speeds of traverse and mandrel rotation and by the width of the band. Tensions in the fibre band are high so as to achieve high levels of volume fraction and to expel entrapped air. Final processing usually involves enveloping the mandrel with a bag or membrane, evacuating and oven curing. Shrink wrapping may also be used. Filament winding using pre-impregnated tapes is also used, particularly in the United States, eliminating the resin bath stage.

Its most common use is in the manufacture of low mass high performance pressure vessels, an application where large tensile hoop stresses must be withstood. In this and other simple parts the process is very efficient and reliable

The most simple machines have only two axes of movement; rotation of the mandrel and traversing of the carriage, whereas the most complex have seven; mandrel rotation, x, y and z motion of the carriage and additional pitching, yawing and rotation of the carriage head. Where this level of control is used with a prepreg tape applicator head the differences between this and a tow placement machine are slight. The primary differences are its inability to either taper thickness by cutting fibres or efficiently lay axial fibres, i.e. along the length of the mandrel. The machines are also un-able to lay materials onto concave tools as tension on the tape being pulled over the surface provides compaction of the part. Costs however are lower at around $300-500k[23]. Manufacturers include McClean Anderson, Entec and Automated Dynamics.

1.7.4.4 Advanced Braiding

Like two dimensional biaxial or triaxial braiding, 3D braiding in its many forms relies on the intertwining or orthogonal interlacing of two or more yarn systems to form an integrated structure. 3D braids are firstly subdivided into two groups multiple track and Cartesian braiding. In multiple track braiding, also called 3D interlock braiding, arrays of carriers are arranged in a predetermined pattern, a rectangular array for a flat braid or as a series or concentric tracks for a circular braid. In the operation of the braider the horn-gears, like in 2D braiding move in a continuous 'maypole' fashion but intertwine in a more complex manner, interchanging carriers between tracks in a repeating fashion to create an integrated structure much like a 2D braid but with intersections. This provides a braid with the desired net-shape and through thickness reinforcement. However because of the size of carriers and the flexibility of movement required, part sizes are limited.

In Cartesian braiding yarn carriers are moved in a sequential discrete manner making the computer control beneficial and necessary. Two basic braiding configurations are used circular and rectangular (Figure 21) The braiding operation includes alternate X and Y displacements (or r and θ) followed by a compacting motion. A large number of carriers can be used and complex fibre architectures created with the ability to change geometry and cross sectional area during manufacture. Stationary axial yarns may also be included and braided around in the same way as triaxial braiding. Cartesian braiders are characterised by being either two, four or multi-step which refers to the number of movements made by each carrier before it returns to its original position.

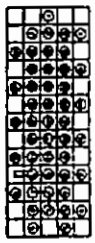

(a) rectangular

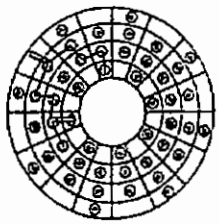

(b) Circular

Figure 21: Cartesian braiding machine schematic

Because of the large number of carriers, the packages of reinforcing fibre tend to be small and consequently parts lengths are constrained to the order of tens of metres.

1.7.4.5 3D weaving

The theoretical benefit of a 3D woven structures is the ability align fibres through the thickness and produce integrated three-dimensional shapes with fibres passing through interconnections creating a net shape structure which can transmit loads through its thickness without risk of delamination. 3D weaving systems can be categorised in a number of ways as presented by Soden and Hill[54] but broadly fall into two categories. Firstly those based upon the 2D weaving process, including 3D layer-to-layer angle interlock (Figure 22a), through thickness angle interlock (Figure 22b) and weaves manufactured flat with interconnections allowing the part to be unfolded. Secondly, 3D orthogonal looms which create the complete part in-situ with a fully orthogonal fibre structure (Figure 23). Radial machines creating similar fibre architectures were among the first to be developed, primarily for carbon/carbon composite rocket nozzle applications.

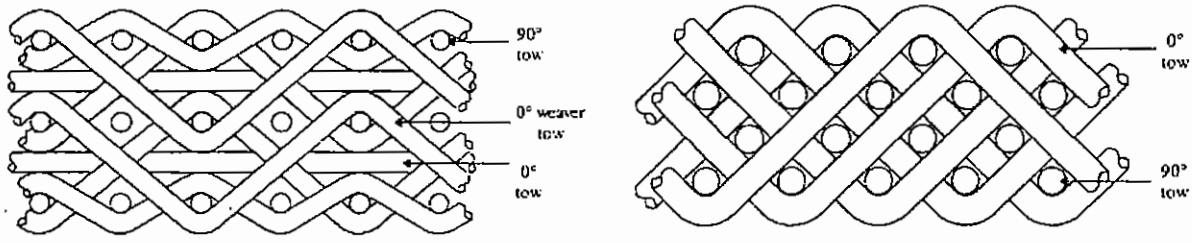

(a) 3D layer-to-layer angle interlock (b) 3D through thickness angle interlock

Figure 22: 3D woven structures based upon the 2D weaving process[39]

2D looms have been used to manufacture fabrics wider than the loom itself for centuries and it is the same principal that is used to allow interconnected folds to be produced in 3D layer interlock structures. These interconnections are however only able to run parallel to the production direction. The only through thickness yarns occur at the intersection points and not in the flat skins or webs which are formed of a layer or layers of woven fabric.

In the 3D orthogonal preforms some the warp (X) yarns are allowed to pass through the entire thickness of the preform creating the Z direction or through thickness yarns. Weft (Y) yarns pass side-to-side in the usual way, but are usually many in number. A 'beat-up' mechanism is also employed as with normal weaving to compress the preform, often to its final 'fibre volume fraction'. Control of the lifting and lowering of individual or groups of warp (X) yarns, typically using a Jacquard device, allows complex fibre architectures to be created. This can include the production of reinforcing preforms which include Integral stiffening blades or changes in thickness across the part width.

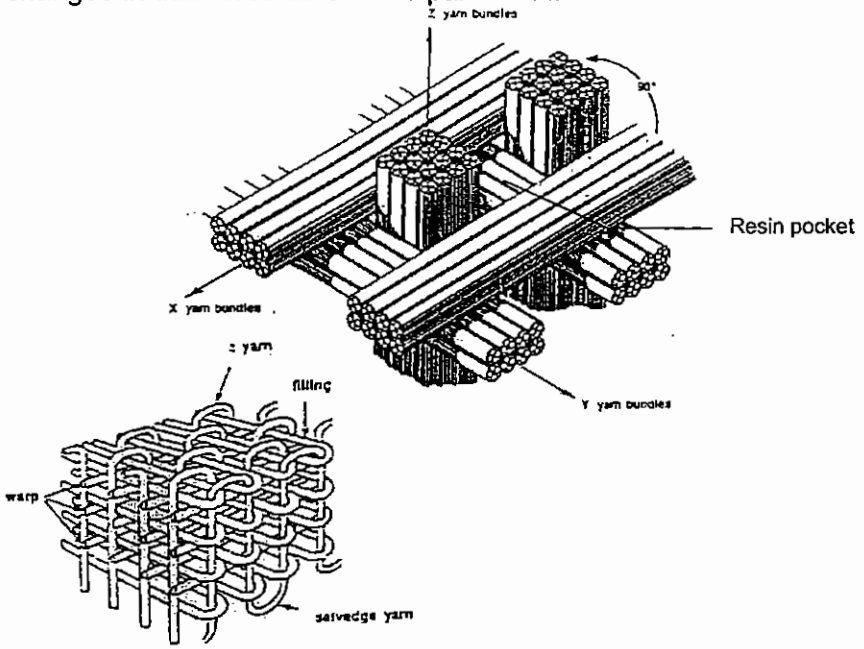

Figure 23: 3D orthogonal weave

The limitation of both 3D layer interlock and orthogonal weaves is their inability, in most cases, to automate the inclusion of off-axis shear load carrying fibres, usually at ±45°. They are also at present slow, have difficulty in economically producing tapered thickness structures, and are only able to produce flat parts. 3D layer interlock weaves suffer the same problems of yarn crimp as 2D woven fabrics, whereas orthogonal 3D woven structures have reliably straight tows when manufactured, however the orthogonal structure produces resin pockets (Figure 23) which if eliminated to raise the fibre volume fraction lead to crimping of the reinforcing tows particularly in the through thickness direction. The

proportion of fibres in each of the orientations (X,Y and Z) can be altered with the X tows becoming Z tows as required.

The most notable machines and applications are as follows:

The only known commercial aircraft 3D woven parts in production are the bonded π joint components (Figure 6) for the Beech Starship wing. Pre-cured 3D layer interlock π sections are bonded into slots routed in the honeycomb cored wing skins to facilitate attachment of ribs and spars. The preforms are manufactured by Fabric Developments Inc, PA, USA.

Mansour Mohammed of North Carolina State University has manufactured five Orthogonal 3D looms, four for research and development and one sold to Daimler Benz Aerospace at Munich[29]. One multi-axial machine has also been produced in which the outer surfaces of the weave have a flattened spiral of ±45° yarns attached using the weft yarns. The process of creating the flat spiral of yarns causes severe abrasion and additionally prevents compaction of the preform as a beat-up mechanism can no longer be used. This machine is only able to produce flat sheets of material.

Keel beam and window belt surround preforms were manufactured by Textile Technologies Industries Inc. in the first phase of the NASA ACT programme. It is believed that these were produced from carbon fibre tow helically wrapped by PVA yarn to give additional control over and protection to the reinforcing fibres during the weaving process. The PVA was then washed from the preform prior to incorporation of the resin matrix.

1.7.5 Assembly of Intermediates

1.7.5.1 Tape Laying

The development of automated tape laying equipment started more than 20 years ago as an alternative to the time consuming lay-up of unidirectional tape by hand. The technique combines the lay-up, compaction and usually the cutting of tape and is widely accepted as the 'state-of-the-art' manufacturing technology for high performance laminated composites. The primary limitations are tape widths limited to between 25-150mm, and the shape of the parts produced. A comprehensive review of pre-preg tape manufacturing technology is presented by Sarh, Moore and Riedel[23].

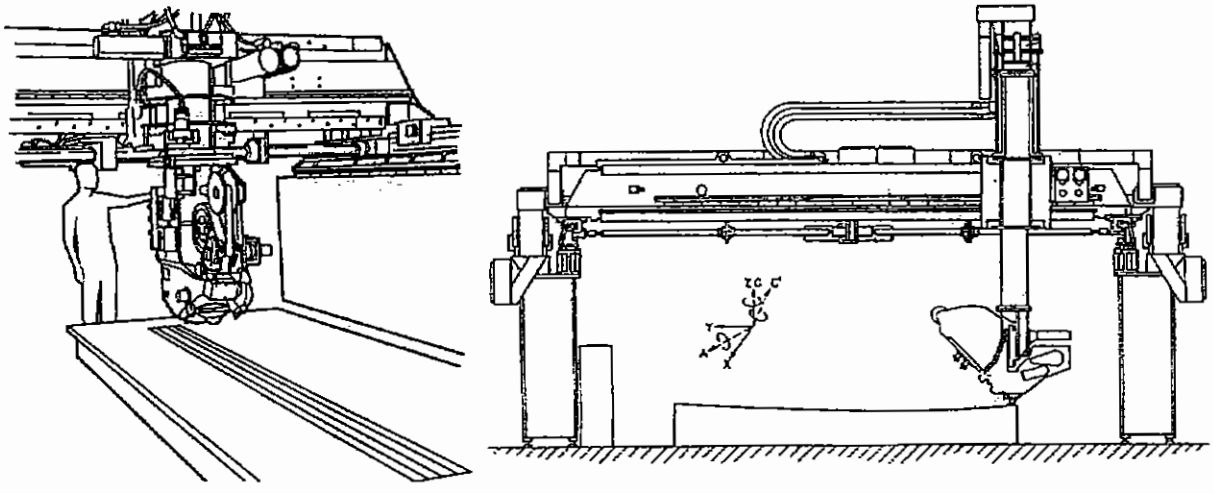

Figure 24: Ingersoll tape-layer schematic[23]

Early machines were limited to flat components and could only cut perpendicular to the laying direction, later machines used 'cassettes' of pre-cut plies. These have largely been replaced by machines able to cut at a range of angles to the direction of lay-down and to lay onto doubly curved surfaces. The most recent machines are able to lay curved fibre paths

allowing double curvature surfaces to be covered without gaps. Machines are available for the application of both thermosetting and thermoplastic (PEEK) pre-impregnated tape and generally apply sufficient compaction during deposition to eliminate the need for de-bulking. The force applied to the tool so as to remove any entrapped air during lay-down is extremely high at around 100kg for a 6" width tape. This requires that part programming is accompanied by a level of adaptive control. Material deposition rates are typically in the range of 3-6kg/hour. Machine costs are typically in the range of $2-4million[23].

1.7.5.2 Hand lay-up and Assisted Hand Lay-up

Hand-lay up has been and remains the most widespread technique for the manufacture of composite components despite material deposition rates being relatively low.

In its most basic form all the operations are performed manually: material un-rolled and cut to shape using a paper or metal template; backing papers removed and layer applied to tool and smoothed to the surface; component de-bulked at regular intervals to eliminate entrapped air. This cycle of cutting laminating and de-bulking being repeated until the component is complete.

Despite the potentially high labour costs, the dexterity required for complex components can often make hand lay-up more cost effective than the use of automated tape laying equipment. The primary limitations of the technique are repeatability and component size. These however have to some extent been overcome with a number of devices which are able to assist the laminator.

1. Automated ply cutting
   Gerber knife, ultrasonic, laser, water-jet and die cutting have all been used to automate the cutting of composite plies prior to lay-up. Gerber knife and more recently ultrasonic cutting are the most widely used in the aircraft industry. This is principally due to their part shape flexibility, speed and absence of a heat or moisture affected region.

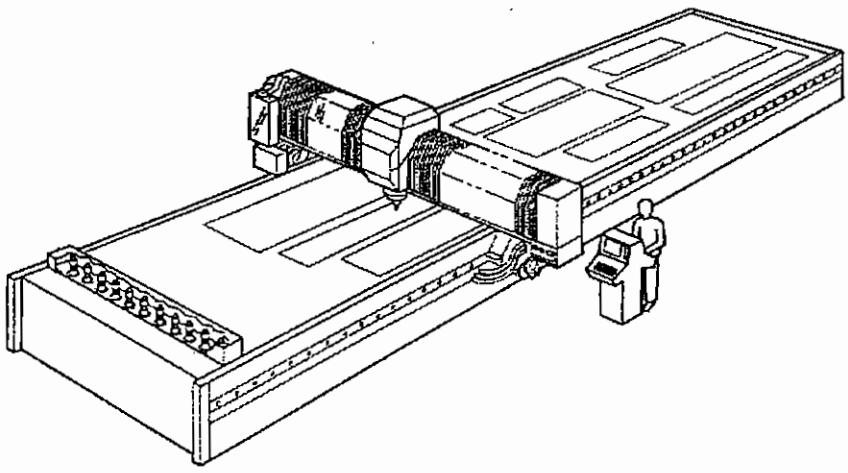

Figure 25: GFM ultrasonic ply cutting gantry schematic[23]

   Ultrasonic cutting systems utilise a cutting blade attached to a 'horn' the resonance of which causes the blade to reciprocate at a high frequency aiding the cutting of the material by the blade.

2. Laser projection systems
   The use of laser projection systems mounted on a gantry above the lay-up tool, projecting instructions and ply-outlines directly onto the tool surface are now well established in a large number of aircraft production facilities.

3. Lay-up modelling software packages
   The use of woven fabrics to assist in the manufacture of particularly curved and doubly curved components requires that some shearing of the material must take place and consequently changes in fibre angle within the fabric. Consequently it becomes necessary to start the lay-up at a particular point of the tool, progress and finish in a particular way so that fibre angles are known and repeatable from part-to-part. This will also mean that the projected area of each ply will not necessarily be that of the tool surface. Commercial software packages such as FiberSIM and Auto-layup are able to perform these functions and contain libraries of the lay-up characteristics of different commonly used composite materials.

1.7.5.3 Pick and Place

Pick and place cells are differentiated on the basis of the method used to pick up and locate plies onto tooling and the method of forming used to create the part shape. Their primary function is to replace the human handling aspect for the manufacture of components using large plies.

In most cases the first stage in the cell is the cutting stage; usually a roll of broadgoods will be unrolled and profiled using an automated CNC cutting device: water jet, laser, Gerber knife or ultrasonic blade. The next step involves either removal of the scrap or sequential removal of the cut plies and transferring them to the tool. Three types of device may be used; vacuum plates or drums[23,55,56], needle grippers[56], or electrostatic attraction[55]. Plies are sequentially lifted and repositioned as desired above the mould tool and deposited. In the case of a drum system the ply will be unrolled onto the tooling surface. Other systems will generally deposit the whole ply at once and rely on manual dexterity or the use of a diaphragm or other tooling to complete the laminating operation. Where plies are small or the part complex the pick and place cell may assemble kits of plies for manual assembly off line.

Pick and Place cells are equally applicable to prepreg parts for autoclave curing and dry preforms for RTM. Consolidation tooling is often used both with prepreg and for RTM preforms where a heat activated binder has been applied. As with hand lay-up, de-bulking is often performed every fifth ply in order to assist the elimination of entrapped air and to minimise the risk of fibre wrinkling and usually performed under a vacuum membrane. This de-bulking stage may include the forming operation where the flat sheet of material is drawn around a former by an diaphragm or membrane. Alternatively the flat sheet may be formed by the application of solid tooling. For dry preforms the forming process generally precludes the use of pre-stitched stacks of material or pre-fused binder materials as they will restrict shear in most cases and particularly if the preform is thick. This was found to be the case in the NASA/McDonnell Douglas ACT ICAPS stitched wing programme where the original intention was to stitch complete wing preforms in the flat and then form them to the wing skin tool. This was abandoned in favour of stitching the wing skin preform in its curved state[4].

1.7.6 Detail attachment and through thickness reinforcement

Mechanical fastening techniques provide additional, usually localised load transfer through the thickness of composite structures, as opposed to relying on the strength of the composite interface or adhesives. They are typically employed to attach discrete components or to transfer loads across major parts of the structure, but may also be used to enhance the resistance to damage initiation or growth caused by defects or in-service damage.

Traditionally, as with metallic structures, both rivets and bolt type fasteners are widely used. However due to problems of galvanic corrosion, when carbon composites are in contact with metals such as aluminium alloys, the use of titanium fasteners can rarely be avoided. This results in a considerable additional weight and cost associated with their purchase and installation. Weight increases result not only from the fastener itself, but include sealant materials and increased local ply thickness because of the stress concentration effect.

Electrically isolating aluminium fasteners from the composite using insulating sleeves or alternatively using composite fasteners are options but are in most situations prohibitively expensive. Other techniques being actively evaluated, because of their potential effectiveness and low cost, are stitching and pinning. Stitching is generally restricted to liquid resin moulding processes, and pinning to more traditional pre-preg manufacturing routes.

1.7.6.1 Stitching

Stitching has been used for more than 20 years to provide through thickness reinforcement to composite structures. The major manufacturing advance in recent years has been the introduction of liquid moulding processes such as Resin Transfer Moulding and Resin Film Infusion. Initial work was carried out on pre-impregnated material and resulted in significant levels of fibre damage. This was attributed to the fibres, held in place by the matrix resin, being damaged by the needle and more particularly the stitching yarn as it is drawn through the material. In dry preforms less fibre damage results since the in-plane fibres are free to move slightly and allow the stitching needle and thread to penetrate the preform. This enhances speed and allows the stitching of thicker preforms.

Three forms of stitching are of interest for structural applications; modified lock stitch, chain stitch and tufting (Figure 26). Both the tufting process and chain stitching use only one stitching thread, whereas the lock stitch requires separate bobbin and needle threads. In the modified lock stitch, the thread tension is adjusted so that the inter-linking of the bobbin and needle threads forms a 'knot' on the outer surface of the laminate, rather than internally. This minimises distortion of the reinforcing fibres within the laminate. The tufting process involves passing the needle and thread through the structure and embedding the thread in a backing material and withdrawing the needle[57].

Both chain stitching and lock stitching may be performed on single needle or multi-needle machines. A single needle lock stitch machine is a 'standard' sewing machine, as commonly used in the garment industry and a multineedle lock stitch machine commonly applied in the manufacture of multilayer quilted fabrics. Multi-needle chain stitching machines are used for quilting and a warp knitting machine similarly performs this function as manufactured by Karl Mayer, Malimo and LIBA.

Dransfield and Baillie[58] in a review of stitching composite laminates provide clear recommendations on stitching threads; a high knot strength for ease of application; tensile strength for delamination resistance; minimum diameter to reduce disruption to the fibre architecture and a abrasion resistant, 'bondable' finish.

For each of these three technologies there are a large number of stitching parameters that can be varied and controlled: Stitching thread (material, tex/denier, finish, twist), Stitching pattern (pitch, row spacing, direction, angle), Stitching process (machine type, thread tension, needle size and type). Various stitching materials have been successfully demonstrated including carbon, glass and Kevlar, with Kevlar being the most popular. Chain stitching, contrary to early NASA studies, causes no more degradation to in-plane properties than modified lock stitch, and has been shown to give similar improvements in damage tolerance properties such as compression after impact strength[27,49].

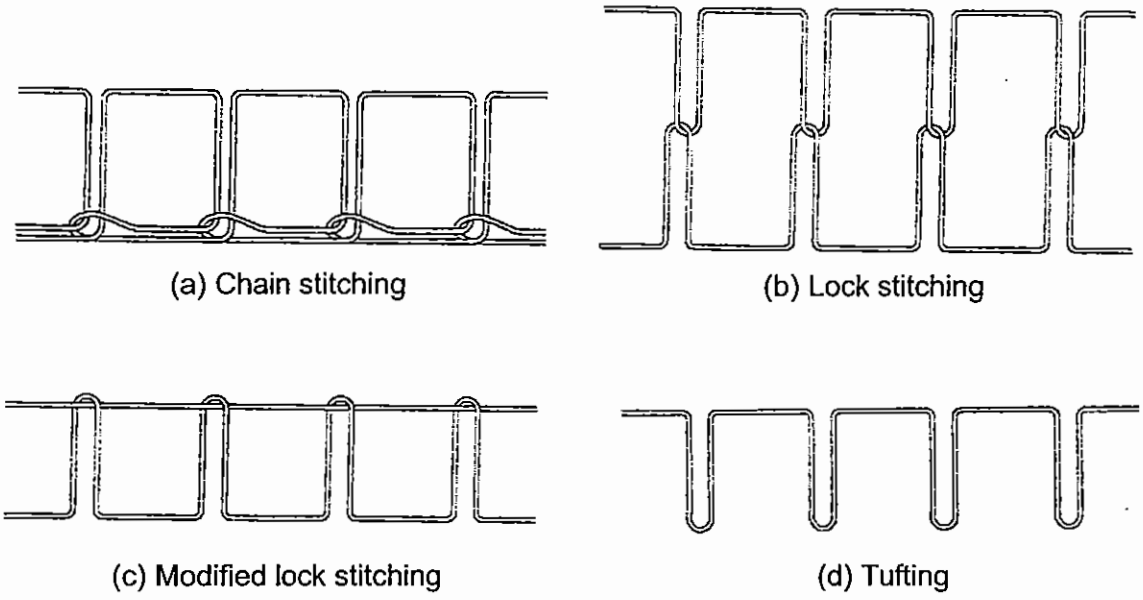

Figure 26: Types of stitching used for though-thickness reinforcement

Tufting is a one sided stitching process suited for attaching details together or providing general through thickness reinforcement when a specialised form tool is used. In the process a needle carrying a thread, in essentially the same way as a sewing machine, penetrates the preform but does not interact with another mechanism at the furthest point of the stroke. Instead the balance of friction between (1) the withdrawing needle and the thread and (2) the thread and the surrounding material into which it has been inserted, encourages the thread to remain in-situ whilst the needle is withdrawn. The tooling material, described as an 'elastic foam', holds both the shape of the preform during the process and the loops of the individual 'tufts' which may be inserted at an angle to the surface if required (Figure 27). The technique and device for insertion of the tufts is a subject of patent protection[57]. The obvious advantage of the process is that it is one-sided but does require special tooling from which it must be removed either before or after curing.

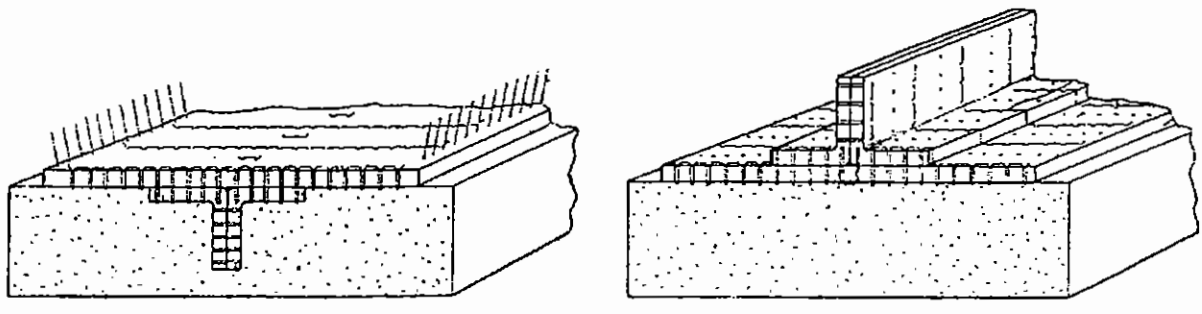

Figure 27: Tufting used to attach and reinforce a stiffened skin structure[57]

1.7.6.1.1 Stitching for Detail Attachment

As well as enhancing damage tolerance, stitching also aids fabrication. Many textile processes generate intermediates that must be formed to shape and attached together to create the final component. Stitching provides a mechanical connection between the preform elements before resin is introduced, allowing the complete preform to be handled

whist maintaining the location of details. In addition stitching compacts the fibre preform closer to the final desired thickness. Less mechanical compression need then be applied to the preform in the tool making it easier to achieve high fibre volume fractions.

The largest stitched composite structure is the McDonnell Douglas (Boeing) NASA ACT funded ICAPS wing box, manufactured with multiaxial non-crimp fabric skins and triaxially braided stiffeners stitched together with spar caps, both for damage tolerance, detail attachment and preform consolidation reasons. A schematic of the stitching machine, capable of stitching a 15m curved wing skin panel, and built by Ingersol and Pathe is shown in Figure 28.

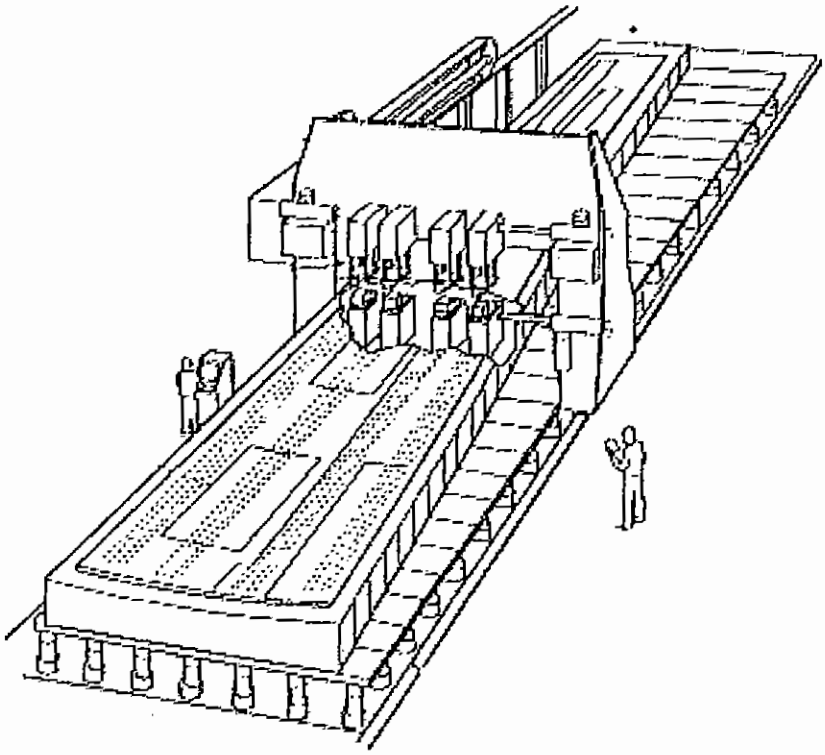

Figure 28: NASA-ACT funded MCD/Boeing ASM machine schematic[6]

The University of Aachen has manufactured secondarily chain stitched preforms consisting of multiple layers of multi-axial warp knit fabric with a blade stiffener attached on one surface. This was accomplished by passing the fabric stack and blade through the warp knitting head of a LIBA machine with the needle and guide elements removed in the location of the blade.

The stitching together of multi-axial warp knit plies to create a flat preform with sufficient stability for handling, but still allowing shearing of layers when placed in a curved mould tool has been developed by Brunel University and British Aerospace[55] and utilises a single curved needle chain stitching device mounted on a CNC controlled 5-axis robot. The unit is able to stitch the material together with access from only one side of the preform.

1.7.6.2 Pinning

The application of mechanical fasteners from one side to join components together is the standard practice is many industries. The use of very small diameter pins manufactured from titanium or unidirectional carbon/epoxy is now being applied to aerospace components in a similar manner. Their small diameter, typically 0.25-0.5mm, minimises disruption to the reinforcing fibres and maximises the surface area transferring load through the thickness of the composite. Rows of pins are inserted through the thickness of the uncured composite

at joints and areas known to require through thickness property enhancement. On curing and loading the pins are able to transfer load through the material thickness or carry higher shear loads than the un-pinned material. In the same way as stitching, different materials, pin diameters and volume percentage of reinforcement may be used.

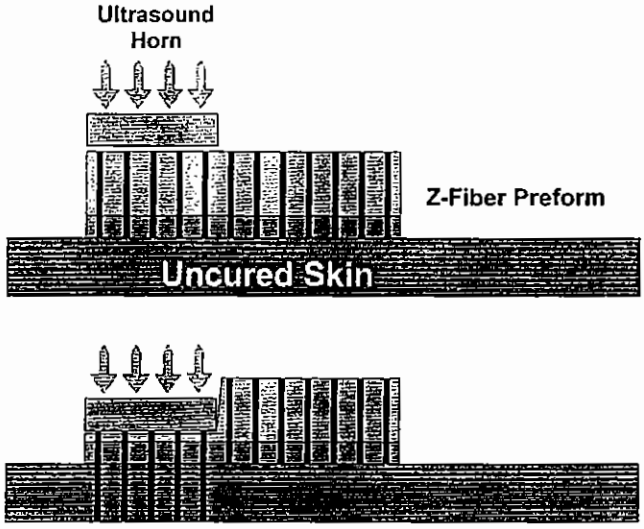

Figure 29: Ultrasonic insertion of Z-Fibers

The principal advantages over stitching are the low disruption to the lay-up due to the absence of stitching loops and knots and its compatibility with pre-impregnated materials which currently form the majority of advanced composite structures in production. Access to the part is only required from one surface, unlike stitching, and so can be easily applied to curved surfaces. The only commercially available pinning system is manufactured by Aztex Inc., who supply preforms of pins embedded at the required spacing and length in a low density foam. The pin preform is placed upon the un-cured component and a gantry or hand held ultrasonic horn used to drive the pins into the component whilst simultaneously heating and softening the resin matrix (Figure 29).

1.7.7 Moulding processes

The process of setting the final properties of the composite structure by adding and/or curing the resin matrix may take several forms, depending on the type of component, anticipated number of parts required, interchangability and performance. Some manufacturing processes restrict the type of moulding process that may be applied, while others are compatible with them all.

Since the introduction of composite aircraft structures there has been a desire to move away from designs with discrete components mechanically fastened together to create the assembled structure, towards integrated co-cured or co-bonded designs as illustrated in Figure 30.

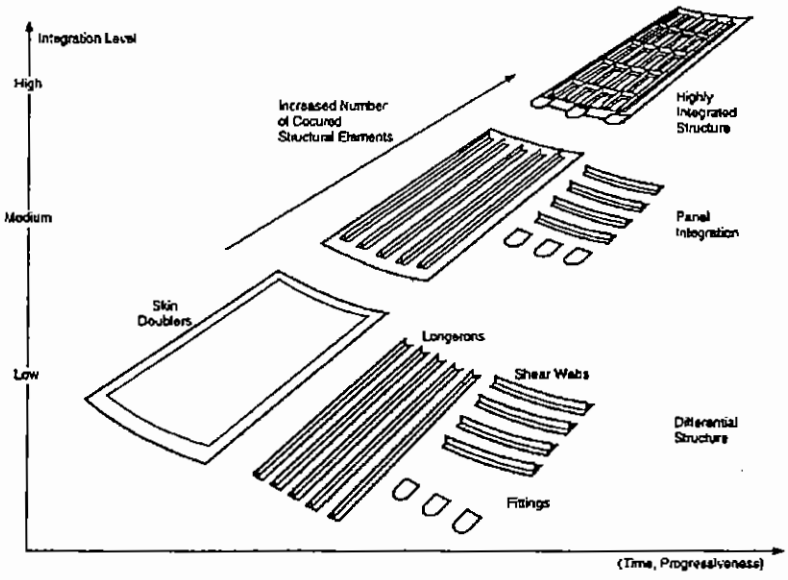

Figure 30: The progression of parts integration during the moulding process[23]

Whilst this reduces the number of components in the final structure and may eliminate the need for hole preparation and shimming for complex components it may markedly increase tooling capital costs and the complexity of tooling assembly/disassembly and increases the process risk. It also severely restricts the ability to make alterations to the component design and makes repair if required less straightforward.

Increasingly manufacturers are moving away from fully autoclave co-cured approaches particularly for large high-value components, towards manufacturing process driven modular designs utilising efficient automation techniques for each modular element. For example tape laying for thin skin components, pultrusion of woven fabrics or braided sections for stiffeners and diaphragm forming techniques for small details and highly curved parts. As well as potential cost benefits in moving away from co-curing, problems such as core slippage and crushing, skin movement and ply wrinkling can also be avoided[3]. Manufacturing discrete parts is typically followed by co-bonding, where un-cured or staged parts are attached to cured components, typically using film adhesives. Secondary bonding where cured parts are later joined using adhesives is less favoured, due to the risk of local disbonds due to joint contamination and the cost of close tolerance machining or shimming of joining surfaces.

1.7.7.1 Autoclave processing

The autoclave processing of usually pre-impregnated composites requires the purchase and maintenance of a heated pressure vessel. Being a batch manufacturing process it should be large enough to contain an economic quantity or size of part. It is a significant capital investment and often ties manufacturers into the autoclave processing route for some period of time. It is however a versatile process and very suited to small volume manufacture of a wide range of parts or where there is a high chance of component modification. Tooling can be relatively inexpensive as it is only subject to hydrostatic pressure but must withstand repeated thermal cycling often to temperatures of around 200°C. Its great advantage over RTM is in the manufacture of skin type components, where the cost of matched tooling for large surface areas would be prohibitive. However the autoclave processing route creates parts with only the tool face moulded accurately, making the part thickness variation dependent on the consistency of fibre and resin content in the composite and on the uniformity of pressure applied by any inner mould line tooling.

An autoclave is also often used in the Resin Film Infusion process to apply pressure to the component after infusion of the resin into the preform in order to close any remaining voids and achieve the fibre volume fractions required in the final structure.

1.7.7.2 Resin Transfer Moulding (RTM)

In the RTM process the preform is placed in a mould with the shape of the final part. A low viscosity resin is then pumped into the cavity through a series of injection ports, vent ports, connected to a vacuum pump in order to, evacuate entrapped air, volatiles and excess resin. The part is then cured at an elevated temperature whilst in the mould. Resin viscosity and injection pressures are kept low to minimise risk of 'fibre wash' and to reduce tooling costs. For high temperature aerospace epoxy matrices such as Hexcel RTM6 or 3M PR500, viscosity at injection temperature is typically around 150-200cps at injection pressures usually restricted to 5 bar. Part cycles times are fairly low, typically 1/5 of that of an autoclave cycle, but require dedicated matched and heated tooling and a heated pressurised resin supply. Parts most suited to RTM are those requiring close thickness tolerance often for reasons of interchangability and relatively high level of part complexity. Components with foam or honeycomb cores may be accommodated, usually requiring the use of a barrier film or cloth to prevent resin ingress but allowing bonding.

Intermediate materials used in RTM are usually in a stable intermediate form laid-up layer-by-layer into the tool itself, usually by hand. Alternatively net-shape preforms may be manufactured off-line and stored until required. Such preforms may be stabilised by stitching, pinning or binding using an adhesive material or be fully integrated 3D woven or braided structures. Adding the matrix resin only at the point of final component manufacture has several advantages; lower storage costs as only the matrix needs temperature controlled storage, lower manufacturing cost as pre-impregnation stage is eliminated and the ability to interchange resin types if required.

Resin flow is controlled both by the permeability of the fibre preform and the viscosity of the resin. Permeability is higher for lower fibre volume fractions but high fibre volume is usually demanded to maximise structural performance. Despite this conflict, high quality parts have been made with fibre volume fractions exceeding 60%.

RTM is considered a high risk process compared with either autoclave curing of pre-impregnated materials or the Resin Film Infusion process. This is due primarily to the difficulties in ensuring complete wetting of the preform, particularly when large or complex. The repeatability of preform permeability and the positioning of injection and vent ports is therefore critical. Alternative methods of reducing process risk and improving the repeatability of RTM preform manufacture have come from the development of fabrics specifically developed to aid resin flow, such as Hexcel Composites Injectex, in the development of specialist consumable materials such as the porous mats used in the Seemann Composite Resin Infusion Moulding Process (SCRIMP), and in better understanding of injection and vent gating in mould design. Monitoring techniques may similarly be applied to identify the arrival of the resin flow front and in some cases monitor the state of cure of the resin itself. Dielectric sensors which measure the response of ions within the matrix resin to an applied electric field may be embedded in the tooling or in the part itself. Reinforcement materials are now being commercialised which contain sensor wires to similarly monitor the resin and its cure state over the whole component surface[129].

1.7.7.3 Resin Film Infusion

Interleaved or thick film forms of this process have both been used in the aircraft industry for many years. In the interleaved RFI process a hot melt resin film, appropriate to the weight of the reinforcing fabric, is usually rolled onto the intermediate, cut to ply shape and placed into

the mould tool. Subsequent layers create an interleaved stack which is very porous in the plane of the fabric such that with the application of vacuum and heat the stack is compacted to near net moulded thickness and air removed.

Porous semi-impregnated fabrics have been used for many years in the manufacture of secondary and tertiary aircraft panels, primarily as a result of difficulties in impregnating thick fabrics by the resin film prepreg route. A review of Resin Film Infusion and a model of the impregnation process is presented by Godbehere[59]. Reliable impregnation of multi-axial warp knit fabrics at fibre volume fractions of 62% using the interleaved RFI process have been demonstrated. This interleaving approach was used by British Aerospace Airbus in the manufacture of demonstration wing-boxes in its AMCAPS I research programme[60].

In the thick film RFI process a separate dry net shape preform and cast film is manufactured. The resin is cast to match the local resin requirement and must be void free. The cast film is placed in the bottom of the mould tool and the dry preform placed above. The closing of the mould; which may be matched metal or semi-rigid, and heating under vacuum causes the void free resin front to infiltrate bottom-upwards as the preform 'floats' on the resin. The semi-rigid upper tooling approach was used extensively by McDonnell Douglas in its NASA ACT funded ICAPS stitched wing programme. Application of stitching through the entire preform thickness made resin inclusion earlier in the manufacturing process undesirable.

Chapter 2

Multiaxial Non-Crimp Fabric Manufacturing Technology

2.1 Introduction

The multi-axial warp knitting process ties tows of reinforcing fibres together in layers with warp (0°), weft (90°) and bias (±θ°) orientations. The knitting is typically performed with fine polyester threads, which amount to a small percentage of the total weight. During knitting, the polyester threads are passed around the reinforcing tows and one another in interpenetrating loops (Figure 31). The mechanical properties of the stack of layers can be controlled by selecting a tow weight in each of the four orientations. The major advantage of the knitting process is its low manufacturing and fabrication cost compared to conventional tape lay-up and the low levels of fibre crimp compared to woven composites. Multiaxial non-crimp fabrics of 2.5m width may be produced by this process, although 1.27m is more common.

As well as including unidirectional fibre layers other materials in sheet form may be introduced. Chopped strand or swirl mat, woven fabrics and even thin Nomex honeycomb have been included. The machines may also be used for the secondary stitching of multiple fabric layers and can even include warp wise stiffener blades by increasing the needle clearance and removing some of the knitting elements.

Work by Hortsing[31] comparing the tensile strength of multiaxial warp knit fabrics with woven fabrics shows a 20-30% increase in tensile strength for fabrics manufactured on LIBA machines. This is attributed to the crimp induced by the weaving of the reinforcing yarns. Similarly the tensile modulus of the LIBA multiaxial warp knit composite was some 20% higher than that of the equivalent woven fabric composite.

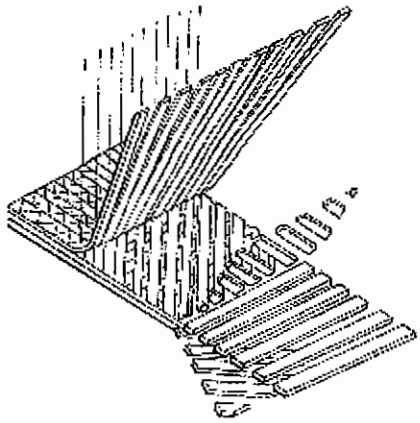

Figure 31: Schematic of a four layer multiaxial warp knit fabric

2.2 Fabric Definition

'Multi-axial warp-knit' (MAWK), 'non-crimp fabrics' (NCF), 'weft inserted warp knit' (WIWK), 'stitch-bonded', 'weft inserted multi-axial gelege' (WIMAG) or 'Directionally Oriented Structures' (DOS) are all terms used in the literature to describe the same material form. In addition to this are added a vast number of tradenames used by manufacturers to differentiate their products. Despite this there are only three basic machine types used to manufacture this class of material; Karl Mayer, Malimo and LIBA.

In Table 7 variables used to define multiaxial non-crimp fabrics were presented. Here, each are described in more detail and used to introduce the capability and limitations of this manufacturing technique described later in the chapter.

2.2.1 Number of Axes

A unidirectional prepreg tape has one primary fibre orientation, a woven cloth two, usually referred to as warp (0°) and weft (90°) and a multiaxial non-crimp fabric up to seven, although in practice this is usually limited to a maximum of four; a warp (0°), weft (90°) and bias (usually ±45°) layers. Their order within the fabric can be altered to some degree with an attendant change in their mechanical performance.

The number of axes used is determined by the application and its requirement for reinforcement in any one direction. A wing skin has requirements, as described in Section 1.6 which favour a four axis 'quadraxial' material containing predominantly 0° and ±45° fibres and some 90° fibres to provide chordwise stiffness primarily where a structure must withstand bolt bearing loads.

As with unidirectional tape or woven fabric lay-up there remains the requirement that the structure be balanced about the mid-plane and symmetric at any point along the span. Stacking a single multiaxial fabric with either three or four axes cannot achieve this even if the fabric is inverted. A second mirror image fabric is therefore required (a handed pair), or some other method found for introducing an additional 0° layer.

The most common method used to achieve a balanced multiaxial fabric is to pass an inverted fabric with a single 0° layer, now on the underside, through the warp knitting machine a second time, whereby the attachment of a second 0° layer creates a balanced symmetric fabric (Figure 32). The resulting fabric however is very thick because of the number of layers and the limitation of layer weight refinement and is not very conformable. The tensile strength of this material is slightly lower that a handed pair of the same layer weights (see section 3.2.1)

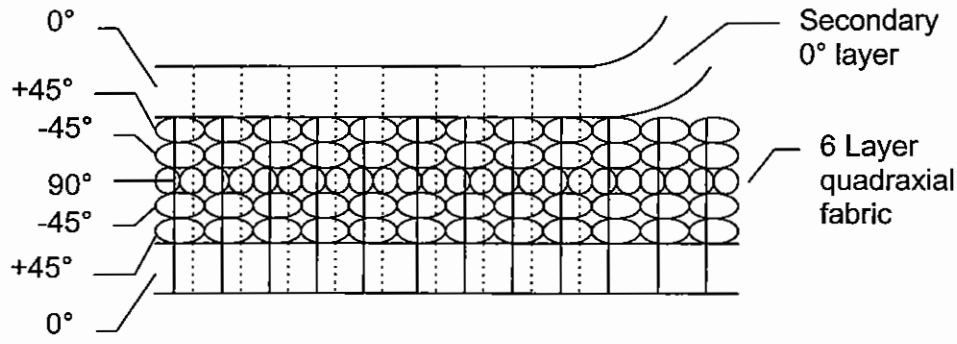

Figure 32: Balanced quadraxial fabric by 'double stitching'

The results indicate that, in tension at least, little additional detriment is caused by stitching the fabric a second time. Using this approach the fabric thickness doubles making it faster to laminate but increasing the minimum step for ply drop-offs in tapered thickness structures and reducing its drapability.

2.2.2 Stitching Geometry

The knitting process may be true warp-knitting, whereby a plurality of adjacent yarns are inter-linked to form a net-like 'Tricot' structure (Figure 33a), or chain stitching, whereby the yarns are not inter-linked and often referred to as stitch-bonding (Figure 33b).

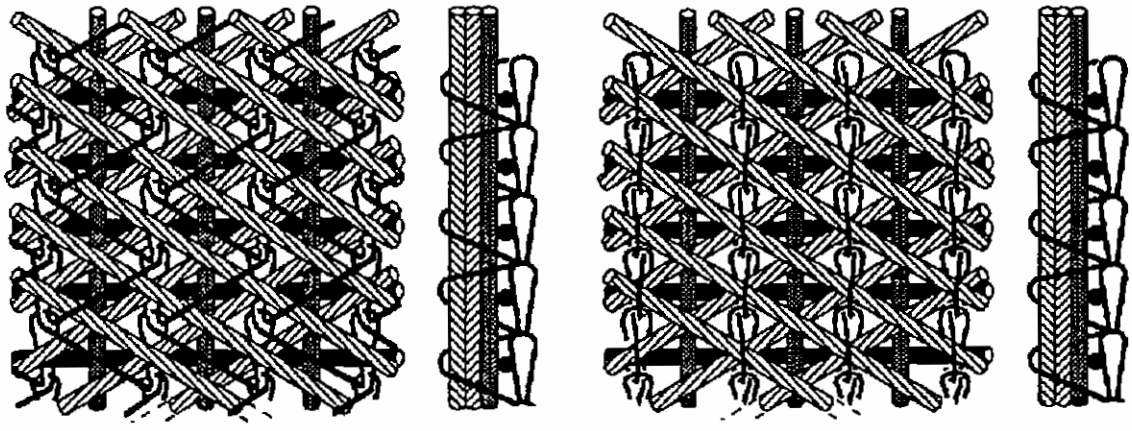

(a) (b)

Figure 33: (a) Warp knitting (b) Chain stitching[61]

These knitting styles have been modified by some fabric manufacturers; Saertex Wagener GmbH manufactures LIBA fabrics with an alternating tricot and chain stitching pattern, the reasons for this modification are not clear. ±45° biaxial and multiaxial non-crimp fabrics, manufactured using a Tricot knitting pattern, have qualitatively better conformance to doubly curved surfaces than equivalent chain stitched ±45° biaxial fabrics and are commercially referred to as 'High Drape'.

Warp knitted or stitch bonded fabrics are often confused with structures stitched through the entire thickness, usually by lock stitching. In a warp knitted or stitch bonded fabric the function of the knitting/stitching yarn is primarily to impart stability to the fabric prior to final moulding and does not, in most cases, provide a significant level of through thickness reinforcement. In lock stitched structures, the secondary process of applying a stitching yarn through the entire thickness of a structure has the primary purpose of providing through-thickness reinforcement. Stitching as an assembly aid and method of providing through thickness reinforcement is described in section 1.7.6.1.

2.2.3 Linearity of Weft and Bias Yarns

The linearity of the fabric is determined by the method of introduction of the bias and weft yarns. Linear or parallel weft/bias fabrics are produced by both Karl Mayer RS2DS and LIBA machines and non-linear (cross-weft or zig-zag) fabrics by Malimo machines. The situation is somewhat different in the USA where there is only one LIBA machine manufacturing linear weft/bias fabrics and owned by Hexcel Composites, and one Mayer RS2DS owned by Milliken. All other producers must manufacture only non-linear (cross-weft) fabrics owing to a patent dispute between Hexcel composites and LIBA; this similarly prevents parallel wefts being exported commercially to the United States.

The visual difference between linear and non-linear fabrics is shown in Figure 34.

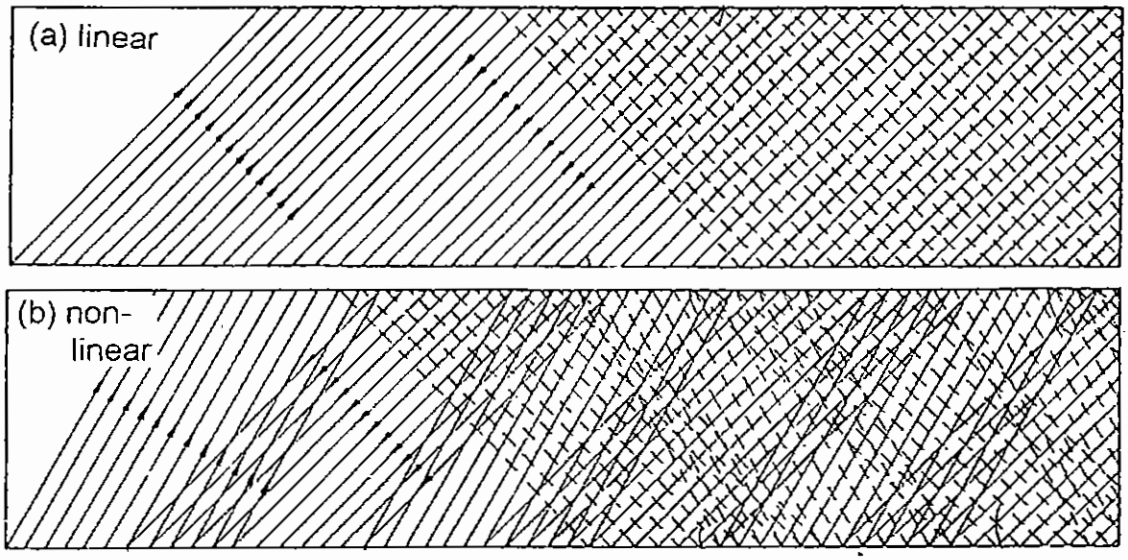

Figure 34: Linear and non-linear weft layers

The mechanism responsible for the creation of the parallel weft/bias yarns is known as the 'shog' and is described in section 2.3.3.2. The properties of un-impregnated fiber-glass linear (Mayer) and non-linear (Malimo) fabrics were studied by Pastore et al[44] and indicate that the initial modulus of the linear fabrics were higher than the non-linear, owing to the variation of angle of the reinforcing fibres, and that the strength of the bias directions was two orders of magnitude higher for the linear fabrics. This result can be attributed to the loading of only a small number of yarns present at the exact bias orientation in the non-linear fabric whereas a large majority would be loaded simultaneously in the linear bias fabric. This situation would not however occur to such a degree in the composite, as load transfer would occur between adjacent yarns and the difference could be expected to be much lower.

2.2.4 Impaled and Non-Impaled yarns

The process of passing a secondary thread through the thickness of layers of dry fibres may be expected to cause fibre breakage, owing to friction between the needle and secondary yarn as it is drawn through the material. Fibre handling during the inlaying process can however prevent needles and yarns piercing fibre bundles. This is done by inlaying the reinforcing fibres as the knit is formed with one reinforcing tow placed between each knitting intersection. The Karl Mayer RS2DS machine inlays all fibres by this method, LIBA multiaxial machines are able to do this only for the warp (0°) tows. Although the reduced fibre breakage appears beneficial, the gaps that form between adjacent fibre tows and where the knitting yarn passes through the thickness results in large resin-rich areas or 'windows' in the impregnated fabric, limiting the achievable fibre volume fraction[6,46]. A second limitation is the more limited layer weight flexibility, as one yarn is required for each knitting yarn intersection.

2.2.5 Layer Weights

In all current multiaxial non-crimp fabric machines, in order to achieve consistent coverage in the weft/bias orientation, the tows which form these layers must be butted together or sufficiently overlapped to eliminate gaps. It has been suggested that gaps caused by low areal weights and by other limitations of the machine may detrimentally affect mechanical performance; primarily by inducing crimp in adjacent fibre layers leading to performance variability and poor compression strength[43].

The minimum areal weights per square metre (g/m²) for a 45° layer on a LIBA machine are as shown in Table 9. Layer weight below the marginal limits indicated result in fabrics where adjacent tows are not butted together.

Table 9: Marginal and optimum ±45° weights (per layer)[62]

Tow Type	Marginal Weight (g/m²)	Optimum Weight (g/m²)
Toray T300 3k	170	190 or above
Toray T300 6k	220	250 or above
Toray T300 12k	300	400 or above

So to minimise the gaps between tows and by inference the tow crimp, heavier weight fabrics could be used. However, in structures such as a wing-skin, thickness tapering using multiaxial fabrics becomes a matter of terminating the whole 'blanket' thickness; the sum of all the layer thicknesses within the fabric. This poses four primary difficulties:

1. Fibre waviness is introduced in the structure by the crimping of adjacent plies
2. Thickness tailoring flexibility is reduced, so excess material may be carried unnecessarily.
3. If a handed fabric is used either areas of un-balanced and un-symmetric lay-up result, or a double ply-drop of twice the thickness must be used
4. The large step and resultant resin area at the end of ply-dropoffs have the potential to fail prematurely due to interlaminar shear and tension stresses.

However these effects can be minimised through judicious design approaches, some of which have been demonstrated and some of which require further validation. Initial tests to examine methods of overcoming these differences in ply-dropoff configuration compared to prepreg tape laminates are presented at the end of the material characterisation chapter.

In addition to the 'ply-dropoff' problem, residual stresses in each of the layers, and stresses induced by laminate bending, cause differential interlaminar shear stresses between layers of different orientations. For this reason design guidelines suggest limits of no more than 4 layers of ud prepreg tape (500-600 g/m² of fibre) of the same orientation should be placed together[28].

Multiaxial warp knit fabrics were manufactured by Hexcel (USA) with Hercules AS4 - 3, 6 and 12k tows, in 850, 1140 and 1695 g/m² weights respectively. Each were manufactured with Kevlar chain knitting and were tested to evaluate the effects of tow size on mechanical properties and damage tolerance. The results reported in [43] showed the following:

1. An average reduction in tensile strength of 15% was observed for all three tow sizes, compared with prepreg tape laminates. Tensile modulus was slightly higher for the 6 and 12k tow sizes.
2. Open hole tensile strength was marginally better than for prepreg tape laminates and favoured the 6k tow based fabric. Open hole compression strength was again similar to the results for prepreg tape but showed increasing strength with tow size.
3. Compression strength results showed an average 25% drop in compression strength, with the 3k based fabric having the highest values. However what was considered 'excessive scatter' was seen in the strength data for the 3k fabric. This was attributed in part to tows filling gaps in adjacent layers. Compression modulus was similar for prepreg tape and all the multiaxial fabrics.
4. Compression after impact results were presented for samples impacted with 12.5mm diameter aluminium spheres at 30 ft-lbs with an air gun. Improvements of 30% in strength were observed compared with prepreg laminates but fell short of design requirements and were subsequently secondarily stitched raising the CAI strength by a further 20%.

2.3 Multiaxial warp knitting machine technology

Three basic manufacturing technologies are used to manufacture these materials, Malimo, Mayer and LIBA. In the USA there are also several machine types, mostly based upon European machines with modifications. Most notable are those of Hexcel, Knytex, Brunswick Technologies and Johnson Industries (formerly Tech Textiles USA). A list of known manufacturers of multiaxial warp knit fabric may be found in Appendix B.

The three European machine types are compared below.

2.3.1 Karl Mayer

Mayer multi-axial non-impaled warp knit fabric is produced using a "multi-axial magazine" weft insertion mechanism in which reinforcing yarns are 'dropped' into the structure as the knit is formed. The attractive feature of this system is the precision of yarn placement with four layers of linear yarns and the inclusion of short fibre mat arranged in a wide range of orientations being possible. Stitches are formed without piercing through the reinforcement yarns and thus reducing the amount of fibre damage. Production rates may be as high as one hundred linear metres per hour[32]. Two basic machine configurations are available; a biaxial (RS3MSU) machine to produce 0°/90° materials and a multi-axial machine (Mayer RS2DS) which is capable of producing 0°/90°/±θ° (4 layers + web) materials and which is a good deal more complex with the machine placed on a rotating platform[63](Figure 35). Ten RS2DS machine have been sold to date (1 to Milliken USA, 9 in Europe and Japan). A new machine aimed at competing directly with the LIBA manufacturing process has been developed by Mayer/Malimo. It is expected that it will in part be based upon Malimo technology as acquired from VEB Kombiant Textima[42].

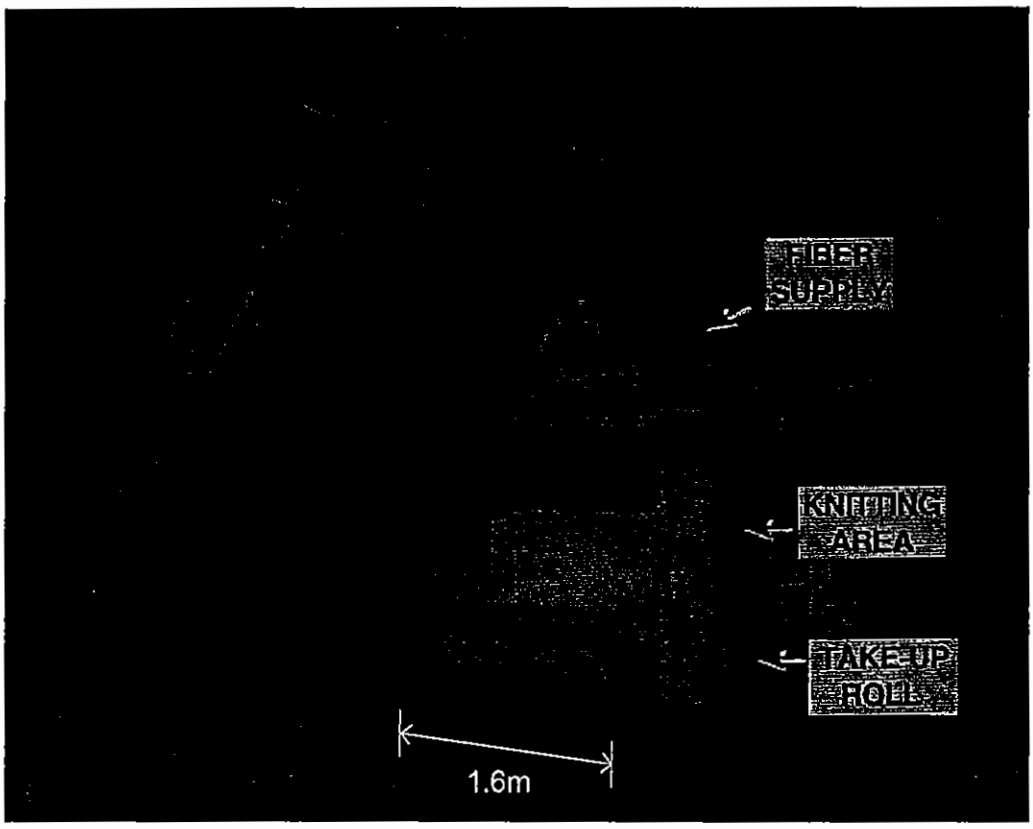

Figure 35: Karl Mayer RS2DS multiaxial warp-knitting machine[64]

2.3.2 Malimo

Malimo was the first type of weft insertion warp knitting machines and was invented by Mauersberger[65]. The machines were manufactured in the former East Germany when the company was known as VEB Kombiant Textima and are described as a stitch-bonding, rather than a warp-knitting machine. Malimo is now owned by Karl Mayer GmbH. Unlike the LIBA machine the reinforcing fibres are bound together in the vertical plane. The weft and bias inlay system is unable to lay fibres at a constant orientation (often referred to as non-linear, zigzag or cross-weft), there being a variation of ±1-6° about the desired angle (see Figure 34b). 0° warp fibres are fed in vertically through a small tube and subject to a small bend radii during insertion into the stitching elements and are hence subject to high levels of fibre damage[31]. The machine type is most often used to manufacture fabrics incorporating chopped or swirl glass mat and fleece backing materials. The stability imparted to the chopped or swirl mat by the stitching process eliminates the need for a binder resin. Malimo have patented machine developments carried out with the University of Dresden which have made it possible to change the warp orientation continuously from the usual 0° to allow curved fibre paths to be laid (US Patent 5140841). This process has been demonstrated on several components including automotive wing and tailgate panels and conical shapes for ESA Ariane rocket components.

2.3.3 LIBA

The LIBA Copcentra multi-axial warp knitting process allows as many as seven weft and one warp layer to be included in the fabric. The maximum weight of the fabric is as high as 4200 g/m²[66] although a more practical limitation is around 2500g/m². The precision of weft orientation is very high owing to a 'shogging' motion whereby the weft inlay carriage moves parallel to the machine as it traverses between the transport pins so as to lay the material in parallel (see Figure 34a). Damage to the reinforcing fibres is minimised as, although pierced through by the knitting needles, the needles on newer machines swing in an arc at the same rate as the layers of fibres being pulled through the machine (US Patent 4723424). The 0° warp inlay system is also flexible, allowing the 0° tows to be deflected away from the stitching yarns avoiding impalement if desired. The cost of purchasing a LIBA machine is approximately 1/3 more than an equivalent Malimo machine (approximately 1 million DM)[67]. The machine is available in two standard gauges 6 or 12 needles/inch 6 being the most common for the manufacture of reinforcement fabrics. Production rates are quoted as being roughly 30-90 linear metres/hour[68].

The machine can be subdivided into five sections by function.
1. Warp knitting head
2. Weft insertion units
3. Fibre supply
4. Knitting yarn supply
5. Fabric sheet transport and batching

Each of these five areas is indicated on the machine schematic in Figure 36 and described in some detail as they relate to the flexibility and quality of the manufactured product.

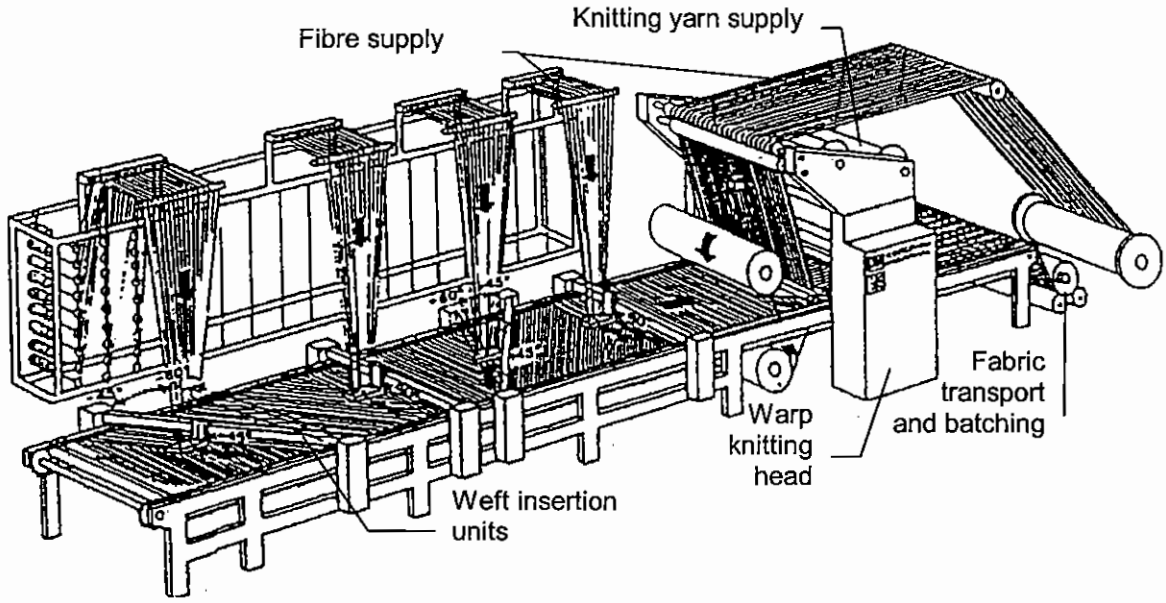

Figure 36: LIBA multiaxial machine with four weft insertion units[69]

2.3.3.1 Warp Knitting Head

This part of the machine takes the individual knitting yarns and, using a series of articulating needle and guide bars, interlinks adjacent yarns in a knitted structure known as a tricot (Figure 37). This structure forms the stabilising structure which holds the reinforcing fibres in place. The knitting yarns are fed from a beam above the knitting head, this beam being driven at a rate which determines the stitching tension in the final product. Axial (0°) material is similarly fed down from the top of the machine over driven rollers and into the knitting area where it passes through the ST bar, a series of guides which control the width and spacing of the reinforcing fibres. The bar may be moved sideways in a reciprocating motion to control the pattern of the 0° surface layer.

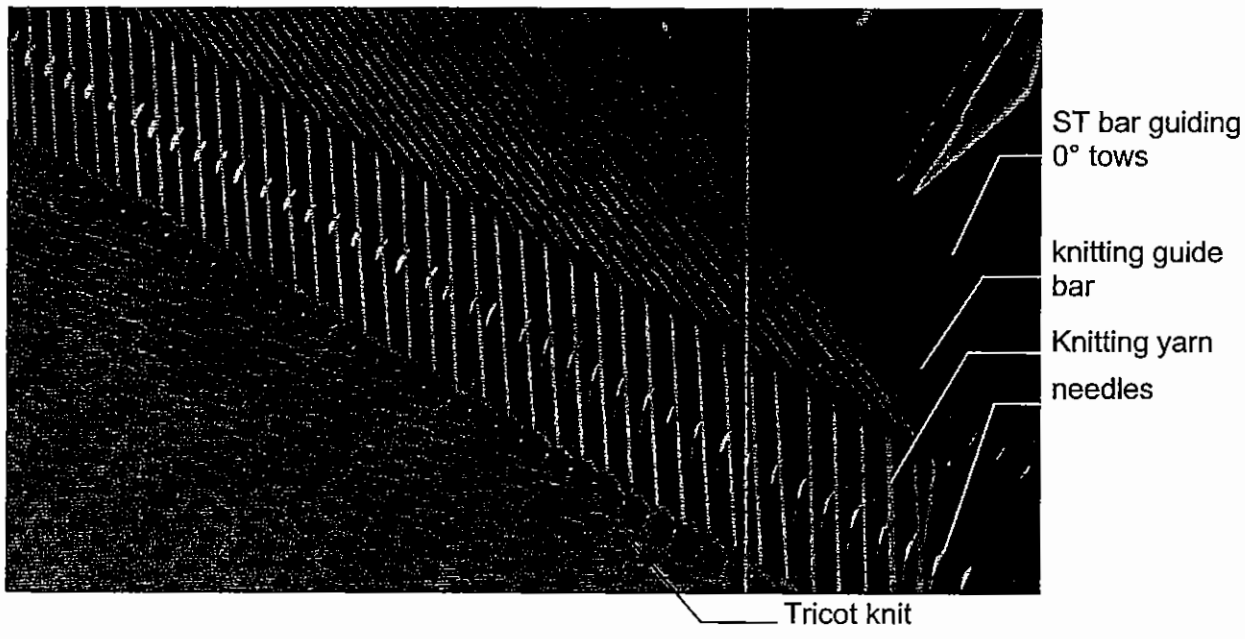

Figure 37: Detailed view of knitting process

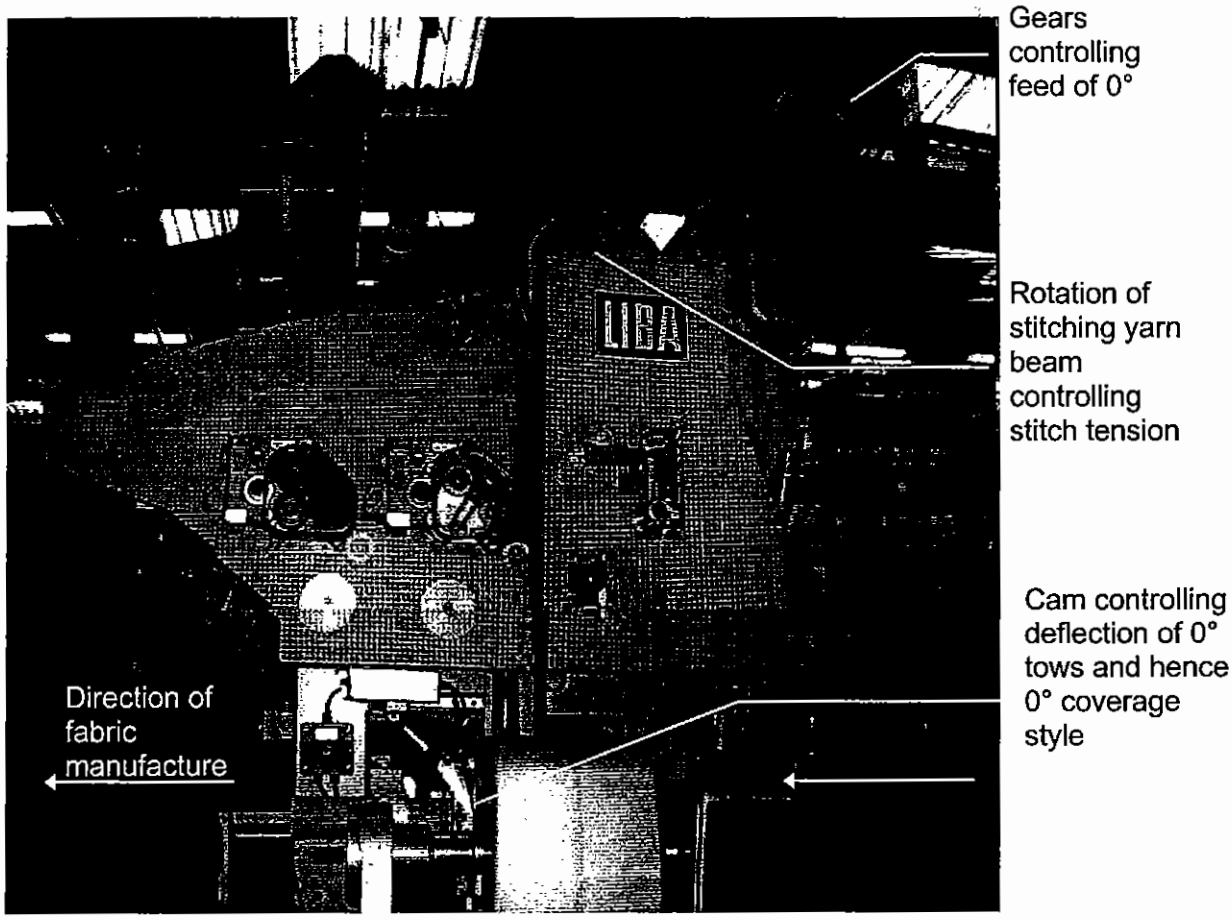

Figure 38: LIBA warp-knitting head (side view)

2.3.3.2 Weft Insertion Units

There are as many as seven weft insertion units on a LIBA machine at different locations and orientations down the length of the machine. Each unit (Figure 39) consists of a guide way along which a carriage is driven via toothed belt and pulleys (a). On this carriage there are eyelets (b) which guide and space the fibre tows, two dancing arm tensioners (c) which maintain tension on the tows during the shog, and a reed (d); a series of equally spaced rollers which dictate the spacing of the tows as they are laid onto the transport pins. Figure 39 shows a unit laying a +45° layer.

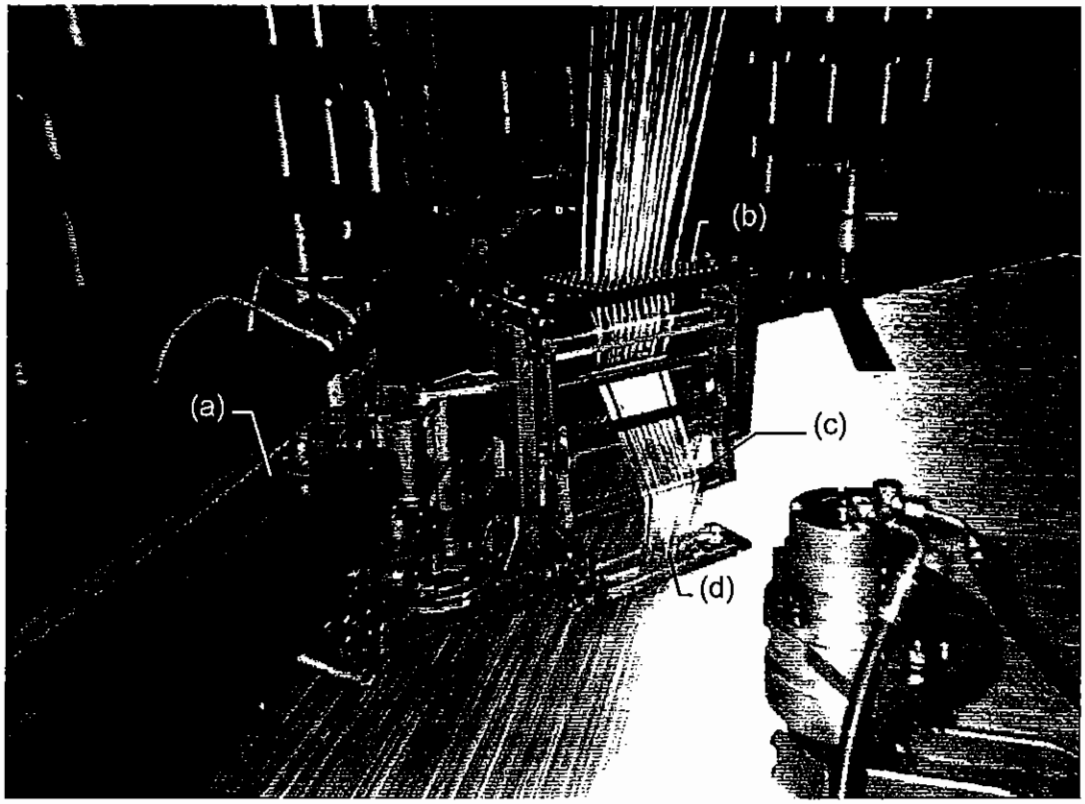

Figure 39: LIBA weft insertion unit applying +45° layer

Not all of the seven units are used at once; fabric lay-up is dependant on the orientation and order of operation of the weft insertion units (Figure 40)

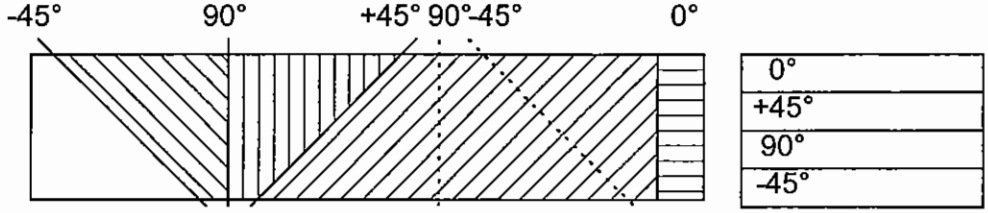

(a) Left handed (A) quadraxial warp knit fabric

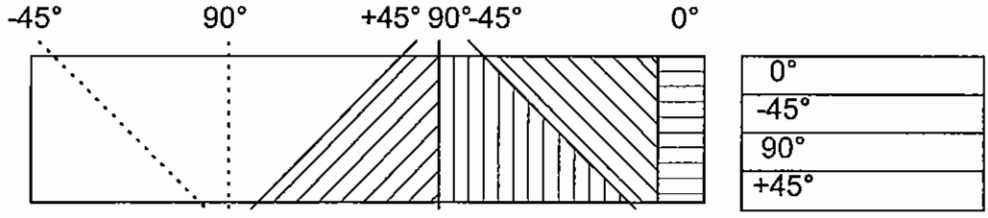

(b) Right handed (B) quadraxial warp knit fabric

Figure 40: Weft insertion units used for handed quadraxial fabric

The most critical area of the weft inlay process is the 'shog'; where the band of tows are moved down the bed of the machine ahead of the transport chain movement in order to produce a layer of parallel fibres as indicated in Figure 41. The 'shogging' process and the placing of the reinforcing fibres over the transport chain pins determines, to a large extent, the quality of the fabric. Pin damage is common and results in gaps and uneven surface coverage.

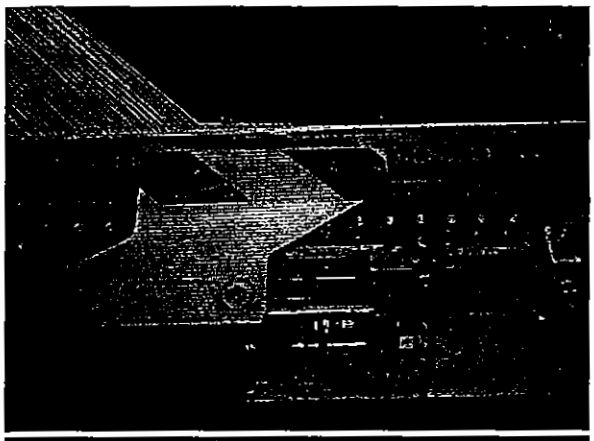

1. Weft insertion carriage approaches pins

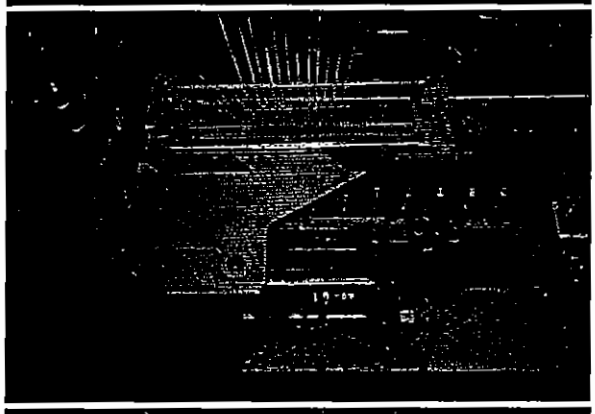

2. Weft insertion unit overshoots pins by approximately 20mm and lowers by 10mm to below level of the pins

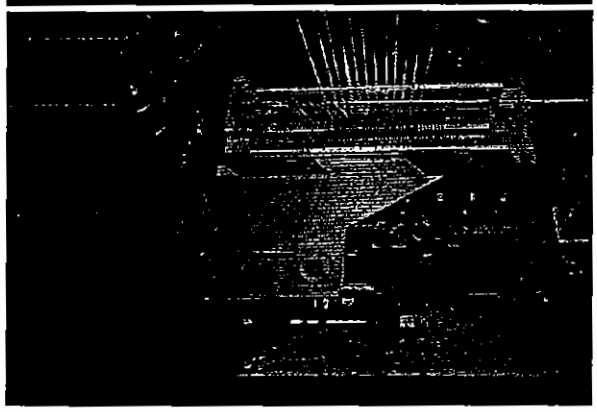

3. Weft insertion unit and rake plate simultaneously 'shog' against direction of fabric manufacture by an amount equal to the width of the band of reinforcing fibres.

   (At the other side of the machine the 'shog' happens with the direction of fabric movement)

   Rake plate holds fibres against back of transport pins during shog

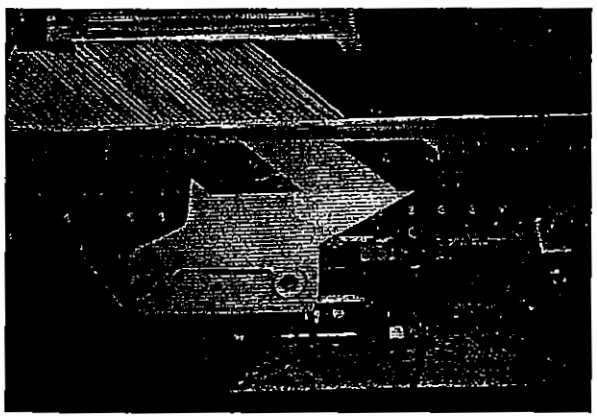

4. Carriage lifts by 10mm above level of the pins and accelerates away. A new band of material is deposited as the tows are pulled off the rake and through the 'new' transport pins.

Figure 41: 'Shogging' movements required to lay parallel 45° layer

2.3.3.3 Fibre Supply

Fibres for both the axial and weft tows are fed from bobbins mounted on creels, that is racks of shelving on which bobbin packages are placed. Tows are pulled 'over-end' from these

packages through eyelets. For the 0° material two 12k tows form each 0° bundle and consequently they share a single eyelet in their path to the knitting unit. 0° axial fibres are pulled of the packages very slowly, at the same linear rate that the fabric is produced. Off-axis weft tows however are unwound much faster, there generally being only fifteen tows per weft as opposed to 600 tows for the 0° material to cover the same surface area in the same time. The action of pulling the fibres off the bobbins 'over end' induces twist in the tow to a greater or lesser extend depending on the orientation of the bobbin. This in turn reduces fibre straightness in the resultant composite and prevents any fibre spreading as the fabric is formed. The alternative to taking material 'over-end' is to use a rotating package as illustrated in Figure 42.

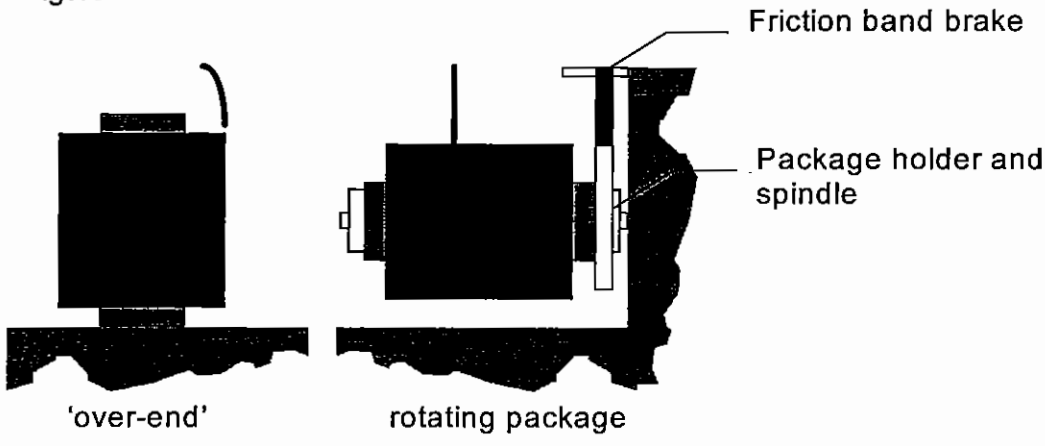

Figure 42: Removal of fibre tows from packages/bobbins

The use of rotating packages requires provision of a support structure, package holders and braking mechanism. This allows it to rotate then material is pulled off but prevents the inertia causing the material to over-run. This is an expensive option for the 0° material as 600 package holders are required for 12k tow at 376 g/m². For the off-axis layers the high feed rate and sinusoidal demand for material makes the use of non-driven rotating packages alone difficult. Attempts to overcome this problem have been developed and trialed by LIBA and a majority of European producers who are aiming their products at the 'high-end' of the market. LIBA and Aachen university co-developed a weft feed system using constant rate rotating bobbins and sprung loaded rollers to act as a accumulator allowing the acceleration/deceleration of the weft insertion unit. It was stated that while this device worked for glass rovings it was too damaging to carbon tows and was hence abandoned by LIBA for commercial use. LIBA also hold patents for other zero twist tow feed systems (US Patent 4411392) and recently with fibre handling equipment specialists Holtex have designed and manufactured a low/constant tension weft feeding device. The unit intermediately feeds material into a hanging loop with the upper and lower limits monitored to trigger the feeder which maintains a ready supply of low tension material for use by the weft carriage[70]. The effectiveness of this device for carbon tows is unknown.

2.3.3.4 Fabric Sheet Transport and Batching

The fibres laid by the weft carriages must be carried along the bed of the machine under tension to the knitting head. This is accomplished by laying the fibres over inclined pins attached to a transport chain which moves along the machine and towards the head. The pins are closely spaced and are subject to damage if subjected to incorrect machine set-up or used for long periods in the manufacture of heavy weight fabrics which results in severe gaps being formed in the fabric.

As the fabric passes each operations weft carriage another layer of material is placed over the same pins above the previous layers. As this 'weft sheet' passes through the knitting head the 0° material is added from above and the knitting elements pass through the

'blanket' of fibres carrying the knitting yarn which is looped with its adjacent yarn forming the knit. As the knitted and stabilised fabric passes through to the front of the machine a pair of rotating diamond impregnated cutting discs shear through the material at each edge next to the pins and the selvedge is removed by a vacuum extraction unit as waste. The material, now locally free from the transport chains is passed through a series of driven rollers and spooled up onto a cardboard tube (Figure 43). When the desired length has been produced, as measured by the number of machine cycles, the machine stops and the fabric is cut from the machine, weighed labelled and bagged.

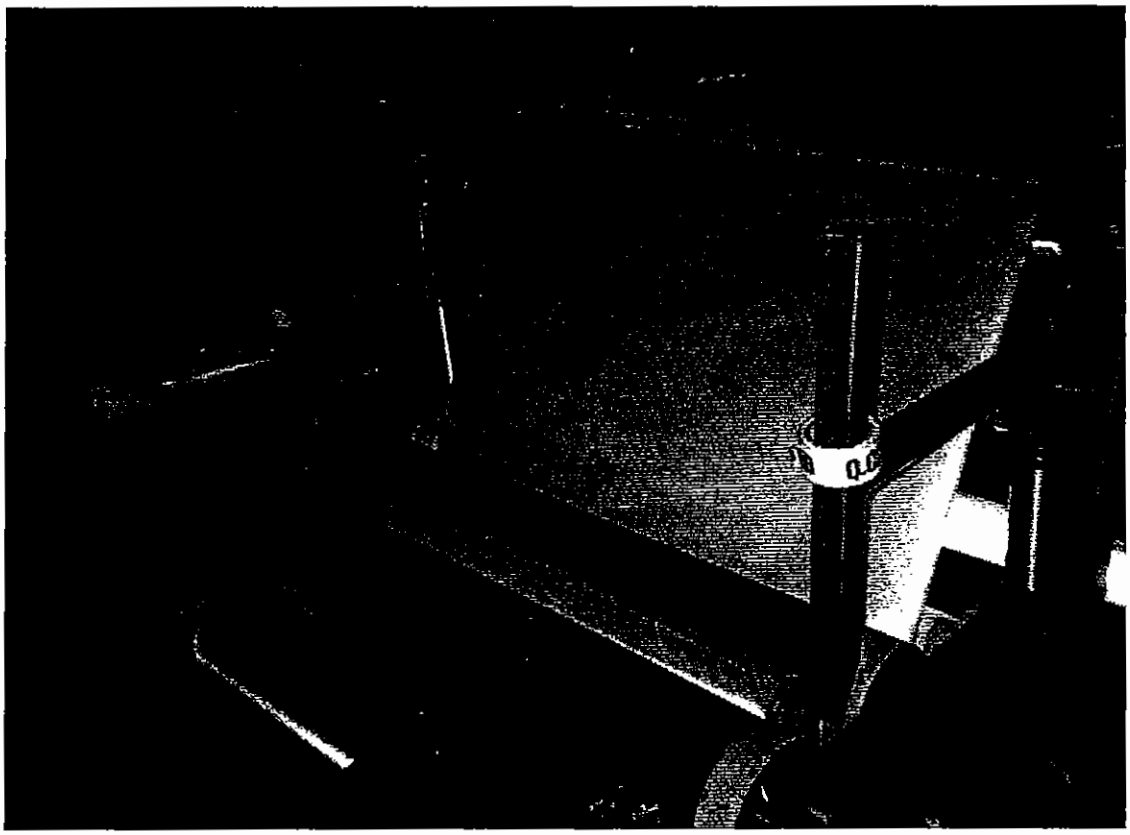

Figure 43: LIBA machine batching unit

Chapter 3

Characterisation Of Structural Composites

3.1 Introduction

Increases in the efficiency of composite materials used in structures may be attained via three routes. Firstly, by good structural design; placing the correct amount of material where it is required in order to accommodate all the stresses that that part of the airframe will see in service. This includes an additional safety factor, to cover for extreme levels of discrete damage and no-growth of un-detectable damage and the presence of bolted repairs. Secondly, by improvements in design allowable stresses based upon statistical confidence in the materials performance. Thirdly, by improving in the constituent properties of the composite itself; stiffness/strength of fibres, toughness of matrix resins.

In order to ascertain how a composite material system will perform in a structure it is necessary to characterise its behaviour using tests. In most cases the statistical interpretation of sets of coupon tests are used to generate design data that is interpolated or extrapolated to the component and loading to which it will be applied. This data will typically be validated, to some extent, by sub-structure tests that represent part of the final component and its in-service loading and finally by limited tests on complete structures.

For coupon test data to be useful the behaviour of the material must be representative of how the material behaves in the structure. For this reason features of the structure, such as lay-up, holes and ply-dropoffs, are usually included at 'coupon level'. This is necessary because the accuracy and confidence in finite element models and failure criteria alone is insufficient to proceed straight from basic fibre and matrix properties to the efficient design of a complete structure.

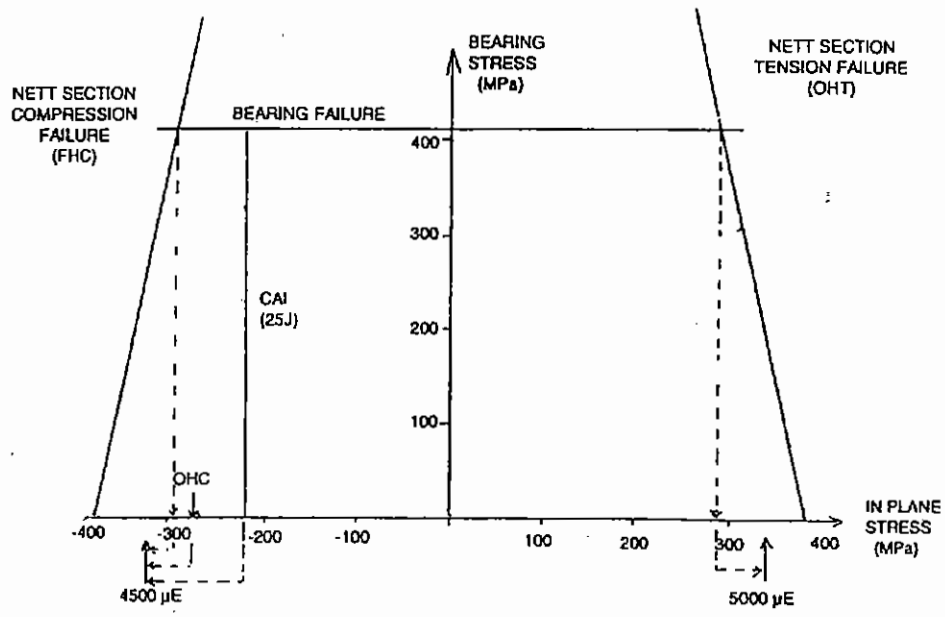

Figure 44: Design allowable envelope for T300/914 prepreg tape composite (50% 0°, 50% ±45° at 80°C)[71]

Figure 44 shows an allowable stress 'envelope' used for the purposes of design for the particular prepreg carbon/epoxy composite used in this study. It illustrates that the 'design allowable stresses' change depending on whether the material in question is loaded in tension, compression, in the presence of holes, fasteners or impact damage. It is clear from this that the gross working stress level of the

damaged structure, rather than the ultimate undamaged strength of the material, that determines the allowable stresses and hence weight efficiency of the structure. There is therefore little benefit to be gained from improving the one type of performance alone as a different failure mechanism may limit the allowable stress[27]. Failure mechanisms may change significantly with fibre type and matrix toughness as well as with the arrangement of the fibres.

For laminated composites characterisation of performance over the entire range of loadings and environments is time consuming and expensive as the constituent properties, lay-up and processing of the material affects its properties both in the short and long term. For textile composites the anisotropy may be in three dimensions and vary in different areas of the part making structural design and modelling a good deal more complex than for most metals or prepreg tape structures. However it does offer the possibility of raising design allowables by improving damage resistance and tolerance and improvements in structural efficiency by tailoring the material strength and stiffness for load transfer through the thickness of the structure.

To allow the range of fibre architectures resulting from the various materials and manufacturing processes to be used effectively in structures, the relationship between fibre architecture and properties and an understanding of the failure mechanisms is thus important. This information may be obtained experimentally or by the creation and use of models; idealised representations of the structure and its behaviour. For textile composites unit-cell models have been created which define the repeating two or three dimensional arrangement of fibres or tows which make up the structure of a composite. They have been extensively developed for woven, braided and more recently multiaxial warp knit materials. The behaviour of some of these models has been subject to validation through experimental examination of property/microstructure relationships.

In this chapter properties measured to characterise the in-plane performance, damage resistance and tolerance, and some microstructural characteristics of composite materials are presented and literature reviewed. In all cases work particularly relevant to the characterisation of multaixial non-crimp fabrics is emphasised. The characterisation of stitched composites is also included as the disruption and fibre damage caused by the stitching process are analogous to the warp knitting of reinforcement fabrics. Previously published data on the performance of LIBA multiaxial non-crimp fabrics with polyester and Kevlar stitching is presented in section 3.5 together with equivalent unidirectional prepreg tape laminate results.

Finally, experimental results are presented on the performance of four different ply/fabric drop-off schemes. These tests were carried out to look at the feasibility of designing tapered structures with very thick (0.8mm) steps as discussed in section 2.2.5.

3.2 In-Plane Property Characterisation

In-plane properties refer to those measured in the plane of the fibres; either along them or at an angle to them. Generally five basic properties are measured; tensile strength and modulus, compression strength and modulus, apparent interlaminar shear strength. In plane shear strength is also often characterised as are holed properties either filled with a fastener or left open. The tests may be carried out at room temperature dry or at elevated temperatures with different levels of relative humidity or in the presence of other substances which may be detrimental to the performance of the structure.

Whatever is measured it is important that the test is carried out in a standardised way which is suitable for the material and that the type of test is relevant to the application of the material in structural use. A comprehensive review of test methods for textile composites[72] noted that the dimensions of repeating unit-cell of the material are important in determining the applicability of test methods to textile composites, this has most influence when considering small sample widths, thickness or gauge lengths. Similarly these internal architecture differences will affect the readings from strain gauges unless they extend over several unit-cell lengths to obtain a measure of strain averaging.

3.2.1 Tensile Strength and Modulus

Tensile strength and modulus are fibre dominated properties and hence sensitive to fibre breakage and misalignment. This is illustrated by the degradation of tensile strength by stitching processes which has been widely reported, although there is some dispute as to whether the primary cause is fibre breakage or fibre misalignment[35].

A designed experiment looking at the effect of five stitching parameters on selected material properties is presented by Dickinson[73] for modified lock-stitched panels within the context of the NASA ACT programme. The five variables considered were; number of plies in the laminate, thread type, thread strength, row spacing and stitch pitch. A Taguchi L_{16} (five parameter, two level) array was chosen and the results of the experiment are shown graphically in Figure 45 for tensile results. Laminates were manufactured by RTM from 3k AS4 carbon fibre uniweave and BP E905L Epoxy matrix and were stitched by Ketema with a modified lock stitch. The observed reduction in tensile strength with increasing thread strength is likely to be caused by the increased crimp or fibre damage due to the large cross sectional area. No significant effect of laminate thickness on the tensile strength of stitched laminates is observed. Previous work[74] had however showed that the surface loop caused by the stitching process adversely affected compression strength; owing to disruption of the surface plies and consequently is more deleterious in thin laminates.

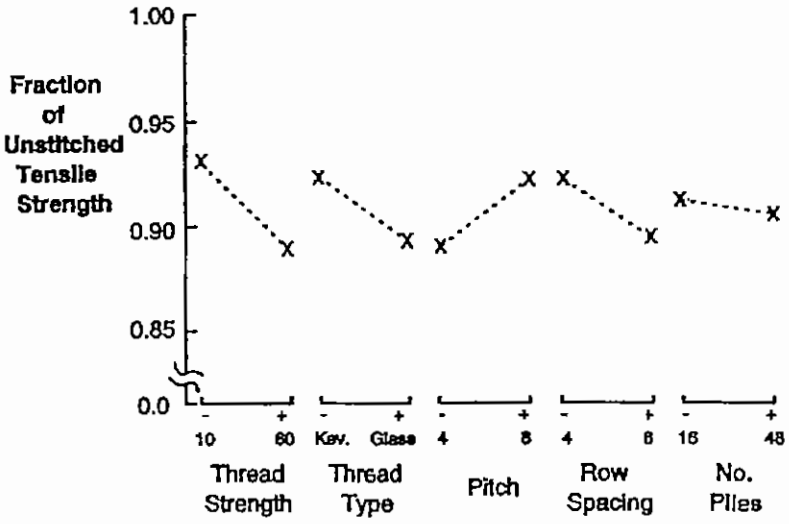

Figure 45: Stitching designed experiment; tensile strength results[73]

Tensile modulus results are presented by Hogg[75] for a wide range of materials including glass chopped strand mat, woven fabrics with thermosetting polyester matrices compared with various biaxial (±45°) and quadriaxial (0°/90°/±45°) non-crimp fabrics. The results indicate that the modulus of the biaxial fabric composites

exceeds those of woven fabrics by as much as 25%. This has been attributed to the reduced crimp in the non crimp fabric material compared with woven reinforcements where each tow is interwoven.

The performance of double stitched multiaxial warp knit non crimp fabrics compared with equivalent single stitched materials shows only a very small degradation in strength caused by the additional stitching process[49]. The double stitching process allows a single material to be used to achieve a balanced symmetric lay-up. Results are presented in Table 10 for a triaxial (0°/±45°) lay-up with 33% 0° in the two fabric configurations shown in Figure 46.

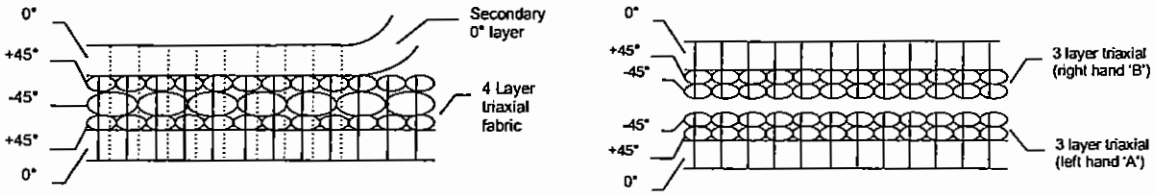

(a) CBTLX1128 - Balanced triaxial (b) CTLX564 - Handed triaxial

Figure 46: Schematic of triaxial balanced and handed pair multiaxial non-crimp fabrics

Table 10: Tensile strength comparison of handed vs. balanced fabric approach

	Tensile Strength (%CV)
CTLX564 multiaxial non-crimp	559 MN/m² (2.7)
CBTLX1128 multiaxial non-crimp	548 MN/m² (8.4)

The results for the two equivalent fabric configurations indicate that, in tension at least, there is little additional detriment caused by stitching the fabric a second time. This implies that the differences in tensile properties observed are not primarily caused by fibre breakage but more likely by differences in fibre architecture caused by the knitting process. Fractographic evidence supports tow crimp at the sites of knitting yarn penetration and tow support as the cause of stress concentration leading to premature failure[65].

3.2.2 Compression Strength and Modulus

The testing of samples in compression requires that the sample be stabilised from globally buckling either using an anti-buckling fixture to constrain the sample, a gauge length which is too short to buckle, or a self supporting shape the sides of which are sufficiently constrained and too short to buckle.

The compressive strength of a material in a given situation will be determined by the failure process which operates at the lowest stress. It is recognised that failure is often initiated by imperfections and that plastic deformation of the matrix[76] coupled with geometric imperfections, such as fibre waviness, voids or cracks[77]are thought to be the probable causes. The mechanism is considered to be that of local buckling instability 'microbuckling' leading to failure due to a lack of shear stiffness at the point of maximum misalignment.

The adverse effects of waviness are further enhanced if adjacent fibre layers have waviness which is in-phase; reducing the stability that might otherwise be offered by adjacent layers. This has been observed by the introduction of intentional crimp in unidirectional materials and from tests on woven materials where the crimp is already present and well defined.

The effect of different percentages of constant amplitude and wavelength 0° layer waviness in unidirectional prepreg tape cross-ply laminates indicated that, above a given fraction of 0° layers containing layer waviness, the reduction in compression strength due to the waviness is constant[78]. Waviness was introduced by applying transverse strips of unidirectional prepreg tape. When more than 33% of the 0° layers contained waviness a 35% strength reduction was consistently observed. For samples with proportions of wavy layers less than 33% the relationship of wavy layer fraction with compression strength appeared linear.

Comparing effects of tow crimp on compression strength Miller[39] observed a linear relationship between standard deviation of tow orientation and compression strength for prepreg tape and non-crimp fabric composites (Figure 47). Compression modulus did not follow the same trend across the materials, although there is some indication of decreasing modulus with increasing tow crimp considering just the triaxial non-crimp fabric data.

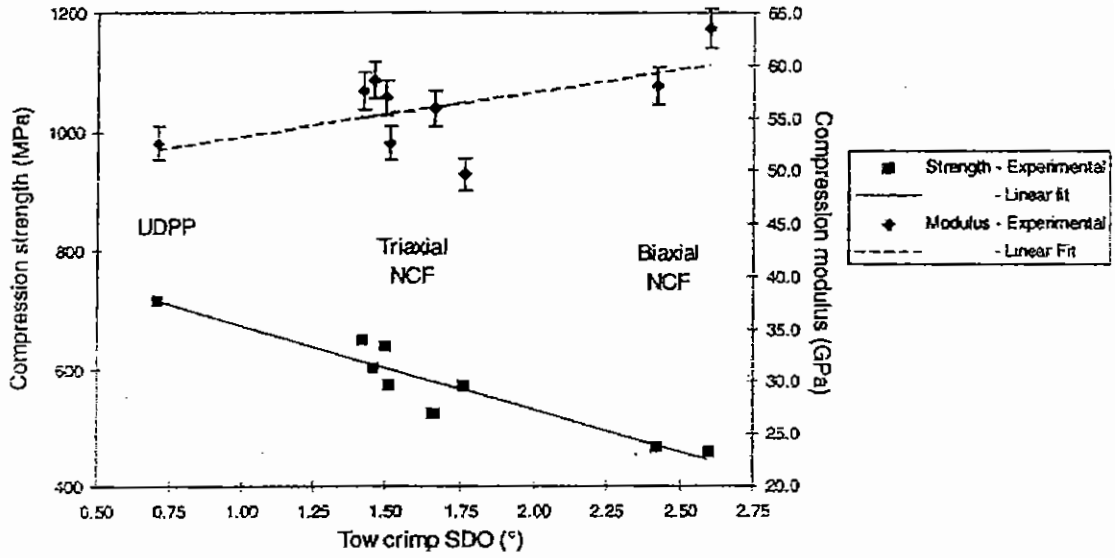

Figure 47: Relationship between compression properties and 0° tow crimp standard deviation[39]

3.2.3 Strength in the Presence of Holes

The stress state in a un-notched multiaxial laminate under in-plane load can be adequately described using the application of laminate theory. In the presence of holes, as at laminate edges, a three dimensional stress state exists. These stresses, and particularly the interlaminar normal stress (through thickness), can attain values which induce delamination between layers. The influence of stacking sequence and relative ply orientations on this free edge stress suggests that the smaller the angular mismatch between adjacent layers the better, and that a spiral stacking sequence is preferred[30]. In a spiral stacking sequence the plies are arranged in repeating sub-laminate groups with ply angles that change by the minimum angular mismatch, like a spiral staircase.

Although increasing the thickness of a laminate by increasing the thickness of the fibre layers may be more cost effective from a fabrication viewpoint, doubling the ply thickness doubles the interlaminar normal stresses[30].

The effect of matrix toughness on notched and un-notched samples indicates that increasing resin toughness leads to increased un-notched tensile strength. However in the presence of a hole the strength reduction for the tougher matrix is more severe than with a more brittle matrix. As hole size increases the tougher matrix shows proportionately less degradation in strength, it is less notch sensitive than the brittle matrix composite[79,80].

The process of damage development in quasi-isotropic laminates has been described as follows[81]. At low loads the sample deforms elastically with no damage, but at some threshold value of load, matrix cracks form at the tip of the 90° plies around the hole. As the load increases the damage spreads to the ±45° plies as both microcracks and delaminations. As the matrix cracks coalesce between ply interfaces; longitudinal splitting between 0° fibres may also occur. Zehn[82] suggests that in this damage zone there are still some fibres (predominantly axial 0°) which retain their original proportion of the load, and as the applied load increases the stress distribution around the hole changes with the stress in the damage zone remaining nearly constant. At some critical maximum load the notch extends rapidly, fibres break and the specimen fails.

Laminates made from woven fabrics tend to be more notch sensitive than unidirectional materials, which is attributed to the weave restricting the size of the damage zone[83]. Damage that is inflicted upon a woven fabric composite cannot easily be dissipated by the growth of intra-ply matrix cracking as the interweaving of the fibres tends to block its propagation and development into delaminations. Damage therefore tends to be dissipated as fibre breakage making the material more notch sensitive than a uni-directional fibre composite where intraply matrix cracks can coalesce to form delaminations as a mechanism of dissipating local stresses.

For textile composites where the fibre architecture comprises discrete tows, as opposed to fibre layers found in unidirectional tape laminates, matrix cracking occurs preferentially between the tows in some materials. Matrix cracking is followed by plastic straightening followed by rupture and eventual pull out of the tows from the composite across the fracture plane[34]. The pull out lengths can be large, as debonding from the surrounding composite occurs over a slip-length which scales as the ratio of the tow's cross sectional area to circumference.

An effect called 'lockup' occurs when the pullout of a fractured tow is opposed by unusually strong friction. This is considered a peculiarity of textile composites and is caused by the impingement of irregular features on neighbouring tows as they are dragged past one another during the pullout process[34].

3.2.4 Interlaminar Shear Strength

For composites which have much higher modulus than the matrix, for a given resin the shear behaviour depends on the stress concentration effects associated with the presence of fibres and voids and on the strength of the interfacial bond[130]. Although increasing the fibre/matrix bond strength increases interlaminar shear strength this only applies up to the point at which failure occurs in the resin rather than at the interface. In most fibre/matrix combinations the fibre surface treatment favours interfacial failures so as to reduce the notch sensitivity of the composite, which would otherwise tend to fail in a brittle manner.

Studies of the effect of fibre volume fraction on interlaminar shear strength show that as the Vf is reduced so the 'additional' resin tends to accumulate in the interlaminar regions[84]. Apparent interlaminar shear strength has been shown to decrease with an increasing free resin volume fraction and also with the thickness of resin layers[39]. Increasing the Vf led to increases in ILSS up to a point at which the strength was observed to drop suddenly[84,85,130]. The sudden load drop is attributed to the stress concentration of the fibres as the resin layer thickness reduces[86,130]. For laminates with brittle resins, the stress concentration effect leads to interlaminar shear strengths in the composite which are lower than that of the neat resin. For tougher systems the shear strength of the composite and neat resin are approximately the same as local stress concentrations are relaxed by local deformation[130].
For multiaxial laminates the shear strength as measured in the short beam shear test is dependent on the strength of each interface when subject to the imposed shear stress, which is at its maximum at the mid-plane. For a given material the level of stress is a function of the fibre orientations at the interface and the thickness of the layers, with the weakest interface determining the shear strength. Hence observation of the plane of failure is important. The test is therefore only useful as an indication of the comparative shear strength for a material system when the lay-up, fibre volume fraction and plane of failure are the same. Other test methods are now considered more reliable indications of shear strengths and modulus. The Iosipescu is often favoured for both in-plane and interlaminar shear testing, as it can be used on a wide range of materials, material thicknesses, lay-up orientations. Difficulties in obtaining a pure shear strain in the test section state have been observed using Moiré Interferometry, and are largely dependent on the chosen lay-up and the constituent properties of the materials being tested[131]. The test also requires careful sample preparation and machining to select the interlaminar shear plane to be tested.

The effect of fibre waviness on interlaminar shear strength is considered to be determined by the possibility that wavy fibres will bridge the interlaminar region and will have to be broken or pulled out to cause failure[87].

3.3 Damage Resistance and Tolerance Characterisation

3.3.1 Introduction

Whereas damage resistance is a measure of the damage incurred by a material or structure due to a particular event, damage tolerance for composites applied to aircraft structures is defined by Baker et al[88] as "the ability of a structure to contain representative weakening defects under representative loading and environment without suffering excessive reduction in residual strength, for some stipulated period of service".

Carbon/epoxy composite structures are highly sensitive to damage from low velocity impact loads which may occur in-service, e.g. dropped tools, runway debris. Different failure mechanisms have been observed under this type of loading, such as breaking fibres, micro cracking of the resin matrix, debonding and delamination. Among these forms the most critical is often delamination. Manufacturing imperfections, such as air entrapment or regions of in-sufficient resin may also give rise to delaminations which can spread to un-damaged areas of structure typically under compressive in-plane loading. Delaminations may also initiate in areas of stress concentration and particularly through thickness tensile stress such as at free edges; notches; holes; ply drop-offs and bonded and bolted joints.

Where design allowable stresses are governed by damage tolerance, airworthiness authorities typically require the structure to withstand two life-times fatigue strength in the presence of barely visible impact damage with no-damage growth. For most materials this restricts the design allowable strains to less than half the ultimate strain to failure of the composite.

Efforts to improve the through thickness properties of composite laminates can broadly be divided into two categories; improvement of constituent material properties as discussed earlier, or modification of the reinforcing fibre architecture usually with the aim of providing reinforcing fibres which pass through the material thickness to limit delaminaton extent and its propagation, i.e. both resistance and tolerance.

Understanding the mechanisms of delamination initiation and growth are typically addressed in two types of test: Firstly, interlaminar fracture tests, which seek to measure the strain energy release rate in a number of loading modes or combination thereof. Secondly, impact tests in which the response of a material to a impact is observed in terms of how load is transferred to the material and the resulting delamination extent. This is typically followed by measuring the residual strength of the material, often in compressive loading.

3.3.2 Mechanisms of Interlaminar Fracture

Wu[126] demonstrated the applicability of Linear Elastic Fracture Mechanics (LEFM) to unidirectional composites containing cracks parallel to the fibres. However, the concept of LEFM is not ideally applicable to composites which exhibit anisotropy and heterogeneous structure at the scale of the crack tip. Instead of using the stress intensity factor, K, as a measure of material toughness, a strain energy release rate, G, defines the work done (Joules) to create a new area of transverse fracture surface (per m^2).

The critical strain energy release rate is representative of the matrix resin toughness influenced by the surroundings (fibres, interface and microstructure). It is also dependant on the mode of the interlaminar stress. There are three basic modes, opening or peel (mode I), shear (mode II), tearing mode (mode III) or a combination thereof (Figure 48).

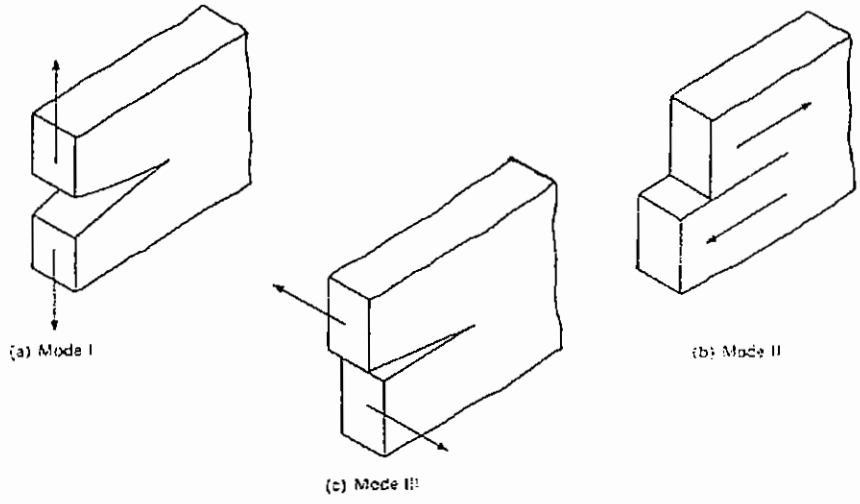

Figure 48: Three basic cracking modes

The failure processes occurring in fracturing composites are complex and will typically include a number of interlaminar failure modes. This is particularly true of

composites subjected to impact, where the failure process is a complex combination of contact stresses, laminate flexure, mode I and mode II delamination initiation and growth, matrix cracking and fibre de-bonding.

The generation of delaminations is associated both with the interlaminar stresses, determined by the geometry of the sample or structure and magnitude of the load, and by the interlaminar strength, dictated by material properties. Thus to improve the resistance to delamination, interlaminar stresses must be reduced or interlaminar strength increased.

The generation of mode I strain energy release rate data is perfomed on a double cantilever beam (DCB) test sample. This consists of a narrow beam with a starter defect running a known length into the sample at the laminate mid-plane. Load is introduced, as shown in Figure 49a, through hinges or hinge blocks bonded to the starter defect end. The crack is developed by pulling apart the hinges at a constant rate during the test. Stable crack growth from the end of the starter defect between the ply interfaces occurs and the resulting force/cross head displacement curve, together with information on the location of the crack tip at intervals during the test, allows the strain energy release rate for crack growth to be calculated for that material system and between that interface.

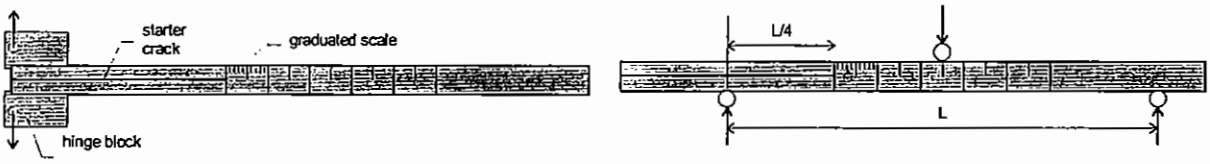

(a) Mode I (crack opening) (b) Mode II (crack shear)

Figure 49: Mode I and Mode II test configurations

The mode II test measures the strain energy release rate for crack growth in shear loading as illustrated in Figure 49b. The test configuration is called End Notched Flexure and uses the same specimen as the mode I DCB test but is loaded in three point bending with the crack tip half way between the mid-span and one knife edge. In this case the crack propagation tends to be unstable and the point of non-linearity on the load displacement curve, the 5% offset point and/or the maximum load achieved tend to be used to characterise the mode II strain energy release rate of the material system.

3.3.2.1 Effect of constituent properties

Interlaminar cracks as well as propagating in neat resin will interact with the fibre surface via an interface. The strength of this interface is often controlled by adapted coatings (sizing) on the fibre surface. As long as the interfacial bond strength is stronger than the resin itself, the crack will tend to propagate only in the matrix.

The role of fibre properties on composite fracture is related primarily to its effect on the compliance of the composite. an applied load will result in a given opening or shear displacement depending on its stiffness and hence stress level at the crack tip.

The effect of resin toughness in relation to the toughness obtained for the composite is related primarily to the constraint, by fibres, of the zone of plastic deformation which surrounds the crack tip. For tough matrices the neat resin plastic zone is larger than the resin layer between plies. This reduces the degree of load re-distribution away from the crack tip, and thus allows the critical strain or stress condition for local failure at the crack tip to be achieved earlier. For resins where the plastic zone ahead of the crack tip is less than or equal to the height of the resin layer between plies, neat resin and composite toughness will be similar.

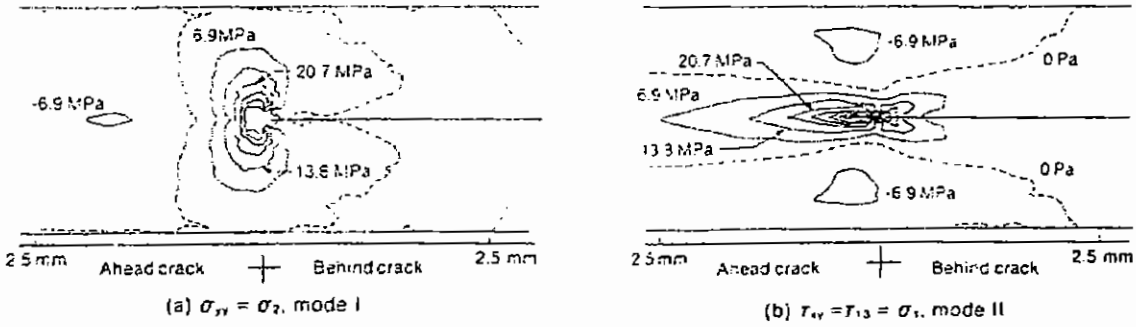

Figure 50: Typical plastic zone stress distribution under mode I and mode II loading

For brittle resins crack growth is more difficult when the crack tip is loaded in shear (mode II). The reason for this is related to the shape of the plastic zone which surrounds the crack tip. Figure 50 shows the difference in stress contours around the crack tip in both mode I and mode II loading for AS4/3501-6 a relatively brittle carbon/epoxy system. It indicates an elongated deformation zone, primarily ahead of the crack tip in mode II loading, giving a more gradual decay of the stress field. In this zone microcracking ahead of the crack tip may lead to local softening and load redistribution. In mode I the stresses are localised above and below the crack tip making them more sensitive to the height of the resin layer. These differences result in the resistance to delamination growth in mode II being much greater than in mode I, particularly for brittle resin systems (neat resin G_{IC}<400J/m²) where the G_{IIC} may be more than three times greater[127]. As neat resin toughness increases the difference between mode I and mode II reduces as the toughness transfer from the resin to composite is compromised by the constraint of the plastic zone by the fibres.

3.3.2.2 Effect of Fibre Architecture

Work to compare the strain energy release rates for both triaxial non-crimp fabrics, with various 0° arrangements and stitching materials, with equivalent lay-ups in unidirectional prepreg tape has showed around 100% increase in mode I strain energy release rate at delamination initiation, compared with unidirectional prepreg tape[89]. The increase in mode I strain energy release rate was attributed to the heterogeneous mesostructure around the fracture surface which resulted in a large fracture surface area and the introduction of a proportion of shear loading as the delamination deviated out-of-plane, around the bundles of fibres. The stitching yarn, texturised polyester, was not considered to play a significant role in the increase in the strain energy release rate at crack initiation, being highly extensible and poorly bonded to the fracture surface.

Through thickness stitching has been shown to increase the strain energy release rate in both mode I and mode II interlaminar fracture. In double cantilever beam tests strain energy release rates were increased by as much as a factor of 30, and in mode II by as much as 15 times. In mode I loaded delamination cracks this increase is attributed to the stitches bridging the cracks and shielding the crack tip from the applied load and hence suppressing crack growth.

In mode II stitching yarns through the thickness bridge the delamination and impose shielding shear tractions on the fracture surfaces. So long as the stitches remain intact the applied load for propagation approaches a steady state independent of the crack length[34]. This is in contrast to un-stitched samples, where crack propagation is typically unstable.

Studies of mode II interlaminar toughness in both glass and carbon laminates have shown that non-crimp laminates have higher G_{IIC} than equivalent laminates manufactured from unidirectional prepreg tape. This has been attributed to the tortuous crack path[89] and the interaction of the knitting yarns[65] with the growing crack front, in the same way as that observed for through thickness stitching increasing the mode II strain energy release rate[34].

3.3.3 Impact and Compression After Impact Testing

Impact damage generally consist of delaminations, matrix cracking and fibre breakage. For low velocity impacts the full extent of damage is usually not visually detectable, consisting mainly of delaminations within the laminate. These delaminations alone can result in significant reductions in strength, particularly when loaded in axial compression. This is due to the reduced buckling stability of the laminate, now locally divided into 'sub-laminates', which are less stable and may exhibit some out of plane deflection due to fibre damage or internal stresses. Resistance to the propagation of delaminations from the buckled sub-laminates is primarily driven by the Mode I strain energy release rate. In the impact event itself the influence of interlaminar fracture properties is more complex and dictated by sample geometry and constraint.

3.3.3.1 Impact damage development

The damage created during an impact event is dependent both on the magnitude of the blow and the constraint of the target. A thin skin with a large span between supports will be relatively free to deflect and the damage introduced is primarily flexural (Figure 51a); large tensile forces on the back face of the material and some localised shear buckling close to the front face adjacent to the impact site. The deflection of the laminate, if sufficiently large, causes transverse cracks between fibres close to the tensile back face of the skin and with increasing deflection these grow and nucleate delaminations where the cracks meet a ply boundary. These delaminations extend in the direction of the lower ply to an extent dependent on the deflection and interlaminar fracture properties of the ply interface. The mode of the delamination growth will be a mixture of mode I and II. Further deflection may cause tensile fibre fracture starting at or close to the back face followed by perforation of the laminate. In cross section the damage is conical with the largest delaminations close to the back face.

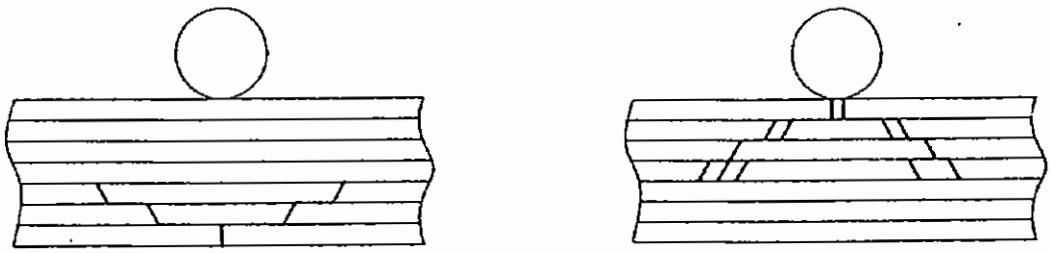

(a) Flexible impact target (b) Rigid impact target

Figure 51: Effect of target stiffness on impact damage development[90]

For rigid targets (Figure 51b) (i.e. thick laminates, or thin laminates which are highly constrained so as to appear rigid), contact damage dominates the failure process with fibre fracture and delaminations cracks generated by shearing of material away from the striker as it indents the surface plies. These delaminations may be conical where their is some deflection of the target as shown, or may posses the largest delamination on the impacted surface as a 'blister' when the target is rigid.

For surfaces loaded primarily in compression, such as an aircraft upper wing skin, delaminations are the most serious aspect of impact damage, whereas for tensile surfaces fibre fracture may be considered more deleterious. As an interlaminar fracture driven process the same factors of constituent and interfacial properties together with the fibre architecture determine the exact nature and extent of the impact damage.

Damage initiation threshold values are important from the point of view of designing against tool drop or small stone impact damage, as these may routinely occur. The threshold force for damage can be obtained from the impact force at the first major load drop on the force/time impact trace.

Effect of material properties

Delamination and matrix cracking are sensitive to matrix toughness and relative resin layer thickness, whereas fibre breakage is sensitive to the properties of the fibres. Experimental results indicate that matrix properties govern the threshold for damage initiation. Damage area however is governed by a combination of matrix properties and fibre strain to failure. Penetration resistance at large impact energies is dominated by fibre properties.

Cantwell et al[92] comparing laminates manufactured with high strain or standard carbon fibres of the same modulus, and manufactured with the same matrix system, showed that fibres with a higher strain to failure exhibit smaller damage areas for the same incident impact energy. The mechanism is the higher impact strain energy absorption made possible in the matrix by extending the strain to failure of the fibres, but keeping the original fibre modulus. Because the fibres had a higher strain to failure the amount of fibre breakage was reduced, increasing the residual tensile properties[91].

Work by Varela[93] on T300/Hexcel 914 and T300/Hexcel M18 multiaxial non-crimp laminates indicated that damage areas were on average 40% smaller for the tougher T300/M18 matrix laminates. However this enhanced damage resistance did not manifest itself as enhanced damage tolerance; the CAI strength for the same damage area being almost equal. Mode I interlaminar fracture tests had indicated similar $G_{IC(NL)}$for both matrix systems but a mode II strain energy release rate G_{IIC} which was almost three times higher for the M18 matrix composite. These differences are attributed to the constraint by the fibres of the plastic zone around the crack tip. This effect being much more severe in mode I loading, resulting in similar G_{IC} values for both systems and consequently similar CAI performance for a given delamination area.

Effect of fibre architecture and lay-up

The onset and extent of impact damage in composite materials is determined by fibre architecture as well as constituent properties. For unidirectional prepreg tapes both the onset and extent of damage is determined by the difference in angle between adjacent plies[94]. The area of delamination increases with increasing mismatch until an angle of around 30° after which no increase in delamination size or initiation load is observed[95]. Delaminations are not observed at ply interfaces of the same orientation[91].

Individual ply thicknesses within a multiaxial laminate also affect the area of delamination due to impact. This is due to the interlaminar shear stress being locally higher at the reduced number of ply interfaces in a laminate comprising large blocks of the same orientation.

Laminates with 0° outer plies are more weakened by delaminations than those with ±45° outer plies[96]. Laminates with woven ±45° plies showed improved delamination resistance and residual strength after impact, compared with laminates manufactured with unidirectional tape ±45° plies[97,98].

Enhanced suppression of delamination damage in non-crimp fabric laminates may be expected on the basis that all the most likely planes of fracture, between layers of differing fibre orientation, are bridged by the through thickness stitching/knitting yarn, providing some crack tip shielding or crack closure force. The use of a 110 tex Kevlar 49 knitting yarn rather than 7 tex polyester has been shown to reduce the delamination damage area under impact loading[65].

Studies of the delamination surfaces of de-plied triaxial carbon non-crimp fabrics indicate similar 'peanut-shaped' delaminations as observed in prepreg tape impact samples. However the delamination surface was 'rippled' and observed to follow the contours of the local fabric architecture[65].

Under impact loading stitched laminates have been shown to offer reduced delamination areas than their unstitched counterparts. This applies both to preforms stitched through the entire thickness and to those in which individual multiaxial non-crimp fabrics were stitched/knitted with Kevlar yarn[65]. Compression after impact strength for secondary stitched multiaxial non-crimp fabric composites can be more than 50 percent higher using the same fabric and 3501-6 matrix and as much as 80% better than 3501-6 unidirectional prepreg tape when the tougher 3M PR500 matrix was used with the multiaxial non-crimp fabric[43,46,47,48].

Impact studies on stitched carbon uni-weave fabrics indicate that there is no significant improvement in the threshold force to initiate damage for thin laminates, and that any increases observed were caused by increases in sample thickness due to the introduction of the stitches. Reductions in damage area of up to 40% were however observed[91].

3.3.3.2 Impact Damage Assessment Techniques

The use of instrumented drop weight impact equipment can be used to identify the nature of the damage and pinpoint the onset of certain fracture mechanisms. Damage initiation for instance is often identified as corresponding to the first load drop on the force-displacement trace[99]. Acoustic emission equipment has been used to identify other mechanisms, such as matrix cracking, which cannot be identified from normal instrumentation of the impactor itself[100]. The use of quasi-static indentation tests has identified matrix cracking preceding delamination initiation[101].

The most common way of assessing the delamination damage to a composite is using ultrasonic techniques, and most commonly a C-scan image of the projected damage area. This is obtained most usually by measurement of the magnitude of a reflected ultrasonic signal whilst the sample is suspended in a bath of fluid, typically water. The transmission of the signal depends on the presence and modulus of the medium though which it passes, hence voids and delaminations which lie parallel to the laminate surface, mask or block the signal, thus identify the location of the anomaly. 'Time of flight' C-scans can be used to locate delaminations and other defects through the thickness, providing a three dimensional image of the damage. The technique measures the time between sending and receiving the ultrasonic

signal to identify the depth. However the signal blocking effect of delaminations prevents any information below a delamination from being collected.

The presence of stitching has been shown to significantly affect the quality and accuracy of standard ultrasonic non-destructive evaluation techniques[35].

X-radiography whilst a routine technique in the inspection of aircraft structures cannot readily be applied to carbon epoxy composites, as both matrix resin and fibres have similar x-ray absorption characteristics so anomalies in material structure are difficult to identify. Delaminations cannot readily be detected as they possess virtually no volume or change in density of the material. However the use of x-ray opaque penetrants such a zinc iodide render delaminations and other cracks observable provided the penetrant can be introduced. This is most readily achieved using a small drilled hole through the centre of the impact site. The damage resolution achieved by this method is higher than with ultrasonic techniques but is expensive and requires that the location of the damage first be identified and the destructive operation of drilling be carried out.

Destructive damage assessment techniques such as de-ply using precipitated gold chloride to identify the delaminations after the sample is partially pyrolised have been successfully used to identify the distribution of delaminations through the sample thickness[102].

3.3.4 The Compression After Impact (CAI) Test

Characterisation of the damage tolerance of polymer matrix composites subject to low velocity impact damage is widely performed by measuring the compression strength of a sample laminate impacted by a falling hemispherical impactor at a known incident energy. To provide the maximum information on the impact event the impactor is often instrumented to provide force/time/deflection data. The test is used to represent the response to delamination damage which might typically occur in service due to dropped tools during assembly or maintenance or other low velocity impact hazards. The 100mm or 4" sample width used in the ACOTEG[103] and Boeing CAI[104] test notionally represents the spacing between stringers, presumably in a military aircraft wing.

Impact induced delaminations can buckle under compressive load and subsequently grow, causing further reductions in the compressive load carrying capacity of the structure. The buckling instability is generally determined by the length of the delaminations. There is evidence that the width of the delamination damage relative to the width of the sample provides a better correlation between damage size and compression strength than either largest delamination length or damage area[65].

In stitched carbon uni-weave laminates, as the damage level increases the stitching tends to improve the CAI performance from an initial degradation to a 400% improvement. It is suggested that sub-laminate buckling which would usually lead to premature failure is suppressed in stitched laminates[105]. The effect of through thickness stitching with polyester has been observed to provide a small increase from 110MN/m² to 125MN/m² compared with the same un-stitched uni-weave impacted with a 40J incident energy impact. The use of Kevlar, glass or carbon stitching yarns increased the CAI strength to around 250 MN/m².

The compression after impact strengths of multiaxial warp knit non-crimp fabrics have been shown to be equivalent to or better than the same lay-up in unidirectional pre-impregnated tape[65] or uni-weave reinforcement[43].

3.4 Microstructural Characterisation

A textile composite has internal structure on several scales. At the molecular scale, both the polymer matrix and the fibres exhibit structural details that profoundly affect strength and stiffness. On a coarser scale typically of the order of 1mm, groups fibres are bundled into yarns and tows. Within the finished composite, each tow behaves as a highly anisotropic solid entity, with far greater stiffness and strength along its axis than in transverse directions. Because tows are rarely packed in straight, parallel arrays, stress and strains often posses strong variations from tow to tow and composite mechanical properties can only be considered approximately uniform on scales that are larger still and of the order of 10mm or higher[34]. This is in some contrast with unidirectional prepreg tape composite where the internal structure of each fibre/resin layer is often considered uniform above the microstructural level.

This uniformity of fibre orientation, straightness and resin distribution in unidirectional prepreg tape composites allows some of the in-plane properties to be relatively simply predicted; at the most basic level by the 'rule-of-mixtures'. Classical Laminate Theory can, with more information, be used successfully to predict the elastic response of combinations of layer orientations to more complicated in-plane loading. However as the internal structure of a textile composite is often more complex, such as the undulating tows seen in woven architectures, these techniques become less applicable and so models to represent their behaviour have been developed. These can generally be considered as Elasticity models and Finite Element models. In both cases the structure of the material is idealised to simplify the analysis task. A review of modelling methods for textile composites is presented by Gowayed and Pastore[106]. A majority of work in this field has concentrated on woven and braided materials as their architectures can be easily controlled during manufacture and they contain high levels of fibre crimp. Multiaxial warp knit non-crimp fabrics however visually appear to fall somewhere between the two extremes of architecture; being formed of layers of unidirectional fibres, created from bundles of tows, which can remain discrete and held in relation to one another by the presence of a fine secondary knitting yarn. Modelling of multiaxial warp knit non-crimp fabrics is less widespread and laminate theory is widely used in the industry for property prediction. More complex models are now being developed which consider the presence of the stitching yarn and tow geometry[107,108].

In this section methods used to characterise composite architectures in the 1mm mesostructural level are described with the results of relevant studies. Much of this work was carried out by Miller[39] who using similar materials developed the image analysis routines which will be used later. The main areas of measurement are the out-of-plane crimp of the 0° tow bundles and resin distribution within the structure of the material.

3.4.1 Tow Crimp and Fibre Misalignment

The causes of fibre misalignment are fourfold: Firstly resulting from the design of the fibre architecture, for instance the crimp caused by the interweaving of fibre bundles in the weaving process. Secondly, they may be caused by the settings selected in the manufacturing process. Thirdly, induced by the design of the structure in which the material is used; if the structure is tapered in thickness these steps will introduce a level of crimp. Finally crimp or misalignment may be caused by uncontrolled, or difficult to control factors,' such as fabric defects or inherent misalignment in the fibre tow as manufactured.

The characterisation of fibre and tow misalignment has been performed in two ways:

1. Measurement of individual fibre orientations
2. Measurement of fibre or tow crimp - waviness.

In the case of measuring individual fibre orientations the method developed by Yurgartis[109] is most widely used. It looks at a discrete cross section of the material cut at an angle to its primary orientation and measures the dimensions of the individual ellipses of the observed fibres. The major length of the oval and its orientation are then used to deduce the path that the section of fibre is taking. Sequential sections through the material can then be taken and used to build up an image of the fibre paths. The main limitations of this technique are its speed and computing power and data storage requirement, as the level of magnification required is large creating a large number of frames, particularly if measurements representative of the material as a whole are required. For certain carbon fibres, Toray T300 being an example, the fibres are 'kidney' shaped in cross-section. This means that the measurement of ovality and hence fibre orientation is compromised by a pre-existing out-of-roundness in the fibres. The error in the calculation of fibre orientation caused by this out of roundness has been calculated at between 10-15°[39].

The effects of out-of-plane tow crimp have been measured using artificially inserted waviness, introduced using either strips of transverse material inserted during cure or pre-curing layers of unidirectional prepreg tape over and under a series or rollers allowing the amplitude and wavelength to be systematically changed[110]. Studies have also been carried out measuring the tow crimp usually from optical microsections cut parallel to the fibre orientation of interest. Measurements of the effect of the crimp have looked at both tension and compression properties. In one study the compression strength was observed to drop as the crimp (defined here as the ratio of crimp amplitude/wavelength) increased. Additionally the study observed that samples were more likely to fail at the location of the crimp as its magnitude increased. Failure was characterised by delamination (or brooming) of the layers starting at the point of maximum crimp angle. Similar effects of crimp amplitude and wavelength are observed when the amount of interweaving is changed in moving from a plain weave to a 5-harness or 8-harness satin weave, or when the filament counts used to manufacture the fabric are changed, altering both the amplitude and wavelength of the crimp.

Tow crimp resulting from the stitching process has been observed and its influence measured by Farley and Dickinson[74]. The relatively poor compression strength of stitched uni-weave fabrics was attributed to the local crimping of the surface plies by the presence of the stitch loop, which interconnects each penetration of the stitch. Removing this loop and the crimped surface layers by machining resulted in a 27% increase in compression strength with no degradation in compression after impact performance. As the same depth of material is likely to be affected by the surface loop irrespective of thickness, the effect will diminish as part thickness increases.

Studies in both thermosetting and thermoplastic matrix composites have revealed a linear relationship between the standard deviation of fibre angle distribution and compression strength. The thermoplastic composites included prepreg tapes, plain weaves and a non-crimp fabric. Similar studies comparing thermoset matrix composite laminates manufactured from prepeg tapes, three different triaxial and one biaxial non-crimp fabrics showed the same linear relationship between the different groups. Prepreg tape laminates having least crimp and the biaxial non-crimp fabric the greatest.

As well as optical techniques glass fibres or metal tracer wires to track the behaviour of carbon fibres using X-radiography have both been reported. Similarly the use of neutron radio-tomography to provide three dimensional images of fibre architectures has been used to reveal the internal structure of textile composite materials[111].

3.4.2 Resin Distribution

As with tow crimp and fibre misalignment, the resin distribution is principally determined by the fibre architecture, but also by the amount of resin applied and the processing conditions.

Studies to evaluate the effect of fibre volume fraction on interlaminar shear properties (section 3.2.4) have indicated that reducing fibre volume fraction encourages resin rich layers to form at ply interfaces[84]. Increasing resin layer thickness has been observed to reduce interlaminar shear strength[39].

Interleaved composites where resin layers of the matrix resin, or more usually a 'tougher' system, are dispersed between unidirectional prepreg tape plies, have been shown to offer large improvements in compression after impact strength as a result of having less internal delamination. Masters[112] presented test results indicating that interleaving produced only nominal increases in G_{IC} but significant improvements in G_{IIC}. This has been attributed to a less constrained plastic zone ahead of the crack which propagates through the resin interleaf. The inclusion of resin interleaves does however require more resin to be carried thus increasing mass and reducing the modulus of the composite[28,90]. An alternative to the use of resin layers is the application of small discrete <20μm diameter thermoplastic polyamide particles as an integral constituent of the prepreg tape and located at the interfaces plies. BMS 8-276 prepreg tape (Toray 3900-2/T800H) used by Boeing on the 777 tailplane and floorbeams incorporates this toughening approach. Seven fold reductions in impact damage area are claimed compared with previous 'equivalent' production materials (BMS 8-212)[113].

Matrix cracking is observed in many instances when laminates are subject to temperature and/or humidity cycling. Cracks occur and propagate predominantly in resin rich areas and particularly in stitched materials where they tend to develop perpendicularly to the stitching fibre and occur both at the laminate surfaces and at the laminate midplane. Their occurrence is thought to be due to thermal shrinkage of large areas of matrix resin and the thermal expansion coefficient of the stitching material, both along the length and radially, where present[114].

Preliminary three dimensional finite element models of the resin pocket observed surrounding the stitch have been created and used to predict the magnitude of the stresses in the matrix. The through thickness stress distributions based on the models when compared with the known shear and tensile strengths of the neat resin allow predictions to be made as to when matrix cracking will occur. Three manufacturing variables have been shown to affect the matrix crack frequency and its appearance; resin systems; stitching threads and process cycles[115]. Degradation of performance (short block compression strength) due to the thermal and humidity cycling is typified by a loss of strength of between 3 and 10% in early cycling[116]. This is believed to be due to the relief of internal stresses through the formation of matrix cracks as described above. The matrix cracking observed in stitched laminates was considered stable in compression-compression fatigue of un-notched and impacted samples, and did not contribute to failure in all but high stress, short life conditions[117].

A remaining concern is the potential effects of long term exposure of microcracks to aviation fuel, both in terms of potential long term leakage paths and in terms of ability to repair fuel soaked structure[115].

3.5 Mechanical performance of CTLX816 baseline vs. UDPT

Tests comparing laminates manufactured by Resin Film Infusion from triaxial carbon multiaxial warp knit non crimp fabrics with equivalent lay-ups in prepreg tape composites indicate similar tensile, open hole and filled hole properties but much lower compression strengths[60]. Similar observations have been made for quadraxial materials manufactured by the LIBA process for the NASA-ACT ICAPS stitched wing programme when compared with uni-weave fabrics[43].

As part of this study a limited investigation was conducted. Table 11 to Table 14 show results for two multiaxial non-crimp fabrics, one stitched/knitted with 7 tex multi-filament texturised polyester and the other manufactured in the same way but with 110 tex continuous filament Kevlar 49. Non-crimp fabric laminates contained nominally 46% 0° fibres and the prepreg tape 43% 0°, the remainder being ±45°. Prepreg tape was laminated so as to replicate as closely as possible the non-crimp fabric lay-up. Data is not corrected for this or fibre volume fraction differences nominally 54% and 60% for the non-crimp and UD tape laminates respectively. Coefficient of variation (%) is given in brackets.

The lay-ups were as follows:

$[+45°_2,-45°_2,0°_6,-45°_2,+45°_2]_s$ 914C-T300-5-34%

$[+45°_{220},-45°_{220},0°_{376},0°_{376},-45°_{220},+45°_{220}]_s$ CTLX816/Fiberdux914 (fibre areal weights (g/m²))

Tow crimp measurements for the same materials made by Miller[39] indicate a 0° tow crimp standard deviation of orientation of 0.7° and 1.4° for the prepreg tape and polyester stitched materials respectively and 1.7° for the Kevlar stitched.

Table 11: Tensile properties of CTLX816 compared with prepreg tape composite

	CTLX 816 (7tex polyester stitch)	CTLX 816 (110tex Kevlar 49 stitch)	UD prepreg tape
Strength (MN/m²)	687 (0.9%)	665 (3.7%)	710 (3.1%)
Modulus (GN/m²)	64.8 (2.1%)	66.2 (3.2%)	61.6 (0.7%)

Table 12: Compression properties of CTLX816 compared with prepreg tape composite

	CTLX 816 (7tex polyester stitch)	CTLX 816 (110tex Kevlar 49 stitch)	UD prepreg tape
Strength (MN/m²)	636 (3.0%)	571 (2.3%)	716 (2.1%)
Modulus (GN/m²)	56.9 (0.8%)	49.7 (1.9%)	52.6 (0.5%)

Table 13: Open Hole Tensile properties of CTLX816 compared with prepreg tape composite

	CTLX 816 (7tex polyester stitch)	CTLX 816 (110tex Kevlar 49 stitch)	UD prepreg tape
Strength (MN/m²)	504 (6.8%)	440 (1.9%)	521 (4.1%)

w:d=6:1 net section strength

Table 14: Filled Hole Compression properties of CTLX816 compared with prepreg tape composite

	CTLX 816 (7tex polyester stitch)	CTLX 816 (110tex Kevlar 49 stitch)	UD prepreg tape
Strength (MN/m^2)	398 (7.1%)	411 (5.7%)	373 (3.5%)

w:d=6:1 countersunk, gross stress, Titanium Hi-lok fastener

Polished cross sections of these materials, parallel to the 0° fibres indicate significant differences in structure. Resin areas and layers particularly around the fibre tows; which retain some of their structure. These effects are particularly strong in the Kevlar stitched material where the coarse thread creates large resin areas and distinct tow bundles.

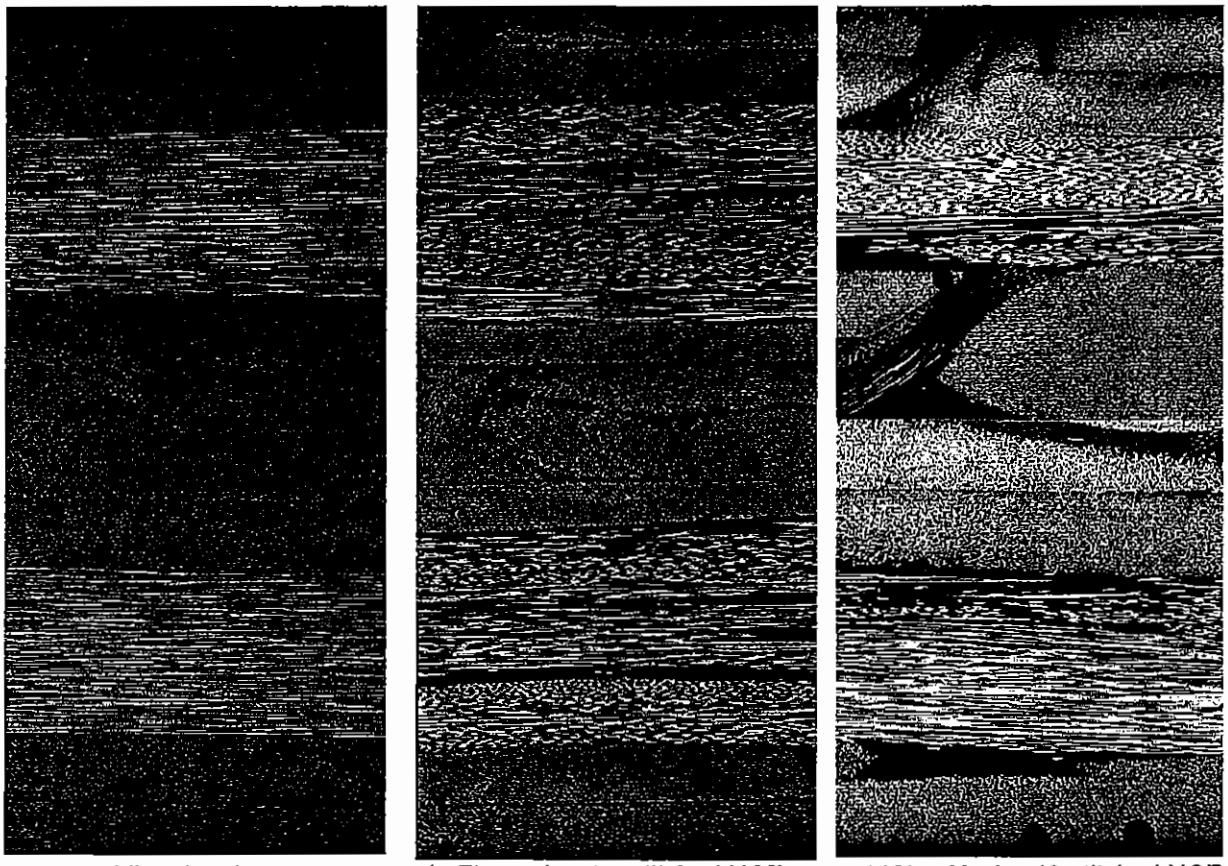

a: unidirectional prepreg b: 7tex polyester stitched NCF c: 110tex Kevlar 49 stitched NCF

Figure 52: Polished microsections parallel to 0° fibres (0°, ±45° lay-up)

Plotting the 0° tow crimp orientation standard deviation against the properties listed we see a strong dependence on the 0° tow crimp (Figure 53), suggesting that it is the changes to the fibre architecture caused by the stitching process that cause the degradation in most properties, the exception being filled hole compression strength. In this case an increase in strength is seen in moving from UD tape through polyester stitching to Kevlar. Work comparing the impact performance of the same materials indicated reduced impact damage as measured using ultrasonic C-scan for the Kevlar stitched material compared with the polyester stitched material. Compression after impact strengths were however worse for the Kevlar material[65] although this may be due to the poor un-notched compression strength.

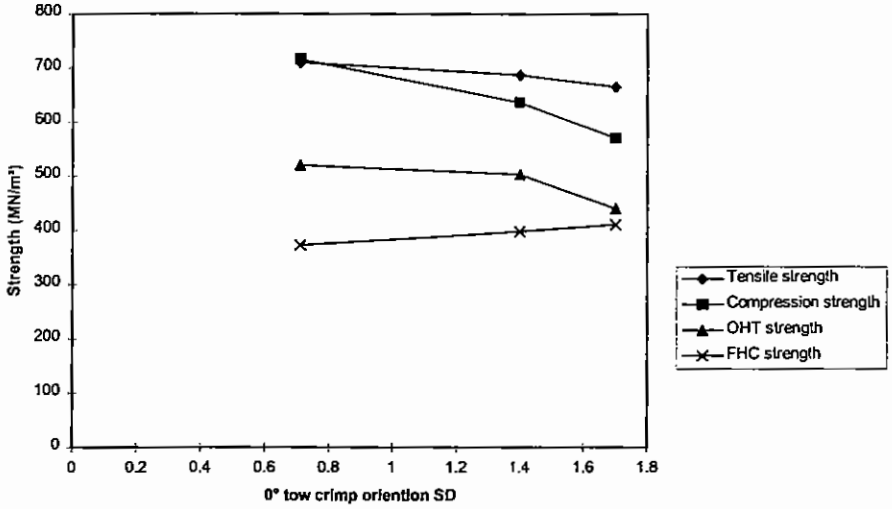

Figure 53: 0° tow crimp and its effect on material properties

On the basis of the poor in-plane performance of the Kevlar knitted material and the observation of microcracks around the Kevlar stitches in some laminates[65] the polyester material remained the preferred material for development activities.

3.6 Thickness Tapering in multiaxial non-crimp fabric composites

Design guidelines for thickness tapering, developed through military aircraft programmes, are outlined in Chapter 1 and suggest the following.

1. To satisfy strength and damage tolerance requirements plies should be dropped-off symmetrically within the stack allowing plies to continue on the top and bottom surface of the laminate.
2. Ply-dropoff rates should be such that they give a maximum gradient of 1 in 20
3. No more than four plies of the same orientation should be placed together
4. Lay-up is best accomplished using repeating balanced ply families

For unidirectional prepreg tape this equates to:
1. 0.125mm steps in thickness (198 g/m² prepreg tape)
2. 1mm step over a 10mm length, if tapered from both sides (1:20 each side - Figure 53)
3. Blocks of prepreg of the same orientation no thicker than 4 plies = 0.5mm

Internal plies dropped-off symmetrically from both sides are shown in
Figure 54 and Figure 55 in theory and in practice, the difference being due to the use of autoclave moulding processes which usually have fixed outer mould line (OML) tooling. This can cause wrinkles to be induced in the continuous plies and particularly on the internal (non-tooled) surface of the part. Kedward[19] suggests that it may be preferable to ply drop from one surface without interspersing dropped plies which would tend to become wrinkled and weakened.

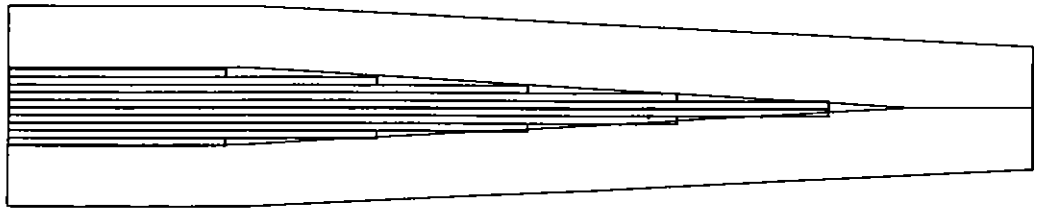

Figure 54: 1:20 ply-dropoff from both sides of a laminate in prepreg tape (theory)

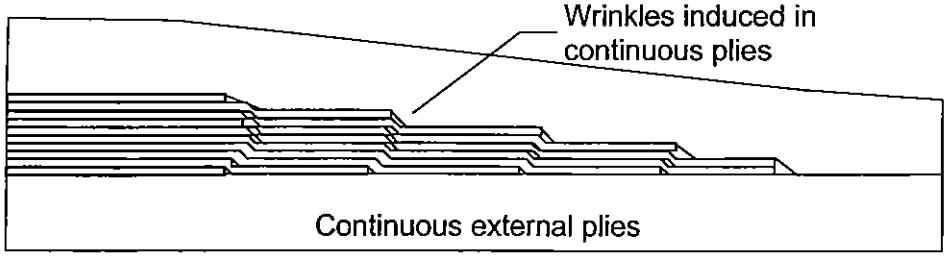

Figure 55: 1:20 ply-dropoff from both sides of a laminate in prepreg tape (practice)

For the multiaxial non-crimp fabrics considered here approximately 800 g/m² (around 0.8mm) of fibre must be dropped in one step and so the above guidelines for prepreg tape laminates cannot be met. If the laminate must also always remain balanced this increases the ply-dropoff steps from 0.8 to 1.6mm.

Tests on single and double 'blanket' ply-dropoffs were carried out as part of this study, together with two schemes it was hoped may improve the ply-drop strength and strain to failure. The approach of tapering thickness from one side of the component and using a full length covering ply over the dropped edges had already been shown as beneficial following earlier ply dropoff trials reported elsewhere[60] . The results are given in Table 15 and some polished cross sections in Figure 56 to Figure 57Figure 58. The configurations are as follows:

1. PSD — plain single 'blanket' ply-dropoff (baseline configuration)
2. PDD — double ply-dropoff (balanced handed-pair dropped together)
3. ASD — plain single ply drop off with film adhesive above and below the dropped blanket (extending 10mm each side)
4. WSD wedge — plain single ply-dropoff with a pre-cured structural paste adhesive (L:t = 10:1) placed as the end of the dropped blanket to soften the transitional step.

In PSD, ASD and WSD a single covering fabric layer continues over the ply-dropoff, this approach having been down-selected from earlier work[65]. In type PDD a balanced handed pair continues over the dropped pliès. Samples were CTLX816/Fiberdux914 processed by interleaved Resin Film Infusion. A cured Airpad sheet was used on the inner laminate surface during curing. Samples were 280mm long as 25mm wide. Tensile load was applied to the samples through bonded aluminium end-tabs.

The stress and strain in the thin section of the sample at initial and net section failure were recorded. Samples types PSD, ASD and WSD were 6.85mm dropping to 6mm thick (8 to 7 fabric layers). Sample type PDD were 6.85 dropping to 5.1mm. Four samples were tested per condition.

Table 15: Ply-dropoff tensile test results

		First indication of failure		Net section failure	
Sample	Description	Stress (MN/m²)	Strain (%)	Stress (MN/m²)	Strain (%)
PSD 01-04	Plain single ply drop with covering blanket	406 (7.4%)	0.6 (2.9%)	592 (3.6%)	0.8 (2.6%)
PDD 01-04	Plain double ply-dropoff with covering blanket	180 (17.9%)	0.3 (21.7%)	487 (6.4%)	0.6 (11.8%)
ASD 01-04	as (PSD) with film adhesive above and below ply-dropoff	583 (3.2%)	0.9 (4.9%)	705 (3.8%)	1 (4.4%)
WSD 01-04	as (PSD) with 1:10 taper structural adhesive wedge	467 (5.7%)	0.7 (1.2%)	754 (2.4%)	1.1 (3.8%)

(Coefficient of variation %)

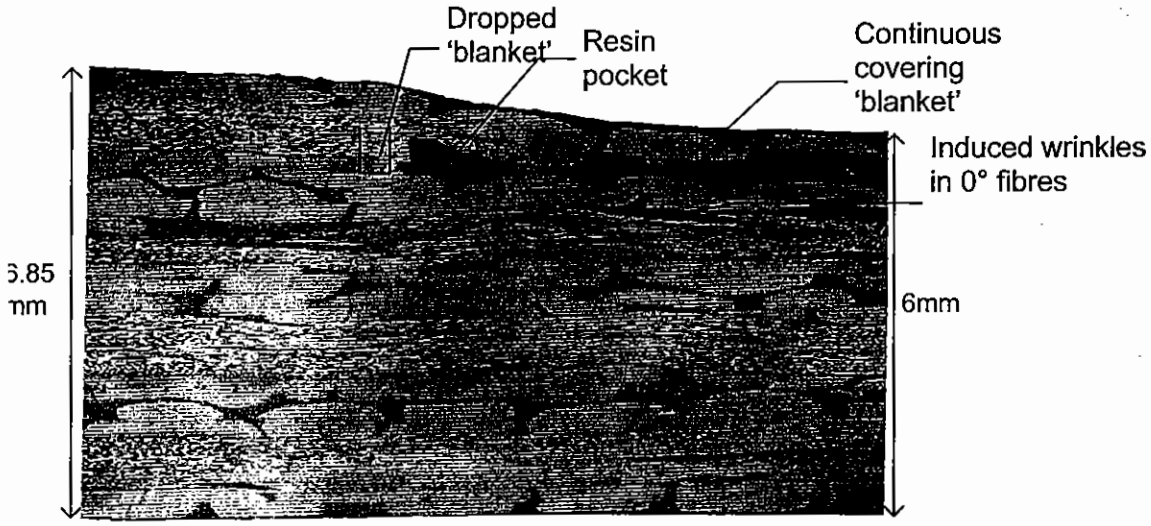

Figure 56: Polished cross section of plain single ply-dropoff (PSD)

Figure 57: Polished cross section of plain double ply-dropoff (PDD)

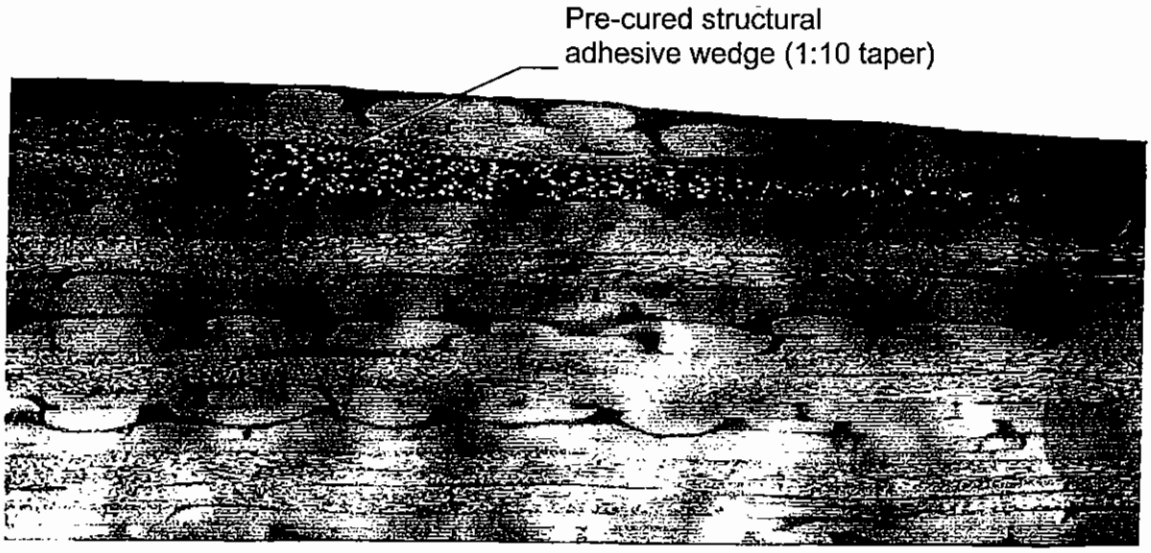

Figure 58: Polished cross section of single ply dropoff with pre-cured structural adhesive wedge (10:1 taper) (WSD)

The results indicate that although the plain single ply-drop does not show signs of failure until 0.6% strain and finally fails at 0.8% (592MN/m²) this is well below the tensile strength of the composite material without a ply-dropoff (796 MN/m²)[65]. For the double ply drop where two layers of fabric are terminated together the performance is extremely poor particularly for the onset of failure. The use of a tougher film adhesive locally around the ply-dropoff region increases the strain at damage initiation and final failure, whereas the pre-cured wedge samples have a similar strain to first failure as the plain samples (PSD) but much enhanced strength approaching that of the plain material despite the high levels of voids observed.

Large benefits have been demonstrated by locally reinforcing ply-dropoff ends using either higher toughness resins or tapered wedges. The former suppresses the onset and subsequent growth of delamination cracks and the latter reduces the interlaminar normal stresses caused by ply straightening in the kinked covering ply and is likely to improve shear load transfer.

It remains to be demonstrated whether these approaches or a combination of them are sufficient to allow the inclusion of these fabrics in flight critical structure. The alternative approaches of applying through thickness reinforcement, adopted by McDonnell Douglas on their stitched wing programme, or the use of much thinner fabrics may also be considered. However the capability of current multiaxial non-crimp fabric machines places a lower limit on the thickness of the fabrics which can be produced. For a triaxial fabric with 50% 0° this is likely to be around 680g/m², some way short of the 0.5mm ply step restriction for prepreg tape laminates.

Chapter 4

Experimental Design Of Fabrics

4.1 Introduction

The use of experimental design techniques to identify the effect of manufacturing or design parameters on performance characteristics has been applied in the optimisation of stitching for composite reinforcements[73] and even aircraft design[15]. Genichi Taguchi popularised the use of orthogonal arrays as an experimental design tool as part of a larger quality engineering philosophy, encompassing conceptual design, experimental design and tolerance design. Orthogonal arrays allow many parameters to be studied simultaneously with a minimum of time and resources.

In this study designed experiments, using orthogonal arrays, are applied to ascertain the effect on composite structure and performance of altering four LIBA machine settings. Two of the parameters involve the density and tension of the polyester knitting yarn which is interlaced around the layers of reinforcing fibres in order to create a stable fabric. The remaining two parameters are concerned with the primary load bearing 0° fibres; how tight they are when inlayed into the fabric and the pattern used to attach them to the surface of the reinforcing fabric. Using the designed experiment technique we can look at the effect changing these four settings on various characteristics of the composite manufactured from them; both on the absolute values and on the variability of performance. This will allow selection of machine settings to produce materials with particular performance characteristics and conversely prediction of a known fabrics performance.

Through the use of image analysis tools we are also able to correlate the effects of machine settings on microstructural features and hence their influence on performance characteristics.

4.2 Taguchi Quality Philosophy

A large amount of engineering effort is consumed in conducting experiments to obtain information needed in making design decisions. Efficiency in generating such information is key to keeping development and manufacturing costs low and producing high quality, robust products.

Taguchi methods, developed by Dr Genichi Taguchi, refer to techniques of quality engineering that embody both statistical process control (SPC) and quality related management techniques. The concepts are based upon two ideas[118]:

1. Quality should be measured by the deviation from a specified target value, rather than by the conformance to preset tolerance limits.

2. Quality cannot be ensured through inspection and rework, but must be built in through the appropriate design of the process and product.

Designed experiments emphasise the attainment of a target value and the minimisation of variation. This is performed by selecting and manipulating control factors to make manufactured products insensitive to uncontrolled variability. This is done through a design process rather than by trial-and-error. In many applications the technique can be used to successfully maximise the performance of a process whilst considering the effect of doing so on variability of performance.

In the application of the process to a composite reinforcement fabric we are considering the optimisation of the material in respect of a number of design criteria. We would therefore expect that the designed experiments will not provide a single fabric which simultaneously provides the optimal mechanical performance however it is loaded. Instead a collection of guidelines are generated which indicate the effect of the machine parameter settings on the

performance characteristics, both the magnitude of their influence and the variability of performance at this setting. Through the use microsectioning techniques some of the mechanisms responsible for the changes in performance are highlighted.

4.3 Baseline Fabric

Design requirements fixed the number of axes to three (0°,±45°) and the proportions of fibre in each orientation at 50% 0°, 50% ±45°. Early studies had shown that the CTLX816 fabric configuration using Toray T300 fibres was a cost effective way of achieving close to 50% 0° material in a triaxial (0°,±45°) fabric. In practice a compromise of 46% 0° fibres was used, as the ±45° layer weight had to be set at 220 g/m² to prevent gaps from forming between tows in the fabric (see section 2.2.5).

The configuration had been developed and used to manufacture wing-box demonstrators and test elements and there existed a large database of mechanical properties including comparisons with equivalent laminates manufactured from unidirectional prepreg tape. Fabric T2 in this study represented the baseline AMCAPS fabric and is used as the reference fabric here. The basic configuration is as shown in Figure 59.

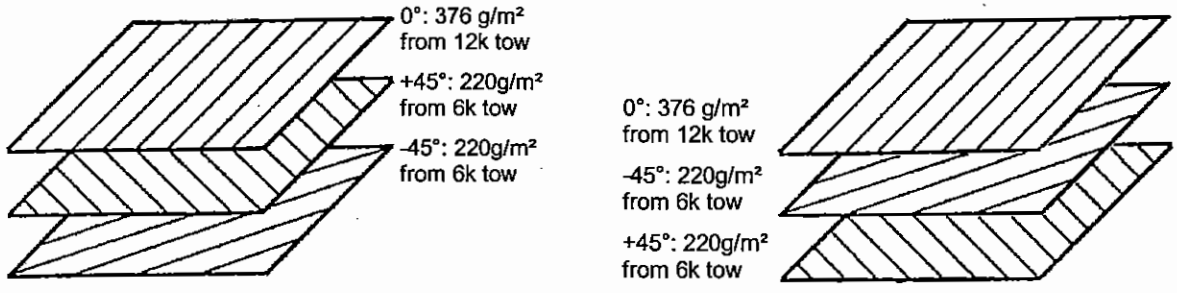

Left Hand - 'A' Fabric Right Hand - 'B' Fabric

Figure 59: CTLX816 fabric configuration

Two fabrics were required per material (A and B) to achieve a balanced symmetric lay-up. Each fabric is manufactured knitted together into a stable dry 'blanket' using 7 tex (g/1000m) texturised multifilament thermoplastic polyester yarn.

4.4 Parameter Selection

As described in section 2.2 the LIBA multiaxial warp knitting machine has a large number of settings and adjustments which affect the material produced upon it. It was decided that the study should maintain the same reinforcing fibre, lay-up and layer weights as the baseline CTLX816 fabric, but use the experimental design process to examine the capability of the LIBA machine in terms of its ability to tailor the reinforcement architecture within that basic fabric. A list of some the possible machine parameters which could have been investigated is shown in Table 16 below.

Table 16: LIBA multiaxial machine parameters

Machine speed	Machine gauge (6 or 12 needles/inch)
Machine cold and machine warm	Width-wise tension at stitching head
Diameter of take up tube	Needles (new or old/blunt)
Batcher tension	Stitch course (pitch)
Tow filament count (3, 6, 12, 24k)	Stitch tension
Fibre feed (rotating or 'over end')	Weft 'shogging' (overlapped or butted)
0° fed from beam or creel	Weft tension
0° Tension	Transport pins (new or old/damaged)
0° coverage style (old 0°, new 0°)	Stitching material and weight

Of these possible parameters some would require the purchase of new hardware or lengthy downtime to make the necessary alterations. The four chosen were selected as the settings were continuously variable and the best setting of each was not predicable and certainly not for the range of properties investigated.

The parameters were as follows:

Stitch Course - stitching pitch (stitches/cm) along the fabric length (0° direction)
Stitch Tension - tension of the stitching yarn
0° Warp Tension - tension of the inlayed 0° fibres
0° Warp Coverage - how much of the inlayed 0° fibres are held by the surface tricot knit

A three level four factor orthogonal array, referred to as an L9 array, was chosen for the experiment as it was hoped that would give the maximum detail from these tests performed. However is does not allow any interactions between parameters to be calculated. Parameter selection was therefore limited to those where no or little interaction was expected.

For each of the nine fabric styles produced a handed pair was manufactured to allow balanced symmetric laminates to be produced for characterisation. Each pair was manufactured with the machine settings given in Table 17.

Table 17: L_9 orthogonal array

	Stitch Course	Stitch Tension	0° Warp Tension	0° Coverage
T1	5	Low	Low	Spread
T2	5	Medium	Medium	50/50
T3	5	High	High	Bunched
T4	7.4	Low	Medium	Bunched
T5	7.4	Medium	High	Spread
T6	7.4	High	Low	50/50
T7	3.5	Low	High	50/50
T8	3.5	Medium	Low	Bunched
T9	3.5	High	Medium	Spread

4.4.1 Levels Selected for Each Parameter

4.4.1.1 Stitch Course

The role of the polyester stitching/knitting material was not well understood, particularly in terms of its role in altering in-plane properties and any possible improvement to damage tolerance/resistance characteristics. The stitch course is the number of needle impalements per linear centimetre of fabric produced. (i.e. linear stitch density).

Because the warp knitting head and fabric transport mechanisms are jointly driven, altering the stitch course alters the fabric transport speed. The weft and bias yarn inlays must be adjusted to compensate for the differences is transport chain speed - this requires that the shog distance along the bed and the number of tow ends be changed. The machine settings for each of the three course settings is given below:

Table 18: Stitch course settings

Stitch Course (penetrations/cm)	Number of Ends per weft layer	Shog Distance (mm)	Bias Weight (g/m^2)
3.5	15	39	216

5	12	32	211
7.4	14	36.5	215

With increasing stitch course the 0° warp side of the fabric is changed by the increased pitch of the tricot knitting pattern (Figure 60). The weft/bias side is characterised by increased fineness of the bundles of fibres held by the stitches.

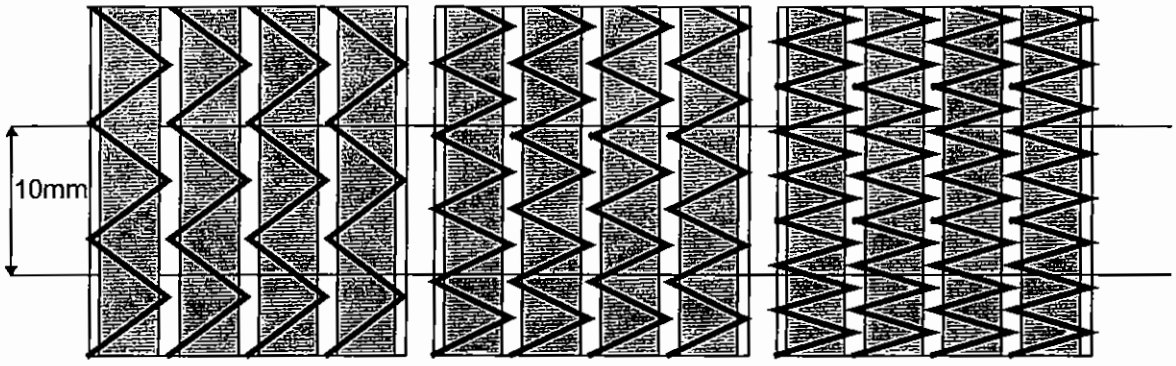

Figure 60: Effect of increasing stitch course on 0° surface of fabric

4.4.1.2 Stitch Tension

Stitch tension cannot be measured directly on the present LIBA machine, although the yarn feed rate can, but is extremely difficult to correlate with the resulting tension in the fabric. Thus the simplest and most robust approach was to look at the highest achievable tension, the setting at which yarns break during the warp knitting process, and the lowest tension at which they 'fall-out' during knitting and an intermediate point in-between considered to be 'normal'. The adjustment is made by changing the relative rotational speed of the stitching yarn beam to that of the main machine drive

4.4.1.3 Warp Tension

The rate of feed of the 0° tows is determined by a drive roller above the warp knitting unit which can be held stationary providing maximum tension, over-fed giving slack to the tows, or fed at the same rate as the feed of the transport chains. This is achieved by the use of different gear wheels on the drive to the feed roller.

Table 19: 0° Tension settings

0° Warp Tension	Gear A	Gear B
Low	58	30
Medium	58	58
High	no gears roll stationary	no gears roll stationary

4.4.1.4 Warp Coverage

The guide bar at the knitting head that directs the 0° warp tows into the knitted structure, called the 'ST bar', can be moved from side to side in order to spread the lay-down of the 0° warp tows within the knitted structure. At one limit, 'spread', the tows are loosely held on the surface of the fabric, only knitted into the structure every 8th needle impalement, whereas in the bunched arrangement the whole tow bundle is held beneath the entire knit structure. At the 50/50 setting half the tow bundle is split between being held under every needle pass and only every 8th impalement. This arrangement encourages the loosely held material to fill the gaps in the surface (Figure 61).

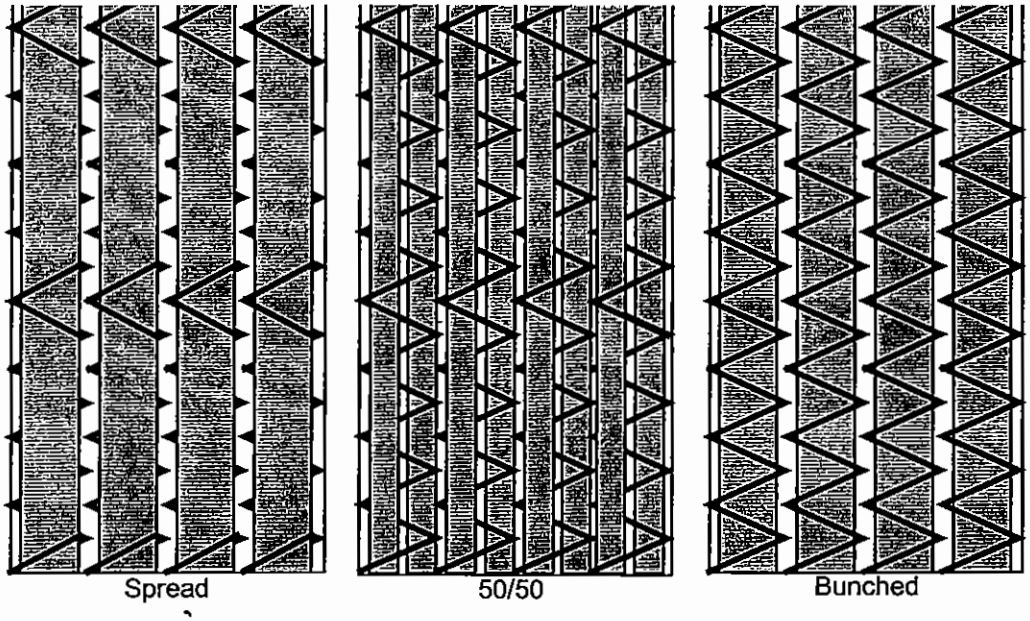

Figure 61: 0° coverage differences schematic

4.5 Materials Produced

Materials were manufactured over a period of five days using the same machine and batch of carbon fibres. In order to reduce set-up time, all the left handed fabrics were produced first and then the right handed materials. Approximately five kilograms of each hand of material was manufactured with three or four materials batched together on each roll. Some waste was produced during the changeover between machine settings. Batch numbers for the fabrics can be seen in Table 20. Six different batches of material were produced, three for each hand of material. The batch numbers allow the carbon fibre used for manufacture and the machine set-up to be traced

Table 20: Fabric batch numbers

	Fabric Batch Numbers	
Fabric Descriptor	Left Hand (A)	Right Hand (B)
CTLX816 - T1	4M-1402	4M-1395
CTLX816 - T2	4M-1402	4M-1395
CTLX816 - T3	4M-1401	4M-1398
CTLX816 - T4	4M-1401	4M-1398
CTLX816 - T5	4M-1401	4M-1398
CTLX816 - T6	4M-1401	4M-1399
CTLX816 - T7	4M-1394	4M-1399
CTLX816 - T8	4M-1394	4M-1395
CTLX816 - T9	4M-1394	4M-1399

Table 21: Resin batch numbers

	Fiberdux 914 (500g/m²) Resin Film Batch number
CTLX816 - T1-T9	199726A-04

Photographs of the front and back face of the nine pairs of fabrics can be seen in Figures 61-69. Visual observations are included with each pair of images. All images are at full scale.

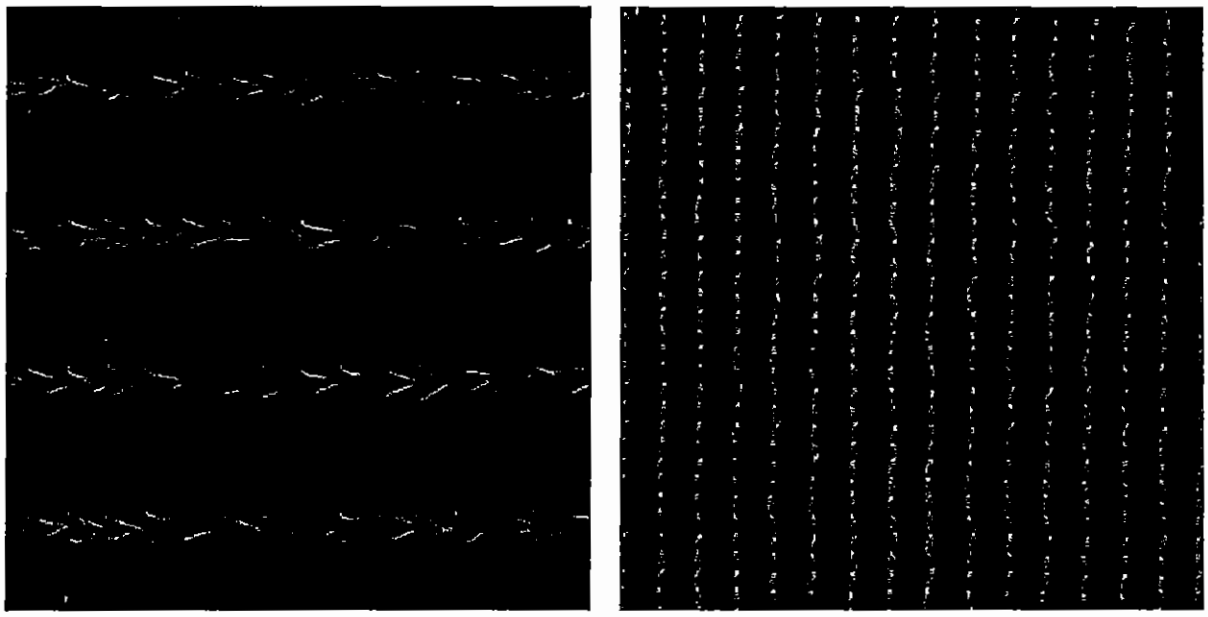

Figure 62: Fabric T1 - front (0°) and back (45°)

Loose feathery stitches, little bunching off 0° fibres observed. Fibre bundles caused by stitching visible on 45° surface.

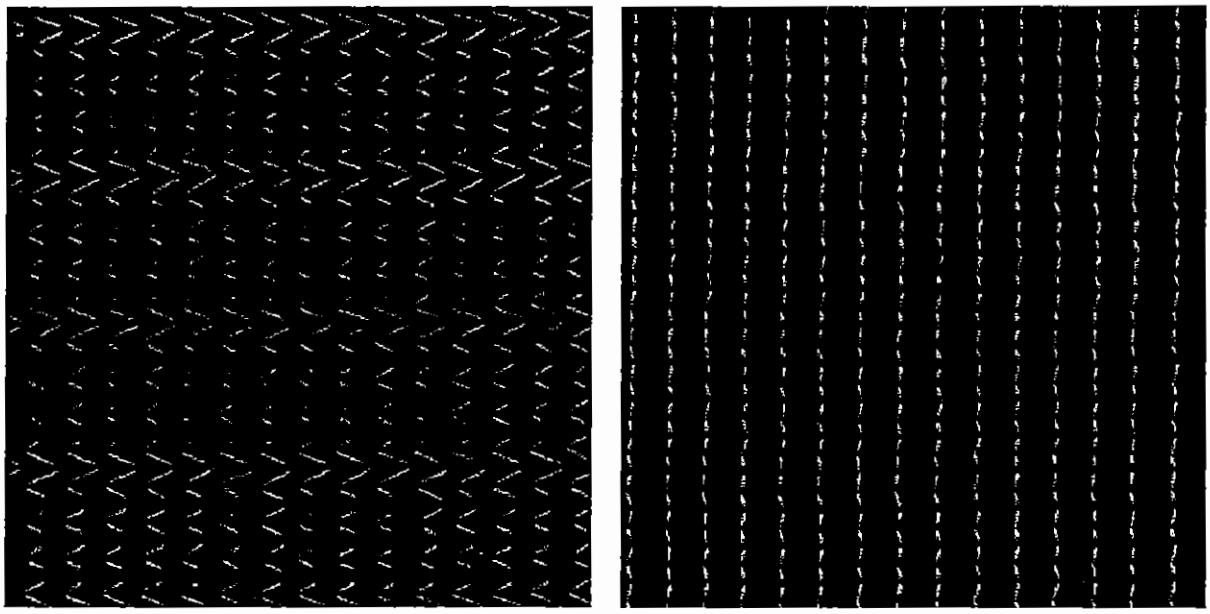

Figure 63: Fabric T2 - front (0°) and back (45°)

Even split between 0° fibres held under all of stitching and those held occasionally. Fibre bundles caused by stitching visible on 45° surface.

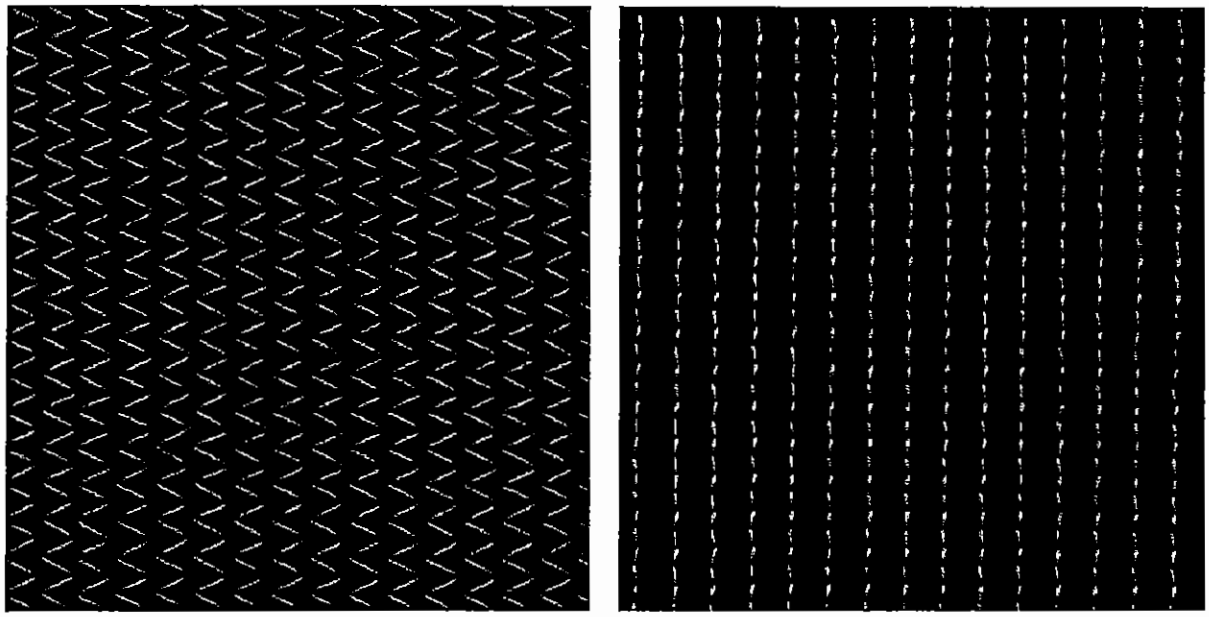

Figure 64: Fabric T3 - front (0°) and back (45°)

0° fibres pulled tightly together by stitching style and tension causing wide gaps between tows. Fibre bundles caused by stitching visible on 45° surface.

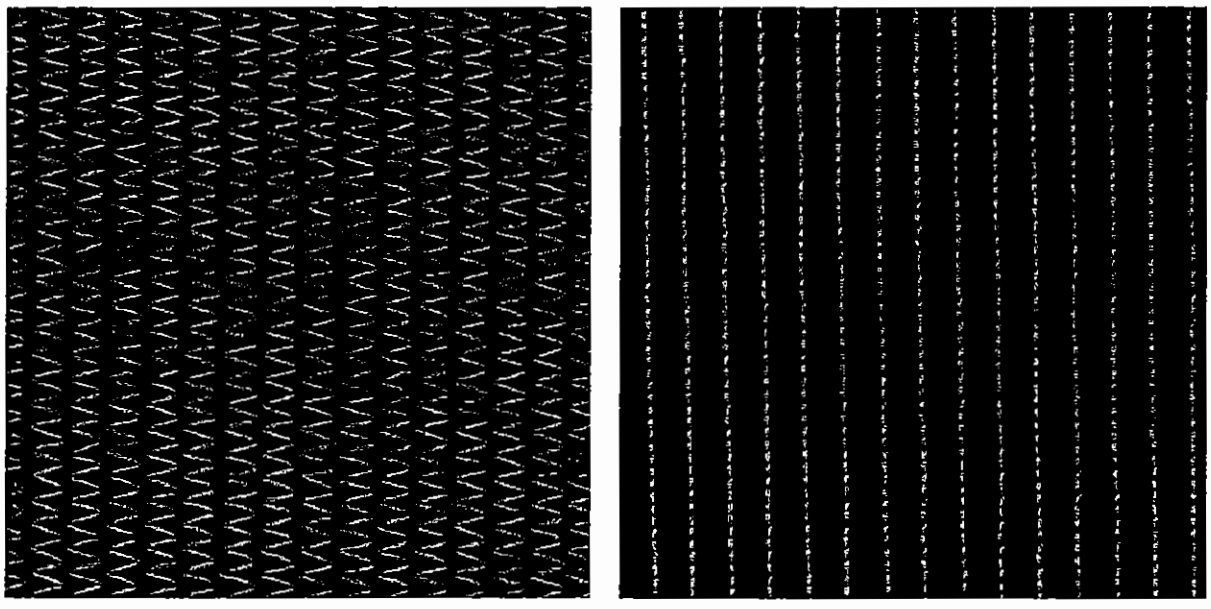

Figure 65: Fabric T4 - front (0°) and back (45°)

0° fibres pulled together by stitching style (less than observed in fabric T3) gaps between tows evident. Finer bunches of 45° fibres than observed in fabrics T1-T3.

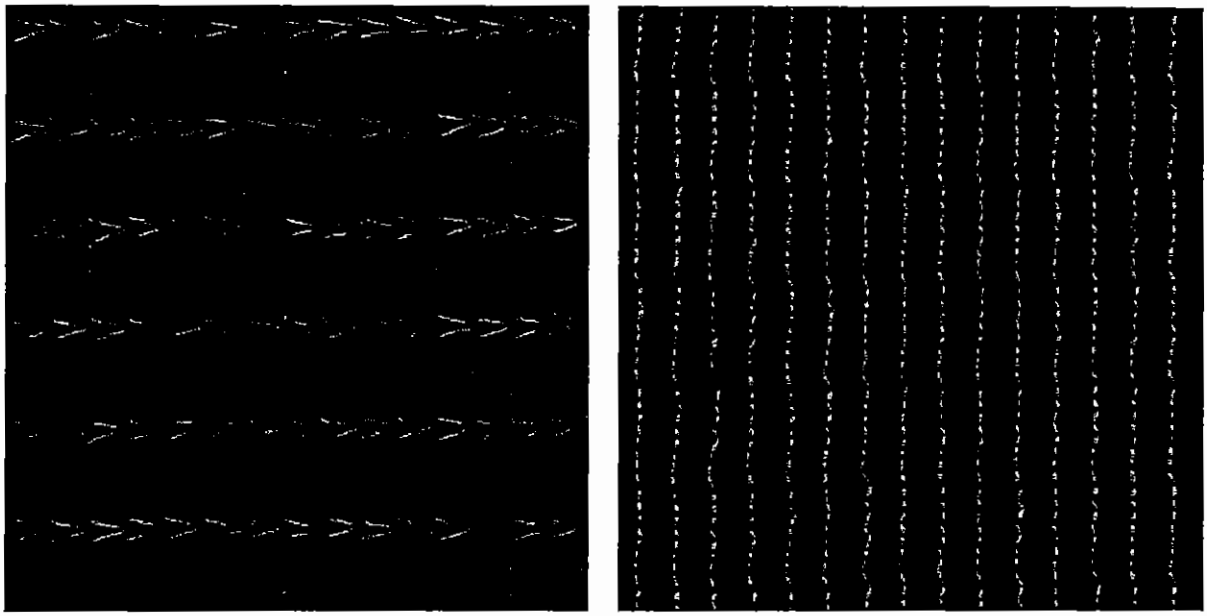

Figure 66: Fabric T5 - front (0°) and back (45°)

Visually similar to fabric T1, 45° surface has finer bundles of fibres than fabrics T1-T3

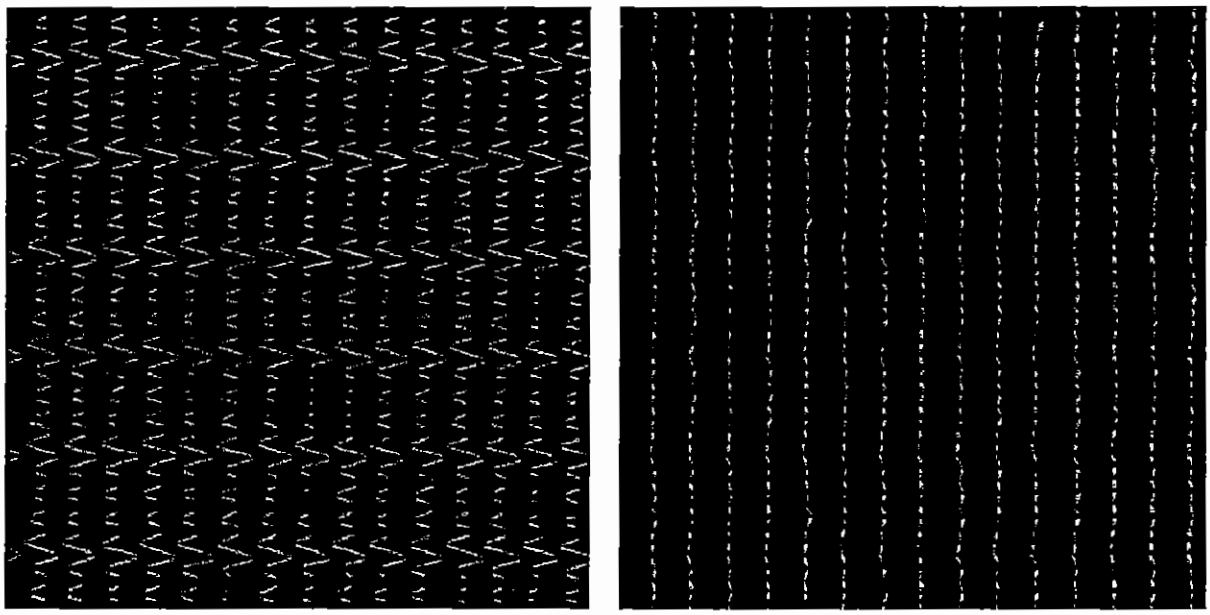

Figure 67: Fabric T6 - front (0°) and back (45°)

Visually similar to fabric T2 with higher frequency of stitching. Small bundles of 45° fibres as T4 and T5

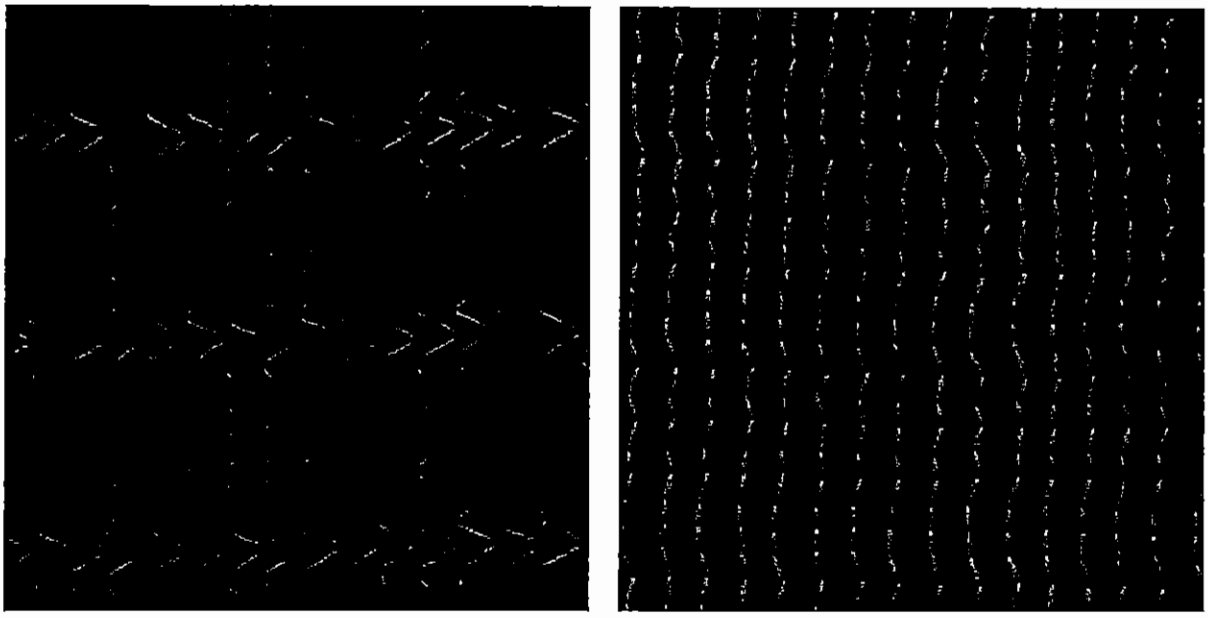

Figure 68: Fabric T7 - front (0°) and back (45°)

0° coverage split has resulted in half the 0° fibres held loosely on the surface spreading out under high 0° tension and low stitch tension. Wavy stitches and 45° fibres evident on 45° surface.

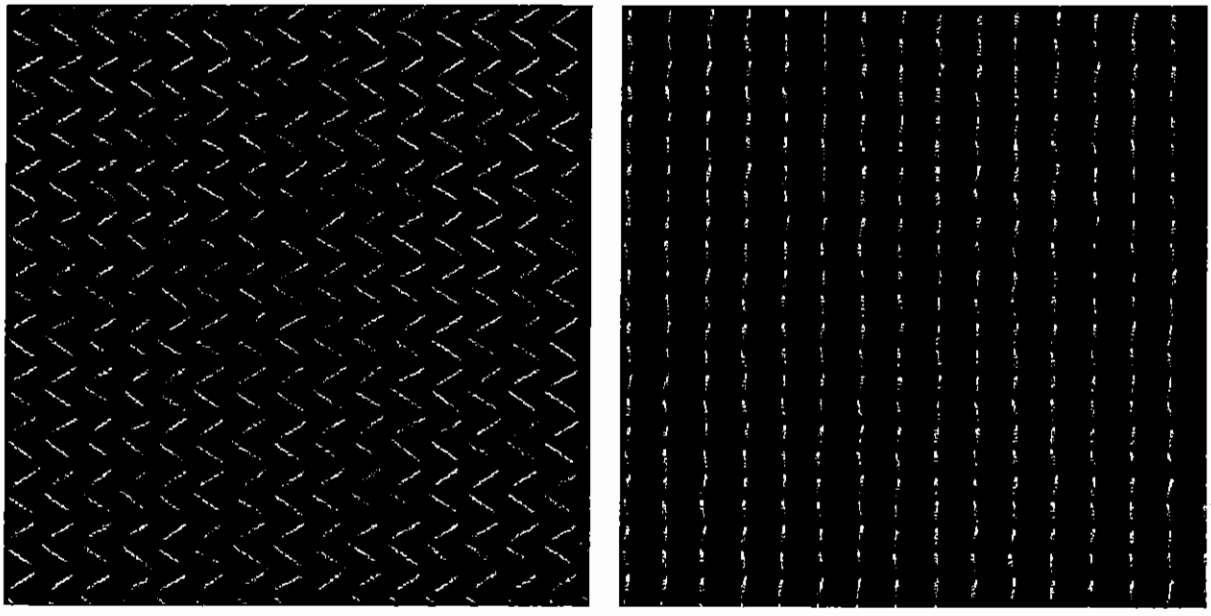

Figure 69: Fabric T8 - front (0°) and back (45°)

Wavy 0° fibres, corresponding tow stitch frequency, with large gaps between bunched 0° tows. Stable 45° back surface, no gaps evident.

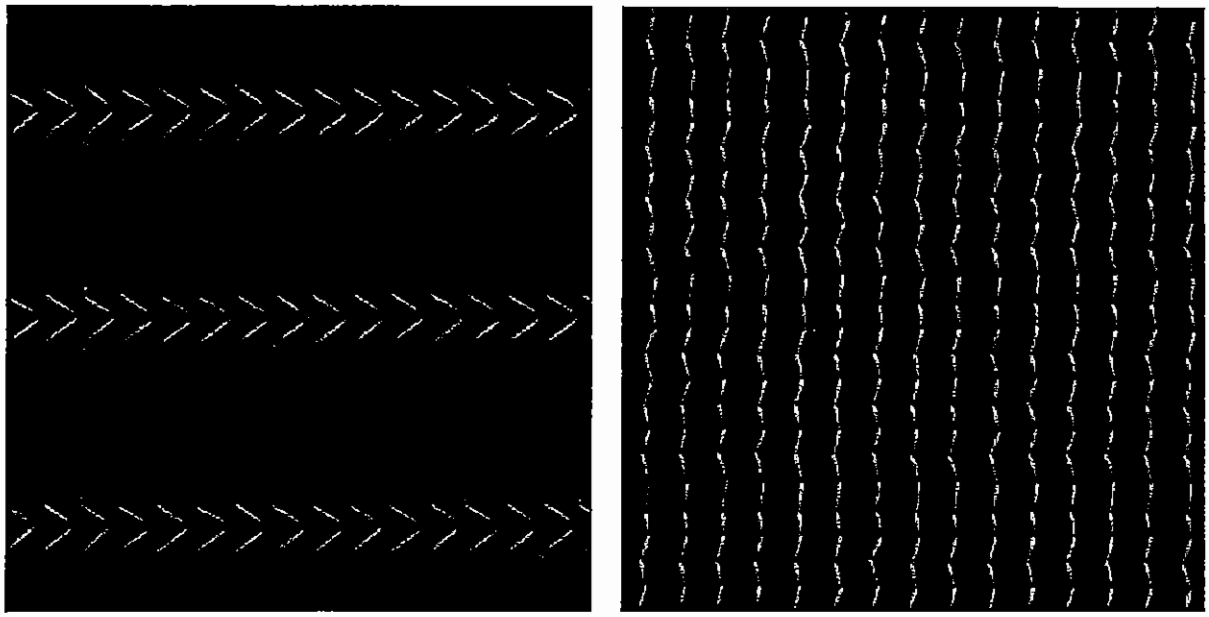

Figure 70: Fabric T9 - front (0°) and back (45°)

Heavily bunched 0° tows at stitch sites, very loosely constrained between stitches. Slightly wavy 45° fibres observed on back surface.

Chapter 5

Manufacturing, Test Procedures And Data Analysis

5.1 Introduction

Three test laminates were manufactured per material and subject to a range of tests in order to measure the influence of the LIBA manufacturing settings. A majority of these measurements were on in-plane and damage tolerance properties. Additionally microstructural measurements of the levels of crimp in the 0° fibre tows and matrix resin distribution within the fibre architecture were made. Information on the tests is presented in three sections; In-Plane Properties, Damage Resistance and Tolerance Properties and finally Microstructural Features. Within each section the test procedure and equipment used is presented along with details of calculations performed on the resulting data. At the end of the chapter the data analysis technique used to deduce the effect of the fabric manufacturing settings on performance is presented.

5.2 Sample Manufacturing

Composite laminates for testing were manufactured using an Interleaved Resin Film Infusion (RFI) process as described by Godbehere[59]. The process involves interleaving matrix resin films between the dry reinforcing fabric layers to create a semi-impregnated fabric 'semi-preg', laminating, subsequently applying heat and vacuum to the stack of material and autoclave processing with applied heat and pressure.

Two fabrics are required per material (A and B) to achieve a balanced symmetric lay-up. These are interleaved with resin as shown in Figure 70 to minimise the risk of lay-up errors.

A nominal fibre volume fraction of 54% was selected for all laminates as this had been shown to provide reliable impregnation by the RFI route at an autoclave pressure of 3 bar (45psi)[59]. The pressure was selected as it is considered acceptable for the manufacture of co-cured Nomex honeycomb cored structures, in which higher curing pressure can cause cell damage.

5.2.1 Manufacture of 'Semi-preg'

A 500g/m² film of Fiberdux 914 matrix resin was cast onto a silicone treated backing paper and spooled up as a continuous roll. This material, manufactured and supplied by Hexcel composites, was packaged and stored in a freezer at below -18°C until required for use, when it was removed from the freezer in its packaging and allowed to defrost for 12 hours.

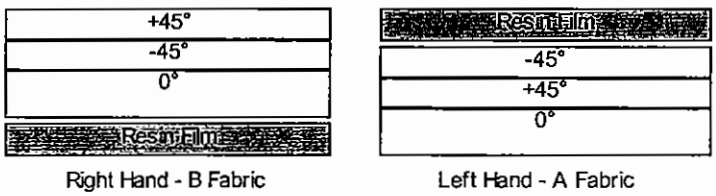

Figure 71: Location of resin films on handed fabrics

1.25 metre lengths of fabric were cut from their rolls and for each, the same length of resin film on its backing paper was cut. Right handed (B) or (+) fabrics (Figure 71) had the resin applied to the 0° surface by placing the fabric on the lay-up table 0° uppermost, inverting the resin film and adhering one complete edge to the fabric. With the adhered edge kept under tension the resin film was lowered progressively onto the fabric surface taking care to avoid distortion of the fabric. When fully in contact the resin and fabric was inverted and any excess resin

trimmed. The process was repeated for the Left handed (A) or (-) fabric (Figure 71) but the resin applied to the -45° surface to aid identification of the fabrics and to prevent air entrapment likely to be caused by placing resin films adjacent with one another.

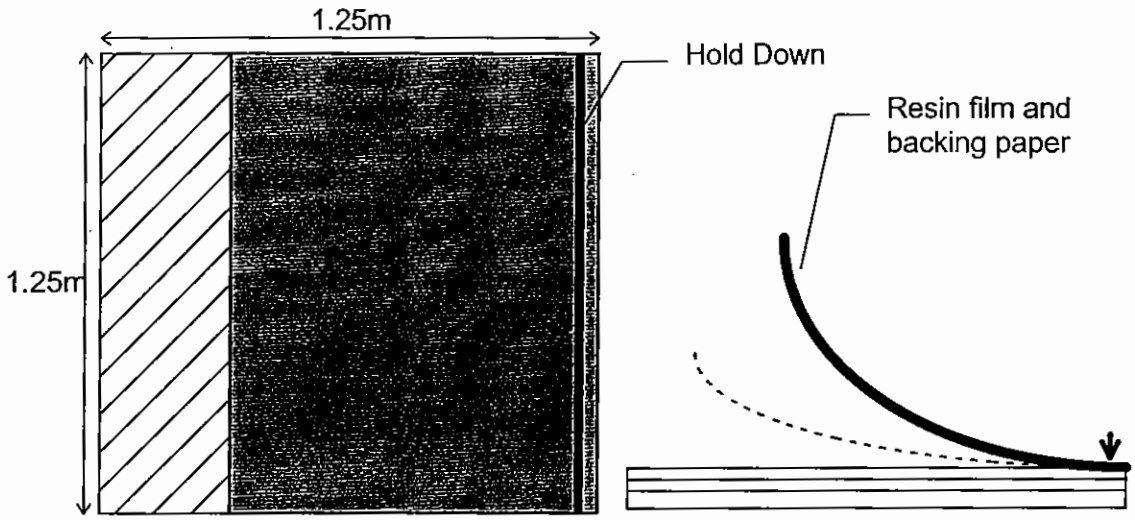

Figure 72: Application of resin film to fabric

5.2.2 Laminate Stacking Sequence

The stacking sequence shown in Figure 73a was used for in-plane test laminates, Figure 73b for Interlaminar Fracture tests on the 0°/0° interface and Figure 73c for Impact and Compression After Impact Tests

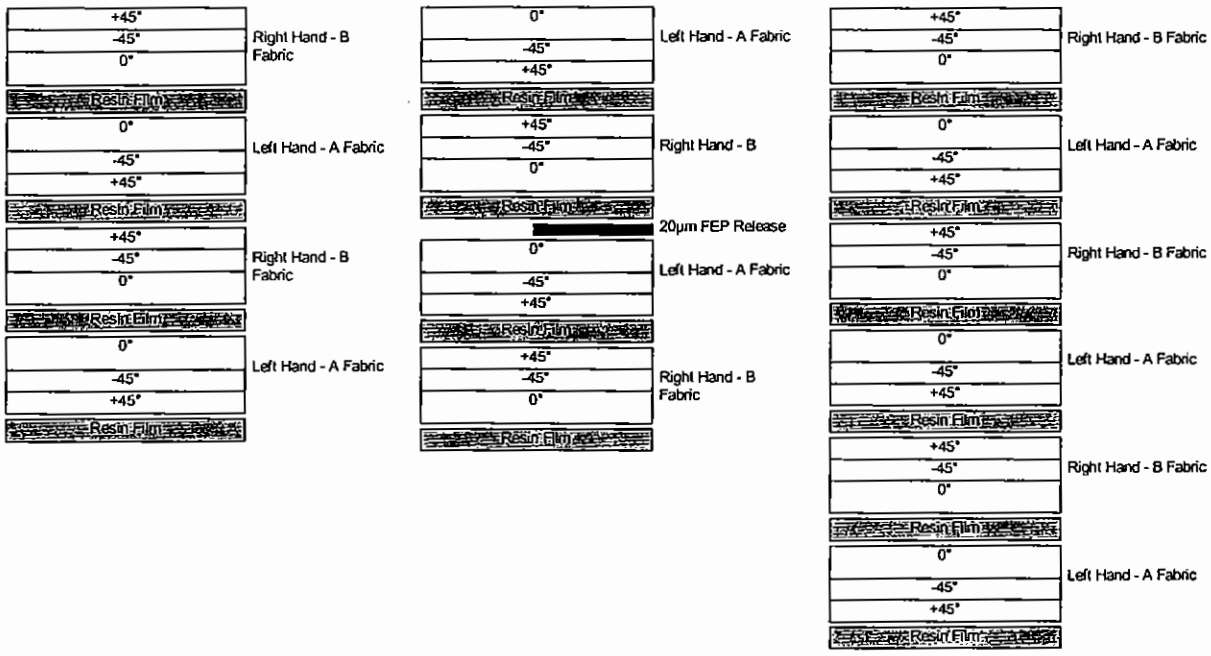

(a) In-Plane test laminate (b) Interlaminar fracture test laminate (c) Compression after impact test laminate

Figure 73: Laminate stacking sequence

Laminates of 4 fabric layers had a nominal cured thickness of 3.4mm, and those of 6 fabric layers 5mm nominal cured thickness. Actual thicknesses can be found in Appendix A.

This laminate stacking sequence was chosen for two reasons:

1. The desire to maintain the same fibre orientations across fabric interfaces, i.e. 0° adjacent to 0°, +45° adjacent to +45° in order to minimise the risk of delaminations between the fabric 'blankets'. This was based upon the assumption that some structural benefit might be achieved from the presence of the stitching yarn bridging the most likely delamination planes.

2. In order that any structure manufactured from the composite could be tapered in thickness from one side of the component as illustrated in Figure 74. This approach minimises the disruption to the continuous un-tapered plies.

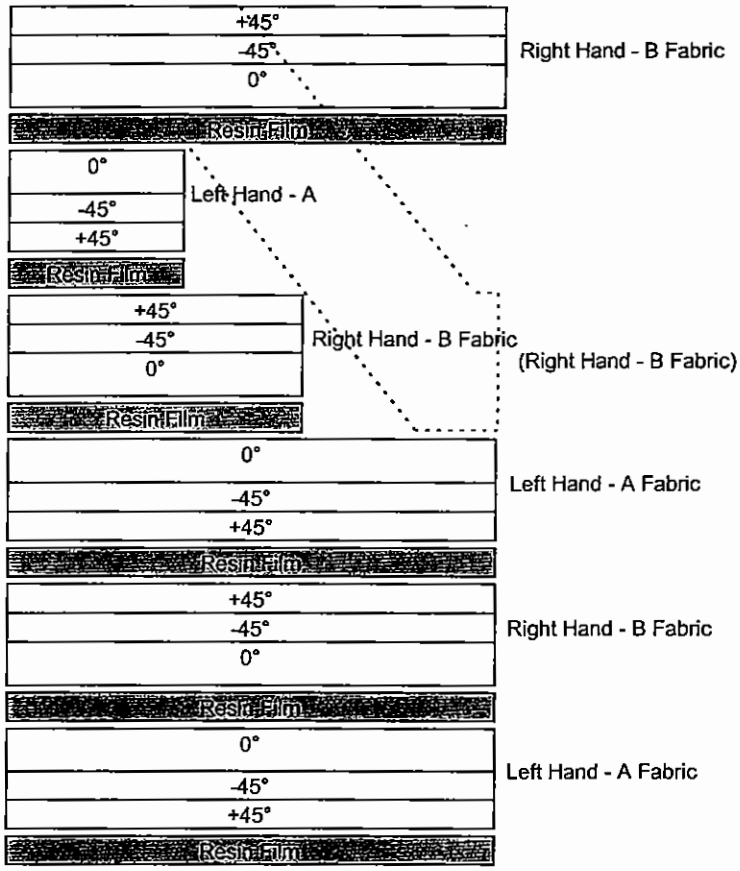

Figure 74: Thickness tapering scheme

In-plane and CAI test laminates of 660 x 360mm were manufactured using a 1.7mm thick steel caul plate of 640 x 340mm, so as to minimise laminate distortion due to any edge bleeding. Interlaminar fracture laminates were manufactured as 360x360mm laminates with a 340 x 340mm caul plate and had a strip of 25µm FEP release film extending 70mm from the laminate edge (50mm from the edge of the caul plate) at the mid-plane of the sample as shown in Figure 73b.

Locating the resin films as shown and using the cure cycles described, with a long dwell below the curing temperature, had been shown by Godbehere[59,60] to produce laminates without observable resin distribution gradients due to the initial location of the resin films.

5.2.3 Autoclave Preparation and Curing

Completed stacks were placed on 25µm FEP film and onto a steel tooling plate placed upon a stiff honeycomb cored aluminium autoclave table. Five laminates were cured in each cycle and bagged as shown in Figure 75. Glass fibre tows were laid along all edges of the laminates, out under the FEP release film and in contact with the breather cloth so as to minimise the risk of air entrapment during infusion and cure.

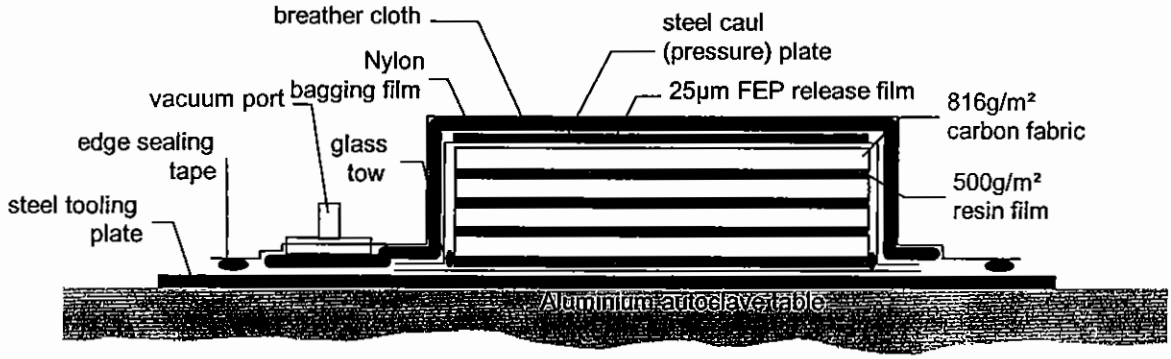

Figure 75: Resin film infusion arrangement for autoclave curing

Autoclave consumable materials used in the manufacture are listed in Table 22.

Table 22: Consumable materials used in the interleaved RFI process

Function	Material	Manufacturer/Supplier
Release film	RF 260R Fluropolymer 25µm	Tygavac
Air path provision	2400tex E-glass roving	PPG
Breather fabric	NW339HA	Tygavac
Edge sealant tape	'Tacky-Tape' Black	'Tacky-Tape'/Tygavac
Vacuum bag	NBF205C Nylon 6	Tygavac

Laminates were cured according to a cure cycle optimised for the RFI process as shown in
Figure 76. The purpose of the dwell for one hour at 110°C under vacuum is to infuse the resin into the dry fabric. Pressure is applied later to minimise the risk of closing off air-pathways.

Figure 76: RFI cure cycle for CTLX816/Fiberdux 914

5.2.4 Sample Preparation and Identification

After manufacture all the laminates were stored in ambient conditions, inspected at Hexcel Composites using their Mecasonics automated ultrasonic C-scan equipment. The results of the scans can be found in Appendix A and were all considered to be of acceptable quality with no evidence of voids observed in any of the panels. The attenuation for some of panels were however different but uniform over the whole panel area. This was attributed to variations in the internal structure of the materials. The panels were subsequently cut using a diamond impregnated slitting wheel, measured using a digital micrometer according to the relevant test procedure, dried at 70°C for at least seven days and subsequently stored in a dessicator. Samples were then removed and tested within 24 hours or returned to the dessicator. Alignment of the cutting with the 0° fibre direction was performed by following the lines of stitching as the 0° layers were hidden. Any samples which deviated by more than one stitch row spacing (4mm) in 280mm length on either face (less than 1°) were discarded.

5.2.4 Sample Preparation and Identification

After manufacture all the laminates were stored in ambient conditions, inspected at Hexcel Composites using their Mecasonics automated ultrasonic C-scan equipment. The results of the scans can be found in Appendix A and were all considered to be of acceptable quality with no evidence of voids observed in any of the panels. The attenuation for some of panels were however different but uniform over the whole panel area. This was attributed to variations in the internal structure of the materials. The panels were subsequently cut using a diamond impregnated slitting wheel, measured using a digital micrometer according to the relevant test procedure, dried at 70°C for at least seven days and subsequently stored in a dessicator. Samples were then removed and tested within 24 hours or returned to the dessicator. Alignment of the cutting with the 0° fibre direction was performed by following the lines of stitching as the 0° layers were hidden. Any samples which deviated by more than one stitch row spacing (4mm) in 280mm length on either face (less than 1°) were discarded.

All sample dimensions and test data can be found in Appendix A arranged according to the type of test. A simple Identification system was used on all samples and their associated documentation:

T1 OHT 02

Fabric ID	Test ID		Sample ID
T1	LT	Longitudinal Tension	01
T2	OHT	Open Hole Tension	02
T3	LC	Longitudinal Compression	03
T4	ILSS	Interlaminar Shear Strength	04
T5	CAI	Compression After Impact	05
T6	DCB	Double Cantilever Beam (mode I)	06
T7			07
T8			08
T9			09
			10
			11
			12

5.3 In-Plane Property Tests

The following in-plane properties were measured for the nine composites produced from the nine pairs of fabrics:

1. Tensile strength and modulus
2. Open hole tensile strength
3. Compression strength and modulus
4. Apparent interlaminar short beam shear strength

5.3.1 Tensile Strength and Modulus

These were measured using the ACOTEG ACO/TP/12 test procedure[119]. The machine used was a 250kN hydraulic test machine with Instron Controller. Hydraulic grips were used with flash hardened spark eroded grip faces precluding the use of end-tabs as allowed in the test standard. Strain measurements were made using an Instron dynamic extensometer with a 50mm gauge length, calibrated before each day's testing using a drum micrometer which itself was calibrated with current NAMAS calibrated gauge blocks. Data acquisition was via PC based Strawberry

Tree 12bit, 8 channel data acquisition hardware running Strawberry Tree Quicklog software. The hardware/software interface had an auto calibration function backed up before use by cross-checking the load display on the Instron controller with that of the Strawberry Tree displayed output.

For each material five samples were tested all cut from the same area of the each panel as manufactured, All samples were tested in position control at an extension rate of 1mm/min with the extensometer left on the samples for the duration of the test. The dimensions and location of the extensometer was as shown in Figure 77. Samples were horizontally and vertically aligned in the test machine grips using a metal jig bolted to the lower jaws.

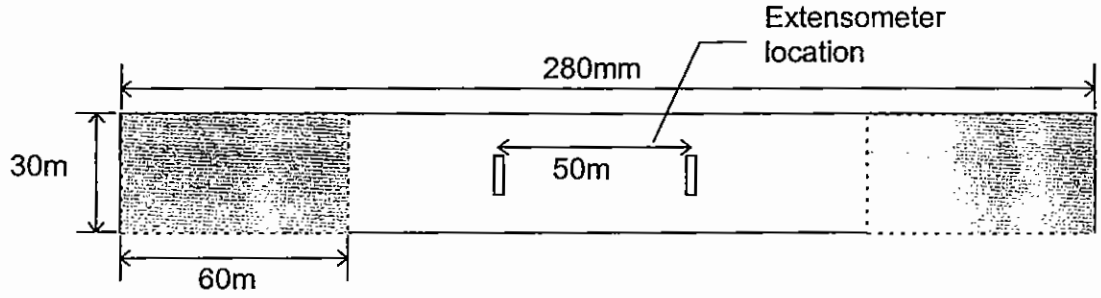

Figure 77: ACOTEG tensile test sample

After test, the data were analysed using Microsoft Excel 5. The ultimate strength was obtained using the dimensions previously measured for each sample and the modulus calculated from the stress/strain data (Figure 78) using the gradient of the line of 'best fit' between 0.1 and 0.5% strain.

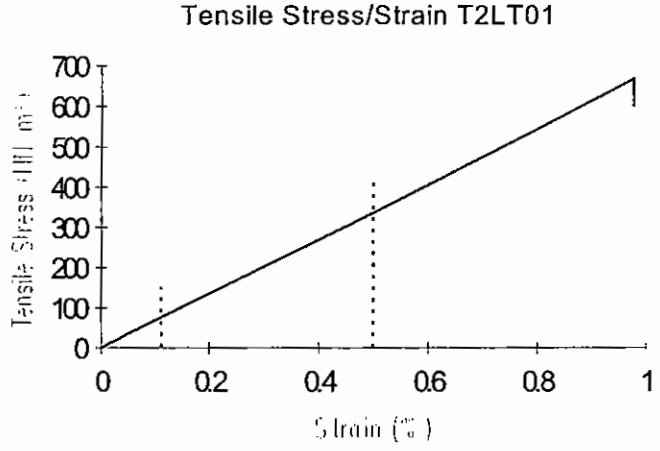

Figure 78: Example stress/strain curve

5.3.2 Open Hole Tensile Strength

The test equipment used for the measurement of open hole tensile strength is as described for un-notched tensile tests, except that an extensometer was not used, as modulus was not to be calculated.

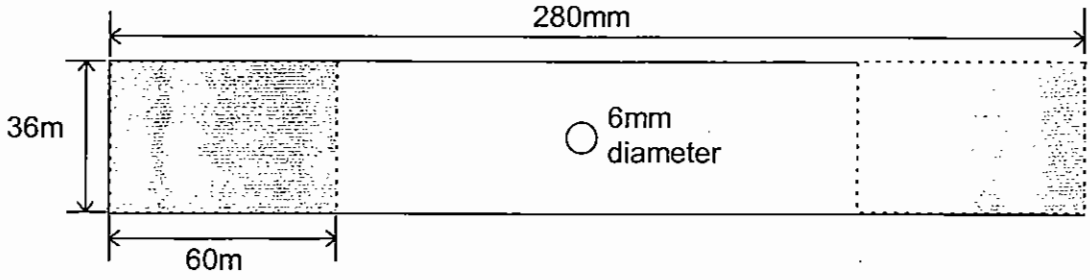

Figure 79: ACOTEG open hole tensile test sample geometry

Samples were 36mm wide with a 6mm plain hole, giving the same cross sectional area of composite across the location of the hole and a width:diameter ratio of 6. Holes were cut using a solid tungsten carbide single flute ball-nose milling cutter. Samples were milled clamped together and aligned in parallel with a scrap carbon/epoxy laminate on the back face to prevent laminate damage when the cutter broke through the back of the samples. Sample hole diameters were individually measured using a bore micrometer.

When analysing the data the stress at failure can be reported in several ways; the gross stress divided by the cross-sectional area away from the hole; or the net stress using the sectional area across the hole. The latter is reported in the results chapter, as it enables the OHT data to be compared with the tensile strength data; both having the same net cross section.

OHT strength was calculated using:

$$\sigma_{OHT} = \frac{P_{max}}{(w-d)t} \qquad (MN/m^2)$$

where P_{max}= maximum load (N)
w = specimen width (mm)
d = hole diameter (mm)
t = specimen thickness (mm)

5.3.3 Compression Strength and Modulus

There are a number of different test methods for compression strength, each of which tend to generate quite different strengths. The tests are of three basic types: Firstly, long gauge length samples supported by anti-buckling guides (ACOTEG, CRAG). Secondly, shear loaded samples with short un-supported gauge lengths (IITRI). Thirdly, end loaded, short gauge length samples which may be solid (NASA short block) or cyclindrical to provide latereal stability.

Unless they are waisted, end-loaded samples tend to fail by 'brooming' at the end of the sample. Short un-supported lengths are inappropriate for some textile composites as the gauge length is often close to the size of the repeating unit cell of the material.

Tests reported in this study were carried out according to the ACOTEG ACO/TP/11 test procedure[120]. This test method requires the use of a patented anti-buckling guide not available at Cranfield University. The tests were performed in the testing laboratories of British Aerospace Defence Ltd, Warton Unit.

Sample size is the same as for tensile coupons at 280 x 30mm and utilises the same method of load application; shear loading through 60mm grip length at each end. The large gauge length (160mm) is supported on both sides by an arrangement of captive roller bearings which provide support against global buckling but allow for elongation of the sample. Strength and modulus results were supplied together with stress/strain curves. Modulus values are calculated from the gradient of the stress/strain curve between 0.1-0.5% strain.

All materials were tested in a self-consistent manner; by the same operator; on the same machine and were of the same nominal lay-up and thickness. The data for the nine materials tested may therefore be considered as self-consistent.

5.3.4 Apparent Interlaminar Short Beam Shear Strength

Samples were tested according to the CRAG test protocol[121]. This is a test method which has received much criticism when used compare materials of different lay-ups, as the resulting strength has much to do with the local fibre architecture at the ply interfaces and cannot reasonably be considered a true material property. Because we are considering materials of the same fibre and resin type, lay-up and nominal fibre volume fraction the differences in shear strength will be due only to differences in fibre architecture and the results are self consistent.

The thickness of the each material was measured at five points along the length to be cut and the width of the samples set to five times the mean thickness. Similarly the length was set to ten times this thickness. The span between the rollers was set to five times thickness for each of the nine materials using digital vernier callipers. Materials were tested on a 50kN hydraulic test machine with Instron controller. Samples were loaded at 1mm/minute in displacement control with the controller set to record the peak load for each sample. Supports and loading roller diameters were all 6mm. Ten samples were tested for each material.

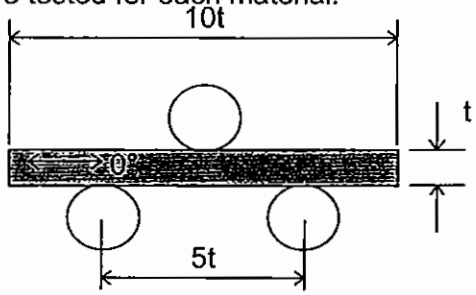

Figure 80: Apparent interlaminar shear test arrangement

The ILSS was calculated using:

$$ILSS = \frac{3P_{max}}{4wt} \qquad (MN/m^2)$$

where P_{max}= maximum load (N)
w = specimen width (mm)
t = specimen thickness (mm)

5.4 Damage resistance/tolerance results

The following damage resistance and tolerance properties were measured for each of the composite materials:

1. Low velocity drop weight impact and compression after impact

2. Mode I interlaminar fracture strain energy release rate

5.4.1 Instrumented low velocity impact

All impact tests were based upon the Boeing BSS7260 CAI test method[104]. Samples of 152.4 x 101.6mm (6" x 4") were cut from 6 blanket thickness panels and impacted at 5, 15 and 25J incident impact energies. A Rosand Instrumented Falling Weight Impact Tester (model 5) was used for the test with a Kistler piezo-electic load cell used to record the impact force during the event. Data acquisition was performed using Rosand software running on an IBM compatible 386 personal computer.

The support frame used to restrain the impact sample was of steel and ply-wood construction with four toggle clamps (Figure 81). This was supported on a 38mm (1½") thick tool steel base and rigid steel columns.

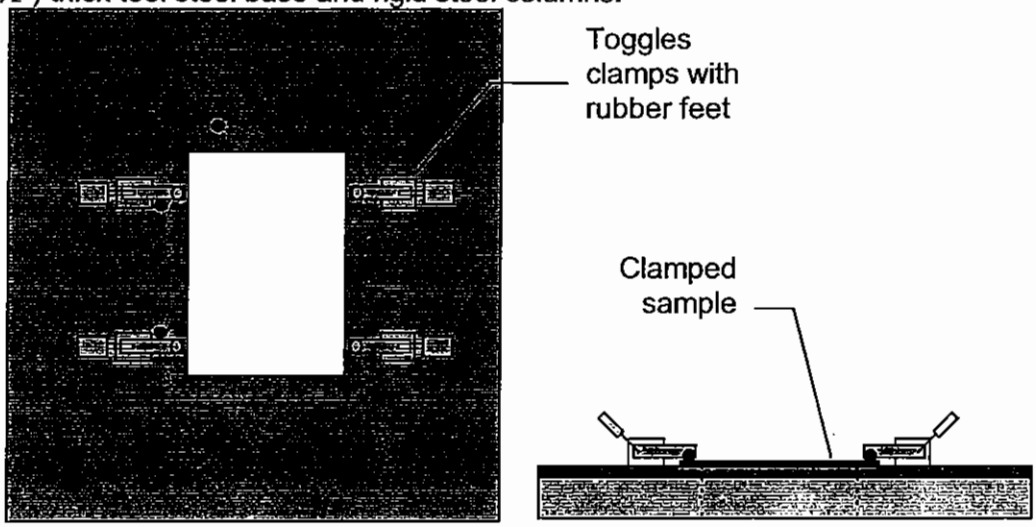

Figure 81: Boeing impact frame schematic

A mass of 6.47 kg was used for all the impact energies examined, and the impactor was prevented from striking the sample more than once. All samples were impacted onto the bottom face of the laminate (tooling side).

5.4.1.1 Absorbed Energy and Peak and Threshold Forces

The incident energy impacting the sample is dissipated by a number of mechanisms as described in Chapter 4, as well as noise and into the supporting structure of the machine. The energy absorbed by the sample is calculated from the force/defection/time data and shows some differences between the materials tested.

Threshold force for delamination is indicated by the first significant drop in the Force/Time curve (Figure 82) and has been correlated with the generation of the first delamination crack.

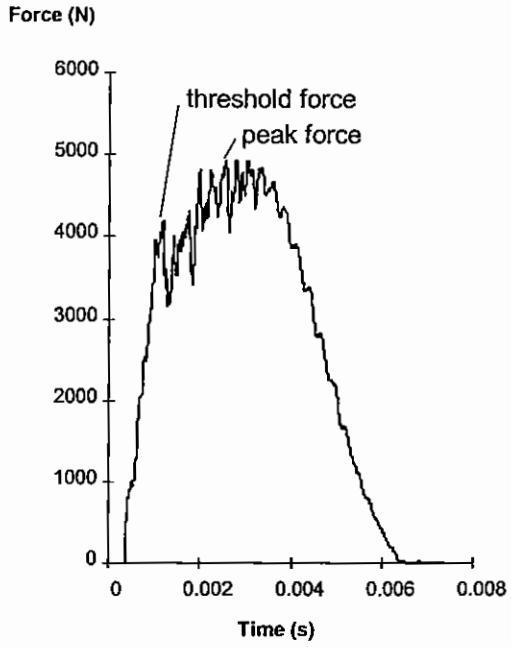

Figure 82: Force/Time graph (T2CAI02)

Threshold force for delamination and peak force were recorded for all the impacted samples. Threshold force for damage is a useful indicator when designing against low velocity impact threats.

5.4.2 Determining impact damage area by ultrasonic C-scan and X-ray

In order to calculate the area of delamination damage caused by the impact event the samples were inspected using ultrasonic C-scan. This was performed, as for the initial quality screening, at Hexcel Composites at Duxford. A Meccasonics water immersion C-scan unit was used with a 5MHz focused probe and glass reflector plate.

Samples were supported 5mm above the glass reflector in edge clamping blocks along the 101mm (4") side. Groups of six samples were scanned at one time and labelled on the image as it was printed. After scanning, the Mecasonics MIDAS v.2 software package was used to calculate the projected impact damage area for each sample. The projected damage area results in mm^2 are summarised in the following chapter.

As a comparison, one 15 J impacted sample from each of the nine fabrics was additionally inspected using Penetrant Enhanced X-Radiography (PEXR) equipment at the University of Sheffield. A 1.5mm diameter hole was drilled through the centre of each impact site and a solution of zinc iodide in iso-propanol and Kodak Photoflow™ allowed to migrate down through the hole and into the damage area over a period of 24 hours. The sample was then placed in an X-ray chamber with X-ray film adhered to the back face of the sample and subjected to a known exposure and the film developed. A contact print was then taken from the negative and compared with the C-scan from the same impacted sample. These detailed images can be found in Appendix A and an example is shown below in Figure 83.

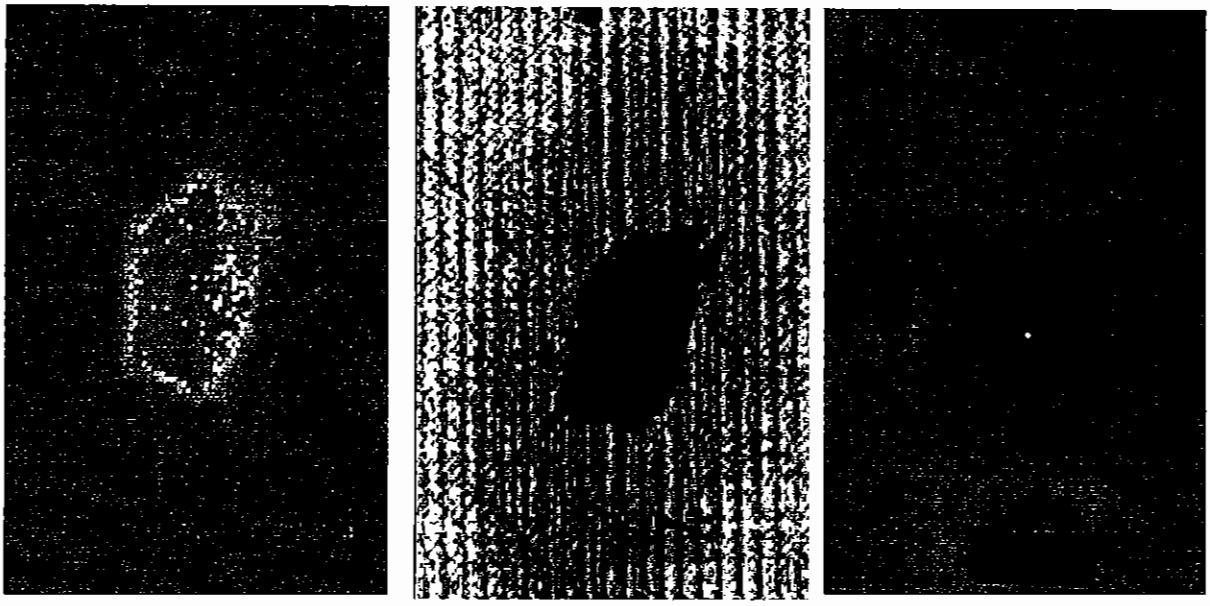

Figure 83: Standard C-scan, high resolution C-scan and penetrant enhanced X-Ray compared (T2CAI06)

5.4.3 Indent Depth

Indent depth, used in routine aircraft inspection and determining the level of damage for BVID (Barely Visible Impact Damage), was recorded for all the impacted samples using a dial gauge mounted on a three footed assembly developed originally for measuring small dents in metallic skin surfaces (Figure 84). For each sample the probe was moved over the surface until the largest displacement was indicated and then recorded.

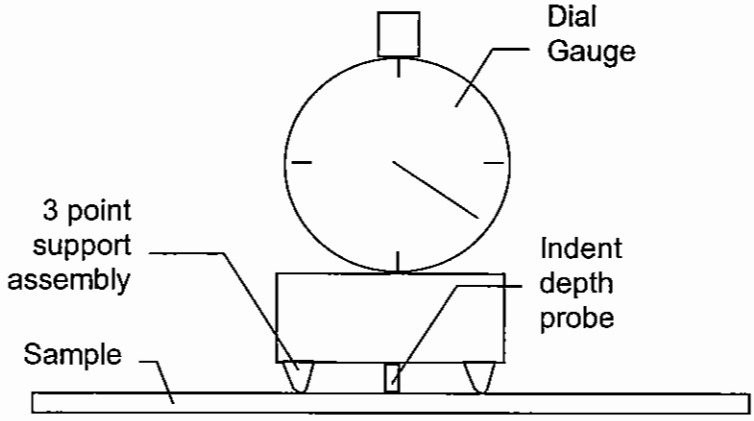

Figure 84: Indent depth measuring assembly

Measurements were taken eight weeks after the impact testing was performed and it is therefore expected that some relaxation of the material may have occurred. The results should therefore be treated with some caution and are consequently only included in Appendix A.

5.4.4 Post impact compression strength

Samples were tested in compression on two machines. Samples impacted at an incident energy of 25J were tested on a 250KN hydraulic machine with Instron 8500Plus controller. However the 15 and 5J samples were compressed on a

1000kN Mayes hydraulic test machine as the 250kN proved insufficient to induce failure in all samples at the lower levels of damage. Both machines used the Strawberry Tree data acquisition system to record load, cross head displacement and on some samples acoustic emission and strain. Samples were supported in a Boeing BS7260[104] type anti buckling fixture (Figure 85) and loaded in position control at a cross-head rate of 1mm/minute.

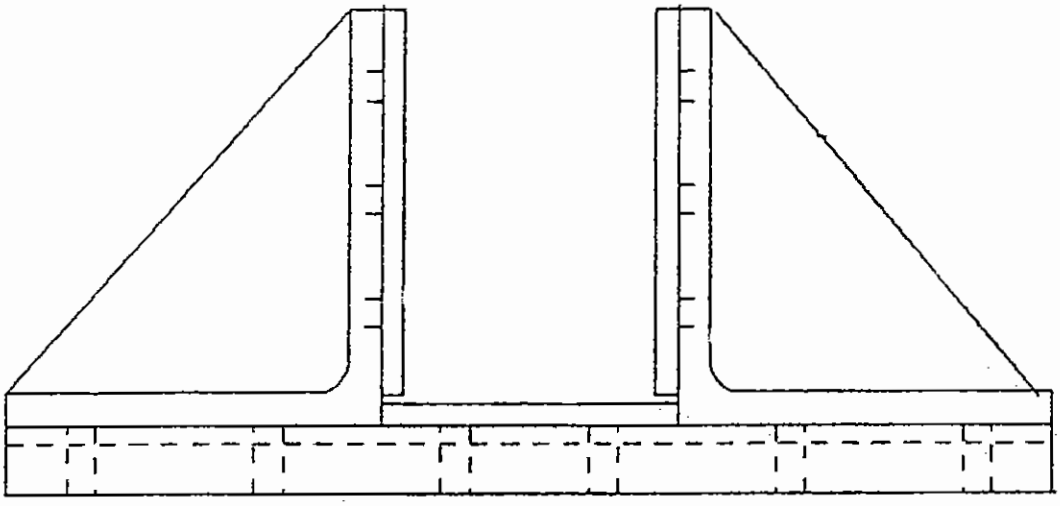

Figure 85: Boeing BSS7260 type CAI anti-buckling fixture

The unreliable failure of the 5J samples due to the low levels damage present precluded their use in the Taguchi analysis but the information is included in Appendix A for reference. All four 25J impacted samples were compressed to failure but only three of the 15J impacted samples, the remaining sample being retained for detailed impact damage evaluation.

5.4.5 Mode I interlaminar fracture (0°/0° interface)

Samples were tested according to the ESIS protocol[122] using a screw driven test machine. The load reading was calibrated using a known mass at the start of each batch of testing and the cross head displacement rate of 1.27mm/min checked using a dial gauge indicator and stop-watch. Samples had correction fluid applied to one side of the sample and a graduated scale marked along 50mm of its length starting at the end of the delamination starter film. For the first 10mm markings were at 1mm intervals followed by 5mm spacing, each marking was numbered to assist in following the crack front.

Load, crack-opening displacement and crack length were recorded on chart paper and manually transferred to Microsoft Excel spreadsheet for data analysis. EMPA software[123] was used for the analysis.

None of the samples tested were pre-cracked, as earlier tests had suggested this to be un-necessary for multiaxial warp-knit composite samples; the load continuing to rise as the crack started to propagate. During the tests it became evident that some of the fabrics exhibited unstable crack growth. However after the crack had arrested the load/displacement curve showed a short linear region followed by non linearity and delamination initiation and growth. In these cases the initial unstable growth was treated as a mode I pre-crack and a line drawn between the origin and the parallel re-loading portion of the curve. This method has previously been used and is reported by Turmel[128]. An illustrative example is provided in Figure 86.

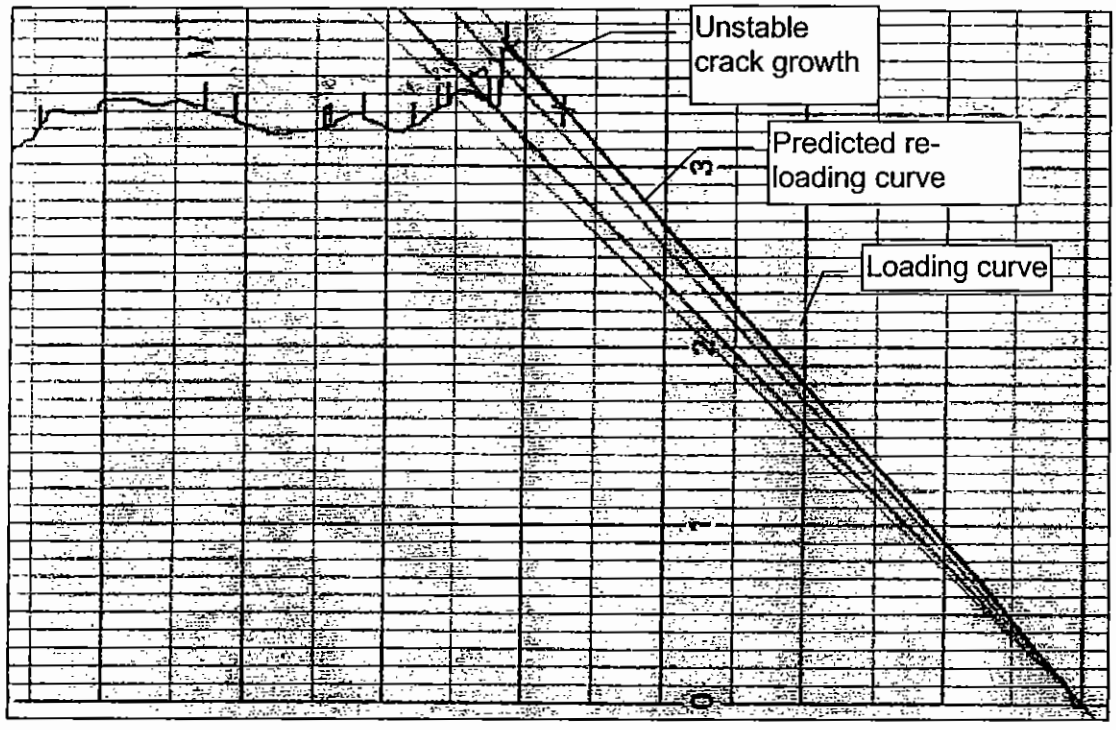

Figure 86: Unstable mode I crack growth observed in some samples (T2DCB01)

The data presented in the results chapter were calculated using Corrected Beam Theory. Four different G_I values are expressed for each of the nine fabrics:

1. $G_{IC(NL)}$ Non-Linear - Strain energy release rate calculated at the point on the load/displacement curve where deviation from a straight line is first observed.

2. $G_{IC(5\%)}$ 5% Compliance Offset - A straight line drawn along the linear region of the loading curve and used to calculate a new line with 5% greater cross head displacement/compliance starting at the same origin. The intersection of this line with the load/displacement line gives the 5% offset strain energy release rate.

3. $G_{I(prop\ max)}$ Propagation Maximum - the single highest G_I value observed during any stage in the 50mm propagation of the delamination crack.

4. $G_{I(10mm\ prop)}$ First 10mm of Propagation - The average strain energy release rate within the detailed first 10mm of propagation data. Where unstable propagation was observed the average over the stable crack length remaining in the first 10mm was used.

Each of these points or averaged results is indicated graphically in Figure 87.

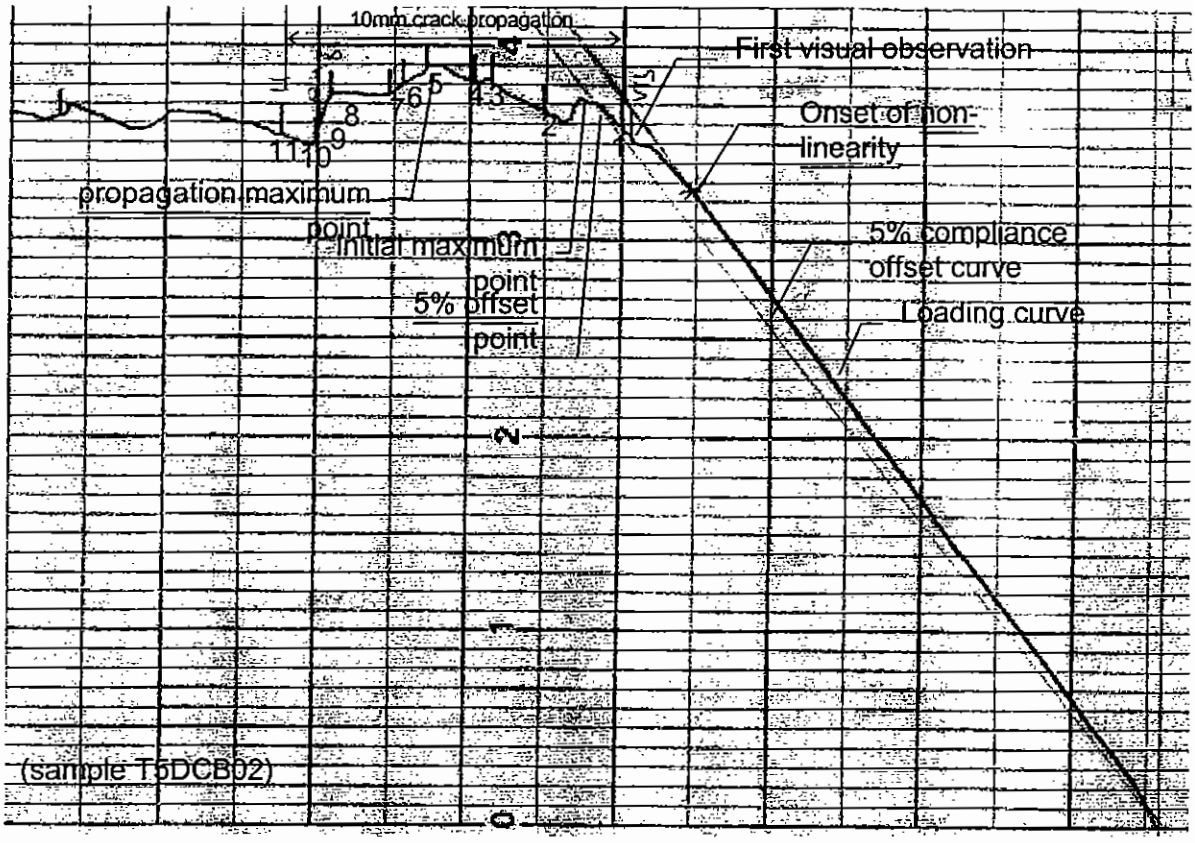

Figure 87: Load/Displacement curve showing the origin of the different G_I Values

G_I and G_{IC} results for the nine materials and the effect of the LIBA manufacturing process settings can be found in the Results and Discussion Chapter. The Chapter similarly contains fracture surface images placed against the load/displacement and strain energy release rate/crack length curves to illustrate the effect of the stitching yarn on the properties.

5.5 Microstructrural results

Two aspects of the composite architecture were characterised for the nine composites; tow-crimp and matrix resin distribution. This data was obtained from polished cross sections taken parallel (0° tow crimp) and perpendicular (matrix resin distribution) to the 0° fibres Automated measurement techniques had been successfully developed and demonstrated by Miller[39] for non-crimp, woven fabrics and unidirectional tape samples. A Leica Quantimat 500 image analyser system with automated microscope and stage was used for gathering and processing the data, presented graphically in summary form using Microsoft Excel 5 spreadsheets.

The same image analysis routines were used here and the technique and assumptions made are summarised below. More in-depth information on the background and development of the routines can be found in reference [39] of which the following sections are an acknowledged condensation.

5.5.1 Specimen Preparation

During the preparation of the in-plane test samples a 160mm long, 10mm wide strip of material was cut from the centre of the same test laminate parallel to the 0° fibre direction for tow crimp measurements and perpendicular for resin distribution analysis. These strips were each subsequently cut into four smaller samples, nominally 40mm in length, using a diamond wafering saw and the samples parallel to each other and mounted in a 50mm diameter block of cold curing two part epoxy

resin. For the tow crimp samples up to five sample blocks were then ground and polished on a Buehler Motopol 12 automatic polisher using the schedule indicated in Table 23.

Table 23: Polishing procedure

Polishing Medium	Relative direction of rotation	Speed (RPM)	Load per sample	Duration (Minutes)
220 SiC paper +water	Complementary	150	12.5lb	until plane
660 SiC paper + water	Complementary	150	12.5lb	2
1200 SiC paper + water	Complementary	150	12.5lb	6
6µm diamond paste - Texmet cloth	Contradictory	120	12.5lb	15
3µm diamond paste - DP Mol Cloth	Contradictory	120	12.5lb	10
Sub-micron colloidal silica - Paper cloth	Complementary	120	12.5lb	5

Difficulties were experienced obtaining a reliable and consistent surface finish in the resin distribution samples when observed at the higher magnifications required for the Image Analysis. The polishing procedure was changed, making use of a Logitech Precision lapping and polishing machine which provided a more uniform surface finish over the whole sample. Polishing materials and consumables were as specified in Table 23, however only three samples were polished at once with a weight of 667 grams per sample. Polishing times were increased by a factor of approximately three.

On completion samples were washed with distilled waster and iso-propanol and parallel mounted on glass slides so that the whole sample would remain in focus on the image analyser.

5.5.2 Out of Plane Tow Crimp

5.5.2.1 Tow detection and Tracking

A x2.5 objective lens was used to give a resolution of 3.36µm/pixel and an image size of 2.42 x 1.72mm. In the images the 0° fibres of interest appear as light streaks; brighter than either the surrounding matrix or the 45° fibres which appear as small ovals. This allows them to be differentiated as illustrated in Figure 88 by (a) sharpening the contrast between fibres and matrix, (b) detecting the horizontal boundary between areas of high contrast, i.e. the boundary between layers of different orientations, increasing the brightness, (c) thresholding so only the brighter fibres of the 0° tow are detected, (d) dilating to merge the boundaries of the detected fibres and fill enclosed holes to create a solid entity. This image is then stored on the hard disk of the computer.

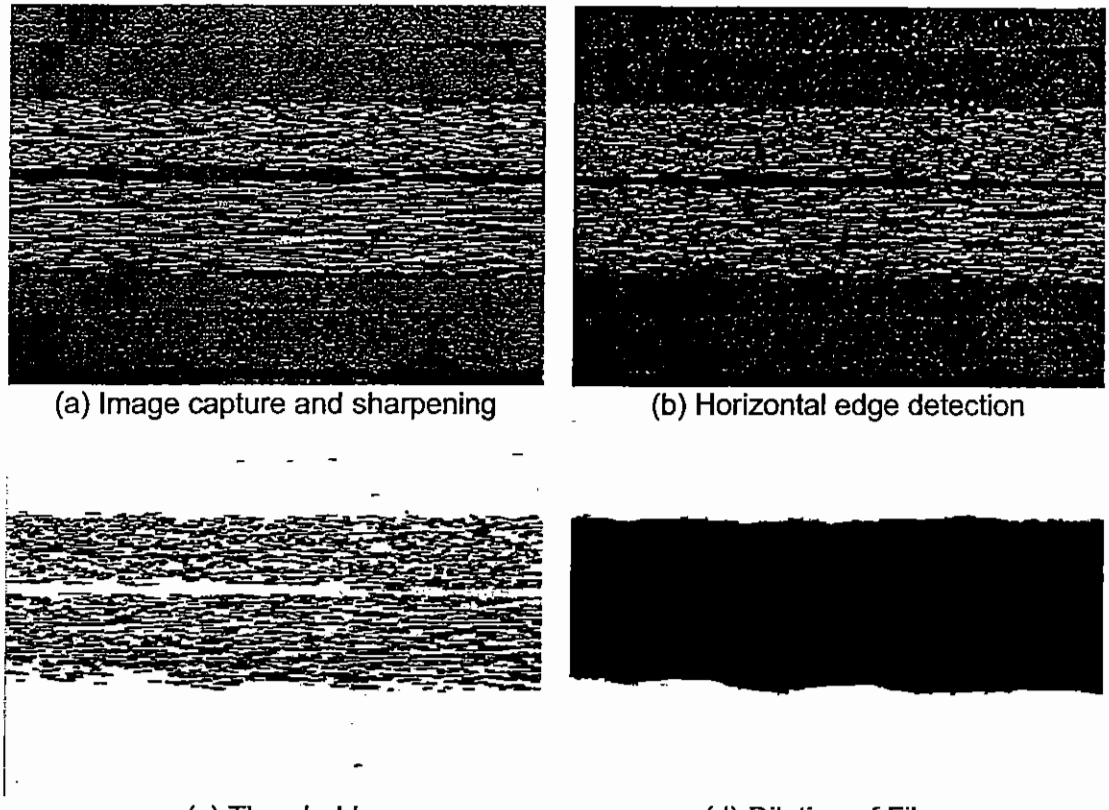

(a) Image capture and sharpening (b) Horizontal edge detection

(c) Threshold (d) Dilation of Fibres

Figure 88: Detection of tows for triaxial non-crimp fabrics[39]

Tow tracking is performed by moving the motorised stage exactly one frame horizontally, refocusing and comparing tow positions at the end of the previous frame to that of the start of the new frame and adjusting vertically to compensate for any tilt of the specimen. When the tow no longer runs across the whole frame that frame is rejected as it has reached the edge of the sample. Automation of this process allows each horizontal pass to be separately identified so that a number of samples can be present on the stage at any one time and scanned sequentially with minimum intervention.

5.5.2.2 Analysis of the Image Data

The tow crimp is presented in two ways; as a distribution of orientations and as a waveform. From the tow orientation distributions two parameters can be calculated; standard deviation of orientation and the range.

In order to obtain this information the stored tow image data had to be reduced into a set of tow paths which could be used to calculate the crimp parameters.

To do this the first frame is loaded and the tow and bottom of the tow in the first column of the image identified and the centre point between the two positions and the thickness calculated. Because the exterior profile of the tow is made up of discrete fibres it is relatively 'jagged'. To overcome this a cubic smoothing spline was fitted to the tow path data and sampled at 0.1mm intervals along its length, to reduce the data storage requirement. The resulting coordinates form the 'tow path' as presented.

Results are presented in summary form for each material in the Results and Discussion Chapter. The orientation distribution histograms are generated from the

cubic spline fitting data and give the orientations of the tow as sampled at 0.1mm intervals. The Fast Fourier Transform (FFT) waveform gives a distribution of frequencies (converted to wavelengths) present in the tow path. The peaks and troughs in the data were also located so that the amplitude of dominant crimps could be calculated.

5.5.3 Resin Distribution

5.5.3.1 Resin Area Detection and measurement

A x5 objective lens was used to capture image frames with a resolution of 1.67μm giving an image size of 1.21 x 0.86mm. Once a suitable polishing procedure had been adopted the image gave good contrast between the brighter fibres and the darker surrounding matrix and only a sharpening filter was required before thresholding. Thesholding was performed by detecting the brighter fibres dilating them so that the tows themselves became the detected objects and then inverting the image leaving the resin areas as the detected objects. To tidy the image resin areas less than 1500μm² were removed and any small holes filled. This process is illustrated in Figure 89.

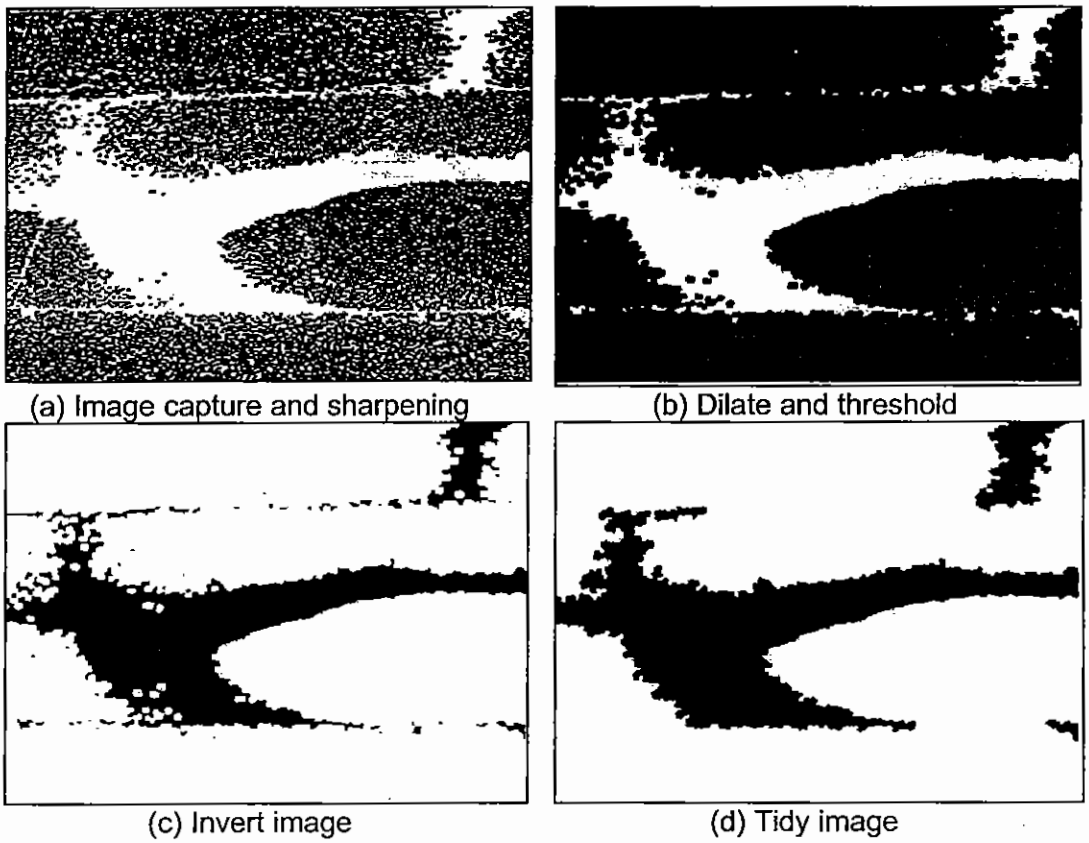

(a) Image capture and sharpening (b) Dilate and threshold

(c) Invert image (d) Tidy image

Figure 89: Detection of resin rich areas[39]

5.5.3.2 Analysis of the Resin Distribution Data

Free resin volume fraction is calculated by dividing the area of detected resin by the total image area. A resin layer is defined here as a portion of resin having a thickness of less than 100μm and a length greater than 200μm. Any resin feature which does not comply with these constraints is considered a resin area.

To identify and measure the resin layers an array of 4 x 4 images is loaded from the hard disk (Figure 90a) and segmented by subtracting a vertical grid with 1 pixel spacing leaving 1 pixel wide columns (Figure 90b). The thickness of the detected resin in each of these columns is measured and all those over 100µm rejected (Figure 90c). The remaining columns are then reformed into larger features by dilating the image in the horizontal direction only (Figure 90d). The remaining features of length less than 200µm are rejected leaving the resin layers to be measured (Figure 90d).

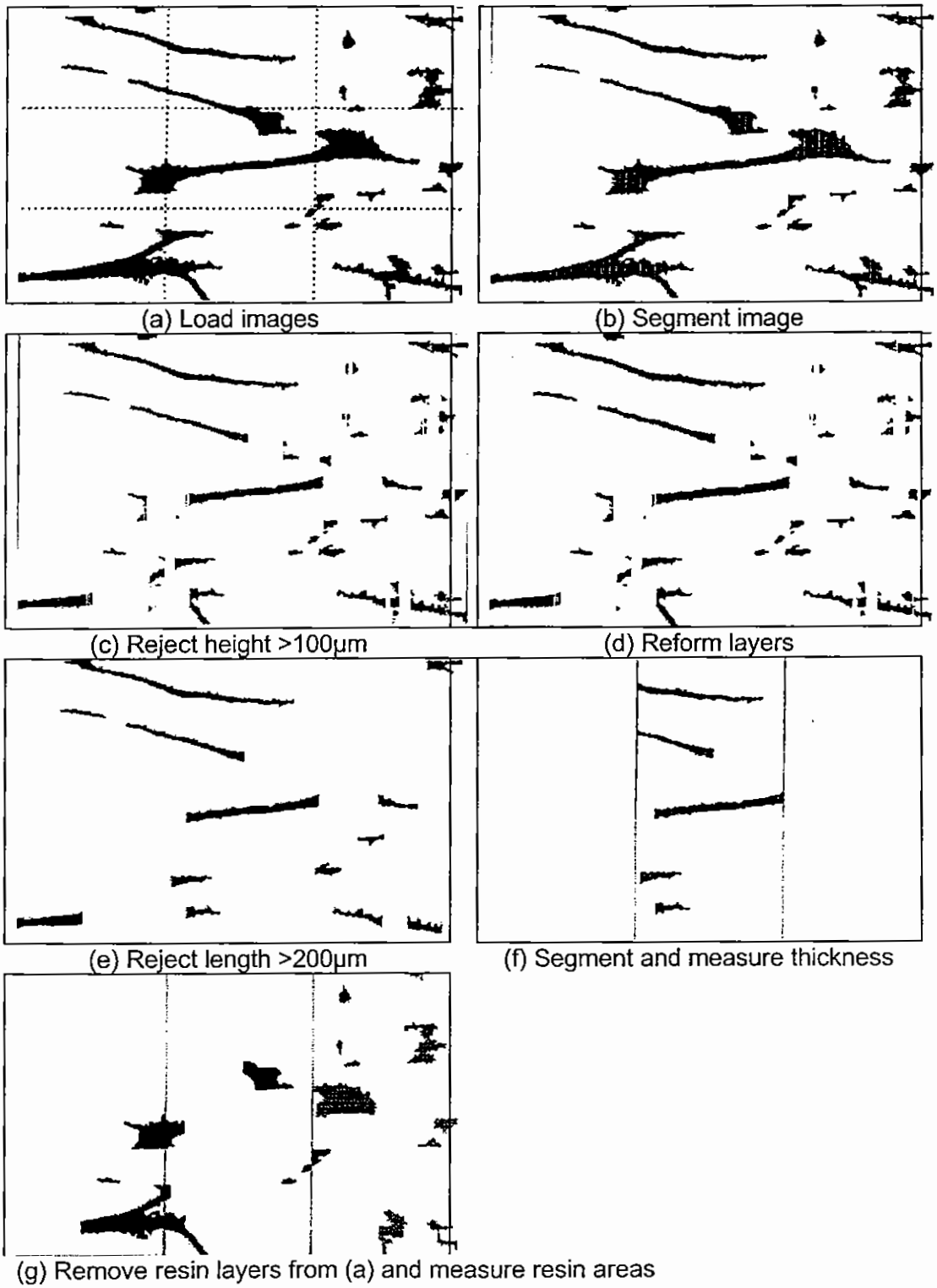

(a) Load images (b) Segment image

(c) Reject height >100µm (d) Reform layers

(e) Reject length >200µm (f) Segment and measure thickness

(g) Remove resin layers from (a) and measure resin areas

Figure 90: Measurement of resin rich layers and areas[39]

A 2 x 4 measuring frame is then imposed on the centre two columns of the array and the features inside the frame detected. The thickness of the features and their position through the thickness are then measured (Figure 90f). To measure the resin areas the accepted resin layer image, above, is subtracted from the original detected resin area image to leave only the resin areas. A measuring frame is again set up in the centre of the image and only those detected areas with their 'Feature Count Points' inside the frame are accepted and then measured. The 'Feature Count Point' defines the x and y coordinate for the feature and is the rightmost pixel (x) and last (bottom) line (y) contained in the detected feature (Figure 90g).

The three measured characteristics; free resin volume fraction, resin layer thickness and location and resin area size are then statistically analysed and presented in a easy to understand summary format using and Microsoft Excel 5 spreadsheet.

5.6 Data Analysis for the Effect of Manufacturing Settings

The analysis of the performance characteristics with respect to LIBA machine settings was performed using Statsoft Statistica V5.1, a commercial statistical analysis software package. Two very similar analyses were performed on the data:

1. 3x3 Greco-Latin Square
2. L_9 Orthogonal Array

The orthogonal array shown in Table 24 was used to determine the parameter settings when the fabrics were manufactured (Table 17). Parameters 1 to 4 represent the different settings on the machine we want to investigate and the numbers 1 to 3 the levels of the machine settings. Runs 1 to 9 are the experiments performed and their settings read across, i.e. Run 2 has parameter settings 1,2,2,2.

Table 24: 3x3 Greco-Latin square or L_9 orthogonal array

	Parameter 1	**Parameter 2**	**Parameter 3**	**Parameter 4**
Run 1	1	1	1	1
Run 2	1	2	2	2
Run 3	1	3	3	3
Run 4	2	1	2	3
Run 5	2	2	3	1
Run 6	2	3	1	2
Run 7	3	1	3	2
Run 8	3	2	1	3
Run 9	3	3	2	1

Both analyses use orthogonal arrays of the same design: The first uses only the mean results from each of the nine materials tested and so does not involve the variability in the data that makes up this mean value. The second technique includes all the individual data points in a signal-to-noise ratio which the analysis in most cases seeks to maximise. When the variability in the data is relatively small and alike for all the materials tested the outcome of both analyses is very similar.

By using a signal-to-noise ratio we can express the relationship between machine setting and performance (signal) and its variability (noise) at the selected parameter settings. For a majority of the tests carried out we want to maximise the performance whilst minimising the variability, so as to maximise the design allowable

for the material. Thus in most cases we wish to maximise the signal-to-noise ratio and this is generally known as a 'larger-the-better' type problem. The signal-to-noise ratio (S/N) in this case is given by Equation 1[118].

$$S/N = -10\log_{10}\left(\frac{1}{n}\sum_{n}^{1}\frac{1}{y_i^2}\right) \qquad \text{Equation 1}$$

For some of the performance characteristics we wish to minimise the characteristic; examples of which are impact damage area and crimp in the 0° fibre tows. In this case we use another equation below (Equation 2)[118].

$$S/N = -10\log_{10}\left(\frac{1}{n}\sum_{n}^{1}y_i^2\right) \qquad \text{Equation 2}$$

where in both cases: for i = 1 to n
n is number of samples
y is the measured value of the performance characteristic

5.6.1 Worked example

By way of illustrating the method of analysis, below is a step-by-step analysis of the results for the open hole tensile strength of the composite materials tested.

Table 25: OHT results for each sample

	OHT01	OHT02	OHT03	OHT04	OHT05
T1	465.1	472.5	483.1	489.2	453.4
T2	507.0	413.1	439.5	428.0	465.9
T3	590.6	579.6	559.7	532.9	563.7
T4	506.9	498.8	511.1	491.6	523.8
T5	425.8	475.8	464.8	495.5	476.0
T6	460.7	438.0	468.9	455.9	491.3
T7	451.2	450.3	445.5	465.7	453.9
T8	471.7	496.2	463.0	476.6	521.3
T9	472.0	495.0	534.3	499.8	535.4

If we superimpose the machine parameters and settings onto Table 24 this becomes clearer and we obtain a list of recipes for making each of the nine fabrics (Table 26).

Table 26: L_9 array with parameters and settings superimposed

	Stitch Course	Stitch Tension	0° Tension	0° Coverage
Fabric 1	5	low	low	spread
Fabric 2	5	medium	medium	50/50
Fabric 3	5	high	high	bunched
Fabric 4	7.4	low	medium	bunched
Fabric 5	7.4	medium	high	spread
Fabric 6	7.4	high	low	50/50
Fabric 7	3.5	low	high	50/50
Fabric 8	3.5	medium	low	bunched

Fabric 9	3.5	high	medium	spread

The feature of orthogonal arrays that allows us to isolate the effect of each parameter is that when we group the fabrics with the same parameter settings, all the other parameters contain each of the three settings thus they have no net effect on that group of results. This can be seen clearly in Table 26 for Stitch Course but is also true for all the other parameters for example Stitch Tension when settings are grouped as shown in Table 27.

Table 27: L_9 array rearranged to group stitch tension settings

	Stitch Tension	**Stitch Course**	**0° Tension**	**0° Coverage**
Fabric 1	Low	5	low	spread
Fabric 4	Low	7.4	medium	bunched
Fabric 7	Low	3.5	high	50/50
Fabric 2	Medium	5	medium	50/50
Fabric 5	Medium	7.4	high	spread
Fabric 8	Medium	3.5	low	bunched
Fabric 3	High	5	high	bunched
Fabric 6	High	7.4	low	50/50
Fabric 9	High	3.5	medium	spread

Looking at the results for one machine parameter at a time and grouping fabrics together with the same settings, Stitch Course results are shown in Table 28.

Table 28: Stitch Course results grouped

	Stitch Course	**OHT01**	**OHT02**	**OHT03**	**OHT04**	**OHT05**	
Fabric 1	5	465.1	472.5	483.1	489.2	453.4	
Fabric 2	5	507.0	413.1	439.5	428.0	465.9	mean = 496.2MN/m²
Fabric 3	5	590.6	579.6	559.7	532.9	563.7	S/N = 53.76dB
Fabric 4	7.4	506.9	498.8	511.1	491.6	523.8	
Fabric 5	7.4	425.8	475.8	464.8	495.5	476.0	mean = 479.0MN/m²
Fabric 6	7.4	460.7	438.0	468.9	455.9	491.3	S/N = 53.57dB
Fabric 7	3.5	451.2	450.3	445.5	465.7	453.9	
Fabric 8	3.5	471.7	496.2	463.0	476.6	521.3	mean = 482.1MN/m²
Fabric 9	3.5	472.0	495.0	534.3	499.8	535.4	S/N = 53.62dB

Similarly for Stitch Tension; grouping fabrics with the same Stitch Tension settings.

Table 29: Stitch Tension results grouped

	Stitch Tension	**OHT01**	**OHT02**	**OHT03**	**OHT04**	**OHT05**	
Fabric 1	Low	465.1	472.5	483.1	489.2	453.4	
Fabric 4	Low	506.9	498.8	511.1	491.6	523.8	mean = 477.5MN/m²
Fabric 7	Low	451.2	450.3	445.5	465.7	453.9	S/N = 53.54dB
Fabric 2	Medium	507.0	413.1	439.5	428.0	465.9	
Fabric 5	Medium	425.8	475.8	464.8	495.5	476.0	mean = 468.0MN/m²
Fabric 8	Medium	471.7	496.2	463.0	476.6	521.3	S/N = 53.35dB
Fabric 3	High	590.6	579.6	559.7	532.9	563.7	

Fabric 6	High	460.7	438.0	468.9	455.9	491.3	mean = 511.9MN/m²
Fabric 9	High	472.0	495.0	534.3	499.8	535.4	S/N = 54.07dB

From this point on the Latin Square analysis and the Taguchi analysis differ slightly. For the Latin square analysis we simply take the mean of each group of fabrics. The effect of a stitch course of 3.5 penetrations/cm is the average result of fabrics 7, 8 and 9 (482.1MN/m²), 5 penetrations/cm fabrics 1, 2 and 3 (496.2MN/m²) and finally for 7.4 penetrations/cm the average of fabrics 4, 5 and 6 (479.0MN/m²).

Similarly for Stitch Tension; for the low setting we take the average of fabrics 1,4 and 7 (477.5MN/m²), medium, fabrics 2, 5 and 8 (468.0MN/m²) and high, 3, 6 and 9 (511.9MN/m²). Doing the same for the remaining parameters produces the graphs as shown in Figure 91.

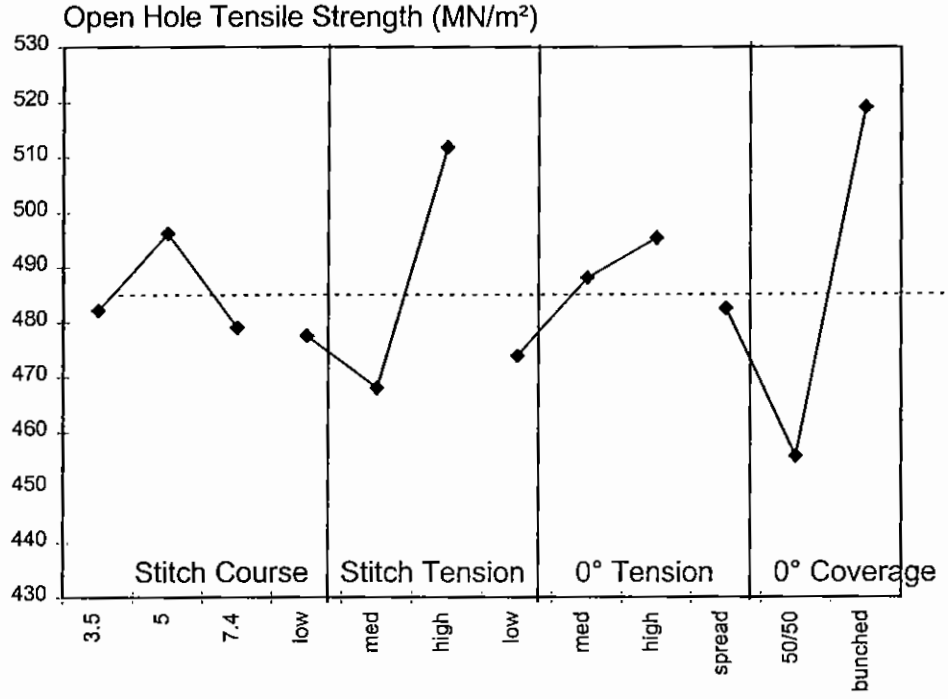

Figure 91: Greco-Latin Square results graph - open hole tensile strength

We now calculate the signal-to-noise ratios using Equation 1, as we wish to maximise the Open Hole Tensile Strength of the material. For the same data (Tables 28 and 29) we obtain the following graphs (Figure 92)

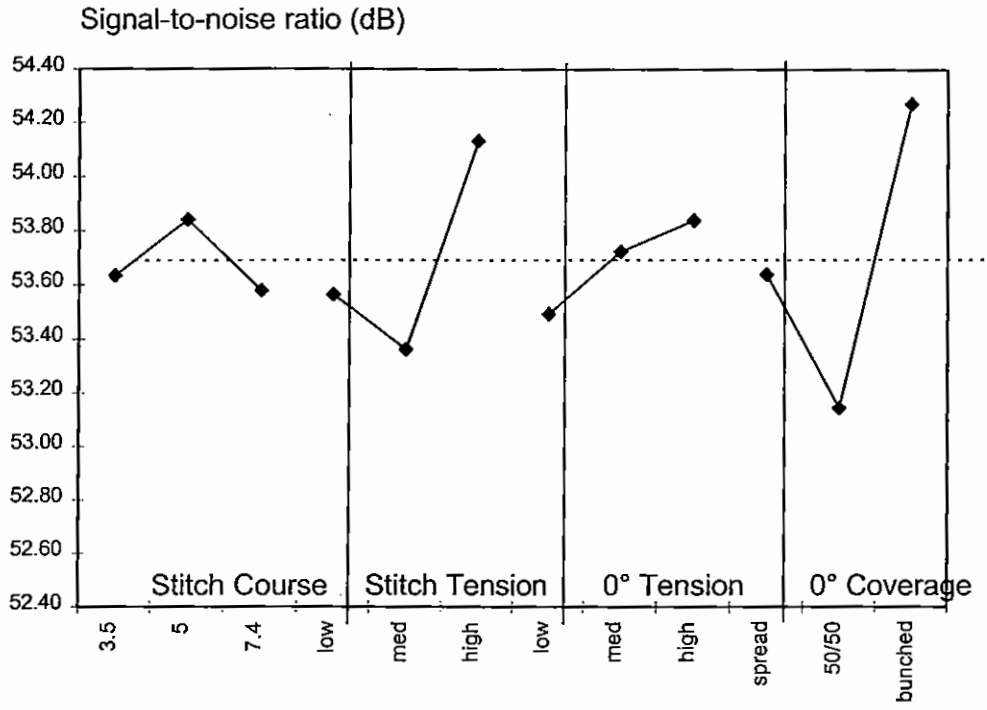

Figure 92: L_9 Array results graph - open hole tensile strength

So the best settings to select in the manufacture of the fabric for open hole tensile strength are:

Parameter	**Best setting**	**signal to noise**
Stitch Course	5 penetrations/cm	53.84
Stitch Tension	High	54.13
0° Tension	High	53.84
0° Coverage	Bunched	54.27
	Best estimate	55.03
	Corresponds to	**564.3 MN/m²**

We can use the Analysis Of Variance, ANOVA, to highlight the parameters which most influence the performance, and can compare this directly with the standard deviation of the mean signal-to-noise ratio as an indication as to how 'significant' the result is. This has been done for all the performance characteristics measured and can be found on each result sheet in Chapter 5. In Figure 91 and Figure 92 we can visually infer that Stitch Course and 0° Tension have relatively little effect on the Open Hole Tensile Strength and that it is principally Stitch Tension and 0° Coverage which control the OHT performance of this material. Furthermore, settings of high stitch tension and bunched 0° coverage will yield the best performance in this respect.

For the open hole tensile strength results:

Mean signal-to-noise ratio = 53.69
Standard deviation = 0.63
Mean squared deviation for each parameter:
Stitch Course = 0.06
Stitch Tension = 0.48
0° Tension = 0.09
0° Coverage = 0.96

We can therefore observe that only the 0° coverage lies outside one standard deviation of the data but with stitch tension relatively close. We can therefore re-calculate our best estimate ignoring the two least significant parameters:

Parameter	**Best setting**	**signal to noise**
~~Stitch Course~~	~~5 penetrations/cm~~	~~53.84~~
Stitch Tension	High	54.13
~~0° Tension~~	~~High~~	~~53.84~~
0° Coverage	Bunched	54.27
	Best estimate	54.72
	Corresponds to	**544.5 MN/m²**

Chapter 6

Results And Discussion

6.1 Introduction

In this chapter the results are as before grouped as in-plane, damage resistance/tolerance properties and microstructural features. For each type of test performed a summary result sheet is presented which contains all the data used to calculate the effect of the machine settings on that particular performance characteristic. This includes the individual data points for each sample, means, coefficient of variation and the signal-to-noise ratios. The results are then combined to give the effect of each setting and estimates of the performance when the best machine settings are selected. Two graphs are also presented of machine settings versus performance characteristic; those based only on the mean results (Greco-Latin Square) and those using the signal-to-noise ratio (Taguchi Analysis). At the end of each grouping of tests they are discussed as a group with reference to the microstructural features and the other performance characteristics presented.

Individual sample details and results are to be found in Appendix A together with results sheets for measured characteristics which were considered to be little affected by the machine settings, but included for completeness.

6.2 Microstructural Results

6.2.1 Optical Microsections

Figure 92 indicates the different features observed in the composite microsections.

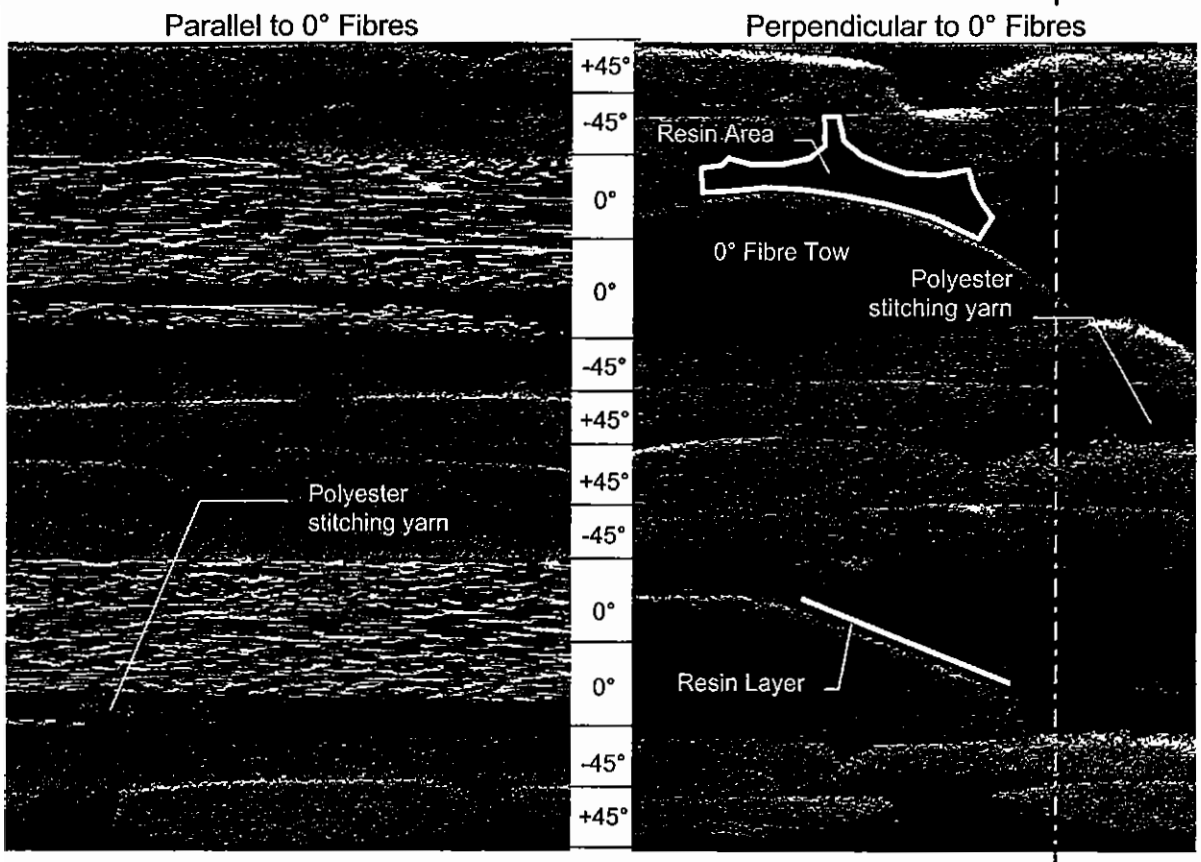

Figure 93: Cross-sections of material T3 showing typical features

Sample microsections for the nine composite materials tested are included in Figure 94 to Figure 111. Images obtained parallel to the 0° fibre tows were used for two crimp measurements and those taken perpendicular, for resin distribution

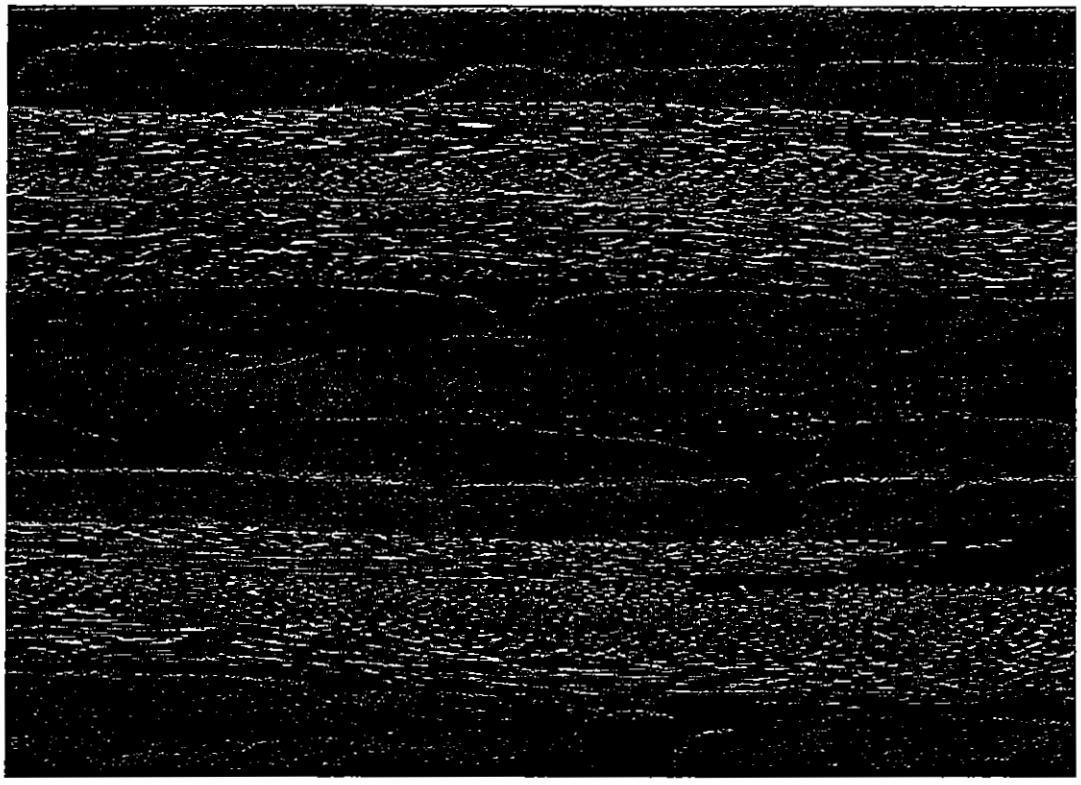

Figure 94 : Material T1 Laminate cross section parallel to 0° fibres

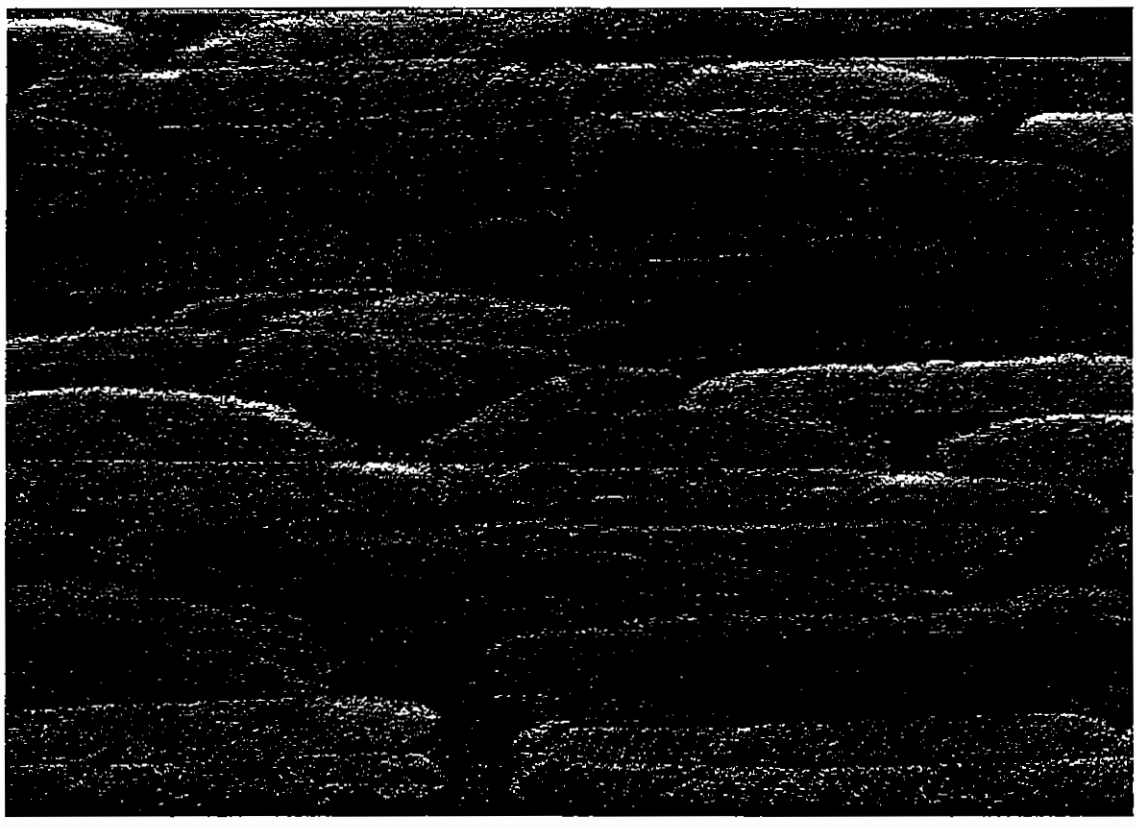

Figure 95: Material T1 Laminate cross section perpendicular to 0° fibres

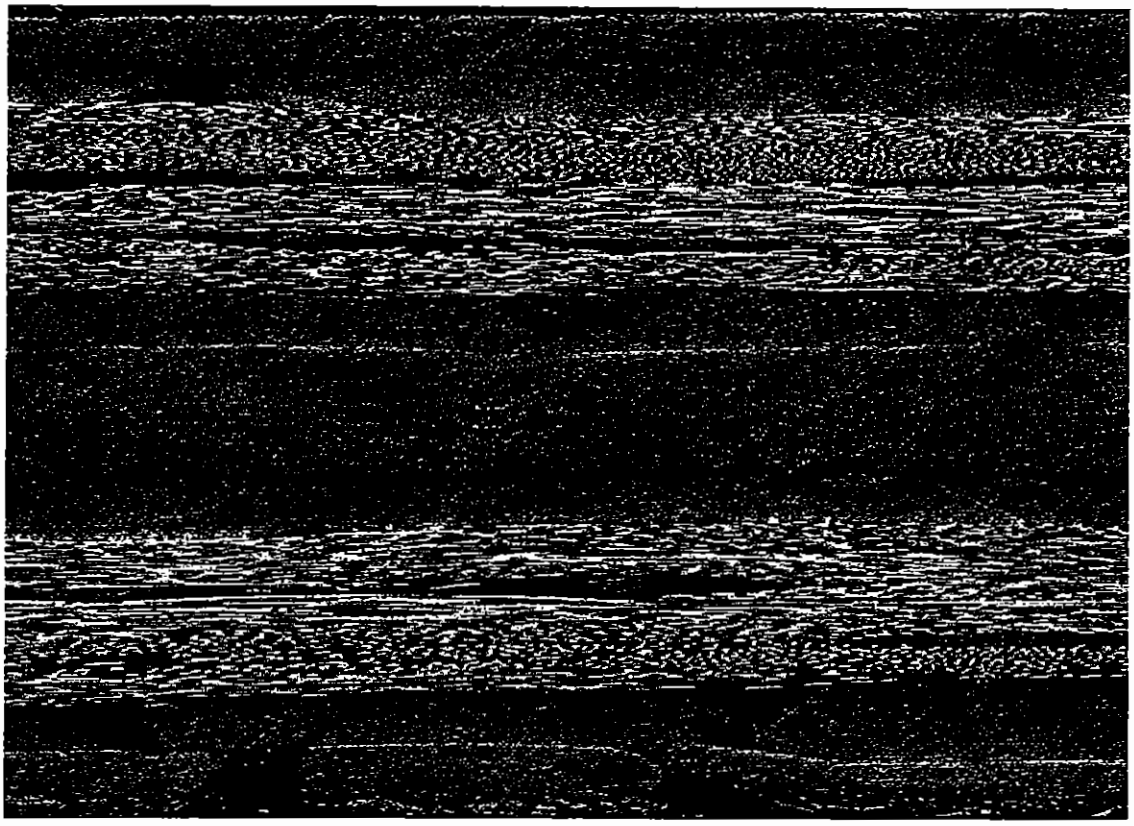

Figure 96: Material T2 Laminate cross section parallel to 0° fibres

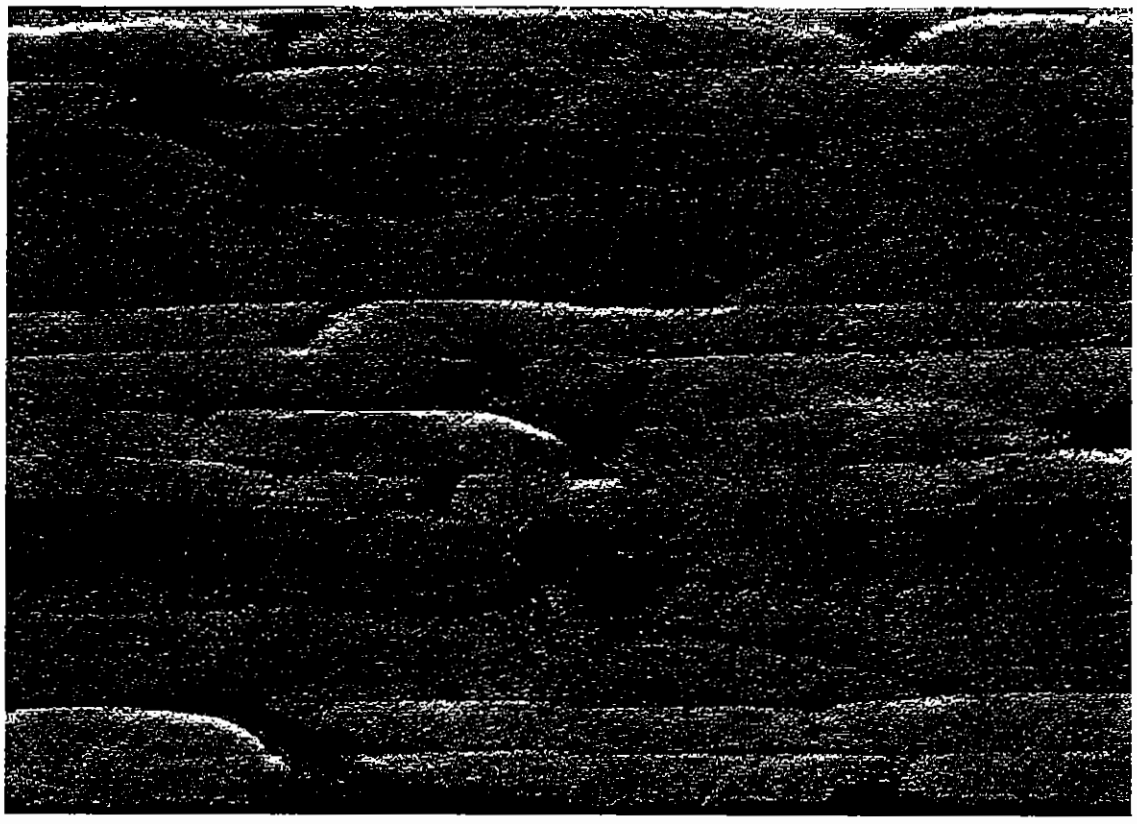

Figure 97: Material T2 Laminate cross section perpendicular to 0° fibres

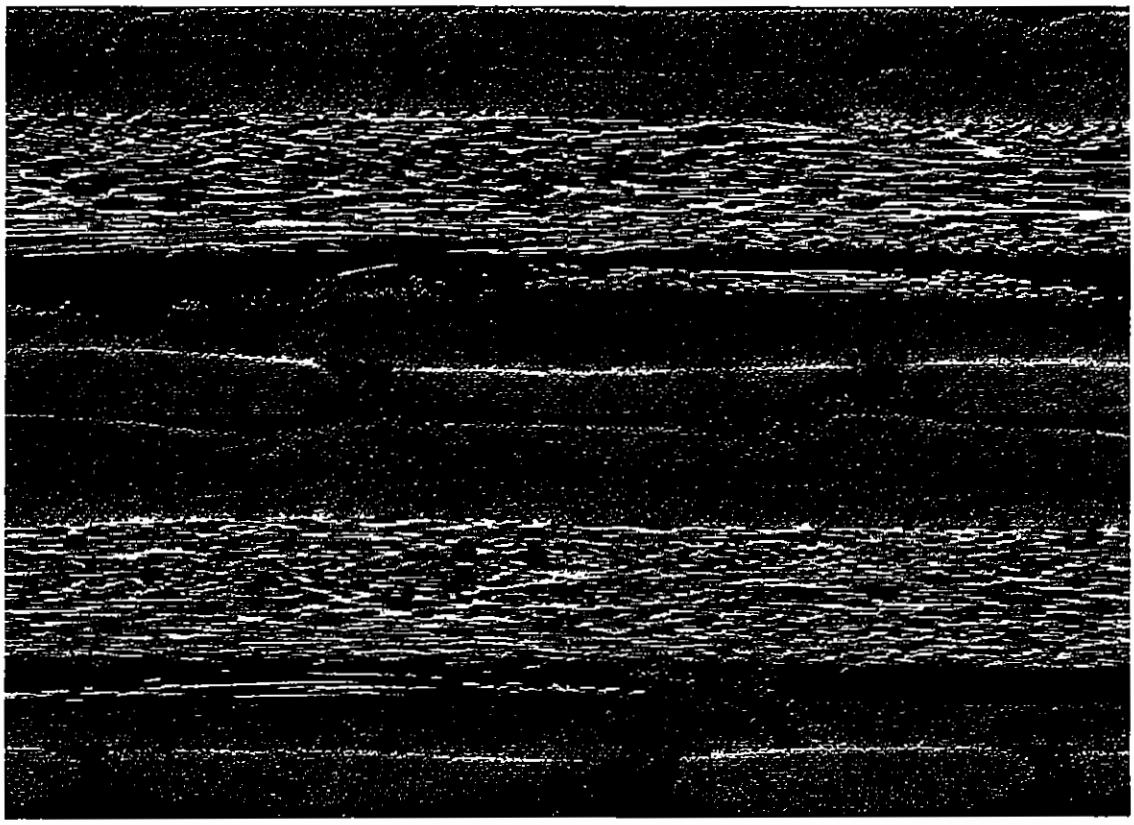

Figure 98: Material T3 Laminate cross section parallel to 0° fibres

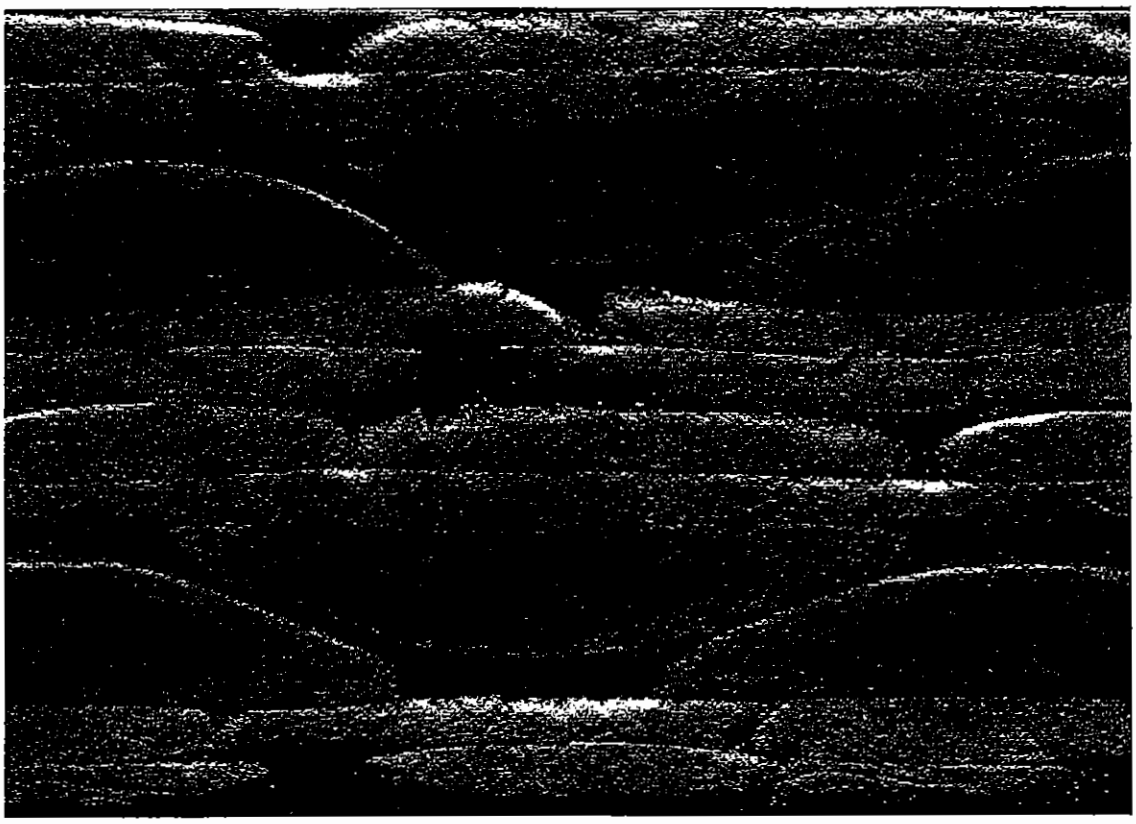

Figure 99: Material T3 Laminate cross section perpendicular to 0° fibres

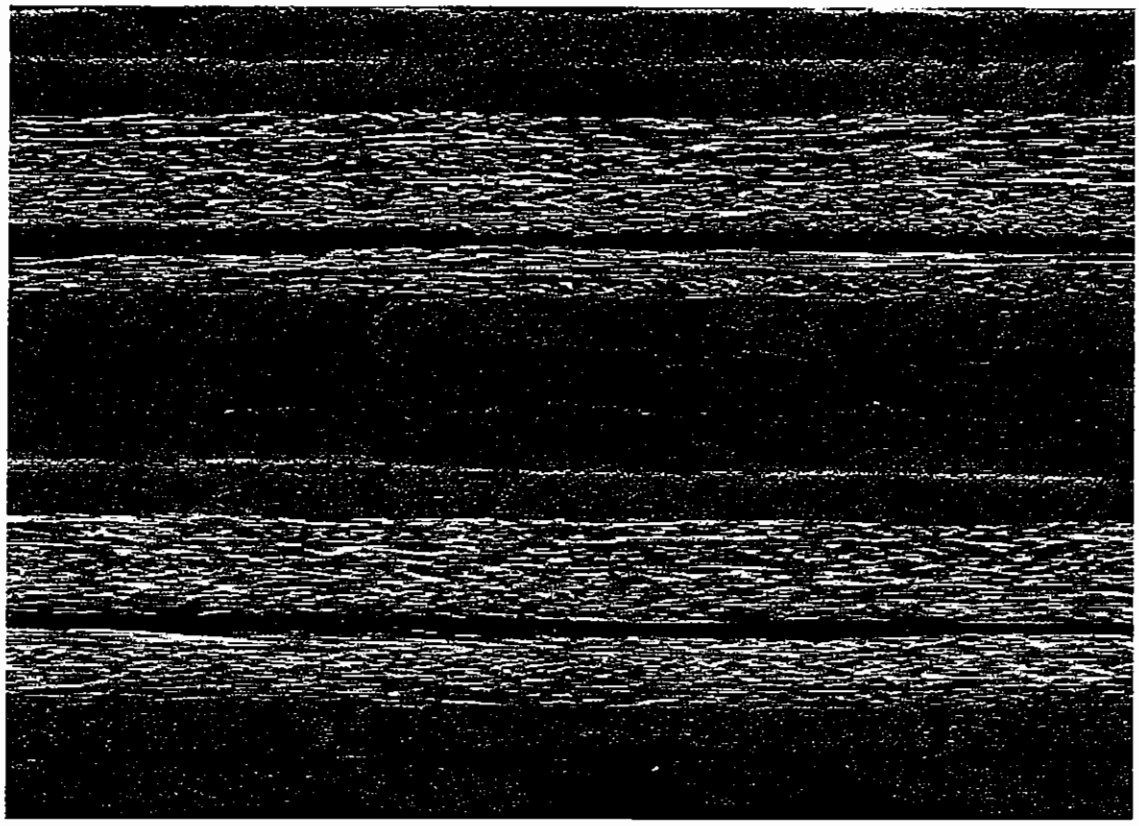

Figure 100: Material T4 Laminate cross section parallel to 0° fibres

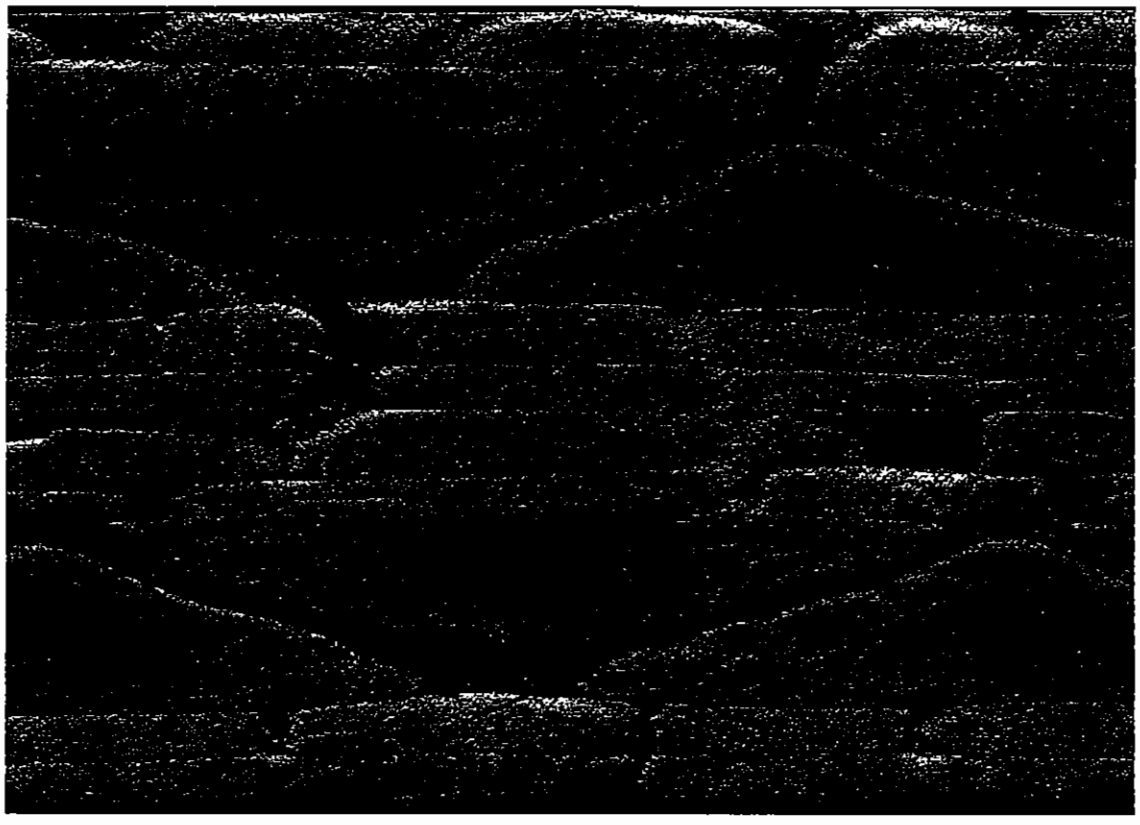

Figure 101: Material T4 Laminate cross section perpendicular to 0° fibres

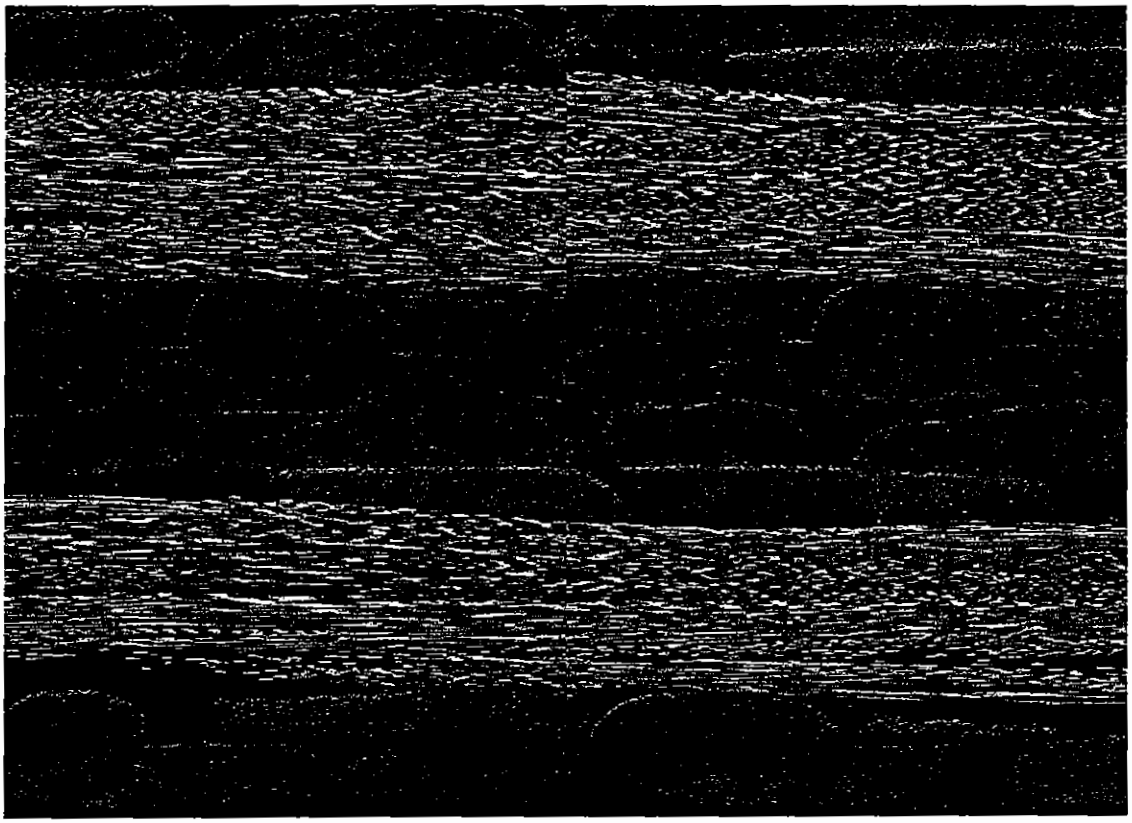

Figure 102: Material T5 Laminate cross section parallel to 0° fibres

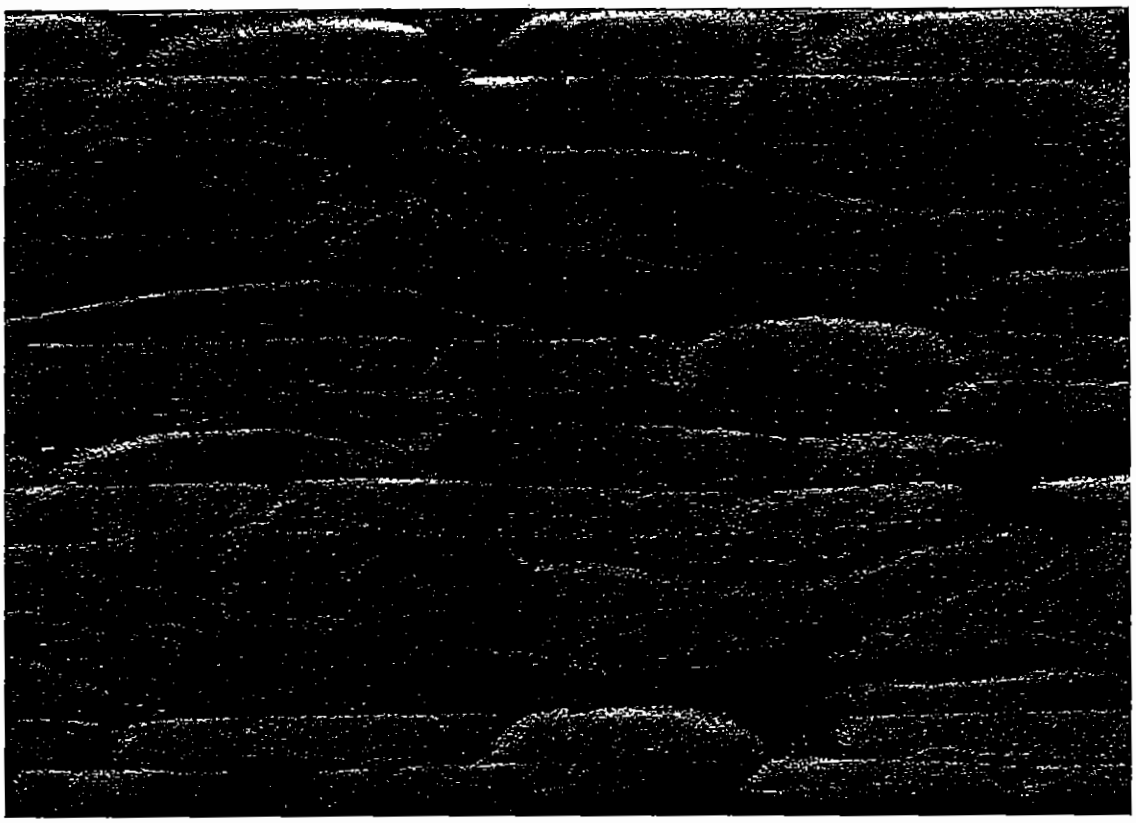

Figure.103: Material T5 Laminate cross section perpendicular to 0° fibres

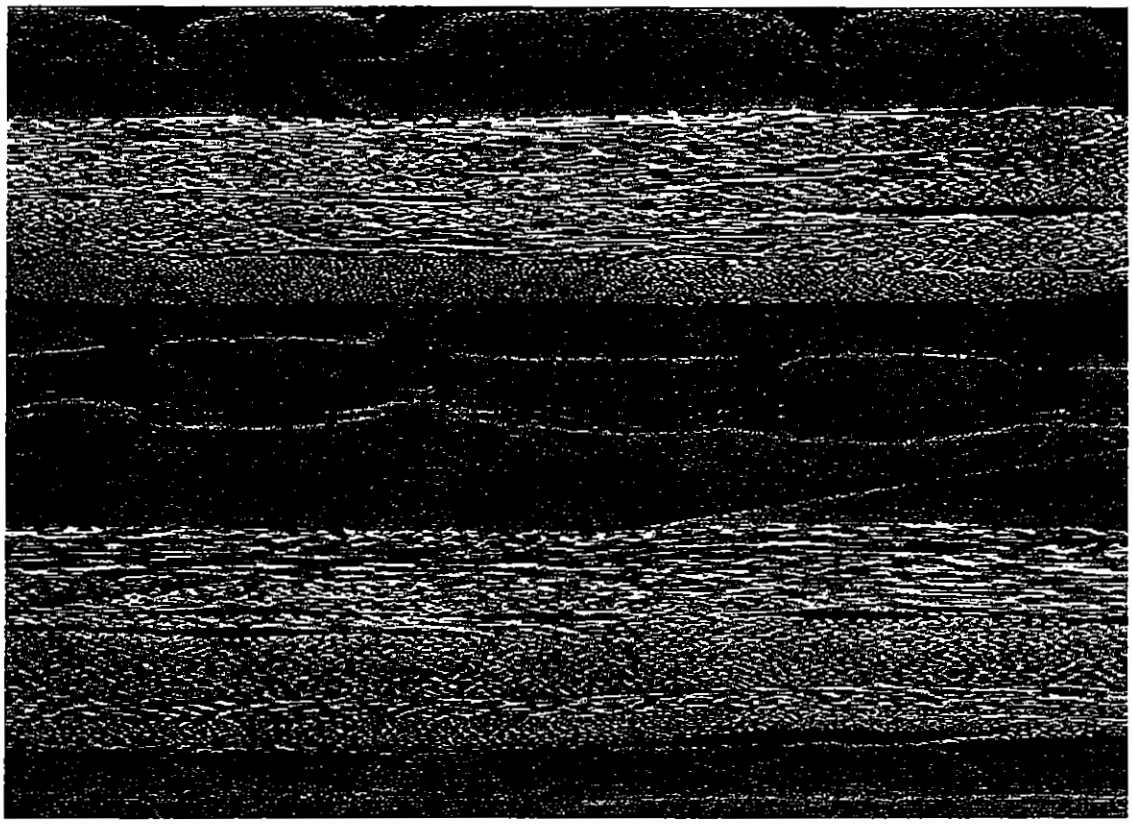

Figure 104: Material T6 Laminate cross section parallel to 0° fibres

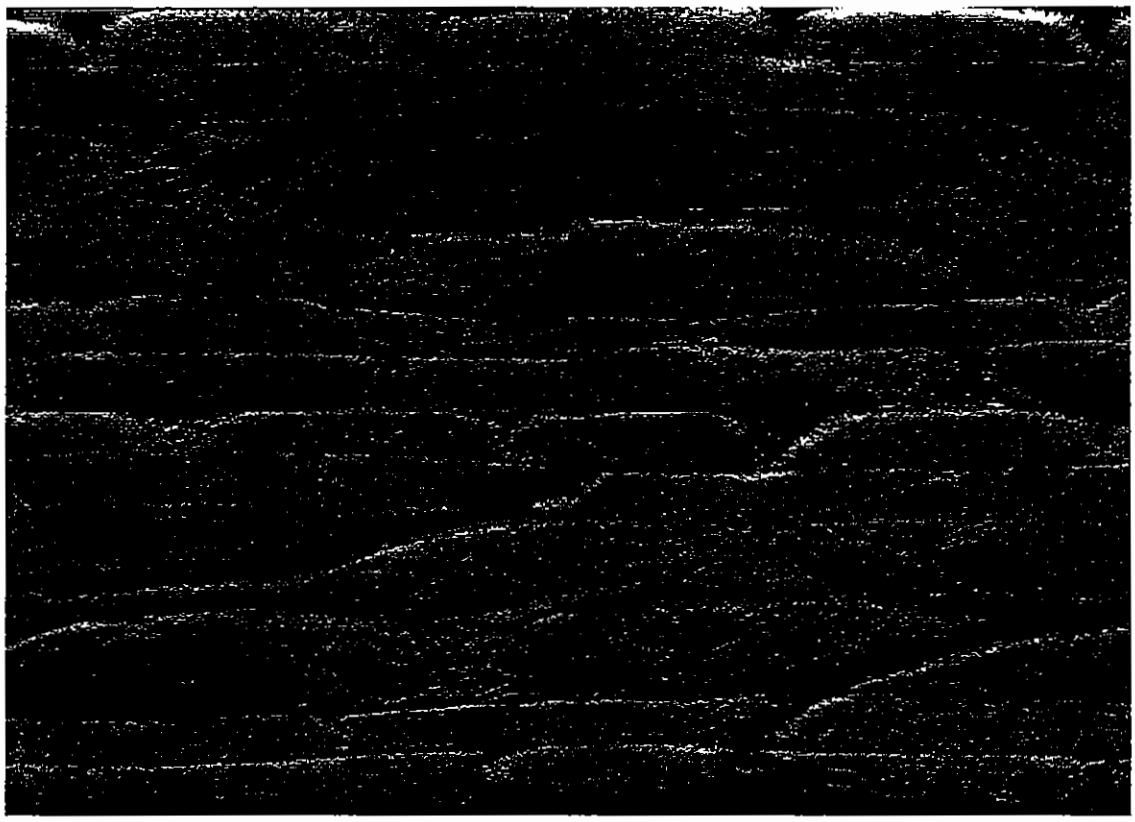

Figure 105: Material T6 Laminate cross section perpendicular to 0° fibres

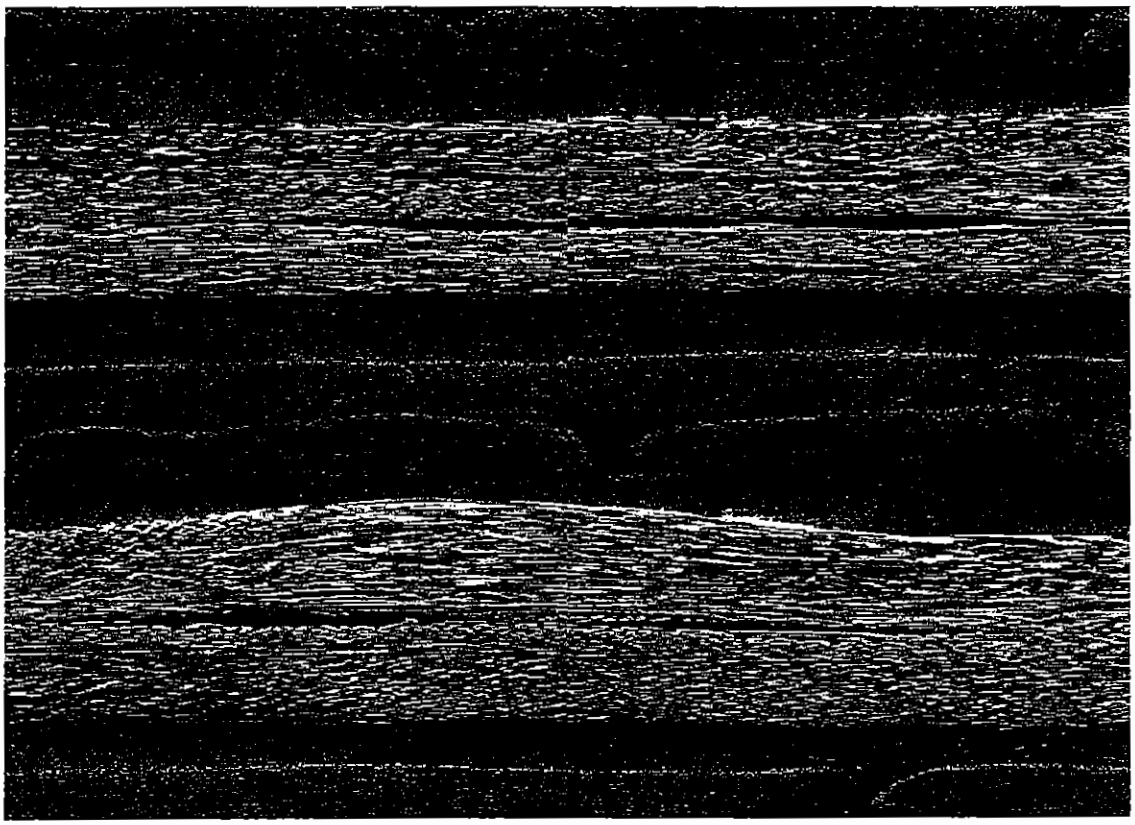

Figure 106: Material T7 Laminate cross section parallel to 0° fibres

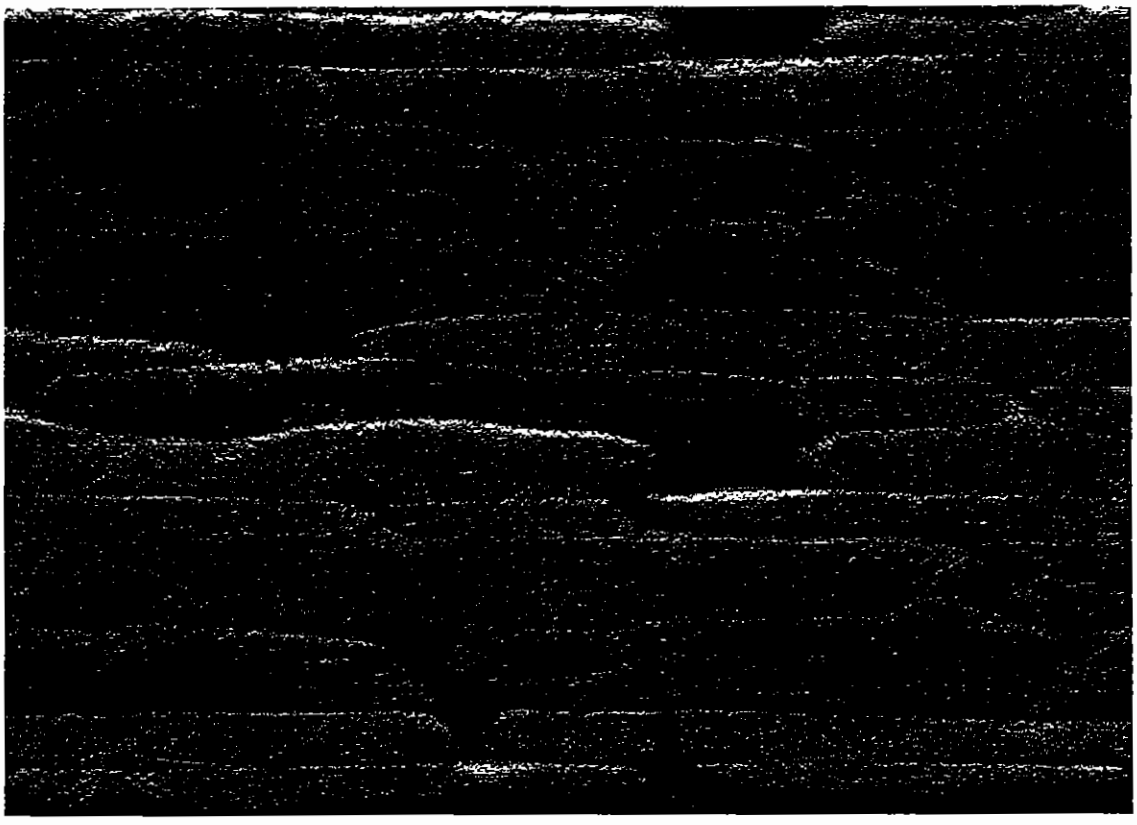

Figure 107: Material T7 Laminate cross section perpendicular to 0° fibres

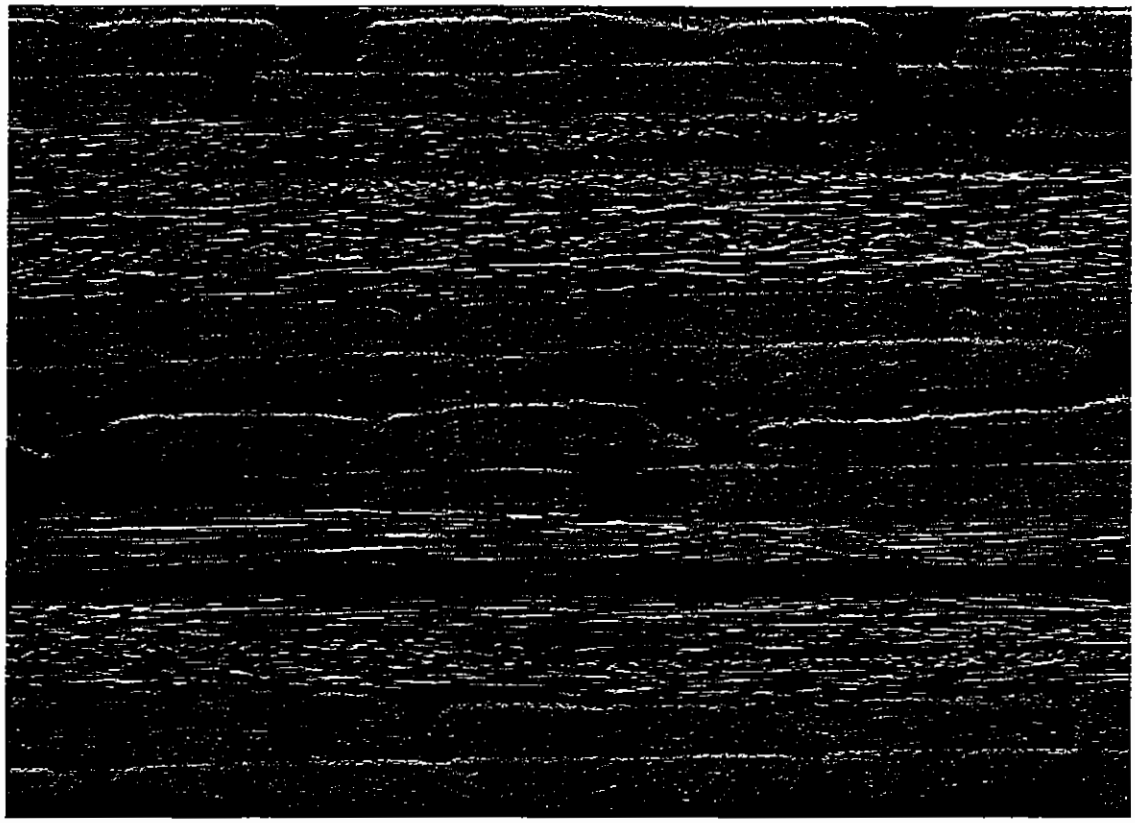

Figure 108: Material T8 Laminate cross section parallel to 0° fibres

Figure 109: Material T8 Laminate cross section perpendicular to 0° fibres

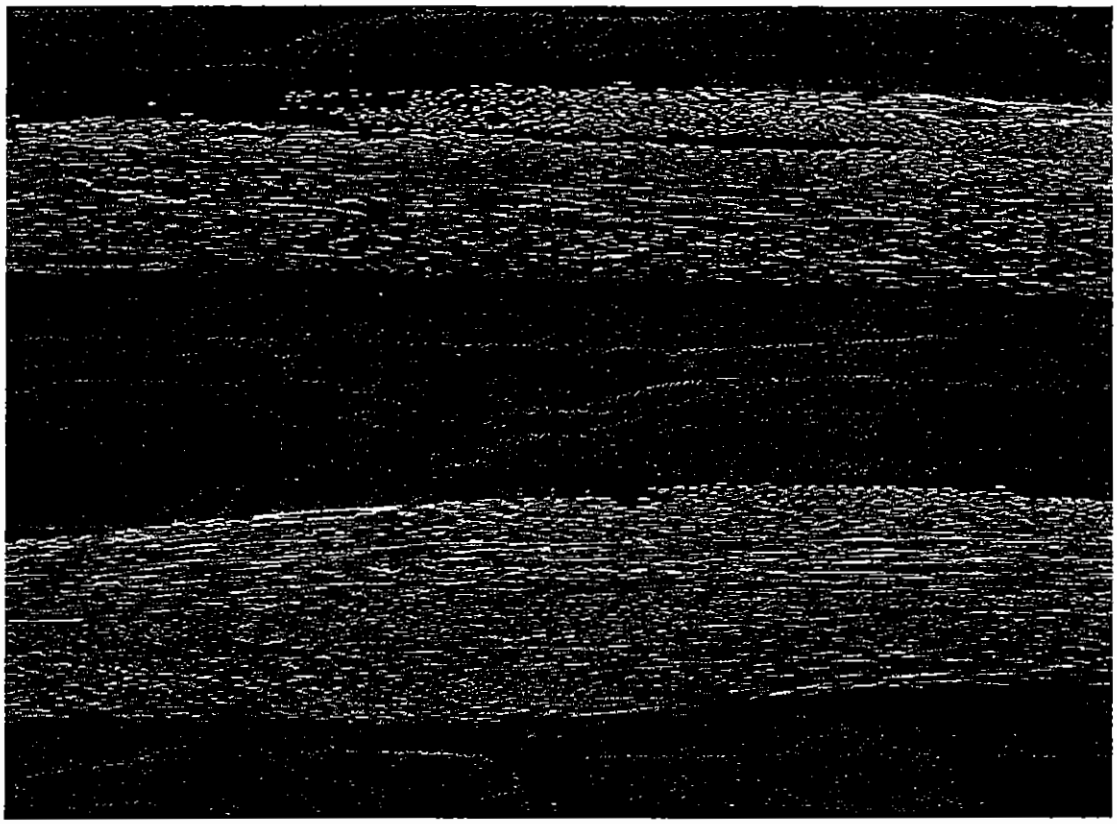

Figure 110: Material T9 Laminate cross section parallel to 0° fibres

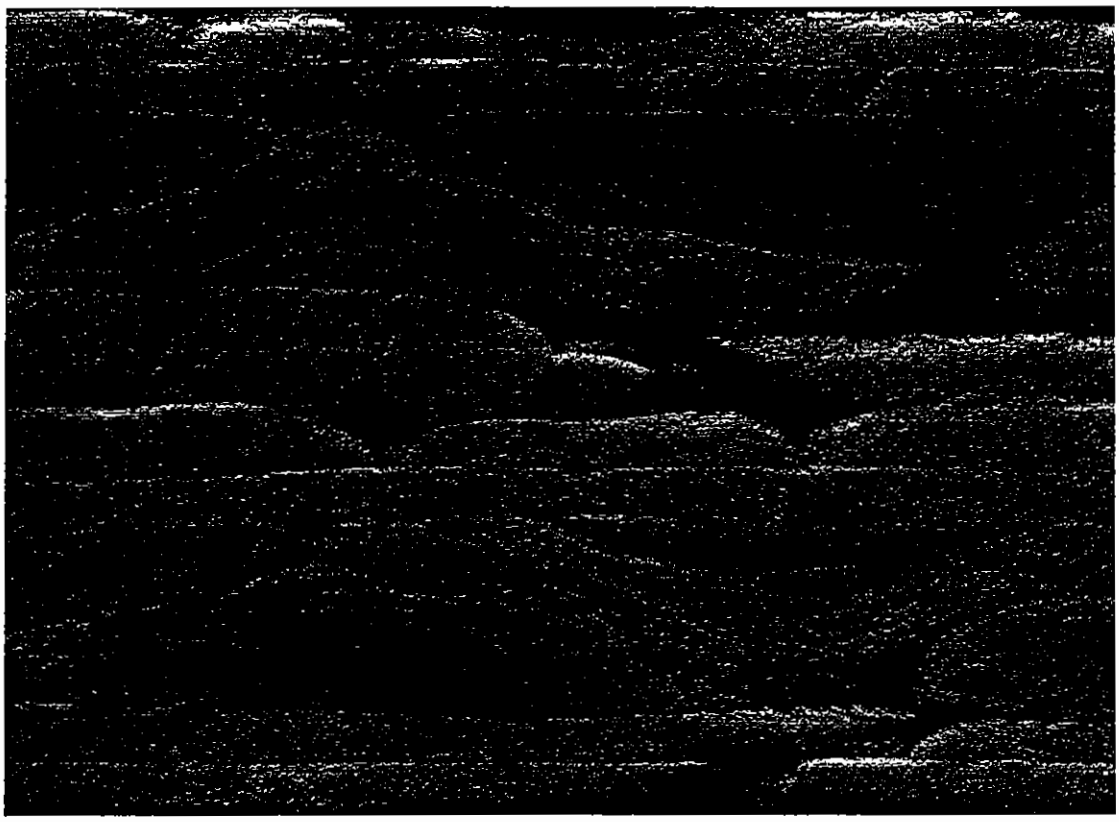

Figure 111: Material T9 Laminate cross section perpendicular to 0° fibres

6.2.1.1 Optical Microsection Visual Observations

As can be seen from Figure 94 to Figure 111 that there exists a broad range of microstructural differences both parallel and perpendicular to the 0° fibre tows. Little information on the 0° tow crimp can be usefully observed from these images and so observations are limited to that of the structure of the fibre bundles and of the resin rich areas and layers.

In Figure 99, Figure 101 and Figure 109 for materials T3, T4 and T8 that large resin layers can be seen running parallel with the 0° tows and caused by the incomplete 'nesting' of the adjacent 0° fibre tows. These were observed as gaps between tows in the dry-fabics in Chapter 5. In Figure 97, Figure 103 and Figure 107 for fabrics T2, 5 and 7 we can see that the 0° tows are more broken up and smaller resin layers are seen within the 0° layer. For fabrics T1, T6 and T9 we in most cases see distinct 0° tows and in Fabric T9 local bunching of the 0° tows due to the tight and infrequent stitching.

In the 45° layers we observe an increasing fineness of the small bundles of 45° fibres as the stitch course is increased. This is caused by the needles and stitching yarn separating the 6k tows into increasingly finer groups as the stitch course is increased. No increase in fibre breakage is observed in the images as the stitch course increases. Bunching of fibres due to the stitch loop is more pronounced on the external surface of the fabric and when the stitching tension is high.

Resin layers for all fabrics tend to be small and infrequent between layers of different orientations but as discussed tend to concentrate around the boundaries of fibre tows of the same orientation which are nested together. The polyester stitching/knitting yarn remains visible in the composite cross sections and tends to spread into a flat layer in those laminates with low stitching tension and to be more bunched where it is manufactured with a high stitching tension.

In the following sections detailed measurements related to the angular mis-orientation 'crimp' of the 0° fibre tows and the matrix resin distribution are presented which cannot readily be observed from the short microsections presented in the above figures.

6.2.2 Tow Crimp Results

Table 30: 0° Tow Crimp Angular Standard Deviation and Range

	Standard Deviation of Orientation °	Range of Orientation °
T1	2.29	14.10
T2	2.55	18.00
T3	2.00	12.67
T4	1.56	8.98
T5	2.12	14.05
T6	2.61	16.87
T7	2.21	15.03
T8	2.82	19.56
T9	2.73	18.08

Following are the summary results for each of the nine materials.

CTLX 816/Hexcel 914 - Designed Fabric (T1) 0° Tow-Crimp

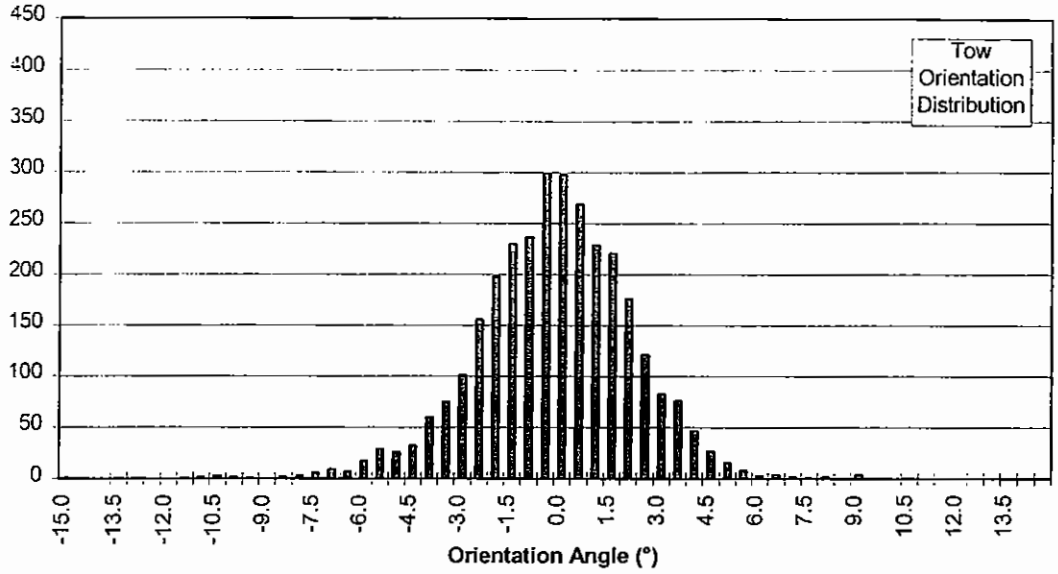

	Specimen	Tow 1	Tow 2	Tow 3	Tow 4	Tow 5	Tow 6	Tow 7	Tow 8
Mean	0.02	0.08	-0.03	0.06	0.03	0.09	0.04	-0.03	-0.06
SD	2.32	2.29	2.86	1.87	2.09	2.21	2.27	1.71	3.00
Min	-14.9	-5.6	-11.0	-6.3	-6.6	-7.5	-7.5	-5.9	-14.9
Max	11.0	6.8	11.0	4.7	4.2	5.4	4.4	4.4	6.7
Range	25.9	12.4	21.9	11.0	10.8	12.9	11.8	10.3	21.6

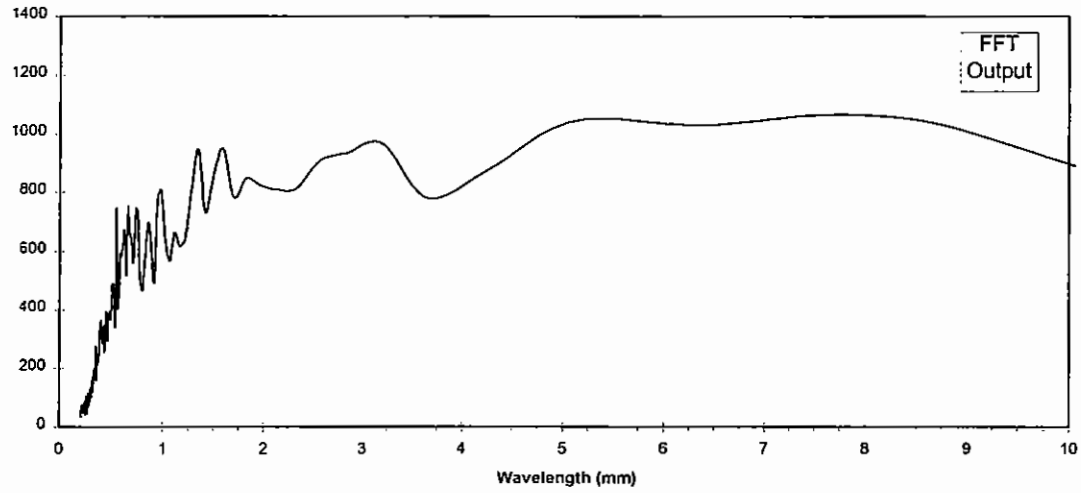

Dominant WaveLengths (mm) = 8.53
5.12

Mean Amplitude (microns) = 426

Amplitude SD (microns) = 3685

Figure 112: Material T1 0° Tow Crimp data summary

CTLX 816/Hexcel 914 - Designed Fabric (T2) 0° Tow-Crimp

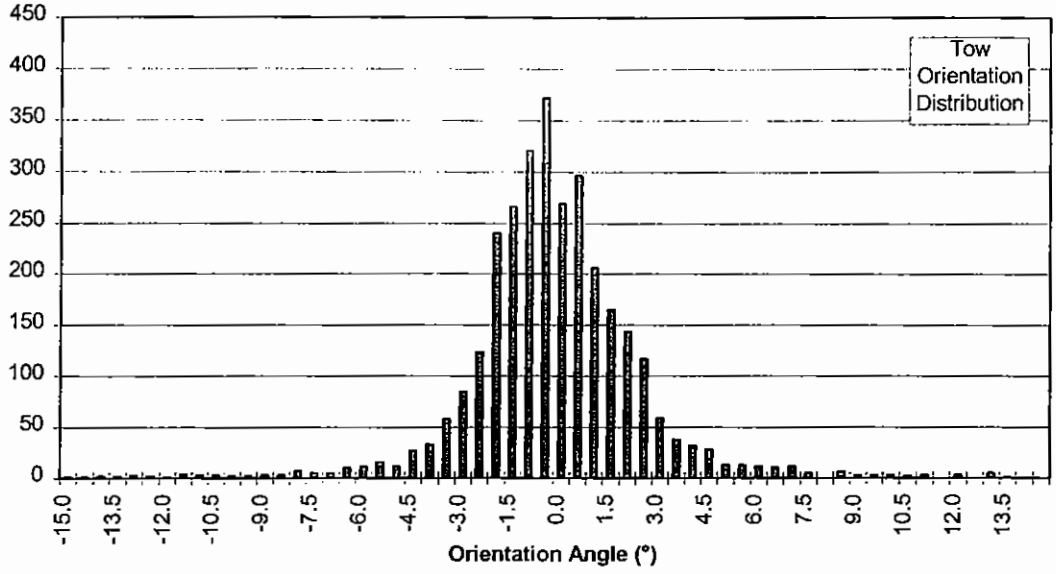

	Specimen	Tow 1	Tow 2	Tow 3	Tow 4	Tow 5	Tow 6	Tow 7	Tow 8
Mean	-0.03	-0.25	0.33	-0.12	-0.40	0.12	0.01	0.11	-0.02
SD	2.66	2.23	3.97	1.39	2.74	1.62	2.81	2.71	2.93
Min	-16.3	-8.5	-16.3	-2.7	-12.4	-5.1	-6.4	-7.8	-12.9
Max	13.6	7.8	13.6	4.6	11.3	7.1	7.7	13.4	6.4
Range	29.9	16.2	29.9	7.3	23.7	12.2	14.2	21.1	19.3

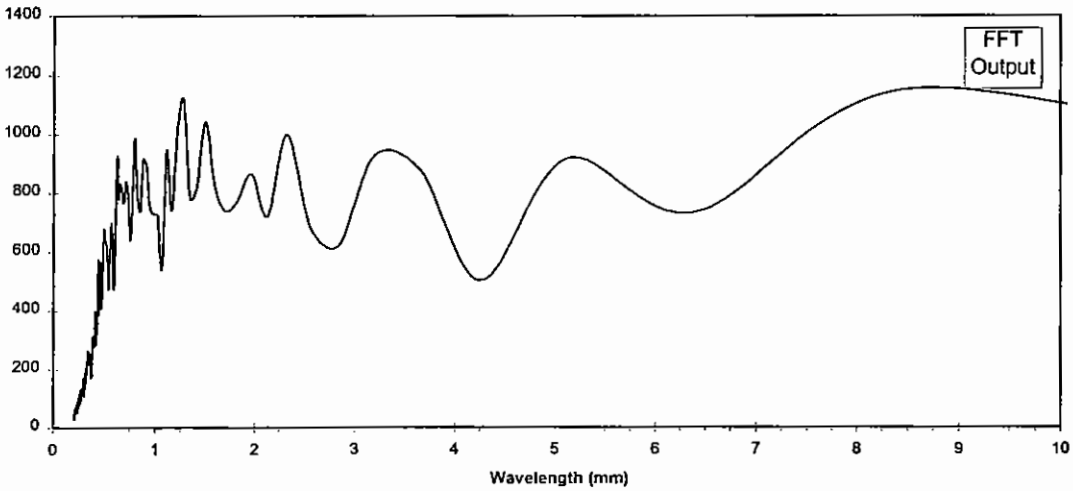

Dominant WaveLengths (mm) = 8.53
1.28

Mean Amplitude (microns) = 418

Amplitude SD (microns) = 3519

Figure 113: Material T2 0° Tow Crimp data summary

CTLX 816/Hexcel 914 - Designed Fabric (T3) 0° Tow-Crimp

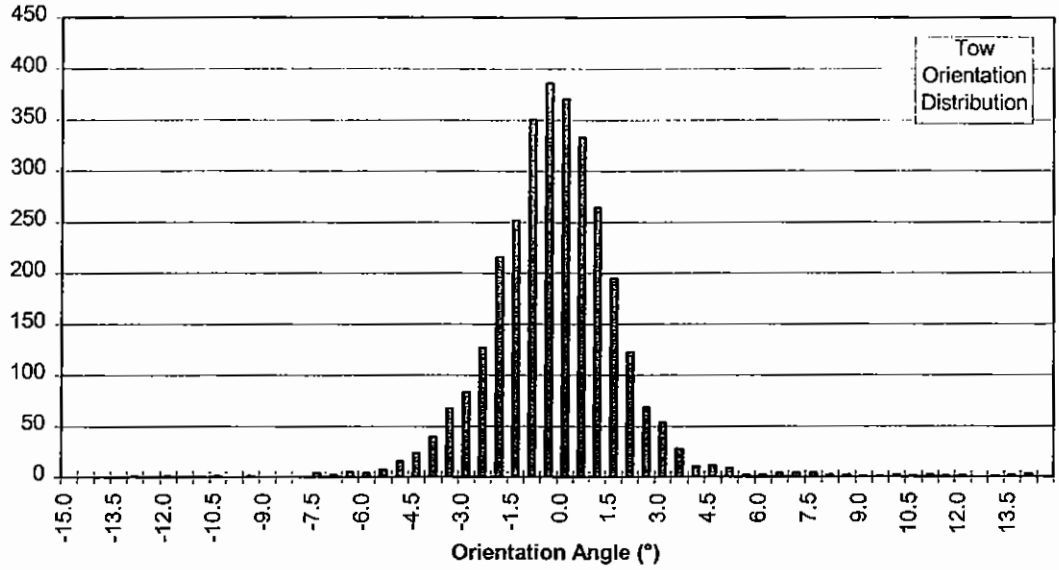

	Specimen	Tow 1	Tow 2	Tow 3	Tow 4	Tow 5	Tow 6	Tow 7	Tow 8
Mean	-0.04	-0.22	-0.21	-0.12	-0.13	0.30	-0.24	-0.06	0.33
SD	2.06	1.82	1.96	1.73	1.67	1.71	1.89	1.95	3.23
Min	-12.7	-4.8	-5.0	-3.9	-5.1	-4.4	-6.1	-12.7	-7.5
Max	17.3	4.3	7.8	3.6	3.8	7.1	5.1	2.8	17.3
Range	30.0	9.2	12.8	7.5	8.9	11.5	11.2	15.4	24.8

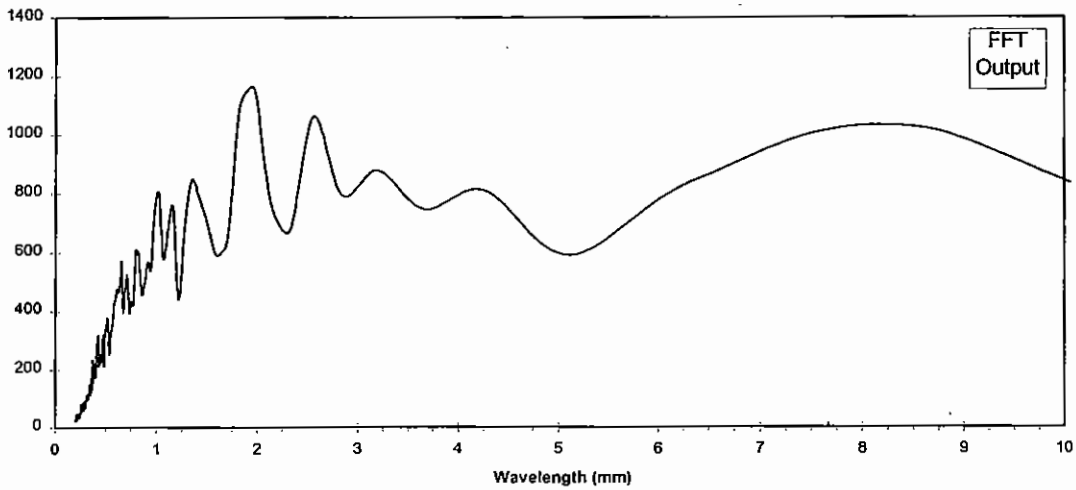

Dominant WaveLengths (mm) = 1.97
2.56

Mean Amplitude (microns) = 43

Amplitude SD (microns) = 39

Figure 114: Material T3 0° Tow Crimp data summary

CTLX 816/Hexcel 914 - Designed Fabric (T4) 0° Tow-Crimp

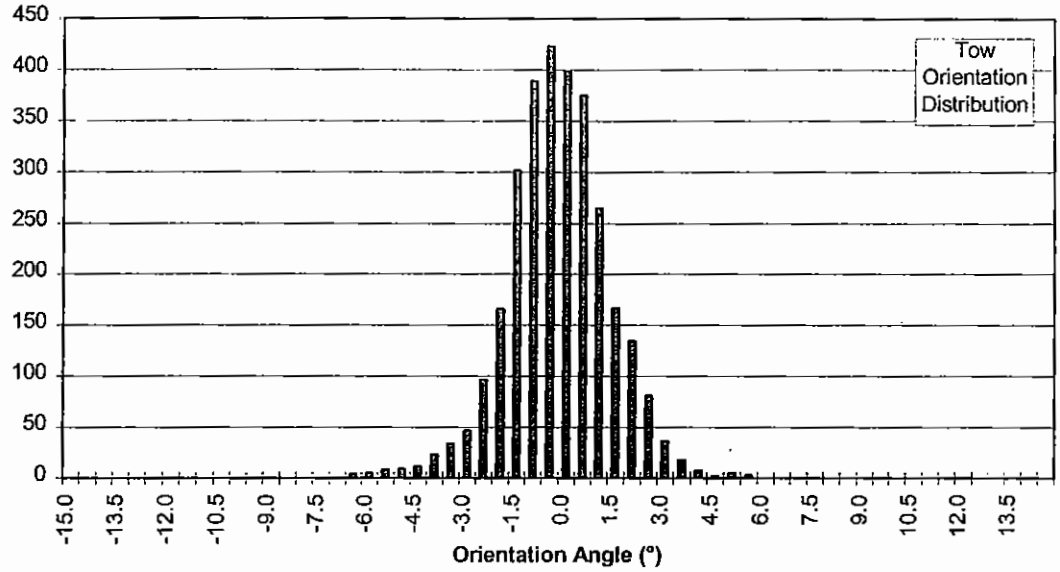

	Specimen	Tow 1	Tow 2	Tow 3	Tow 4	Tow 5	Tow 6	Tow 7	Tow 8
Mean	-0.09	-0.28	-0.09	-0.20	-0.05	-0.16	0.02	0.00	0.03
SD	1.58	1.71	1.60	1.94	1.31	1.75	1.19	1.52	1.48
Min	-6.4	-6.4	-4.4	-6.0	-4.0	-6.3	-2.7	-5.0	-4.7
Max	6.0	3.6	3.6	6.0	3.4	5.4	3.2	3.5	3.9
Range	12.4	10.0	7.9	11.9	7.3	11.7	5.9	8.5	8.5

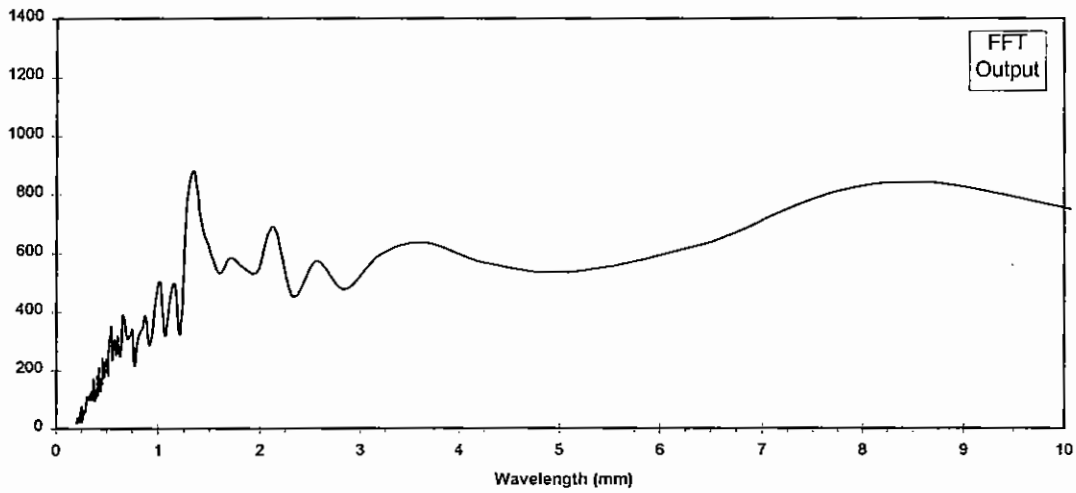

Dominant WaveLengths (mm) = 1.35
8.53

Mean Amplitude (microns) = 277

Amplitude SD (microns) = 2842

Figure 115: Material T4 0° Tow Crimp data summary

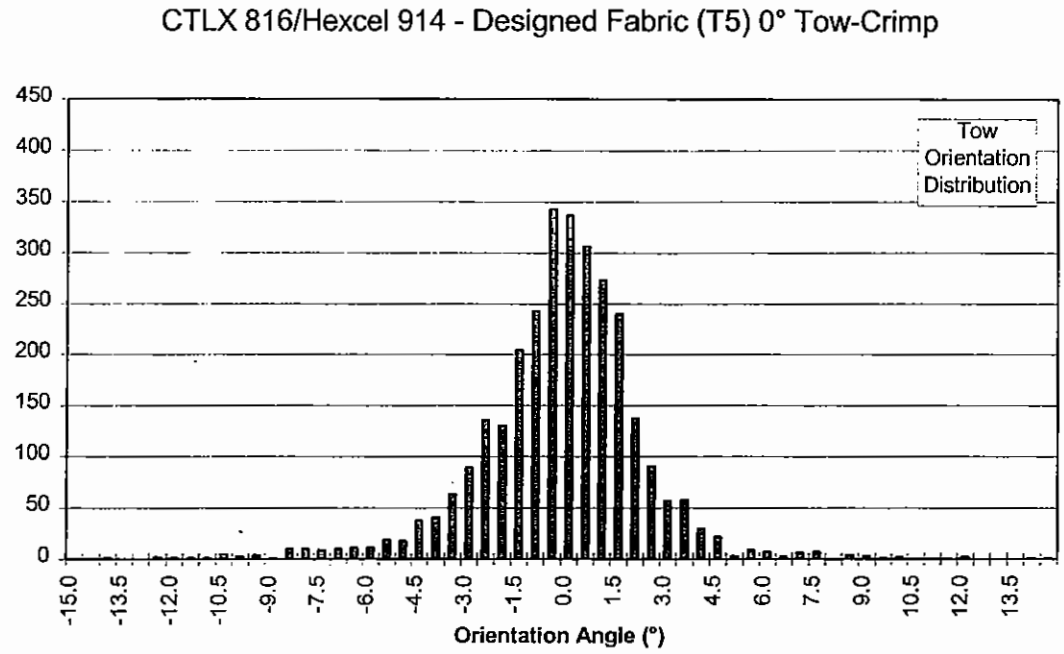

	Specimen	Tow 1	Tow 2	Tow 3	Tow 4	Tow 5	Tow 6	Tow 7	Tow 8
Mean	0.22	0.05	0.67	0.20	0.49	0.14	0.27	-0.09	0.00
SD	2.17	2.38	2.19	2.09	2.53	2.25	1.39	2.62	1.53
Min	-12.0	-7.5	-3.9	-8.4	-9.3	-10.3	-2.5	-12.0	-7.7
Max	10.2	8.7	10.2	6.4	9.3	3.7	5.7	4.3	2.6
Range	22.2	16.1	14.0	14.8	18.6	14.0	8.2	16.3	10.3

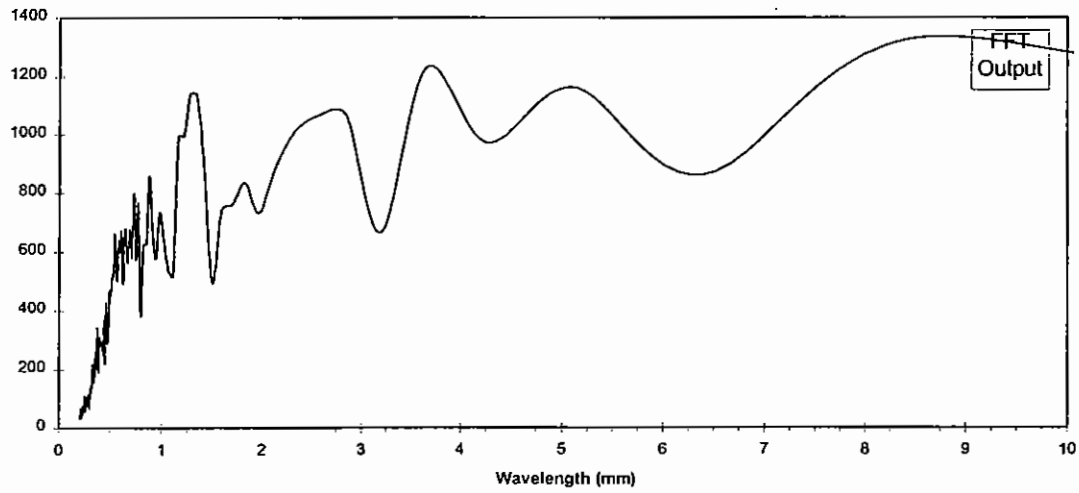

Dominant WaveLengths (mm) = 8.53
3.66

Mean Amplitude (microns) = 50

Amplitude SD (microns) = 49

Figure 116: Material T5 0° Tow Crimp data summary

CTLX 816/Hexcel 914 - Designed Fabric (T6) 0° Tow-Crimp

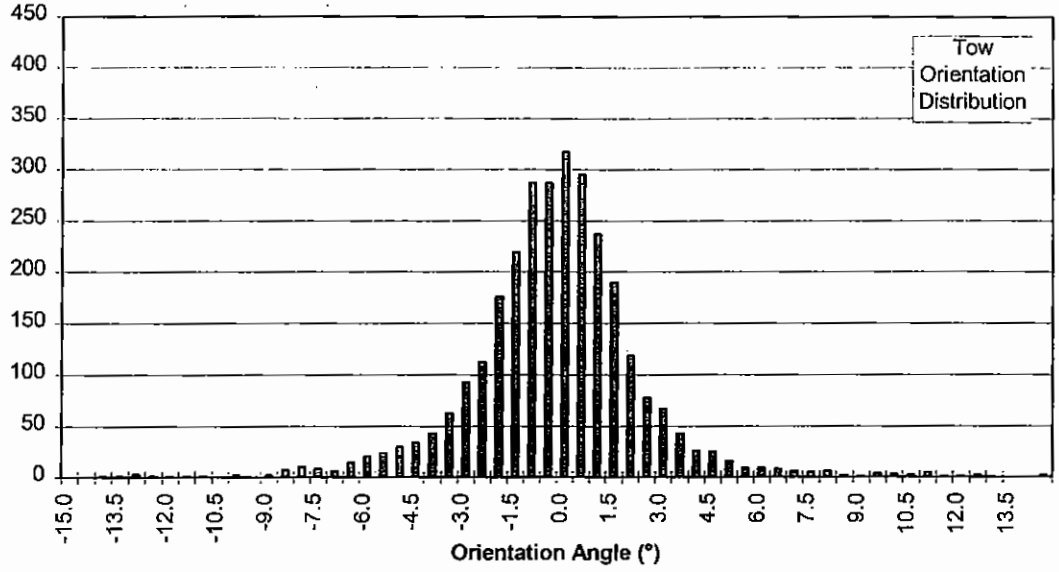

	Specimen	Tow 1	Tow 2	Tow 3	Tow 4	Tow 5	Tow 6	Tow 7	Tow 8
Mean	-0.07	0.00	0.11	-0.56	0.10	-0.14	-0.07	0.14	-0.10
SD	2.75	2.11	3.50	2.34	2.33	1.62	3.27	1.63	4.12
Min	-13.8	-6.5	-8.4	-6.7	-7.9	-5.8	-13.8	-4.0	-12.8
Max	19.6	4.6	11.7	6.4	9.5	4.4	8.5	4.5	19.6
Range	33.4	11.1	20.1	13.0	17.4	10.2	22.3	8.5	32.3

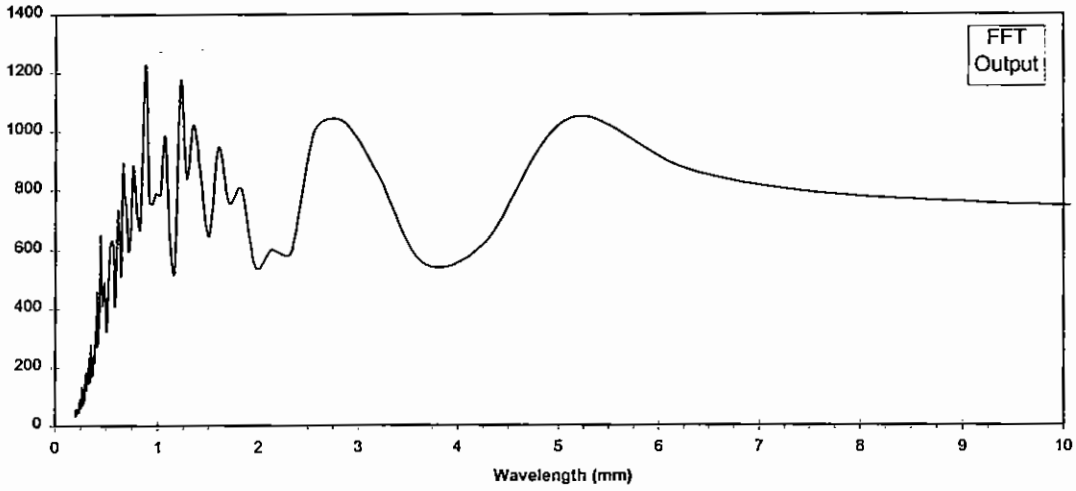

Dominant WaveLengths (mm) = 0.88
1.22

Mean Amplitude (microns) = 222

Amplitude SD (microns) = 2378

Figure 117: Material T6 0° Tow Crimp data summary

CTLX 816/Hexcel 914 - Designed Fabric (T7) 0° Tow-Crimp

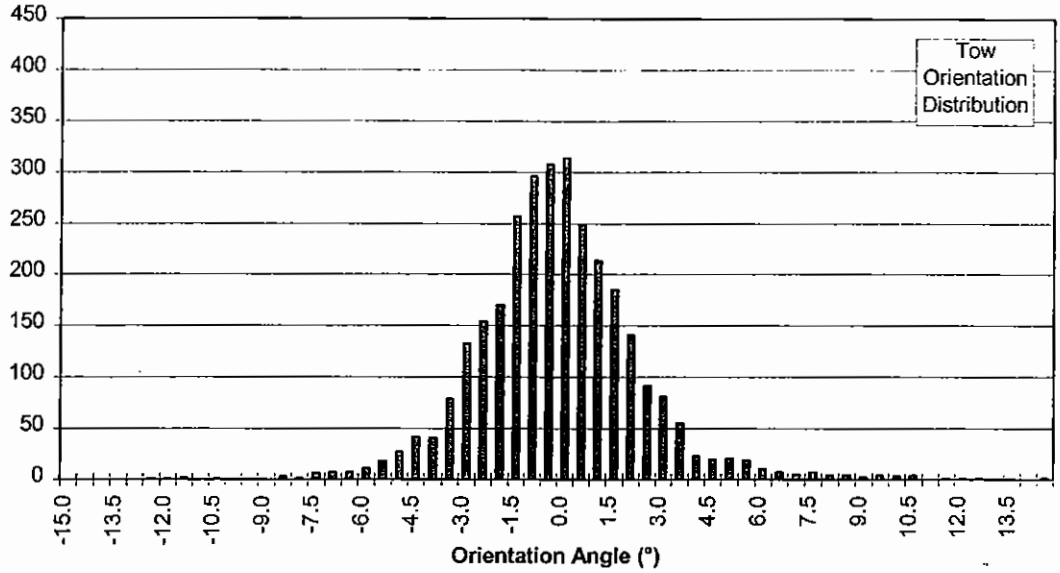

	Specimen	Tow 1	Tow 2	Tow 3	Tow 4	Tow 5	Tow 6	Tow 7	Tow 8
Mean	-0.12	-0.35	0.16	-0.31	-0.18	0.11	-0.10	0.16	-0.48
SD	2.30	3.33	1.92	1.97	2.29	1.80	1.38	3.00	1.97
Min	-16.1	-16.1	-3.9	-8.1	-4.0	-5.6	-5.0	-11.4	-5.3
Max	14.6	10.3	6.1	6.1	14.6	5.2	3.8	9.3	5.3
Range	30.8	26.4	10.0	14.2	18.6	10.9	8.8	20.8	10.6

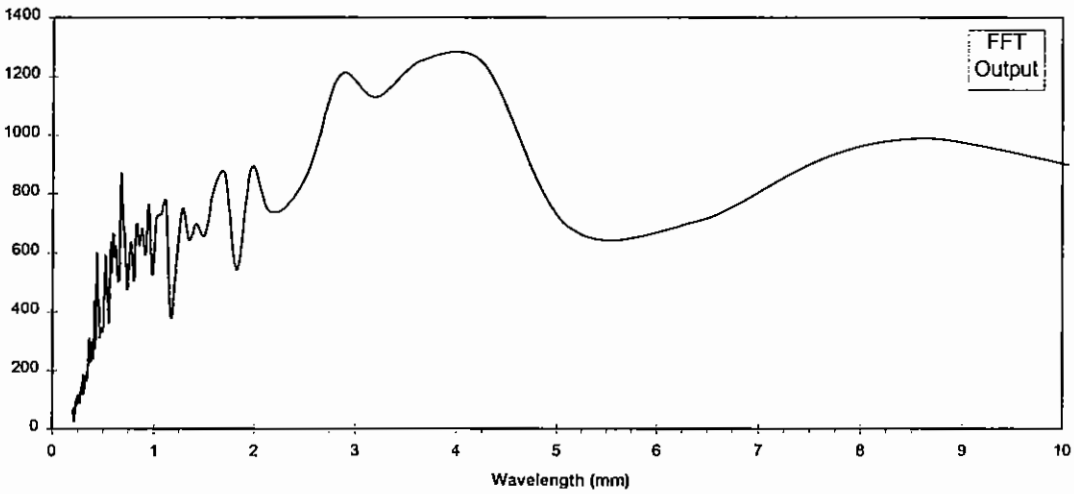

Dominant WaveLengths (mm) = 3.66
2.84

Mean Amplitude (microns) = 48

Amplitude SD (microns) = 42

Figure 118: Material T7 0° Tow Crimp data summary

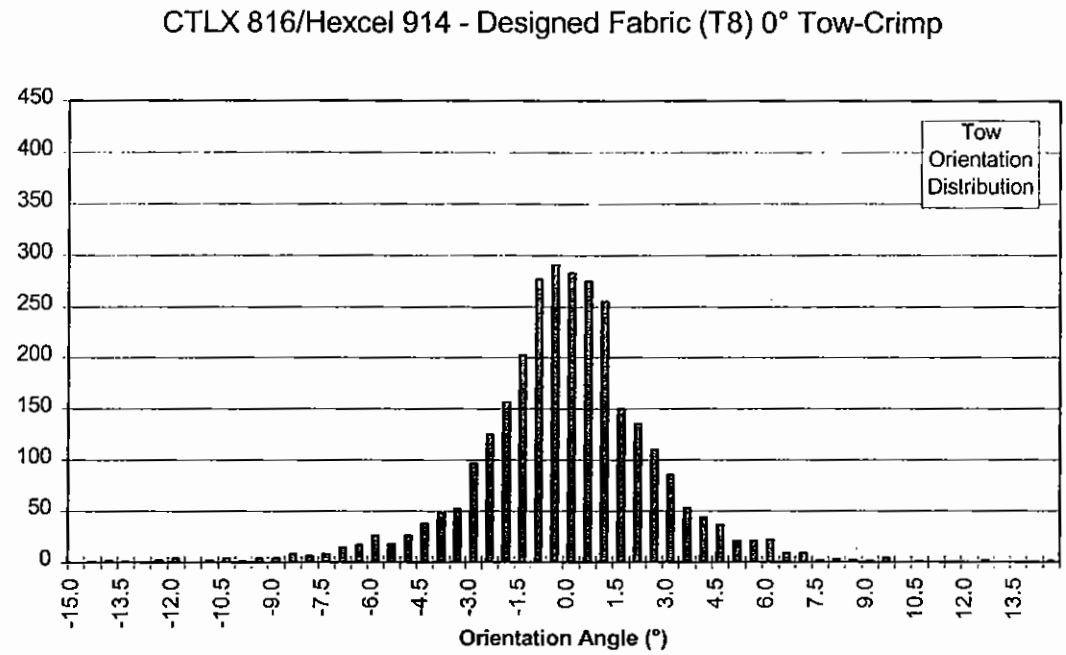

	Specimen	Tow 1	Tow 2	Tow 3	Tow 4	Tow 5	Tow 6	Tow 7	Tow 8
Mean	0.05	0.15	0.12	0.19	0.06	0.10	-0.06	-0.27	0.07
SD	2.84	2.61	2.58	2.30	3.09	2.52	3.41	3.01	3.05
Min	-16.3	-6.7	-8.3	-7.4	-13.8	-10.3	-10.7	-16.3	-12.4
Max	14.6	14.6	7.4	10.6	9.8	6.1	8.6	6.3	7.0
Range	30.9	21.4	15.7	18.0	23.7	16.4	19.4	22.6	19.4

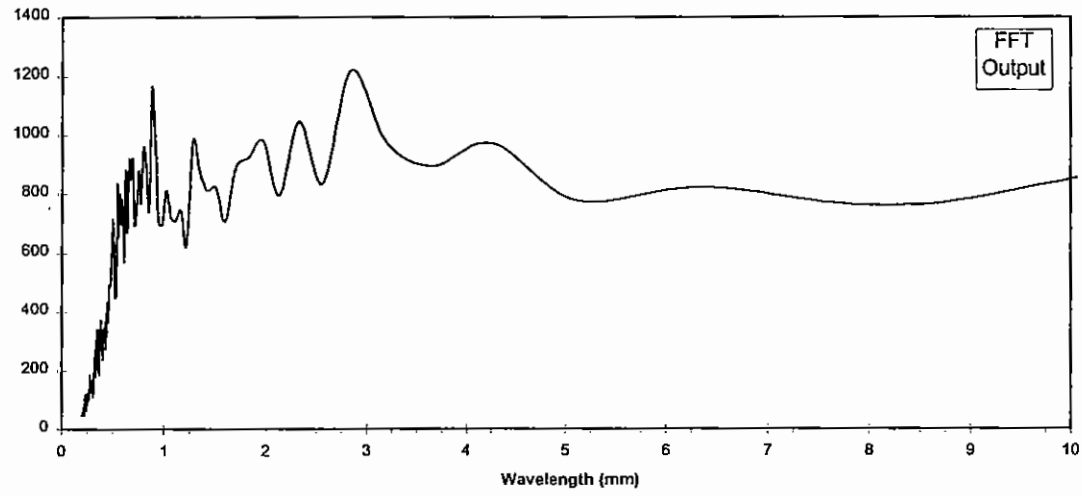

Dominant WaveLengths (mm) = 2.84
0.88

Mean Amplitude (microns) = 737

Amplitude SD (microns) = 4945

Figure 119: Material T8 0° Tow Crimp data summary

CTLX 816/Hexcel 914 - Designed Fabric (T9) 0° Tow-Crimp

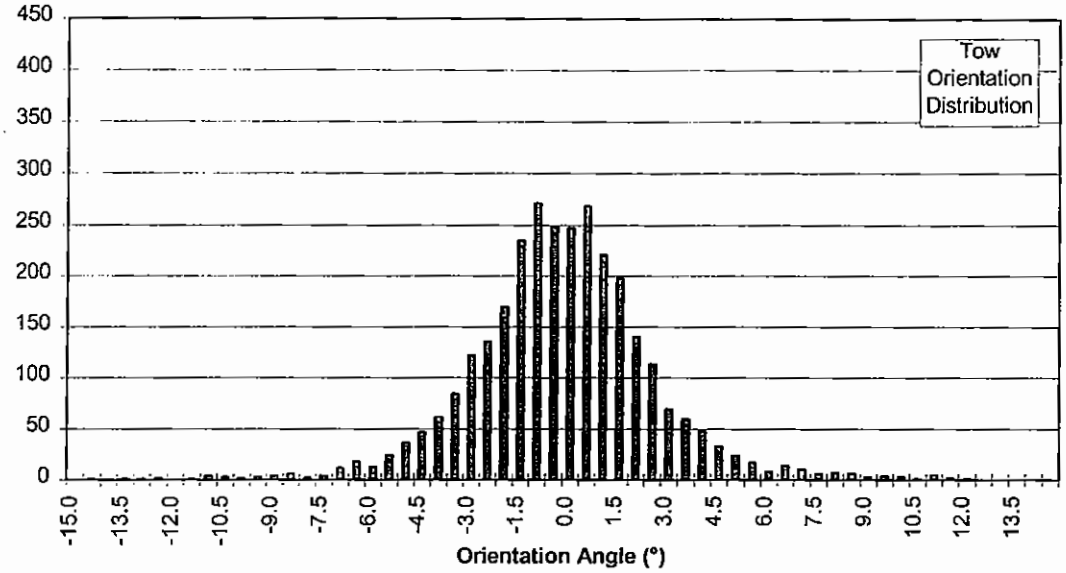

	Specimen	Tow 1	Tow 2	Tow 3	Tow 4	Tow 5	Tow 6	Tow 7	Tow 8
Mean	0.18	-0.16	0.66	0.14	0.23	0.23	0.06	0.08	0.18
SD	2.80	3.23	3.29	3.18	2.42	1.91	3.14	1.69	2.97
Min	-15.3	-13.0	-6.8	-15.3	-8.0	-4.0	-10.9	-6.6	-10.3
Max	12.2	12.2	11.4	9.9	8.7	5.9	11.7	2.9	6.9
Range	27.6	25.2	18.2	25.3	16.7	9.9	22.6	9.5	17.2

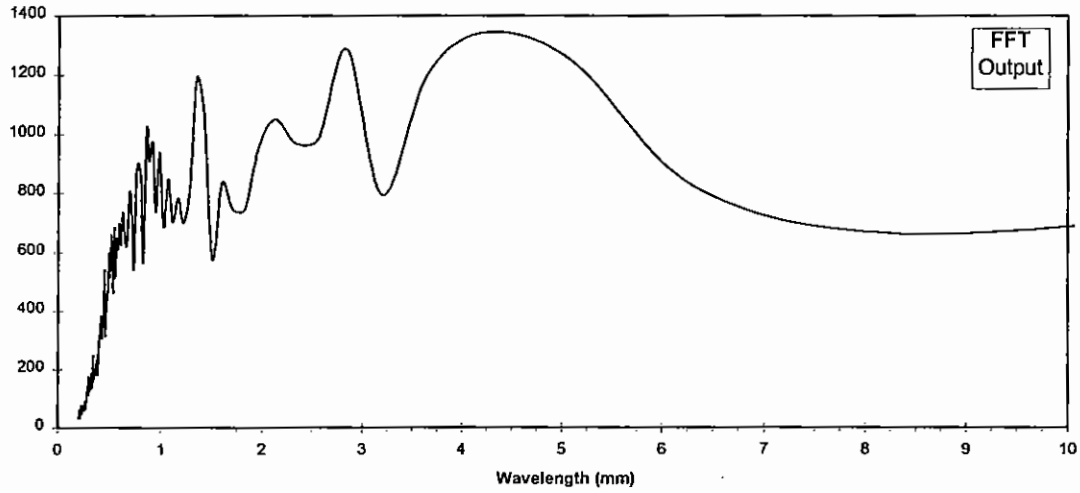

Dominant WaveLengths (mm) = 4.27
2.84

Mean Amplitude (microns) = 52

Amplitude SD (microns) = 38

Figure 120: Material T9 0° Tow Crimp data summary

6.2.2.1 Observations

The histograms of tow mis-orientation occurrence show some differences for the nine materials tested. Material T4 has the most precisely oriented tows, having the smallest standard deviation and lowest range. Its manufacturing settings are; bunched 0° tows, high stitch course and low stitching tension. T9 conversely has the

6.2.2.2 Effect of Fabric Manufacturing Settings

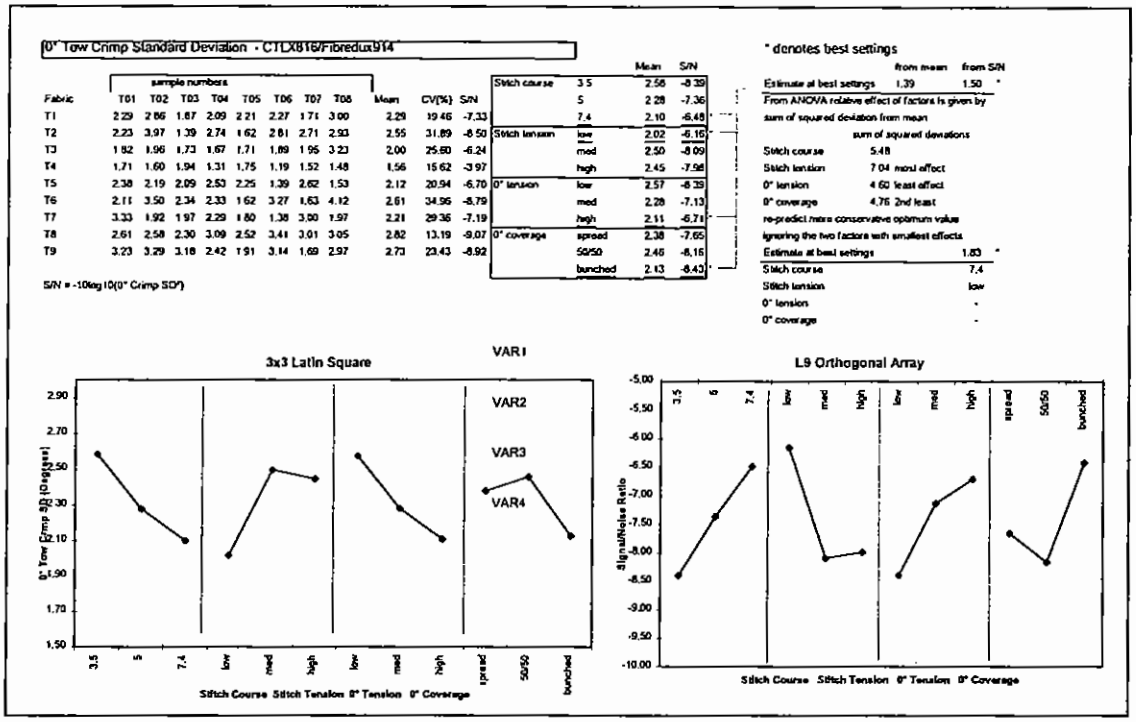

Figure 122: 0° Tow Crimp Angular Standard Deviation Results Summary

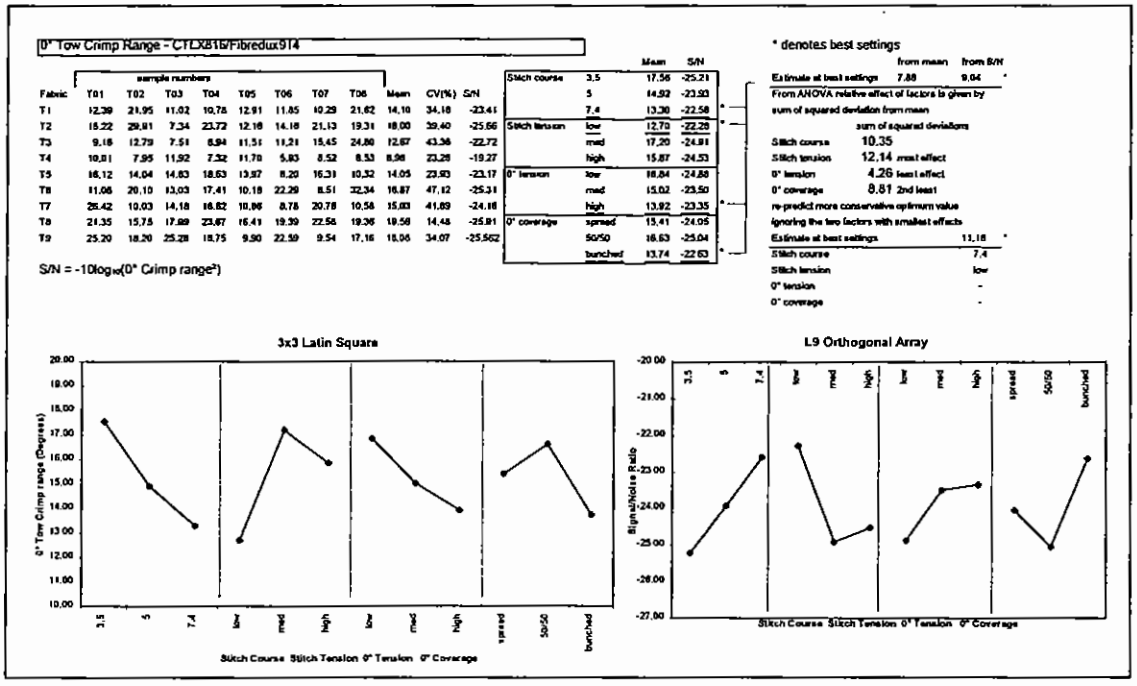

Figure 123: 0° Tow Crimp Angular Deviation Range Results Summary

The magnitude of the effect of the different LIBA machine parameters on both the standard deviation and its range is similar, with stitch tension and stitch course having slightly more effect. Increasing stitch course progressively reduces the angular deviation and range; a similar response is observed with increasing the 0° tension. A low stitch tension is much preferred to either the medium or high settings. The 50/50 split of the 0° coverage is detrimental to both standard deviation and range; not expected as the compression strength is maximised with this setting. It

would therefore appear that the 0° crimp is minimised when the 0° tows are inlayed tight, and consequently straightened, fully cradled by as much stitching yarn as possible, but only held loosely so as not to induce crimp by adversely bunching the fibre tows.

6.2.3 Resin Distribution

Table 31: Resin Distribution Results

	Free Resin Volume %	Mean resin area μm²	Maximum resin area μm²	Mean resin layer thickness μm
T1	11.4	77000	503000	44.3
T2	13.5	64000	377000	51.0
T3	14.9	132000	717000	52.9
T4	18.2	101000	831000	57.2
T5	15.2	72000	549000	58.1
T6	19.5	65000	540000	56.3
T7	9.8	60000	324000	51.2
T8	15.5	155000	1046000	51.4
T9	13.8	116000	767000	50.0

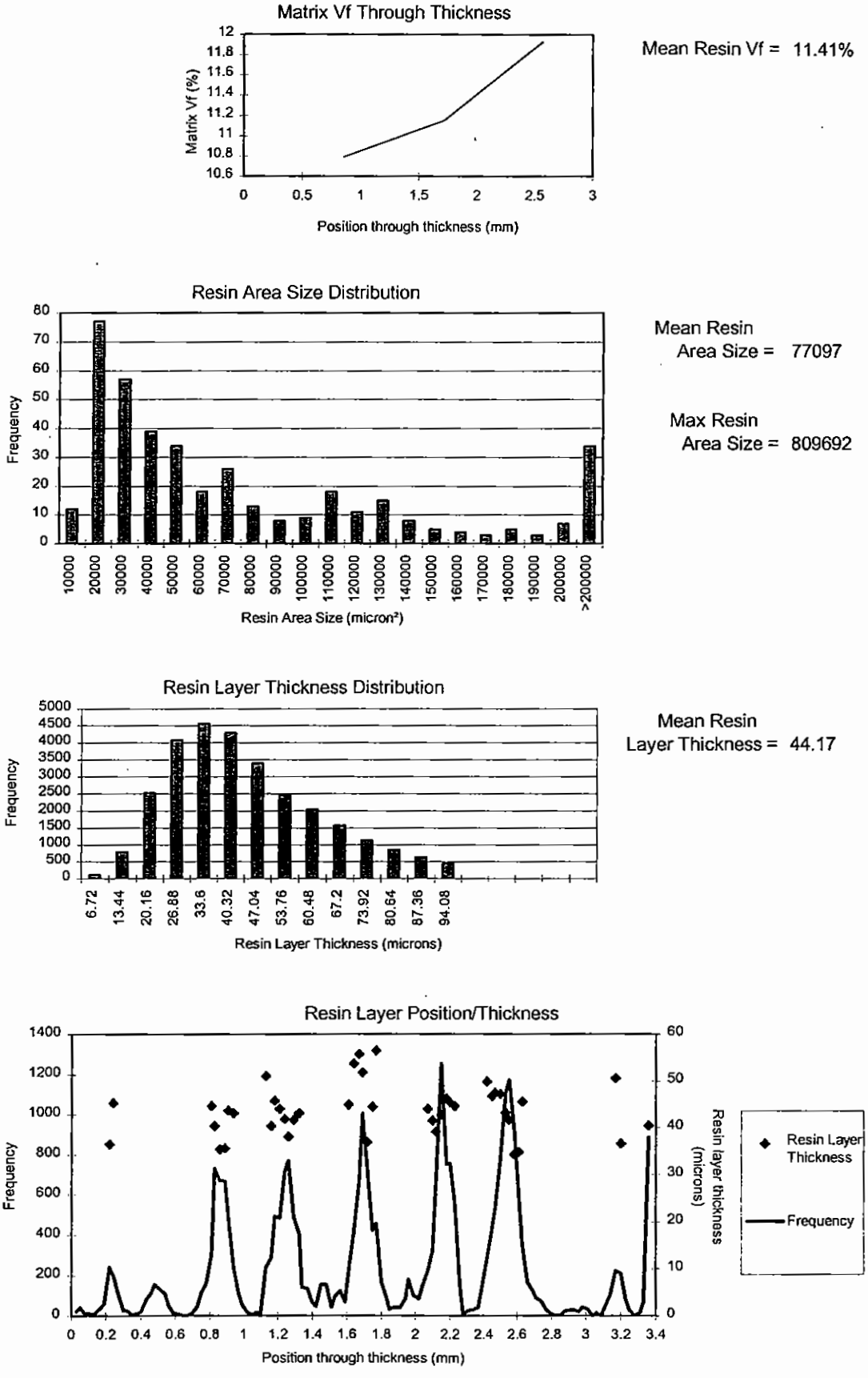

Figure 124 :Material T1 Resin Distribution data summary

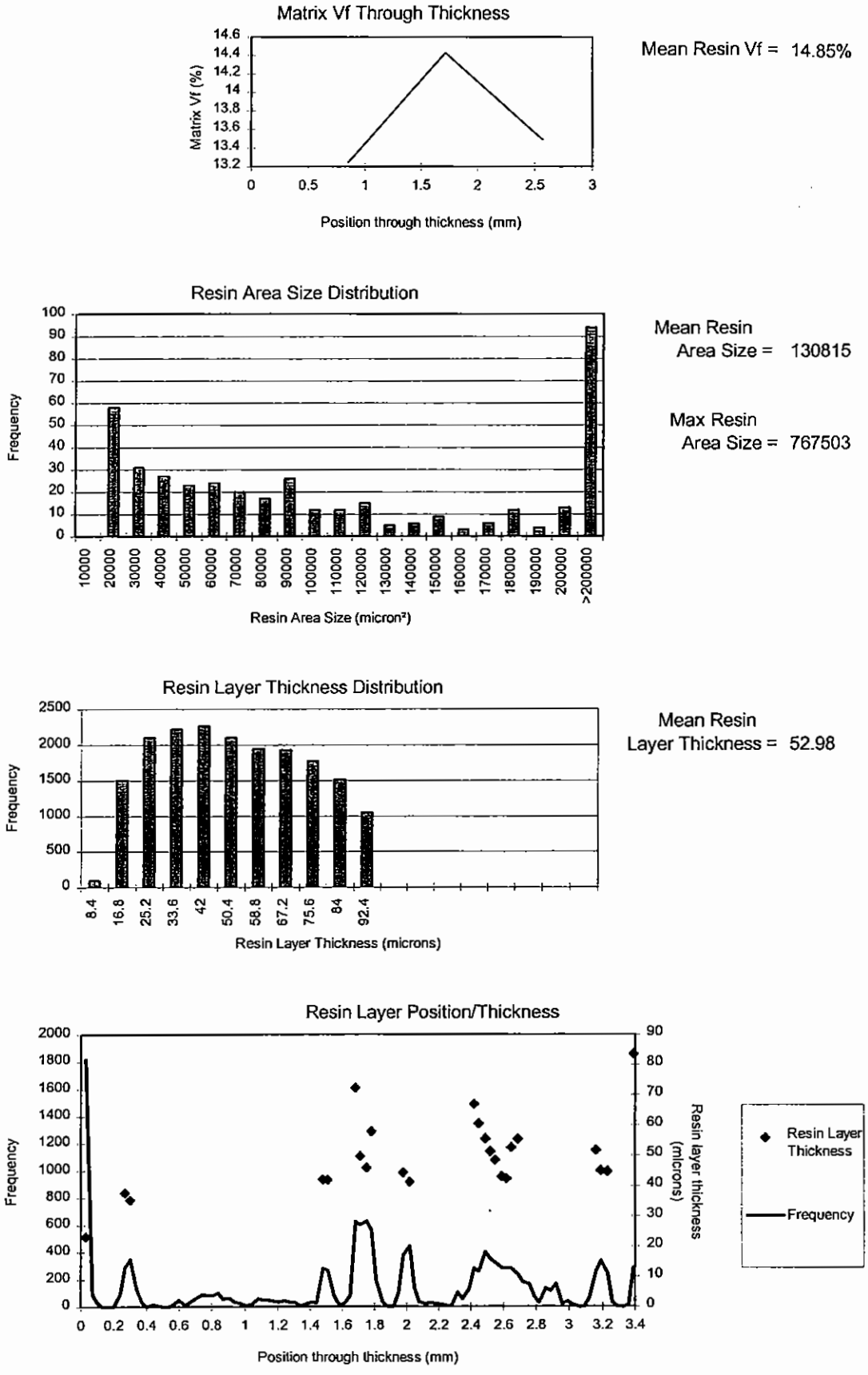

Figure 126:Material T3 Resin Distribution data summary

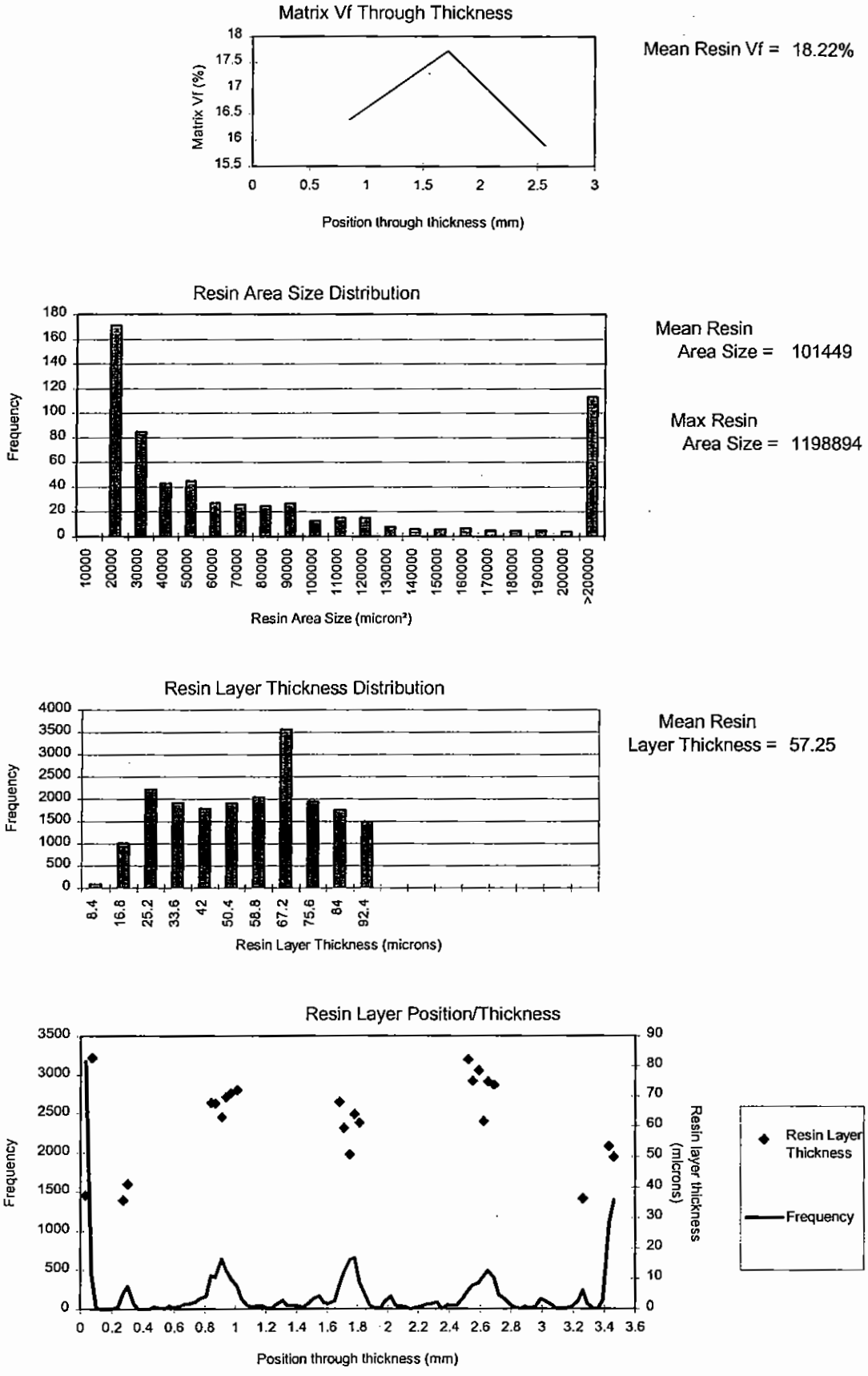

Figure 127 :Material T4 Resin Distribution data summary

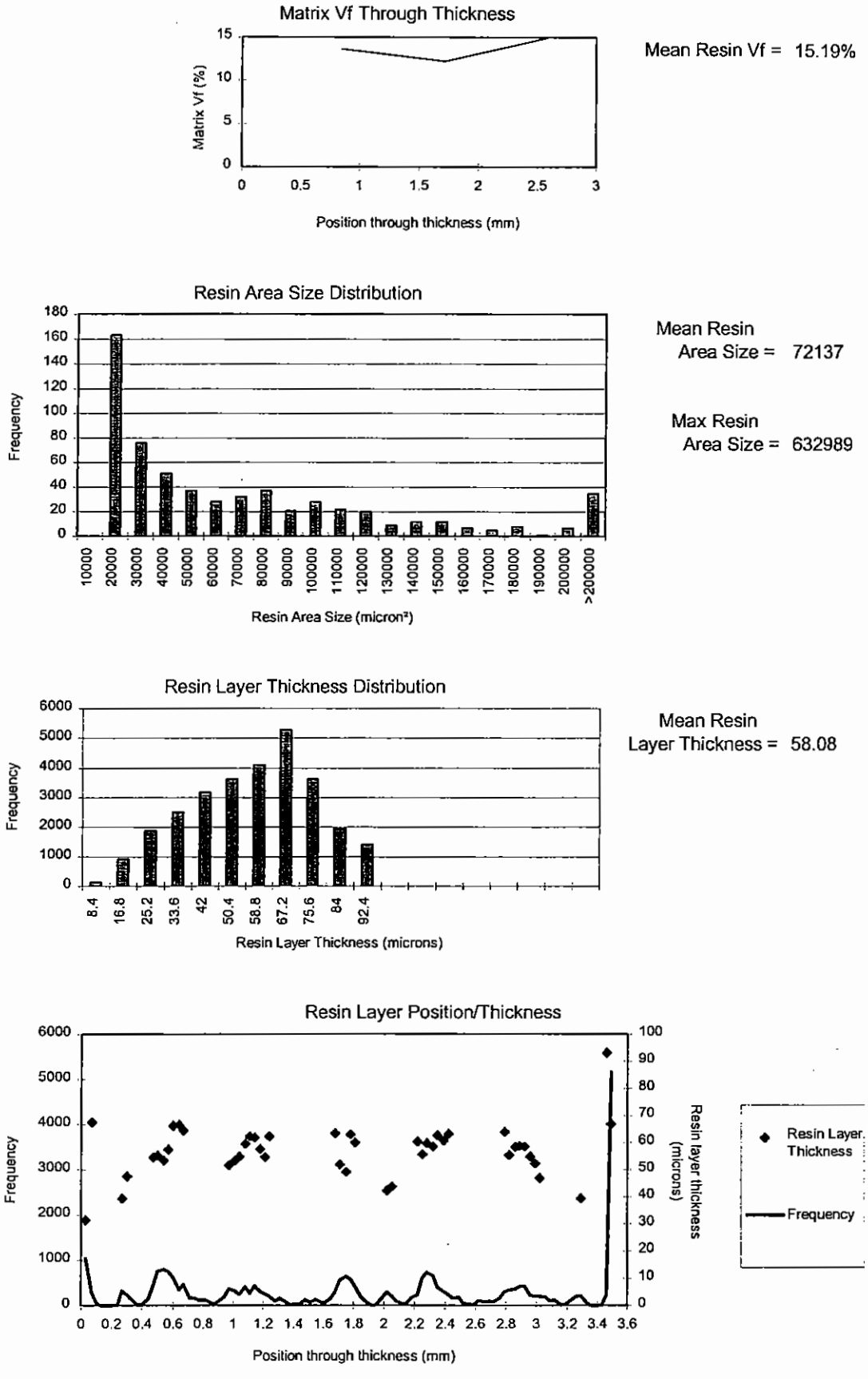

Figure 128 :Material T5 Resin Distribution data summary

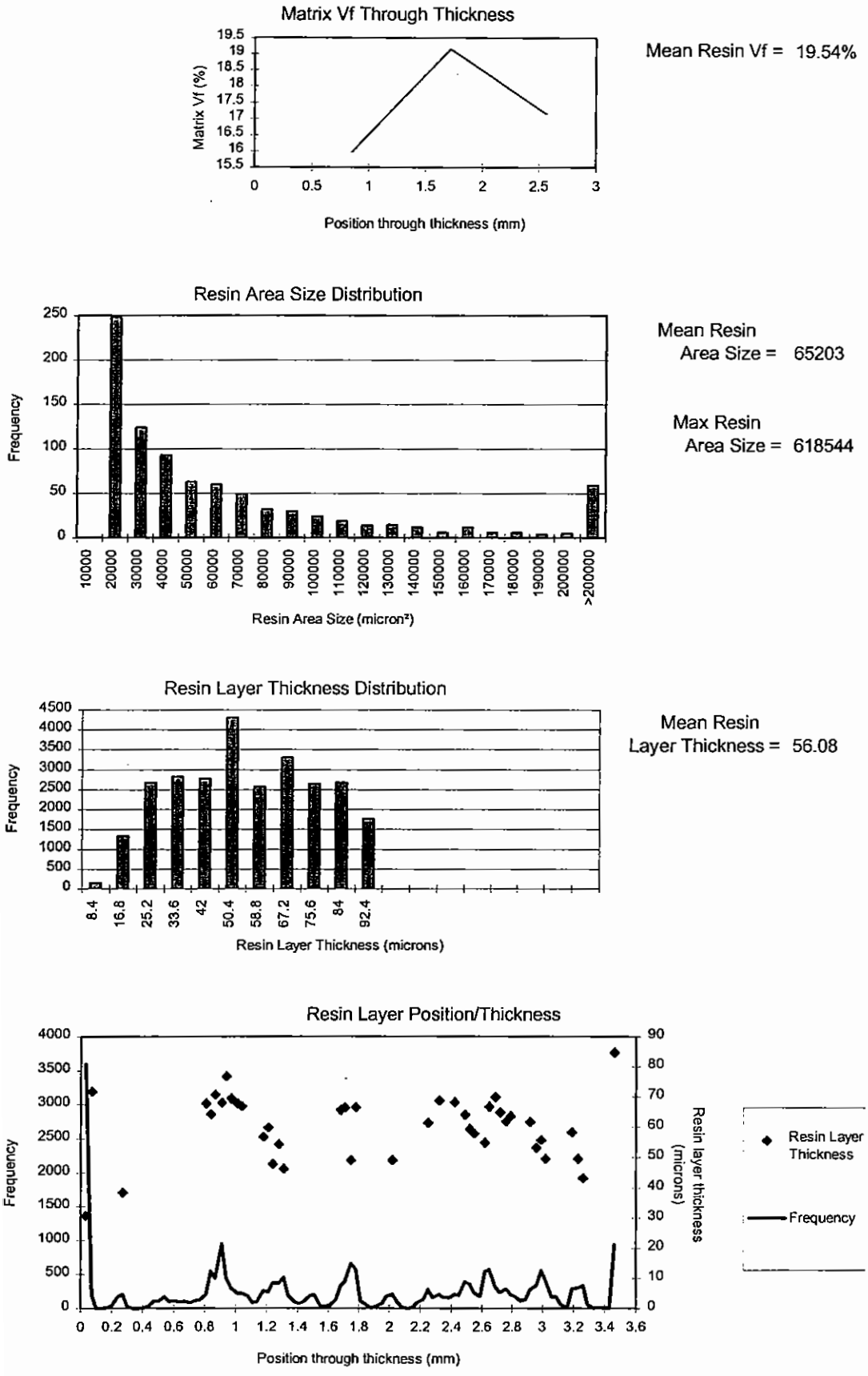

Figure 129 :Material T6 Resin Distribution data summary

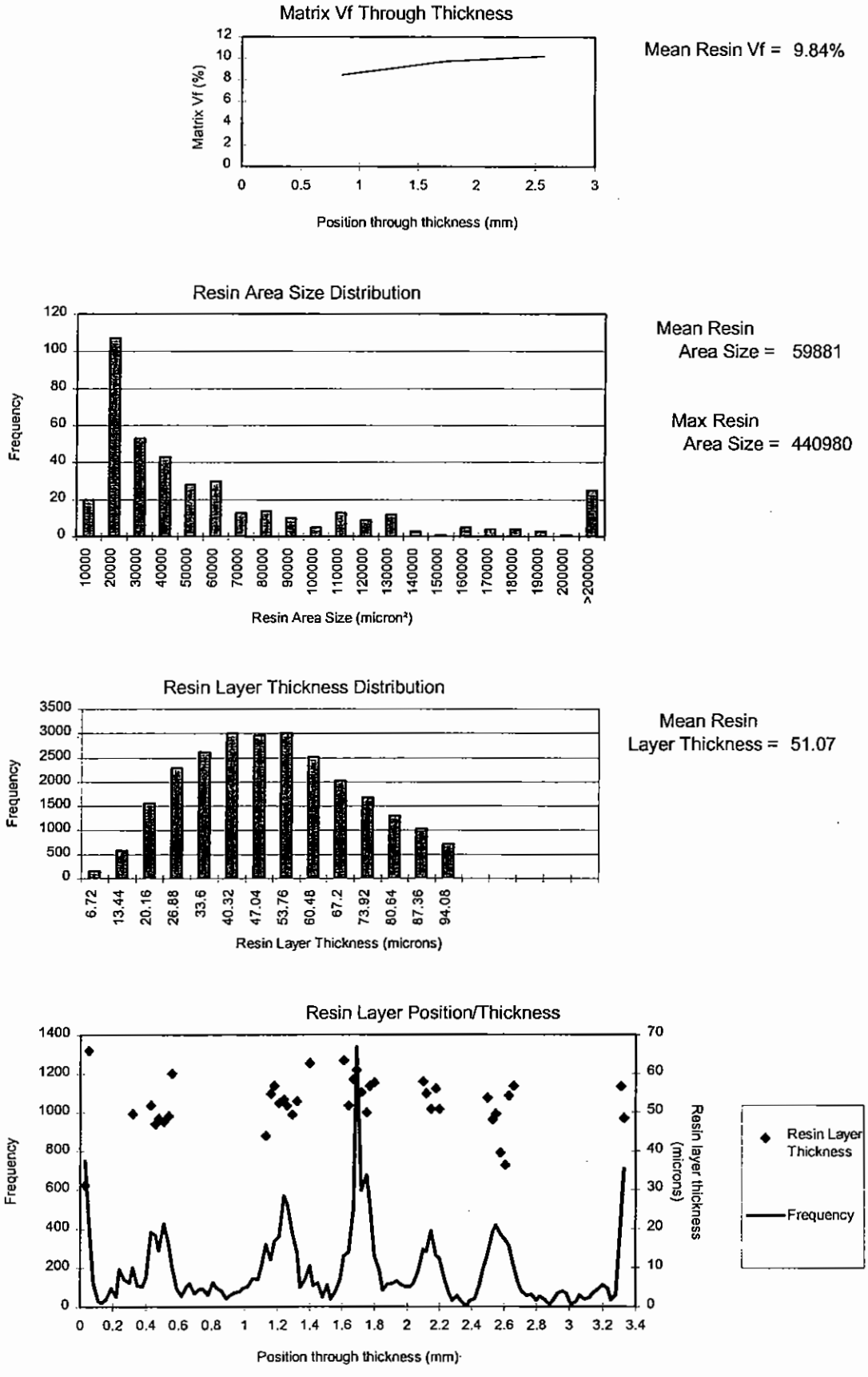

Figure 130 :Material T7 Resin Distribution data summary

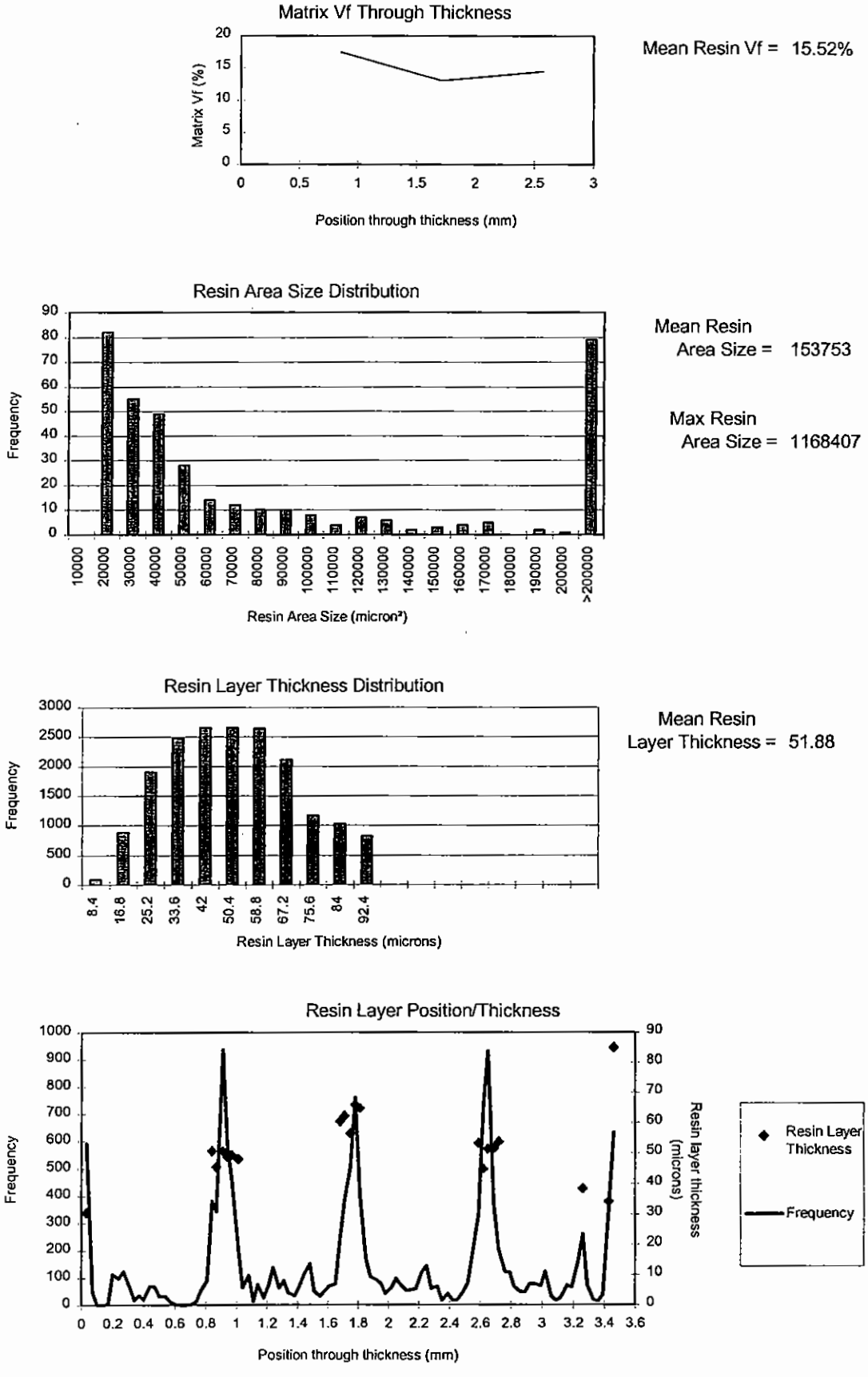

Figure 131 :Material T8 Resin Distribution data summary

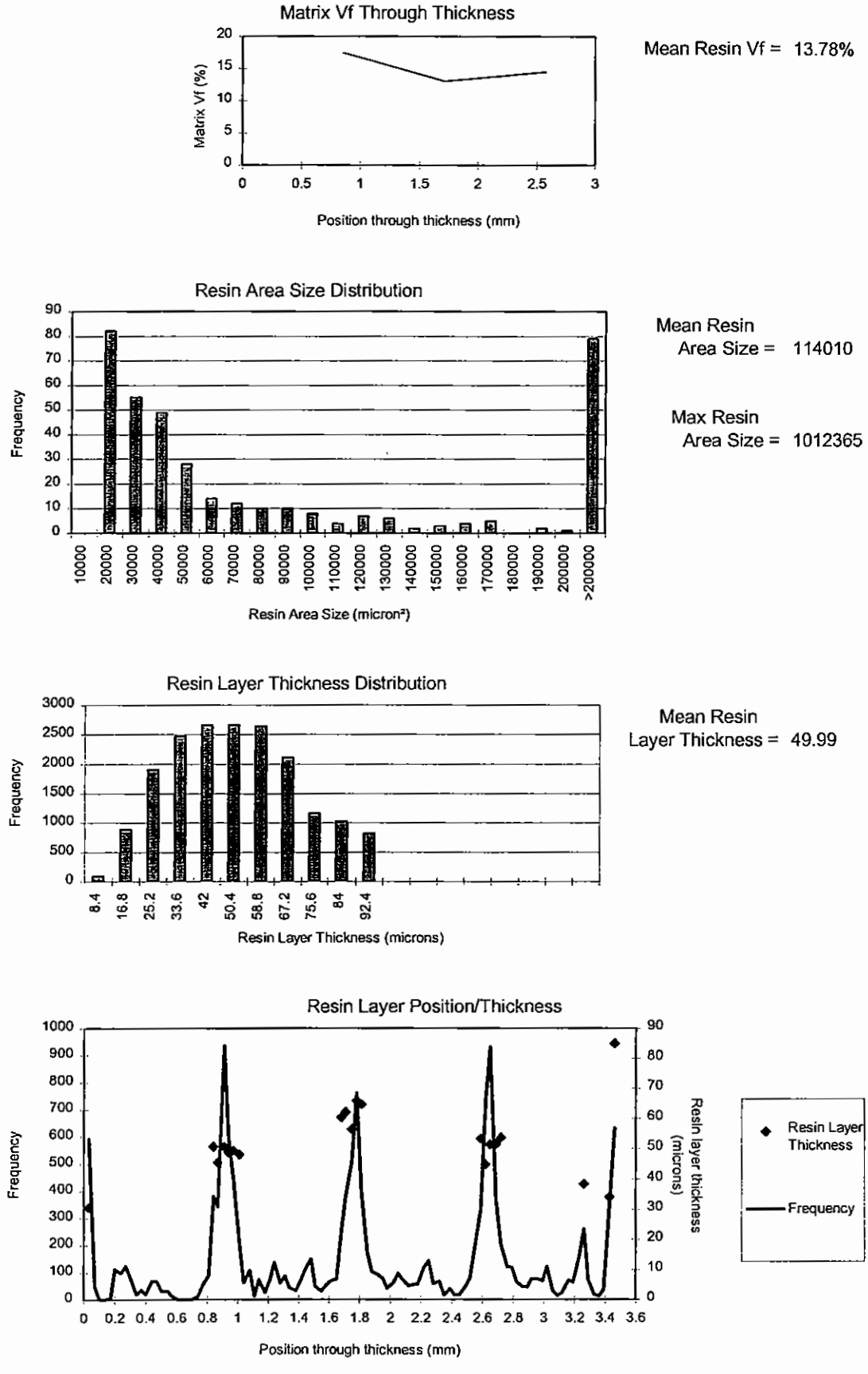

Figure 132 :Material T9 Resin Distribution data summary

6.2.3.1 Resin Distribution Observations

Four principal results were measured and analysed; free resin volume fraction, mean resin area size, maximum resin area size, and the mean resin layer thickness. The free resin volume is the percentage of the total volume of resin that is distributed as discrete areas of neat resin (areas and layers). The differences in measured characteristics between materials are very large with factors of between two and three differences in mean and maximum resin area size for materials T7 and T8.

Of the graphs presented in Figure 124 to Figure 132 the most useful is that of the resin layer position and frequency through the thickness. In general it is likely that resin areas and layers close to delamination planes (typically ±45° and 0°/45° interfaces) will affect damage resistance and tolerance properties and apparent interlaminar shear strength as failure tends to occur in those planes. The height of the resin layer is likely to have some effect on the interlaminar fracture properties, particularly in impact damage development. For other properties such as compression strength the resin areas surrounding the 0° tows are likely to affect the buckling stability of the axial 0° tows.

For all the materials, thick resin layers tended to occur at the interface between adjacent fabrics, forming resin rich 0°/0° or 45°/45° interfaces. These tended to form as channels in fabrics T3, T4 and T8 where the 0° tows are bunched. Similar concentrations of resin layers are observed at the laminate centre (45°/45°) interface (Materials T7, T8 and T9). The most likely explanation for this is the pre-compaction of the individual fabric blankets provided by the knitting/stitching process. When infused with matrix resin to the 54% fibre volume used here, the pre-compaction provides some excess resin which tends to occupy the area between the blankets as observed.

6.2.3.2 Effect of Fabric Manufacturing Settings

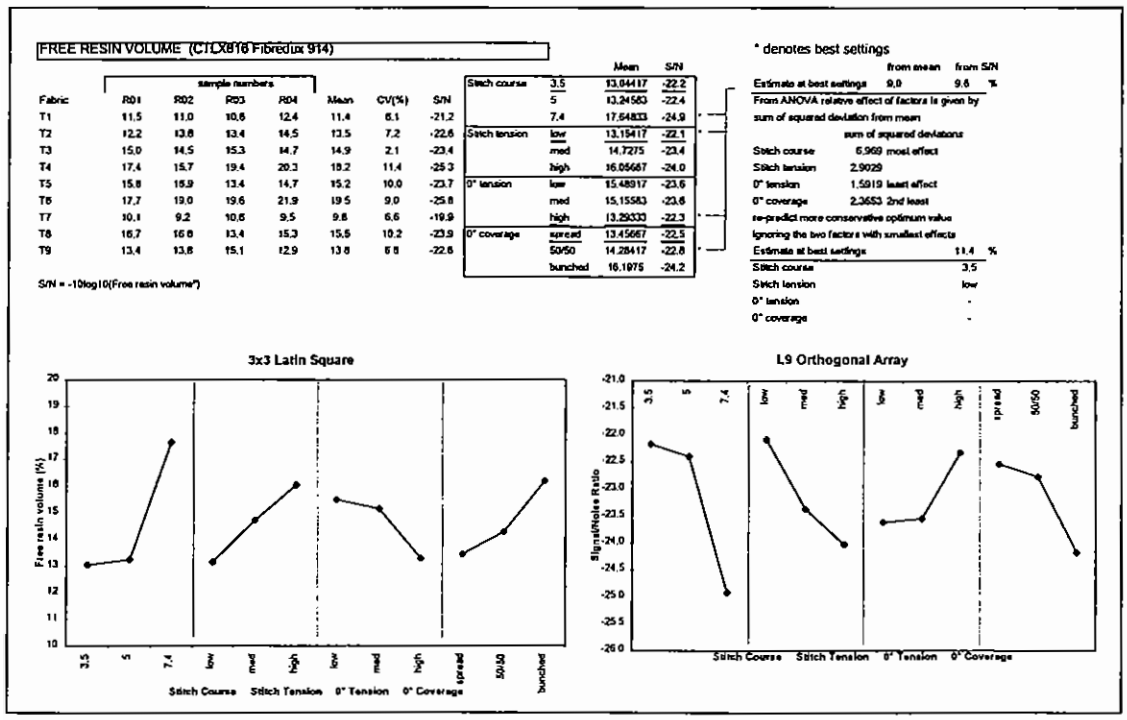

Figure 133: Free Resin Volume Results Summary

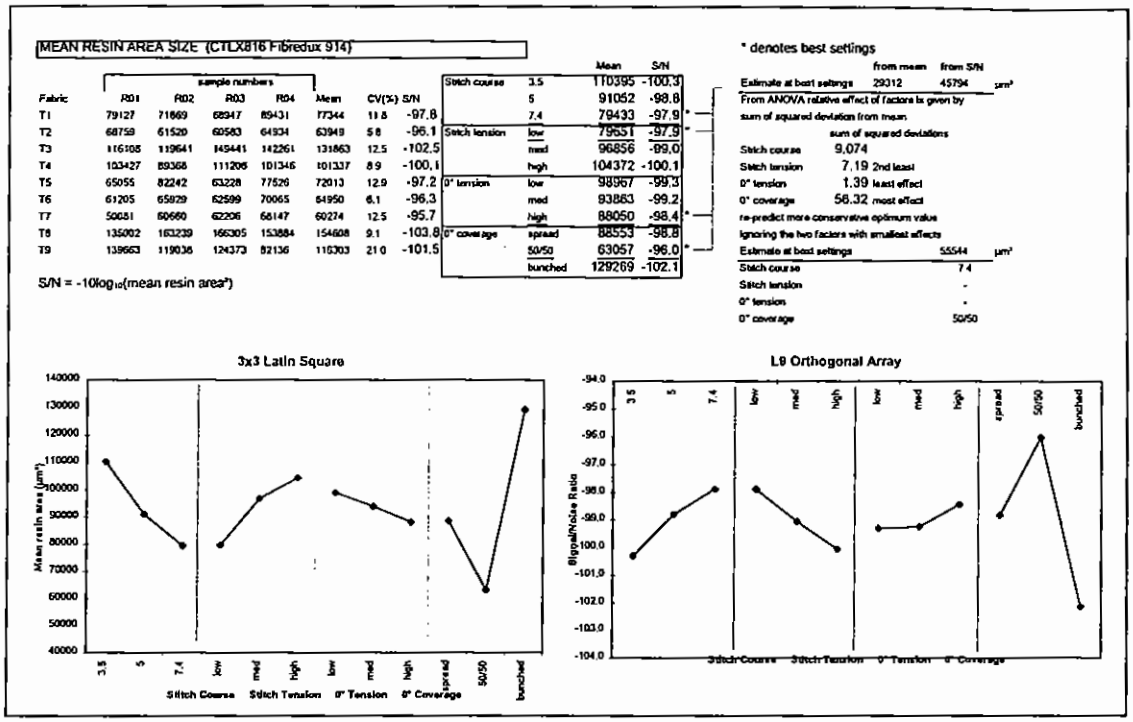

Figure 134: Mean Resin Area Size Results Summary

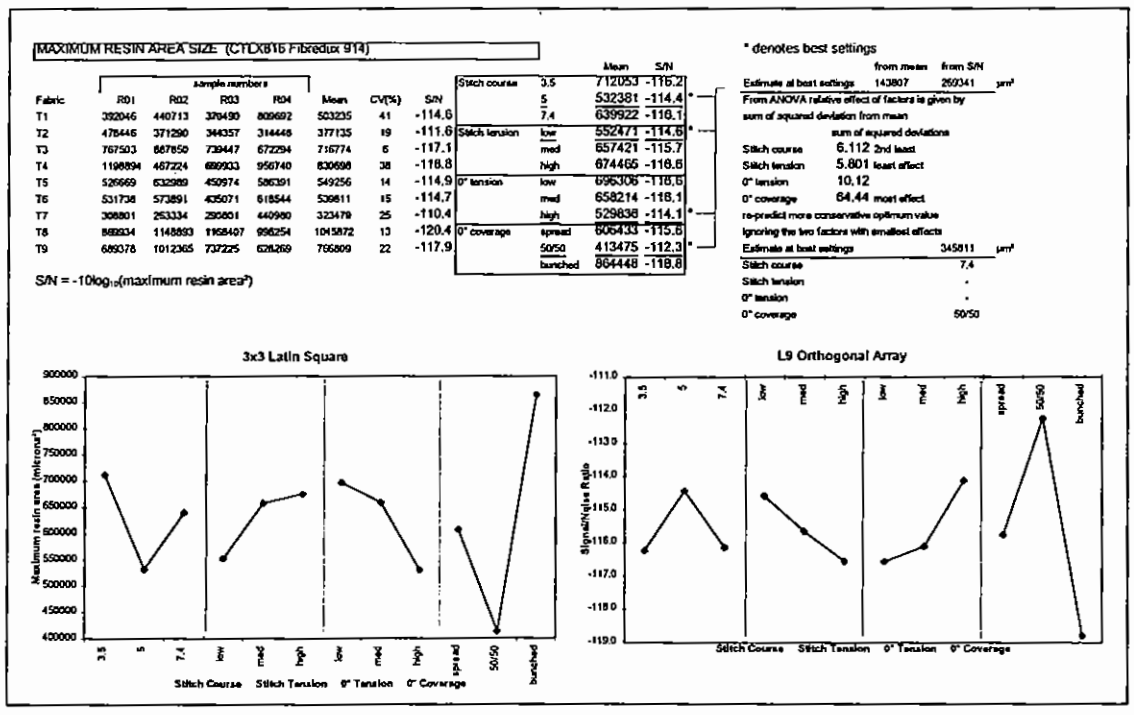

Figure 135: Maximum Resin Area Size Results Summary

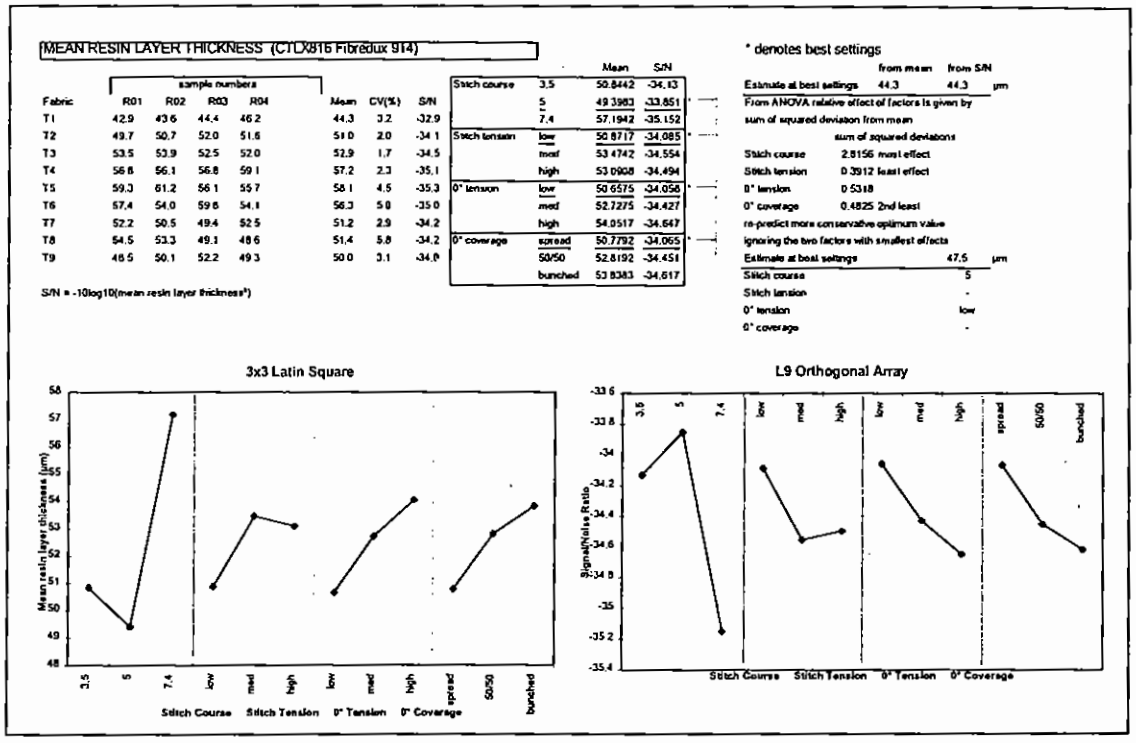

Figure 136: Mean Resin Layer Thickness Results Summary

With reference to Figure 133, free resin volume fraction within the structure increases markedly for materials with a high stitch course. For fabrics T4 and T6 a majority of the free resin is located towards the centre of the laminates whereas in Fabric T5 it is more evenly distributed through the thickness. Increasing stitch tension causes the reinforcing fibres to be held more closely together and thus appears to increase the free resin volume. Applying a high tension to the 0° tows appears to counteract the bunching effect of the stitching. Moving from a spread 0° coverage to a bunched one causes an increase in free resin volume presumably because the 0° tows are more constrained, and there are strong indications that the resin layers in these fabrics are prevalent around the nested together 0° tows as can be seen in the mean resin layer thickness summary sheet (Figure 136).

With reference to the resin layer summary sheet (Figure 136), by far the strongest effect is that of stitch course with a setting of 7.4 leading to a large increase in layer thickness. This increase in layer thickness is concentrated around the 0° tows, with the resin distribution within each fabric being fairly consistent. The reason for the increase in layer thickness with 0° tension is not obvious but the increasing layer thickness with 0° coverage, moving from spread to bunched, may be due to the increasing difficulty in getting the 0° surfaces to nest closely together and causing resin layers to be generated.

Looking at the summary graph for mean resin area size (Figure 134) we see the same trend for stitch tension and 0° tension as seen with the free resin volume. This time however the effect of stitch course is reversed and increasing the stitch course appears to break up the resin areas into small sizes, as could logically be expected. For 0° coverage the 50/50 splitting of the 0° tows is effective and does minimise the mean resin area size, as is the intention of this 0° style. The influence of the parameter settings on the maximum resin area size (Figure 135) is very similar to that for the mean area size.

6.2.4 Microstructural Results Discussion

Interrelationships between microstructural features are as follows:

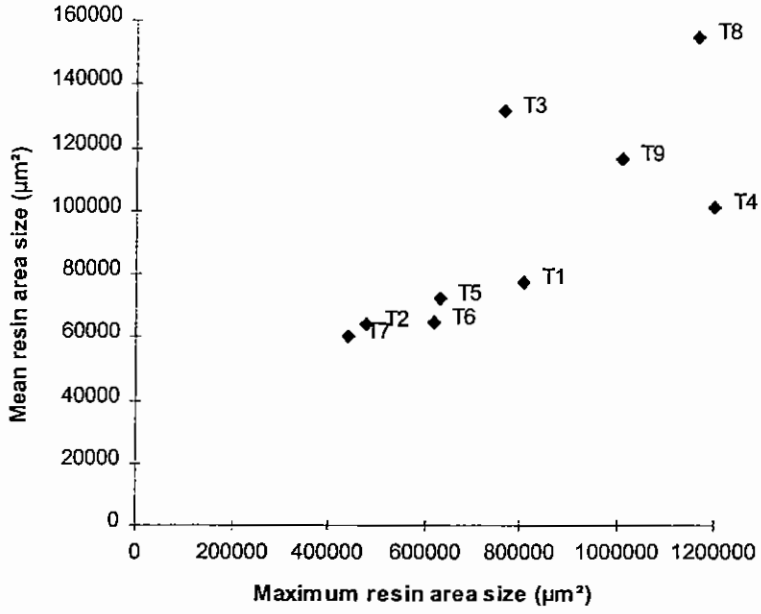

Figure 137: Relationship between mean and maximum resin area size

For a majority of the materials the relationship between mean and maximum resin area size is linear (Figure 137), however for the samples with bunched 0° coverage and where the tightness of the stitching causes localised bunching we observe large mean resin area sizes as the excess matrix caused by the pre-compaction of the fabrics tends to be retained the fabric interfaces.

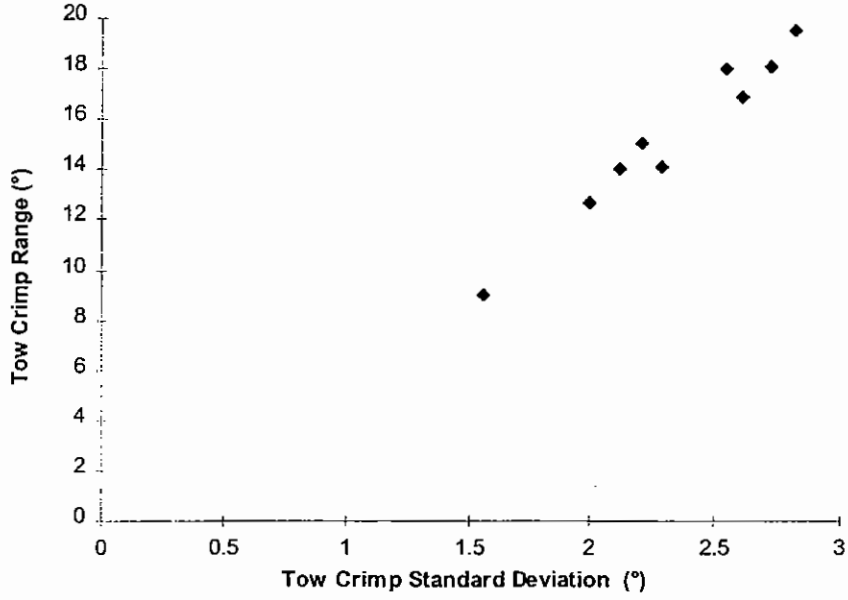

Figure 138: Relationship between Tow Crimp Standard Deviation and Range

The relationship between tow crimp standard deviation and range is linear, suggesting that the behaviour of the tow is primarily controlled by the manufacture of the fabric, and not subject to significant uncontrolled variation.

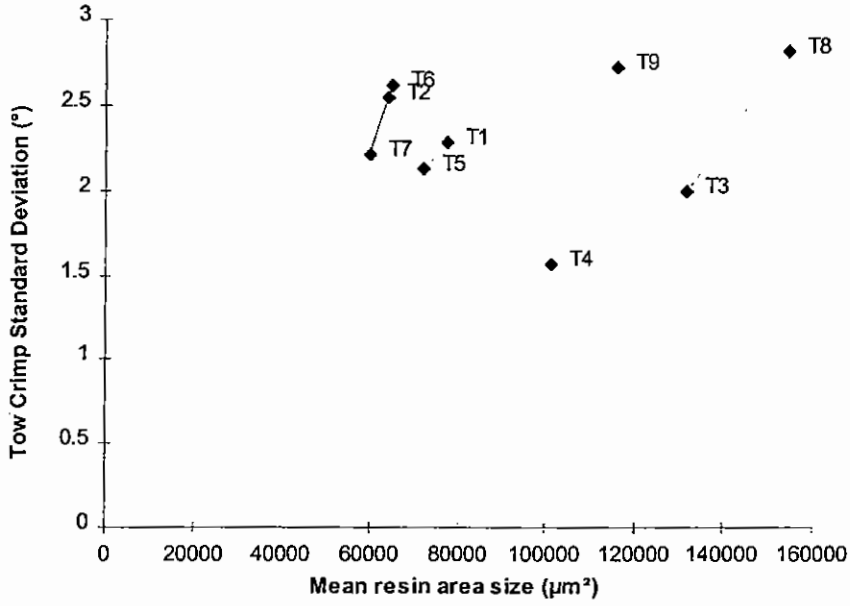

Figure 139: Relationship between mean resin area size and tow-crimp SD

There is evidence of a relationship between the resin area size and tow crimp but dependent on the 0° coverage style as shown in Figure 139. For all types of 0° coverage we observe an increase in resin area size with increasing tow-crimp. For the spread and bunched configuration the increases in resin area size and crimp are associated with reducing stitch course, i.e. less frequent stitching. For the 50/50 0° coverage configuration however the dependence on stitch course is completely reversed. This may be due to the increased disruption to the 0° structure with increasing stitch course which in turn produces more resin rich areas.

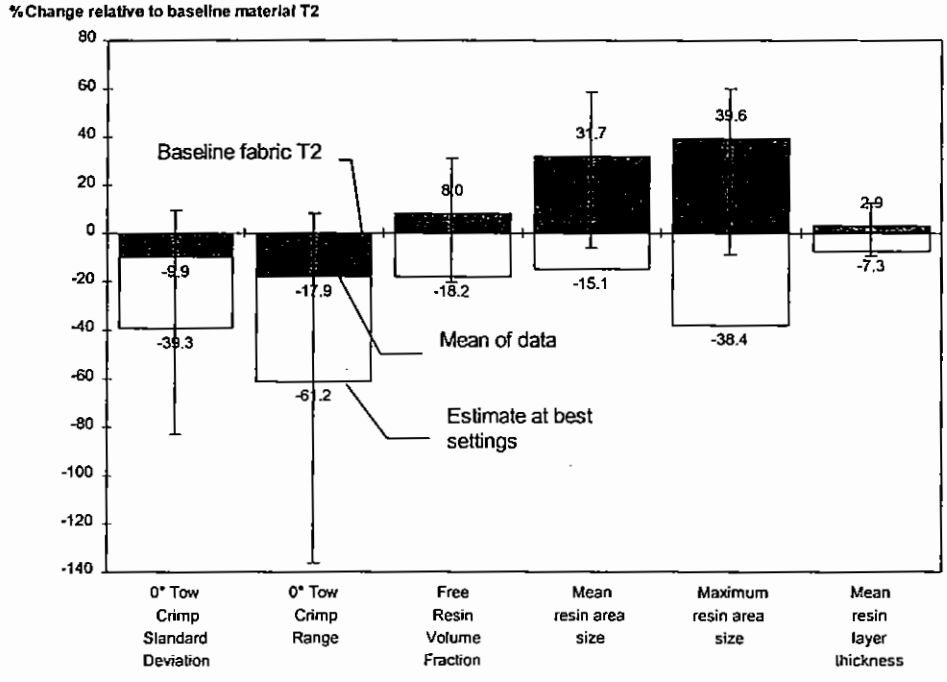

Figure 140: Predicted 'best' microstructure relative to baseline (T2) and mean

Figure 140 indicates that some reduction in tow crimp is predicted when the best settings are selected, but that the reduction is small in relation to the range of the data. This suggests that the level of experimental variation is quite large or that another uncontrolled factor is influencing the level of tow crimp. Large reductions in resin areas are predicted using a 50/50 0° coverage to prevent bunching of the 0° tows, a low stitch tension again to prevent bunching, and a high stitch course presumably to break up resin areas into a smaller size. Resin layer thickness is minimised with a low or medium stitch course, and low stitch and 0° tensions and spread 0° coverage.

The relationships between the measured microstructural features and other mechanical properties can be found in the discussion of the in-plane and the damage resistance and tolerance results.

6.3 In-Plane Property Results

6.3.1 Tensile Strength and Modulus

Table 32: Tensile strength results

Material	Tensile Strength MN/m²	Standard Deviation MN/m²	Coefficient of Variation %
T1	708.3	13.5	1.9
T2	665.8	24.1	3.6
T3	708.9	21.5	3.0
T4	695.5	29.6	4.3
T5	652.1	21.6	3.3
T6	643.3	39.1	6.1
T7	665.1	15.7	2.4
T8	652.2	36.4	5.6
T9	661.0	28.2	4.3

Table 33: Tensile modulus results

Material	Tensile Modulus GN/m²	Standard Deviation GN/m²	Coefficient of Variation %
T1	57.5	1.0	1.7
T2	57.4	1.2	2.2
T3	56.4	0.6	1.1
T4	55.2	0.5	0.9
T5	54.3	2.0	3.6
T6	55.8	2.3	4.0
T7	54.8	1.7	3.1
T8	55.4	1.7	3.0
T9	57.4	1.5	2.6

6.3.1.1 Effect of Manufacturing Settings

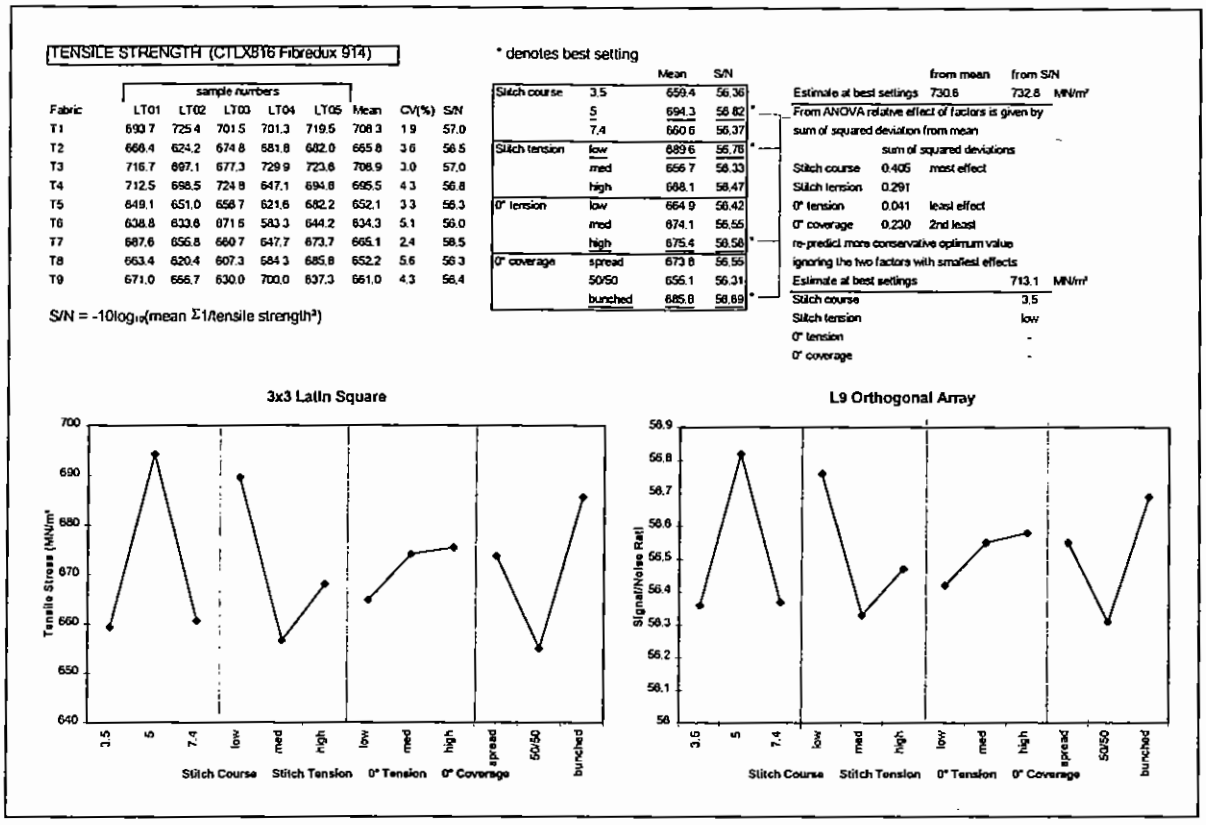

Figure 141: Tensile Strength Results Summary

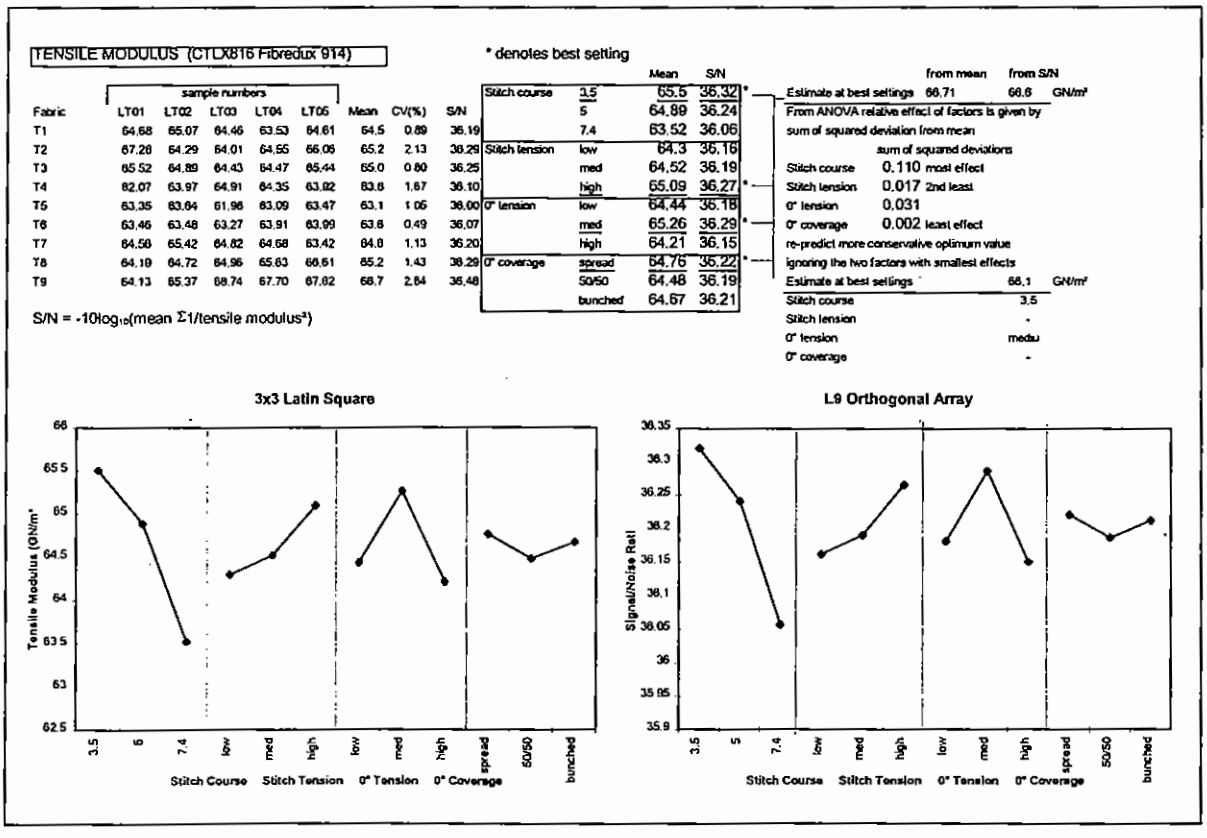

Figure 142: Tensile Modulus Results Summary

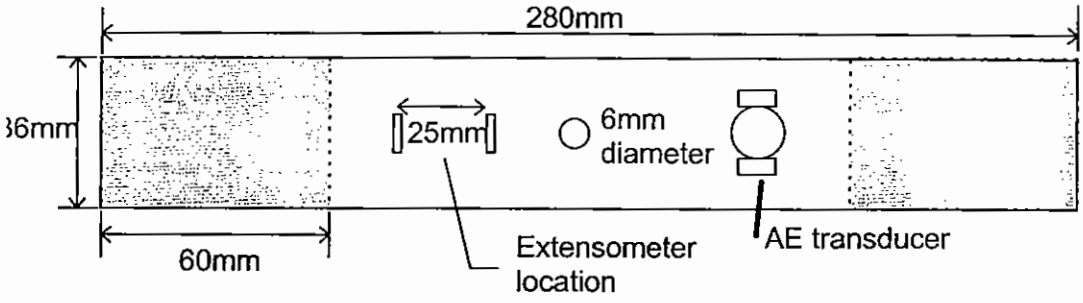

Figure 143: Extensometer and AE transducer locations on interrupted OHT tests

The sample was then loaded until acoustic emissions were first recorded whereupon the sample was immediately unloaded and ultrasound C-scanned again. After scanning the sample was re-loaded, this time to 0.4% strain, un-loaded and C-scanned (acoustic emissions started at between 0.3 and 0.4% strain). This was repeated at 0.1% strain increments until the increment before failure (0.6% strain). The stresses, strains and C-scan images are shown below in Table 35.

Table 35: Results for interrupted OHT tests of materials T2

Sample 2T2OHT5

	As Manufactured	First acoustic emission	0.4% strain (nominal)	0.5% strain (nominal)	0.6% strain (nominal)
Strain (%)	-	0.38	0.44	0.51	0.61
Stress(MN/m²)	-	281.5	322.6	387.5	496.0
		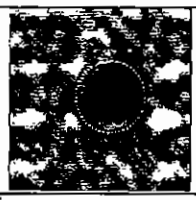	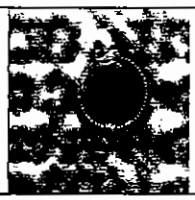	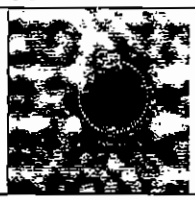	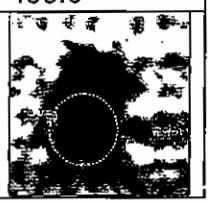

Sample 2T2OHT6

	As Manufactured	First acoustic emission	0.4% strain (nominal)	0.5% strain (nominal)	0.6% strain (nominal)
Strain (%)	-	0.41	0.44	0.51	0.58
Stress MN/m²)	-	320.0	347.6	401.0	460.9
	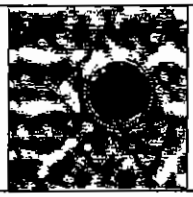	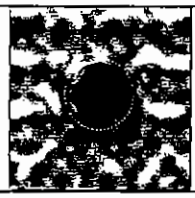		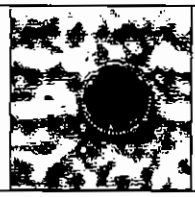	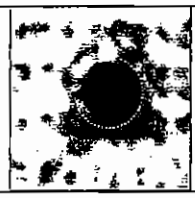

Table 36: Results for interrupted OHT tests of materials T3

Sample 2T3OHT5

	As Manufactured	First acoustic emission	0.4% strain (nominal)	0.5% strain (nominal)	0.6% strain (nominal)
Strain (%)	-	0.35	0.41	0.50	0.60
Stress MN/m²)	-	270.5	319.6	393.8	477.8
		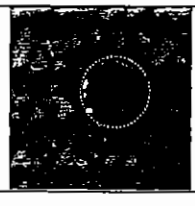	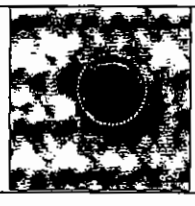	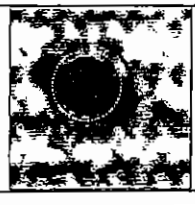	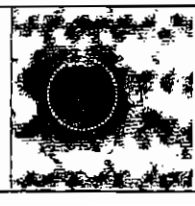

Sample 2T3OHT6

	As Manufactured	First acoustic emission	0.4% strain (nominal)	0.5% strain (nominal)	0.6% strain (nominal)
Strain (%)	-	0.32	0.42	0.50	0.60
Stress MN/m²)		240.3	322.7	399.9	481.7
		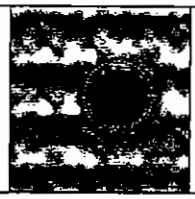	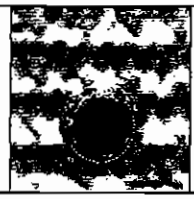	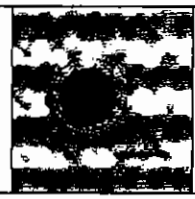	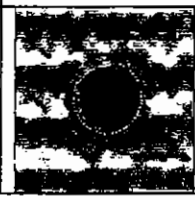

Additional tests were also carried out on two hole OHT samples as shown in Figure 144. The rationale is that the at the samples would fail preferentially at the weakest hole but leave the remaining hole intact but damaged having been subject to the same stress and strain.

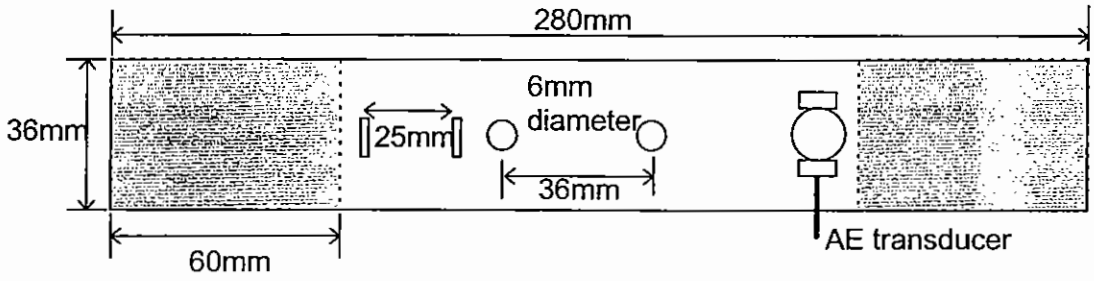

Figure 144: Two hole OHT sample configuration

Samples were only C-scanned after failure and are shown below in Table 37.

Table 37: Two hole OHT results and C-scan images of damaged hole

Sample Identification	C-Scan Image	Failure Stress (MN/m²)
2T2OHT7		469.1
2T2OHT8	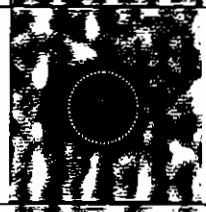	475.2
2T3OHT7	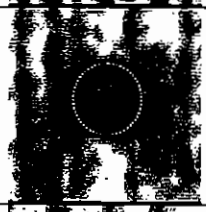	594.3
2T3OHT8	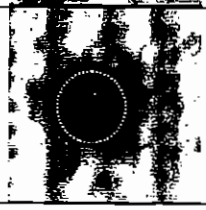	563.2

6.3.2.2 Interrupted and Two Hole OHT Test Observations

The results of the interrupted tests (Table 35 and Table 36) show that damage, observed by acoustic emission and C-scan, occurs at lower strains for fabric T3. However subsequent re-loading at 0.1% strain increments shows no visible signs of damage and no observable growth despite what appears to pre-existing manufacturing defect around the hole in sample 2T3OHT5 (Table 36). In material T2 damage detected by acoustic emission is observed progressively growing with increasing strain, presumably as matrix cracking or delamination from the free edge of the drilled hole.

The two hole OHT results (Table 37) again show failure at lower stresses for the T2 material with a little obvious damage growth around the un-failed holes. For material T3, strengths are much higher, as previously observed, and damage either side of the un-failed hole is clearly visible. This damage appears to follow, and be constrained in width by, the large resin channels running parallel to the 0° tows which are a particular feature of material T3.

In both cases the strain in the material away from the hole when damage is first detected is relatively low at between 0.32 and 0.41% strain. This is below current design allowable strains for composite wing structure.

6.3.2.3 Effect of Manufacturing Settings

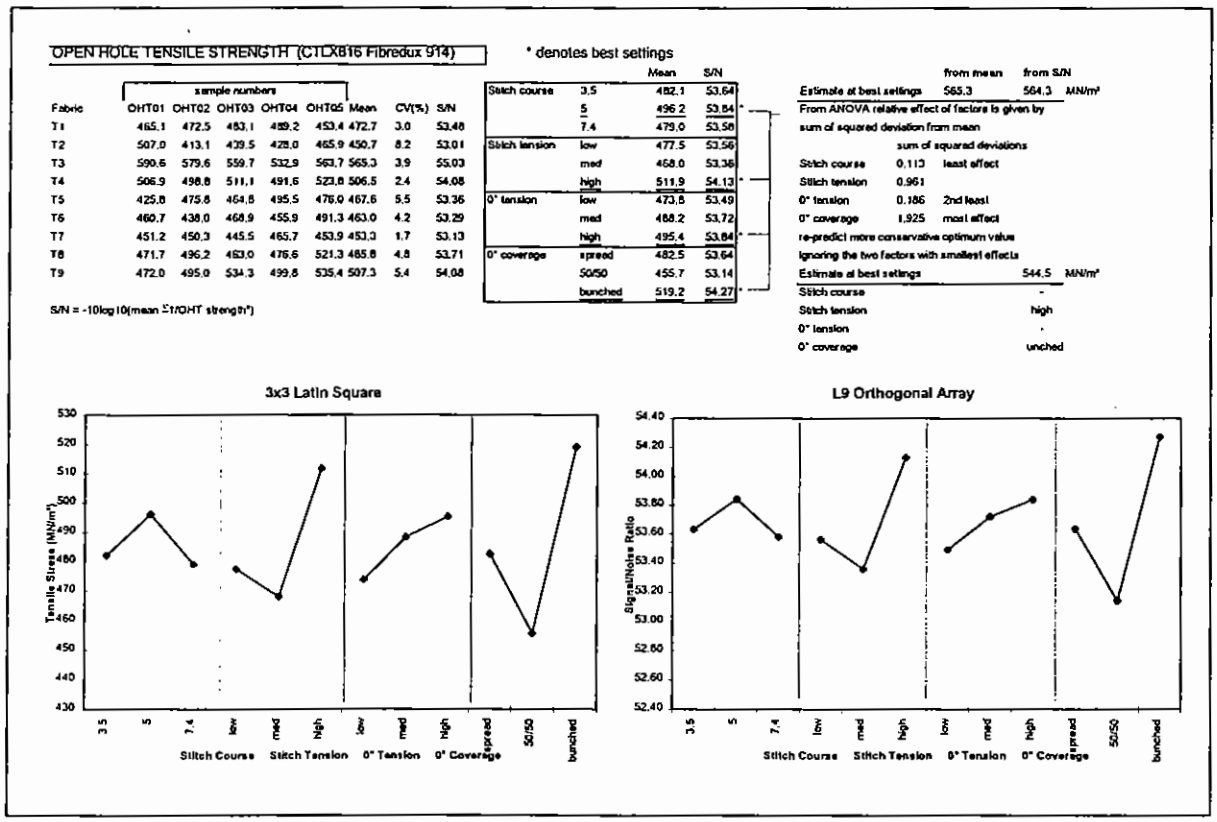

Figure 145: Open Hole Tensile Strength Summary

The effect of the machine parameters and their settings are very similar to those for the tensile tests as may be expected, but with the effect of stitching tension reversed in favour of a high tension. The relative magnitude of the effects is also changed;

with a much smaller effect from the stitch course and a large effect from the 0° coverage which strongly favours a bunched tow 0° coverage.

The failure process for holed laminates is related to both the tensile performance of the material and its response to the interlaminar tensile (normal) stresses at the hole edge. These will be dictated primarily by the mode I interlaminar fracture performance. Both open hole tensile strength and mode I strain energy release rate favour a high stitch tension and bunched 0° coverage

6.3.3 Compression Strength and Modulus

Table 38:Compression strength results

Material	Compression Strength MN/m²	Standard Deviation MN/m²	Coefficient of Variation %
T1	584.5	11.7	2.0
T2	606.8	27.6	4.5
T3	556.3	22.6	4.1
T4	575.4	13.1	2.3
T5	526.3	46.8	8.9
T6	569.6	14.0	2.5
T7	596.9	12.2	2.0
T8	552.7	26.6	4.8
T9	553.1	13.5	2.4

Table 39:Compression modulus results

Material	Compression Modulus GN/m²	Standard Deviation GN/m²	Coefficient of Variation %
T1	57.5	1.0	1.7
T2	57.4	1.2	2.1
T3	56.4	0.6	1.1
T4	55.2	0.5	0.9
T5	54.3	2.0	3.7
T6	55.8	2.2	3.9
T7	54.8	1.7	3.1
T8	55.4	1.7	3.1
T9	57.4	1.5	2.6

6.3.3.1 Effect of Manufacturing Settings

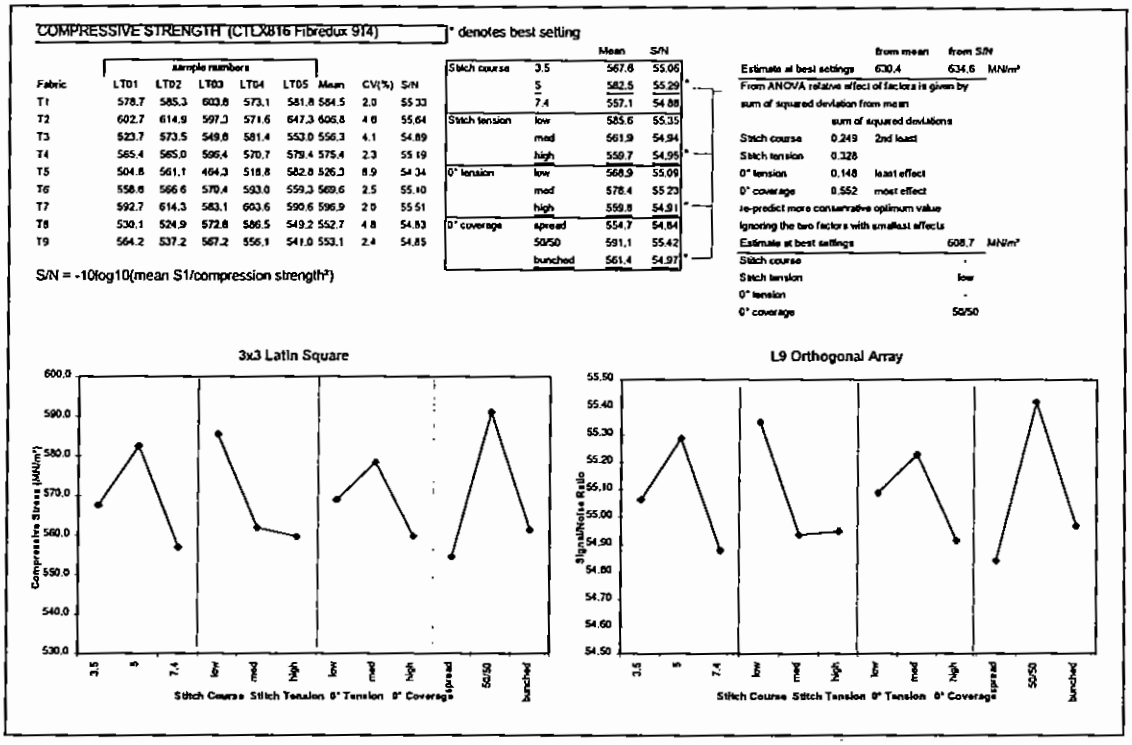

Figure 146: Compression Strength Results Summary

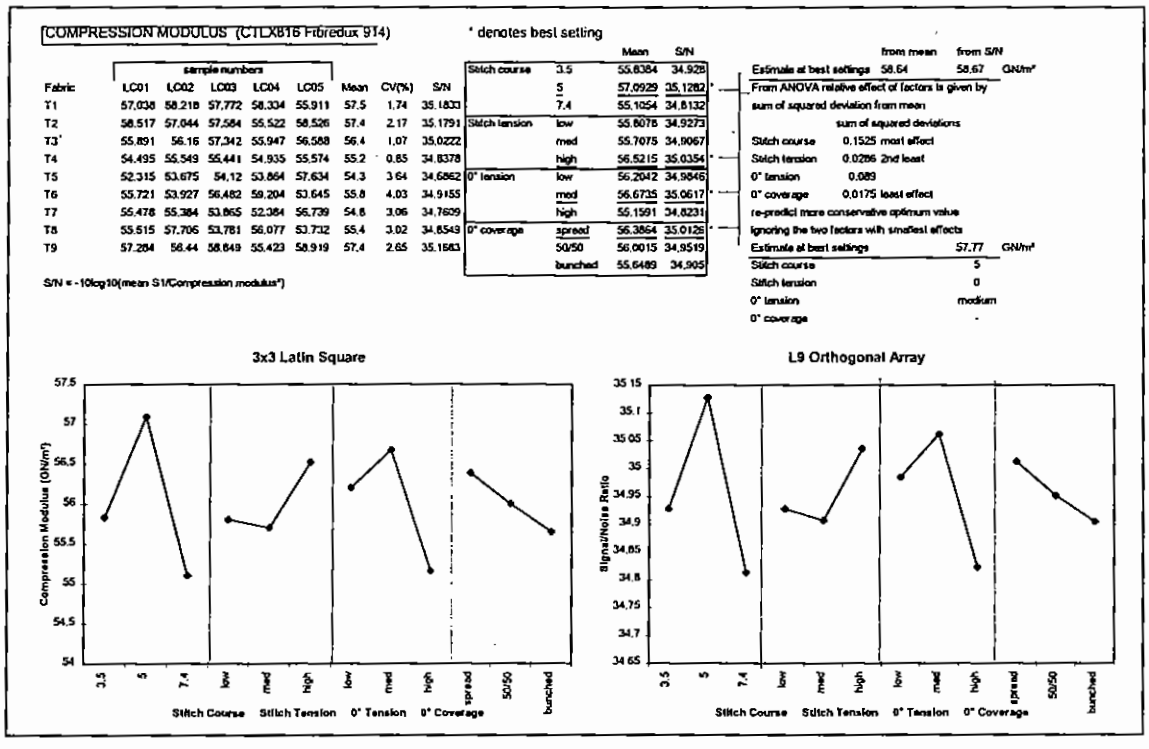

Figure 147: Compression Modulus Results Summary

The effects of the machine settings on compression strength (Figure 146) indicate the best fabric to have a stitch course of 5 penetrations/cm, a low stitch tension, medium 0° tension and a 50/50 split 0° coverage, in contrast to the bunched structure favoured for tensile strength. These settings are the same as the baseline fabric T2 but with the stitching tension reduced. The parameters having most effect are stitch tension and 0° coverage and the estimated best compression strength

predicted at these settings is slightly higher than that of the baseline T2 fabric. For compression modulus (Figure 147) as with strength the stitch course of 5 gives the best performance. The role of stitch tension is reversed with a high tension favoured, and a spread 0° resulting in the highest stiffness.

6.3.4 Apparent Interlaminar Shear Strength and Modulus

Table 40: Apparent interlaminar shear strength

Material	Apparent Interlaminar Shear Strength MN/m²	Standard Deviation MN/m²	Coefficient of Variation %
T1	54.3	2.7	5.0
T2	59.9	3.8	6.3
T3	54.7	3.2	5.9
T4	57.2	2.7	4.7
T5	59.0	2.3	3.9
T6	60.6	3.4	5.6
T7	59.4	3.1	5.2
T8	56.6	2.3	4.1
T9	55.9	3.8	6.8

6.3.4.1 Effect of Manufacturing Settings

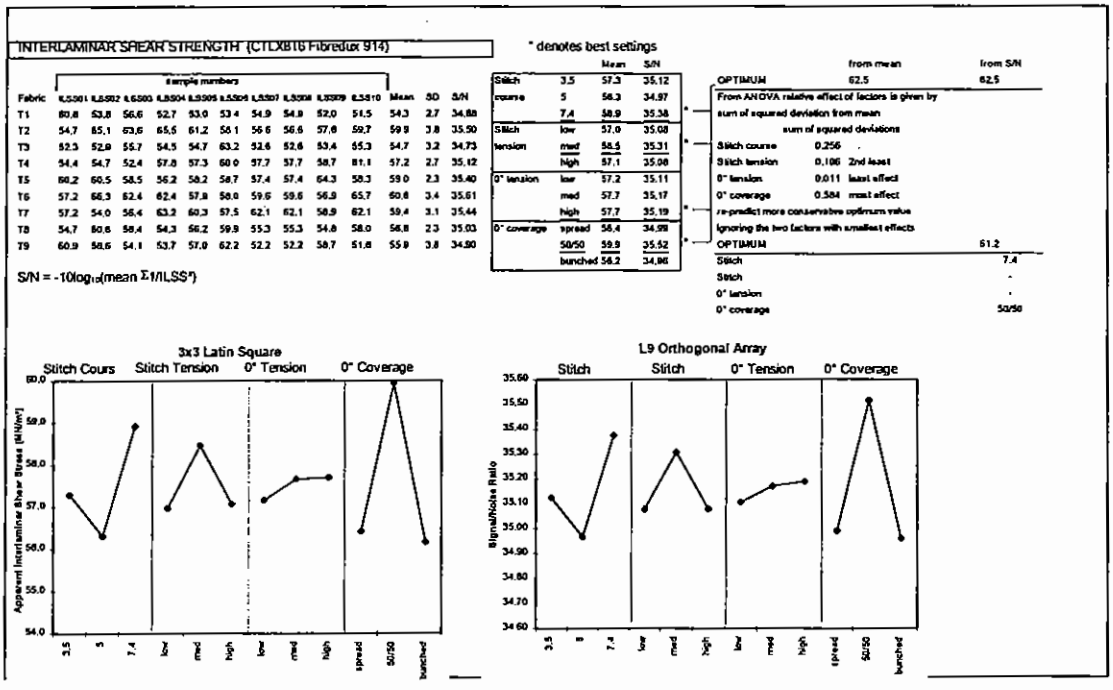

Figure 148: Apparent ILSS Results Summary

The apparent interlaminar shear strength results indicate a benefit from increasing the stitch course to 7.4 penetrations/cm and from a 50/50 split 0° coverage. A small benefit is also indicated from a medium stitch tension although 0° tension has negligible effect. Overall the effect of changing the manufacturing settings is small in relation to the experimental scatter, despite 30 test results forming each data point on the graphs.

6.3.5 In-Plane Properties Discussion

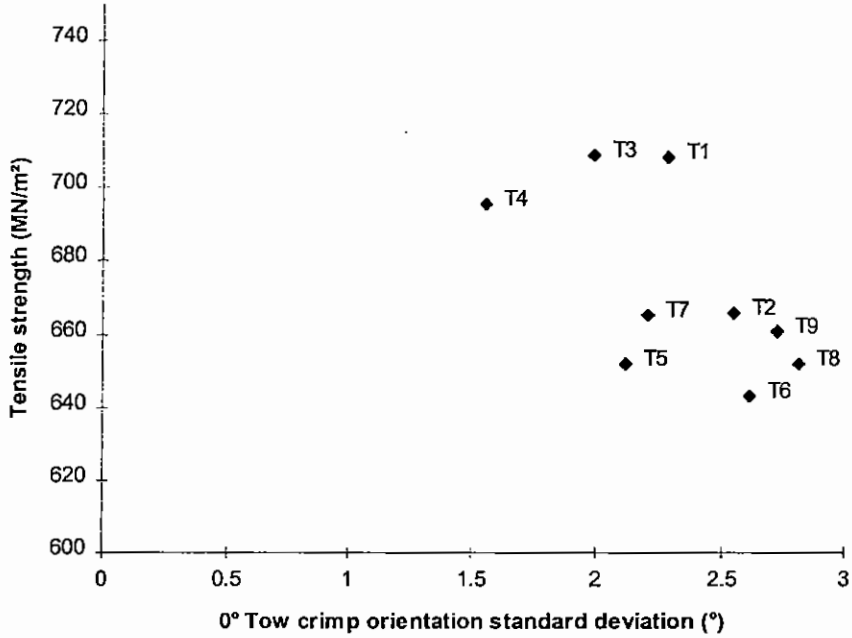

Figure 149: Relationship between 0° Tow Crimp Orientation Standard Deviation and Tensile Strength

Although not a particularly strong trend, the tensile strength is observed to reduce with increasing tow crimp, for both standard deviation and range (Figure 149). No such relationship is observed for tensile modulus. Similarly resin distribution properties did not appear to significantly affect the tensile properties.

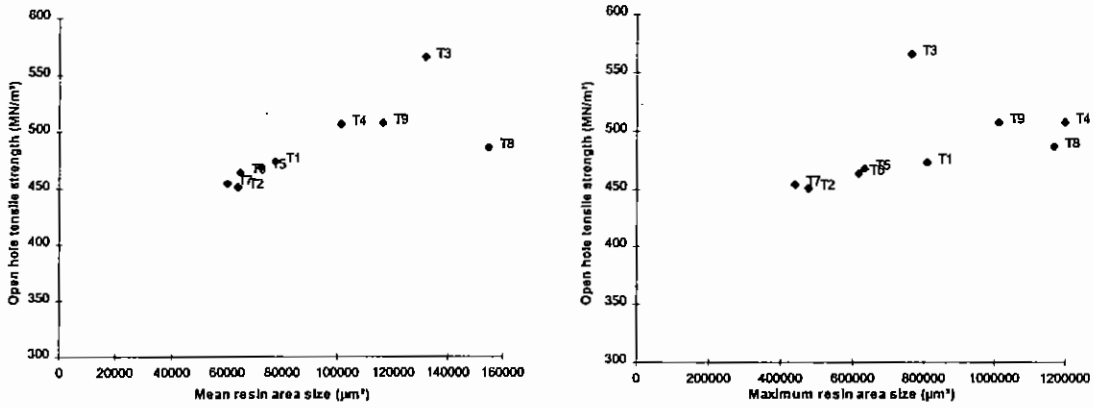

Figure 150: Relationships between resin area size and open hole tensile strength

The relationship between open hole tensile strength and resin area size indicates a strong dependence of strength on the size of the resin areas (Figure 150). No such relationship is seen with changes in free resin volume or resin layer thickness.

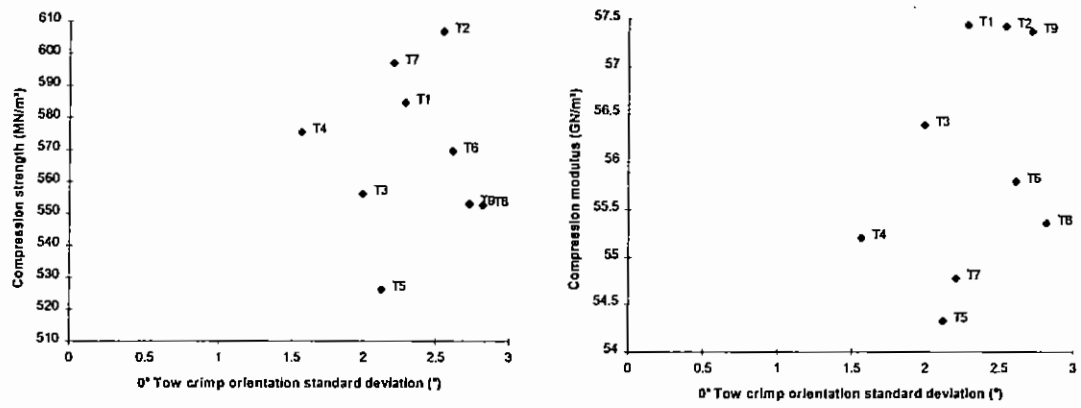

Figure 151: Relationship between compression properties and tow crimp

No well defined relationship was observed between the compression strength and modulus and tow crimp (Figure 151). Some grouping of data into possible relationships can be seen. However the reasons for the particular groupings cannot readily be explained from the manufacturing settings.

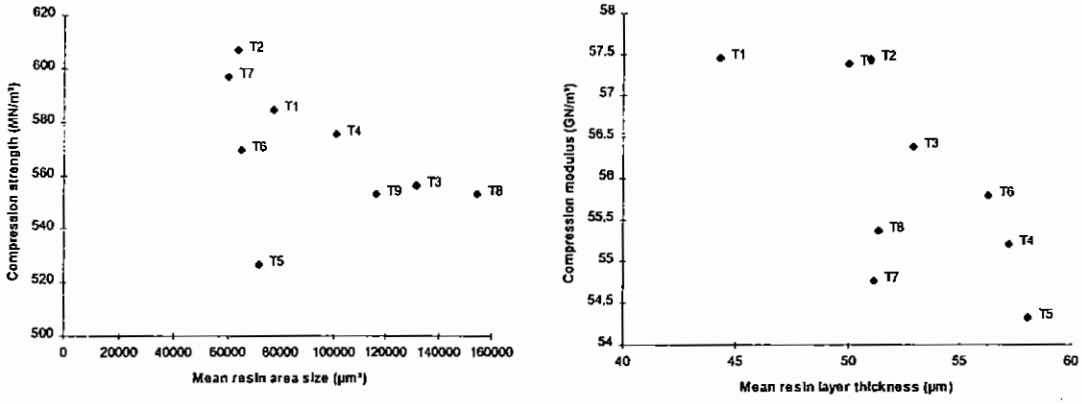

Figure 152: Relationships between resin distribution and compression properties

The compression strength appears to influenced by the mean resin area size and the modulus by the thickness of the resin layers (Figure 152). It is possible that increases in the amount of resin surrounding the 0° tows reduce the lateral support they receive from the surrounding fibres leading to earlier microbuckling and failure. The thickness of resin over which this effect extends may be small at the relatively low level of strain at which the modulus is calculated (0.25% strain). This would explain the more clearly defined relationship between the modulus and resin layer thickness rather than mean resin area. Conversely the influence of resin support may be larger at the higher strains of compression failure hence the clearer relationship to mean resin area size.

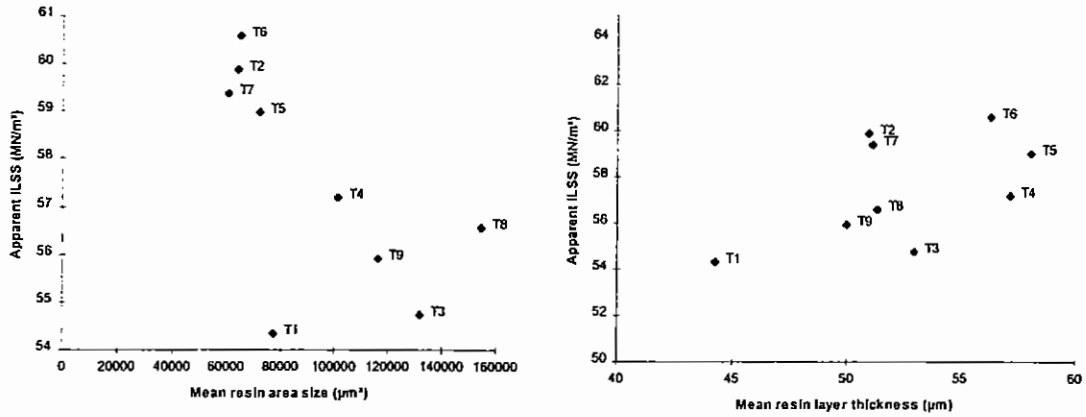

Figure 153: Relationships between resin distribution and apparent ILSS

A clear relationship is observed between mean resin area size and apparent ILSS; strength decreasing with increasing mean area size (Figure 153). However no clear trends can be observed in the relationship with resin layer thickness. This is likely to result from the resin layers concentrating at the nested fabric interfaces (0°/0°) and (45°/45°) in materials with the highest stitch course (T4, T5 and T6) where interlaminar shear failure did not occur.

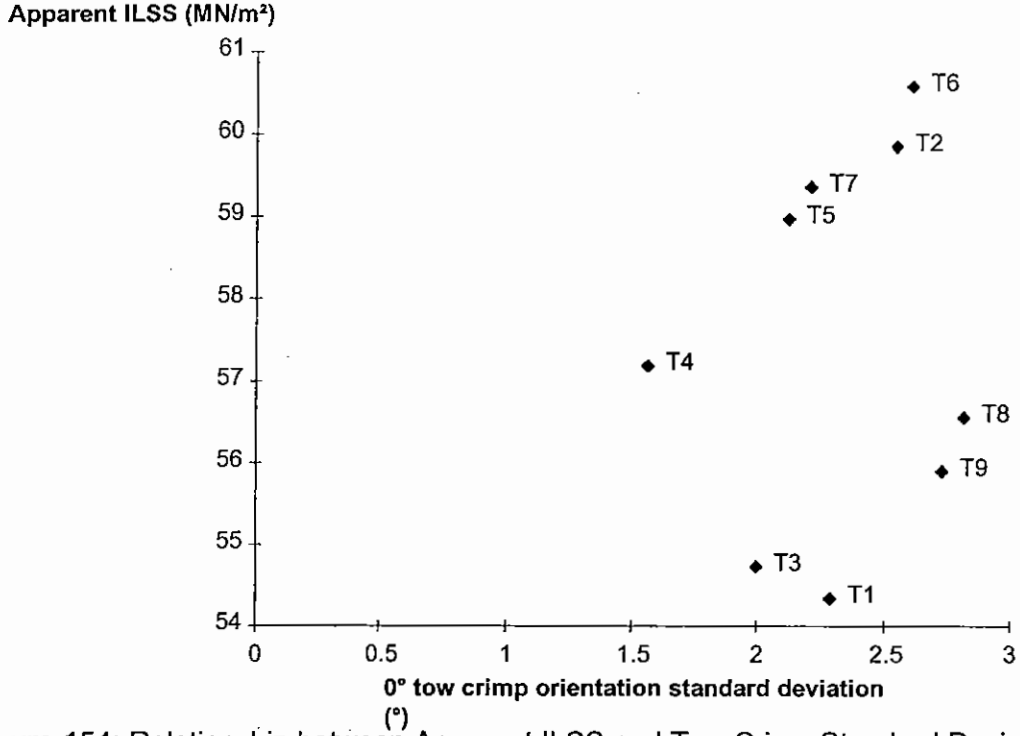

Figure 154: Relationship between Apparent ILSS and Tow Crimp Standard Deviation

The relationship between tow crimp and interlaminar shear strength in unidirectional samples was thought to be governed by the introduction of crimped fibres to bridge the shear failure surface thus increasing the shear strength[87]. In the multiaxial samples tested here failure was uniformly between ±45° interfaces with cracks extending into 0° and 45° interface always in the fabrics adjacent to the sample mid-plane. Consequently carbon fibres are unlikely to bridge and embed between these layers, as they are of different orientations. The only fibres bridging the fracture plane are those of the polyester knitting yarn, the amount bridging being dependant on the stitch course and the 0° coverage. The grouping to the left hand side of Figure 154 are all fabrics with 50/50 0° coverage or those with high stitch course and

those on the right, fabrics with spread or bunched 0° coverage and low or medium stitch course. It is also possible that increasing 0° tow crimp presents an increasingly undulating shear plane, providing a degree of mechanical 'keying' between the layers and thus increasing the apparent ILSS.

In summary, Figure 155 indicates the predicted in-plane performance of a 'notional' fabric manufactured with the best settings of each manufacturing parameter for that particular in-plane test. The results are presented relative to the baseline fabric T2, also included are the mean results for all nine materials and their range.

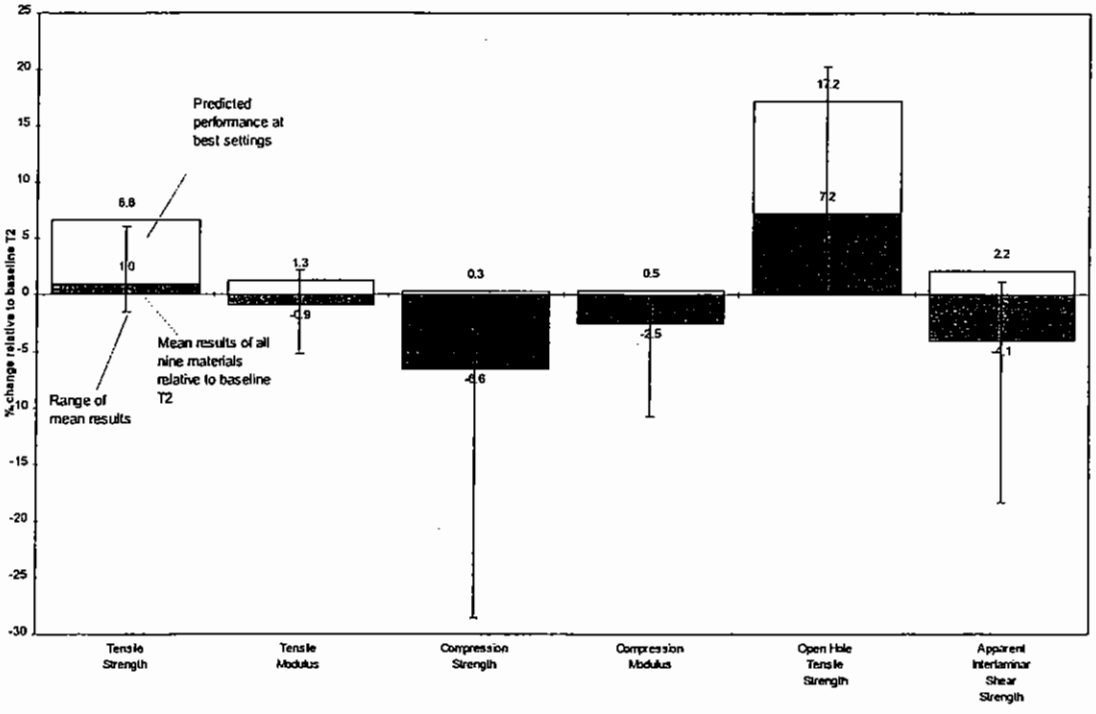

Figure 155: Predicted best In-plane performance relative to baseline (T2) and mean

From the graph we can make several observations:

Between 5 and 6% improvement over the mean performance is expected to be achieved for tensile strength and compression strength by selecting the best parameter settings. For compression strength the baseline T2 fabric has the best machine settings. A 17% and 7% increase in open hole tensile strength is predicted compared with the baseline (T2) material and mean results respectively.

The small predicted improvements in both tension and compression modulus through altering the machine settings suggest that the effect of settings is relatively small or that the observed range of the data may be due to other factors or uncontrolled variation.

As seen in the 'Effect of Manufacturing Settings' summary sheets, settings that maximise tensile strength (Figure 141) and open hole tensile strength (Figure 145) tend to be the opposite of those which maximise compression properties (Figure 146) and it appears also interlaminar shear strength (Figure 148), for which the baseline material T2 has close to the best settings.

6.4 Damage Resistance and Tolerance Results

6.4.1 Threshold Force for Delamination Damage

Table 41: Delamination Threshold Force Results

	Delamination Threshold 15J (kN)	SD (kN)	CV (%)	Delamination Threshold 25J (kN)	SD (kN)	CV (%)
T1	5.58	0.41	7.33	5.80	0.25	4.38
T2	5.57	0.25	4.54	5.63	0.12	2.12
T3	4.67	0.14	2.91	4.66	0.33	7.14
T4	4.98	0.22	4.39	5.91	0.18	3.07
T5	5.85	0.16	2.75	5.84	0.13	2.23
T6	5.83	0.39	6.74	5.66	0.23	4.15
T7	5.67	0.56	9.83	5.96	0.18	3.06
T8	4.75	0.26	5.56	5.33	0.60	11.33
T9	4.77	0.31	6.52	4.85	0.18	3.76

6.4.1.1 Threshold Force for damage observations

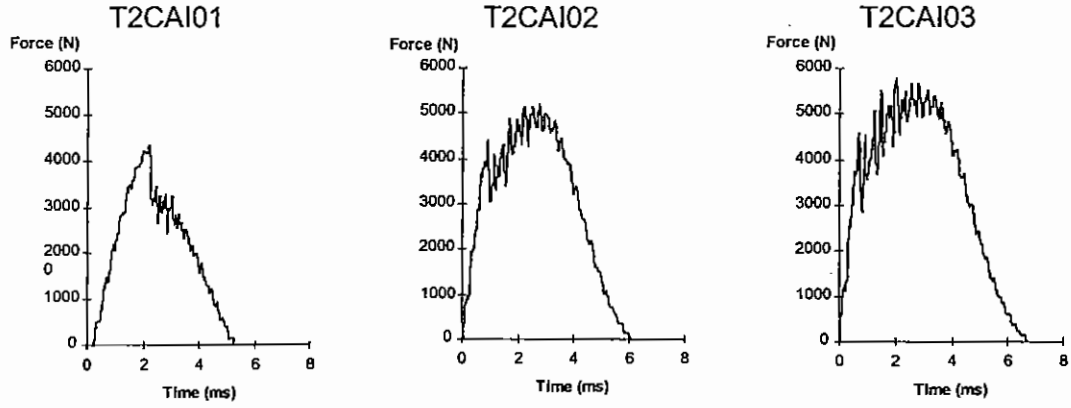

(a) 5J incident energy (b) 15J incident energy (c) 25J incident energy

Figure 156: Typical changes in Force/Time traces with increasing Impact energy

Force vs. Time traces were typically as shown in Figure 156, with a characteristic threshold force for delamination which remained reasonably constant for each material and is presented here as a damage resistance characteristic. The threshold force was observed to increase with increasing impact energy. However, because the indentor mass remained constant, irrespective of impact energy, the velocity of the impact increased, which may explain the slight increase in force observed.

For some of the 5J impacted samples with the highest stitch course (materials T4,T5 and T6), the impact force was insufficient to generate a delamination (so as to

identify the threshold force at 5J). The 5 Joule impact samples are therefore not included in the analysis. Data can however be found in Appendix A.

6.4.1.2 Effect of Manufacturing Settings

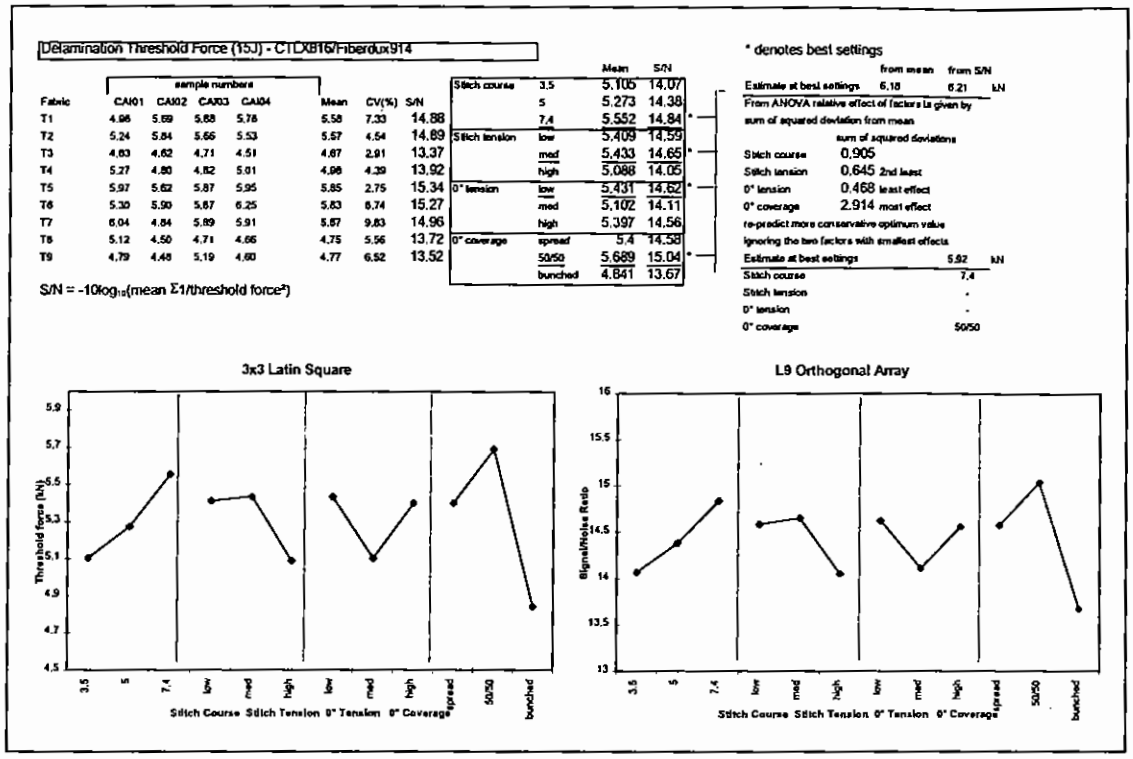

Figure 157: Threshold Force at 15J Impact Results Summary

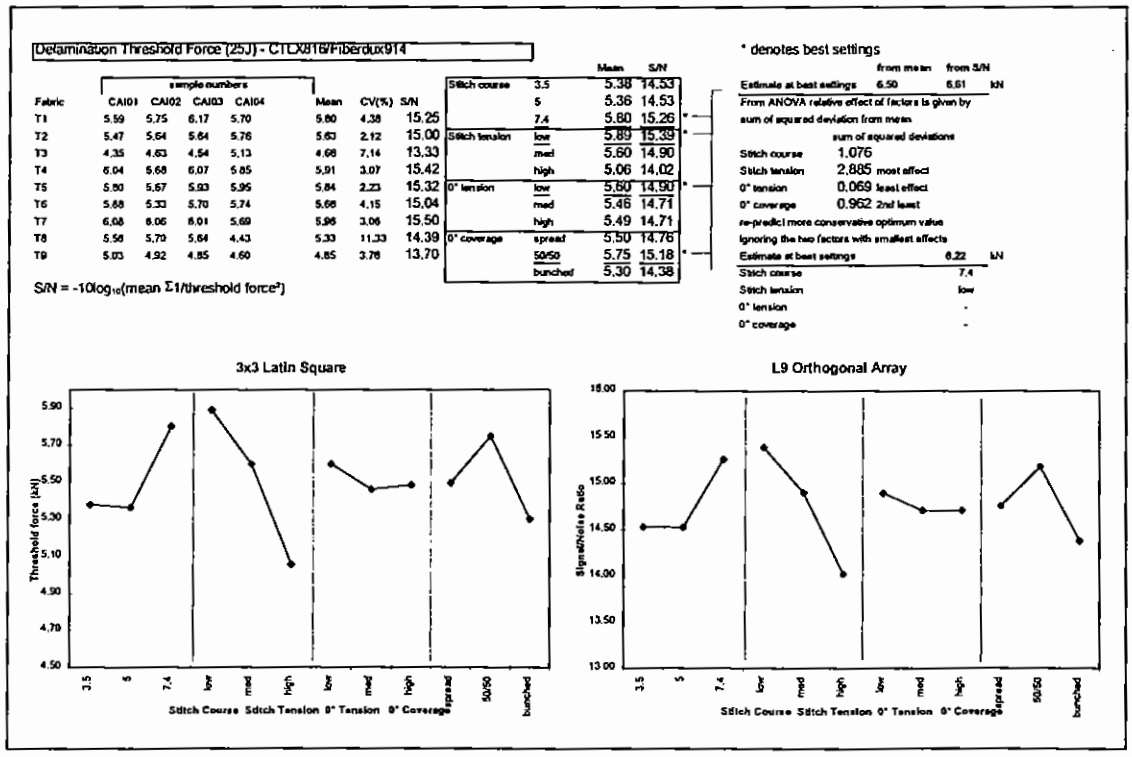

Figure 158: Threshold Force at 25J Impact Results Summary

Best resistance to delamination damage as measured using the threshold force is provided by the high stitch course (7.4 penetrations/cm), low stitching tension and

50/50 0° coverage. The influence of the 0° coverage is more pronounced at the 15J energy, whereas at 25J the stitch tension has more effect, strongly favouring a low tension.

6.4.2 Impact Damage areas

Ultrasonic C-scan images for all the samples as used for damage area measurement calculation can be found in Appendix A along with all other impact data recorded. 15J impacted samples with the closest incident impact energy were selected for detailed analysis. Overview sheets comparing the X-ray and detailed C-scan (0.25mm step scans) images for the nine materials are shown in Figure 159 and Figure 160.

The results for projected damage area measurement are shown in Table 42.

Table 42: Impact damage projected area results

Material	5J Incident Energy mm²	15J Incident Energy mm²	25J Incident Energy mm²
T1	399	1353	2463
T2	394	1238	2189
T3	478	1310	2191
T4	335	1149	1940
T5	162	1127	2123
T6	329	1127	2009
T7	282	1103	2002
T8	454	1425	2326
T9	486	1440	2411

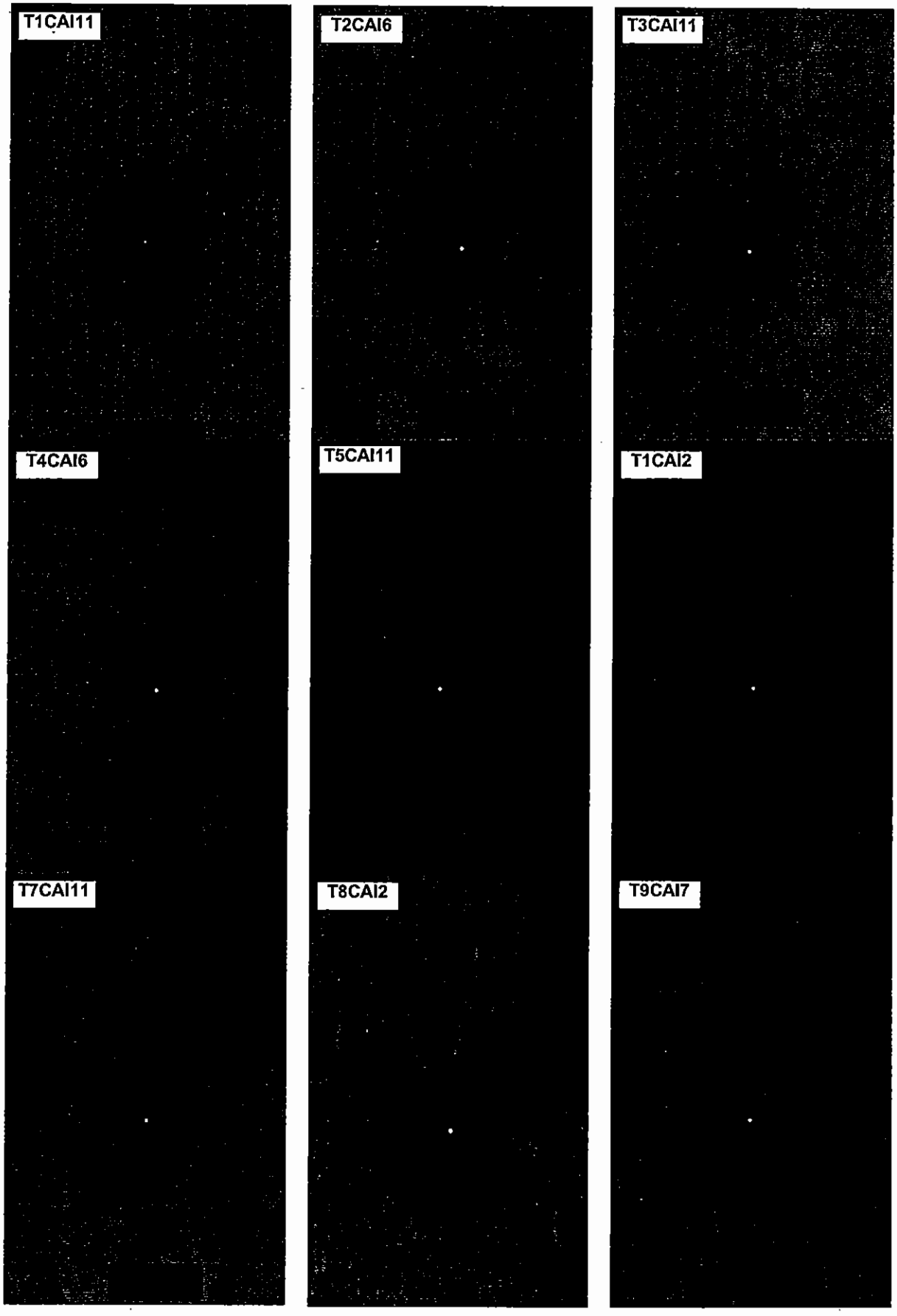

Figure 159: Penetrant Enhanced X-Radiographs of CAI Laminates T1-T9

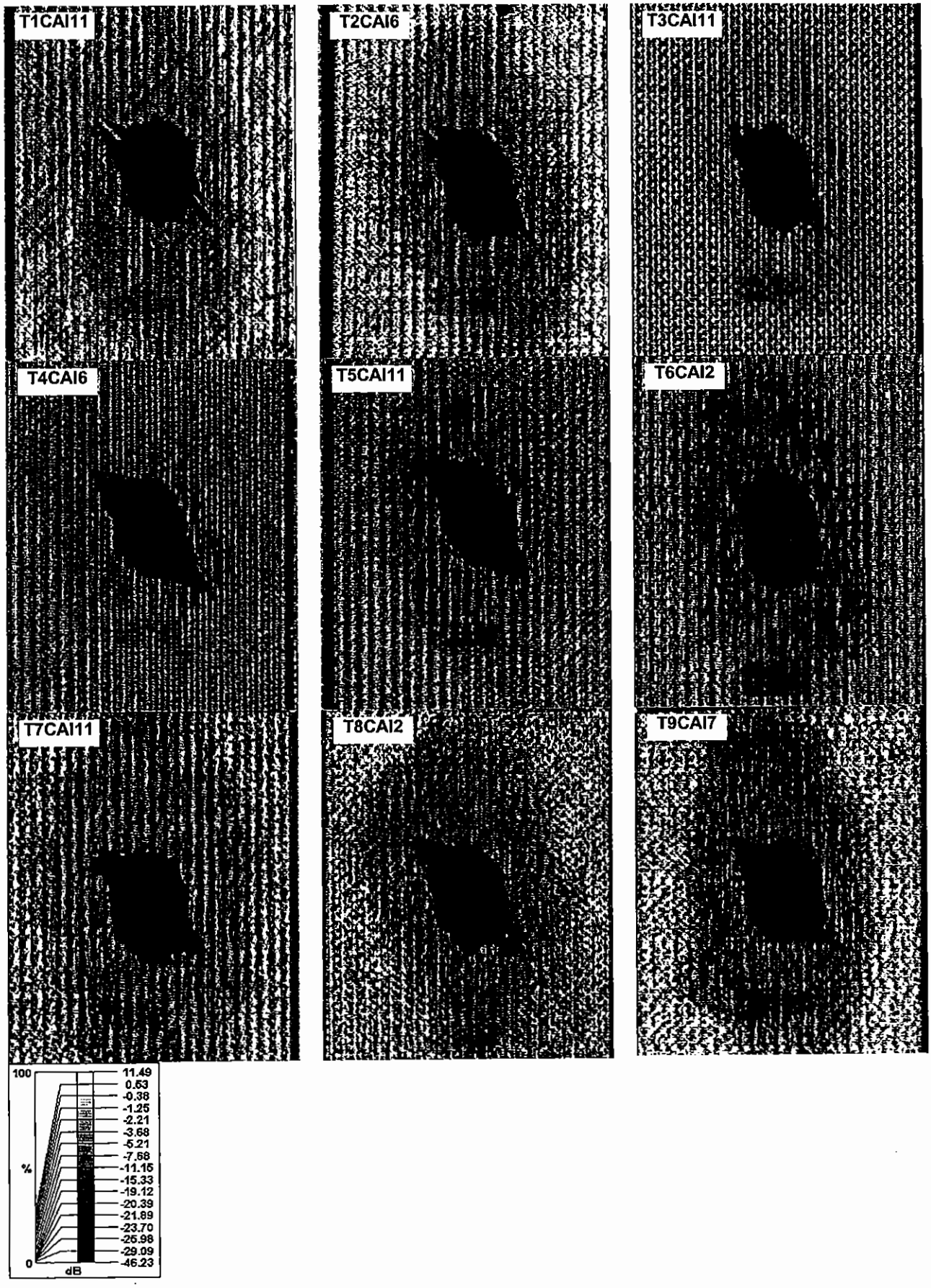

Figure 160: High Resolution C-scans of CAI Laminates T1-T9

6.4.2.1 Impact damage area observations

Projected damage areas in all cases are shaped as would be expected; generally elongated in the major load bearing axis (0°) with a characteristic back face delamination and split in the last ±45° layer. As can be observed in the X-ray images the delaminations in the other plies emanate from the impact site and are 'petal' or 'peanut' shaped as widely observed for prepreg tape laminates. Transverse microcracks can be clearly seen in the X-ray images both in and extending beyond the delaminated plies in ±45° and 0° directions. These cracks are longest in the 0° direction and extend in width to approximately that of the indentor diameter.

In the X-ray image of material T1, a large 'halo' of microcracks can be observed around the impact site and not seen in the initial C-scan images. The microcracks are principally in the ±45° directions and appear to originate from the points at which the stitching yarns penetrate the fabric blankets. High resolution C-scans however indicate its presence on all the samples to varying degrees. Its invisibility in a majority of the X-ray images suggests that the cracks are not physically connected to the delaminations but exist as discrete cracks distributed through the thickness of the material. Their presence on the X-ray of T1 may suggest that they are surface breaking, either only that sample or because X-ray opaque penetrant may have been wiped inadvertently into that surface.

6.4.2.2 Effect of Manufacturing Settings

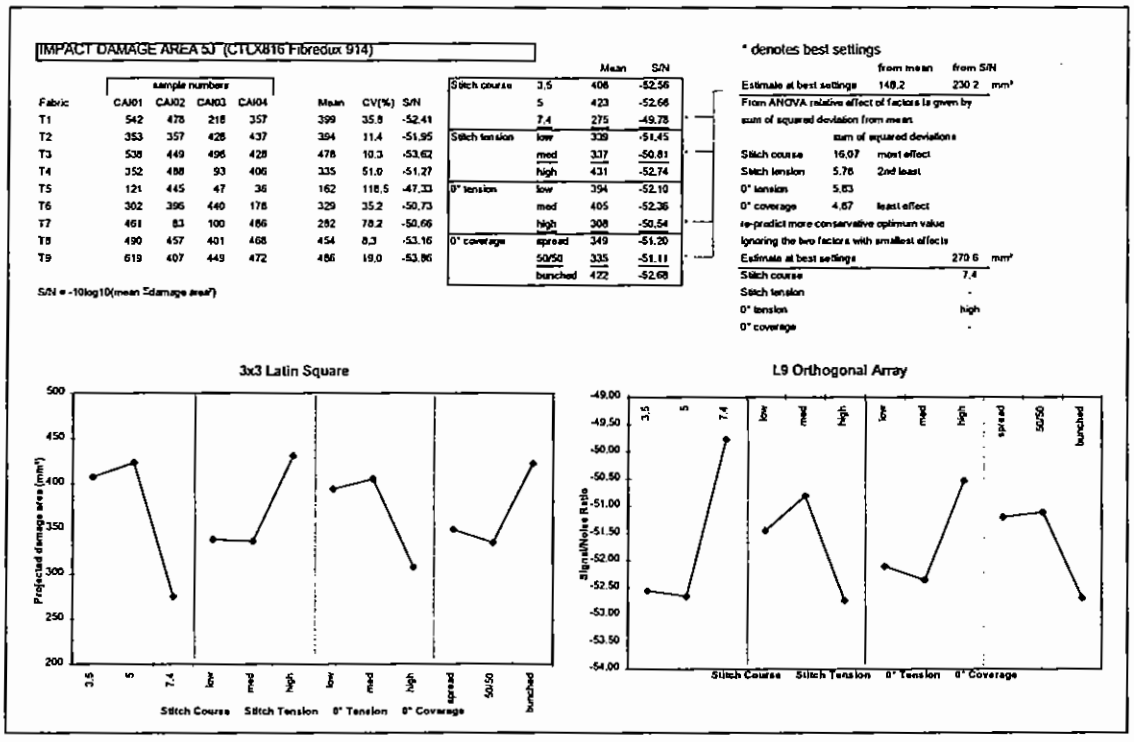

Figure 161: Projected damage area at 5J Impact Results Summary

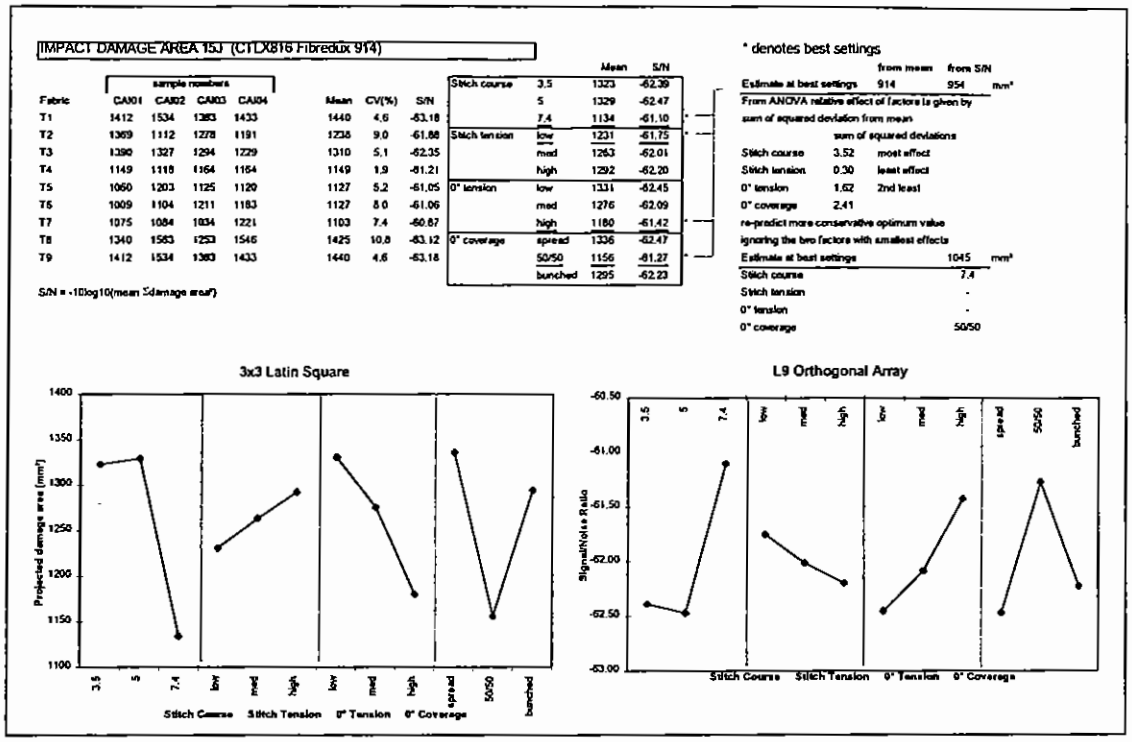

Figure 162: Projected damage area at 15J Impact Results Summary

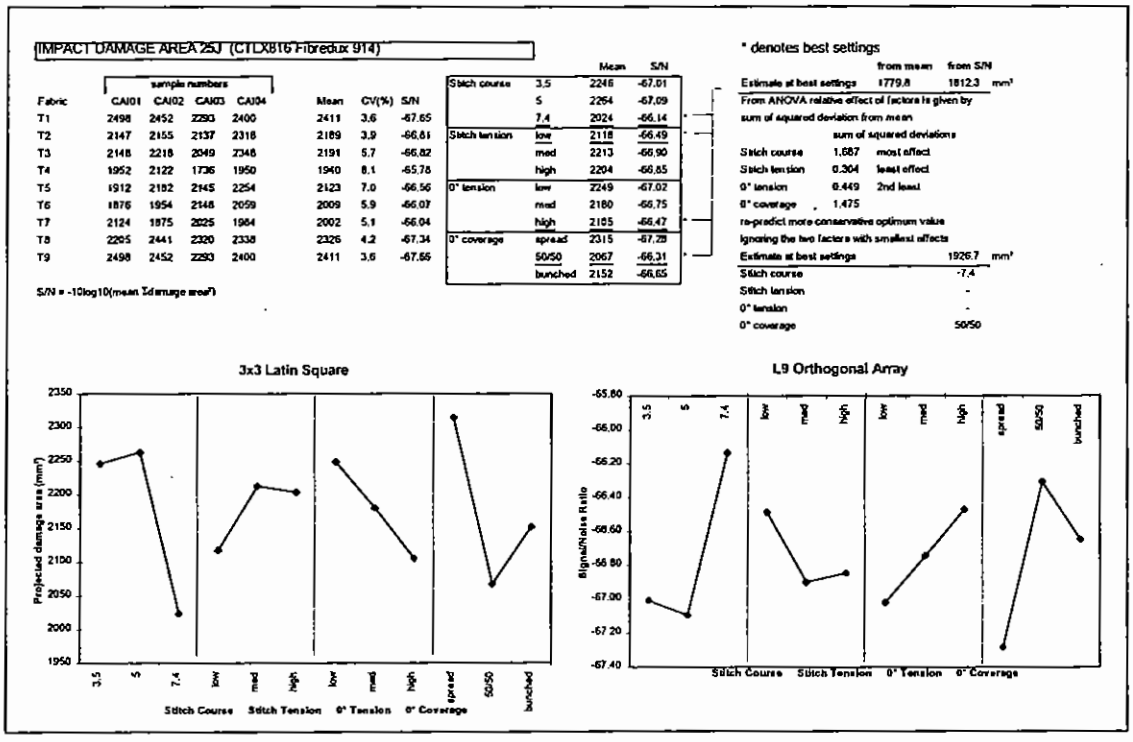

Figure 163: Projected damage area at 25J Impact Results Summary

Across all three energies tested the 7.4 stitch course provides a large reduction in damage area. Similarly the 50/50 0° coverage configuration in all cases minimises the damage area as does the lowest stitch tension during manufacture. In all cases these settings match those to maximise the delamination threshold force. A high 0° setting appears to minimise the delamination area but has little effect on the delamination threshold force.

6.4.3 Compression After Impact Strength

During testing of the 5 Joule impacted samples, a large number of samples had to be discarded, having failed in the un-supported gap between the anti-buckling guides and the upper load application fixture. The compression after impact testing of 5J samples was therefore abandoned and hence is not reported.

The summary results for the 15 and 25J incident energy impacts are found in Table 43. Four 25J impacted samples were tested but only three 15J samples; the remaining one was retained for impact damage evaluation as described earlier.

Table 43: Compression After Impact Strength Results

Material	15J Impact CAI Strength MN/m²	SD (MN/m²)	CV (%)	25J Impact CAI Strength MN/m²	SD (MN/m²)	CV (%)
T1	302.2	14.0	4.6	262.1	7.5	2.9
T2	311.0	5.8	1.9	259.0	4.0	1.5
T3	307.6	20.2	6.6	268.1	4.4	1.6
T4	314.0	15.2	4.8	277.6	13.8	5.0
T5	317.3	4.7	1.5	273.2	5.1	1.9
T6	322.9	19.6	6.1	272.4	5.7	2.1
T7	302.6	23.0	7.6	251.3	6.3	2.5
T8	317.1	10.6	3.3	265.2	11.9	4.5
T9	290.1	10.1	3.5	254.3	2.7	1.1

6.4.3.1 Effect of Manufacturing Settings

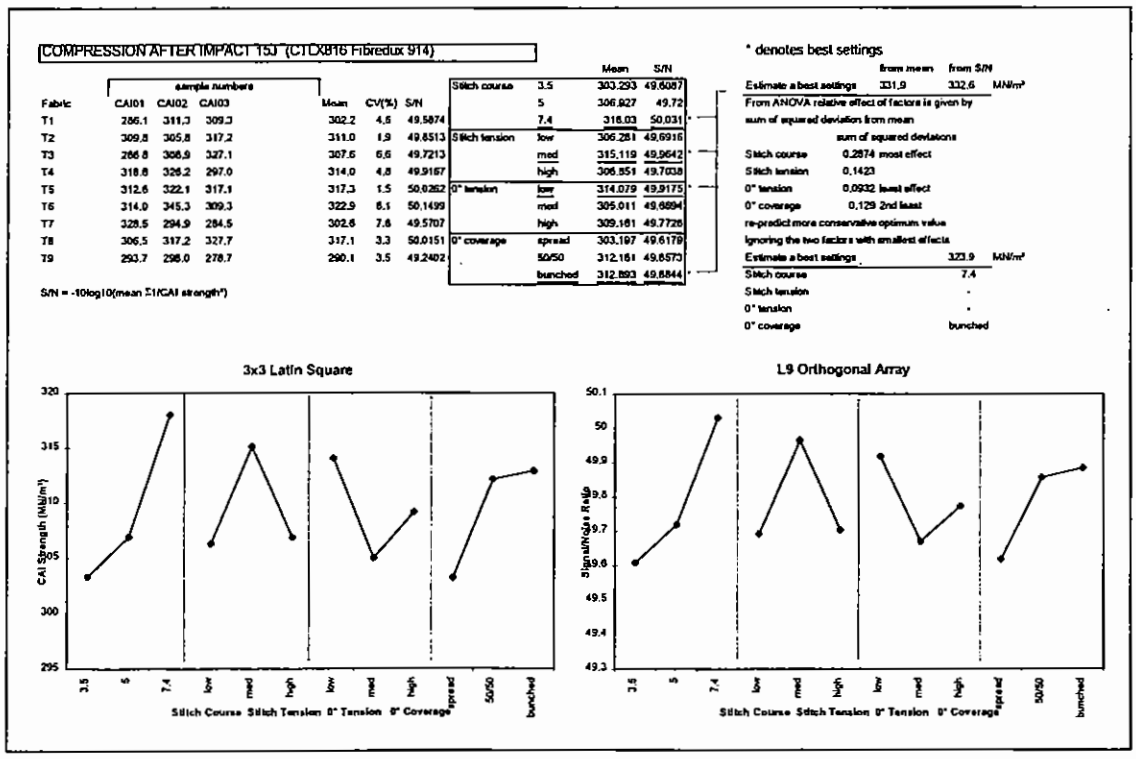

Figure 164: Compression Strength After 15J Impact Results Summary

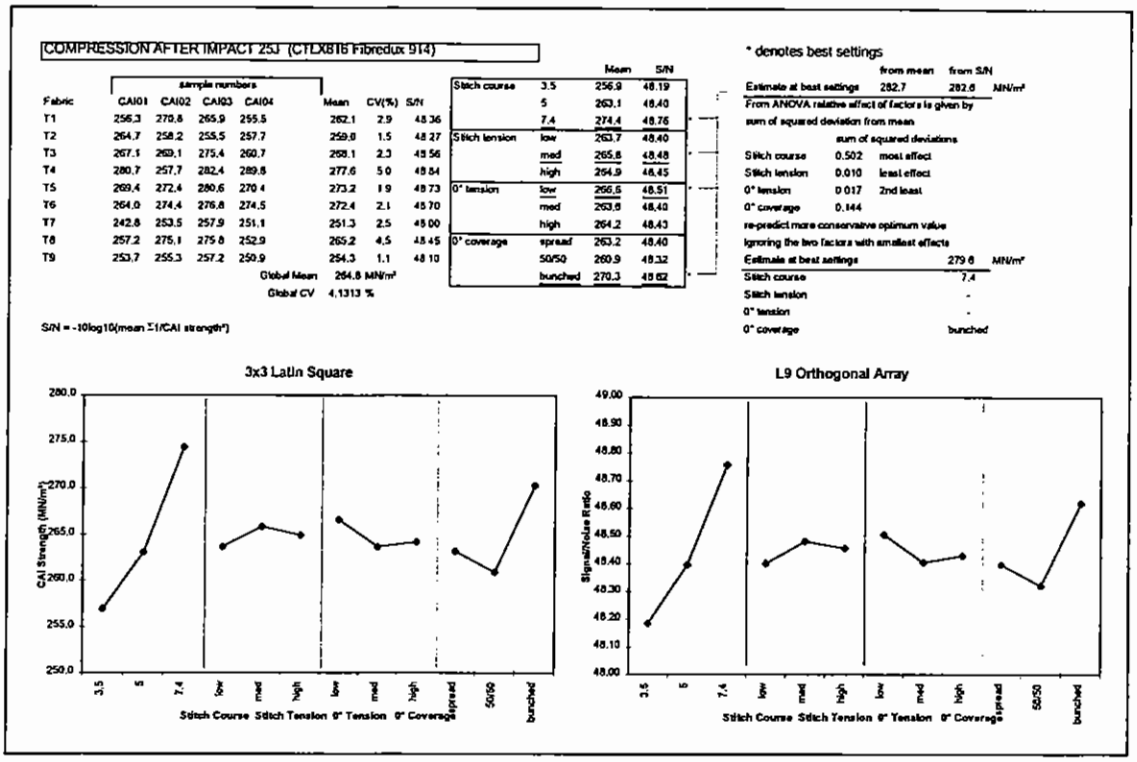

Figure 165: Compression Strength After 25J Impact Results Summary

At both 15 and 25J impact energies the Compression After Impact Strength is enhanced by the highest stitch course and the bunched 0° coverage. The role of stitch and 0° tension diminishes at the 25J energy. The beneficial effect of the 0° coverage being bunched is unexpected as compression strength was maximised and damage area minimised at the 50/50 coverage setting.

6.4.4 Mode I Interlaminar Fracture

Strain energy release rates calculated using Corrected Beam Theory can be found in Table 44.

Table 44: Mode I strain energy release rates (0°/0° interface)

	G_{IC} (non-linear) J/m²	G_{IC} (5% offset) J/m²	G_I (propagation maximum) J/m²	G_I (average for first 10mm of propagation) J/m²
T1	232	265	389	301
T2	238	262	375	289
T3	274	320	475	361
T4	226	284	580	424
T5	250	309	528	325
T6	213	273	441	347
T7	256	269	337	261
T8	235	267	436	318
T9	208	245	493	255

For one sample of each material the fracture surface was optically scanned and enlarged to match that of the load/crack opening displacement graphs and placed adjacent to one another . A graph of the resulting strain energy release rate against delamination crack length was then superimposed on the fracture surface. From this we can observe the effect of the polyester stitching/knitting yarn on both crack

growth rate and strain energy release rate during delamination propagation. These images and graphs are shown in Figure 166 to Figure 174.

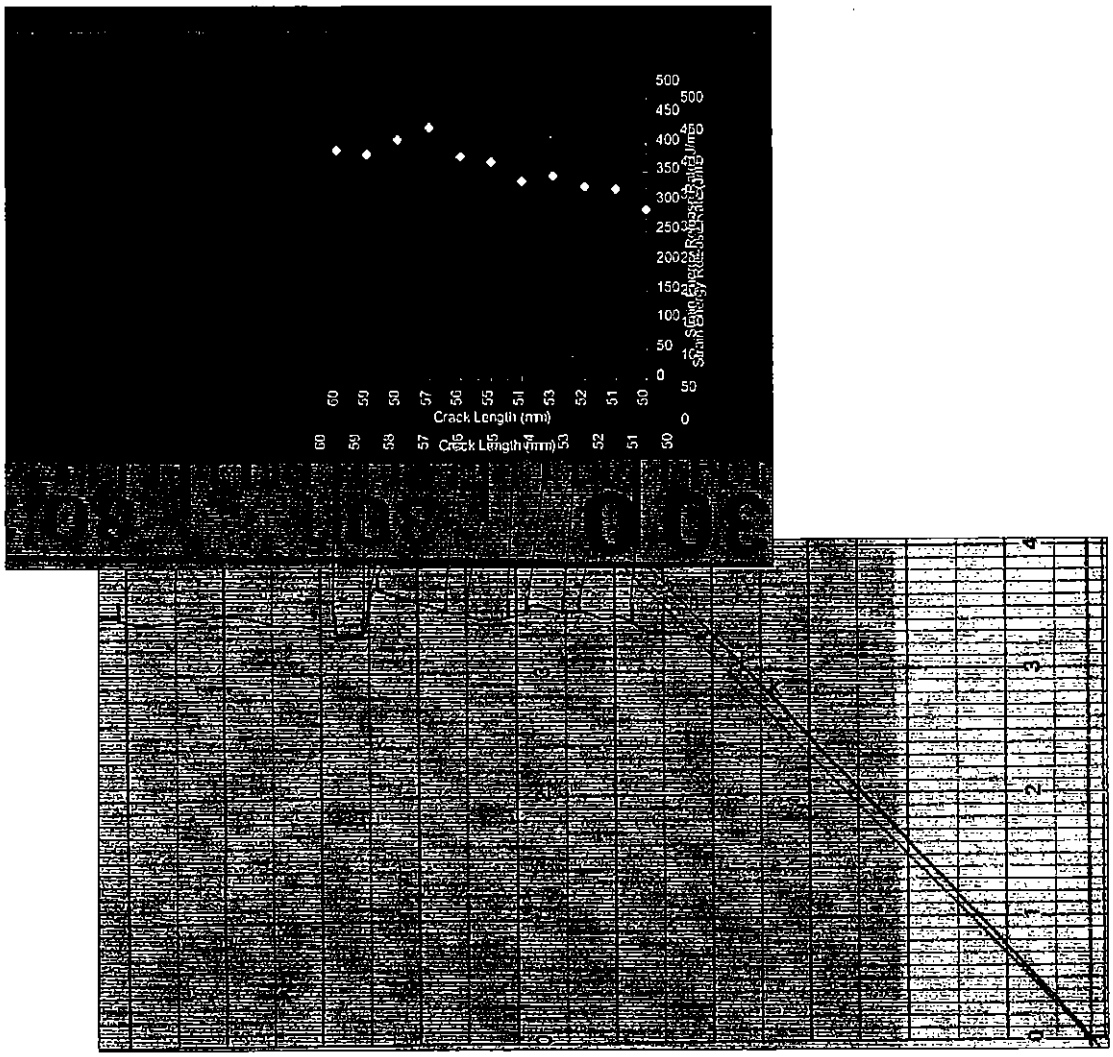

Figure 166: Sample T1DCB03 Mode I Fracture Map

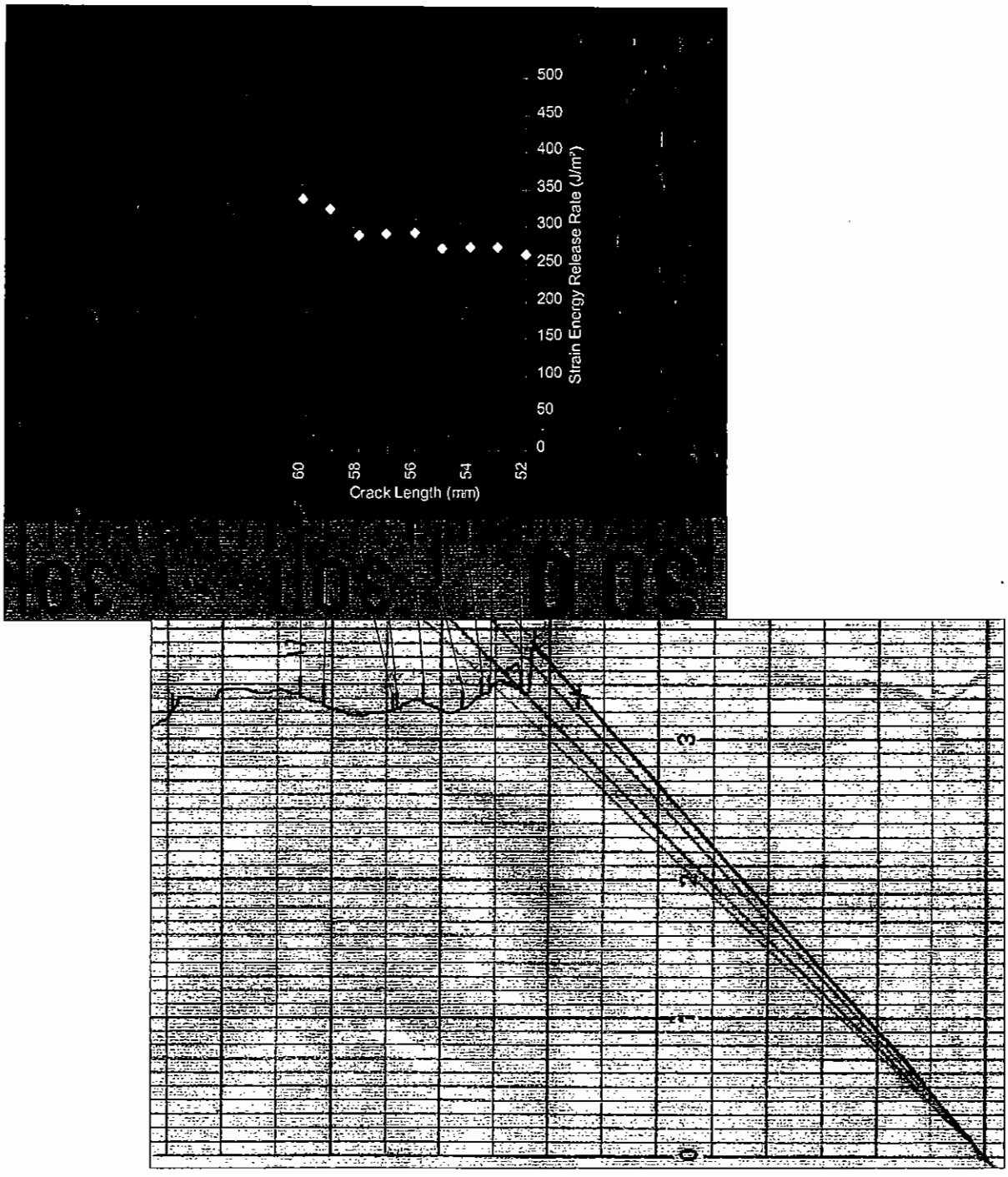

Figure 167: Sample T2DCB03 Mode I Fracture Map

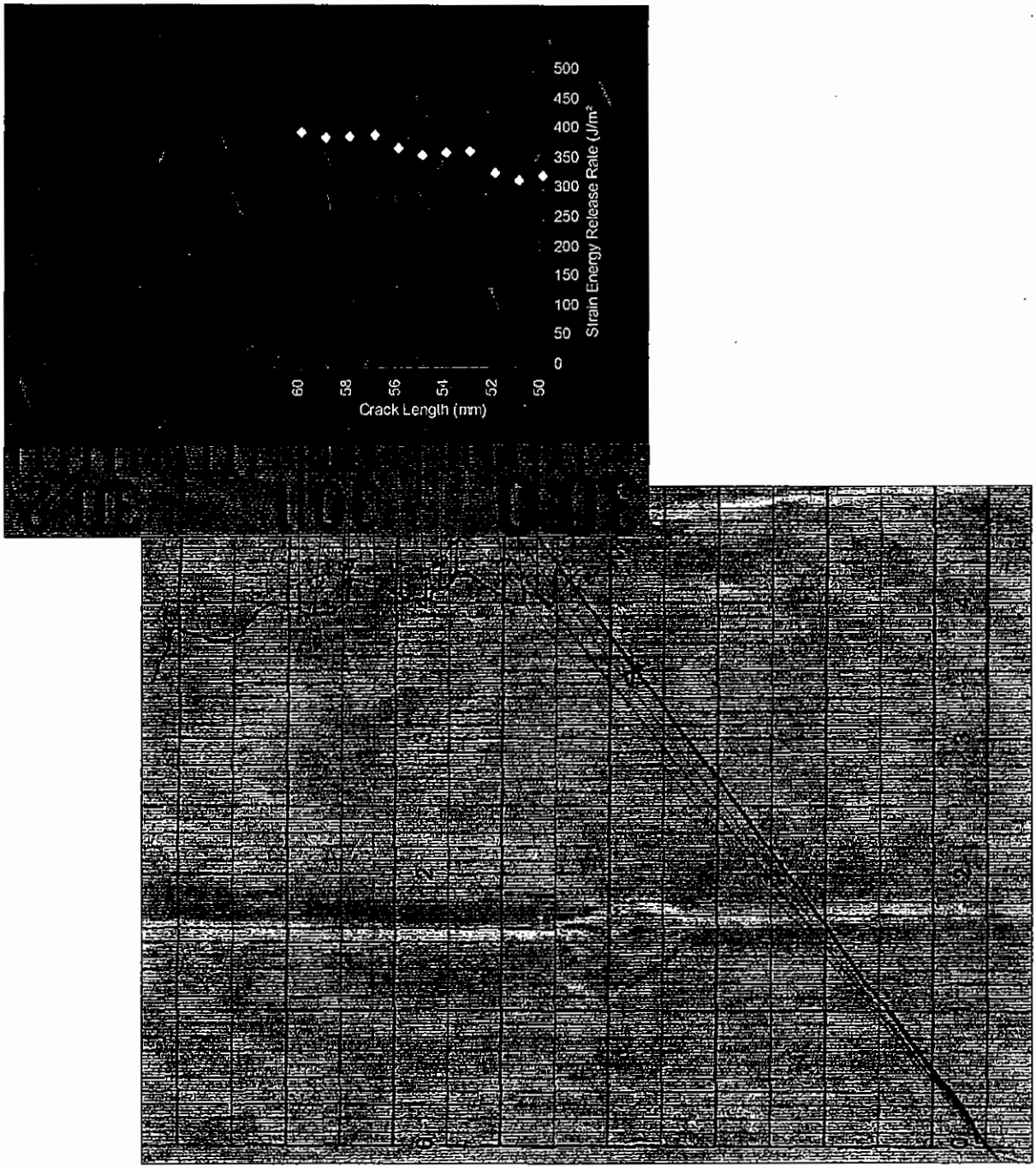

Figure 168: Sample T3DCB03 Mode I Fracture Map

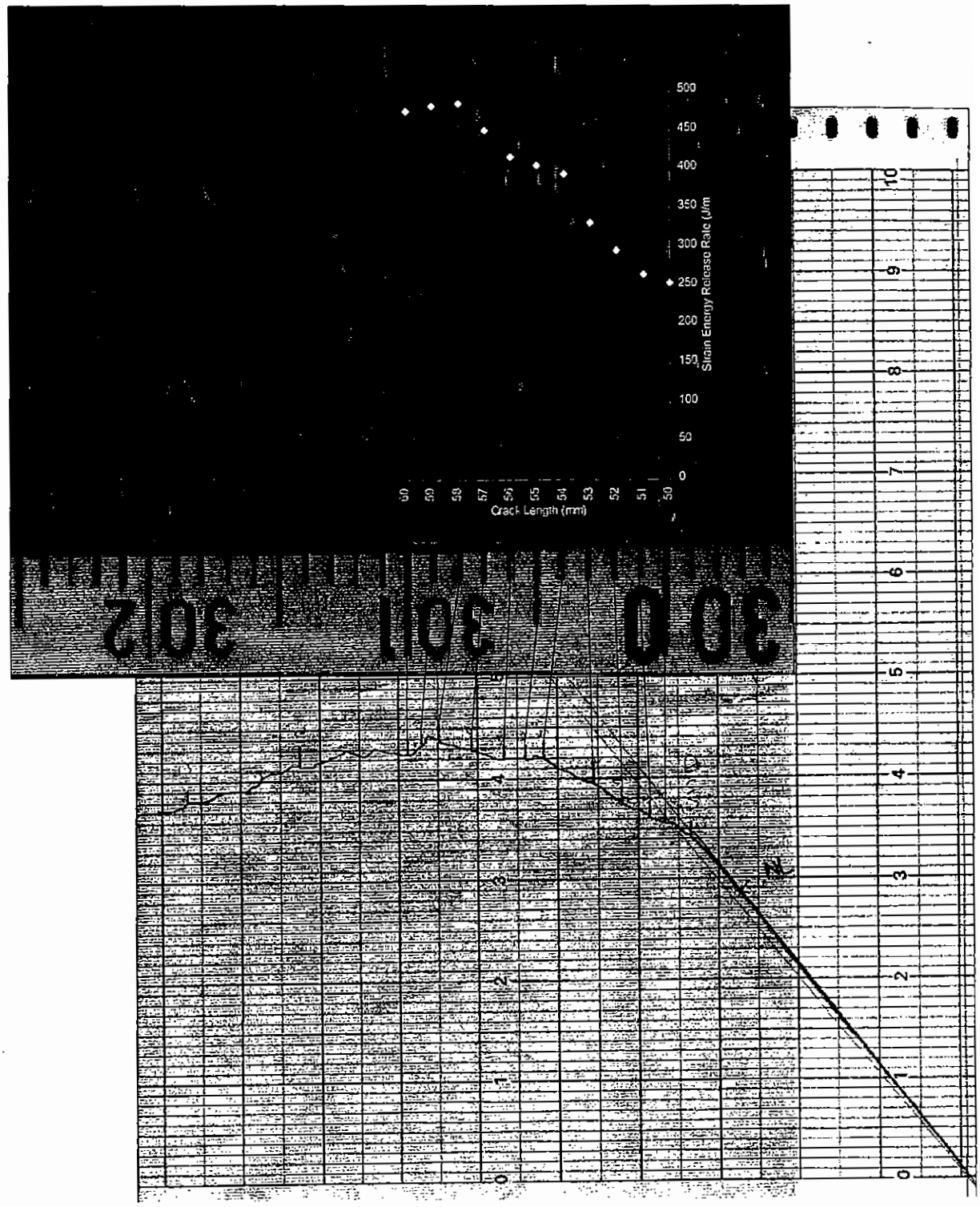

Figure 169: Sample T4DCB02 Mode I Fracture Map

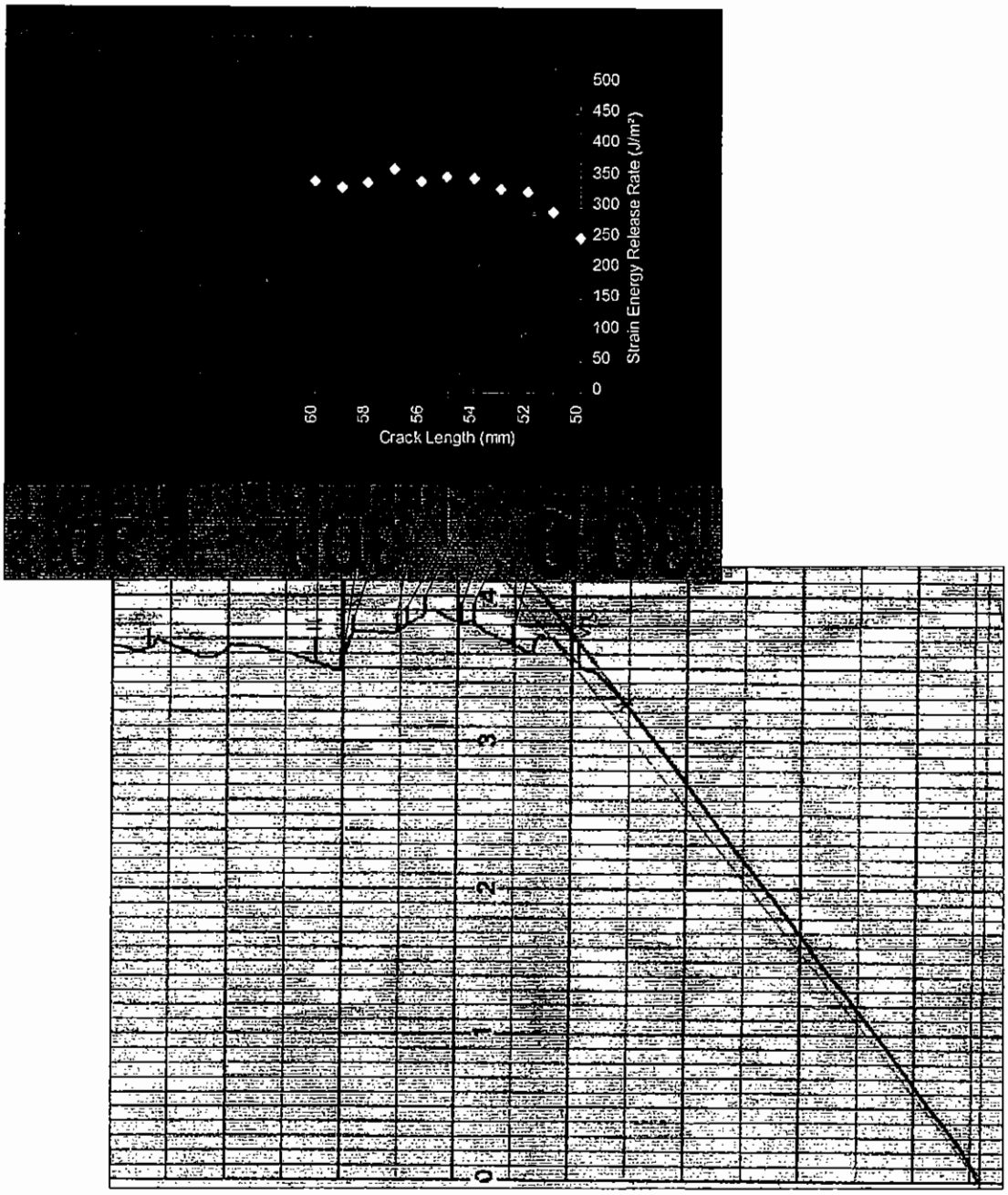

Figure 170: Sample T5DCB02 Mode I Fracture Map

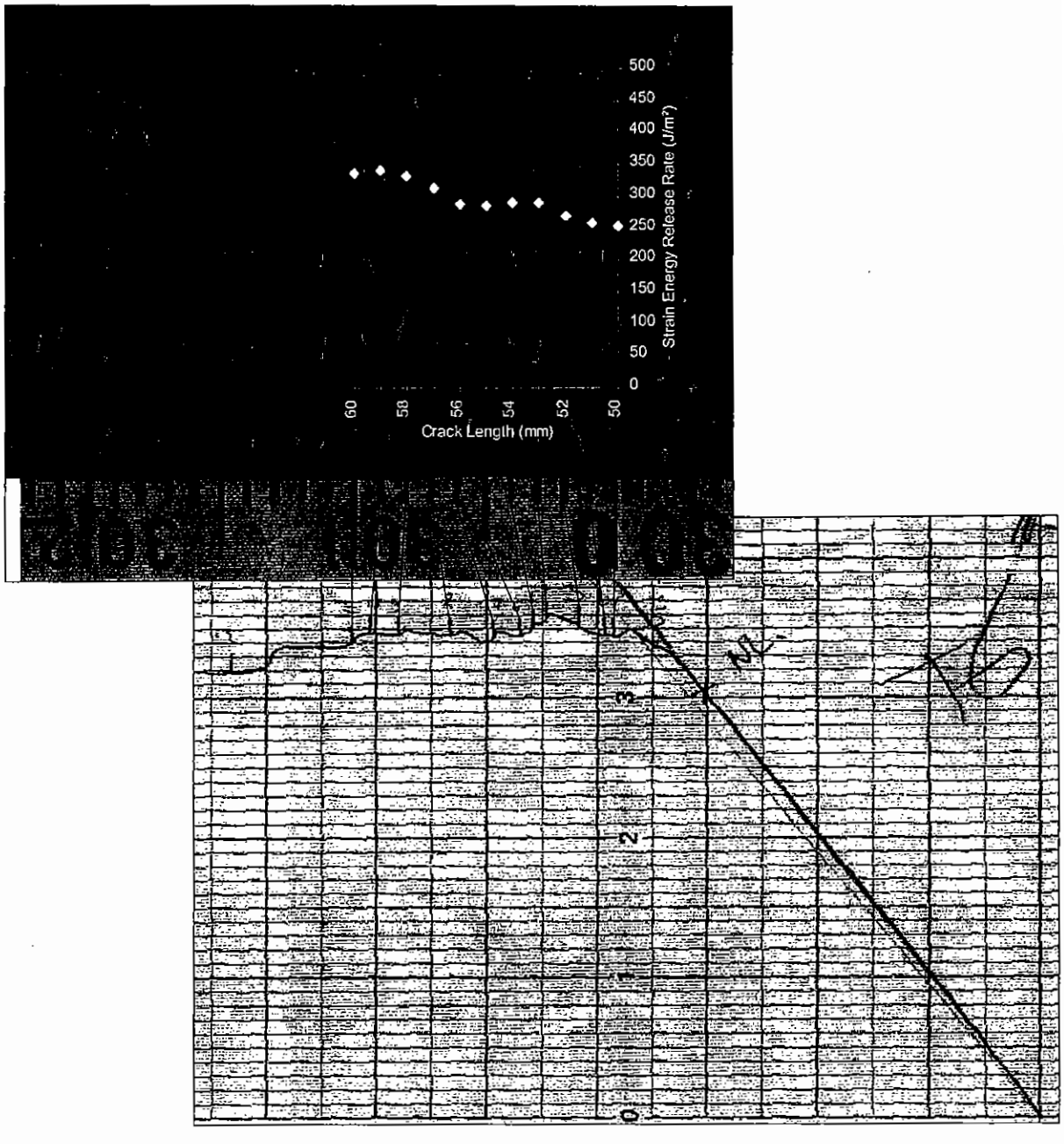

Figure 171: Sample T6DCB02 Mode I Fracture Map

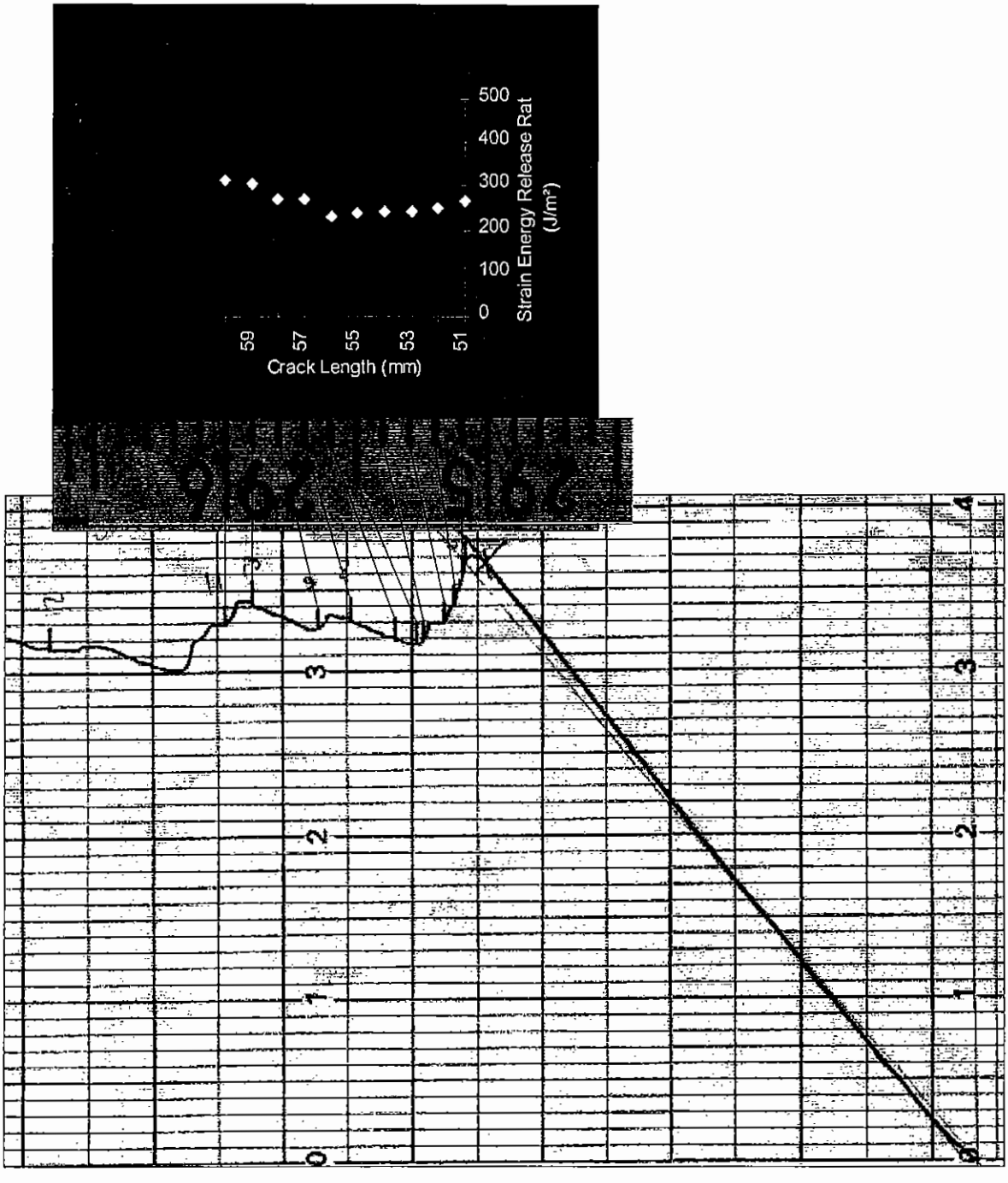

Figure 172: Sample T7DCB02 Mode I Fracture Map

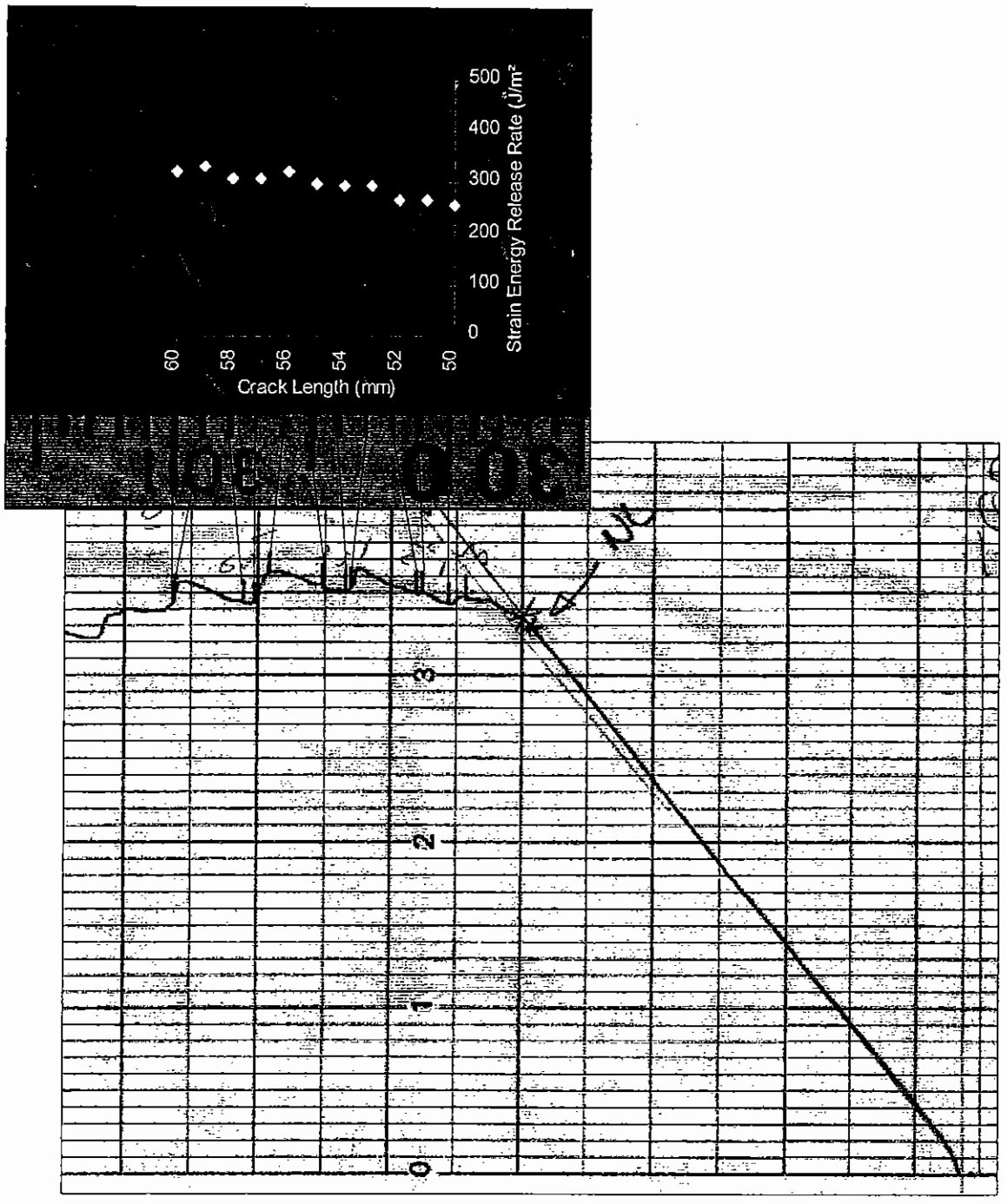

Figure 173: Sample T8DCB02 Mode I Fracture Map

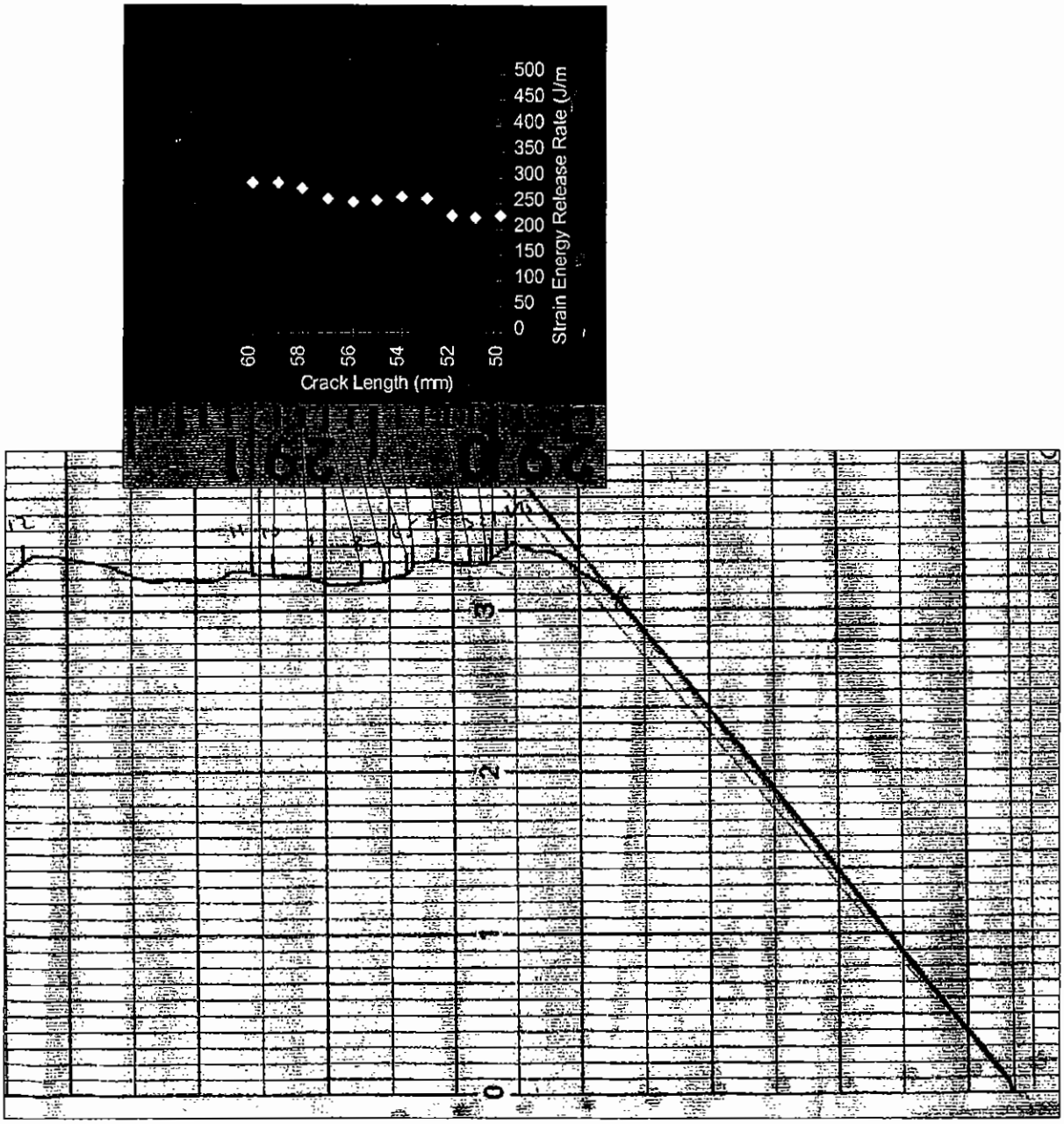

Figure 174: Sample T9DCB02 Mode I Fracture Map

6.4.4.1 Mode I Interlaminar Fracture Observations

Mode I strain energy release rates calculated using the point of non-linearity of the load displacement curve (NL) are broadly similar for all the fabrics tested, similarly 5% offset values are again similar for all materials. During propagation of the crack however we see a wider range of values both for the maximum propagation strain energy release rate and the mean value in the first 10mm of propagation. The mean strain energy release rate for the first 10mm of propagation was used it is only for this crack length that we have 1mm resolution of the crack location. During the test polyester fibres are observed bridging the delamination crack. They were observed to remain attached across the two arms of the sample as the crack propagated several millimetres ahead, before they were broken or pulled from the matrix. The effect of this polyester bridging the crack front can be observed particularly in the fracture maps of Figure 167, Figure 171 and Figure 172 where the delamination

propagates through an area with few polyester fibres at the interface until it reaches an area with more polyester, whereby the strain energy release rate increases.

Bridging of carbon fibres across the delamination was only observed in material T4 and only as the crack length had propagated to around 5mm.

The change in strain energy release as the delamination propagates suggests that the role of the stitching/knitting yarn is small at crack initiation but larger as the crack propagates. The presence of the stitching/knitting yarn at the point of initiation does not significantly increase the initiation strain energy release rates (NL, 5% offset).

Delamination growth rate is rapid in where there is little polyester knitting yarn but slows as the polyester stitching/knitting yarn bridges the delamination after which the load/opening displacement increases. This is most clearly observed in sample T1DCB03 (Figure 168) where on reaching the end of the polyester on the surface the strain energy release rate continues to increase for, in this case 2mm. At this point, as can be seen for the load/crack opening displacement graph, there is a sudden reduction in load and crack propagation as the polyester yarn either breaks or is pulled out of the fracture surface.

We can therefore observe that the propagation strain energy release rate is determined by the amount of polyester yarn at the fracture surface which is a function of the stitch course (stitch penetrations/centimetre) and the 0° coverage (how much of the 0° tows are encompassed by the knitting yarn). The polyester stitching yarn primarily affects the crack propagation by bridging the crack front and providing crack closure force.

6.4.4.1.1 Effect of Manufacturing Settings

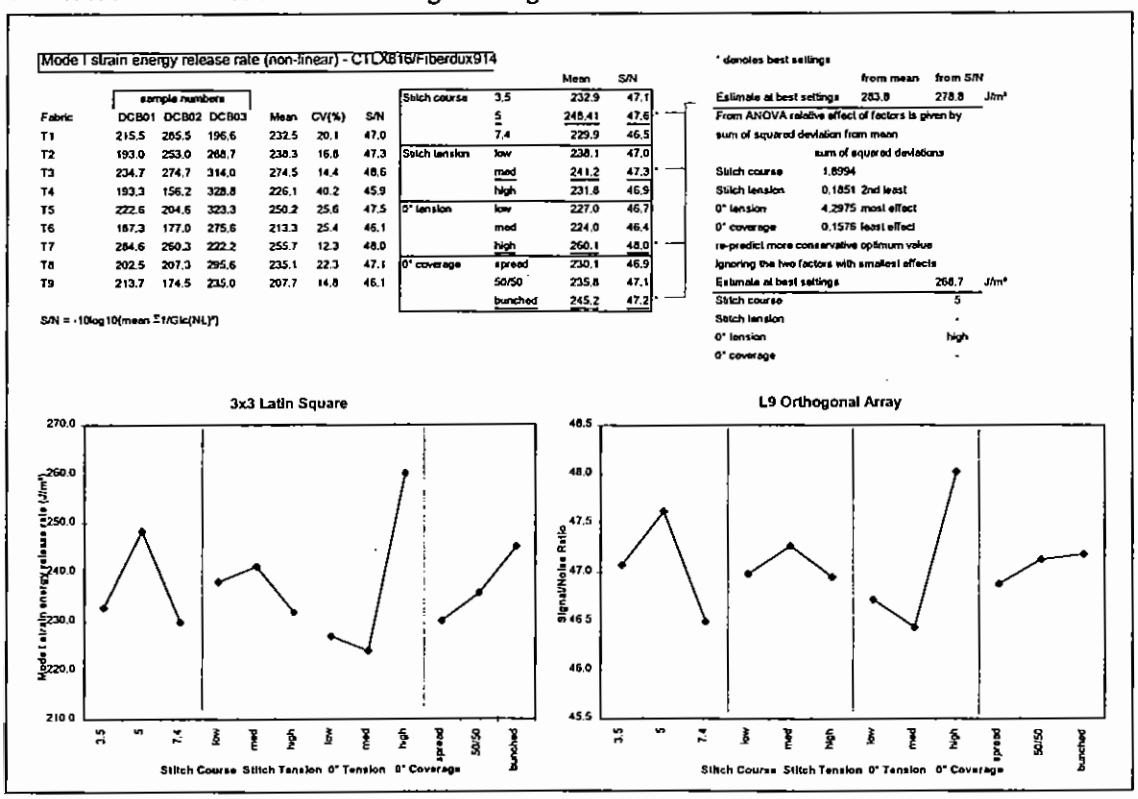

Figure 175: Mode I at Non-Linear Point Results Summary

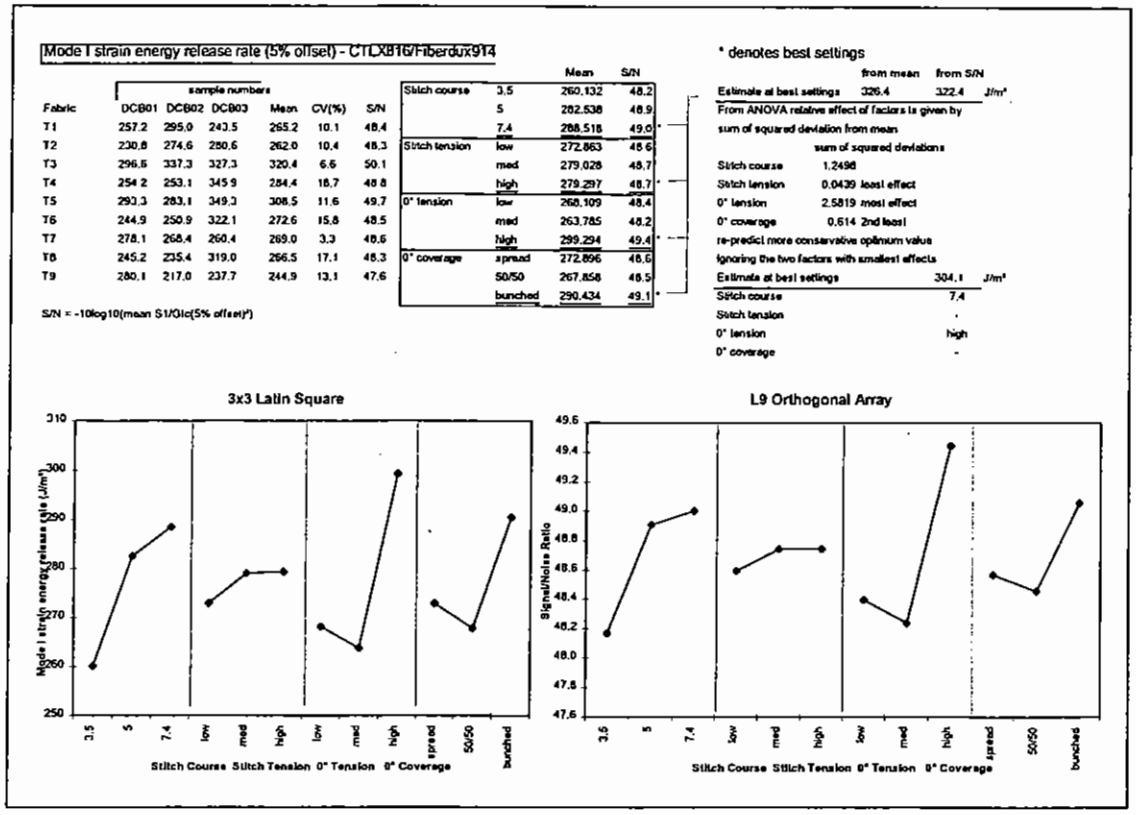

Figure 176: Mode I 5% Compliance Offset Results Summary

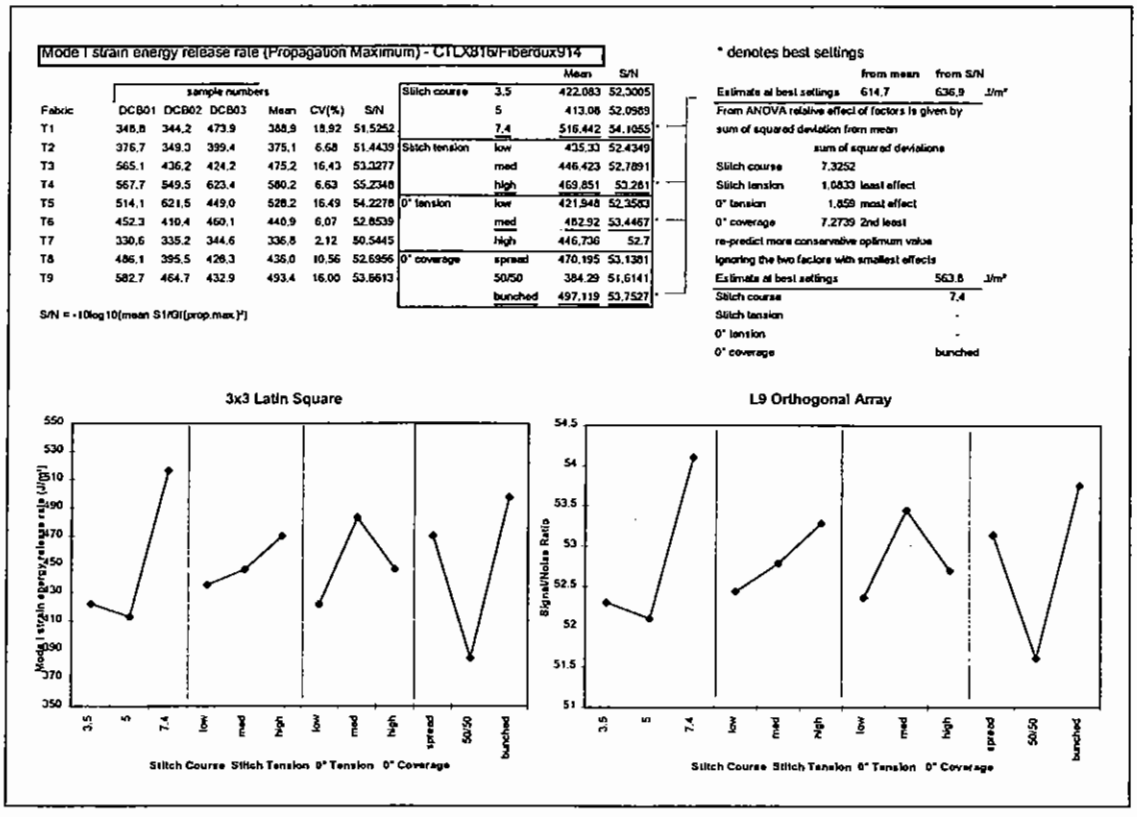

Figure 177: Mode I Propagation Maximum Results Summary

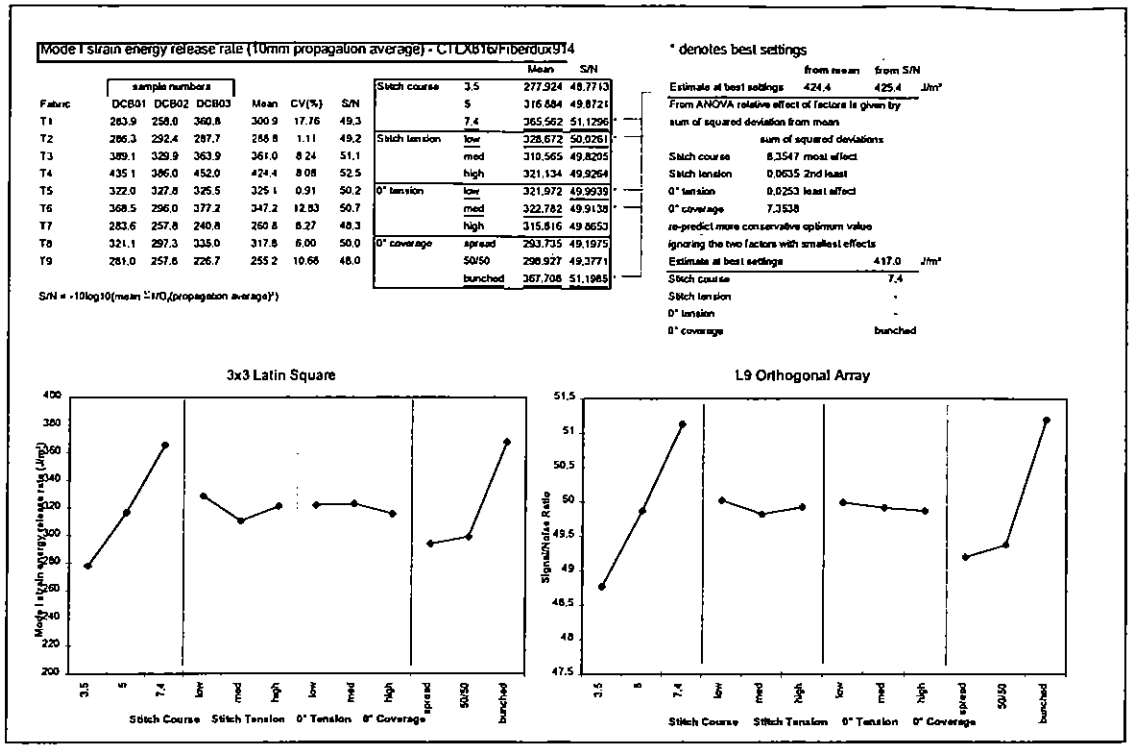

Figure 178: Mode I 10mm Propagation Average Results Summary

As observed from the fracture maps, increasing the stitch course and consequently the amount of polyester bridging the fracture increases the strain energy release rate. Stitch tension has little effect on any of the measured characteristics but 0° tension appears to have a large effect on both the critical strain energy release rate calculated from the point of non-linearity on the load/displacement curve and from the 5% compliance offset point. The influence of the 0° coverage at these points is also small but as the delamination propagates the bunched 0° coverage is favoured as it provides more polyester yarns which bridge the propagating delamination.

6.4.5 Damage Resistance and Tolerance Discussion

The delamination threshold force increases as the mean resin area size reduces as shown in Figure 179. This effect is weak but two groupings can be observed: Firstly at 15J, materials with bunched 0° fibres and consequently large resin channels have a lower threshold for damage. Secondly, at 25J only the materials with bunched 0° tows and high stitch tension have low threshold force for delamination damage.

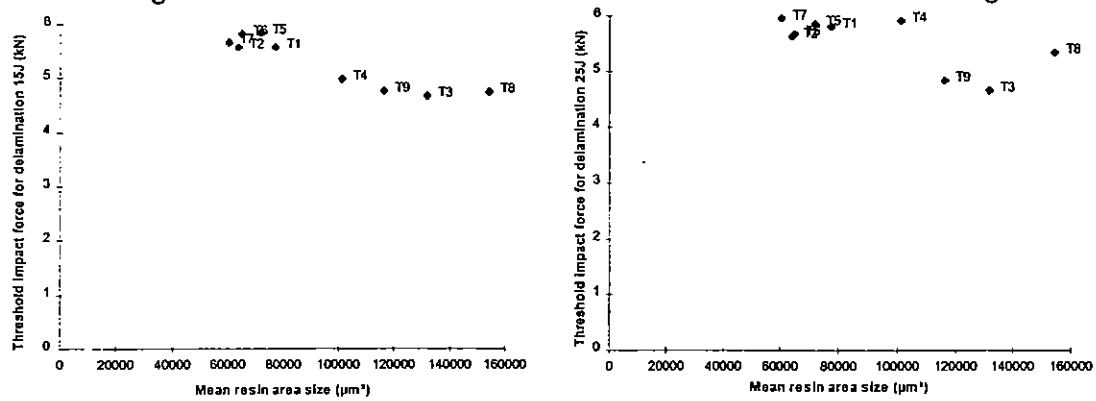

(a) 15J Impact (a) 25J Impact

Figure 179: Relationship between delamination threshold force and mean resin area size

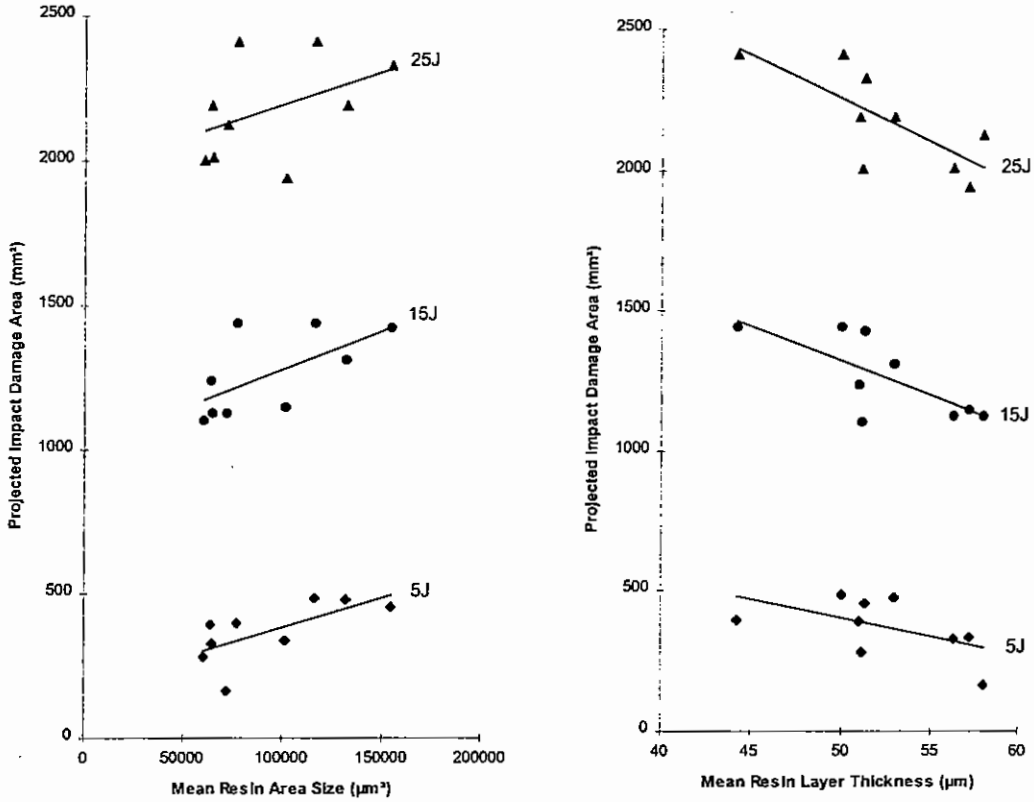

Figure 180: Relationships between resin distribution and impact damage area

In Figure 180 we observe different influences of the resin distribution on impact damage area. Increasing mean resin area size corresponds to an increase in the projected delamination area as observed by ultrasonic C-scan. However as the resin layer thickness increases we see the damage area reducing. This effect is not caused by a relationship between mean resin area size and mean layer thickness as they appear independent (Figure 181). These observations suggest that to minimise impact delamination area, all the free resin in the structure should exist as resin layers, rather than areas.

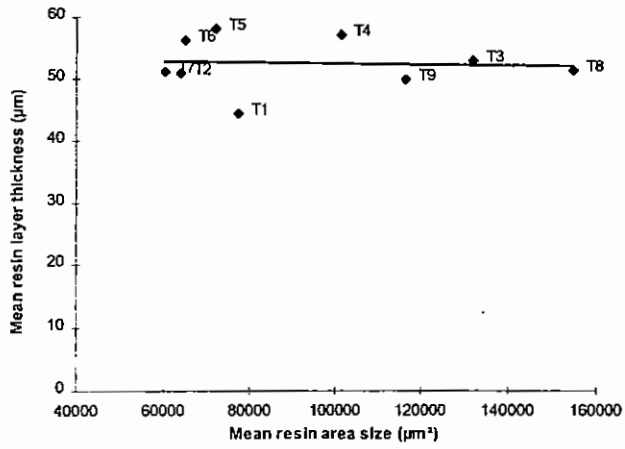

Figure 181: Relationship between mean resin area size and mean layer thickness

Considering the effect of damage area, resin layer thickness and mean resin area size on compression after impact strength (Figure 182 and Figure 183) we observe a dependence of CAI strength on impact damage area. The line is not straight as we know that the manufacturing settings of the fabric will modify the response. The

effect of mean resin area size shows no clear relationship with CAI strength but increasing the resin layer thickness increases the CAI strength. This is likely to be a result of the relationship between resin layer thickness and damage area, plus any affect of the resin layer thickness on damage development during the CAI test. This is likely to be primarily crack opening (mode I). Evidence from interlaminar fracture testing would suggest that for a brittle matrix, such as Hexcel 914, that resin layer thickness will have more effect in mode II (a primary influence in impact damage development) than mode I (damage growth in CAI test) as the zone of plasticity around the crack tip is more elongated.

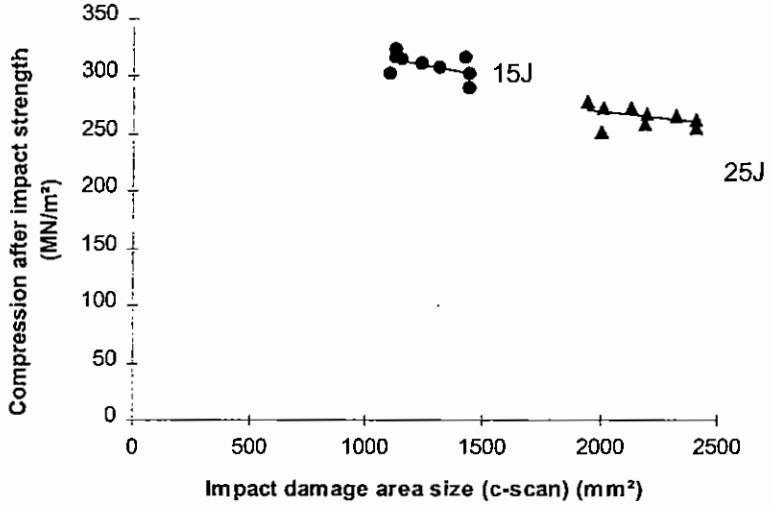

Figure 182: Relationship between Impact damage area (C-scan) and CAI strength

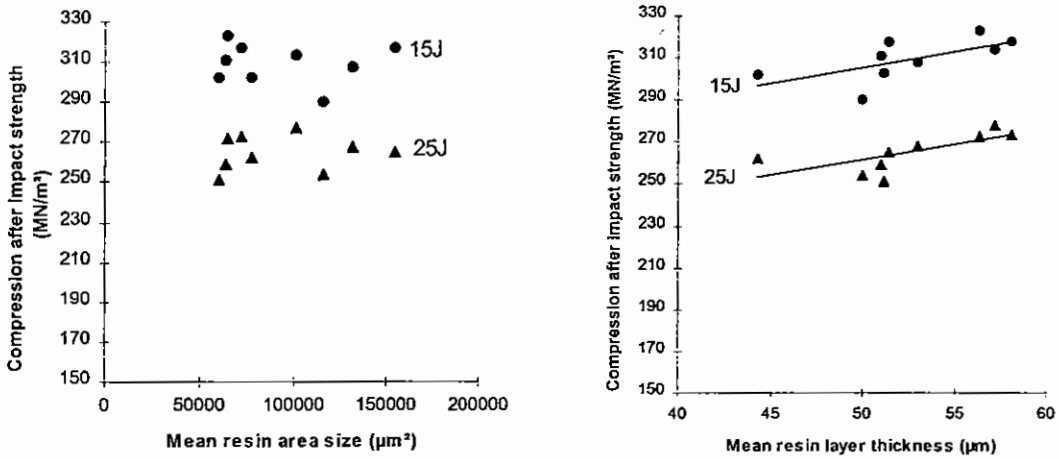

Figure 183: Relationships between CAI strength and resin distribution properties

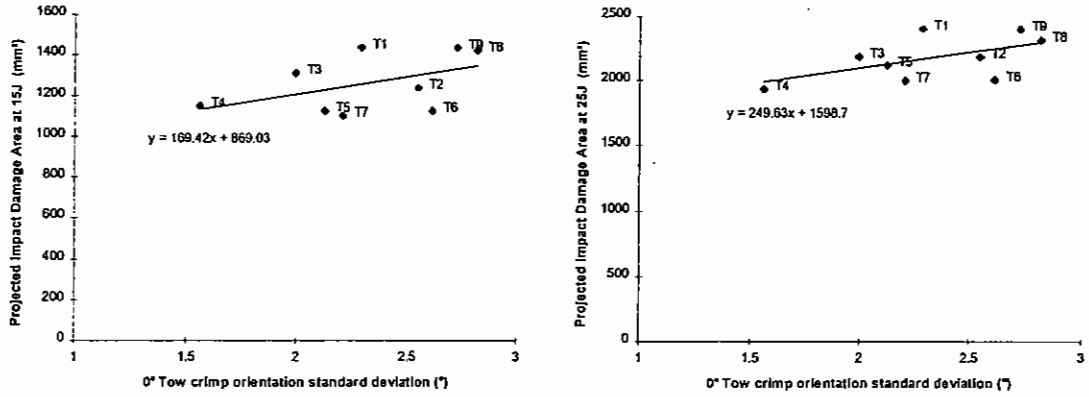

Figure 184: Relationship between tow-crimp standard deviation of orientation and impact damage area

Figure 184 indicates increasing impact damage area with increasing 0° tow crimp, this may be a real effect or may be due to the relationship between tow crimp and resin distribution as indicated in Figure 139. However a similar relationship is observed between tow-crimp and Mode I strain energy release rate as shown below.

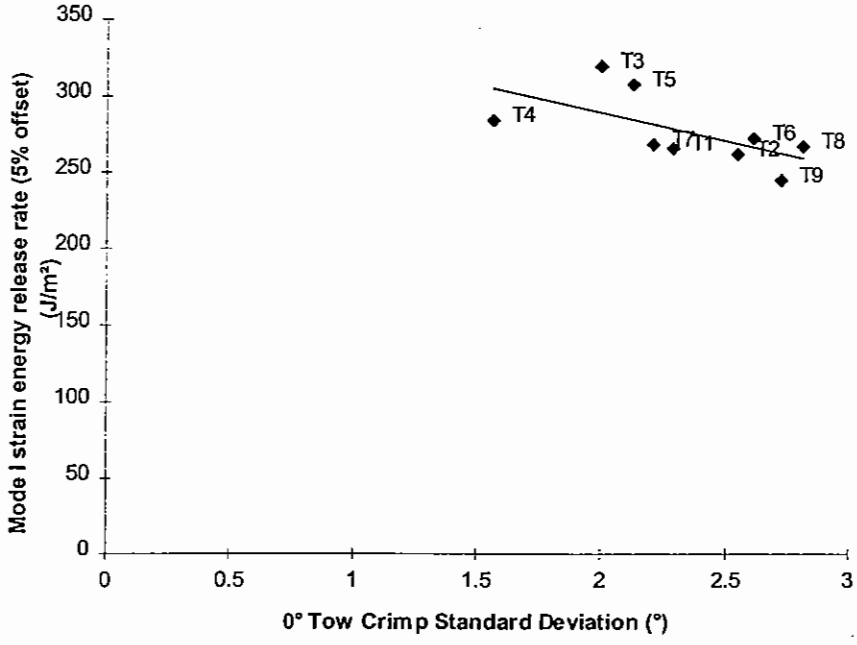

Figure 185: Relationship between 0° tow crimp and mode I strain energy release rate (5% compliance offset)

We have seen that the tighter the 0° tension during the manufacture of the fabric the lower the tow crimp resulting in the composite, and that the high 0° tension setting corresponds to the highest critical strain energy release rate. These two observations are confirmed by the above Figure. The mechanism responsible is however not obvious from the optical microsections or from the fracture maps.

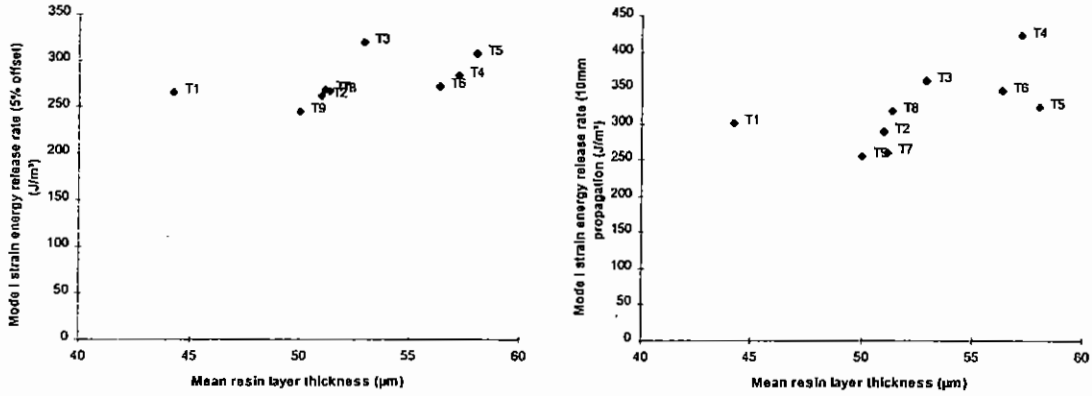

Figure 186: Relationships between resin distribution and Mode I strain energy release rate

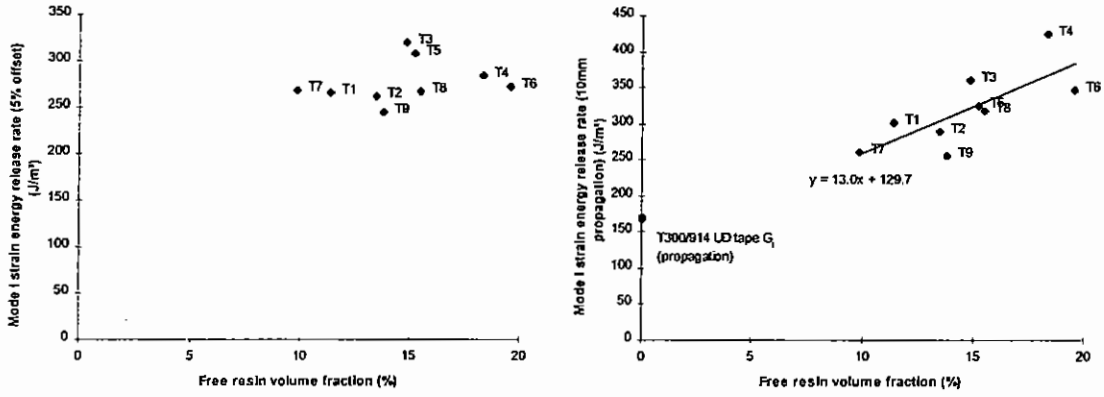

Figure 186: Relationships between resin distribution and Mode I strain energy release rate (continued)

In Figure 186 we see that increasing the mean resin layer thickness increases the strain energy release rate both for crack initiation and propagation. Increasing free resin volume similarly increases the propagation strain energy release rate, but no such relationship is observed when using the 5% offset point for comparison. Stronger relationships between resin layer thickness and strain energy release rate are likely to be observed in mode II loading. Test samples were prepared but not tested, due to lack of time.

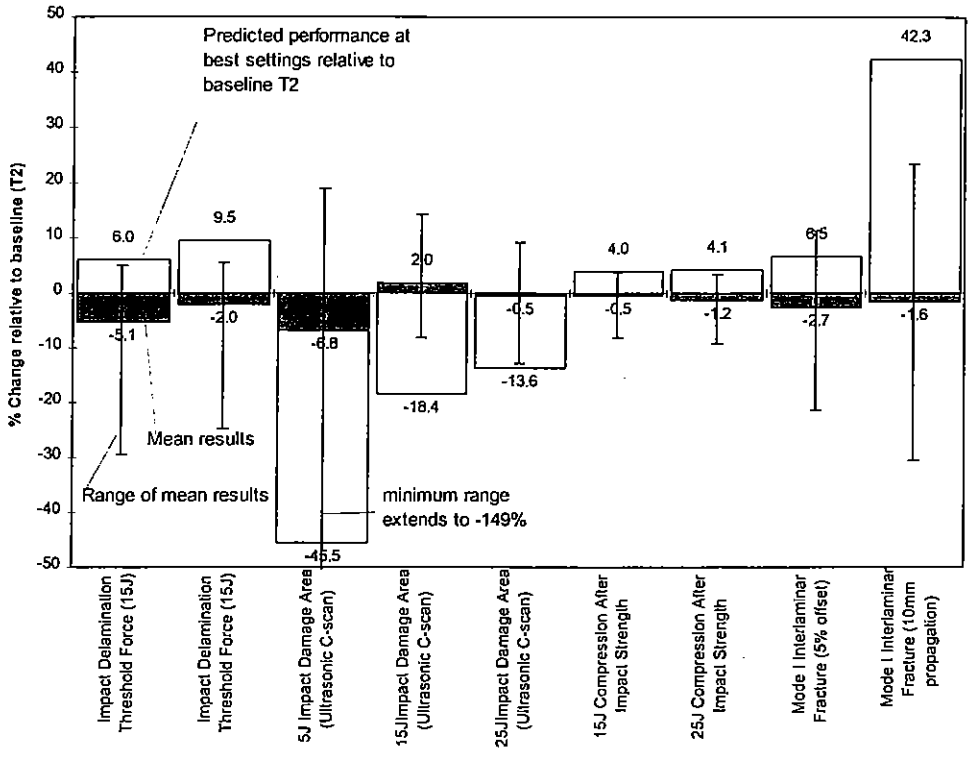

Figure 187: Predicted best damage resistance and tolerance performance relative to baseline T2 and mean

We can observe from Figure 187 that a 12% increase in threshold force is predicted above the mean performance of the fabric, an 9.5% above that of material T2 (baseline). This response corresponds to a high stitch course (high stitching density) and 50/50 split of the 0° coverage between being fully encapsulated and held occasionally by the stitching yarn. The same settings similarly minimise the impact damage area. As impact energy increases from 5 to 25J the possible reduction in damage area diminishes from 46 to 14%.

During the compression after impact test again the high stitch course maximises the residual strength but this time with a preference for a fully bunched 0° coverage. In the Mode I interlaminar fracture tests we observe the same preference for the fully bunched 0° coverage and high stitch course in most cases.

The tension at which the 0° material in inlayed into the fabric has an apparently strong influence on strain energy release rate for crack initiation (non-linear and 5% compliance offset). The same effect was observed on the impact damage area. In both cases progressively increasing the 0° tension results in increasing strain energy release rates and reducing damage areas.

Chapter 7

Non-Crimp Fabric Competitive Environment

7.1 Introduction

Strategic analysis is concerned with understanding the strategic position of an organisation. What changes are going on in the environment, and how will they affect the organisation's competitive position in the market

The multiaxial warp knitted non-crimp textile industry is a relatively new one and there is evidence to suggest that it could revolutionise the manufacture of cost effective high performance composite structures. In order to take advantage of this emerging interest, the nature of the competitive environment and those forces acting upon it are described. How an organisation responds to environmental change and how it proactively seeks to alter the competitive environment will ultimately determine its position and profitability within the market.

Strategic decisions are concerned with defining the scope of an organisation's activities and how these activities are tailored to the environment in which it operates including issues of matching its activities to is resource capability.

In this Chapter a model of the competitive environment is presented and used to describe the current shape of the multiaxial fabric industry. Emphasis is placed on competitive forces acting particularly in respect of high performance markets, although others are discussed as they affect the behaviour of an organisation as a whole.

7.2 Industry Overview

The main geographic markets for multiaxial warp knit fabrics can be divided into three, North America, Europe and Asia Pacific including Australasia. Among these Europe has the largest concentration of manufacturers and the most diverse applications. Information presented here concentrates on the European market, although many companies have international agents and the use of European manufactured fabrics in high profile North American programmes will also be discussed. Table 45 lists the geographic locations of European non-crimp fabric manufacturers together with machine details where known. Contact details for companies known to be manufacturing multiaxial warp knit non-crimp fabrics worldwide are given in Appendix B.

Table 45:Industry competitors and capability

	Machine details			Location
	LIBA	Mayer	Malimo	
Devold AMT	yes	no	no	Norway
Gamma Tensor	yes	-	-	Spain
Hexcel Composites	yes	no	yes	France
Saertex Wagener GmbH	yes	yes	yes	Germany
Selcom NV	yes	no	yes	Italy
Syncoglas NV	yes	-	-	Belgium
Tech Textiles International Ltd	yes	no	no	UK
Ahlsrom Glassfibre Ltd	-	-	-	Finland
Flemmings Industrial Fabrics (FIF)	0/90	-	-	UK-Scotland
Welbeck Advanced Material Systems	no	0/90	no	UK

Buyer markets are relatively similar for all companies and are quite diverse as described in Chapter 1.

7.3 Structural Analysis - Porters Five Forces Model

The 'five-forces' approach proposed by Porter[124] is a structured means of examining the competitive environment of an organisation and the forces that impinge upon it (Figure 188). It is the collective strength of these five forces that determines the profit potential of the industry. Knowledge of these underlying sources of competitive pressure highlights the critical strengths and weaknesses of an organisation, illustrates its position within the industry and clarifies the areas where strategic change may prove beneficial.

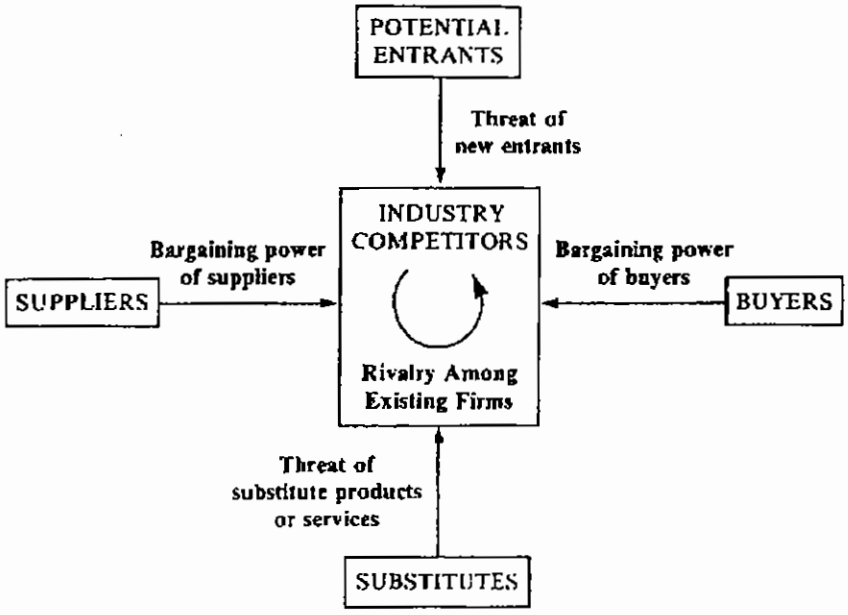

Figure 188: Five forces driving industry competition[124]

Each of these five forces; threat of new entrants, threat of substitute products, bargaining power of suppliers, bargaining power of buyers and rivalry between current competitors are described below in relation to the multiaxial warp knit fabric industry. An overview of the five forces operating in the industry is given in Figure 189.

Each company's 'strength and weakness' with respect to the underlying causes of each competitive pressure define its competitive position. In the face of these five forces each company takes either offensive or defensive action in order to maintain a defensible position within the market. Defensive moves involve positioning the company within the marketplace so that its current capabilities provide the best defence against the five forces acting upon it. Alternatively, influencing the balance of forces through strategic moves or by anticipating shifts in the factors underlying the forces and adopting a new and more appropriate strategy enables the company to exploit the changes before its competitors.

7.3.1 Threat of New Entrants

New entrants into an industry bring new capacity, a desire to gain market share and often substantial resources and new equipment. However within the existing competitive group there are likely to be barriers to reduce the threat of new entrants into the market.

For entry into the multiaxial warp-knit industry, capital requirements are large with machines costing upwards of 1 million Deutsch Marks. However the switching costs

are low within most market sectors as products are identical and produced on the same basic equipment. Differentiation of products has been attempted in some market sectors mostly without success due to obvious product similarity. As companies look towards higher value markets such as aerospace some proprietary product technology has been developed to increase product quality and flexibility and some significant experience/learning curve advantages developed particularly in long established firms. Access to raw materials is also important with shortages common in both glass and carbon fibre materials; companies with established relationships with end user customers generally gaining favourable access to raw materials. Geographic location is important as at present the number of companies are small and widely spread throughout Europe, Asia, and North America. Currency fluctuations therefore have a large impact on product price and profitability, as do import taxes. The North American market is however quite separate from the European one, due to a patent dispute between LIBA and Hexcel which was settled by an agreement preventing sale of LIBA multiaxial machines and parallel weft fabrics and fabrics in North America, and conversely Hexcel being unable to sell fabrics into Europe from the United States. This restriction has recently been lifted allowing both the supply of materials and machines to and from the United States. Economies of scale are not a strong barrier to entry as the production capacity of the machines are high with many companies competing successfully with a single machine.

7.3.2 Rivalry Between Existing Competitors

The multiaxial warp-knit industry is characterised by the relatively large number of equally balanced competitors who are prone to strong competition with one another due in part to currency fluctuations. The profit margins on 'near commodity' products which form the bulk of production throughput is relatively low with product generally offered on a cost plus basis. (manufacturing cost, plus a small margin). Large volumes of material are sold in this way to relatively promiscuous customers who move between suppliers, so forcing the price downward. Competitors have started to differentiate themselves largely based upon added value services such as design advice or application development. As interest has been stimulated in high performance markets, where profit margins are significantly higher, partnerships and alliances have formed usually between government funding bodies, universities and potential customers. These alliances have tended to be along geographic boundaries and are only now beginning to bear fruit in terms of large volume sales of high value, usually carbon, multiaxial warp-knit fabrics.

7.3.3 Pressure from Substitute Products

All firms in an industry are competing with industries producing substitute products. Substitutes limit the potential returns of an industry by placing a ceiling on the prices firms in the industry can profitably charge. The more attractive the price-performance alternative offered by substitutes, the lower the profit potential of the industry.

As a relatively new product into the composite structural materials market, multiaxial warp-knit fabrics are seen as substitutes for random mat products, woven reinforcements and, increasingly, unidirectional tapes. However as manufacturing technologies have developed, direct fibre placement manufacturing technologies may become more cost competitive as waste becomes more important. Triaxial braiding for example has been demonstrated as offering a cost benefit over the cutting, folding and stitching of multiaxial warp-knit fabrics for wing stiffeners in the

NASA ACT ICAPS stitched wing programme[6], despite a modest reduction in component performance. The intermediate materials and direct methods described in detail in Chapter 1 are all potential substitute technologies, 3D weaving for example offers the future promise of net-shape fully integrated structures in a single operation, without the current problems of delamination crack growth. However at present, questions remain whether the technology can be made to operate with sufficient flexibility and at production rates which improve the current price/performance ratio to an acceptable level.

7.3.4 Bargaining Power of Buyers

Buyers compete with the industry by forcing down prices, bargaining for high quality or more services, and playing competitors against each other - all at the expense of industry profitability. The power of the industries buyer groups depends on the relative importance of its purchases relative to its overall business. High performance products form only a small volume of total sales but as a fraction of the fabrication cost of the finished component form a large proportion. This means that buyers will tend to purchase very selectively in order to obtain a favourable price, particularly as at present the products of the industry are essentially undifferentiated and hence switching costs are low. Concerns over backward integration by buyers has always been a concern of the industry and hence full information on the manufacture of the product, proprietary knowledge and skills, tend to be withheld or protected by patents or confidentiality agreements.

However the product itself is of critical importance to the quality of the buyers product, which here works in favour of those who can provide a measurably consistent product and service. Such relationships within the aerospace industry tend to be long term due to the high costs of switching once a material has passed through qualification, and hence a decision to pursue such buyer groups can be highly profitable, particularly by finding buyers with the least power to influence it adversely.

7.3.5 Bargaining Power of Suppliers

Suppliers can exert bargaining power over participants in an industry by threatening to raise prices or withhold supply of materials. Powerful suppliers can therefore squeeze profitability out of an industry unable to recover cost increases in its own prices. In the multiaxial warp-knit fabric industry raw material supply is dominated, by a small number of large companies to whom the industry is a relatively un-important customer but whose product is the primary input to the business. Material tends therefore to be purchased when it is available leading to large inventories of material whose prices fluctuate strongly, due principally to currency market changes. Forward integration was adopted by Hexcel and glass fibre manufacturer Owens Corning in 1988, when they set up Knytex, a 50:50 joint venture, manufacturing multiaxial warp-knit glass fabrics for the US market.

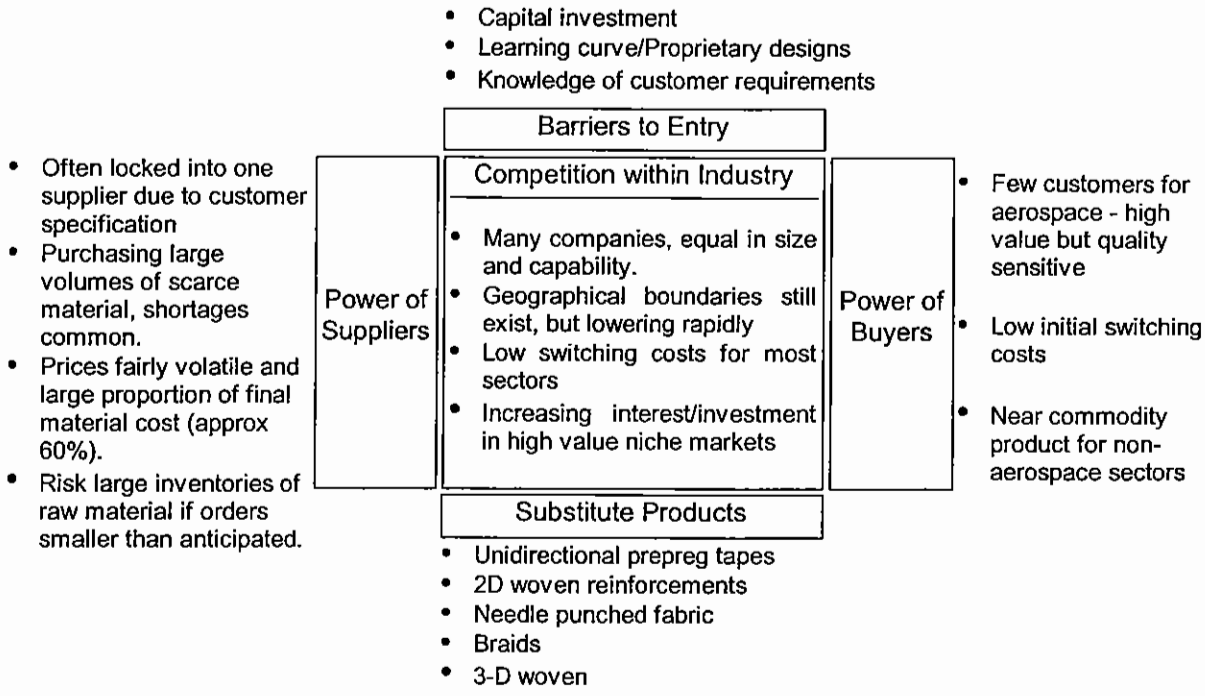

Figure 189: Porters Five Forces Model of the Multiaxial fabric industry

7.4 Conclusions

Having reviewed the industry and the competitive forces acting upon it the following conclusions can be drawn as to the key influences on market competition and industry profitability.

Shortages of 3 and 6k tow are becoming widespread with no indication that production volumes will be increased in the future. 12 and 24k tow are becoming increasingly available at reducing cost, as well as higher tow count fibres 48 -240k. Primary technical innovations are in the use of high filament count fibres both for light fabrics and heavy weight materials. Fibre costs are likely to continue to fall and volume usage increases.

Aerospace manufacturers now entering into material qualification for non-crimp fabrics, increasing pressure on fabric manufacturers to deliver quality and consistent products. Therefore competing companies can expect fierce competition for large, high value orders. This situation may offer the potential to create high switching costs, particularly if the customer product or processes are reliant on in-house technologies. Increasing pressure from customers to licence in-house technologies to allow dual sourcing of product.

Possible Competitive Strategy

Commodity goods - Improve production rates for commodity products, possible outsourcing of production overseas allowing business to concentrate on higher margin products. This approach may also take control of the competition posed by new entrants in low cost markets and make market entry less favourable.

High value products - where material specification fixed and reliant on scarce resources, develop alliances with suppliers to gain favourable access to raw

materials. Separate production and marketing of high value goods; separate machines and quality equipment and procedures; value added technical support and design advice.

Gain technical lead with developments allowing use of high filament count tows for lightweight and heavy fabrics. This will improve margins, where customers will bare costs, and will allow price reductions to gain in market share and growth of market. Risks are however present when material and production costs are transparent to customers, as prices can be forced down. This is the case only if customer is reliant on the product and an equivalent can be purchased elsewhere. It is therefore important to protect Intellectual Property.

Chapter 8

Conclusions

Nine pairs of LIBA multiaxial non-crimp fabrics were designed using an L_9 Taguchi orthogonal array to study the effect of machine settings on composite performance and microstructure. These carbon fibre reinforcement fabrics were converted to composite laminates by the interleaved Resin Film Infusion route using Fibredux 914 matrix resin. Differences between the nine pairs of fabrics was restricted to the settings of four manufacturing parameters; stitch course (needle penetrations/cm); stitch tension, 0° tension and 0° coverage (amount of constraint on the 0° material provided by the stitch). Three settings were used for each of the parameters; each representing the upper and lower limits, and standard setting.

Observations of the fabric structure and measurements of the crimp of the 0° tows and matrix resin distribution in the composite indicated the following .

- Changes to the manufacturing settings had a large effect on both the visual appearance of the fabrics and the observed microstructure, both parallel and perpendicular to the 0° fibres

- 0° tow crimp is minimised when the 0° tows are inlayed under high tension and fully cradled (bunched) by as much stitching yarn as possible (high stitch course), but only held by a loose stitch tension so as not to locally bunch the fibre tows, thus inducing crimp. The mean crimp of the non-crimp fabric samples at 2.32° is significantly larger than for the same lay-up in UD prepreg tape at 0.71° as measured by Miller[39].

- Mean and maximum resin area size is minimised when the 0° coverage is split 50/50 between being constrained by all the stitch and only being held occasionally. Similarly increasing the stitch course leads to smaller mean and maximum resin area sizes.

  Relative to the reference material T2, the standard CTLX816 fabric, a reduction in mean resin area size of 46% is predicted when the best combination of settings is selected. This corresponds to using a 50/50 0° coverage to prevent bunching of the 0° tows, a low stitch tension again to prevent bunching, and a high stitch course presumably to break up resin areas into a smaller mean size. Resin layer thickness is minimised with a 3.5 or 5 stitch course, and low stitch and 0° tensions and spread 0° coverage. It is maximised with a stitch course of 7.4, medium stitch tension, high 0° tension and bunched 0° structure.

- A relationship is observed between the mean resin area size and 0° tow crimp. However the relationship is dependant on the 0° coverage setting selected. In all cases an increase in mean resin area size corresponds to increasing tow-crimp.

The best settings for each of the measured characteristics is shown below.

Table 46: Best manufacturing settings for microstructure

	minimised					
	0° tow crimp SD	0° tow crimp range	Free resin volume fraction	Mean resin area size	Maximum resin area size	Mean resin layer thickness
Stitch Course	7.4	7.4	3.5	~~7.4~~	5	~~5~~
Stitch Tension	low	low	low	low	low	low
0° Tension	~~high~~	~~high~~	~~high~~	high	~~high~~	~~low~~
0° Coverage	~~bunched~~	~~bunched~~	~~spread~~	~~50/50~~	~~50/50~~	spread
predicted % change (c.f. T2)	-39%	-61%	-18%	-15%	-38%	-7%

settings with line through (~~hence~~) have least effect

In all cases, assuming that the measured microstructural features should be minimised, Stitch Course and Stitch Tension dominate the control of the microstructure. In all cases a low stitch tension is preferred. Crimp is minimised with a high stitch course whereas the response is mixed for the resin distribution characteristics measured. 0° tension, although having a weaker effect, should be kept high and the 0° coverage should be bunched to minimise tow crimp but split 50/50 or spread to minimise the resin distribution characteristics.

From the measurements of the composites' in-plane properties the following conclusions can be drawn.

- A strong dependence is observed in the relationship between open hole tensile strength and mean resin area; strength increasing with mean area size. A 17% increase in strength is predicted over the baseline fabric T2 when the best machine settings are selected (Table 47). The same stitch tension and 0° coverage setting maximises both mean resin area size, mode I interlaminar fracture (5% offset), and OHT strength. The same stitch course and 0° tension settings maximises both OHT and un-notched tensile strength.

- No well defined relationship was observed between the compression strength and modulus and 0° tow crimp. However compression strength appears to influenced by the mean size of the resin areas around the tows and the modulus by the thickness of the resin layers. It is possible that increases in the amount of resin surrounding the 0° tows reduce the lateral support they receive from surrounding fibres. The thickness of resin over which this effect extends may be small at the relatively low level of strain at which the modulus is calculated (0.1-0.5%), and may explain the more clearly defined relationship between the modulus and resin layer thickness rather than mean resin area.

- Reducing mean resin area size increases the apparent interlaminar shear strength. The machine settings that minimise the mean resin area size generally maximise the interlaminar shear strength (except stitch tension). No such relationship is observed for reducing the resin layer thickness, although this is likely to be a result of the resin layers occurring primarily away from the interlaminar shear plane where failure occurred.

The best settings for each of the measured characteristics is shown below.

Table 47: Best manufacturing settings for in-plane properties

	Maximised					
	Tensile Strength	Tensile Modulus	Compression Strength	Compression Modulus	Open Hole Tensile Strength	Apparent ILSS (short beam)
Stitch Course	5	3.5	~~5~~	5	~~5~~	7.4
Stitch Tension	low	~~high~~	low	~~high~~	high	~~medium~~
0° Tension	~~high~~	medium	~~medium~~	medium	~~high~~	~~high~~
0° Coverage	~~bunched~~	~~50/50~~	50/50	~~spread~~	bunched	50/50
predicted % change (c.f. T2)	+6%	+1%	+0%	+1%	+17%	+2%

settings with line through (~~hence~~) have least effect

Conclusions on the influence of manufacturing settings on damage resistance and tolerance properties are as follows.

- The best resistance to impact damage initiation, as measured using the delamination threshold force, is provided by a high stitch course (7.4 penetrations/cm), low stitching tension and 50/50 0° coverage. The influence of the 0° coverage is more pronounced at the 15J energy, whereas at 25J the stitch tension has more effect strongly favouring a low tension.

- Across the range of impact energies investigated a high stitch course (7.4 penetrations/cm) provides a large reduction in damage area (C-scan). Similarly the 50/50 0° coverage configuration in all cases minimises the damage area as does the lowest stitch tension during manufacture. In all cases these settings match those to maximise the delamination threshold force. A high 0° tension setting appears to minimise the delamination area but has little effect on the delamination threshold force.

- At both 15 and 25J impact energies the Compression After Impact Strength is enhanced by the highest stitch course and the bunched 0° coverage. The role of stitch and 0° tension diminishes at the 25J energy. The beneficial effect of the 0° coverage being bunched is unexpected as compression strength was maximised and damage area minimised at the 50/50 coverage setting.

- Measurements of the Mode I strain energy release rate at crack initiation suggest that the role of the stitching/knitting yarn is initially small. However as the delamination propagates, bridging by polyester stitching yarns occurs; pulled out of the fracture surface providing a crack closure force which raises the propagation strain energy release rate G_I. Little bridging by carbon fibres across the delamination was observed.

  We can therefore conclude that the propagation strain energy release rate is determined by the amount of polyester yarn at the fracture surface. This is a function of the stitch course (stitch penetrations/centimetre) and the 0° coverage (how much of the 0° tows are encompassed by the knitting yarn).

- Increasing mean resin area size reduces the threshold force for impact delamination and correspondingly leads to an increase in the projected delamination area as observed by ultrasonic C-scan. However as the resin layer thickness increases the damage area reduces.

- Increasing resin layer thickness increases the CAI strength. This is likely to be a results of both the relationship between resin layer thickness and damage area and any effect during the growth of the delamination damage during subsequent compressive loading likely to be affected by the mode I strain energy release rate. The mode I strain energy release rate is observed to increase with increasing mean resin layer thickness.

The best settings for each of the measured characteristics is shown below.

Table 48: Best manufacturing settings for damage resistance and tolerance properties

	maximise		minimise		
	impact delamination threshold 15J	impact delamination threshold 25J	impact damage area 5J	impact damage area 15J	impact damage area 25J
Stitch course	7.4	7.4	7.4	7.4	7.4
stitch tension	~~medium~~	low	~~medium~~	~~low~~	~~low~~
0° tension	~~low~~	~~low~~	high	~~high~~	~~high~~
0° coverage	50/50	~~50/50~~	~~50/50~~	50/50	50/50

predicted % change (c.f. T2)	+6%	+10%	-46%	-18%	-14%

settings with line through (~~hence~~) have least effect

	maximise			
	CAI strength 15J	CAI strength 25J	Mode I fracture (5% offset) (initiation)	Mode I fracture (10mm of propagation average)
Stitch course	7.4	7.4	7.4	7.4
stitch tension	~~medium~~	~~medium~~	~~high/medium~~	~~low~~
0° tension	~~low~~	~~low~~	high	~~low~~
0° coverage	bunched	bunched	~~bunched~~	bunched
predicted % change (c.f. T2)	+4%	+4%	+7%	+42%

settings with line through (~~hence~~) have least effect

All the damage resistance and tolerance characteristics were enhanced with the highest stitch course of 7.4 penetrations/cm. Both stitch course and 0° coverage overall had the largest effect on these characteristics, with a 50/50 split 0° coverage maximising the impact threshold force and minimising the Impact damage areas, whereas a bunched 0° structure maximised both the Mode I strain energy release rate and the compression after impact strength.

Stitch tension and 0° tension where they had a large effect were in-line with the observed effect on the microstructural features; a low stitch tension and high 0° tension being favoured.

Penetrant enhanced X-ray and high resolution C-scan images of impact damage show a large 'halo' of microcracks extending beyond the delamination damage. This damage was not observed in the initial C-scan images. The microcracks are principally in the ±45° directions and appear to originate from the points at which the stitching yarns penetrate the fabric blankets. The effect and origin of this damage is not known but may be caused by the polyester stitching yarn and its poor bond to the epoxy matrix.

General Conclusions

For applications where tensile, open hole tensile performance is imperative and where there may be peel stresses at free edges (the structure is not subject to compression loads or impact threats), the following material is likely to give the best performance:

Manufacturing setting	**Level**
Stitch Course	5 stitches/cm
Stitch Tension	Low
0° Tension	High
0° Coverage	Bunched

The performance of a composite manufactured with these settings, relative to the baseline fabric T2, is given in Table 49.

Table 49: Recommended fabric (1) performance

		recommended fabric	baseline (T2)	predicted difference (%)
Tensile Strength	(MN/m²)	733	666	+10%
Tensile Modulus	(GN/m²)	64.1	65.2	-2%
Compression Strength	(MN/m²)	581	607	-4%
Compression Modulus	(GN/m²)	55.7	57.4	-3%
Open Hole Tensile Strength	(MN/m²)	528	451	+17%

Apparent ILSS	(MN/m²)	54.5	59.9	-9%
Impact delamination Threshold (15J)	(kN)	4.96	5.57	-11%
Impact Damage Area (15J)	(mm²)	1246	1238	+1%
CAI Strength (15J)	(MN/m²)	306	311	-2%
Mode I Fracture (5% offset)	(J/m²)	313	262	+19%
Mode I Fracture (10mm prop. average)	(J/m²)	363	289	+26%

For applications where resistance to impact damage is of primary importance, the following material is likely to give the best performance:

Manufacturing setting	**Level**
Stitch Course	7.4 stitches/cm
Stitch Tension	Low
0° Tension	High
0° Coverage	50/50

The performance of a composite manufactured with these settings, relative to the baseline fabric T2, is given in Table 50.

Table 50: Recommended fabric (2) performance

		recommended fabric	baseline (T2)	predicted difference (%)
Tensile Strength	(MN/m²)	666	666	0%
Tensile Modulus	(GN/m²)	62.7	65.2	-4%
Compression Strength	(MN/m²)	584	607	-4%
Compression Modulus	(GN/m²)	54.0	57.4	-6%
Open Hole Tensile Strength	(MN/m²)	450	451	0%
Apparent ILSS	(MN/m²)	61.0	59.9	+2%
Impact delamination Threshold (15J)	(kN)	6.12	5.57	+10%
Impact Damage Area (15J)	(mm²)	950	1238	-23%
CAI Strength (15J)	(MN/m²)	310	311	0%
Mode I Fracture (5% offset)	(J/m²)	295	262	+13%
Mode I Fracture (10mm prop. average)	(J/m²)	340	289	+18%

With the cost of unidirectional prepreg tape currently around £60/kg compared with current prices of around £35-45/kg for multiaxial non-crimp fabric composite and resin film, there is the potential for large material cost savings if the design allowable stresses are acceptable and the design rules established to cope with this new class of material.

Furthermore because of the pre-orientation of plies and relatively thick fabrics, fast uni-directional laminating may be possible leading to the potential of large fabrication cost savings if suitable handling equipment is developed. Laminating broadgoods of this size (1.27m width) at rates that at least match uni-directional prepreg tape laying 3-5kg/hour is thought feasible.

From the static (RT/dry) tests reported and reviewed here there is little difference in tensile and notched properties, the same or improved damage resistance and tolerance, compared with equivalent UD tape based laminates. The strength of ply-dropped samples have shown that strength approaching that of the plain material can be achieved, albeit with additional cost and changes in design approach. Through the experimental design process it has been shown that there is scope to further improve and tailor mechanical performance by controlling the manufacturing parameter settings.

Chapter 9

Future Work

Having studied the effects of the manufacturing settings on composite performance, validation of the results analysis would be desirable. This could be performed by manufacturing and testing the performance of composites laminates manufactured from fabrics with the 'best' settings, as identified in the analyses.

Multi-criteria optimisation of the fabric design based upon the desired combination of composite properties. This is desirable as structural components may be simultaneously subject to a range of loadings and damage threats.

Characterisation of the mode II interlaminar fracture performance of the composites. This is likely to show more effect, than observed in mode I, of the changes to the resin distribution and resin layer thickness caused by the manufacturing settings. This may create the ability to tailor the interlaminar fracture performance of the structure by controlling the height of the resin layer thickness using the manufacturing settings of the reinforcing fabric.

Characterisation of the processing performance of the designed fabrics. The effect of manufacturing settings and microstructure on the permeability of the fabric during the Resin Transfer Moulding process. The effect of structure and manufacturing on the forming characteristics, as measured using drapability assessment techniques.

Extension of the manufacturing/microstructure/property relationships including other fabric configurations; different number of layers, stacking sequence and layer weights. Fibre volume fraction effects.

The role of the stitching yarn in enhancing the damage resistance and tolerance properties may also provide a route for further toughness enhancement through the optimisation of the stitching yarn. Studies by Hayashi and Sugimori[125] using threads of thermoplastic polyamide at ply interfaces in a Bismaleimide (BMI) matrix composites have led to large increases in both mode I and mode II strain energy release rates. Polyamide particles have also been successfully employed commercially as a interfacial toughening mechanism[113]. The use of higher strength yarns, such as Kevlar or polyamide, could be used in conjunction with the manufacturing setting guidelines, to maximise the damage tolerance benefits whilst minimising in-plane property degradation.

Studies to see whether or not prepreg derived design guidelines on ply-dropoff step heights and restrictions to the number of plies placed together of the same orientation are appropriate in multiaxial non-crimp fabric materials. If appropriate the creation of design guidelines for the use of non-crimp fabric materials, particularly lay-up schemes and guidelines for thickness tapering.

Investigation into the market potential of multiaxial non-crimp fabrics with performance tailored for the application during fabric manufacture.

References

REFERENCES

1. Bashford D P, The Potential of Composite Materials in Industry, Composite Materials In Aircraft Structures, Middleton D H (Ed.),Published By Longman Scientific And Technical, ISBN 0-582-01712-2, 1990

2. Green W, Swanborough G, Mowinski J, Modern Commercial Aircraft, Published by Portland House Publishers, ISBN 0-517-63369-8, 1987

3. Hadcock R N, Vosteen L F, Composite Chronicles: A Study of the Lessons Learned in the Development, Production, and Service of Composite Structures, NASA Contractor Report 4620, November 1994

4. Hawley A V, Preliminary Design of an Advanced Technology Composite Wing for a Transport Aircraft, Presented at 53rd Annual International Conference on Mass Properties Engineering, Society of Allied Weight Engineers Inc., Long Beach, California, USA, 23-25 May 1994

5. Kinder R H, Impact of Composites on Future Transport Aircraft, Third NASA Advanced Composites Technology Conference, Volume 1, Part 1, NASA Conference Publication 3178, 1992

6. Davis J, Dexter H B, The NASA-ACT program: Examining Innovative Textiles for Composites, presented at IFAI Workshop on Advanced Textile Composites, Anaheim, California, USA, March 1996

7. Anon, Design and Manufacture of Low Cost Composites - Wings Initiative, Contract No F33615-91-C-5720, Air Force Research Laboratory Manufacturing Technology 1998 Project Book, Public release reference ASC/PA#97-361, 1998, pp165

8. Middleton D H, Composite Materials in Aircraft Structures, Published by Longman Scientific and Technical, ISBN 0-582-01712-2, 1990

9. Ardolino J B, Mallow C L, Resin Transfer Moulding Implementation for the F/A-18 E/F Aircraft, Proceedings of the 40th International SAMPE Symposium, Anaheim, California, USA, May 8-11, 1995

10. Middleton D H, Composite Developments in Aircraft Structures - Part 2, Aircraft Engineering, June 1992, pp6-11

11. Mills A R, Manufacturing Technology Development for Aerospace Composite Structures, The Aeronautical Journal of the Royal Aeronautical Society, December 1996, pp539-545

12. Anon, Design and Manufacture of Low Cost Composites - Bonded Wing Initiative, Contract No F33615-91-C-5729, Air Force Research Laboratory Manufacturing Technology 1998 Project Book, Public release reference ASC/PA#97-361, 1998

13. Davis J G, Advanced Composites Technology Program, Third NASA Advanced Composites Technology Conference, Volume 1, Part 1, NASA Conference Publication 3178, 1992, pp49-85

14. Anon, Composites Affordability Initiative, ALOG Number 1433, Air Force Research Laboratory Manufacturing Technology 1998 Project Book, Public release reference ASC/PA#97-361, 1998

15. Holzwarth R C, An Overview of the Advanced Lightweight Aircraft Fuselage Structures (ALAFS) Program, American Institute of Aeronautics and Astronautics, AIAA-96-1573-CP, 1996

16. Luce S, Composites Technology, Published by Society of Manufacturing Engineers, Reference Publications Division, One SME Drive, PO Box 930, Dearborn, Michigan 48121, USA

17. Bailey J E, Chapter 1 - Origins of Composite Materials, Composite Materials in Aircraft Structures, ed. Middleton D H, Published by Longman Scientific and Technical, ISBN 0-582-01712-2, 1990

18. Schwartz M M, Composite Materials Handbook - 2nd edition, McGraw-Hill Book Company, ISBN 0-07-055819-1, 1992

19. Kedward K T, Composite Structures Theory vs. Practice: Some Personal Experiences, presented at Bristol University, Aerospace Engineering Department, Bristol, England, 10th November 1989.

20. Iden M, Pham D, Boeing 777 Empennage Manufacturing, 40th International SAMPE Symosium, Volume 40, Book 1, ISBN 0-938994-72-7, May 8-11, 1995 pp421-432

21. Markus A, Thrash P, Rohwer K, Progress in Manufacturing Large Aircraft Structures Using the Stitching/RTM Process, Third NASA Advanced Composites Technology Conference, Volume 1, Part 1, NASA Conference Publication 3178, 1992

22. Turner G F, Advanced Composite Materials in European Aircraft Present and Future, 40th International SAMPE Symposium, Volume 40, Book 1, ISBN 0-938994-72-7, May 8-11, 1995, pp366-380.

23. Sarh B, Moore B, Riedell J, Advanced Manufacturing Technologies for Composite Aircraft Structures Based on Prepreg Materials, 40th International SAMPE symposium, May 8-11, Volume 40, Book 1, 1995

24. Reckers B, Deutsche Airbus, private communication

25. Navas G, Petitin J P, ATR-72: The First Civil Aircraft with a Carbon Fibre Reinforced Plastic Wing, European SAMPE International Conference, 1987

26. Kolax M W, Testing a Composite Wing Box, European SAMPE International Conference, 1994, pp279-287

27. Hawley A V, Development of Stitched/RTM Primary Structures for Transport Aircraft, NASA Contractor Report 191441, July 1993

28. Whiteside J, Designing Out Failure in Composites, presented at Designing Out Failure in Composites, 23rd, Seminar 177, IMechE HQ, London, November 1994

29. Brandt J, Dreschler K, Application of Composites in the Transportation Industry. Proceedings of the third international symposium on new textiles for composites - Texcomp 3, University of Aachen, Germany, December 9-11, 1996.

30. Tsai S W, Patterson J M, Design Rules and Techniques for Composite Materials, Ch 8, Composite Materials in Aircraft Structures, Middleton D H (ed.), Published by Longman Scientific and Technical, ISBN 0-582-01712-2, 1990

31. Horsting K, Wulhorst B, Franzke G, Offermann P, New Types of Textile Fabrics for Fibre Composites, SAMPE Journal, Volume 29 Number 1, January/February 1993

32. Ko F K, Advanced Textile Structural Composites, in Advanced Topics in Materials Science and Engineering, Moran-Lopez J L, Sanchez J M, eds., Plenum Press, NY, 1993, pp117-137

33. Scardino F L, Advanced Stitching Technology, The Fifth Conference on Advanced Engineering Fibers and Textile Structures for Composites. NASA Langley Research Centre, Hampton, Virginia, NASA Conference Publication 3176, 5th October 1992, pp77-86

34. Cox B N, Flanagan G, Handbook of Analytical Methods for Textile Composites, NASA Contractor Report 4750, March 1997.

35. Dickinson L C, Trans-Laminar Reinforced Composites, PhD Thesis, College of William and Mary, Virginia, USA, 1997

36. Lowe J, Tenax Fibres GmbH, private communication

37. Brailsford B, Advanced Fiber Placement Program for Aircraft Structures, Proceedings of the 10th Annual ASM/ESD Advanced Composites Conference, Dearborn, Michigan, USA, 7-10th November 1994, pp 299-304

38. Anderson R L, Grant C G, Advanced Tow Placement of Composite Fuselage Structure, Ninth Dod/NASA/FAA Conference on Fibrous Composites in Structural Design, 4-7th November 1991, Lake Tahoe, Nevada, USA, pp1211-1221

39. Miller A J, The Effect of Microstructural Parameters on the Mechanical Properties of Non-Crimp Fabric Composites, M.Phil Thesis, School of Industrial and Manufacturing Science, Cranfield University, Bedford, UK, August 1996

40. Bishop S M, Strength and Failure of Woven Carbon Fibre Reinforced Plastics for High Performance Applications, Textile Structural Composites, Elsevier, 1987, pp173-207

41. Boniface L, Gao F, Marsden W M, Ogin S L, Smith P A, Greaves R P, Matrix Cracking Phenomena in Glass and Carbon Woven Fabric Composites, Proceedings of 3rd International Conference on Deformation and Fracture of Composites, University of Surrey, Guildford, UK, March 1995

42. Scardino F, Warp Knits for Composites, IFAI Textile Composite Workshop, SAMPE Anaheim, California, USA, May 1996

43. Dexter H B, Hasko G H, Performance of Resin Transfer Moulded Multiaxial Warp Knit Composites, Third NASA Advanced Composites Technology Conference, Volume 1, Part 1, NASA Conference Publication 3178, 1992, pp231-261

44. Pastore C M, Whyte D W, Soebruto H, Ko F K, Design and Analysis of Multiaxial Warp Knit Fabrics for Composites, Journal of Industrial Fabrics, Volume 5, Number 14, 1986, pp4-14

45. Kaufmann J R, Industrial Applications of Multiaxial Warp Knit Composites, Proceedings of The 5th Conference on Advanced Engineering Fibers and Textile Structures for Composites, Fibertex 1991, Raleigh, North Carolina, USA, pp77-86

46. Dexter H B, Hasko G H, Cano R J, Characterisation of Multiaxial Warp Knit Composites, First NASA Advanced Composites Technology Conference, Part II, NASA Langley research Centre, Hampton, Virginia, USA, January 1991

47. Dexter H B, Harris C E, Johnston N J, Recent Progress in NASA Langley Textile Reinforced Composites Program, NASA Advanced Composites Technology Conference, NASA ACT2, NASA Langley research Centre, Hampton, Virginia, USA, June 1992

48. Dexter H B, An Overview of the NASA Textile Composites Program, Fibre-Tex 1992, The sixth Conference on Advanced Engineering Fibers and Textile Structures for Composites, Philadelphia, Pennsylvania , USA, October 1992

49. Harris H, Schinske N, Krueger R, Swanson B, Multiaxial Stitched Preform Reinforcements for RTM Fabrication, 36th International SAMPE Symposium, April 15-18 1991, San Diego, Covina, California, USA

50. Godbehere A P, Mills A R, Irving P E, Non Crimped Fabrics Versus Prepreg CRFP Composites - A comparison of mechanical performance, Fibre Reinforced Composites FRC'94, Newcastle, UK, March 29-31, 1994

51. Sharpless G, Fiber Innovations Inc, private communication

52. Anon, Fiber Placement Benchmark and Technology Roadmap, Co-operative agreement number F33615-95-2-5563, Air Force Research Laboratory Manufacturing Technology 1998 Project Book, Public release reference ASC/PA#97-361, 1998

53. Brailsford B, Fiber Steering, Great Lakes Composites Consortium Current Programs, Project TDL 96-09

54. Soden J A, Hill B J, The Manufacture of Shaped Preforms for Engineering Composites on a Conventional Loom, Fifth International Conference on Automated Composites, ISBN 1-86125-003-7, 4-5 September 1997

55. Sarhadi M, Mitchell, McCarthy R A F, Robotic Lay-up of High-Quality Composite Preforms, Proceedings of the 14th International European Chapter Conference of the Society for the Advancement of Materials and Process Engineering, Birmingham, England, October 19-21, 1993, pp215-225

56. Newell G C, Buckingham R O, Khodabanehloo, The Automated Manufacture of Prepreg Broadgoods Components - a Review of Literature, Composites Part A, 27A, No3 3, 1996, pp211-217

57. Darrieux J-L, Method for Producing a Fiber Reinforcement For a Component of Composite Material and Composite Component Comprising Such a Reinforcement, US Patent 5429853, 4th July 1995

58. Dransfield K, Baillie C, Mai Y-W, Improving the Delamination Resistance of CFRP by Stitching - A Review, Composites Science and Technology, Volume 50, 1994, pp305-317

59. Godbehere A P, The Manufacture of Composites by Resin Film Infusion of Non Crimp Fabrics, PhD Thesis, School of Industrial and Manufacturing Science, Cranfield University, Bedford UK, March 1995

60. British Aerospace Cranfield Manufacturing Centre, AMCAPS Quarterly Reports, 1992-1995, School of Industrial and Manufacturing Science, Cranfield University, Bedford UK

61. Ko F K, The Role of Textile Preforms in Composites, IFAI Textile Composite Workshop, SAMPE symposium, Anaheim, California, USA, May 1996

62. Lee M, Tech Textiles International Ltd, private communication, 1996

63. Anon, Multi-axial Structures with Web Inserts and Diagonal Yarns in Alternate Directions, Kettenwirk-Praxis, March 1988, pp5-10

64. Dexter H B, Hasko G H, Mechanical Properties and Damage Tolerance of Multiaxial Warp-Knit Composites, Composites Science and Technology, Volume 56, pp367-380, 1996

65. Bibo G A, Deformation and Fracture of Non-Crimp Fabric Composites, PhD Thesis, Queen Mary and Westfield College, University of London, London, UK, April 1997

66. Deas S, CoTech Non-Crimp Fabrics in the Marine Industry, Proceedings of the 14th International SAMPE European Chapter Conference, Birmingham, UK, October 1993, pp317-328

67. Thomas Bischoff, Institute for Technical Textiles (ITA), RWTH Aachen, private communication, 1996

68. Iyer C, Manufacture and Application of Bisaxial and Multiaxial Knits as Textile Reinforcements in Composite Materials, International Symposium on Textile Composites 1992, Technical Research Centre of Finland, June 1992, pp147-156

69. Anon, Copcentra Multi Axial - New model from Liba has up to seven weft insertion systems for technical warp knits, Knitting International, October 1991

70. Kimpton-Smith C, Tex-Kimp Ltd, personal communication, 1997

71. Heath B, British Aerospace Airbus Ltd, Filton, personal communication, 1996

72. Minguet P J, Fedro M J, Gunther C K, Test Methods for Textile Composites, NASA Contractor Report 4609, July 1994

73. Dickinson L C, A Designed Experiment in Stitched/RTM Composites, Third NASA Advanced Composites Technology Conference, Volume 1, Part 1, NASA Conference Publication 3178, 1992, pp381-397

74. Farley G L, Dickinson L C, Mechanical Response of Composite Materials with Through-The-Thickness Reinforcement. In Fibre-tex 1991, NASA Conference Publication 3176, Oct 1991,

75. Hogg P J, Multiaxial Non-Crimp Fabrics, The Future of Composite Reinforcement?, Materials Technology 8(3/4), Elsevier Science Publishing, pp51-56, 1993

76. Piggott M R, Harris B, Compression Strength of Carbon, Glass and Kevlar-49 Fiber Reinforced Polyester Resins, Journal of Material Science, Volume 15, 1980, pp2523-2538

77. Budianski B, Fleck N A, Compressive Kinking of Fibre Composites, Journal of the Mechanics and Physics of Solids, Volume 41, Number 1, pp183-211, 1997

78. Adams D, Bell S J, Compression Strength Reduction in Composite Laminates Due to Multiple-Layer Waviness, Composite Science and Technology, 53, (1995), pp 207-212

79. Cano R J, Dow M B, Properties of Five Toughened Matrix Composite Materials, NASA TP-3254, Oct 1992

80. Smith D L, Dow M B, Properties of Three Graphite/Toughened Resin Composites, NASA TP-3102, Sept 1991

81. Lo K H, Wu E M, Konish D Y, Failure Strength of Notched Composites, Journal of Composite Laminates, Journal of Composite Materials, Volume 17, Number 5, pp 384-398, (1983)

82. Zehn S, The D Criterion Theory of Notched Composite Laminates, Journal of Reinforced Plastics and Composites, Volume 2, Number 2, 1983, pp98-110

83. Dorey G, The Fibre-Matrix Interface and Composite Strength, Ch.5, Composite Materials in Aircraft Structures, Middleton D H ed, Longman Scientific and Technical, ISBN 0-582-01712-2, 1990

84. Shu W-Y, Lin K-F, The Effects of Additives on Curing Properties, Resin Contents and Mechanical Properties of Graphite/Epoxy Composites, Polymer Composites, Volume 13, Number 3, 1992, pp213-222

85. Lundahl C E, Kreiner J H, Effect of Composite Properties on Interlaminar Shear Strength, 31st International SAMPE Symposium and Exhibition, Los Angeles, California, USA, 7-10 April 1986, pp1299-1503

86. Hull D, Strength of Composite Laminae, An Introduction to Composite Materials, Cambridge University Press, 1981, pp163-164.

87. Piggot M R, The Effect of Fibre Waviness on the Mechanical Properties of Unidirectional Fibre Composites: A Review, Composites Science and Technology, Volume 53, 1995, pp 201-205

88. Baker A A, Jones R, Callinan R J, Damage Tolerance of Graphite/Epoxy Composites, Composite Structures, Volume 4, 1985, pp15-44

89. Backhouse R, Blakeman C, Irving P E, Mechanisms of Toughness Enhancement in Carbon Fibre Non-Crimp Fabrics, Proceedings of 3rd International Conference on

Deformation and Fracture of Composites, University of Surrey, Guildford, UK, March 1995

90. Abrate S, Impact on Laminated Composite Materials, Applied Mechanics Review, 44, Number 74, April 1991, pp155-190

91. Poe C C, Jackson M A, Portanova M A, Masters J E, Damage Tolerance of Textile composites, Proceedings of the Fourth NASA.DoD Advanced Composites Technology Conference, Salt Lake City, Utah, USA, June 7-11, 1993

92. Cantwell W, Curtis P, Morton J, An Assessment of the Impact Performance of CFRP Reinforced with High-strain Carbon Fibres, Composite Science and Technology, Volume 25, Number 2, 1986, pp133-148

93. Varela J A P, Compression After Impact and Damage Tolerance in NCF Composites. MSc Thesis, Cranfield University, Bedford, UK, 1995

94. Hull D, Shi Y B, Damage mechanism characterisation in composite damage tolerance investigations, Composite Structures, Volume 23, 1993, pp90-120

95. Finn S R, He Y-F, Springer G S, Delaminations in Composite Plates under transverse static loads - Experimental Results, Composite Structures, 23, 1993, pp191-204

96. Baker A A, Jones R, Callinan R J, Damage tolerance of graphite/epoxy composites, Composite Structures, 4, 1985, pp15-44

97. Curtis P T, Bishop S M, An assessment of the potential of woven carbon fibre reinforced plastics for high performance applications, Composites, Volume 15, Number 4, 1984, pp259-264

98. Cantwell W, Curtis P, Morton J, Post impact fatigue performance of carbon fibre laminates with non-woven and mixed woven layers, Composites, Volume 14, Number 3, 1983, pp301-305

99. Madan R C, in Composite Materials: Fatigue and Fracture, Volume 3, ASTM STP1110, O'Brien T K ed., 1991, pp457-475

100. Gardiner D S, Pearson L H, Acoustic Emission monitoring of composite damage occurring under static and impact loading, Experimental Techniques, Volume 9, November 1985, pp22-28

101. Lammerant L, Verpost I, The interaction between matrix cracks and delaminations during quasi-static impact of composites, Composites Science and Technology, Volume 51, 1994, pp505-516

102. Levin K, Effect of low velocity impact on compressive strength of quazi-isotropic laminate, 1st Technical Conference of the American Society for Composites, Dayton, Ohio, USA, 1986, pp313-326.

103. Test Procedure for the Determination of the Post Impact Compression Strength of Multidirectional Laminates, ACOTEG New Materials and Standardisation Working Group, ACOTEG/TP/10 Issue P, October 1992

104. Advanced Composite Compression Tests, Boeing Specification Support Standard (BSS) 7260, Boeing Airplane Company, Seattle, Washington, USA, 1986.

105. Ogo Y, The effect of stitching in in-plane and interlaminar properties of carbon-epoxy fabric laminates, CCM report 87-17, Centre for Composite Materials, University of Delaware, Newark, May 1987.

106. Gowayed Y A, Pastore C M, Analytical Techniques for the Prediction of Elastic Properties of Textile Reinforced Composites, Composites Science and Technology, 5, 1992, pp579-596

107. Ko F, Lei C, Rahman A, Du G W, Cai Y-J, Unit Cell Geometry of Multiaxial Preforms for Structural Composites, NASA Contractor Report 197294, November 1993

108. Kuhl N, Osswald T A, Wulfhorst B, Horsting K, A Finite Element Model and Simulation of the Deformation of Multi-Axial Multi-Layer Warp Knits, Proceedings of the SPE 50th Annual Technical Conference, ANTECH '92, 1992, pp 1700-1704

109. Yurgartis S W, Measurements of Small Angle Fiber Misalignments in Continuous Fiber Composites, Composites Science and Technology, Volume 30, 1987, pp279-293

110. Mrse A M, Piggott M R, Compressive Properties of Unidirectional Carbon Fibre Laminates: II. The Effects of Unintentional and Intentional Fibre Misalignments. Composites Science and Technology, Volume 46, 1993, pp 219-227

111. Pastore C M, Quantification of Processing Artefacts in Textile Composites, Composites Manufacturing, Volume 4, Number 4, 1993, pp217-226

112. Masters J E, Correlation of impact and delamination resistance in interleaved laminates, Proceedings of 6th International Conference on Composite Materials, and 2nd European Conference on Composite Materials, Imperial College of Science and Technology, London, UK, Volume 3, July 1987,pp96-107

113. Quinlivan J, Challenges and Payoff of Composites in Transport Aircraft: 777 Empennage and Future Applications, Third NASA Advanced Composites Technology Conference, Volume 1, Part 1, NASA Conference Publication 3178, 1992

114. Shim S B, Ahn K, Seferis J C, Berg A J, Hudson W, Cracks and microcracks in stitched structural composites manufactured with the resin film infusion process, Journal of Advanced Materials, Volume 26, Number 4, July 1995, pp48-62

115. Walker J, Roundy L, Goering J, Effects of Thermal and Moisture Cycling on the Internal Structure of Stitched RTM Laminates, Third NASA Advanced Composites Technology Conference, Volume 1, Part 1, NASA Conference Publication 3178, 1992

116. Cano R J, Furrow K W, Effects of Temperature and Humidity Cycling on the Strengths of Textile Reinforced Carbon/Epoxy Composite Materials, Third NASA Advanced Composites Technology Conference, Volume 1, Part 1, NASA Conference Publication 3178, 1992

117. Portanova M A, Poe C C, Whicomb J D, Open Hole and Postimpact Compression Fatigue of Stitched and Unstitched Carbon-Epoxy Laminates. Composite Materials: Testing and Design (Tenth Volume), Gen C Grimes, Ed., American Society for Testing and Materials, Philadelphia, Pennsylvania, USA, 1992, pp37-53

118. Phadke M S, Quality Engineering Using Robust Design, Published by Prentice Hall PTR, Englewood Cliffs, New Jersey 07632, USA, ISBN 0-13-745167-9,1989

119. Test Procedure for the Determination of Notched and Unnotched Tensile Strength of Multidirectional Laminates, ACOTEG New Materials and Standardisation Working Group, ACOTEG/TP/12 Issue P, October 1992

120. Test Procedure for the Determination of Notched and Unnotched Compression Strength of Multidirectional Laminates, ACOTEG New Materials and Standardisation Working Group, ACOTEG/TP/11 Issue P, October 1992

121. CRAG Test Methods for the Measurement of the Engineering Properties of Fibre Reinforced Plastics, RAe Technical Report 88012, HMSO, London, 1988

122. Davies P (ed.), Protocols for Interlaminar Fracture Testing of Composites, European Structural Integrity Society (ESIS), 1993

123. EMPA spreadsheet for the analysis of Mode I DCB samples, Version 1.0, Available from EMPA, St.Tanner, Abteilung 114, CH-8600 Dubendorf, Switzerland, 1992

124. Porter M E, Competitive Strategy: Techniques for Analysing Industries and Competitors, Published by Free Press, ISBN 0-02-925360-8, 1980

125. Hayashi S, Sugimore M, Properties of Carbon Fibre/Bismaleimide Prepreg System Toughened With Thermoplastic Polyamide Fibers, 40th International SAMPE Symposium, Volume 40, Book 1, ISBN 0-938994-72-7, May 8-11, 1995, pp621-631.

126. Wu E N, Application of Fracture Mechanics to Anisotropic Plates, Journal of Applied Mechanics, Volume 34, 1967, pp967-975

127. Jordan M W, Bradley W L, Micromechanisms of Fracture in Toughened Graphite-Epoxy Laminates, Toughened Composites, N Johnson (ed), ASTM STP937, 1987

128. Turmel D J-P, Szpicak J-A, Singh S, Partridge I K, Crack Initiators and Pre-Cracking Techniques for Fracture Testing of Polymer Matrix Composites, Proceedings of 3rd International Conference on Deformation and Fracture of Composites, University of Surrey, Guildford, UK, March 1995

129. Gillespie J W, Don R C, Bernetich K R, Fink B K, Lounderback M, Large Scale Implementation of Flow and Cure Sensing in a Thermoset Resin Infused Composite Structure, Proceedings of the 43rd SAMPE Symposium, Anaheim, CA, USA, May 1998

130. Hull D, An introduction to Composite Materials, Cambridge University Press, ISBN 0521239915, 1981

131. Ho H, Budiman H T, Tsai M-Y, Morton J, Farley G L, Composite Material Shear Property Measurement Using the Iosipescu Specimen, Composite Materials Testing and Design, Camponeschi E T (ed.), Volume 11, ASTM STP 1206, 1993, pp70-89

Appendix A

Supplementary Test Data

Tensile Test Data

Material T1

Coupon		width (mm)	thickness (mm)	length (mm)	mass (g)	Strength (MN/m²)	Modulus (GN/m²)
T1LT01	1	30.12	3.41	280.3	44.4	693.70	64.68
	2	30.06	3.43				
	3	30.08	3.41				
T1LT02	1	30.14	3.41	279.8	44.4	725.35	65.07
	2	30.11	3.40				
	3	30.15	3.41				
T1LT03	1	30.14	3.42	279.82	44.4	701.47	64.46
	2	30.05	3.43				
	3	30.07	3.44				
T1LT04	1	30.05	3.38	280.17	44.0	701.26	63.53
	2	30.04	3.38				
	3	30.14	3.41				
T1LT05	1	30.04	3.34	280.17	43.2	719.52	64.61
	2	30.05	3.34				
	3	30.14	3.34				
Mean		**30.09**	**3.40**	**280.05**	**44.1**	**708.26**	**64.47**

Material T2

Coupon		width (mm)	thickness (mm)	length (mm)	mass (g)	Strength (MN/m²)	Modulus (GN/m²)
T2LT01	1	30.14	3.35	280.30	43.0	666.35	67.28
	2	30.02	3.32				
	3	30.00	3.34				
T2LT02	1	29.94	3.40	279.86	43.9	624.15	64.29
	2	30.06	3.43				
	3	30.07	3.40				
T2LT03	1	30.03	3.38	280.03	43.7	674.75	64.01
	2	29.98	3.39				
	3	30.02	3.42				
T2LT04	1	30.06	3.40	279.88	43.9	681.75	64.55
	2	29.97	3.41				
	3	30.00	3.40				
T2LT05	1	30.12	3.30	279.91	42.8	682.01	66.06
	2	30.01	3.30				
	3	30	3.34				
Mean		**30.028**	**3.372**	**280.10**	**43.5**	**665.80**	**65.24**

Material T3

Coupon		width (mm)	thickness (mm)	length (mm)	mass (g)	Strength (MN/m²)	Modulus (GN/m²)
T3LT01	1	30.10	3.44	279.8	44.4	716.73	65.52
	2	30.08	3.42				
	3	30.05	3.43				
T3LT02	1	30.00	3.46	279.86	44.2	697.13	64.89
	2	30.01	3.45				
	3	30.06	3.40				
T3LT03	1	30.06	3.47	280.06	44.5	677.34	64.43
	2	30.01	3.46				
	3	30.03	3.43				
T3LT04	1	30.09	3.44	279.86	44.8	729.94	64.47
	2	30.04	3.48				
	3	30.13	3.44				
T3LT05	1	30.12	3.47	279.92	44.7	723.60	65.44
	2	30.00	3.48				
	3	30.03	3.41				
Mean		**30.05**	**3.45**	**279.90**	**44.5**	**708.95**	**64.95**

Material T4

Coupon		width (mm)	thickness (mm)	length (mm)	mass (g)	Strength (MN/m²)	Modulus (GN/m²)
T4LT01	1	30.05	3.45	279.97	44.2	712.53	62.07
	2	29.97	3.45				
	3	29.94	3.42				
T4LT02	1	30.09	3.47	279.84	44.7	698.52	63.97
	2	30.06	3.46				
	3	30.09	3.45				
T4LT03	1	30.06	3.40	279.86	43.9	724.75	64.91
	2	30.06	3.39				
	3	30.04	3.35				
T4LT04	1	30.05	3.44	280.01	44.5	647.06	64.35
	2	30.06	3.44				
	3	30.05	3.43				
T4LT05	1	30.09	3.46	279.83	44.9	694.55	63.92
	2	30.03	3.47				
	3	30.05	3.47				
Mean		**30.05**	**3.44**	**279.90**	**44.4**	**695.48**	**63.84**

Material T5

Coupon		width (mm)	thickness (mm)	length (mm)	mass (g)	Strength (MN/m²)	Modulus (GN/m²)
T5LT01	1	30.06	3.47	280.16	44.6	649.13	63.35
	2	30.07	3.46				
	3	30.11	3.43				
T5LT02	1	30.03	3.49	279.82	45.0	651.00	63.64
	2	30.03	3.49				
	3	30.06	3.51				
T5LT03	1	30.05	3.49	279.95	45.0	656.67	61.98
	2	30.04	3.48				
	3	30.07	3.56				
T5LT04	1	30.08	3.48	279.85	45.0	621.56	63.09
	2	30.06	3.49				
	3	30.05	3.48				
T5LT05	1	29.99	3.45	279.91	44.4	682.23	63.47
	2	29.98	3.47				
	3	30.08	3.46				
Mean		**30.05**	**3.48**	**279.94**	**44.8**	**652.12**	**63.11**

Material T6

Coupon		width (mm)	thickness (mm)	length (mm)	mass (g)	Strength (MN/m²)	Modulus (GN/m²)
T6LT01	1	30.10	3.50	279.83	45.1	638.75	63.46
	2	30.00	3.48				
	3	30.03	3.48				
T6LT02	1	30.13	3.50	279.85	45.2	633.6	63.48
	2	30.08	3.49				
	3	30.06	3.49				
T6LT03	1	30.10	3.50	279.82	45.2	671.58	63.27
	2	30.03	3.49				
	3	30.05	3.50				
T6LT04	1	30.08	3.51	279.87	45.0	583.32	63.91
	2	30.00	3.48				
	3	30.03	3.47				
T6LT05	1	30.10	3.49	279.88	45.1	644.17	63.99
	2	30.02	3.48				
	3	30.02	3.50				
Mean		**30.06**	**3.49**	**279.85**	**45.1**	**634.28**	**63.62**

Material T7

Coupon		width (mm)	thickness (mm)	length (mm)	mass (g)	Strength (MN/m²)	Modulus (GN/m²)
T7LT01	1	30.07	3.49	280.09	45.0	687.61	64.56
	2	30.00	3.50				
	3	29.99	3.49				
T7LT02	1	30.02	3.46	280.17	44.4	655.78	65.42
	2	30.10	3.48				
	3	30.03	3.47				
T7LT03	1	30.11	3.49	279.89	45.2	660.72	64.82
	2	30.05	3.51				
	3	30.04	3.50				
T7LT04	1	30.06	3.47	280.02	44.8	647.7	64.68
	2	30.05	3.48				
	3	30.05	3.47				
T7LT05	1	30.10	3.53	279.88	45.3	673.69	63.42
	2	30.06	3.5				
	3	30.04	3.49				
Mean		**30.05**	**3.49**	**280.01**	**44.9**	**665.10**	**64.58**

Material T8

Coupon		width (mm)	thickness (mm)	length (mm)	mass (g)	Strength (MN/m²)	Modulus (GN/m²)
T8LT01	1	30.11	3.50	279.88	44.6	663.42	64.19
	2	30.06	3.48				
	3	30.04	3.44				
T8LT02	1	30.10	3.43	279.88	44.2	620.43	64.72
	2	30.00	3.46				
	3	30.01	3.40				
T8LT03	1	30.08	3.45	279.87	44.8	607.26	64.96
	2	30.04	3.49				
	3	30.01	3.50				
T8LT04	1	30.06	3.49	280.01	44.8	684.28	65.63
	2	30.00	3.51				
	3	30.00	3.48				
T8LT05	1	29.93	3.42	280.16	44.5	685.79	66.61
	2	29.94	3.41				
	3	30.06	3.41				
Mean		**30.03**	**3.46**	**279.96**	**44.6**	**652.24**	**65.22**

Material T9

Coupon		width (mm)	thickness (mm)	length (mm)	mass (g)	Strength (MN/m²)	Modulus (GN/m²)
T9LT01	1	30.02	3.38	279.84	44.0	671.02	64.13
	2	30.00	3.38				
	3	30.02	3.42				
T9LT02	1	29.99	3.42	279.93	43.6	666.68	65.37
	2	29.95	3.37				
	3	30.00	3.34				
T9LT03	1	30.02	3.41	279.97	43.8	629.99	68.74
	2	30.01	3.39				
	3	30.01	3.44				
T9LT04	1	30.02	3.39	280.08	43.7	699.96	67.7
	2	29.99	3.37				
	3	30.02	3.33				
T9LT05	1	29.99	3.38	280.00	44.0	637.28	67.62
	2	29.95	3.38				
	3	30.02	3.43				
Mean		**30.00**	**3.39**	**279.96**	**43.8**	**660.99**	**66.71**

TENSILE STRENGTH (CTLX816 Fibredux 914)

	sample numbers							
Fabric	LT01	LT02	LT03	LT04	LT05	Mean	CV(%)	S/N
T1	693.7	725.4	701.5	701.3	719.5	708.3	1.9	57.0
T2	666.4	624.2	674.8	681.8	682.0	665.8	3.6	56.5
T3	716.7	697.1	677.3	729.9	723.6	708.9	3.0	57.0
T4	712.5	698.5	724.8	647.1	694.6	695.5	4.3	56.8
T5	649.1	651.0	656.7	621.6	682.2	652.1	3.3	56.3
T6	638.8	633.6	671.6	583.3	644.2	634.3	5.1	56.0
T7	687.6	655.8	660.7	647.7	673.7	665.1	2.4	56.5
T8	663.4	620.4	607.3	684.3	685.8	652.2	5.6	56.3
T9	671.0	666.7	630.0	700.0	637.3	661.0	4.3	56.4

$S/N = -10\log_{10}(\text{mean } \Sigma 1/\text{tensile strength}^2)$

* denotes best settings

		Mean	S/N	
Stitch course	3.5	659.4	56.36	
	5	694.3	56.82	*
	7.4	660.6	56.37	
Stitch tension	low	689.6	56.76	*
	med	656.7	56.33	
	high	668.1	56.47	
0° tension	low	664.9	56.42	
	med	674.1	56.55	
	high	675.4	56.58	*
0° coverage	spread	673.8	56.55	
	50/50	655.1	56.31	
	bunched	685.6	56.69	*

	from mean	from S/N	
Estimate at best settings	730.6	732.8	MN/m²

From ANOVA relative effect of factors is given by sum of squared deviation from mean

	sum of squared deviations	
Stitch course	0.405	most effect
Stitch tension	0.291	
0° tension	0.041	least effect
0° coverage	0.230	2nd least

re-predict more conservative optimum value ignoring the two factors with smallest effects

Estimate at best settings	713.1	MN/m²
Stitch course	3.5	
Stitch tension	low	
0° tension	-	
0° coverage	-	

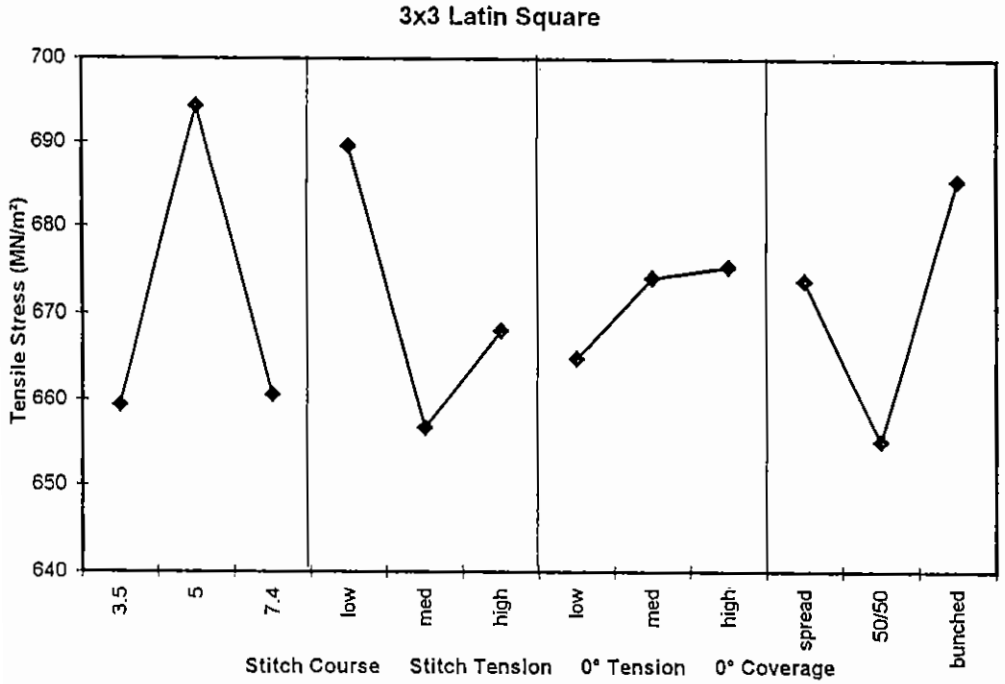

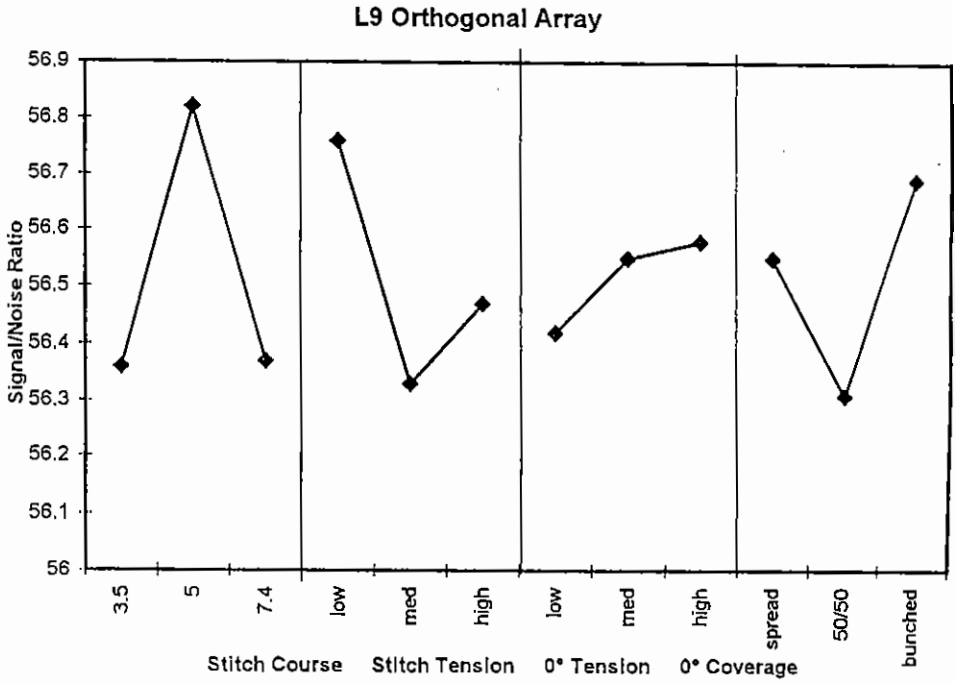

TENSILE MODULUS (CTLX816 Fibredux 914)

Fabric	sample numbers LT01	LT02	LT03	LT04	LT05	Mean	CV(%)	S/N
T1	64.68	65.07	64.46	63.53	64.61	64.5	0.89	36.19
T2	67.28	64.29	64.01	64.55	66.06	65.2	2.13	36.29
T3	65.52	64.89	64.43	64.47	65.44	65.0	0.80	36.25
T4	62.07	63.97	64.91	64.35	63.92	63.8	1.67	36.10
T5	63.35	63.64	61.98	63.09	63.47	63.1	1.05	36.00
T6	63.46	63.48	63.27	63.91	63.99	63.6	0.49	36.07
T7	64.56	65.42	64.82	64.68	63.42	64.6	1.13	36.20
T8	64.19	64.72	64.96	65.63	66.61	65.2	1.43	36.29
T9	64.13	65.37	68.74	67.70	67.62	66.7	2.84	36.48

$S/N = -10\log_{10}(\text{mean } \Sigma 1/\text{tensile modulus}^2)$

* denotes best settings

		Mean	S/N	
Stitch course	3.5	65.5	36.32	*
	5	64.89	36.24	
	7.4	63.52	36.06	
Stitch tension	low	64.3	36.16	
	med	64.52	36.19	
	high	65.09	36.27	*
0° tension	low	64.44	36.18	
	med	65.26	36.29	*
	high	64.21	36.15	
0° coverage	spread	64.76	36.22	*
	50/50	64.48	36.19	
	bunched	64.67	36.21	

	from mean	from S/N	
Estimate at best settings	66.71	66.6	GN/m²

From ANOVA relative effect of factors is given by sum of squared deviation from mean

	sum of squared deviations	
Stitch course	0.110	most effect
Stitch tension	0.017	2nd least
0° tension	0.031	
0° coverage	0.002	least effect

re-predict more conservative optimum value ignoring the two factors with smallest effects

Estimate at best settings	66.1	GN/m²
Stitch course	3.5	
Stitch tension	0	
0° tension	medium	
0° coverage	-	

3x3 Latin Square

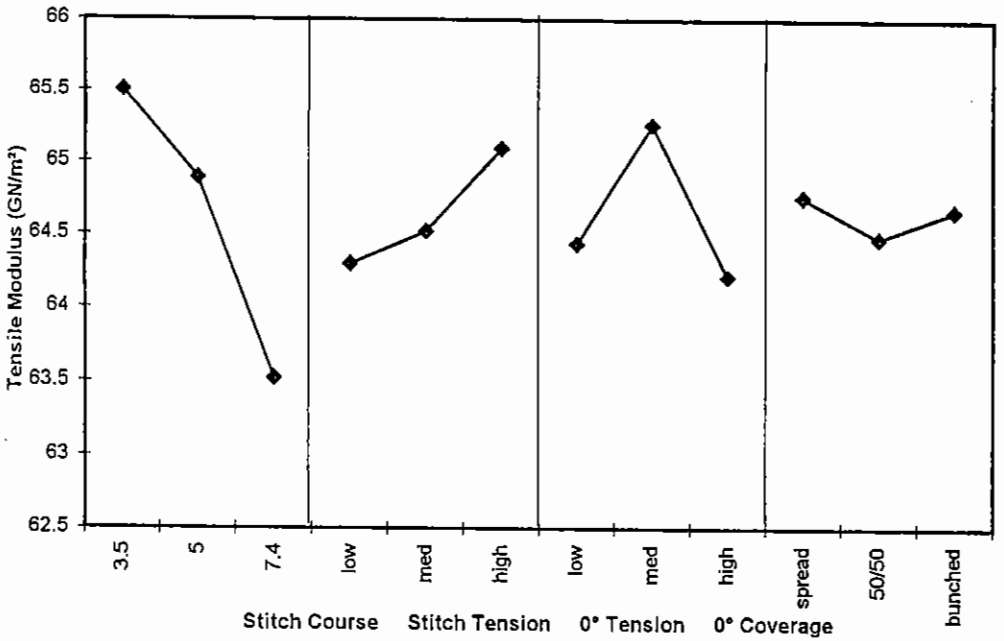

L9 Orthogonal Array

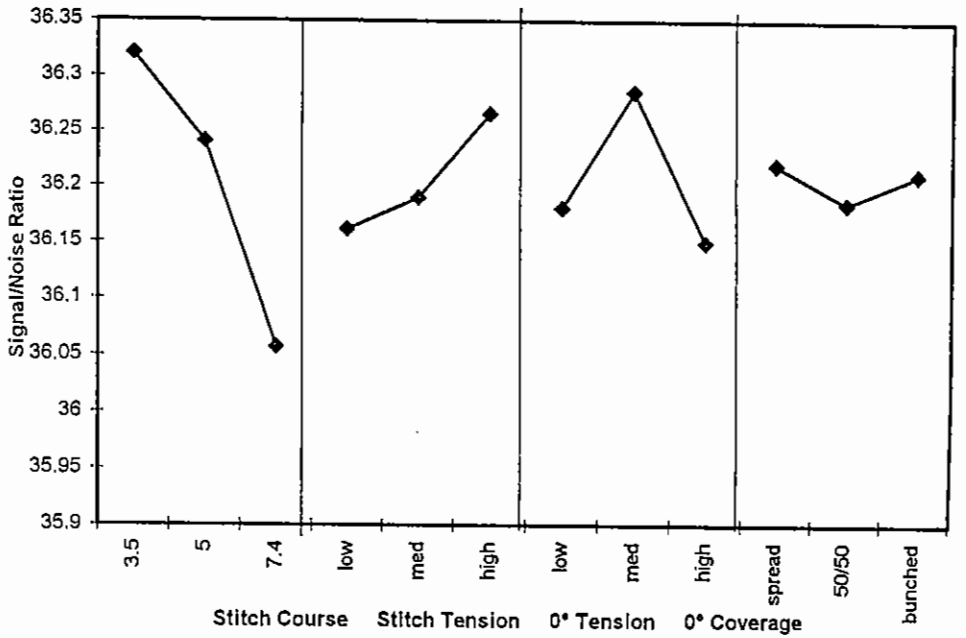

Compression Test Data

Material T1

Coupon		width (mm)	thickness (mm)	length (mm)	mass (g)	Strength (MN/m²)	Modulus (GN/m²)
T1LC01	1	29.95	3.41	280.26	44.3	578.72	57.038
	2	29.97	3.47				
	3	30.10	3.43				
T1LC02	1	29.97	3.42	280.19	44.3	585.27	58.218
	2	30.02	3.4				
	3	30.10	3.42				
T1LC03	1	30.11	3.41	280.19	44.2	603.8	57.772
	2	30.00	3.38				
	3	30.03	3.41				
T1LC04	1	30.03	3.42	280.23	44.5	573.10	58.334
	2	30.04	3.44				
	3	30.11	3.42				
T1LC05	1	29.98	3.35	280.42	43.8	581.79	55.911
	2	29.99	3.38				
	3	30.05	3.39				
Mean		**30.03**	**3.41**	**280.26**	**44.2**	**584.50**	**57.45**

Material T2

Coupon		width (mm)	thickness (mm)	length (mm)	mass (g)	Strength (MN/m²)	Modulus (GN/m²)
T2LC01	1	30.08	3.34	279.97	43.8	602.71	58.52
	2	29.97	3.35				
	3	29.95	3.35				
T2LC02	1	30.02	3.35	280.22	43.5	614.88	57.04
	2	29.95	3.35				
	3	30.03	3.39				
T2LC03	1	30.03	3.38	279.9	43.9	597.27	57.58
	2	29.96	3.39				
	3	30.02	3.36				
T2LC04	1	30.04	3.35	280.13	43.6	571.56	55.52
	2	29.97	3.36				
	3	29.94	3.39				
T2LC05	1	30.02	3.37	279.91	43.6	647.33	58.53
	2	29.94	3.38				
	3	29.95	3.38				
Mean		**29.99**	**3.37**	**280.03**	**43.6**	**606.75**	**57.44**

Material T3

Coupon		width (mm)	thickness (mm)	length (mm)	mass (g)	Strength (MN/m²)	Modulus (GN/m²)
T23LC01	1	30.06	3.35	280.11	43.8	523.66	55.89
	2	30.07	3.27				
	3	30.02	3.27				
T3LC02	1	30.04	3.40	279.96	44.4	573.51	56.16
	2	29.95	3.42				
	3	29.98	3.40				
T3LC03	1	30.05	3.43	279.79	44.4	549.83	57.34
	2	29.94	3.40				
	3	29.97	3.38				
T3LC04	1	30.01	3.37	279.83	44.4	581.36	55.95
	2	29.90	3.41				
	3	29.85	3.45				
T3LC05	1	29.83	3.41	279.86	44.6	552.97	56.59
	2	30.00	3.45				
	3	29.95	3.44				
Mean		**29.97**	**3.39**	**279.91**	**44.3**	**556.27**	**56.39**

Material T4

Coupon		width (mm)	thickness (mm)	length (mm)	mass (g)	Strength (MN/m²)	Modulus (GN/m²)
T4LC01	1	29.97	3.44	280.11	44.6	565.39	54.50
	2	29.98	3.41				
	3	29.98	3.43				
T4LC02	1	30.06	3.45	279.86	44.6	564.95	55.55
	2	30.03	3.41				
	3	29.98	3.41				
T4LC03	1	30.02	3.46	279.85	44.9	596.4	55.44
	2	29.99	3.46				
	3	29.95	3.44				
T4LC04	1	30.05	3.44	279.85	44.9	570.72	54.94
	2	29.99	3.44				
	3	30.00	3.44				
T4LC05	1	29.95	3.40	280.15	44.4	579.36	55.57
	2	29.94	3.44				
	3	30.02	3.43				
Mean		**29.99**	**3.43**	**279.96**	**44.7**	**575.36**	**55.20**

Material T5

Coupon		width (mm)	thickness (mm)	length (mm)	mass (g)	Strength (MN/m²)	Modulus (GN/m²)
T5LC01	1	29.97	3.45	280.03	45.1	504.79	52.32
	2	29.94	3.46				
	3	30.04	3.48				
T5LC02	1	29.99	3.47	279.94	44.9	561.05	53.68
	2	29.98	3.49				
	3	29.99	3.44				
T5LC03	1	29.98	3.50	279.94	45.1	464.28	54.12
	2	30.02	3.46				
	3	30.01	3.45				
T5LC04	1	29.99	3.47	279.87	45.0	518.75	53.86
	2	30.02	3.45				
	3	30.03	3.48				
T5LC05	1	29.99	3.43	280.12	45.0	582.79	57.63
	2	29.98	3.46				
	3	30.00	3.48				
Mean		**30.00**	**3.46**	**279.98**	**45.0**	**526.33**	**54.32**

Material T6

Coupon		width (mm)	thickness (mm)	length (mm)	mass (g)	Strength (MN/m²)	Modulus (GN/m²)
T6LC01	1	30.06	3.46	279.8	45.3	558.59	55.72
	2	29.99	3.47				
	3	30.00	3.49				
T6LC02	1	30.04	3.48	280.03	44.9	566.57	53.93
	2	30.00	3.47				
	3	29.99	3.44				
T6LC03	1	30.07	3.39	280.08	44.5	570.35	56.48
	2	29.97	3.39				
	3	30.01	3.43				
T6LC04	1	30.02	3.40	279.91	44.4	593.04	59.20
	2	29.96	3.41				
	3	29.94	3.41				
T6LC05	1	30.06	3.47	279.95	45.0	559.30	53.65
	2	30.00	3.48				
	3	30.00	3.45				
Mean		**30.01**	**3.44**	**279.95**	**44.8**	**569.57**	**55.80**

Material T7

Coupon		width (mm)	thickness (mm)	length (mm)	mass (g)	Strength (MN/m²)	Modulus (GN/m²)
T7LC01	1	29.96	3.47	279.92	44.2	592.68	55.48
	2	29.97	3.50				
	3	30.04	3.47				
T7LC02	1	30.00	3.47	279.86	45.2	614.28	55.38
	2	29.99	3.51				
	3	30.03	3.50				
T7LC03	1	30.03	3.45	279.87	45.0	583.09	53.87
	2	29.98	3.50				
	3	29.96	3.48				
T7LC04	1	30.01	3.48	279.90	45.1	603.58	52.38
	2	30.02	3.51				
	3	30.07	3.45				
T7LC05	1	29.96	3.50	279.97	45.1	590.62	56.74
	2	29.91	3.50				
	3	30.00	3.48				
Mean		**30.00**	**3.48**	**279.90**	**44.9**	**596.85**	**54.77**

Material T8

Coupon		width (mm)	thickness (mm)	length (mm)	mass (g)	Strength (MN/m²)	Modulus (GN/m²)
T8LC01	1	30.01	3.46	280.08	44.9	530.13	55.52
	2	30.00	3.49				
	3	30.13	3.47				
T8LC02	1	30.05	3.49	279.92	45.0	524.91	57.71
	2	30.01	3.49				
	3	30.00	3.46				
T8LC03	1	30.09	3.46	279.87	45.0	572.8	53.78
	2	30.05	3.48				
	3	30.01	3.51				
T8LC04	1	30.02	3.40	280.24	43.9	586.49	56.08
	2	29.99	3.40				
	3	29.99	3.35				
T8LC05	1	30.04	3.50	279.84	44.8	549.17	53.73
	2	30.00	3.49				
	3	29.99	3.46				
Mean		**30.03**	**3.46**	**279.99**	**44.72**	**552.7**	**55.36**

Material T9

Coupon		width (mm)	thickness (mm)	length (mm)	mass (g)	Strength (MN/m²)	Modulus (GN/m²)
T9LC01	1	30.01	3.37	280.14	43.3	564.17	57.28
	2	30.00	3.37				
	3	29.93	3.38				
T9LC02	1	30.04	3.40	280.02	44.0	537.20	56.44
	2	30.04	3.39				
	3	30.04	3.44				
T9LC03	1	30.00	3.40	280.01	43.6	567.16	58.85
	2	29.95	3.39				
	3	29.98	3.36				
T9LC04	1	30.00	3.41	280.00	43.9	556.09	55.42
	2	30.00	3.39				
	3	30.04	3.37				
T9LC05	1	30.05	3.34	280.10	43.3	541.01	58.92
	2	30.01	3.32				
	3	30.05	3.41				
Mean		**30.01**	**3.38**	**280.05**	**43.6**	**553.13**	**57.38**

COMPRESSIVE STRENGTH (CTLX816 Fibredux 914)

* denotes best settings

	sample numbers							
Fabric	LT01	LT02	LT03	LT04	LT05	Mean	CV(%)	S/N
T1	578.7	585.3	603.8	573.1	581.8	584.5	2.0	55.33
T2	602.7	614.9	597.3	571.6	647.3	606.8	4.6	55.64
T3	523.7	573.5	549.8	581.4	553.0	556.3	4.1	54.89
T4	565.4	565.0	596.4	570.7	579.4	575.4	2.3	55.19
T5	504.8	561.1	464.3	518.8	582.8	526.3	8.9	54.34
T6	558.6	566.6	570.4	593.0	559.3	569.6	2.5	55.10
T7	592.7	614.3	583.1	603.6	590.6	596.9	2.0	55.51
T8	530.1	524.9	572.8	586.5	549.2	552.7	4.8	54.83
T9	564.2	537.2	567.2	556.1	541.0	553.1	2.4	54.85

S/N = -10log10(mean S1/compression strength²)

		Mean	S/N	
Stitch course	3.5	567.6	55.06	
	5	582.5	55.29	*
	7.4	557.1	54.88	
Stitch tension	low	585.6	55.35	
	med	561.9	54.94	
	high	559.7	54.95	*
0° tension	low	568.9	55.09	
	med	578.4	55.23	
	high	559.8	54.91	*
0° coverage	spread	554.7	54.84	
	50/50	591.1	55.42	
	bunched	561.4	54.97	*

	from mean	from S/N	
Estimate at best settings	630.4	634.6	MN/m²

From ANOVA relative effect of factors is given by sum of squared deviation from mean

	sum of squared deviations	
Stitch course	0.249	2nd least
Stitch tension	0.328	
0° tension	0.148	least effect
0° coverage	0.552	most effect

re-predict more conservative optimum value ignoring the two factors with smallest effects

Estimate at best settings	608.7	MN/m²
Stitch course	-	
Stitch tension	low	
0° tension	-	
0° coverage	50/50	

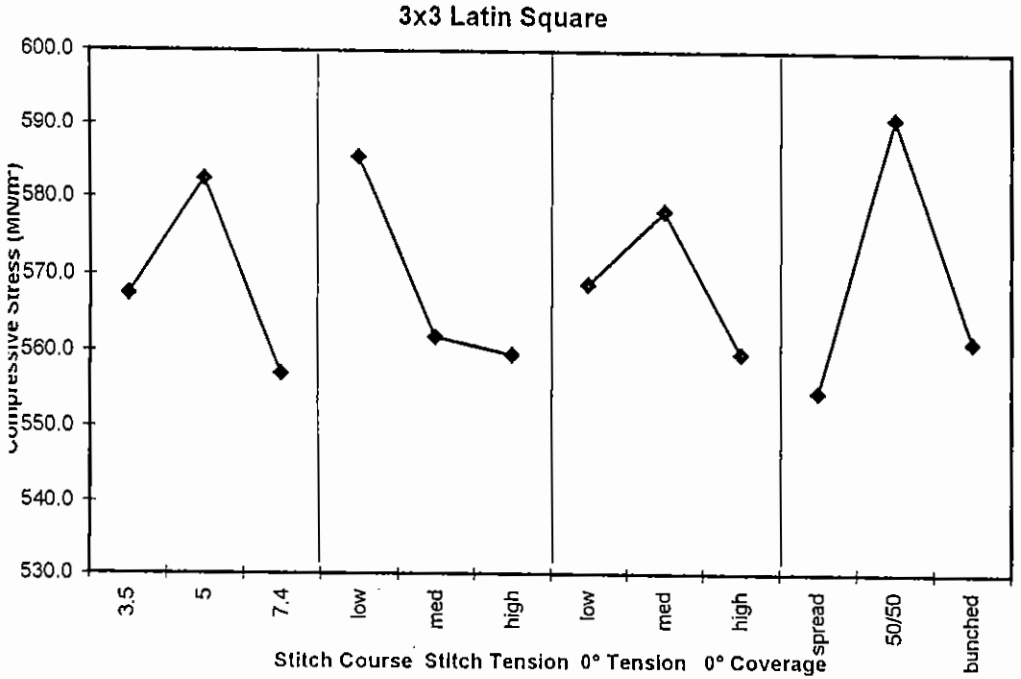

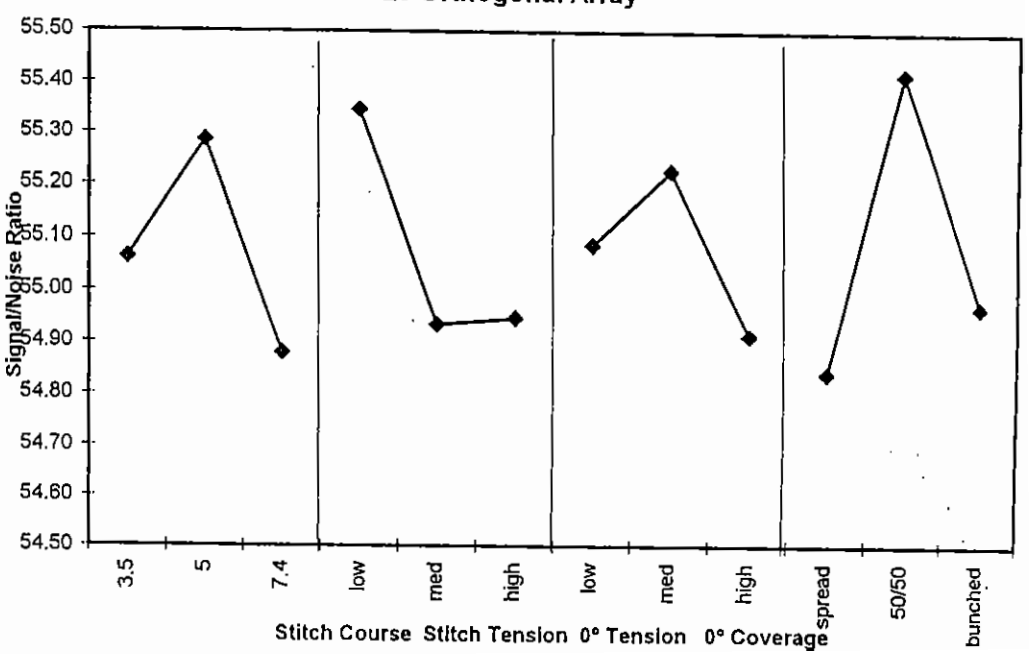

COMPRESSION MODULUS (CTLX816 Fibredux 914)

	sample numbers							
Fabric	LC01	LC02	LC03	LC04	LC05	Mean	CV(%)	S/N
T1	57.038	58.218	57.772	58.334	55.911	57.5	1.74	35.1833
T2	58.517	57.044	57.584	55.522	58.526	57.4	2.17	35.1791
T3	55.891	56.16	57.342	55.947	56.588	56.4	1.07	35.0222
T4	54.495	55.549	55.441	54.935	55.574	55.2	0.85	34.8378
T5	52.315	53.675	54.12	53.864	57.634	54.3	3.64	34.6862
T6	55.721	53.927	56.482	59.204	53.645	55.8	4.03	34.9155
T7	55.478	55.384	53.865	52.384	56.739	54.8	3.06	34.7609
T8	55.515	57.706	53.781	56.077	53.732	55.4	3.02	34.8549
T9	57.284	56.44	58.849	55.423	58.919	57.4	2.65	35.1683

S/N = -10log10(mean S1/Compression modulus²)

* denotes best settings

		Mean	S/N	
Stitch course	3.5	55.8384	34.928	
	5	57.0929	35.128	*
	7.4	55.1054	34.813	
Stitch tension	low	55.8078	34.927	
	med	55.7075	34.907	
	high	56.5215	35.035	*
0° tension	low	56.2042	34.985	
	med	56.6735	35.062	*
	high	55.1591	34.823	
0° coverage	spread	56.3864	35.013	*
	50/50	56.0015	34.952	
	bunched	55.6489	34.905	

	from mean	from S/N	
Estimate at best settings	58.64	58.67	GN/m²

From ANOVA relative effect of factors is given by sum of squared deviation from mean

	sum of squared deviations	
Stitch course	0.1525	most effect
Stitch tension	0.0286	2nd least
0° tension	0.089	
0° coverage	0.0175	least effect

re-predict more conservative optimum value

Ignoring the two factors with smallest effects

Estimate at best settings	57.77	GN/m²
Stitch course	5	
Stitch tension	0	
0° tension	medium	
0° coverage	-	

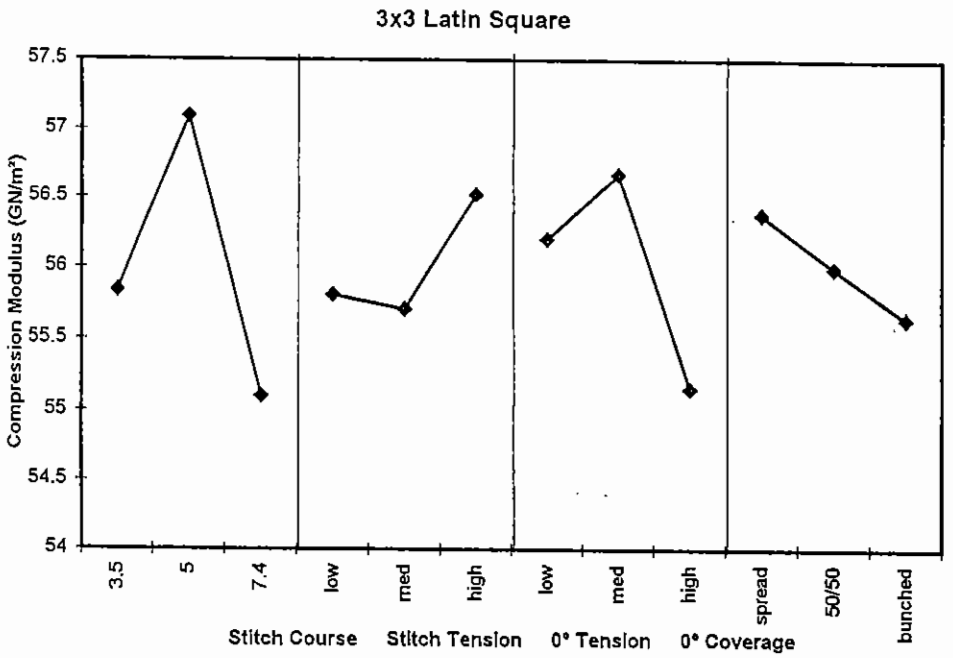

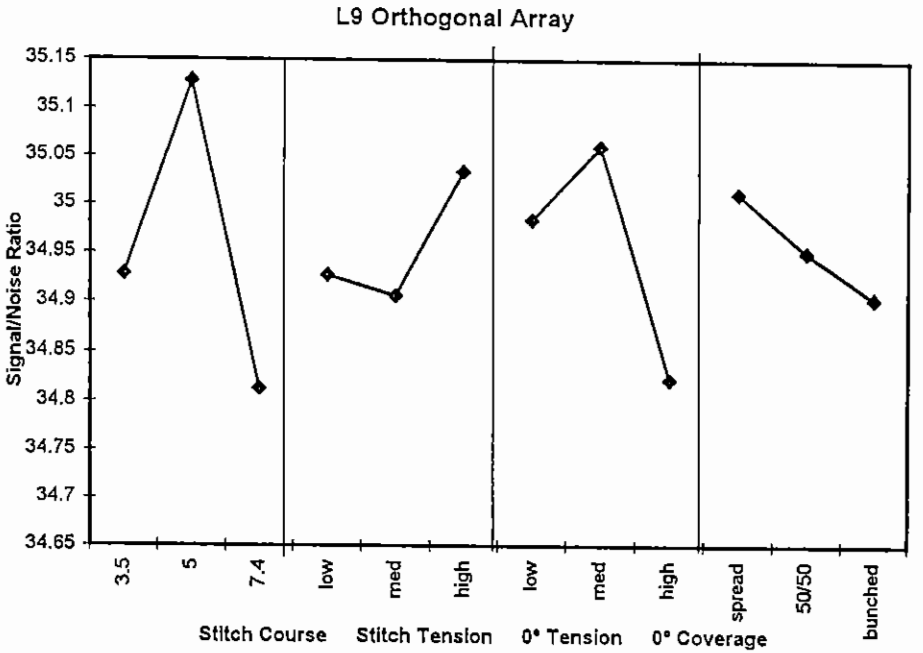

Open Hole Tensile Test Data

Material T1

Coupon		width (mm)	thickness (mm)	length (mm)	mass (g)	Hole Dia (mm)	Ult. Load (kN)	Strength (MN/m²)
T1OHT01	1	36.02	3.40	279.90	52.7	6.01	47.56	465.14
	2		3.41					
	3		3.41					
T1OHT02	1	36.05	3.40	279.80	53	6.01	48.47	472.48
	2		3.42					
	3		3.43					
T1OHT03	1	36.02	3.40	279.80	52.9	6.01	49.52	483.15
	2		3.42					
	3		3.43					
T1OHT04	1	36.03	3.44	279.81	52.9	6.00	50.31	489.19
	2		3.43					
	3		3.41					
T1OHT05	1	35.98	3.41	279.82	52.8	6.00	46.32	453.39
	2		3.40					
	3		3.42					
Mean		**36.02**	**3.41**	**279.83**	**52.86**	**6.01**	**48.44**	**472.67**

Material T2

Coupon		width (mm)	thickness (mm)	length (mm)	mass (g)	Hole Dia (mm)	Ult. Load (kN)	Strength (MN/m²)
T2OHT01	1	36.14	3.29	279.90	51.6	5.99	50.27	506.99
	2		3.26					
	3		3.32					
T2OHT02	1	36.18	3.39	279.92	52.5	6.00	42.18	413.05
	2		3.39					
	3		3.37					
T2OHT03	1	36.13	3.41	279.91	53.0	6.00	45.32	439.51
	2		3.42					
	3		3.44					
T2OHT04	1	36.11	3.41	279.89	52.9	6.00	44.08	427.99
	2		3.42					
	3		3.44					
T2OHT05	1	36.14	3.40	279.90	52.9	6.00	47.84	465.88
	2		3.41					
	3		3.42					
Mean		**36.14**	**3.38**	**279.90**	**52.6**	**6.00**	**45.94**	**450.68**

Material T3

Coupon		width (mm)	thickness (mm)	length (mm)	mass (g)	Hole Dia (mm)	Ult. Load (kN)	Strength (MN/m²)
T3OHT01	1	36.16	3.45	279.91	53.3	6.00	60.95	590.56
	2		3.40					
	3		3.42					
T3OHT02	1	36.21	3.44	279.77	53.7	6.01	60.38	579.57
	2		3.45					
	3		3.46					
T3OHT03	1	36.21	3.44	279.78	53.4	6.01	58.12	559.67
	2		3.43					
	3		3.45					
T3OHT04	1	36.19	3.47	279.90	53.6	6.01	55.45	532.95
	2		3.45					
	3		3.42					
T3OHT05	1	36.21	3.41	279.78	53.5	6.01	58.35	563.72
	2		3.42					
	3		3.45					
Mean		**36.19**	**3.44**	**279.83**	**53.5**	**6.01**	**58.65**	**565.29**

Material T4

Coupon		width (mm)	thickness (mm)	length (mm)	mass (g)	Hole Dia (mm)	Ult. Load (kN)	Strength (MN/m²)
T4OHT01	1	36.21	3.46	279.87	54.0	5.99	53.27	506.92
	2		3.48					
	3		3.49					
T4OHT02	1	36.21	3.46	279.94	53.8	6.02	52.15	498.81
	2		3.47					
	3		3.46					
T4OHT03	1	36.21	3.47	279.85	53.9	5.99	54.12	511.14
	2		3.50					
	3		3.55					
T4OHT04	1	36.18	3.51	279.83	54.0	6.00	52.37	491.59
	2		3.55					
	3		3.53					
T4OHT05	1	36.18	3.46	279.84	54.0	6.01	54.97	523.82
	2		3.49					
	3		3.49					
Mean		**36.20**	**3.49**	**279.87**	**53.9**	**6.00**	**53.38**	**506.46**

Material T5

Coupon		width (mm)	thickness (mm)	length (mm)	mass (g)	Hole Dia (mm)	Ult. Load (kN)	Strength (MN/m²)
T5OHT01	1	36.19	3.51	279.79	54.4	6.00	45.16	425.75
	2		3.51					
	3		3.52					
T5OHT02	1	36.19	3.48	279.91	54.0	6.00	49.99	475.82
	2		3.48					
	3		3.49					
T5OHT03	1	36.19	3.46	279.92	53.4	6.01	48.46	464.79
	2		3.46					
	3		3.45					
T5OHT04	1	36.21	3.50	279.80	54.3	6.00	52.39	495.55
	2		3.51					
	3		3.49					
T5OHT05	1	36.23	3.49	279.79	54.2	6.00	50.22	476.02
	2		3.51					
	3		3.48					
Mean		**36.20**	**3.49**	**279.84**	**54.1**	**6.00**	**49.24**	**467.59**

Material T6

Coupon		width (mm)	thickness (mm)	length (mm)	mass (g)	Hole Dia (mm)	Ult. Load (kN)	Strength (MN/m²)
T6OHT01	1	36.20	3.49	279.79	54.5	5.99	48.86	460.75
	2		3.52					
	3		3.52					
T6OHT02	1	36.21	3.52	279.84	54.6	6.00	46.47	438.00
	2		3.50					
	3		3.52					
T6OHT03	1	36.21	3.50	279.83	54.4	6.00	49.61	468.86
	2		3.50					
	3		3.51					
T6OHT04	1	36.20	3.51	279.80	54.5	6.01	48.47	455.95
	2		3.51					
	3		3.54					
T6OHT05	1	36.22	3.43	279.85	53.8	6.01	51.02	491.31
	2		3.43					
	3		3.45					
Mean		**36.21**	**3.50**	**279.82**	**54.4**	**6.00**	**48.89**	**462.97**

Material T7

Coupon		width (mm)	thickness (mm)	length (mm)	mass (g)	Hole Dia (mm)	Ult. Load (kN)	Strength (MN/m²)
T7OHT01	1	36.14	3.48	279.83	53.4	6.00	47.47	451.18
	2		3.50					
	3		3.50					
T7OHT02	1	36.20	3.50	279.88	54.4	6.01	47.70	450.34
	2		3.51					
	3		3.51					
T7OHT03	1	36.20	3.51	279.86	54.5	6.00	47.32	445.49
	2		3.52					
	3		3.52					
T7OHT04	1	36.21	3.51	279.92	54.5	6.01	49.38	465.65
	2		3.52					
	3		3.51					
T7OHT05	1	36.19	3.51	279.91	54.5	6.01	48.06	453.93
	2		3.50					
	3		3.51					
Mean		**36.19**	**3.51**	**279.88**	**54.3**	**6.00**	**47.99**	**453.32**

Material T8

Coupon		width (mm)	thickness (mm)	length (mm)	mass (g)	Hole Dia (mm)	Ult. Load (kN)	Strength (MN/m²)
T8OHT01	1	36.19	3.50	279.79	54.1	6.01	49.96	471.70
	2		3.50					
	3		3.53					
T8OHT02	1	36.20	3.42	279.91	53.5	5.99	51.57	496.21
	2		3.43					
	3		3.47					
T8OHT03	1	36.19	3.47	279.78	54.3	6.02	48.84	463.03
	2		3.49					
	3		3.53					
T8OHT04	1	36.19	3.51	279.79	54.5	6.01	50.53	476.64
	2		3.51					
	3		3.52					
T8OHT05	1	36.18	3.53	279.90	54.4	6.01	55.46	521.33
	2		3.53					
	3		3.52					
Mean		**36.19**	**3.50**	**279.83**	**54.2**	**6.01**	**51.27**	**485.78**

Material T9

Coupon		width (mm)	thickness (mm)	length (mm)	mass (g)	Hole Dia (mm)	Ult. Load (kN)	Strength (MN/m²)
T9OHT01	1	36.18	3.42	279.84	53.3	6.03	48.95	472.04
	2		3.44					
	3		3.46					
T9OHT02	1	36.19	3.47	279.9	53.5	6.05	51.45	495.05
	2		3.46					
	3		3.42					
T9OHT03	1	36.19	3.48	279.95	53.7	6.06	56.03	534.29
	2		3.48					
	3		3.48					
T9OHT04	1	36.19	3.42	279.9	53.4	6.00	52.06	499.80
	2		3.45					
	3		3.48					
T9OHT05	1	36.21	3.43	279.86	53.0	5.98	55.40	535.42
	2		3.43					
	3		3.41					
Mean		**36.19**	**3.45**	**279.89**	**53.4**	**6.02**	**52.78**	**507.32**

OPEN HOLE TENSILE STRENGTH (CTLX816 Fibredux 914)

Fabric	sample numbers OHT01	OHT02	OHT03	OHT04	OHT05	Mean	CV(%)	S/N
T1	465.1	472.5	483.1	489.2	453.4	472.7	3.0	53.48
T2	507.0	413.1	439.5	428.0	465.9	450.7	8.2	53.01
T3	590.6	579.6	559.7	532.9	563.7	565.3	3.9	55.03
T4	506.9	498.8	511.1	491.6	523.8	506.5	2.4	54.08
T5	425.8	475.8	464.8	495.5	476.0	467.6	5.5	53.36
T6	460.7	438.0	468.9	455.9	491.3	463.0	4.2	53.29
T7	451.2	450.3	445.5	465.7	453.9	453.3	1.7	53.13
T8	471.7	496.2	463.0	476.6	521.3	485.8	4.8	53.71
T9	472.0	495.0	534.3	499.8	535.4	507.3	5.4	54.08

S/N = -10log10(mean Σ1/OHT strength²)

* denotes best settings

		Mean	S/N	
Stitch course	3.5	482.1	53.64	
	5	496.2	53.84	*
	7.4	479.0	53.58	
Stitch tension	low	477.5	53.56	
	med	468.0	53.36	
	high	511.9	54.13	*
0° tension	low	473.8	53.49	
	med	488.2	53.72	
	high	495.4	53.84	*
0° coverage	spread	482.5	53.64	
	50/50	455.7	53.14	
	bunched	519.2	54.27	*

	from mean	from S/N	
Estimate at best settings	565.3	564.3	MN/m²

From ANOVA relative effect of factors is given by sum of squared deviation from mean

	sum of squared deviations	
Stitch course	0.113	least effect
Stitch tension	0.961	
0° tension	0.186	2nd least
0° coverage	1.925	most effect

re-predict more conservative optimum value ignoring the two factors with smallest effects

Estimate at best settings	544.5	MN/m²
Stitch course	-	
Stitch tension	high	
0° tension	-	
0° coverage	unched	

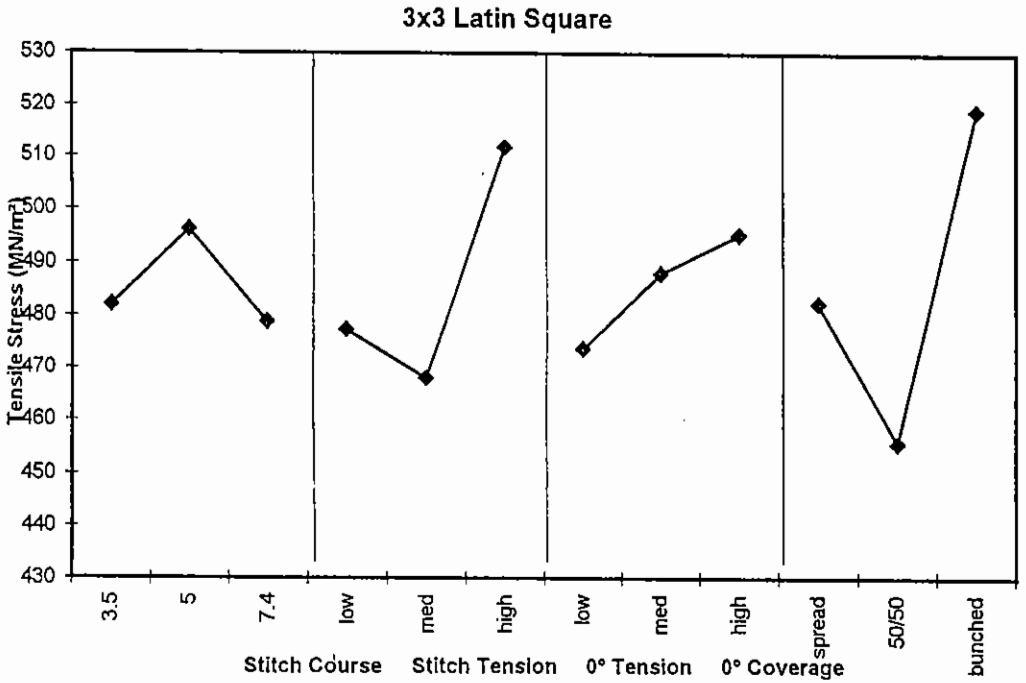

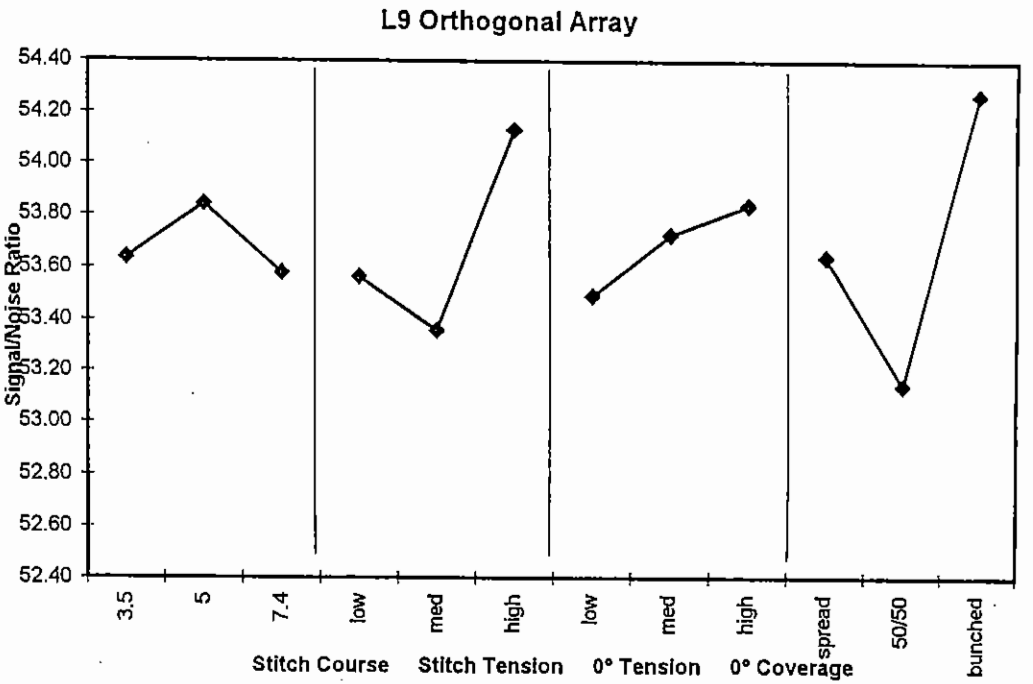

Apparent Interlaminar Shear Strength Test Data

Material T1

Coupon		width (mm)	thickness (mm)	length (mm)	mass (g)	load (kN)	ILSS (MN/m²)
T1ILS01	1	17.043	3.384	34.260			
	2	17.037	3.380	34.240			
	mean	17.040	3.382	34.250	3.029	4.65	60.57
T1ILS02	1	17.034	3.357	34.280			
	2	17.032	3.365	34.290			
	mean	17.033	3.361	34.285	3.019	4.10	53.77
T1ILS03	1	17.023	3.361	34.280			
	2	17.032	3.361	34.290			
	mean	17.028	3.361	34.285	3.016	4.32	56.61
T1ILS04	1	17.019	3.352	34.280			
	2	17.026	3.351	34.280			
	mean	17.023	3.352	34.280	3.010	4.01	52.72
T1ILS05	1	17.041	3.363	34.280			
	2	17.035	3.351	34.280			
	mean	17.038	3.357	34.280	3.016	4.04	52.96
T1ILS06	1	17.072	3.391	34.260			
	2	17.067	3.389	34.270			
	mean	17.070	3.390	34.265	3.041	4.12	53.44
T1ILS07	1	17.041	3.388	34.280			
	2	17.039	3.382	34.240			
	mean	17.040	3.385	34.260	3.035	4.23	54.94
T1ILS08	1	17.016	3.368	34.260			
	2	17.035	3.368	34.290			
	mean	17.026	3.368	34.275	3.020	4.18	54.66
T1ILS09	1	17.025	3.382	34.290			
	2	17.021	3.386	34.300			
	mean	17.023	3.384	34.295	3.030	4.00	52.01
T1ILS10	1	17.003	3.334	34.280			
	2	17.015	3.338	34.290			
	mean	17.009	3.336	34.285	2.997	3.89	51.46
	Mean	**17.033**	**3.368**	**34.276**	**3.021**	**4.15**	**54.31**

Material T2

Coupon		width (mm)	thickness (mm)	length (mm)	mass (g)	load (kN)	ILSS (MN/m²)
T2ILS01	1	17.040	3.431	34.220			
	2	17.044	3.431	34.300			
	mean	17.042	3.431	34.260	3.066	4.26	54.66
T2ILS02	1	16.996	3.420	34.230			
	2	17.035	3.429	34.300			
	mean	17.016	3.425	34.265	3.061	5.06	65.10
T2ILS03	1	17.033	3.408	34.270			
	2	17.034	3.400	34.290			
	mean	17.034	3.404	34.280	3.046	4.92	63.64
T2ILS04	1	17.035	3.426	34.280			
	2	17.025	3.419	34.310			
	mean	17.030	3.423	34.295	3.058	5.09	65.55
T2ILS05	1	17.064	3.430	34.290			
	2	17.023	3.430	34.280			
	mean	17.044	3.430	34.285	3.062	4.77	61.17
T2ILS06	1	17.019	3.405	34.270			
	2	17.025	3.399	34.290			
	mean	17.022	3.402	34.280	3.043	4.48	58.06
T2ILS07	1	17.044	3.434	34.310			
	2	17.039	3.440	34.240			
	mean	17.042	3.437	34.275	3.077	4.42	56.61
T2ILS08	1	17.039	3.378	34.300			
	2	17.047	3.376	34.300			
	mean	17.043	3.377	34.300	3.025	4.66	60.76
T2ILS09	1	17.044	3.428	34.250			
	2	17.034	3.429	34.310			
	mean	17.039	3.429	34.280	3.064	4.48	57.55
T2ILS10	1	17.036	3.423	34.260			
	2	17.038	3.426	34.280			
	mean	17.037	3.425	34.270	3.060	4.64	59.70
	Mean	**17.035**	**3.418**	**34.279**	**3.056**	**4.68**	**60.28**

Material T3

Coupon		width (mm)	thickness (mm)	length (mm)	mass (g)	load (kN)	ILSS (MN/m²)
T3ILS01	1	17.036	3.471	34.200			
	2	17.038	3.468	34.260			
	mean	17.037	3.470	34.230	3.103	4.13	52.34
T3ILS02	1	17.045	3.483	34.270			
	2	17.035	3.470	34.250			
	mean	17.040	3.477	34.260	3.102	4.18	52.95
T3ILS03	1	17.069	3.486	34.260			
	2	17.050	3.467	34.280			
	mean	17.060	3.477	34.270	3.113	4.41	55.71
T3ILS04	1	17.040	3.388	34.250			
	2	17.050	3.386	34.250			
	mean	17.045	3.387	34.250	3.022	4.19	54.46
T3ILS05	1	17.022	3.377	34.280			
	2	17.024	3.388	34.180			
	mean	17.023	3.383	34.230	3.020	4.20	54.69
T3ILS06	1	17.040	3.344	34.280			
	2	17.060	3.352	34.270			
	mean	17.050	3.348	34.275	3.003	4.81	63.20
T3ILS07	1	17.024	3.387	34.270			
	2	17.030	3.379	34.260			
	mean	17.027	3.383	34.265	3.025	4.04	52.63
T3ILS08	1	17.067	3.438	34.290			
	2	17.081	3.457	34.290			
	mean	17.074	3.448	34.290	3.090	4.33	55.16
T3ILS09	1	17.047	3.466	34.290			
	2	17.035	3.431	34.220			
	mean	17.041	3.449	34.255	3.084	4.18	53.36
T3ILS10	1	17.060	3.356	34.260			
	2	17.064	3.356	34.240			
	mean	17.062	3.356	34.250	3.006	4.22	55.29
	Mean	**17.046**	**3.418**	**34.258**	**3.057**	**4.27**	**54.98**

Material T4

Coupon		width (mm)	thickness (mm)	length (mm)	mass (g)	load (kN)	ILSS (MN/m^2)
T4ILS01	1	17.022	3.422	34.280			
	2	17.038	3.405	34.220			
	mean	17.030	3.414	34.250	3.067	4.22	54.38
T4ILS02	1	17.049	3.469	34.230			
	2	17.058	3.449	34.310			
	mean	17.054	3.459	34.270	3.111	4.30	54.71
T4ILS03	1	17.012	3.382	34.300			
	2	17.015	3.399	34.250			
	mean	17.014	3.391	34.275	3.045	4.03	52.36
T4ILS04	1	17.040	3.397	34.250			
	2	17.063	3.402	34.310			
	mean	17.052	3.400	34.280	3.057	4.47	57.84
T4ILS05	1	17.041	3.429	34.290			
	2	17.053	3.396	34.250			
	mean	17.047	3.413	34.270	3.067	4.45	57.33
T4ILS06	1	17.021	3.407	34.270			
	2	17.018	3.388	34.290			
	mean	17.020	3.398	34.280	3.052	4.63	60.04
T4ILS07	1	17.034	3.455	34.290			
	2	17.036	3.460	34.240			
	mean	17.035	3.458	34.265	3.099	4.53	57.70
T4ILS08	1	17.065	3.420	34.280			
	2	17.070	3.426	34.290			
	mean	17.068	3.423	34.285	3.078	4.73	60.72
T4ILS09	1	17.070	3.453	34.260			
	2	17.058	3.459	34.270			
	mean	17.064	3.456	34.265	3.108	4.62	58.74
T4ILS10	1	17.017	3.475	34.290			
	2	17.014	3.460	34.250			
	mean	17.016	3.468	34.270	3.106	4.81	61.08
	Mean	**17.040**	**3.428**	**34.271**	**3.079**	**4.48**	**57.49**

Material T5

Coupon		width (mm)	thickness (mm)	length (mm)	mass (g)	load (kN)	ILSS (MN/m^2)
T5ILS01	1	17.029	3.535	34.280			
	2	17.019	3.536	34.250			
	mean	17.024	3.536	34.265	3.175	4.83	60.21
T5ILS02	1	17.039	3.492	34.260			
	2	17.037	3.493	34.280			
	mean	17.038	3.493	34.270	3.133	4.80	60.55
T5ILS03	1	17.046	3.497	34.260			
	2	17.068	3.496	34.220			
	mean	17.057	3.497	34.240	3.115	4.65	58.50
T5ILS04	1	17.076	3.454	34.300			
	2	17.048	3.461	34.310			
	mean	17.062	3.458	34.305	3.099	4.42	56.23
T5ILS05	1	17.040	3.538	34.240			
	2	17.042	3.522	24.290			
	mean	17.041	3.530	29.265	3.167	4.67	58.21
T5ILS06	1	17.055	3.521	34.220			
	2	17.026	3.520	34.270			
	mean	17.041	3.521	34.245	3.147	4.70	58.71
T5ILS07	1	17.028	3.526	34.300			
	2	17.019	3.505	34.280			
	mean	17.024	3.516	34.290	3.130	4.58	57.45
T5ILS08	1	17.035	3.498	34.290			
	2	17.012	3.510	34.220			
	mean	17.024	3.504	34.255	3.132	4.81	60.46
T5ILS09	1	17.036	3.517	34.220			
	2	17.025	3.538	34.260			
	mean	17.031	3.528	34.240	3.149	5.15	64.27
T5ILS10	1	17.059	3.451	34.270			
	2	17.044	3.473	34.270			
	mean	17.052	3.462	34.270	3.104	4.59	58.29
	Mean	**17.039**	**3.504**	**33.765**	**3.135**	**4.72**	**59.29**

Material T6

Coupon		width (mm)	thickness (mm)	length (mm)	mass (g)	load (kN)	ILSS (MN/m²)
T6ILS01	1	17.033	3.485	34.250			
	2	17.041	3.481	34.260			
	mean	17.037	3.483	34.255	3.114	4.52	57.15
T6ILS02	1	17.054	3.505	34.300			
	2	17.053	3.499	34.290			
	mean	17.054	3.502	34.295	3.144	5.28	66.27
T6ILS03	1	17.031	3.495	34.280			
	2	17.063	3.490	34.290			
	mean	17.047	3.493	34.285	3.131	4.95	62.38
T6ILS04	1	17.027	3.492	34.280			
	2	17.040	3.497	34.300			
	mean	17.034	3.495	34.290	3.134	4.95	62.42
T6ILS05	1	17.027	3.499	34.280			
	2	17.028	3.496	34.250			
	mean	17.028	3.498	34.265	3.135	4.60	57.88
T6ILS06	1	17.052	3.475	34.310			
	2	17.050	3.461	34.300			
	mean	17.051	3.468	34.305	3.101	4.58	58.03
T6ILS07	1	17.020	3.496	34.290			
	2	17.036	3.496	34.280			
	mean	17.028	3.496	34.285	3.123	4.73	59.55
T6ILS08	1	17.042	3.492	34.270			
	2	17.061	3.476	34.280			
	mean	17.052	3.484	34.275	3.118	4.62	58.33
T6ILS09	1	17.054	3.505	34.220			
	2	17.020	3.492	34.270			
	mean	17.037	3.499	34.245	3.121	4.52	56.86
T6ILS10	1	17.043	3.501	34.170			
	2	17.062	3.493	34.240			
	mean	17.053	3.497	34.205	3.125	5.22	65.69
	Mean	**17.042**	**3.491**	**34.271**	**3.125**	**4.80**	**60.46**

Material T7

Coupon		width (mm)	thickness (mm)	length (mm)	mass (g)	load (kN)	ILSS (MN/m²)
T7ILS01	1	17.066	3.528	34.300			
	2	17.044	3.507	34.280			
	mean	17.055	3.518	34.290	3.156	4.58	57.23
T7ILS02	1	17.072	3.487	34.280			
	2	17.053	3.495	34.300			
	mean	17.063	3.491	34.290	3.126	4.29	53.99
T7ILS03	1	17.024	3.524	34.220			
	2	17.037	3.519	34.300			
	mean	17.031	3.522	34.260	3.145	4.51	56.39
T7ILS04	1	17.055	3.513	34.330			
	2	17.060	3.501	34.290			
	mean	17.058	3.507	34.310	3.136	5.04	63.19
T7ILS05	1	17.041	3.532	34.230			
	2	17.040	3.522	34.310			
	mean	17.041	3.527	34.270	3.155	4.83	60.26
T7ILS06	1	17.041	3.495	34.300			
	2	17.056	3.478	34.300			
	mean	17.049	3.487	34.300	3.110	4.56	57.52
T7ILS07	1	17.036	3.557	34.260			
	2	17.008	3.555	34.320			
	mean	17.022	3.556	34.290	3.154	5.01	62.08
T7ILS08	1	17.030	3.501	34.290			
	2	17.032	3.508	34.290			
	mean	17.031	3.505	34.290	3.135	4.38	55.01
T7ILS09	1	17.055	3.500	34.310			
	2	17.057	3.487	34.310			
	mean	17.056	3.494	34.310	3.125	4.68	58.88
T7ILS10	1	17.082	3.518	34.290			
	2	17.066	3.486	34.320			
	mean	17.074	3.502	34.305	3.143	4.95	62.14
	Mean	**17.048**	**3.511**	**34.292**	**3.139**	**4.68**	**58.67**

Material T8

Coupon		width (mm)	thickness (mm)	length (mm)	mass (g)	load (kN)	ILSS (MN/m²)
T8ILS01	1	17.042	3.500	34.240			
	2	17.041	3.495	34.320			
	mean	17.042	3.498	34.280	3.138	4.35	54.70
T8ILS02	1	17.027	3.463	34.250			
	2	17.031	3.469	34.300			
	mean	17.029	3.466	34.275	3.094	4.79	60.83
T8ILS03	1	17.026	3.464	34.220			
	2	17.032	3.479	34.340			
	mean	17.029	3.472	34.280	3.105	4.44	56.36
T8ILS04	1	17.029	3.494	34.280			
	2	17.041	3.485	34.180			
	mean	17.035	3.490	34.230	3.109	4.31	54.34
T8ILS05	1	17.009	3.497	34.310			
	2	17.049	3.506	34.300			
	mean	17.029	3.502	34.305	3.137	4.47	56.22
T8ILS06	1	17.031	3.510	34.330			
	2	17.036	3.501	34.120			
	mean	17.034	3.506	34.225	3.129	4.77	59.86
T8ILS07	1	17.047	3.492	34.310			
	2	17.028	3.497	34.300			
	mean	17.038	3.495	34.305	3.125	4.39	55.30
T8ILS08	1	17.054	3.434	34.200			
	2	16.953	3.422	34.210			
	mean	17.004	3.428	34.205	3.056	4.28	55.07
T8ILS09	1	17.062	3.501	34.310			
	2	17.065	3.509	34.260			
	mean	17.064	3.505	34.285	3.130	4.37	54.76
T8ILS10	1	17.015	3.437	34.300			
	2	16.985	3.449	34.260			
	mean	17.000	3.443	34.280	3.074	4.53	58.01
	Mean	**17.030**	**3.480**	**34.267**	**3.110**	**4.47**	**56.55**

Material T9

Coupon		width (mm)	thickness (mm)	length (mm)	mass (g)	load (kN)	ILSS (MN/m^2)
T9ILS01	1	17.040	3.423	34.280			
	2	17.031	3.416	34.250			
	mean	17.036	3.420	34.265	3.071	4.73	60.89
T9ILS02	1	17.036	3.409	34.300			
	2	17.028	3.374	34.280			
	mean	17.032	3.392	34.290	3.040	4.36	56.65
T9ILS03	1	16.985	3.411	24.280			
	2	17.032	3.414	24.260			
	mean	17.009	3.413	24.270	3.064	4.18	54.06
T9ILS04	1	17.034	3.431	34.220			
	2	17.017	3.442	34.270			
	mean	17.026	3.437	34.245	3.089	4.19	53.67
T9ILS05	1	17.053	3.338	34.290			
	2	17.063	3.365	34.280			
	mean	17.058	3.352	34.285	3.028	4.34	56.97
T9ILS06	1	17.063	3.377	34.290			
	2	17.072	3.372	34.280			
	mean	17.068	3.375	34.285	3.044	4.78	62.18
T9ILS07	1	17.015	3.456	34.330			
	2	17.024	3.448	34.290			
	mean	17.020	3.452	34.310	3.088	4.09	52.19
T9ILS08	1	17.043	3.426	34.280			
	2	17.036	3.440	34.220			
	mean	17.040	3.433	34.250	3.069	4.47	57.30
T9ILS09	1	17.043	3.444	34.300			
	2	17.040	3.448	34.270			
	mean	17.042	3.446	34.285	3.086	4.59	58.66
T9ILS10	1	16.999	3.466	34.310			
	2	17.013	3.470	34.290			
	mean	17.006	3.468	34.300	3.112	4.06	51.64
	Mean	**17.033**	**3.419**	**33.279**	**3.069**	**4.38**	**56.42**

NTERLAMINAR SHEAR STRENGTH (CTLX816 Fibredux 914)

	sample numbers												
abric	ILSS01	ILSS02	ILSS03	ILSS04	ILSS05	ILSS06	ILSS07	ILSS08	ILSS09	ILSS10	Mean	SD	S/N
1	60.6	53.8	56.6	52.7	53.0	53.4	54.9	54.9	52.0	51.5	54.3	2.7	34.68
2	54.7	65.1	63.6	65.5	61.2	58.1	56.6	56.6	57.6	59.7	59.9	3.8	35.50
3	52.3	52.9	55.7	54.5	54.7	63.2	52.6	52.6	53.4	55.3	54.7	3.2	34.73
4	54.4	54.7	52.4	57.8	57.3	60.0	57.7	57.7	58.7	61.1	57.2	2.7	35.12
5	60.2	60.5	58.5	56.2	58.2	58.7	57.4	57.4	64.3	58.3	59.0	2.3	35.40
6	57.2	66.3	62.4	62.4	57.9	58.0	59.6	59.6	56.9	65.7	60.6	3.4	35.61
7	57.2	54.0	56.4	63.2	60.3	57.5	62.1	62.1	58.9	62.1	59.4	3.1	35.44
8	54.7	60.8	56.4	54.3	56.2	59.9	55.3	55.3	54.8	58.0	56.6	2.3	35.03
9	60.9	56.6	54.1	53.7	57.0	62.2	52.2	52.2	58.7	51.6	55.9	3.8	34.90

i/N = -10log$_{10}$(mean Σ1/ILSS^2)

* denotes best settings

		Mean	S/N	
Stitch course	3.5	57.3	35.12	
	5	56.3	34.97	
	7.4	58.9	35.38	*
Stitch tension	low	57.0	35.08	
	med	58.5	35.31	*
	high	57.1	35.08	
0° tension	low	57.2	35.11	
	med	57.7	35.17	
	high	57.7	35.19	*
0° coverage	spread	56.4	34.99	
	50/50	59.9	35.52	*
	bunched	56.2	34.96	

	from mean		from S/N
OPTIMUM	62.5		62.5
From ANOVA relative effect of factors is given by			
sum of squared deviation from mean			
sum of squared deviations			
Stitch course	0.256		
Stitch tension	0.106	2nd least	
0° tension	0.011	least effect	
0° coverage	0.584	most effect	
re-predict more conservative optimum value			
Ignoring the two factors with smallest effects			
OPTIMUM			61.2
Stitch			7.4
Stitch			-
0° tension			-
0° coverage			50/50

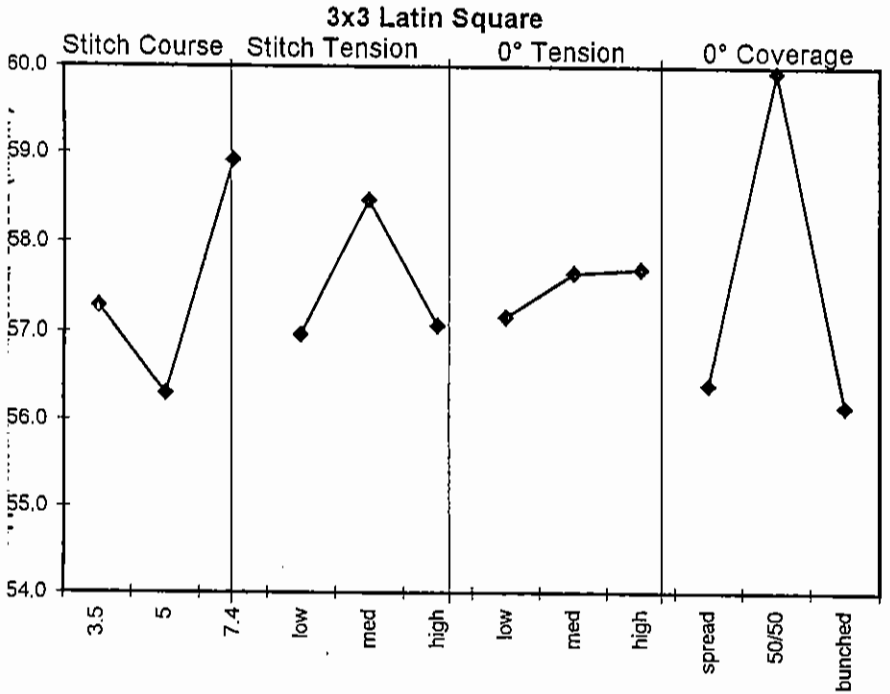

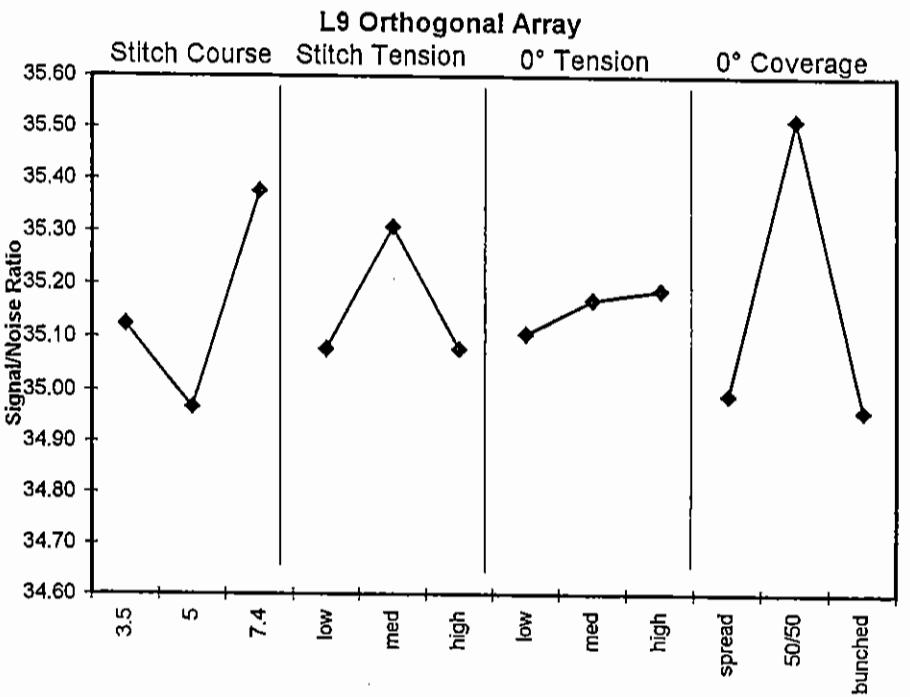

Impact and Compression After Impact Test Data

Material T1

Coupon		width (mm)	thickness (mm)	length (mm)	mass (g)	impact energy (J)	Threshold Force (kN)	Peak Force (kN)	Absorbed Energy (J)	Damage area (mm²)	Damage width (mm)	Damage Length (mm)	Indent Depth (mm)	CAI (MN/m²)
T1CAI01	1	101.65	5.00	152.68	120.7	5.15	4.70	5.02	3.14	542	24	36	0.06	-
	2	101.64	5.08	152.66										
	3	101.68	5.11	152.63										
T1CAI02	1	101.61	5.03	152.68	121.3	15.66	4.98	5.86	11.33	1350	52	52	0.18	286.06
	2	101.65	5.09	152.66										
	3	101.70	5.10	152.69										
T1CAI03	1	101.63	4.97	152.68	120.4	25.97	5.59	6.87	20.34	2263	72	76	0.39	256.29
	2	101.62	5.00	152.72										
	3	101.66	5.08	152.69										
T1CAI04	1	101.68	5.11	152.75	121.5	25.74	5.75	7.01	19.72	2203	76	74	0.39	270.81
	2	101.66	5.10	152.72										
	3	101.68	5.12	152.73										
T1CAI05	1	101.68	5.14	152.73	122.5	5.15	5.11	5.14	3.17	478	23	31	0.05	-
	2	101.65	5.13	152.68										
	3	101.69	5.12	152.68										
T1CAI06	1	101.66	5.12	152.62	121.6	15.53	5.69	6.25	11	1213	44	50	0.17	311.32
	2	101.62	5.09	152.64										
	3	101.60	5.08	152.64										
T1CAI07	1	101.59	5.15	152.68	121.6	15.31	5.88	6.31	10.73	1330	42	52	0.15	309.32
	2	101.60	5.13	152.70										
	3	101.69	5.08	152.71										
T1CAI08	1	101.66	5.14	152.70	123.0	25.92	6.17	6.98	20.51	2764	73	76	0.39	265.89
	2	101.66	5.16	152.71										
	3	101.59	5.13	152.70										
T1CAI09	1	101.69	5.07	152.70	121.8	5.12	5.30	5.3	2.13	218	16	26	0.00	-
	2	101.65	5.10	152.70										
	3	101.59	5.08	152.66										
T1CAI10	1	101.63	5.06	152.64	119.9	5.20	5.25	5.25	2.12	357	15	38	0.00	-
	2	101.64	5.04	152.69										
	3	101.65	4.98	152.63										
T1CAI11	1	101.69	5.10	152.70	121.4	15.43	5.78	6.03	11.03	1517	45	59	0.17	-
	2	101.67	5.10	152.72										
	3	101.68	5.00	152.69										
T1CAI12	1	101.63	5.06	152.72	120.7	25.74	5.7	7.13	20.37	2621	75	81	0.38	255.49
	2	101.67	5.03	152.70										
	3	101.64	5.02	152.68										

Material T2

Coupon		width (mm)	thickness (mm)	length (mm)	mass (g)	impact energy (J)	Threshold Force (kN)	Peak Force (kN)	Absorbed Energy (J)	Damage area (mm²)	Damage width (mm)	Damage Length (mm)	Indent Depth (mm)	CAI (MN/m²)
T2CAI01	1	101.56	5.03	152.72	120.4	5.19	4.44	4.64	2.93	353	20	28	0.06	-
	2	101.49	5.01	152.69										
	3	101.55	5.06	152.68										
T2CAI02	1	101.59	5.03	152.72	120.7	15.54	5.24	6.16	11.04	1369	49	49	0.20	309.84
	2	101.57	5.03	152.71										
	3	101.57	5.07	152.70										
T2CAI03	1	101.57	5.05	152.65	120.2	25.97	5.47	6.9	20.73	2147	74	66	0.42	264.75
	2	101.48	5.06	152.70										
	3	101.46	5.07	152.70										
T2CAI04	1	101.57	5.06	152.73	121.3	25.93	5.64	6.79	21.14	2155	76	75	0.54	258.22
	2	101.54	5.04	152.69										
	3	101.52	5.04	152.65										
T2CAI05	1	101.54	5.07	152.69	121.3	5.01	5.11	5.15	2.9	357	20	28	0.07	-
	2	101.53	5.06	152.69										
	3	101.53	5.07	152.71										
T2CAI06	1	101.52	5.03	152.71	120.5	15.43	5.84	6.17	10.89	1112	37	47	0.18	-
	2	101.47	5.08	152.67										
	3	101.50	5.08	152.61										
T2CAI07	1	101.57	5.02	152.72	120.9	15.55	5.66	6.23	11.3	1278	67	48	0.18	305.85
	2	101.59	5.06	152.71										
	3	101.65	5.06	152.68										
T2CAI08	1	101.62	5.06	152.72	121.3	25.74	5.64	6.81	20.91	2137	70	69	0.49	255.51
	2	101.62	5.1	152.71										
	3	101.64	5.05	152.71										
T2CAI09	1	101.56	5.07	152.74	121	5.08	5.21	5.21	3.07	428	19	32	0.07	-
	2	101.61	5.07	152.70										
	3	101.66	5.07	152.70										
T2CAI10	1	101.64	5.06	152.75	120.3	5.16	5.17	5.17	3.33	437	21	30	0.08	-
	2	101.55	4.99	152.73										
	3	101.6	4.97	152.69										
T2CAI11	1	101.60	5.07	152.70	120.3	15.55	5.53	6.03	11.19	1191	41	47	0.18	317.22
	2	101.57	5.02	152.71										
	3	101.51	5.02	152.69										
T2CAI12	1	101.55	5.10	152.69	120.3	25.72	5.76	6.62	20.75	2318	72	79	0.46	257.72
	2	101.49	5.05	152.70										
	3	101.46	5.02	152.67										

Material T3

Coupon		width (mm)	thickness (mm)	length (mm)	mass (g)	impact energy (J)	Threshold Force (kN)	Peak Force (kN)	Absorbed Energy (J)	Damage area (mm²)	Damage width (mm)	Damage Length (mm)	Indent Depth (mm)	CAI (MN/m²)
T3CAI01	1	102.05	5.23	152.72	125.1	5.09	4.75	4.75	3.17	538	23	37	0.05	-
	2	102.00	5.25	152.72										
	3	101.96	5.23	152.67										
T3CAI02	1	101.76	5.22	152.72	124.6	15.51	4.83	6.17	11.2	1390	45	53	0.17	286.76
	2	101.88	5.22	152.71										
	3	101.93	5.22	152.66										
T3CAI03	1	101.92	5.13	152.7	123.9	25.71	4.35	6.84	20.21	2148	62	64	0.35	267.12
	2	101.97	5.16	152.73										
	3	101.95	5.18	152.74										
T3CAI04	1	101.92	5.2	152.74	124.2	25.73	4.63	7.07	20.14	2218	64	62	0.33	269.13
	2	101.96	5.19	152.74										
	3	101.98	5.19	152.73										
T3CAI05	1	101.8	5.21	152.76	124.6	5.16	4.8	4.8	3.22	449	21	35	0.06	-
	2	101.88	5.22	152.72										
	3	101.95	5.2	152.6										
T3CAI06	1	101.94	5.16	152.74	122.8	15.24	4.62	6.15	10.75	1327	41	48	0.17	308.92
	2	101.76	5.16	152.73										
	3	101.65	5.17	152.72										
T3CAI07	1	101.86	5.18	152.72	123.6	15.44	4.71	6.27	10.95	1294	41	49	0.38	327.07
	2	101.88	5.17	152.72										
	3	101.92	5.13	152.72										
T3CAI08	1	102.05	5.16	152.7	123.4	25.91	4.54	7.3	20.59	2049	66	65	0.07	275.38
	2	102.02	5.13	152.71										
	3	102.02	5.12	152.72										
T3CAI09	1	101.69	5.1	152.67	122.5	5.09	4.71	4.71	3.22	496	21	33	0.18	-
	2	101.6	5.12	152.7										
	3	101.51	5.12	152.72										
T3CAI10	1	101.93	5.09	152.6	120.9	5.16	4.8	4.8	3.13	428	21	30	0.07	-
	2	101.95	5.05	152.67										
	3	101.97	4.96	152.7										
T3CAI11	1	101.95	5.11	152.72	121.3	15.43	4.51	6.18	10.81	1229	41	47	0.17	-
	2	101.98	5.07	152.7										
	3	101.98	4.98	152.65										
T3CAI12	1	101.98	5.11	152.72	121.5	25.93	5.13	6.94	21.12	2348	62	65	0.43	260.69
	2	101.99	5.06	152.72										
	3	101.93	4.97	152.73										

Material T4

Coupon		width (mm)	thickness (mm)	length (mm)	mass (g)	impact energy (J)	Threshold Force (kN)	Peak Force (kN)	Absorbed Energy (J)	Damage area (mm^2)	Damage width (mm)	Damage Length (mm)	Indent Depth (mm)	CAI (MN/m^2)
T4CAI01	1	101.88	5.12	152.72	124	5.01	5.08	5.08	3.03	352	20	26	0.06	-
	2	101.95	5.19	152.71										
	3	101.99	5.18	152.66										
T4CAI02	1	101.92	5.11	152.72	124.3	15.71	5.27	6.25	11.36	1149	38	45	0.17	318.77
	2	101.96	5.20	152.73										
	3	102.01	5.21	152.67										
T4CAI03	1	101.95	5.09	152.71	123.8	25.86	6.04	7.18	19.71	1952	69	69	0.34	280.71
	2	101.97	5.15	152.72										
	3	101.95	5.15	152.71										
T4CAI04	1	101.98	5.20	152.74	124.6	25.51	5.68	7.21	20.1	2122	72	70	0.36	257.74
	2	101.94	5.21	152.71										
	3	101.98	5.22	152.69										
T4CAI05	1	101.94	5.23	152.74	125.1	5.17	5.20	5.2	3.37	488	23	32	0.07	-
	2	101.96	5.22	152.72										
	3	101.92	5.22	152.72										
T4CAI06	1	101.94	5.19	152.77	124.3	15.4	4.80	6.23	10.9	1118	42	46	0.17	-
	2	101.95	5.20	152.72										
	3	101.92	5.18	152.7										
T4CAI07	1	101.92	5.24	152.72	124.4	15.31	4.82	6.35	10.92	1164	38	47	0.17	326.16
	2	101.90	5.21	152.72										
	3	101.87	5.20	152.72										
T4CAI08	1	102.03	5.23	152.75	125.1	25.93	6.07	7.08	20.87	1736	66	61	0.44	282.42
	2	101.99	5.23	152.72										
	3	101.95	5.22	152.71										
T4CAI09	1	101.98	5.15	152.76	124.1	5.09	5.33	5.33	2.24	93	10	18	0.00	-
	2	101.98	5.15	152.71										
	3	102.02	5.22	152.68										
T4CAI10	1	101.97	5.2	152.66	123.5	5.16	5.02	5.02	3.15	406	21	27	0.06	-
	2	101.94	5.17	152.68										
	3	101.96	5.13	152.72										
T4CAI11	1	101.94	5.21	152.75	123.9	15.5	5.01	6.29	11.15	1164	37	46	0.17	296.96
	2	101.99	5.18	152.73										
	3	101.96	5.12	152.70										
T4CAI12	1	101.94	5.20	152.74	123.7	25.91	5.85	7.15	20.32	1950	65	60	0.31	289.64
	2	101.95	5.19	152.72										
	3	101.88	5.12	152.69										

Material T5

Coupon		width (mm)	thickness (mm)	length (mm)	mass (g)	impact energy (J)	Threshold Force (kN)	Peak Force (kN)	Absorbed Energy (J)	Damage area (mm²)	Damage width (mm)	Damage Length (mm)	Indent Depth (mm)	CAI (MN/m²)
T5CAI01	1	102.03	5.14	152.71	123.9	5.02	5.37	5.37	2.23	120.5	12	17	0.00	-
	2	101.97	5.22	152.72										
	3	101.86	5.24	152.70										
T5CAI02	1	102.01	5.17	152.65	124.7	15.33	5.97	6.08	11.02	1060	36	41	0.16	312.61
	2	101.97	5.22	152.70										
	3	101.88	5.24	152.74										
T5CAI03	1	101.86	5.14	152.68	123.8	25.72	5.80	6.90	20.9	1912	58	60	0.39	269.41
	2	101.91	5.19	152.73										
	3	101.97	5.18	152.73										
T5CAI04	1	101.93	5.24	152.72	125.1	25.93	5.67	6.86	21.09	2182	72	69	0.36	272.43
	2	101.97	5.24	152.73										
	3	101.98	5.24	152.70										
T5CAI05	1	101.89	5.23	152.73	125.3	5.17	5.20	5.2	3.22	445	21	32	0.05	-
	2	101.97	5.23	152.69										
	3	102.01	5.24	152.65										
T5CAI06	1	101.96	5.22	152.67	124.5	15.41	5.62	6.16	11.31	1203	43.5	48	0.17	322.10
	2	101.94	5.22	152.68										
	3	101.97	5.22	152.65										
T5CAI07	1	101.97	5.25	152.69	124.7	15.42	5.87	6.00	12.06	1125	40.5	45	0.17	317.06
	2	101.93	5.23	152.69										
	3	101.89	5.23	152.67										
T5CAI08	1	101.95	5.23	152.72	125.2	25.73	5.93	6.98	20.73	2145	63.5	68	0.32	280.61
	2	101.97	5.23	152.65										
	3	101.95	5.24	152.59										
T5CAI09	1	102.00	5.20	152.56	124.4	5.09	5.36	5.36	2.36	47	6.5	11	0.00	-
	2	101.95	5.23	152.63										
	3	101.88	5.22	152.66										
T5CAI10	1	101.93	5.22	152.66	123.7	4.97	5.30	5.30	2.13	36	6.5	12	0.00	-
	2	101.93	5.20	152.67										
	3	101.95	5.15	152.69										
T5CAI11	1	101.96	5.22	152.73	124.3	15.42	5.95	6.21	11.22	1120	36	44	0.18	-
	2	101.96	5.21	152.66										
	3	101.89	5.14	152.62										
T5CAI12	1	102.03	5.20	152.65	123.7	25.73	5.95	6.72	20.51	2254	67	68	0.34	270.35
	2	101.93	5.19	152.68										
	3	101.75	5.16	152.72										

Material T6

Coupon		width (mm)	thickness (mm)	length (mm)	mass (g)	impact energy (J)	Threshold Force (kN)	Peak Force (kN)	Absorbed Energy (J)	Damage area (mm²)	Damage width (mm)	Damage Length (mm)	Indent Depth (mm)	CAI (MN/m²)
T6CAI01	1	101.99	5.13	152.73	123.8	5.03	4.94	4.94	2.98	302	18	24	0.05	-
	2	101.95	5.20	152.69										
	3	101.97	5.23	152.64										
T6CAI02	1	101.96	5.15	152.65	124.4	15.43	5.30	6.16	10.93	1009	35	39	0.18	-
	2	101.96	5.22	152.67										
	3	101.96	5.25	152.73										
T6CAI03	1	101.98	5.15	152.75	123.9	25.7	5.88	6.87	20.84	1876	67	66	0.46	264.00
	2	101.95	5.21	152.72										
	3	101.98	5.25	152.67										
T6CAI04	1	101.99	5.24	152.67	124.5	25.92	5.33	6.81	21.15	1954	70	71	0.43	274.43
	2	101.91	5.24	152.70										
	3	101.94	5.24	152.74										
T6CAI05	1	101.99	5.25	152.70	125.5	5.17	5.28	5.28	3.29	396	20	27	0.05	-
	2	101.99	5.25	152.71										
	3	101.91	5.25	152.73										
T6CAI06	1	101.96	5.23	152.67	124.8	15.42	5.90	6.44	10.87	1104	36	43	0.17	313.99
	2	101.88	5.22	152.71										
	3	101.87	5.25	152.70										
T6CAI07	1	101.91	5.24	152.74	124.9	15.41	5.87	6.17	11.27	1211	42	43	0.19	345.33
	2	101.98	5.25	152.71										
	3	102.02	5.25	152.69										
T6CAI08	1	102.00	5.25	152.75	125.5	25.92	5.70	7.1	21.18	2148	70	69	0.40	276.79
	2	102.00	5.27	152.72										
	3	101.94	5.26	152.72										
T6CAI09	1	101.95	5.27	152.55	125.3	5.02	5.32	5.32	3.3	440	22	30	0.06	-
	2	101.96	5.27	152.66										
	3	101.94	5.23	152.73										
T6CAI10	1	102.00	5.24	152.73	123.9	5.12	5.36	5.36	2.19	178	14	21	0.00	-
	2	101.91	5.22	152.72										
	3	101.87	5.15	152.68										
T6CAI11	1	101.95	5.26	152.70	124.8	15.51	6.25	6.27	11.56	1183	41	44	0.20	309.30
	2	101.98	5.23	152.72										
	3	101.97	5.15	152.74										
T6CAI12	1	101.93	5.13	152.70	124.0	25.93	5.74	6.92	20.85	2059	70	66	0.45	274.46
	2	101.96	5.22	152.72										
	3	101.98	5.23	152.73										

Material T7

Coupon		width (mm)	thickness (mm)	length (mm)	mass (g)	impact energy (J)	Threshold Force (kN)	Peak Force (kN)	Absorbed Energy (J)	Damage area (mm²)	Damage width (mm)	Damage Length (mm)	Indent Depth (mm)	CAI (MN/m²)
T7CAI01	1	101.68	5.07	152.66	123.4	5.01	5.28	5.28	3.44	461	21.5	30	0.06	-
	2	101.77	5.22	152.62										
	3	101.76	5.24	152.59										
T7CAI02	1	101.68	5.13	152.66	124.1	15.61	6.04	6.62	11.26	1075	35	46	0.19	328.49
	2	101.77	5.22	152.67										
	3	101.77	5.26	152.67										
T7CAI03	1	101.79	5.05	152.58	122.6	25.71	6.08	7.01	20.83	2124	72.5	72	0.45	242.81
	2	101.79	5.13	152.63										
	3	101.79	5.22	152.64										
T7CAI04	1	101.8	5.26	152.68	124.7	25.93	6.06	7.32	20.73	1875	67	62	0.38	253.52
	2	101.80	5.26	152.67										
	3	101.79	5.24	152.64										
T7CAI05	1	101.68	5.26	152.66	125.6	5.02	5.36	5.36	2.31	83	11	11	0.02	-
	2	101.77	5.28	152.66										
	3	101.8	5.26	152.64										
T7CAI06	1	101.71	5.22	152.65	124.1	15.61	4.84	6.26	11.20	1084	32	46	0.19	294.94
	2	101.79	5.21	152.65										
	3	101.81	5.21	152.63										
T7CAI07	1	101.80	5.25	152.64	124.3	15.33	5.89	6.29	11.22	1034	36.5	44	0.18	284.51
	2	101.77	5.24	152.64										
	3	101.20	5.24	152.64										
T7CAI08	1	101.72	5.26	152.67	125.2	25.921	6.01	7.08	20.63	2025	75.5	74	0.36	257.88
	2	101.74	5.25	152.66										
	3	101.80	5.25	152.66										
T7CAI09	1	101.80	5.17	152.66	124.1	4.92	5.27	5.27	2.34	100	12	16	0.00	-
	2	101.78	5.22	152.66										
	3	101.80	5.21	152.64										
T7CAI10	1	101.81	5.10	152.66	123.6	5.05	5.33	5.33	3.39	486	22	33	0.07	-
	2	101.74	5.23	152.60										
	3	101.64	5.26	152.59										
T7CAI11	1	101.78	5.25	152.63	124.4	15.42	5.91	6.41	10.98	1221	40.5	47	0.16	-
	2	101.76	5.23	152.65										
	3	101.71	5.10	152.65										
T7CAI12	1	101.79	5.23	152.64	123.1	25.69	5.69	6.94	20.37	1984	72	70	0.33	251.06
	2	101.75	5.18	152.63										
	3	101.65	5.08	152.59										

Material T8

Coupon		width (mm)	thickness (mm)	length (mm)	mass (g)	impact energy (J)	Threshold Force (kN)	Peak Force (kN)	Absorbed Energy (J)	Damage area (mm²)	Damage width (mm)	Damage Length (mm)	Indent Depth (mm)	CAI (MN/m²)
T8CAI01	1	102.02	5.05	152.82	122.5	4.95	4.42	4.42	3.34	490	22.5	34	0.08	-
	2	102.00	5.16	152.77										
	3	101.97	5.20	152.72										
T8CAI02	1	101.97	5.07	152.74	123.1	15.45	5.12	6.07	11.69	1340	48	49	0.18	-
	2	101.80	5.14	152.74										
	3	101.82	5.21	152.73										
T8CAI03	1	102.00	5.12	152.56	122.4	25.91	5.56	7.09	21.27	2205	73.5	73	0.35	257.21
	2	101.99	5.15	152.78										
	3	101.93	5.22	152.72										
T8CAI04	1	102.02	5.18	152.77	122.8	25.92	5.70	7.31	21.41	2441	74.5	73	0.40	275.05
	2	102.02	5.18	152.77										
	3	102.01	5.18	152.88										
T8CAI05	1	101.99	5.20	152.78	124.4	4.99	4.66	4.66	3.40	457	21.5	32	0.05	-
	2	101.99	5.20	152.79										
	3	101.96	5.19	152.78										
T8CAI06	1	102.01	5.18	152.74	123.7	15.26	4.50	6.07	11.70	1563	42.5	58	0.15	306.49
	2	102.01	5.19	152.79										
	3	101.98	5.18	152.73										
T8CAI07	1	101.91	5.20	152.77	122.9	15.23	4.71	6.07	11.60	1252	45	56	0.19	317.18
	2	101.93	5.18	152.77										
	3	101.97	5.15	152.87										
T8CAI08	1	102.00	5.13	152.76	123.2	26.1	5.64	6.99	21.17	2320	71	75	0.30	275.77
	2	101.94	5.10	152.76										
	3	101.93	5.10	152.80										
T8CAI09	1	102.03	5.16	152.81	122.4	5.00	4.43	4.43	3.45	401	20	30	0.05	-
	2	102.04	5.14	152.79										
	3	102.02	5.11	152.76										
T8CAI10	1	101.92	5.16	152.71	122.5	5.04	4.68	4.68	3.43	468	20.5	33	0.06	-
	2	101.97	5.18	152.78										
	3	102.00	5.10	152.77										
T8CAI11	1	101.94	5.13	152.72	122.9	15.17	4.66	6.00	11.38	1546	46.5	64	0.19	327.73
	2	101.97	5.15	152.72										
	3	101.94	5.13	152.70										
T8CAI12	1	101.99	5.08	152.81	120.9	26.14	4.43	7.08	21.54	2338	75.5	76	0.36	252.92
	2	101.97	5.05	152.77										
	3	101.91	5.00	152.73										

Material T9

Coupon		width (mm)	thickness (mm)	length (mm)	mass (g)	impact energy (J)	Threshold Force (kN)	Peak Force (kN)	Absorbed Energy (J)	Damage area (mm²)	Damage width (mm)	Damage Length (mm)	Indent Depth (mm)	CAI (MN/m²)
T9CAI01	1	101.87	4.93	152.73	120.2	4.93	5.11	5.11	3.71	619	24	43	0.07	-
	2	101.83	5.02	152.71										
	3	101.82	5.07	152.70										
T9CAI02	1	101.82	5.00	152.65	120.8	15.33	4.79	5.76	11.81	1412	45	52	0.19	293.65
	2	101.79	5.06	152.64										
	3	101.81	5.06	152.61										
T9CAI03	1	101.77	4.95	152.34	119.9	25.93	5.03	6.75	21.3	2498	76	80	0.38	253.66
	2	101.76	5.05	152.32										
	3	101.80	5.06	152.19										
T9CAI04	1	101.84	5.09	152.65	121.8	25.92	4.92	6.72	21.42	2452	74.5	76	0.45	255.27
	2	101.82	5.11	152.66										
	3	101.82	5.11	152.68										
T9CAI05	1	101.78	5.08	152.68	122.1	4.97	4.69	4.69	3.22	407	19	34	0.06	-
	2	101.75	5.13	152.74										
	3	101.83	5.14	152.72										
T9CAI06	1	101.81	5.08	152.70	121.6	15.38	4.48	5.79	11.86	1534	48.5	56	0.19	297.97
	2	101.77	5.10	152.69										
	3	101.78	5.09	152.66										
T9CAI07	1	101.81	5.12	150.71	120.6	15.44	5.19	6.07	12.12	1383	43.5	50	0.20	
	2	101.78	5.12	150.72										
	3	101.84	5.11	150.71										
T9CAI08	1	101.80	5.14	152.66	122.3	25.93	4.85	6.94	21.62	2293	73.5	70	0.39	257.22
	2	101.76	5.12	152.67										
	3	101.77	5.11	152.67										
T9CAI09	1	101.8	5.09	150.69	120	4.99	4.32	4.32	3.31	449	21.5	31	0.05	-
	2	101.79	5.08	150.68										
	3	101.82	5.07	150.66										
T9CAI10	1	101.81	5.10	150.71	119.3	4.99	4.56	4.56	3.33	472	31	36	0.05	-
	2	101.83	5.07	150.69										
	3	101.85	5.01	150.68										
T9CAI11	1	101.81	5.08	150.71	119.5	15.56	4.6	6.06	11.77	1433	51	52	0.20	278.68
	2	101.78	5.08	150.68										
	3	101.76	5.01	150.64										
T9CAI12	1	101.83	5.07	150.72	118.9	25.93	4.6	6.83	21.72	2400	79.5	98	0.46	250.86
	2	101.81	5.05	150.71										
	3	101.84	4.91	150.70										

Delamination Threshold Force (15J) - CTLX816/Fiberdux914

Fabric	sample numbers CAI01	CAI02	CAI03	CAI04	Mean	CV(%)	S/N
T1	4.98	5.69	5.88	5.78	5.58	7.33	14.88
T2	5.24	5.84	5.66	5.53	5.57	4.54	14.89
T3	4.83	4.62	4.71	4.51	4.67	2.91	13.37
T4	5.27	4.80	4.82	5.01	4.98	4.39	13.92
T5	5.97	5.62	5.87	5.95	5.85	2.75	15.34
T6	5.30	5.90	5.87	6.25	5.83	6.74	15.27
T7	6.04	4.84	5.89	5.91	5.67	9.83	14.96
T8	5.12	4.50	4.71	4.66	4.75	5.56	13.72
T9	4.79	4.48	5.19	4.60	4.77	6.52	13.52

$S/N = -10\log_{10}(\text{mean } \Sigma 1/\text{threshold force}^2)$

		Mean	S/N	
Stitch course	3.5	5.105	14.07	
	5	5.273	14.38	
	7.4	5.552	14.84	*
Stitch tension	low	5.409	14.59	
	med	5.433	14.65	*
	high	5.088	14.05	
0° tension	low	5.431	14.62	*
	med	5.102	14.11	
	high	5.397	14.56	
0° coverage	spread	5.4	14.58	
	50/50	5.689	15.04	*
	bunched	4.841	13.67	

* denotes best settings

	from mean	from S/N	
Estimate at best settings	6.18	6.21	kN

From ANOVA relative effect of factors is given by sum of squared deviation from mean

	sum of squared deviations	
Stitch course	0.9	
Stitch tension	0.65	2nd least
0° tension	0.47	least effect
0° coverage	2.91	most effect

re-predict more conservative optimum value ignoring the two factors with smallest effects

Estimate at best settings	5.92	kN
Stitch course	7.4	
Stitch tension	-	
0° tension	-	
0° coverage	50/50	

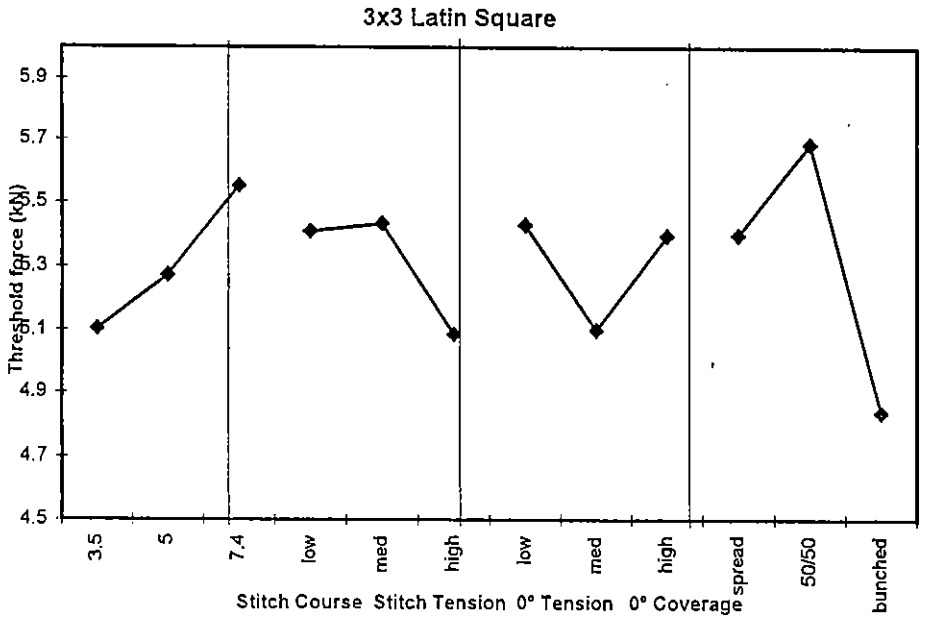

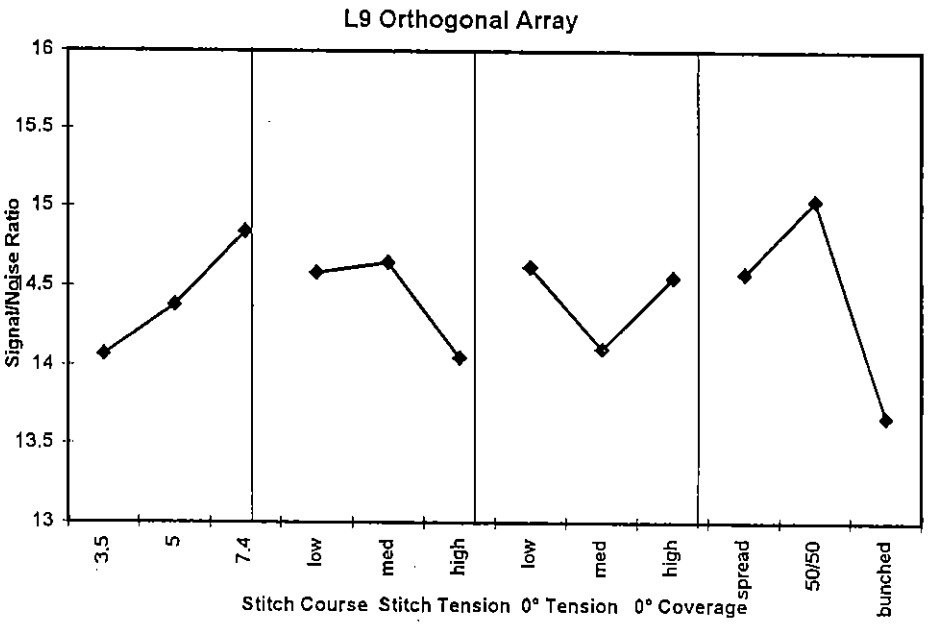

Delamination Threshold Force (25J) - CTLX816/Fiberdux914

Fabric	sample numbers CAI01	CAI02	CAI03	CAI04	Mean	CV(%)	S/N
T1	5.59	5.75	6.17	5.70	5.80	4.38	15.25
T2	5.47	5.64	5.64	5.76	5.63	2.12	15.00
T3	4.35	4.63	4.54	5.13	4.66	7.14	13.33
T4	6.04	5.68	6.07	5.85	5.91	3.07	15.42
T5	5.80	5.67	5.93	5.95	5.84	2.23	15.32
T6	5.88	5.33	5.70	5.74	5.66	4.15	15.04
T7	6.08	6.06	6.01	5.69	5.96	3.06	15.50
T8	5.56	5.70	5.64	4.43	5.33	11.33	14.39
T9	5.03	4.92	4.85	4.60	4.85	3.76	13.70

$S/N = -10\log_{10}(\text{mean } \Sigma 1/\text{threshold force}^2)$

		Mean	S/N	
Stitch course	3.5	5.38	14.53	
	5	5.36	14.53	
	7.4	5.80	15.26	*
Stitch tension	low	5.89	15.39	*
	med	5.60	14.90	
	high	5.06	14.02	
0° tension	low	5.60	14.90	*
	med	5.46	14.71	
	high	5.49	14.71	
0° coverage	spread	5.50	14.76	
	50/50	5.75	15.18	*
	bunched	5.30	14.38	

* denotes best settings

	from mean	from S/N	
Estimate at best settings	6.50	6.61	kN

From ANOVA relative effect of factors is given by sum of squared deviation from mean

	sum of squared deviations	
Stitch course	1.076	
Stitch tension	2.885	most effect
0° tension	0.069	least effect
0° coverage	0.962	2nd least

re-predict more conservative optimum value ignoring the two factors with smallest effects

Estimate at best settings	6.22	kN
Stitch course	7.4	
Stitch tension	low	
0° tension	-	
0° coverage	-	

3x3 Latin Square

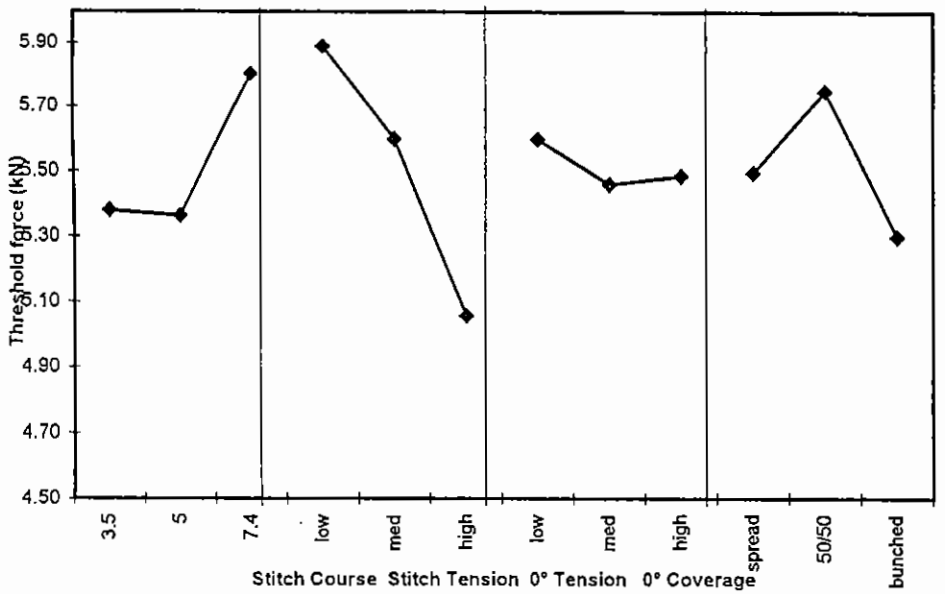

L9 Orthogonal Array

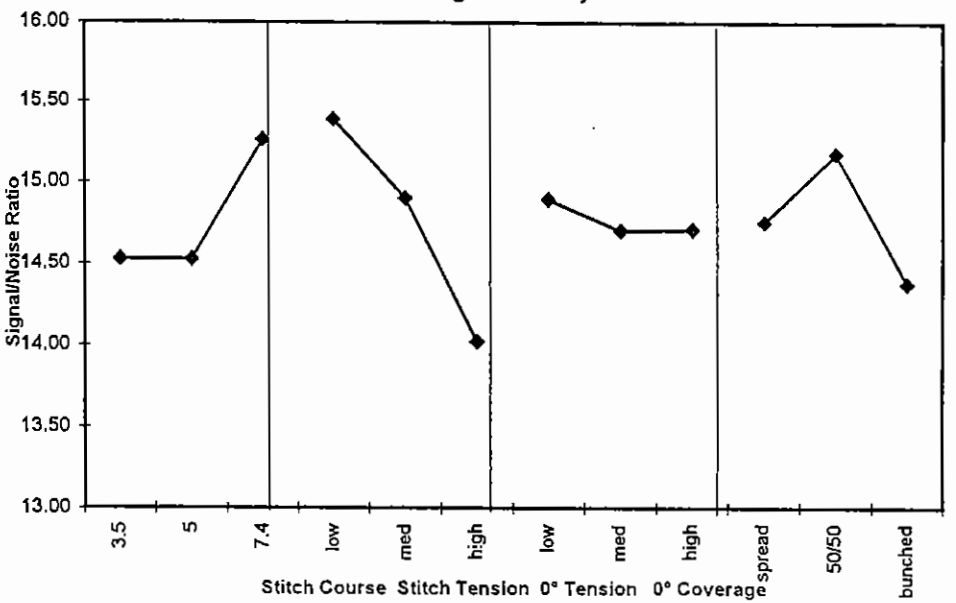

mpact Peak Force (15J) - CTLX816/Fiberdux914

Fabric	sample numbers CAI01	CAI02	CAI03	CAI04	Mean	SD	S/N
F1	5.86	6.25	6.31	6.03	6.11	0.21	15.71
F2	6.16	6.17	6.23	6.03	6.15	0.08	15.77
F3	6.17	6.15	6.27	6.18	6.19	0.05	15.84
F4	6.25	6.23	6.35	6.29	6.28	0.05	15.96
F5	6.08	6.16	6.00	5.95	6.05	0.09	15.63
F6	6.16	6.44	6.17	6.27	6.26	0.13	15.93
F7	6.62	6.26	6.29	6.41	6.40	0.16	16.11
F8	6.07	6.07	6.07	6.00	6.05	0.04	15.64
F9	5.76	5.79	6.07	6.06	5.92	0.17	15.44

$S/N = -10\log_{10}(\text{mean } \Sigma 1/\text{peak force}^2)$

		Mean	S/N	
Stitch course	3.5	6.122	15.73	
	5	6.151	15.77	
	7.4	6.196	15.84	*
Stitch tension	low	6.262	15.93	*
	med	6.082	15.68	
	high	6.124	15.73	
0° tension	low	6.142	15.76	
	med	6.116	15.72	
	high	6.212	15.86	*
0° coverage	spread	6.027	15.59	
	50/50	6.267	15.94	*
	bunched	6.175	15.81	

* denotes best settings

	from mean	from S/N	
OPTIMUM	6.5	6.5	kN

From ANOVA relative effect of factors is given by sum of squared deviation from mean

	sum of squared deviations	
Stitch course	0.018	
Stitch tension	0.102	2nd least
0° tension	0.03	least effect
0° coverage	0.181	most effect

re-predict more conservative optimum value ignoring the two factors with smallest effects

OPTIMUM	6.4	kN
Stitch course	-	
Stitch tension	low	
0° tension	-	
0° coverage	50/50	

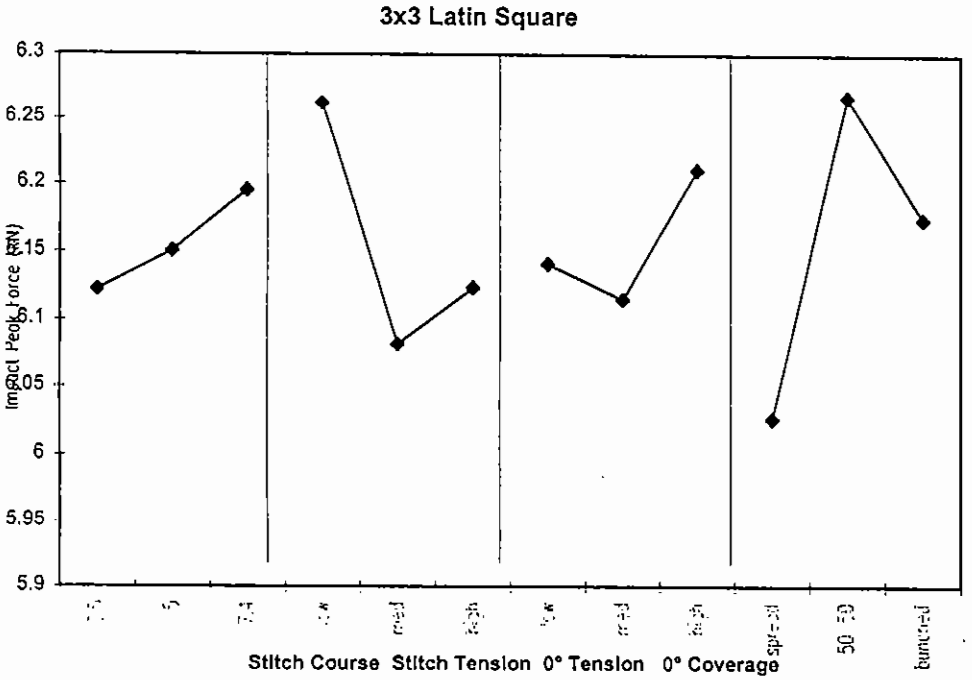

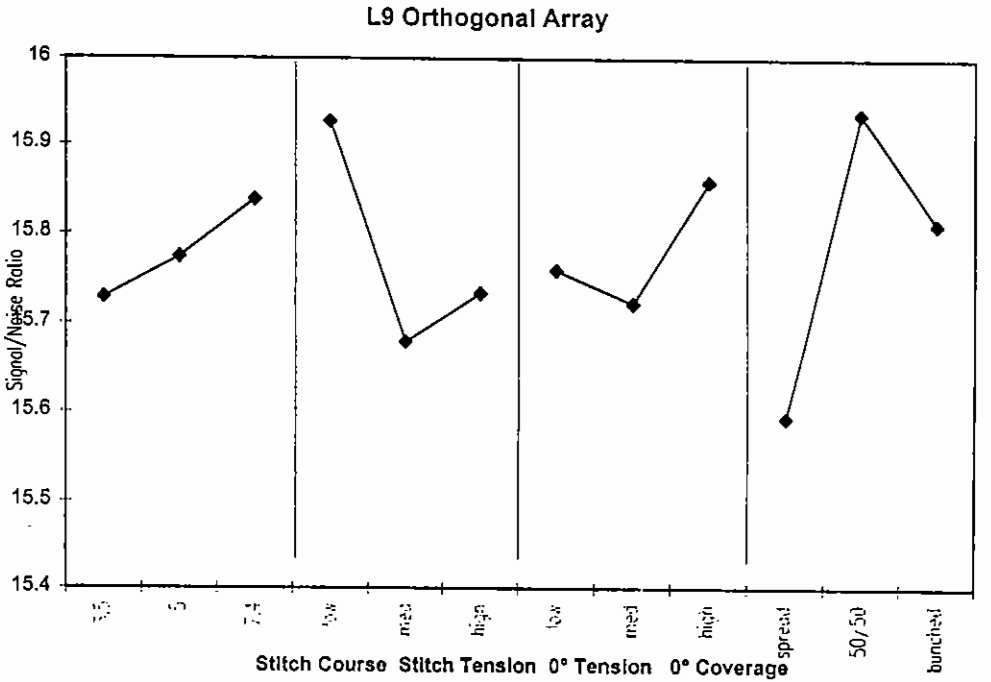

mpact Peak Force (25J) - CTLX816/Fiberdux914

abric	sample numbers CAI01	CAI02	CAI03	CAI04	Mean	SD	S/N
1	6.87	7.01	6.98	7.13	7.00	0.11	16.90
2	6.90	6.79	6.81	6.62	6.78	0.12	16.62
3	6.84	7.07	7.30	6.94	7.04	0.20	16.94
4	7.18	7.21	7.08	7.15	7.16	0.06	17.09
5	6.90	6.86	6.98	6.72	6.87	0.11	16.73
6	6.87	6.81	7.10	6.92	6.93	0.13	16.81
7	7.01	7.32	7.08	6.94	7.09	0.17	17.00
8	7.09	7.31	6.99	7.08	7.12	0.14	17.04
9	6.75	6.72	6.94	6.83	6.81	0.10	16.66

S/N = -10log$_{10}$(mean Σ1/peak force^2)

		Mean	S/N	
Stitch course	3.5	7.005	16.9	*
	5	6.938	16.82	
	7.4	6.982	16.88	
Stitch tension	low	7.08	17	*
	med	6.921	16.8	
	high	6.924	16.8	
0° tension	low	7.013	16.91	*
	med	6.915	16.79	
	high	6.997	16.89	
0° coverage	spread	6.891	16.76	
	50/50	6.931	16.81	
	bunched	7.103	17.03	*

* denotes best settings

	from mean	from S/N	
OPTIMUM	7.3	7.3	kN

From ANOVA relative effect of factors is given by sum of squared deviation from mean

	sum of squared deviations	
Stitch course	0.011	least effect
Stitch tension	0.078	
0° tension	0.026	2nd least
0° coverage	0.117	most effect

re-predict more conservative optimum value ignoring the two factors with smallest effects

OPTIMUM	7.2	kN
Stitch course	7.4	
Stitch tension	low	
0° tension	-	
0° coverage	-	

3x3 Latin Square

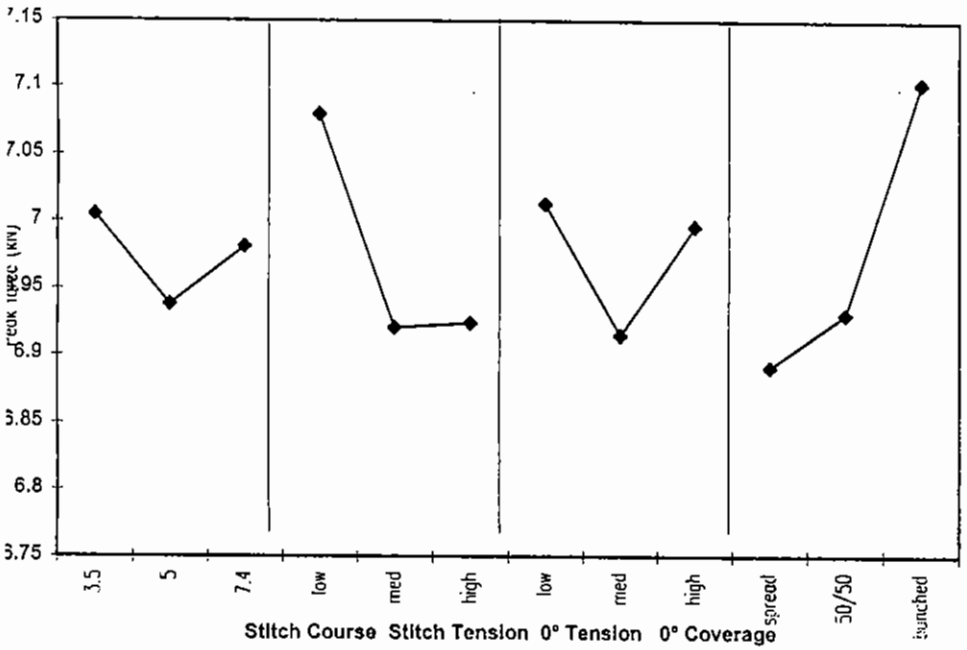

L9 Orthogonal Array

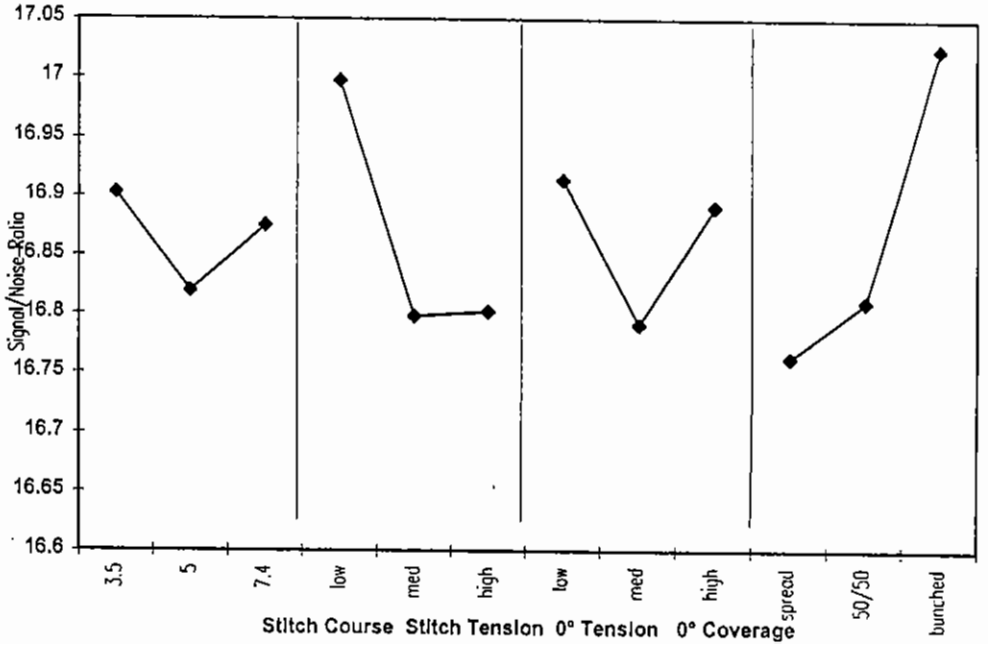

IMPACT DAMAGE AREA 5J (CTLX816 Fibredux 914)

Fabric	sample numbers CAI01	CAI02	CAI03	CAI04	Mean	CV(%)	S/N
T1	542	478	218	357	399	35.8	-52.41
T2	353	357	428	437	394	11.4	-51.95
T3	538	449	496	428	478	10.3	-53.62
T4	352	488	93	406	335	51.0	-51.27
T5	121	445	47	36	162	118.5	-47.33
T6	302	396	440	178	329	35.2	-50.73
T7	461	83	100	486	282	78.2	-50.66
T8	490	457	401	468	454	8.3	-53.16
T9	619	407	449	472	486	19.0	-53.86

S/N = -10log10(mean Σdamage area²)

		Mean	S/N	
Stitch course	3.5	408	-52.56	
	5	423	-52.66	
	7.4	275	-49.78	*
Stitch tension	low	339	-51.45	
	med	337	-50.81	*
	high	431	-52.74	
0° tension	low	394	-52.10	
	med	405	-52.36	
	high	308	-50.54	*
0° coverage	spread	349	-51.20	
	50/50	335	-51.11	*
	bunched	422	-52.68	

* denotes best settings

	from mean	from S/N	
Estimate at best settings	148.2	230.2	mm²

From ANOVA relative effect of factors is given by sum of squared deviation from mean

	sum of squared deviations	
Stitch course	16.07	most effect
Stitch tension	5.76	2nd least
0° tension	5.83	
0° coverage	4.67	least effect

re-predict more conservative optimum value ignoring the two factors with smallest effects

Estimate at best settings	270.6	mm²
Stitch course	7.4	
Stitch tension	-	
0° tension	high	
0° coverage	-	

3x3 Latin Square

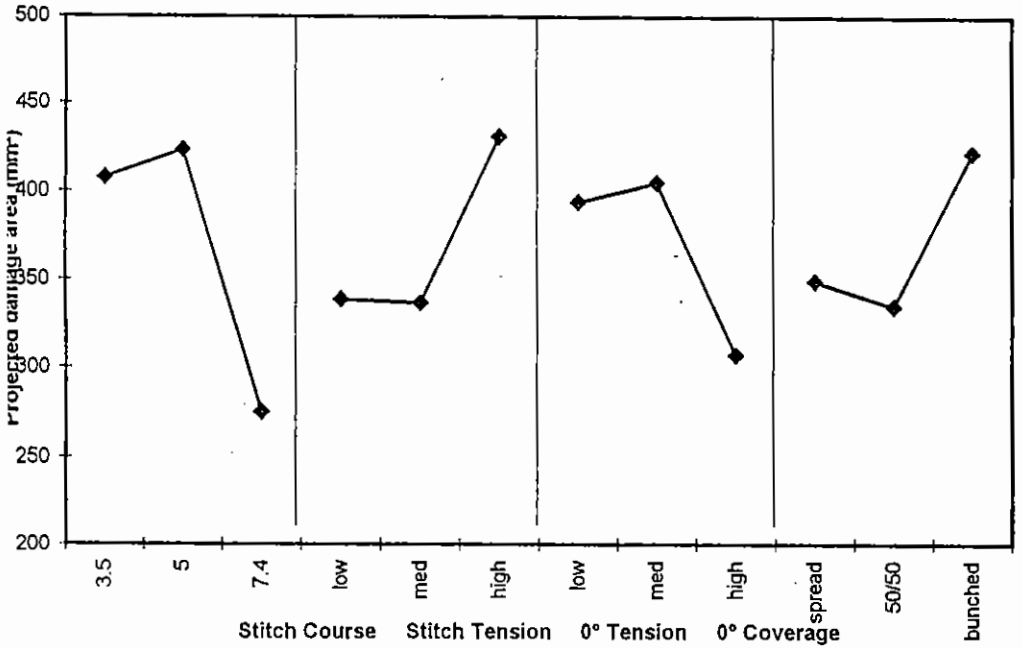

L9 Orthogonal Array

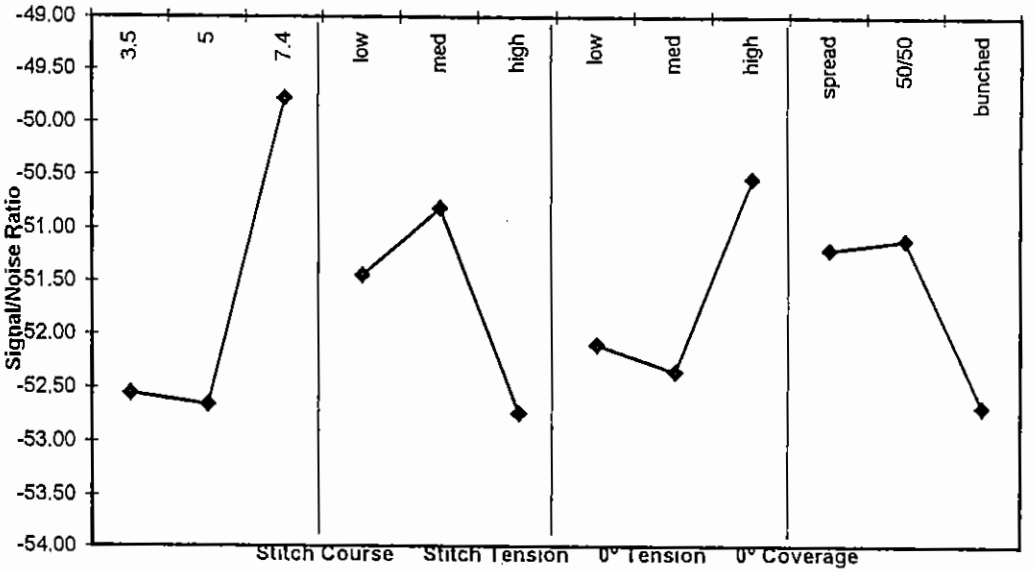

IMPACT DAMAGE AREA 15J (CTLX816 Fibredux 914)

Fabric	sample numbers CAI01	CAI02	CAI03	CAI04	Mean	CV(%)	S/N
T1	1412	1534	1383	1433	1440	4.6	-63.18
T2	1369	1112	1278	1191	1238	9.0	-61.88
T3	1390	1327	1294	1229	1310	5.1	-62.35
T4	1149	1118	1164	1164	1149	1.9	-61.21
T5	1060	1203	1125	1120	1127	5.2	-61.05
T6	1009	1104	1211	1183	1127	8.0	-61.06
T7	1075	1084	1034	1221	1103	7.4	-60.87
T8	1340	1563	1253	1546	1425	10.8	-63.12
T9	1412	1534	1383	1433	1440	4.6	-63.18

S/N = -10log10(mean Σdamage area²)

		Mean	S/N	
Stitch course	3.5	1323	-62.39	
	5	1329	-62.47	
	7.4	1134	-61.10	*
Stitch tension	low	1231	-61.75	*
	med	1263	-62.01	
	high	1292	-62.20	
0° tension	low	1331	-62.45	
	med	1276	-62.09	
	high	1180	-61.42	*
0° coverage	spread	1336	-62.47	
	50/50	1156	-61.27	*
	bunched	1295	-62.23	

* denotes best settings

	from mean	from S/N	
Estimate at best settings	914	954	mm²

From ANOVA relative effect of factors is given by sum of squared deviation from mean

	sum of squared deviations	
Stitch course	3.52	most effect
Stitch tension	0.30	least effect
0° tension	1.62	2nd least
0° coverage	2.41	

re-predict more conservative optimum value ignoring the two factors with smallest effects

Estimate at best settings	1045	mm²
Stitch course	7.4	
Stitch tension	-	
0° tension	-	
0° coverage	50/50	

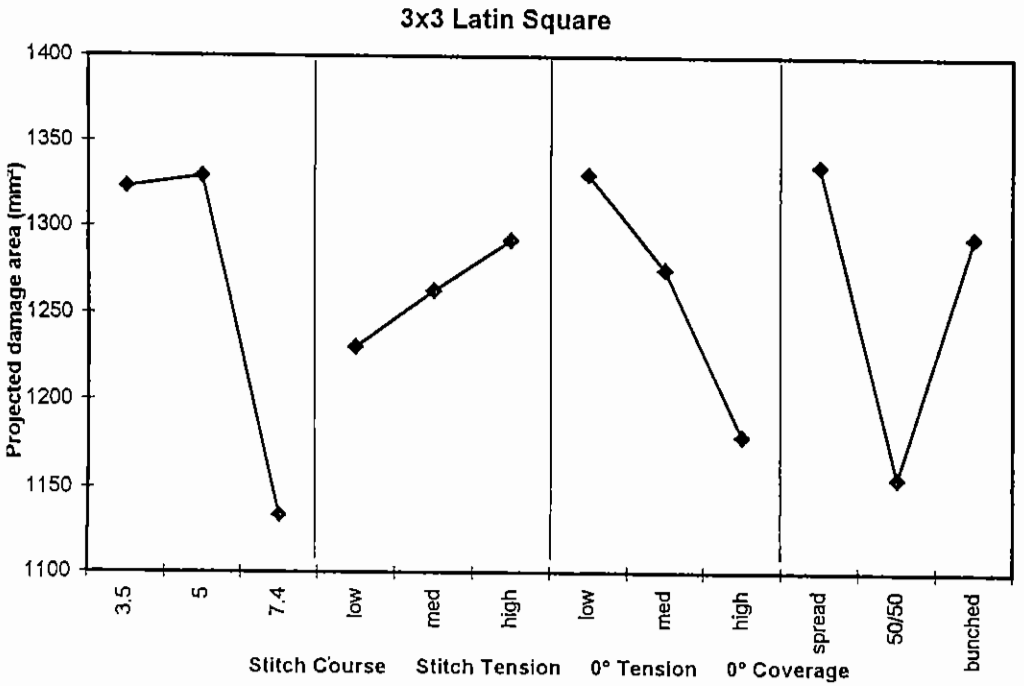

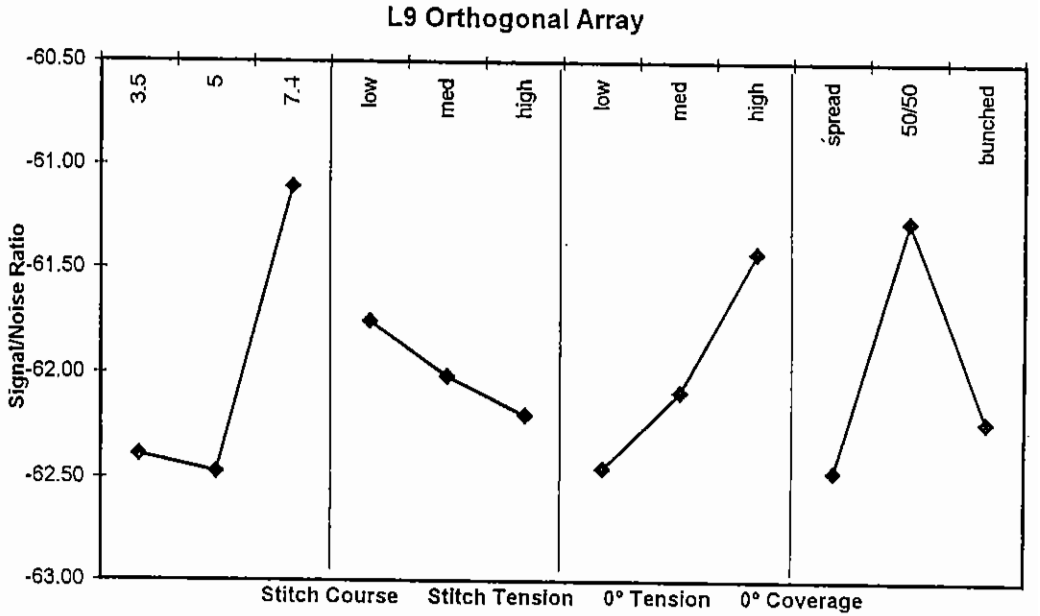

IMPACT DAMAGE AREA 25J (CTLX816 Fibredux 914)

Fabric	sample numbers CAI01	CAI02	CAI03	CAI04	Mean	CV(%)	S/N
T1	2498	2452	2293	2400	2411	3.6	-67.65
T2	2147	2155	2137	2318	2189	3.9	-66.81
T3	2148	2218	2049	2348	2191	5.7	-66.82
T4	1952	2122	1736	1950	1940	8.1	-65.78
T5	1912	2182	2145	2254	2123	7.0	-66.56
T6	1876	1954	2148	2059	2009	5.9	-66.07
T7	2124	1875	2025	1984	2002	5.1	-66.04
T8	2205	2441	2320	2338	2326	4.2	-67.34
T9	2498	2452	2293	2400	2411	3.6	-67.65

S/N = -10log10(mean Σdamage area²)

		Mean	S/N	
Stitch course	3.5	2246	-67.01	
	5	2264	-67.09	
	7.4	2024	-66.14	*
Stitch tension	low	2118	-66.49	*
	med	2213	-66.90	
	high	2204	-66.85	
0° tension	low	2249	-67.02	
	med	2180	-66.75	
	high	2105	-66.47	*
0° coverage	spread	2315	-67.28	
	50/50	2067	-66.31	*
	bunched	2152	-66.65	

* denotes best settings

	from mean	from S/N	
Estimate at best settings	1779.8	1812.3	mm²

From ANOVA relative effect of factors is given by sum of squared deviation from mean

	sum of squared deviations	
Stitch course	1.687	most effect
Stitch tension	0.304	least effect
0° tension	0.449	2nd least
0° coverage	1.475	

re-predict more conservative optimum value
Ignoring the two factors with smallest effects

Estimate at best settings	1926.7	mm²
Stitch course	7.4	
Stitch tension	-	
0° tension	-	
0° coverage	50/50	

3x3 Latin Square

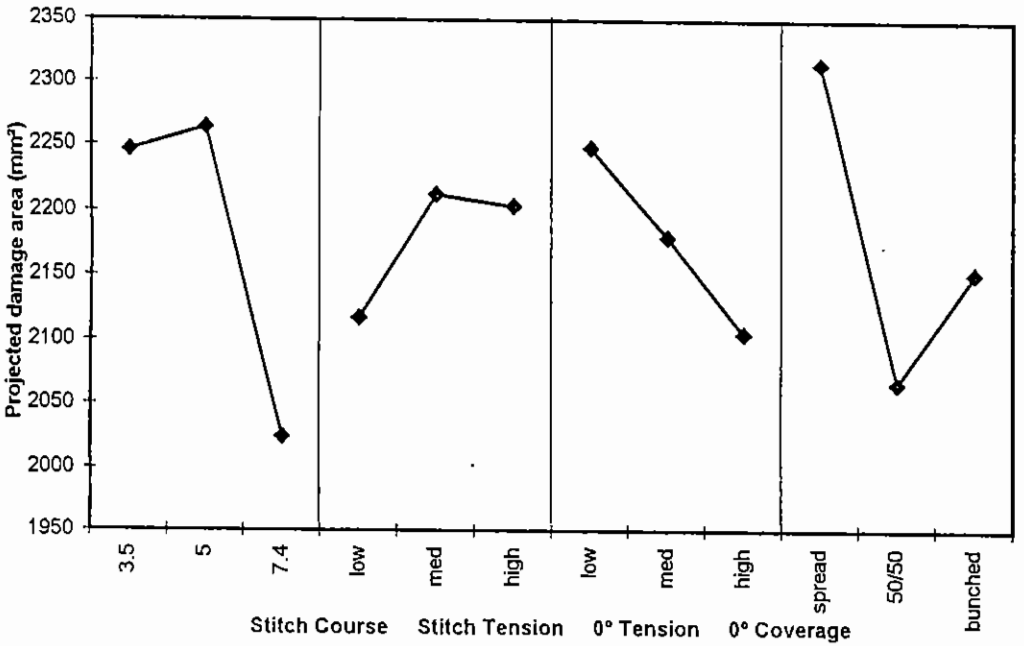

L9 Orthogonal Array

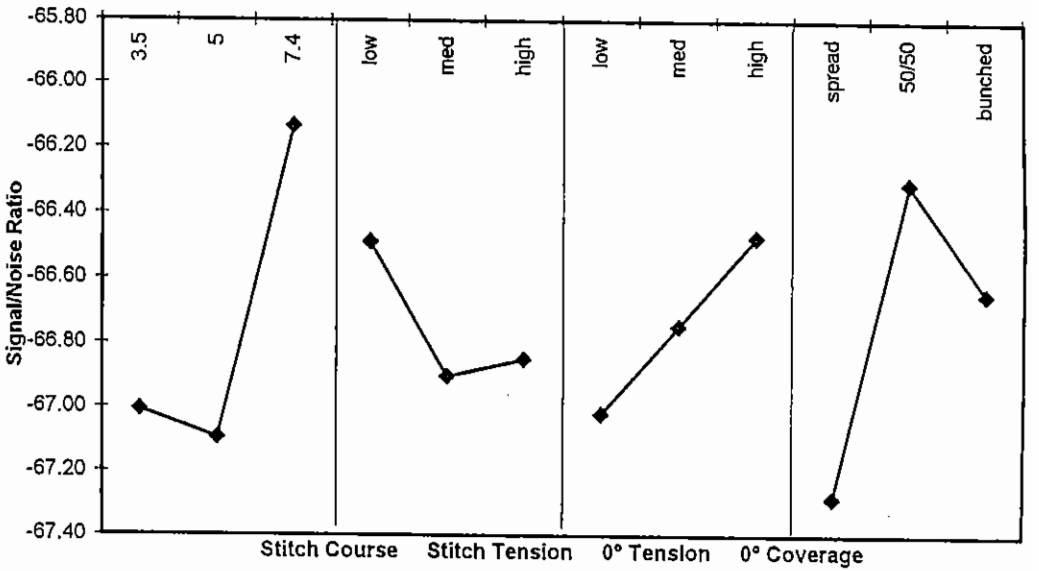

COMPRESSION AFTER IMPACT 15J (CTLX816 Fibredux 914)

Fabric	sample numbers CAI01	CAI02	CAI03	Mean	CV(%)	S/N
Γ1	286.1	311.3	309.3	302.2	4.6	49.5874
Γ2	309.8	305.8	317.2	311.0	1.9	49.8513
Γ3	286.8	308.9	327.1	307.6	6.6	49.7213
Γ4	318.8	326.2	297.0	314.0	4.8	49.9167
Γ5	312.6	322.1	317.1	317.3	1.5	50.0262
Γ6	314.0	345.3	309.3	322.9	6.1	50.1499
Γ7	328.5	294.9	284.5	302.6	7.6	49.5707
Γ8	306.5	317.2	327.7	317.1	3.3	50.0151
Γ9	293.7	298.0	278.7	290.1	3.5	49.2402

S/N = -10log10(mean Σ1/CAI strength²)

		Mean	S/N	
Stitch course	3.5	303.293	49.609	
	5	306.927	49.72	
	7.4	318.03	50.031	*
Stitch tension	low	306.281	49.692	
	med	315.119	49.964	*
	high	306.851	49.704	
0° tension	low	314.079	49.917	*
	med	305.011	49.669	
	high	309.161	49.773	
0° coverage	spread	303.197	49.618	
	50/50	312.161	49.857	
	bunched	312.893	49.884	*

* denotes best settings

	from mean	from S/N	
Estimate a best settings	331.9	332.6	MN/m²

From ANOVA relative effect of factors is given by sum of squared deviation from mean

	sum of squared deviations	
Stitch course	0.2874	most effect
Stitch tension	0.1423	
0° tension	0.0932	least effect
0° coverage	0.129	2nd least

re-predict more conservative optimum value ignoring the two factors with smallest effects

Estimate a best settings	323.9	MN/m²
Stitch course	7.4	
Stitch tension	-	
0° tension	-	
0° coverage	bunched	

3x3 Latin Square

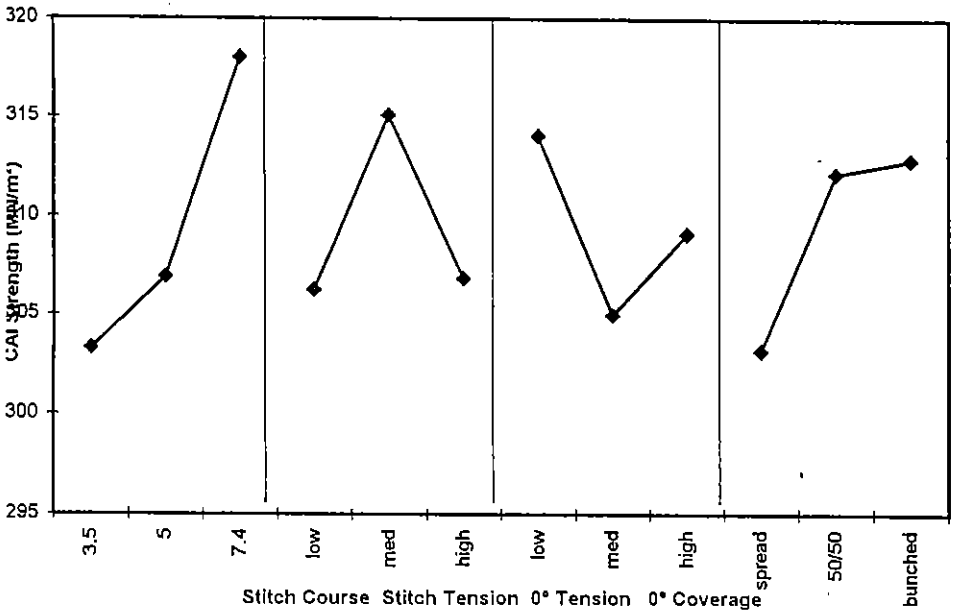

L9 Orthogonal Array

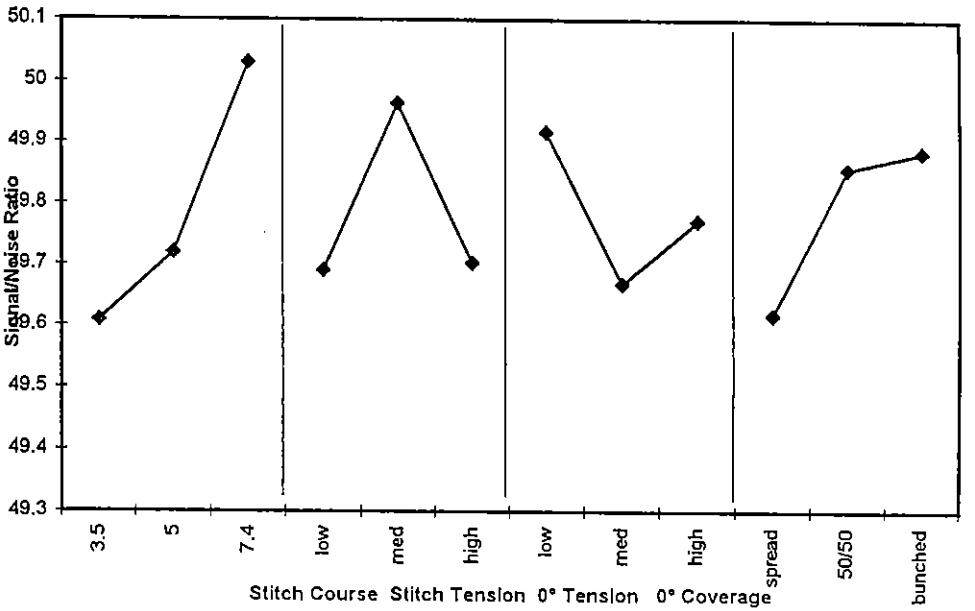

COMPRESSION AFTER IMPACT 25J (CTLX816 Fibredux 914)

abric	sample numbers CAI01	CAI02	CAI03	CAI04	Mean	CV(%)	S/N
1	256.3	270.8	265.9	255.5	262.1	2.9	48.36
2	264.7	258.2	255.5	257.7	259.0	1.5	48.27
3	267.1	269.1	275.4	260.7	268.1	2.3	48.56
4	280.7	257.7	282.4	289.6	277.6	5.0	48.84
5	269.4	272.4	280.6	270.4	273.2	1.9	48.73
6	264.0	274.4	276.8	274.5	272.4	2.1	48.70
7	242.8	253.5	257.9	251.1	251.3	2.5	48.00
8	257.2	275.1	275.8	252.9	265.2	4.5	48.45
9	253.7	255.3	257.2	250.9	254.3	1.1	48.10
				Global Mean	264.8	MN/m²	
				Global CV	4.1313	%	

		Mean	S/N	
Stitch course	3.5	256.9	48.19	
	5	263.1	48.40	
	7.4	274.4	48.76	*
Stitch tension	low	263.7	48.40	
	med	265.8	48.48	*
	high	264.9	48.45	
0° tension	low	266.6	48.51	*
	med	263.6	48.40	
	high	264.2	48.43	
0° coverage	spread	263.2	48.40	
	50/50	260.9	48.32	
	bunched	270.3	48.62	*

* denotes best settings

	from mean	from S/N	
Estimate at best settings	282.7	282.6	MN/m²

From ANOVA relative effect of factors is given by sum of squared deviation from mean

	sum of squared deviations	
Stitch course	0.502	most effect
Stitch tension	0.010	least effect
0° tension	0.017	2nd least
0° coverage	0.144	

re-predict more conservative optimum value ignoring the two factors with smallest effects

Estimate at best settings	279.6	MN/m²
Stitch course	7.4	
Stitch tension	-	
0° tension	-	
0° coverage	bunched	

i/N = -10log10(mean sum(1/compression strength²))

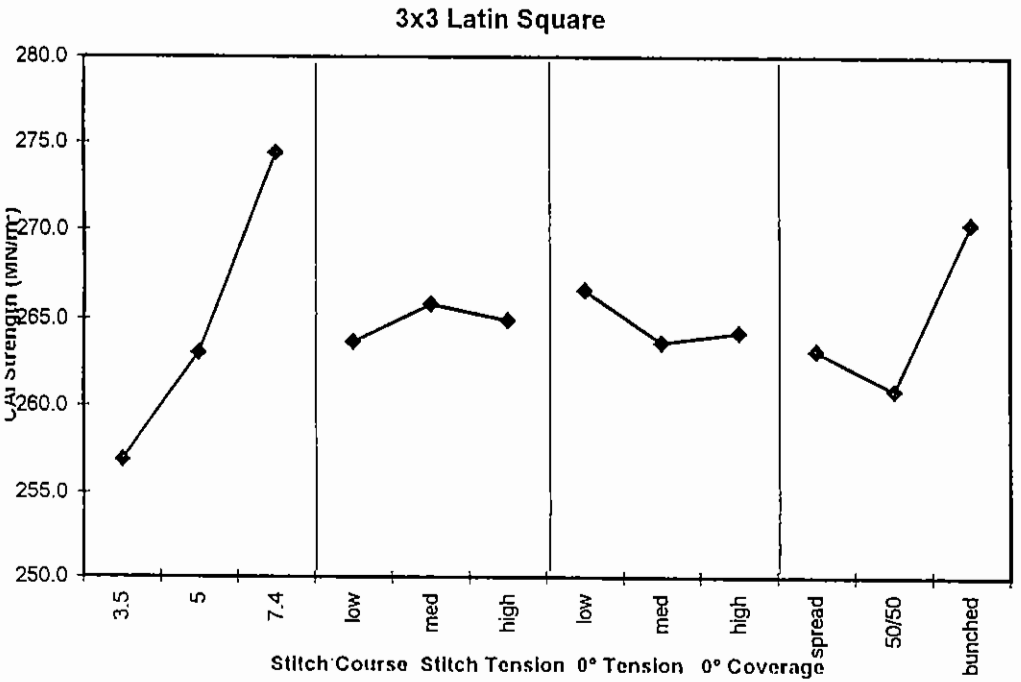

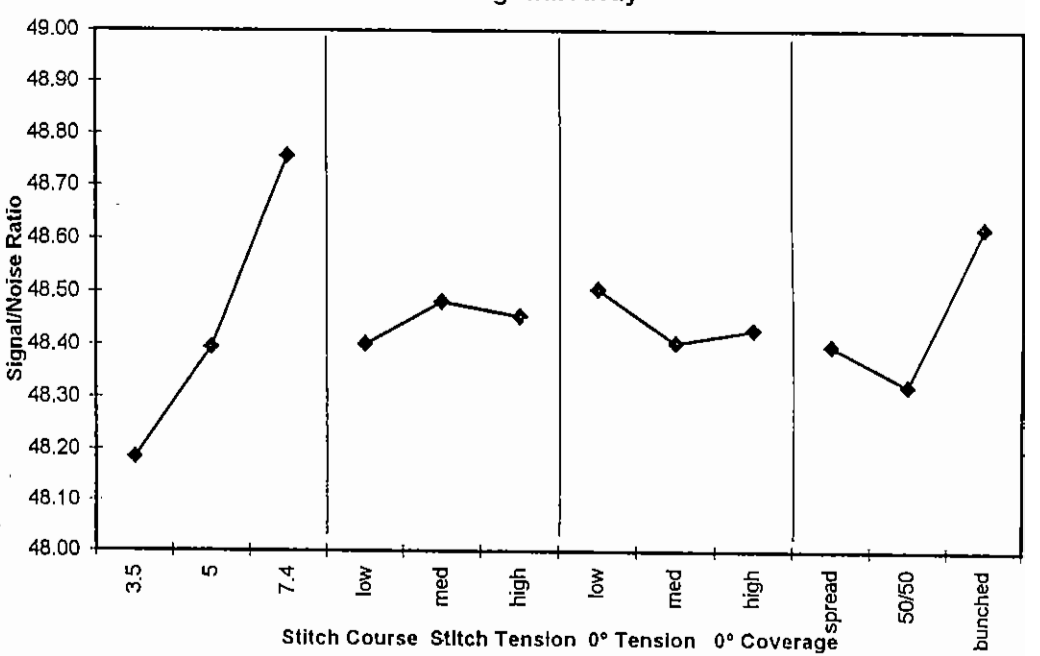

Mode I strain energy release rate (non-linear) - CTLX816/Fiberdux914

	sample numbers					
Fabric	DCB01	DCB02	DCB03	Mean	CV(%)	S/N
T1	215.5	285.5	196.6	232.5	20.1	47.0
T2	193.0	253.0	268.7	238.3	16.8	47.3
T3	234.7	274.7	314.0	274.5	14.4	48.6
T4	193.3	156.2	328.8	226.1	40.2	45.9
T5	222.6	204.6	323.3	250.2	25.6	47.5
T6	187.3	177.0	275.6	213.3	25.4	46.1
T7	284.6	260.3	222.2	255.7	12.3	48.0
T8	202.5	207.3	295.6	235.1	22.3	47.1
T9	213.7	174.5	235.0	207.7	14.8	46.1

S/N = -10log10(mean Σ1/Glc(NL)²)

		Mean	S/N	
Stitch course	3.5	232.9	47.1	
	5	248.41	47.6	*
	7.4	229.9	46.5	
Stitch tension	low	238.1	47.0	
	med	241.2	47.3	*
	high	231.8	46.9	
0° tension	low	227.0	46.7	
	med	224.0	46.4	
	high	260.1	48.0	*
0° coverage	spread	230.1	46.9	
	50/50	235.8	47.1	
	bunched	245.2	47.2	*

* denotes best settings

	from mean	from S/N	
Estimate at best settings	283.8	278.8	J/m²

From ANOVA relative effect of factors is given by sum of squared deviation from mean

	sum of squared deviations	
Stitch course	1.8994	
Stitch tension	0.1851	2nd least
0° tension	4.2975	most effect
0° coverage	0.1576	least effect

re-predict more conservative optimum value ignoring the two factors with smallest effects

Estimate at best settings	268.7	J/m²
Stitch course	5	
Stitch tension	-	
0° tension	high	
0° coverage	-	

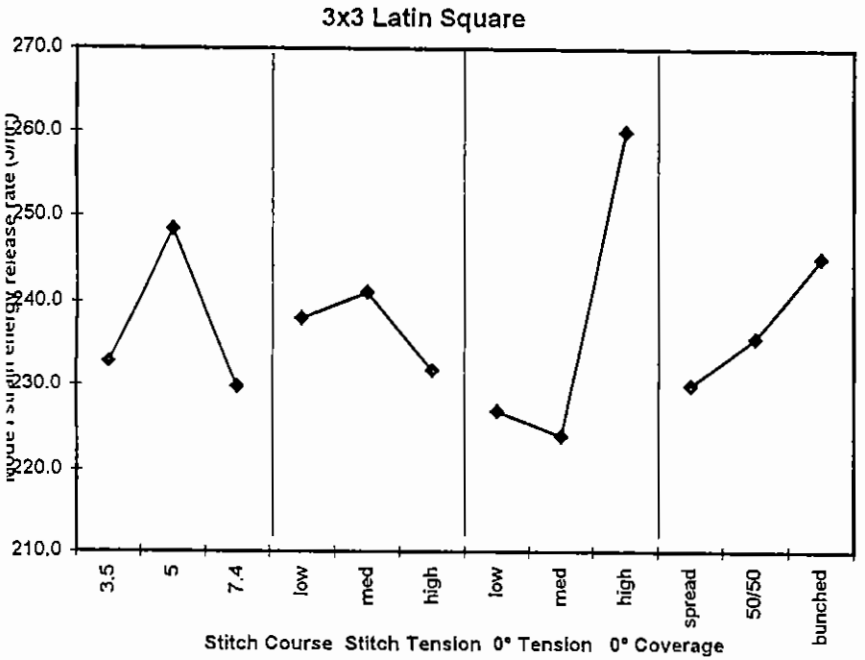

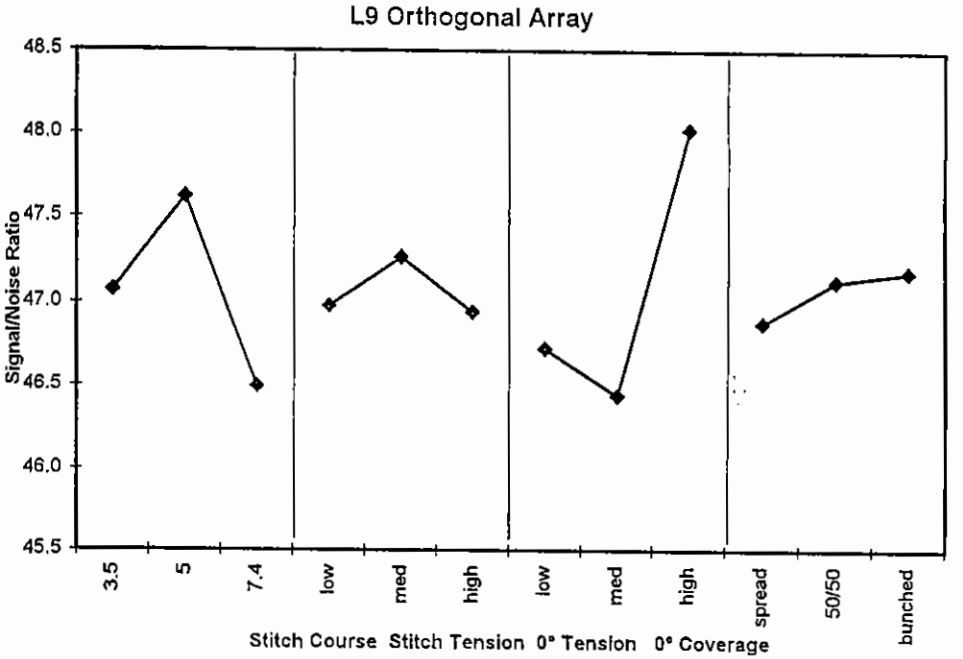

Mode I strain energy release rate (5% offset) - CTLX816/Fiberdux914

Fabric	sample numbers DCB01	DCB02	DCB03	Mean	CV(%)	S/N
T1	257.2	295.0	243.5	265.2	10.1	48.4
T2	230.8	274.6	280.6	262.0	10.4	48.3
T3	296.6	337.3	327.3	320.4	6.6	50.1
T4	254.2	253.1	345.9	284.4	18.7	48.8
T5	293.3	283.1	349.3	308.5	11.6	49.7
T6	244.9	250.9	322.1	272.6	15.8	48.5
T7	278.1	268.4	260.4	269.0	3.3	48.6
T8	245.2	235.4	319.0	266.5	17.1	48.3
T9	280.1	217.0	237.7	244.9	13.1	47.6

S/N = -10log10(mean S1/Glc(5% offset)²)

		Mean	S/N	
Stitch course	3.5	260.132	48.2	
	5	262.538	48.9	
	7.4	288.518	49.0	*
Stitch tension	low	272.863	48.6	
	med	279.028	48.7	
	high	279.297	48.7	*
0° tension	low	268.109	48.4	
	med	263.785	48.2	
	high	299.294	49.4	*
0° coverage	spread	272.896	48.6	
	50/50	267.858	48.5	
	bunched	290.434	49.1	*

* denotes best settings

	from mean	from S/N	
Estimate at best settings	326.4	322.4	J/m²

From ANOVA relative effect of factors is given by sum of squared deviation from mean

	sum of squared deviations	
Stitch course	1.2498	
Stitch tension	0.0439	least effect
0° tension	2.5819	most effect
0° coverage	0.614	2nd least

re-predict more conservative optimum value
Ignoring the two factors with smallest effects

Estimate at best settings	304.1	J/m²
Stitch course	7.4	
Stitch tension	-	
0° tension	high	
0° coverage	-	

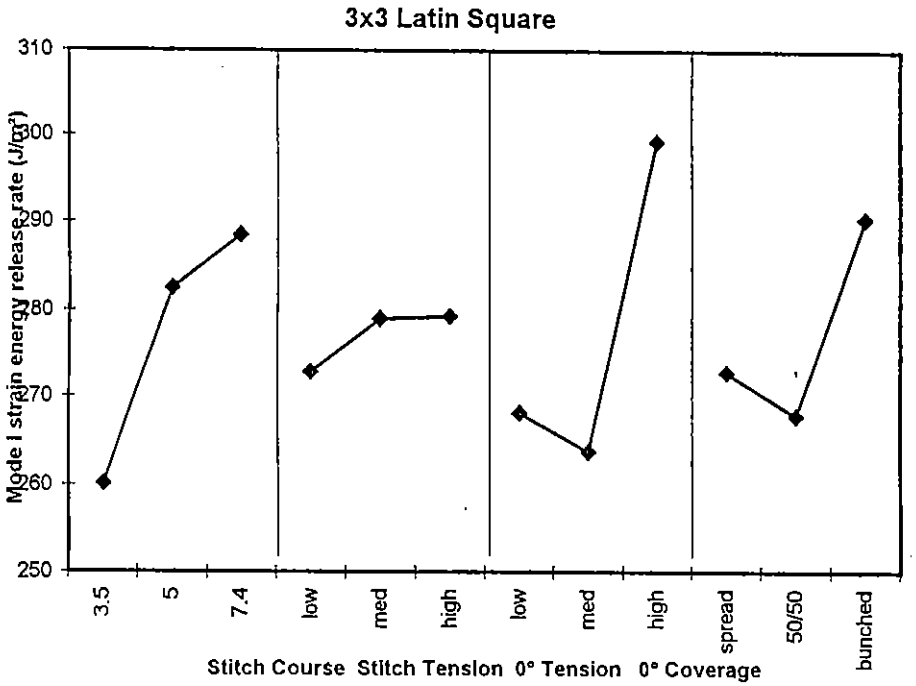

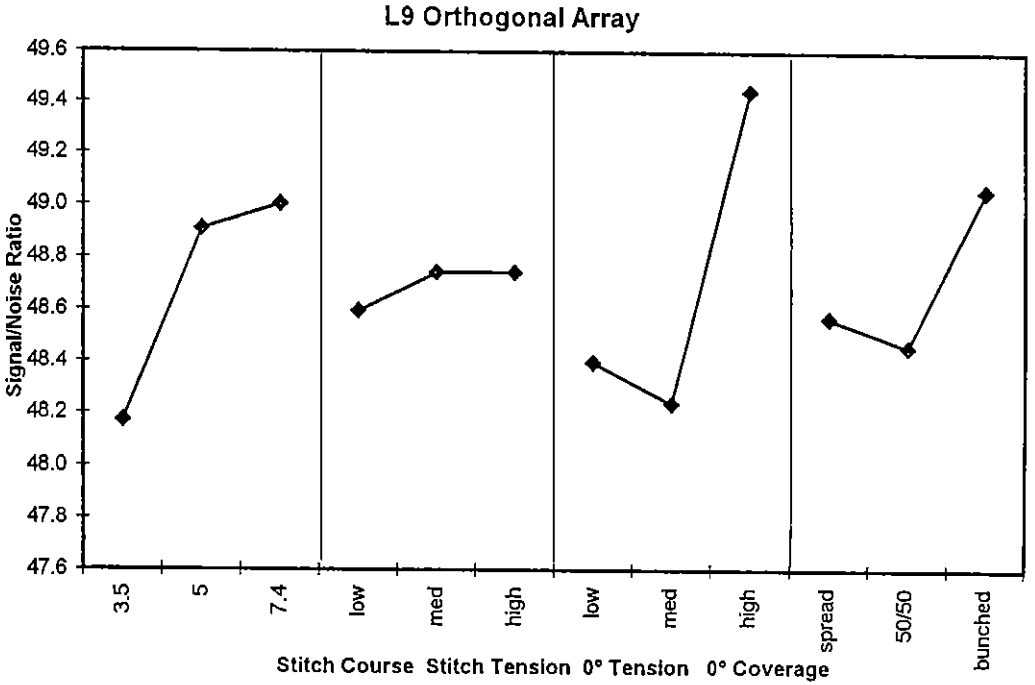

Mode I strain energy release rate (10mm propagation average) - CTLX816/Fiberdux914

Fabric	sample numbers DCB01	DCB02	DCB03	Mean	CV(%)	S/N
T1	283.9	258.0	360.8	300.9	17.76	49.3
T2	286.3	292.4	287.7	288.8	1.11	49.2
T3	389.1	329.9	363.9	361.0	8.24	51.1
T4	435.1	386.0	452.0	424.4	8.08	52.5
T5	322.0	327.8	325.5	325.1	0.91	50.2
T6	368.5	296.0	377.2	347.2	12.83	50.7
T7	283.6	257.8	240.8	260.8	8.27	48.3
T8	321.1	297.3	335.0	317.8	6.00	50.0
T9	281.0	257.8	226.7	255.2	10.68	48.0

S/N = -10log10(mean S1/GI(propagation average)²)

		Mean	S/N	
Stitch course	3.5	277.924	48.771	
	5	316.884	49.872	
	7.4	365.562	51.13	*
Stitch tension	low	328.672	50.026	*
	med	310.565	49.82	
	high	321.134	49.926	
0° tension	low	321.972	49.994	*
	med	322.782	49.914	*
	high	315.616	49.865	
0° coverage	spread	293.735	49.197	
	50/50	298.927	49.377	
	bunched	367.708	51.198	*

* denotes best settings

	from mean	from S/N	
Estimate at best settings	424.4	425.4	J/m²

From ANOVA relative effect of factors is given by sum of squared deviation from mean

	sum of squared deviations	
Stitch course	8.3547	most effect
Stitch tension	0.0635	2nd least
0° tension	0.0253	least effect
0° coverage	7.3538	

re-predict more conservative optimum value ignoring the two factors with smallest effects

Estimate at best settings	417.0	J/m²
Stitch course	7.4	
Stitch tension	-	
0° tension	-	
0° coverage	bunched	

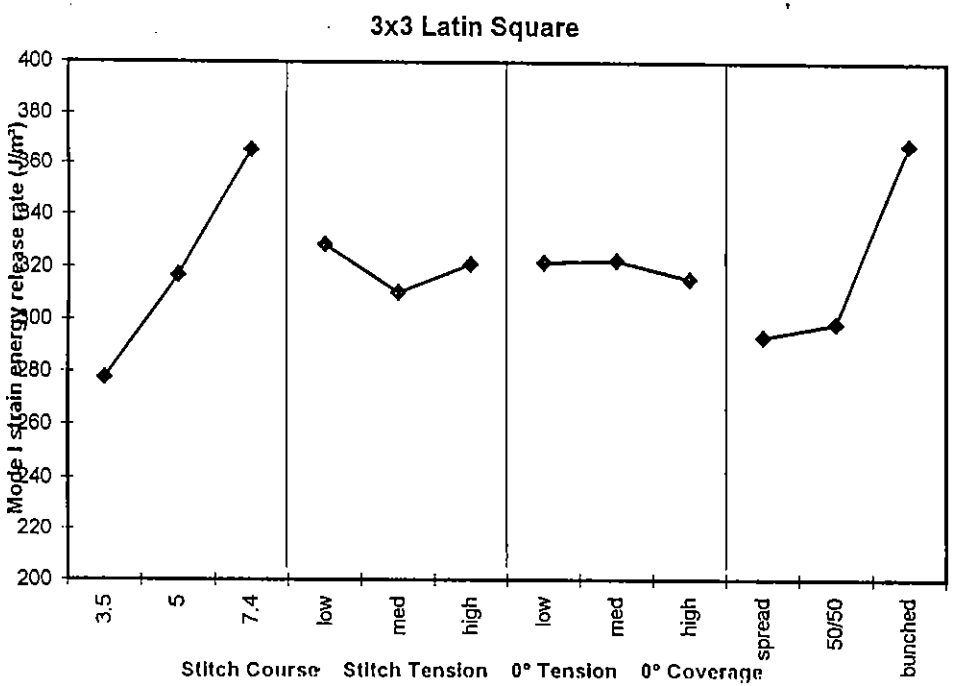

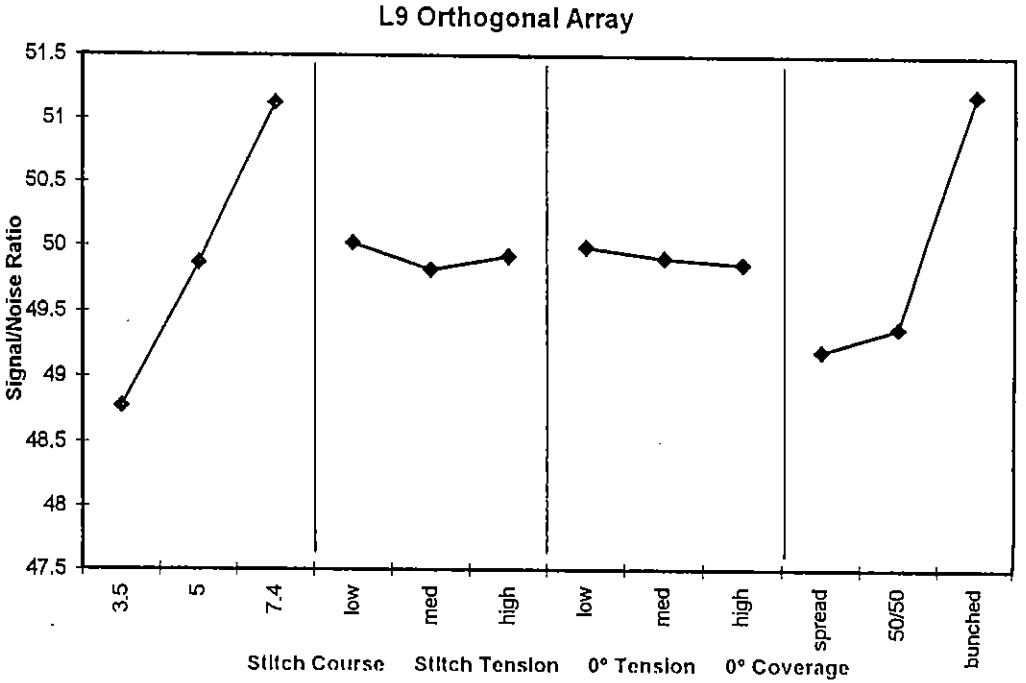

Mode I strain energy release rate (Propagation Maximum) - CTLX816/Fiberdux914

	sample numbers					
Fabric	DCB01	DCB02	DCB03	Mean	CV(%)	S/N
T1	348.8	344.2	473.9	388.9	18.92	51.5252
T2	376.7	349.3	399.4	375.1	6.68	51.4439
T3	565.1	436.2	424.2	475.2	16.43	53.3277
T4	567.7	549.5	623.4	580.2	6.63	55.2348
T5	514.1	621.5	449.0	528.2	16.49	54.2278
T6	452.3	410.4	460.1	440.9	6.07	52.8539
T7	330.6	335.2	344.6	336.8	2.12	50.5445
T8	486.1	395.5	426.3	436.0	10.56	52.6956
T9	582.7	464.7	432.9	493.4	16.00	53.6613

S/N = -10log10(mean S1/GI(prop.max.)²)

		Mean	S/N	
Stitch course	3.5	422.083	52.3	
	5	413.08	52.099	
	7.4	516.442	54.106	*
Stitch tension	low	435.33	52.435	
	med	446.423	52.789	
	high	469.851	53.281	*
0° tension	low	421.948	52.358	
	med	482.92	53.447	*
	high	446.736	52.7	
0° coverage	spread	470.195	53.138	
	50/50	384.29	51.614	
	bunched	497.119	53.753	*

* denotes best settings

	from mean	from S/N	
Estimate at best settings	614.7	636.9	J/m²

From ANOVA relative effect of factors is given by sum of squared deviation from mean

	sum of squared deviations	
Stitch course	7.3252	
Stitch tension	1.0833	least effect
0° tension	1.859	most effect
0° coverage	7.2739	2nd least

re-predict more conservative optimum value ignoring the two factors with smallest effects

Estimate at best settings	563.8	J/m²
Stitch course	7.4	
Stitch tension	-	
0° tension	-	
0° coverage	bunched	

3x3 Latin Square

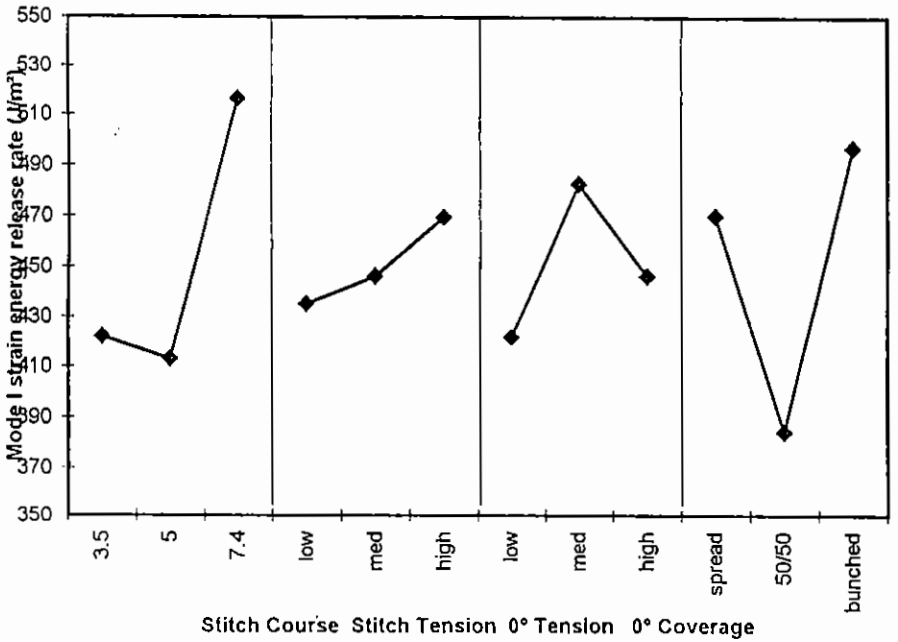

L9 Orthogonal Array

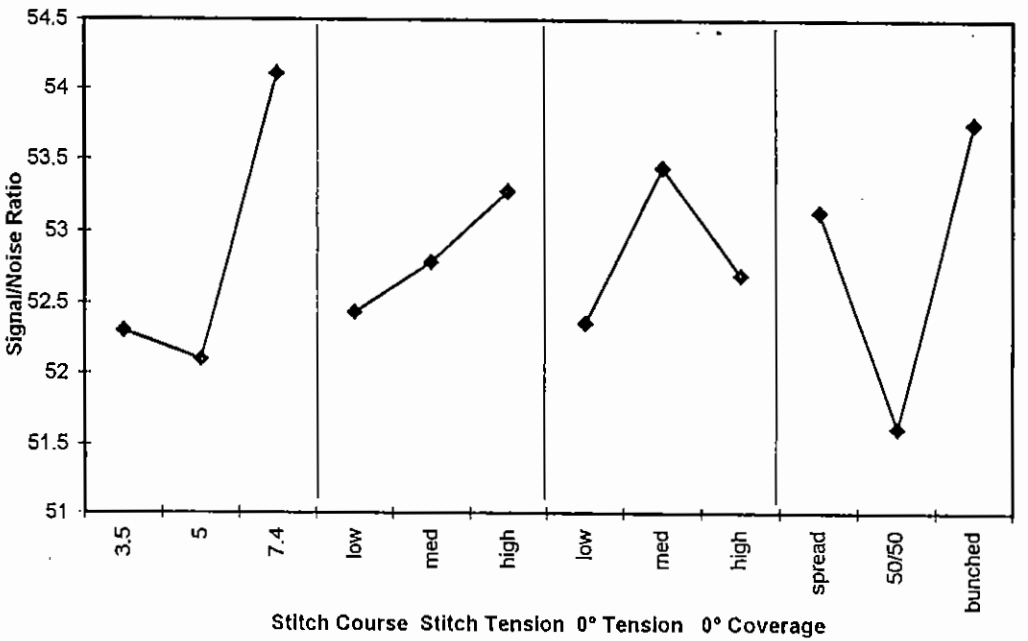

0° Tow Crimp Standard Deviation - CTLX816/Fibredux914

Fabric	sample numbers T01	T02	T03	T04	T05	T06	T07	T08	Mean	CV(%)	S/N
T1	2.29	2.86	1.87	2.09	2.21	2.27	1.71	3.00	2.29	19.46	-7.33
T2	2.23	3.97	1.39	2.74	1.62	2.81	2.71	2.93	2.55	31.89	-8.50
T3	1.82	1.96	1.73	1.87	1.71	1.89	1.95	3.23	2.00	25.60	-6.24
T4	1.71	1.80	1.94	1.31	1.75	1.19	1.52	1.48	1.56	15.62	-3.97
T5	2.38	2.19	2.09	2.53	2.25	1.39	2.62	1.53	2.12	20.94	-6.70
T6	2.11	3.50	2.34	2.33	1.62	3.27	1.63	4.12	2.61	34.98	-8.79
T7	3.33	1.92	1.97	2.29	1.80	1.38	3.00	1.97	2.21	29.36	-7.19
T8	2.61	2.58	2.30	3.09	2.52	3.41	3.01	3.05	2.82	13.19	-9.07
T9	3.23	3.29	3.18	2.42	1.91	3.14	1.69	2.97	2.73	23.43	-8.92

S/N = -10log10(0° Crimp SD²)

		Mean	S/N	
Stitch course	3.5	2.28	-7.36	
	5	2.10	-6.48	*
	7.4	2.58	-8.39	
Stitch tension	low	2.02	-6.16	*
	med	2.50	-8.09	
	high	2.45	-7.98	
0° tension	low	2.57	-8.39	
	med	2.28	-7.13	
	high	2.11	-6.71	*
0° coverage	spread	2.38	-7.65	
	50/50	2.48	-8.16	
	bunched	2.13	-8.43	*

* denotes best settings

	from mean	from S/N	
Estimate at best settings	1.4	1.5	*

From ANOVA relative effect of factors is given by sum of squared deviation from mean

	sum of squared deviations	
Stitch course	5.48	
Stitch tension	7.04	most effect
0° tension	4.60	least effect
0° coverage	4.78	2nd least

re-predict more conservative optimum value
Ignoring the two factors with smallest effects

Estimate at best settings	1.8	*
Stitch course	5	
Stitch tension	low	
0° tension	-	
0° coverage	-	

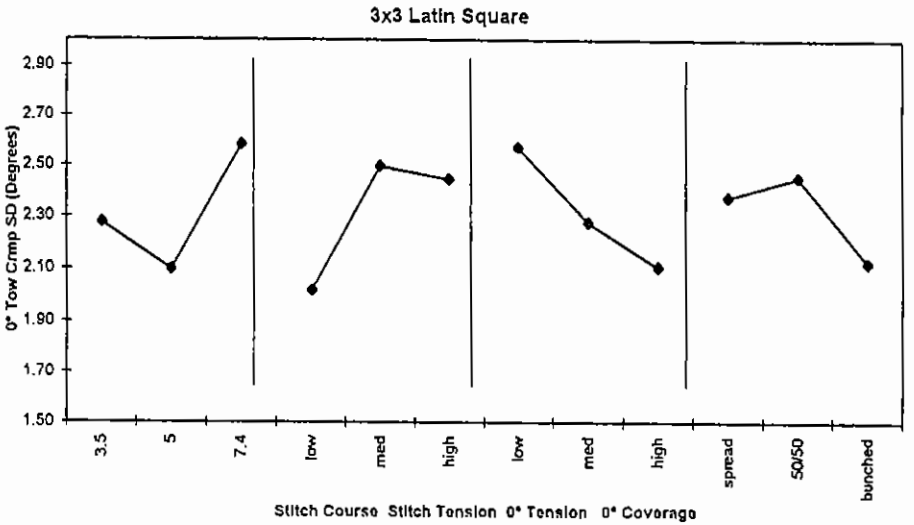

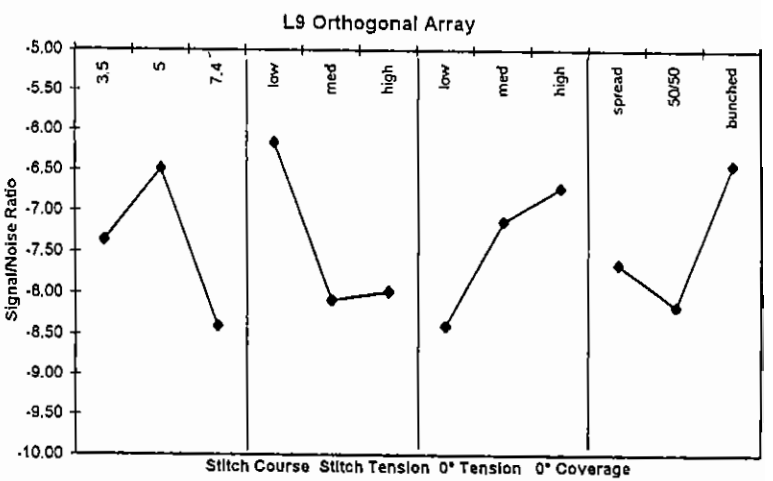

0° Tow Crimp Range - CTLX816/Fibredux914

	sample numbers										
Fabric	T01	T02	T03	T04	T05	T06	T07	T08	Mean	CV(%)	S/N
T1	12.39	21.95	11.02	10.78	12.91	11.85	10.29	21.62	14.10	34.18	-23.41
T2	16.22	29.91	7.34	23.72	12.16	14.16	21.13	19.31	18.00	39.40	-25.66
T3	9.16	12.79	7.51	8.94	11.51	11.21	15.45	24.80	12.67	43.36	-22.72
T4	10.01	7.95	11.92	7.32	11.70	5.93	8.52	8.53	8.98	23.28	-19.27
T5	16.12	14.04	14.83	18.63	13.97	8.20	16.31	10.32	14.05	23.93	-23.17
T6	11.08	20.10	13.03	17.41	10.18	22.29	8.51	32.34	16.87	47.12	-25.31
T7	26.42	10.03	14.18	18.62	10.86	8.78	20.76	10.58	15.03	41.89	-24.16
T8	21.35	15.75	17.99	23.67	16.41	19.39	22.58	19.36	19.56	14.48	-25.91
T9	25.20	18.20	25.28	16.75	9.90	22.59	9.54	17.16	18.08	34.07	-25.562

$S/N = -10\log_{10}(0° \text{ Crimp range}^2)$

		Mean	S/N	
Stitch course	3.5	17.56	-25.21	
	5	14.92	-23.93	
	7.4	13.30	-22.58	*
Stitch tension	low	12.70	-22.28	*
	med	17.20	-24.91	
	high	15.87	-24.53	
0° tension	low	16.84	-24.88	
	med	15.02	-23.50	
	high	13.92	-23.35	*
0° coverage	spread	15.41	-24.05	
	50/50	16.63	-25.04	
	bunched	13.74	-22.63	*

* denotes best settings

	from mean	from S/N	
Estimate at best settings	7.9	9.0	*

From ANOVA relative effect of factors is given by sum of squared deviation from mean

	sum of squared deviations	
Stitch course	10.35	
Stitch tension	12.14	most effect
0° tension	4.26	least effect
0° coverage	8.81	2nd least

re-predict more conservative optimum value ignoring the two factors with smallest effects

Estimate at best settings	11.2 *
Stitch course	7.4
Stitch tension	low
0° tension	-
0° coverage	-

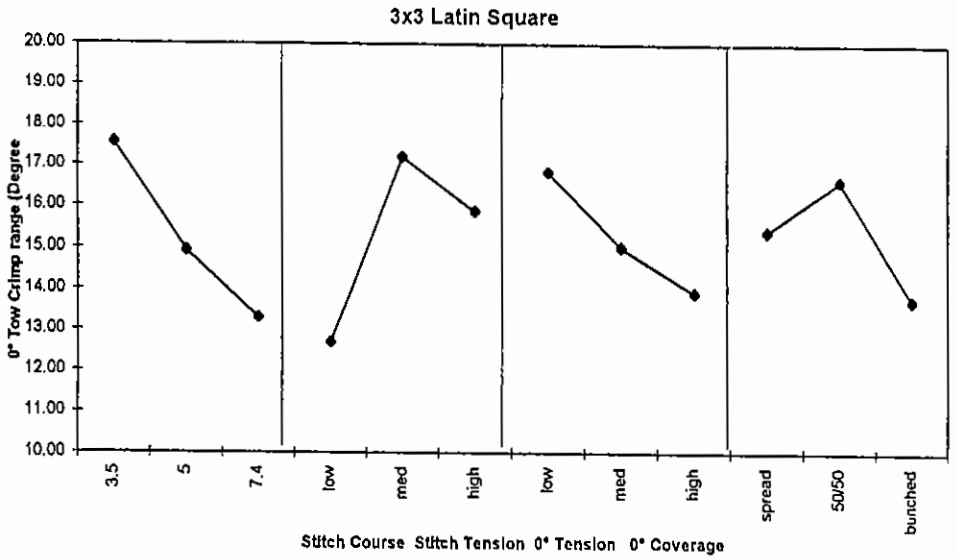

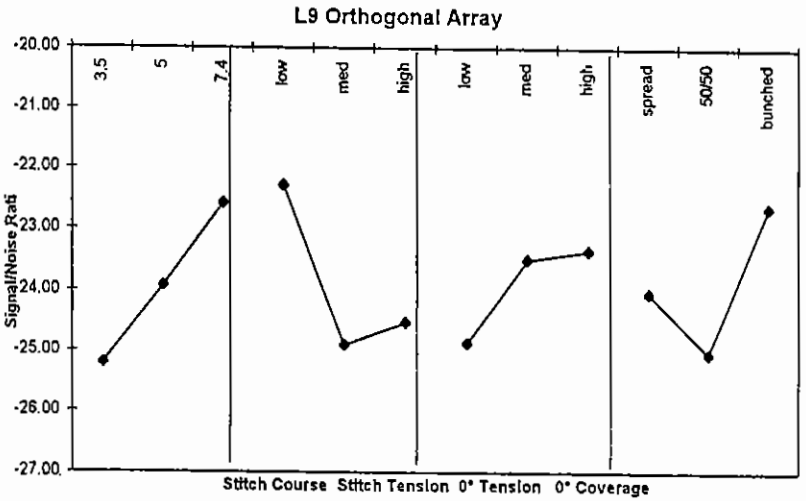

FREE RESIN VOLUME (CTLX816 Fibredux 914)

Fabric	sample numbers R01	R02	R03	R04	Mean	CV(%)	S/N
T1	11.5	11.0	10.8	12.4	11.4	6.1	-21.2
T2	12.2	13.8	13.4	14.5	13.5	7.2	-22.6
T3	15.0	14.5	15.3	14.7	14.9	2.1	-23.4
T4	17.4	15.7	19.4	20.3	18.2	11.4	-25.3
T5	15.8	16.9	13.4	14.7	15.2	10.0	-23.7
T6	17.7	19.0	19.6	21.9	19.5	9.0	-25.8
T7	10.1	9.2	10.6	9.5	9.8	6.6	-19.9
T8	16.7	16.8	13.4	15.3	15.5	10.2	-23.9
T9	13.4	13.8	15.1	12.9	13.8	6.8	-22.8

S/N = -10log10(Free resin volume²)

		Mean	S/N	
Stitch course	3.5	13.04417	-22.2	
	5	13.24583	-22.4	
	7.4	17.64833	-24.9	*
Stitch tension	low	13.15417	-22.1	*
	med	14.7275	-23.4	
	high	16.05667	-24.0	
0° tension	low	15.48917	-23.6	
	med	15.45583	-23.6	
	high	13.29333	-22.3	*
0° coverage	spread	13.45667	-22.5	
	50/50	14.28417	-22.8	*
	bunched	16.1975	-24.2	

* denotes best settings

	from mean	from S/N	
Estimate at best settings	9.0	9.6	%

From ANOVA relative effect of factors is given by sum of squared deviation from mean

	sum of squared deviations	
Stitch course	6.989	most effect
Stitch tension	2.9029	
0° tension	1.5919	least effect
0° coverage	2.3653	2nd least

re-predict more conservative optimum value ignoring the two factors with smallest effects

Estimate at best settings	11.4	%
Stitch course	3.5	
Stitch tension	low	
0° tension	-	
0° coverage	-	

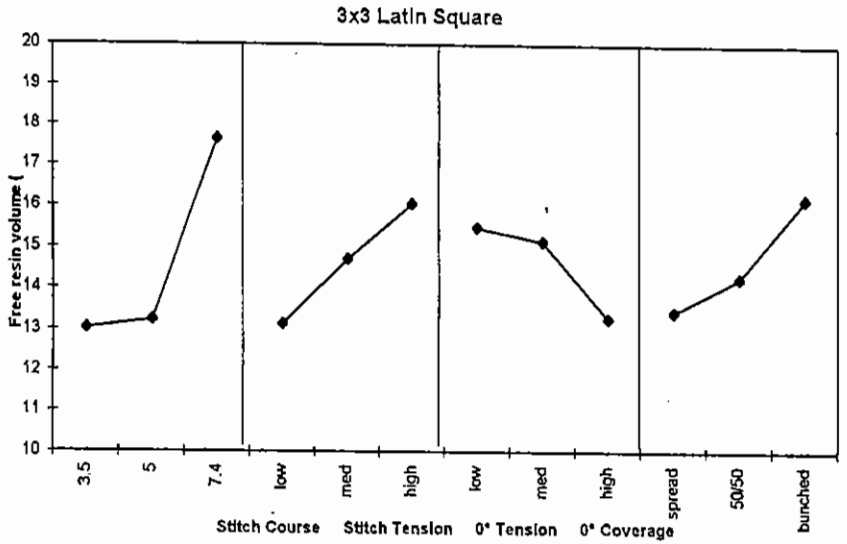

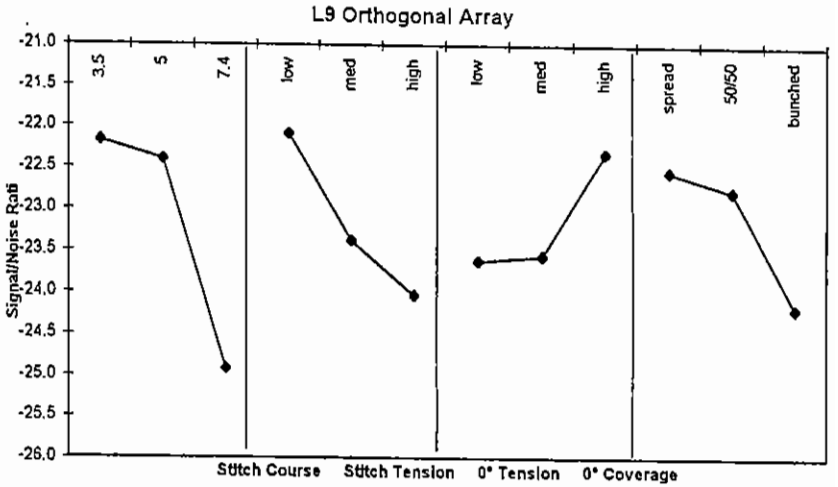

MEAN RESIN AREA SIZE (CTLX816 Fibredux 914)

Fabric	sample numbers R01	R02	R03	R04	Mean	CV(%)	S/N
T1	79127	71869	68947	89431	77344	11.8	-97.8
T2	68759	61520	60583	64934	63949	5.8	-96.1
T3	116108	119641	149441	142261	131863	12.5	-102.5
T4	103427	89368	111206	101346	101337	8.9	-100.1
T5	65055	82242	63228	77526	72013	12.9	-97.2
T6	61205	65929	62599	70065	64950	6.1	-96.3
T7	50081	60660	62206	68147	60274	12.5	-95.7
T8	135002	163239	166305	153884	154608	9.1	-103.8
T9	139663	119038	124373	82136	116303	21.0	-101.5

$S/N = -10\log_{10}(\text{mean resin area}^2)$

		Mean	S/N	
Stitch course	3.5	110395	-100.3	
	5	91052	-98.8	
	7.4	79433	-97.9	*
Stitch tension	low	79651	-97.9	*
	med	96856	-99.0	
	high	104372	-100.1	
0° tension	low	98967	-99.3	
	med	93863	-99.2	
	high	88050	-98.4	*
0° coverage	spread	88553	-98.8	
	50/50	63057	-96.0	*
	bunched	129269	-102.1	

* denotes best settings

	from mean	from S/N	
Estimate at best settings	29312	45794	µm²

From ANOVA relative effect of factors is given by sum of squared deviation from mean

	sum of squared deviations	
Stitch course	9.074	
Stitch tension	7.19	2nd least
0° tension	1.39	least effect
0° coverage	56.32	most effect

re-predict more conservative optimum value ignoring the two factors with smallest effects

Estimate at best settings	55544	µm²
Stitch course	7.4	
Stitch tension	-	
0° tension	-	
0° coverage	50/50	

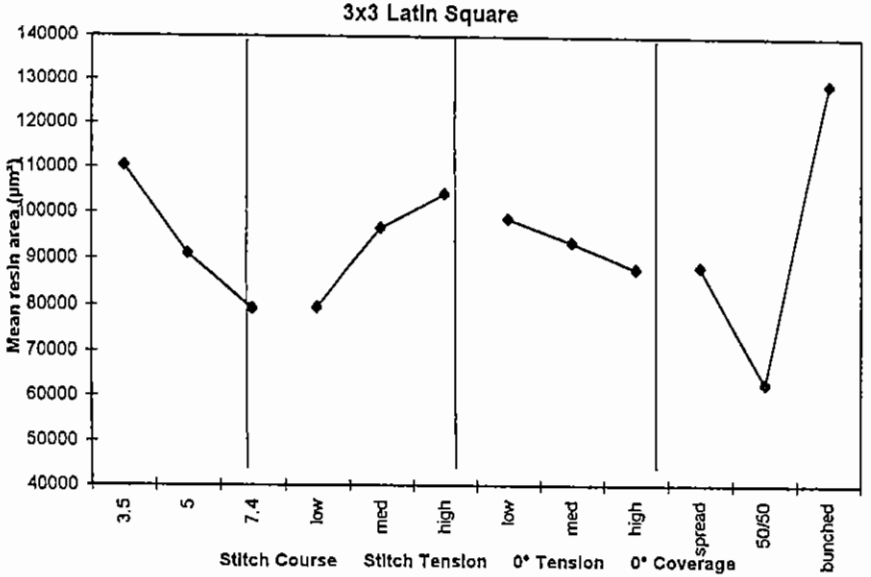

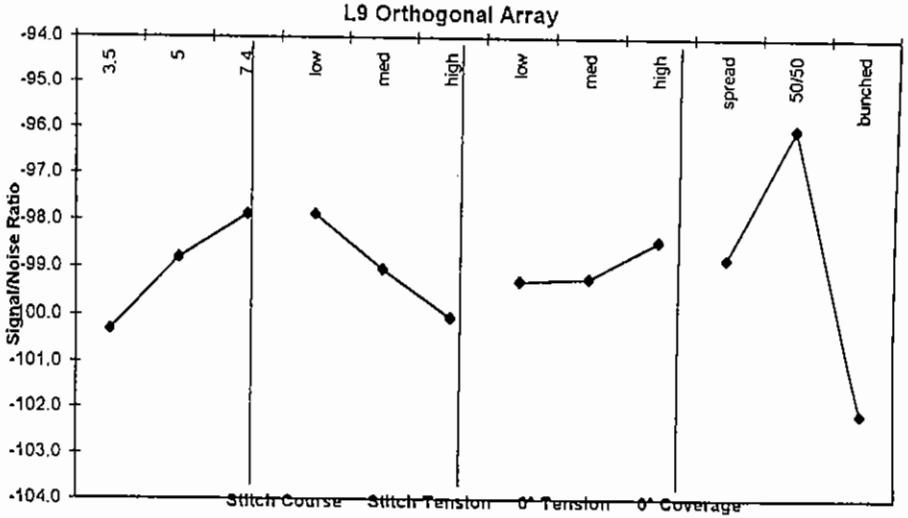

MAXIMUM RESIN AREA SIZE (CTLX816 Fibredux 914)

	sample numbers							
Fabric	R01	R02	R03	R04	Mean	CV(%)	S/N
T1	392046	440713	370490	809692	503235	41	-114.6
T2	478446	371290	344357	314446	377135	19	-111.6
T3	767503	687850	739447	672294	716774	6	-117.1
T4	1198894	467224	699933	956740	830698	38	-118.8
T5	526669	632989	450974	586391	549256	14	-114.9
T6	531738	573891	435071	618544	539811	15	-114.7
T7	308801	253334	290801	440980	323479	25	-110.4
T8	869934	1148893	1168407	996254	1045872	13	-120.4
T9	689378	1012365	737225	628269	766809	22	-117.9

S/N = -10log$_{10}$(maximum resin area^2)

		Mean	S/N	
Stitch course	3.5	712053	-116.2	
	5	532381	-114.4	*
	7.4	639922	-116.1	
Stitch tension	low	552471	-114.6	*
	med	657421	-115.7	
	high	674465	-116.6	
0° tension	low	696306	-116.6	
	med	658214	-116.1	
	high	529836	-114.1	*
0° coverage	spread	606433	-115.8	
	50/50	413475	-112.3	*
	bunched	864448	-118.8	

* denotes best settings

	from mean	from S/N	
Estimate at best settings	143807	269341	µm^2

From ANOVA relative effect of factors is given by sum of squared deviation from mean

	sum of squared deviations	
Stitch course	6.112	2nd least
Stitch tension	5.801	least effect
0° tension	10.12	
0° coverage	64.44	most effect

re-predict more conservative optimum value ignoring the two factors with smallest effects

Estimate at best settings	345811	µm^2
Stitch course	7.4	
Stitch tension	-	
0° tension	-	
0° coverage	50/50	

3x3 Latin Square

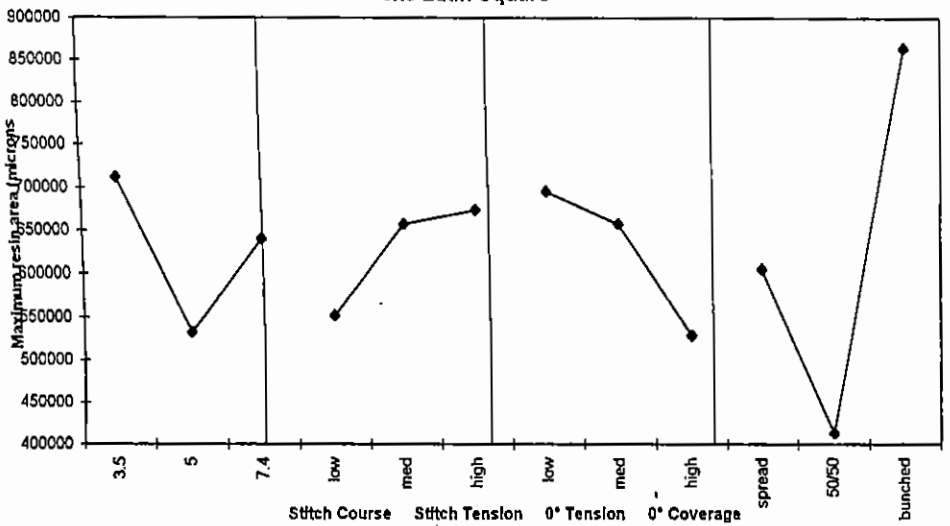

L9 Orthogonal Array

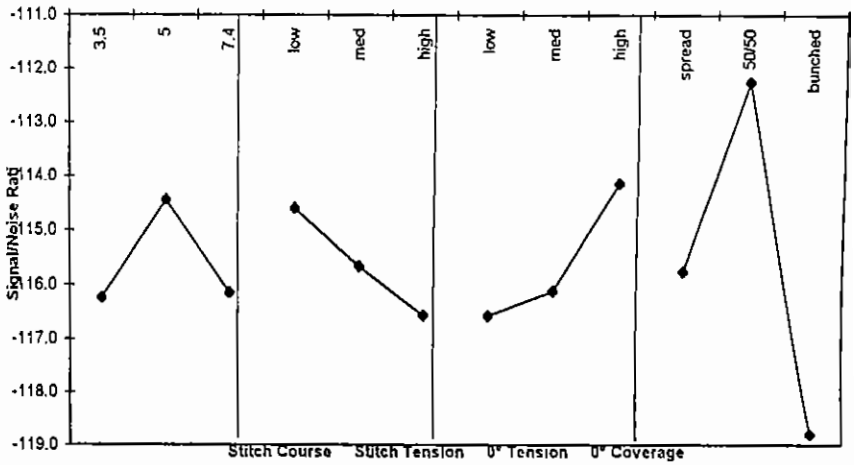

MEAN RESIN LAYER THICKNESS (CTLX816 Fibredux 914)

Fabric	sample numbers R01	R02	R03	R04	Mean	CV(%)	S/N
T1	42.9	43.6	44.4	46.2	44.3	3.2	-32.9
T2	49.7	50.7	52.0	51.6	51.0	2.0	-34.1
T3	53.5	53.9	52.5	52.0	52.9	1.7	-34.5
T4	56.8	58.1	56.8	59.1	57.2	2.3	-35.1
T5	59.3	61.2	56.1	55.7	58.1	4.5	-35.3
T6	57.4	54.0	59.8	54.1	56.3	5.0	-35.0
T7	52.2	50.5	49.4	52.5	51.2	2.9	-34.2
T8	54.5	53.3	49.1	48.6	51.4	5.8	-34.2
T9	48.5	50.1	52.2	49.3	50.0	3.1	-34.0

S/N = -10log10(mean resin layer thickness^2)

		Mean	S/N	
Stitch course	3.5	50.8442	-34.13	
	5	49.3983	-33.851	*
	7.4	57.1942	-35.152	
Stitch tension	low	50.8717	-34.085	*
	med	53.4742	-34.554	
	high	53.0908	-34.494	
0° tension	low	50.6575	-34.058	*
	med	52.7275	-34.427	
	high	54.0517	-34.647	
0° coverage	spread	50.7792	-34.065	*
	50/50	52.8192	-34.451	
	bunched	53.8383	-34.617	

* denotes best settings

	from mean	from S/N	
Estimate at best settings	44.3	44.3	µm

From ANOVA relative effect of factors is given by sum of squared deviation from mean

	sum of squared deviations	
Stitch course	2.8156	most effect
Stitch tension	0.3912	least effect
0° tension	0.5318	
0° coverage	0.4825	2nd least

re-predict more conservative optimum value ignoring the two factors with smallest effects

Estimate at best settings	47.5	µm
Stitch course	5	
Stitch tension	-	
0° tension	low	
0° coverage	-	

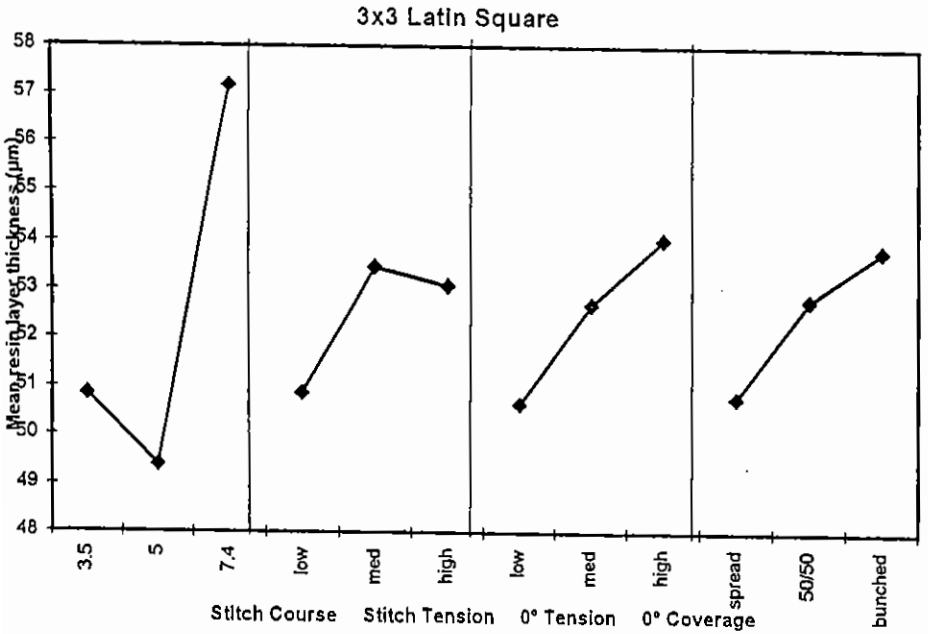

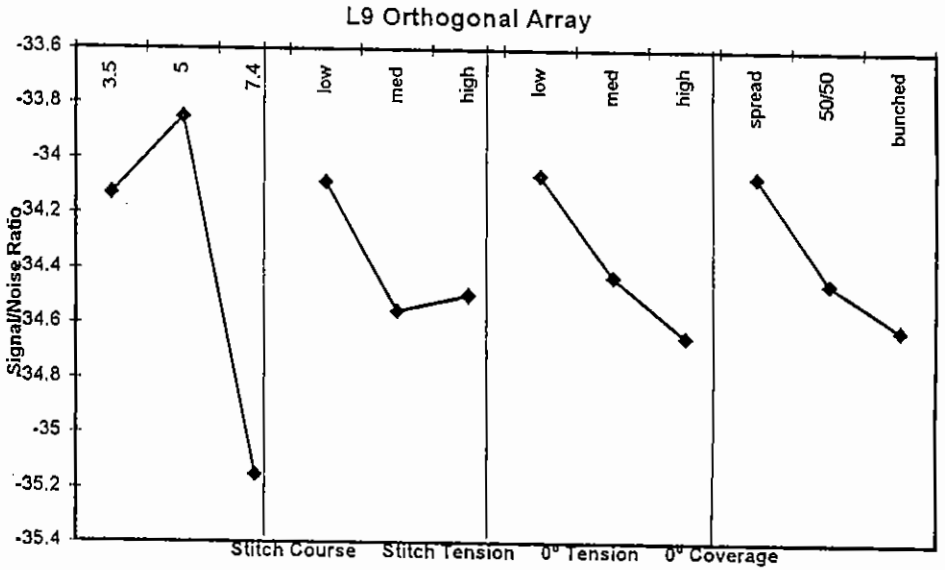

Laminate Quality Assurance C-scans

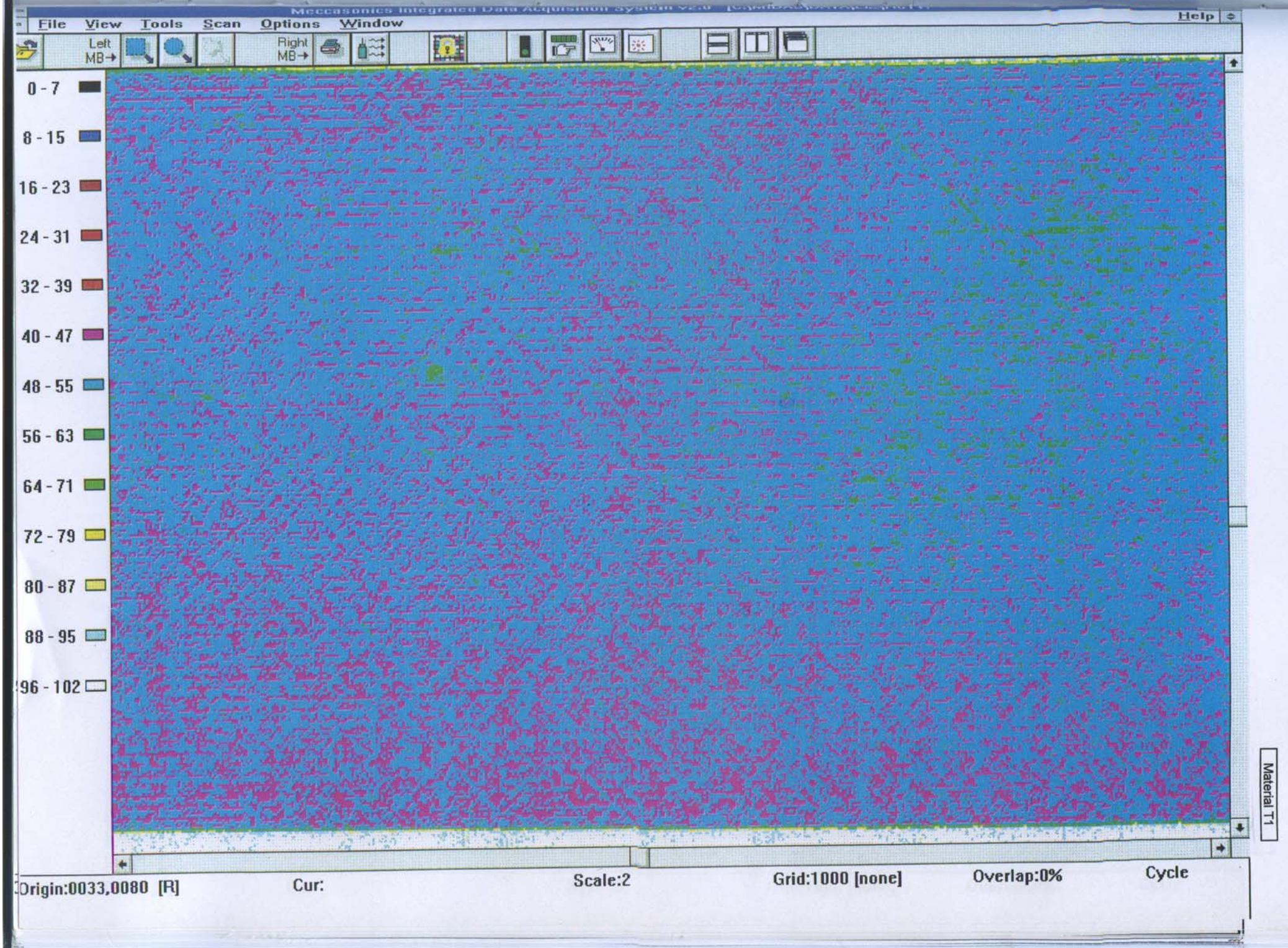
Meccasonics Integrated Data Acquisition System
File
View
Tools
Scan
Options
Window
Help
Left MB→
Right MB→
0 - 7
8 - 15
16 - 23
24 - 31
32 - 39
40 - 47
48 - 55
56 - 63
64 - 71
72 - 79
80 - 87
88 - 95
96 - 102
Material T1
Origin:0033,0080 [R]
Cur:
Scale:2
Grid:1000 [none]
Overlap:0%
Cycle

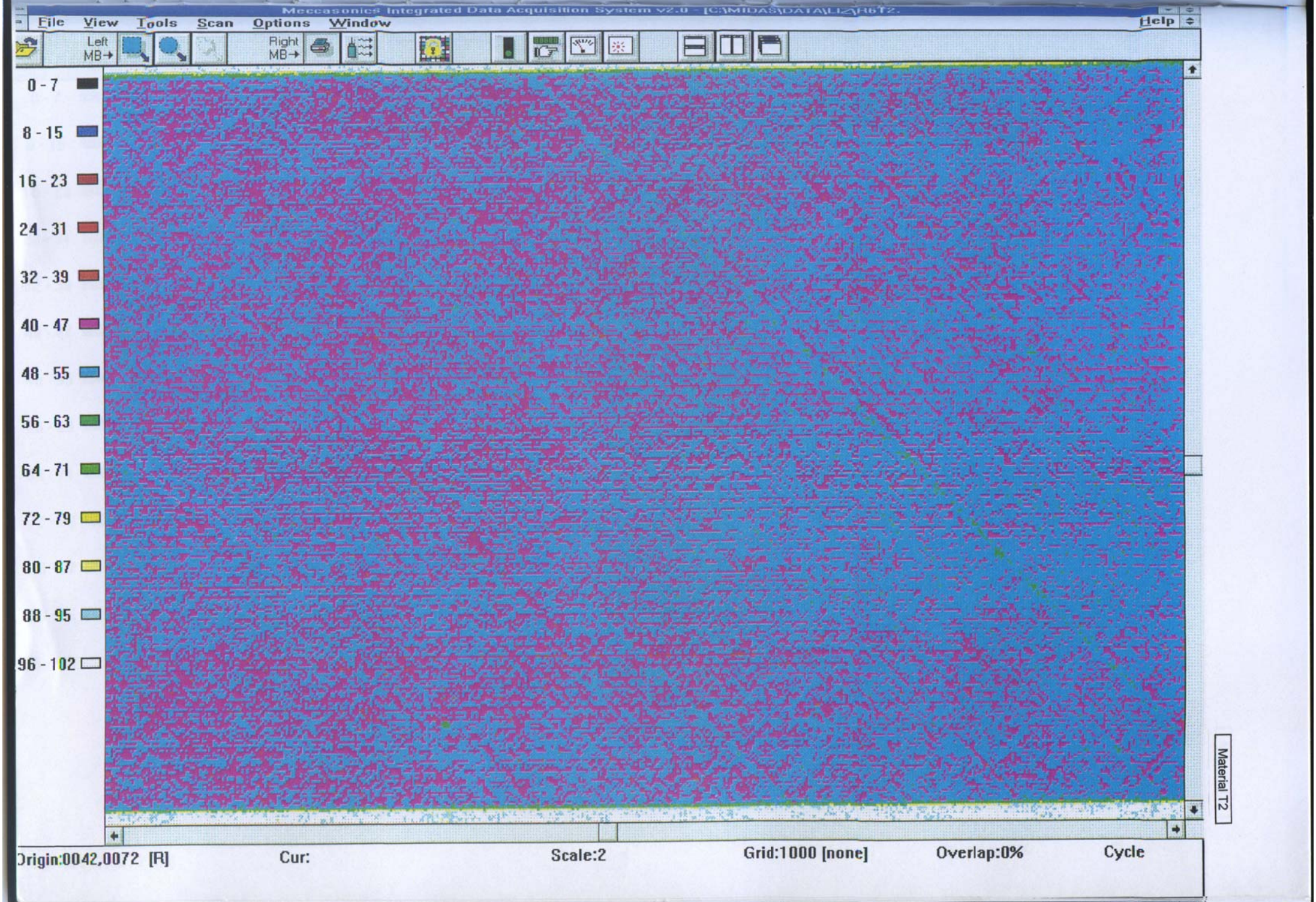
Meccasonics Integrated Data Acquisition System v2.0 - [C:\MIDAS\DATA\LI...R6T2.
File
View
Tools
Scan
Options
Window
Help
Left MB→
Right MB→
0 - 7
8 - 15
16 - 23
24 - 31
32 - 39
40 - 47
48 - 55
56 - 63
64 - 71
72 - 79
80 - 87
88 - 95
96 - 102
Material T2
Origin:0042,0072 [R]
Cur:
Scale:2
Grid:1000 [none]
Overlap:0%
Cycle

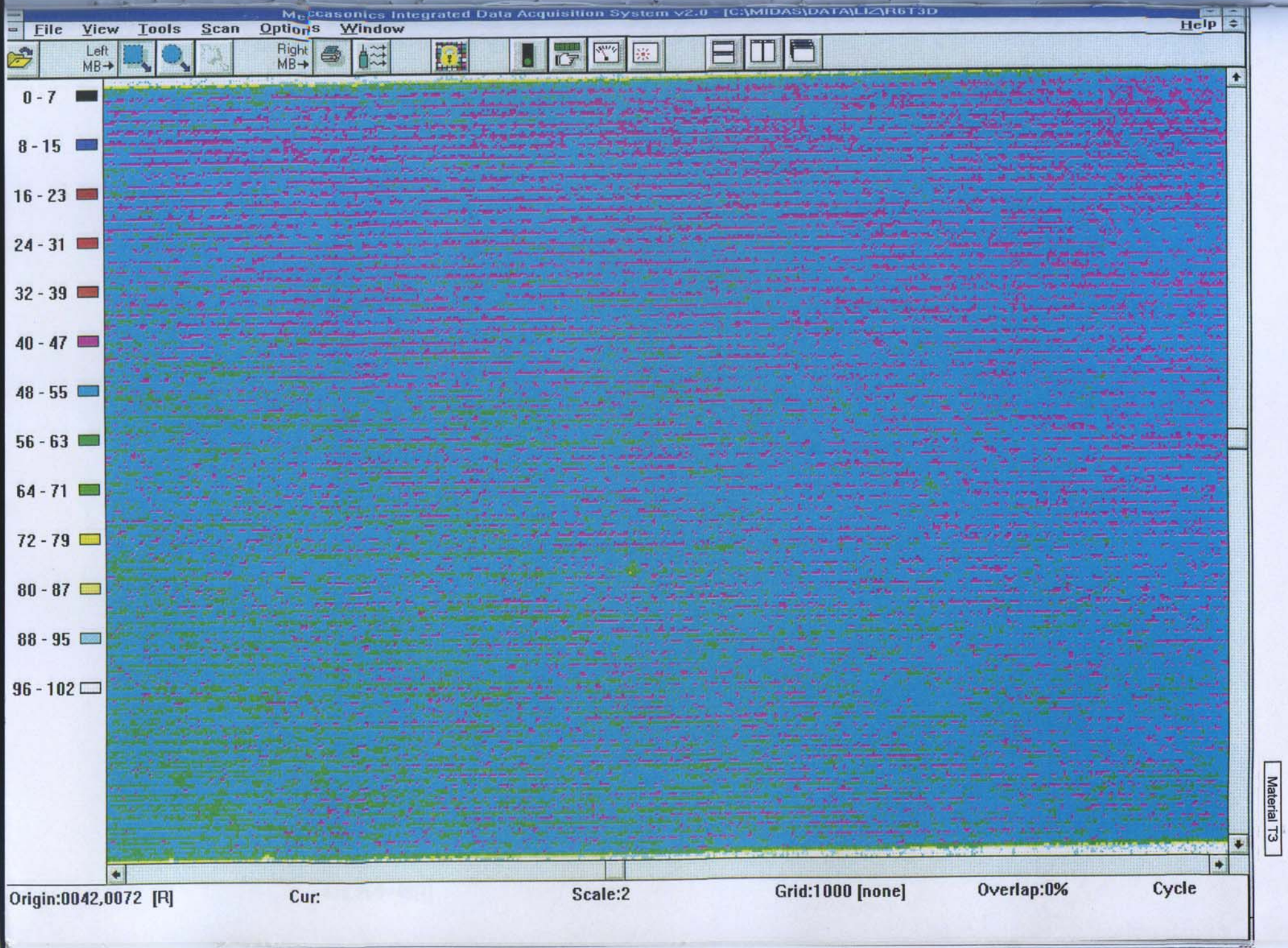
Mecasonics Integrated Data Acquisition System v2.0 - [C:\MIDAS\DATA\LIZ\R6T3D
File View Tools Scan Options Window Help
Left MB→
Right MB→
0 - 7
8 - 15
16 - 23
24 - 31
32 - 39
40 - 47
48 - 55
56 - 63
64 - 71
72 - 79
80 - 87
88 - 95
96 - 102
Origin:0042,0072 [R]
Cur:
Scale:2
Grid:1000 [none]
Overlap:0%
Cycle
Material T3

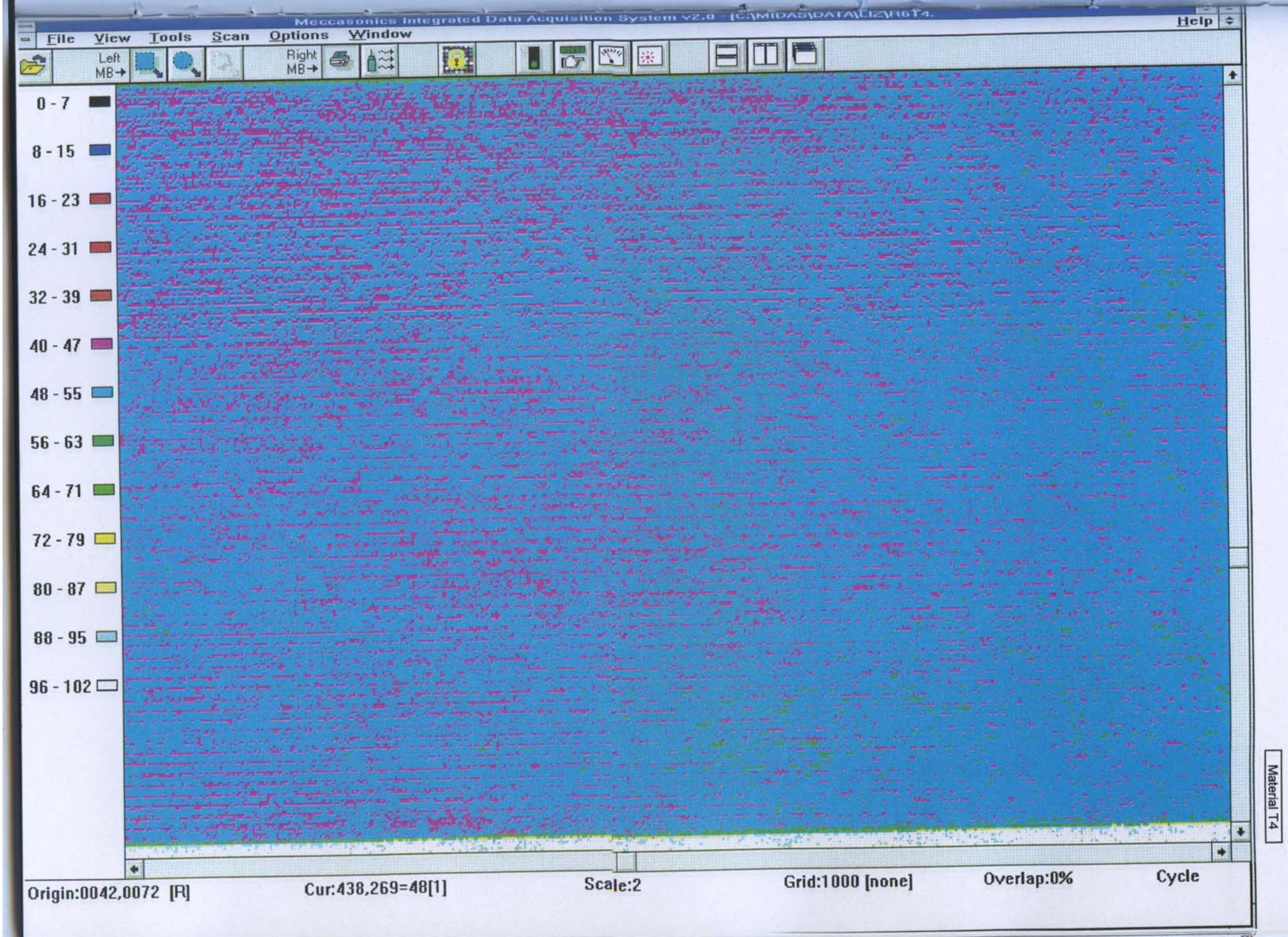
Meccasonics Integrated Data Acquisition System v2.0 - [C:\MIDAS\DATA\C1C\R6T4.
Help
File View Tools Scan Options Window
Left MB→
Right MB→
0 - 7
8 - 15
16 - 23
24 - 31
32 - 39
40 - 47
48 - 55
56 - 63
64 - 71
72 - 79
80 - 87
88 - 95
96 - 102
Material T4
Origin:0042,0072 [R]
Cur:438,269=48[1]
Scale:2
Grid:1000 [none]
Overlap:0%
Cycle

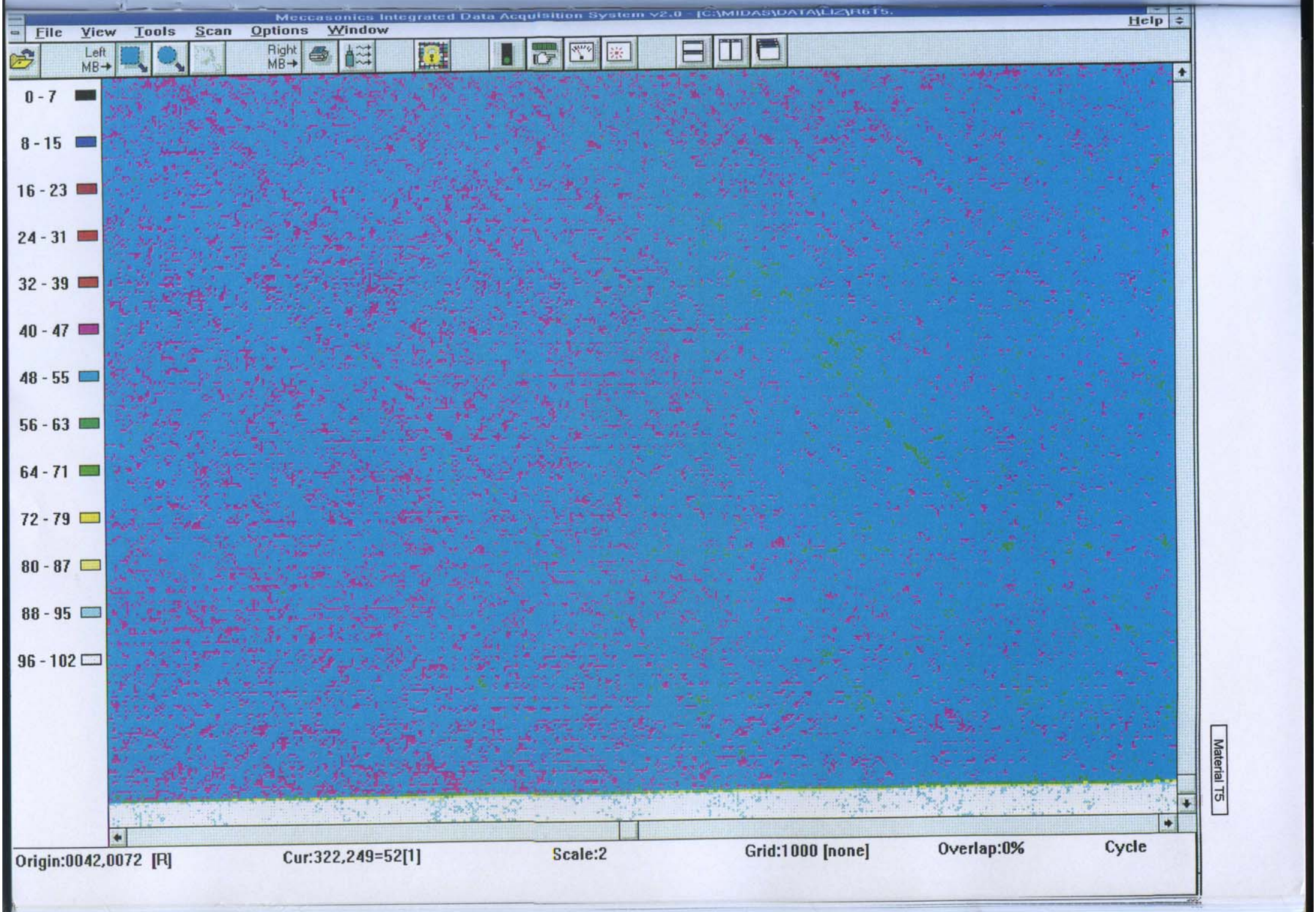
Meccasonics Integrated Data Acquisition System v2.0 - [C:\MIDAS\DATA\LIZ\R6T5.
File View Tools Scan Options Window
Help
Left MB→
Right MB→
0 - 7
8 - 15
16 - 23
24 - 31
32 - 39
40 - 47
48 - 55
56 - 63
64 - 71
72 - 79
80 - 87
88 - 95
96 - 102
Material T5
Origin:0042,0072 [R]
Cur:322,249=52[1]
Scale:2
Grid:1000 [none]
Overlap:0%
Cycle

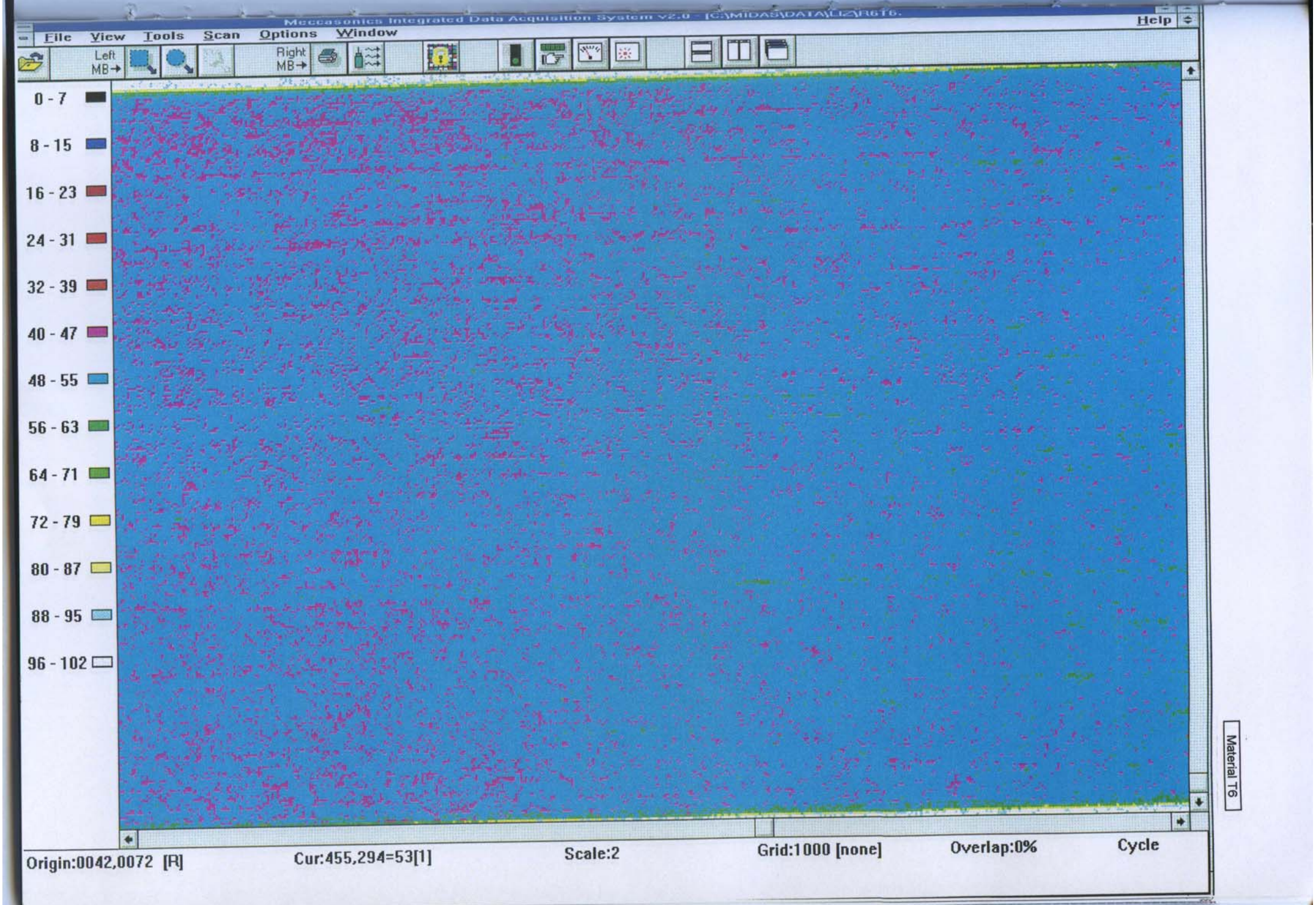
Meccasonics Integrated Data Acquisition System v2.0 - [C:\MIDAS\DATA\LI2\R6T6.
File View Tools Scan Options Window
Help
Left MB→
Right MB→
0 - 7
8 - 15
16 - 23
24 - 31
32 - 39
40 - 47
48 - 55
56 - 63
64 - 71
72 - 79
80 - 87
88 - 95
96 - 102
Material T6
Origin:0042,0072 [R]
Cur:455,294=53[1]
Scale:2
Grid:1000 [none]
Overlap:0%
Cycle

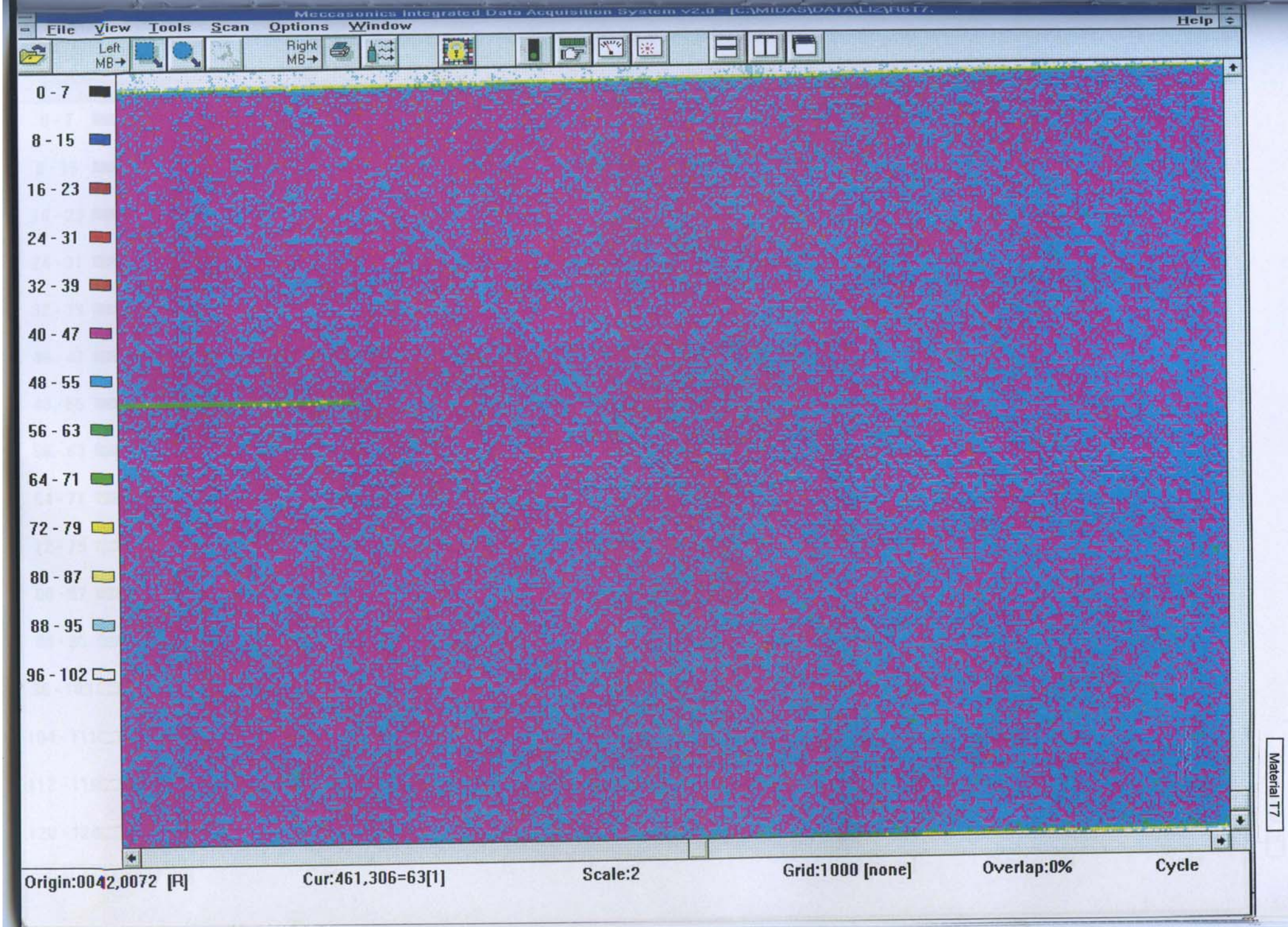
Meccasonics Integrated Data Acquisition System v2.0 - [C:\MIDAS\DATA\LI2\R6T7.
File
View
Tools
Scan
Options
Window
Help
Left MB→
Right MB→
0 - 7
8 - 15
16 - 23
24 - 31
32 - 39
40 - 47
48 - 55
56 - 63
64 - 71
72 - 79
80 - 87
88 - 95
96 - 102
Origin:0042,0072 [R]
Cur:461,306=63[1]
Scale:2
Grid:1000 [none]
Overlap:0%
Cycle
Material T7

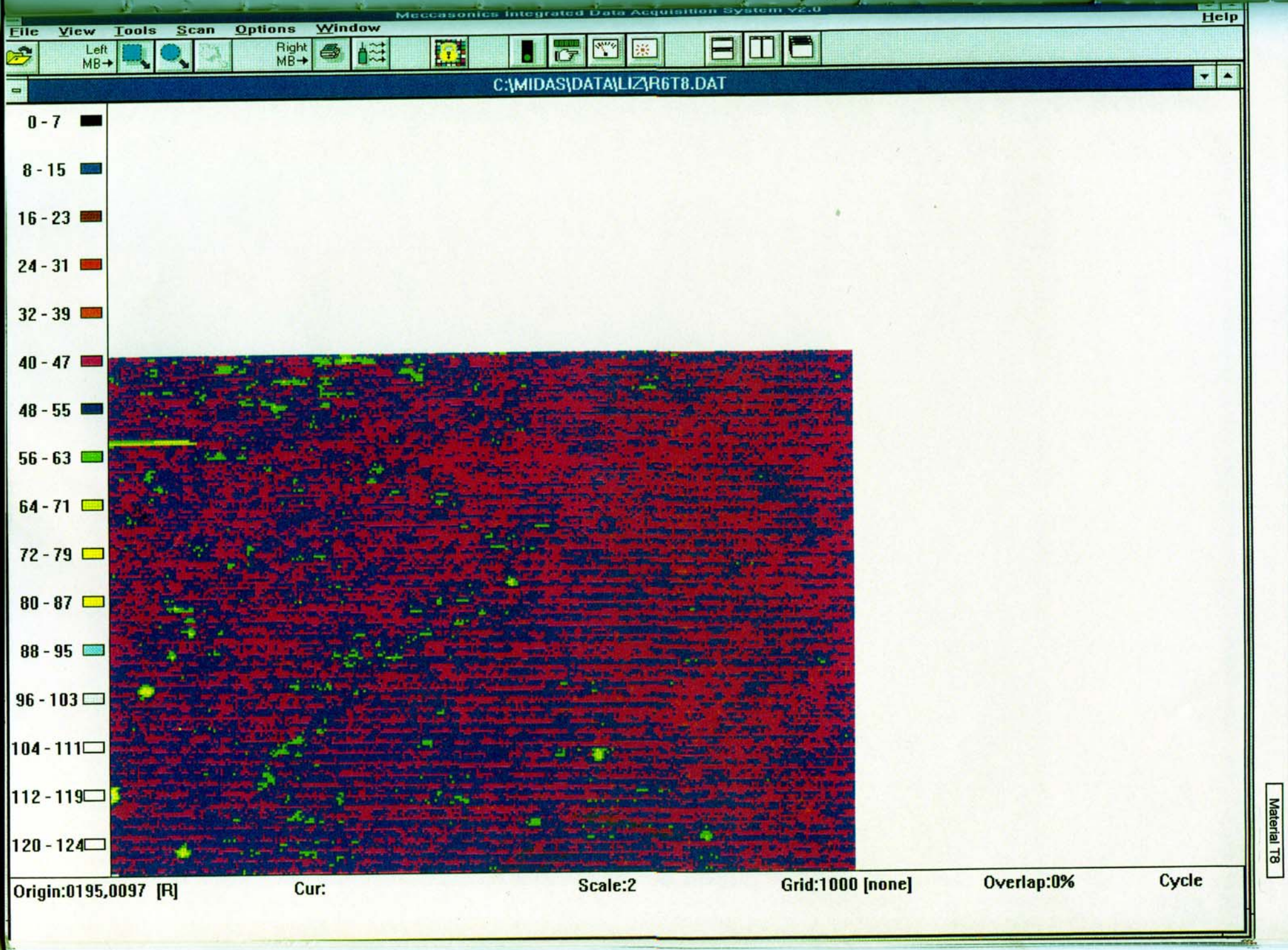
Meccasonics Integrated Data Acquisition System V2.0
File View Tools Scan Options Window Help
Left MB→
Right MB→
C:\MIDAS\DATA\LIZ\R6T8.DAT
0 - 7
8 - 15
16 - 23
24 - 31
32 - 39
40 - 47
48 - 55
56 - 63
64 - 71
72 - 79
80 - 87
88 - 95
96 - 103
104 - 111
112 - 119
120 - 124
Origin:0195,0097 [R]
Cur:
Scale:2
Grid:1000 [none]
Overlap:0%
Cycle
Material T8

Impact Sample C-scans and Penetrant Enhanced X-ray Images

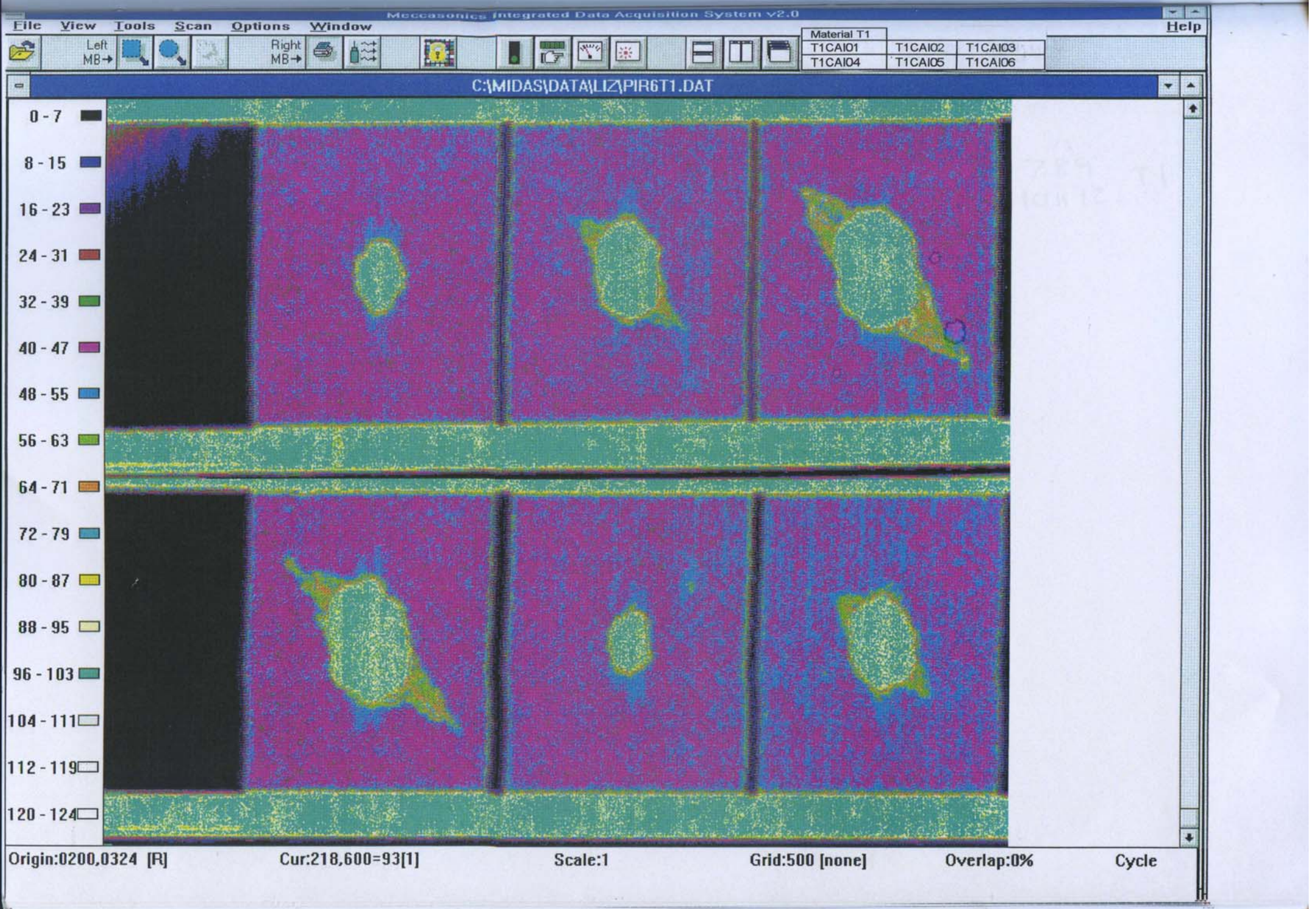
Meccasonics Integrated Data Acquisition System v2.0
File View Tools Scan Options Window Help
Left MB→
Right MB→
Material T1
T1CAI01 T1CAI02 T1CAI03
T1CAI04 T1CAI05 T1CAI06
C:\MIDAS\DATA\LIZ\PIR6T1.DAT
0 - 7
8 - 15
16 - 23
24 - 31
32 - 39
40 - 47
48 - 55
56 - 63
64 - 71
72 - 79
80 - 87
88 - 95
96 - 103
104 - 111
112 - 119
120 - 124
Origin:0200,0324 [R]
Cur:218,600=93[1]
Scale:1
Grid:500 [none]
Overlap:0%
Cycle

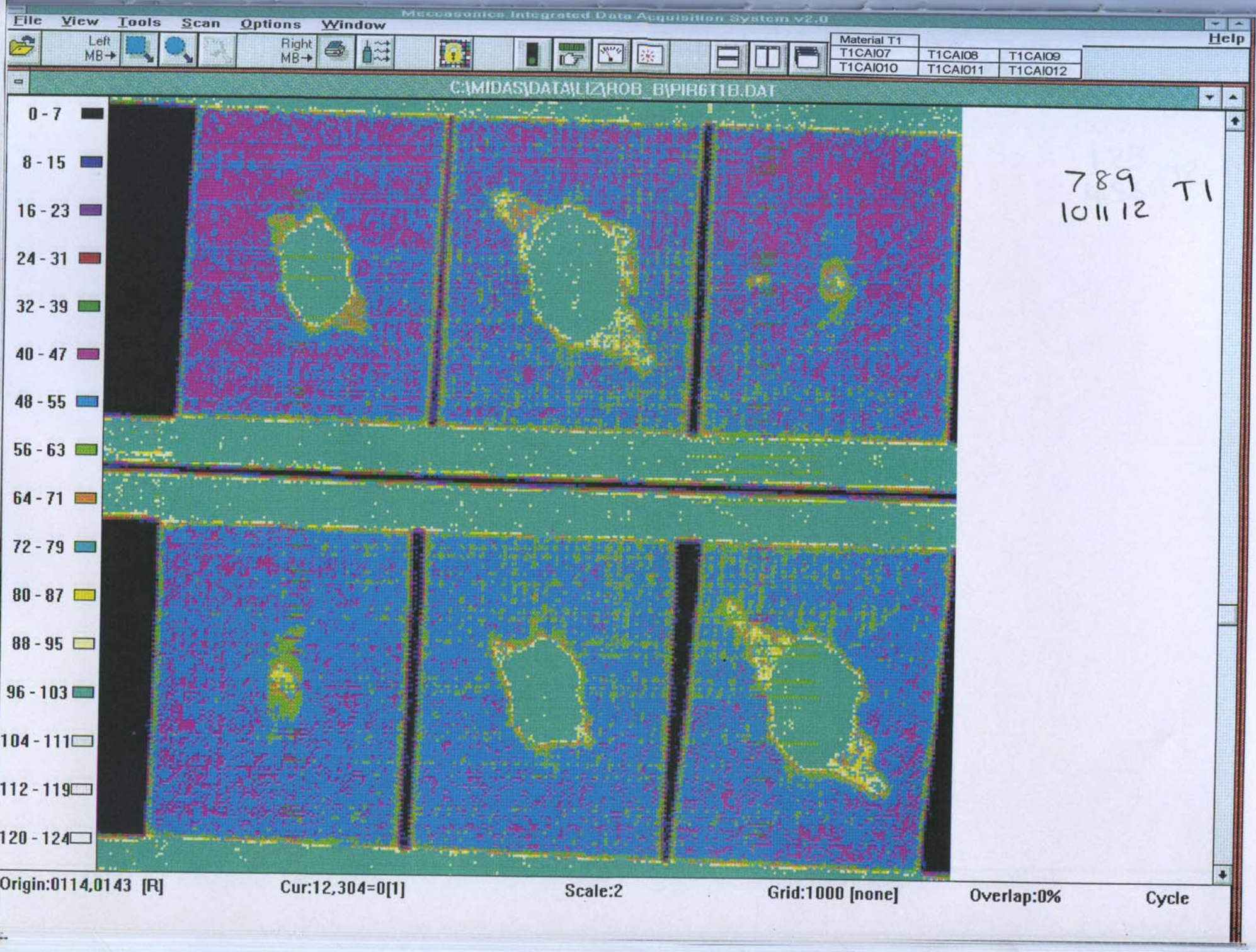
Meccasonics Integrated Data Acquisition System v2.0
File View Tools Scan Options Window
Help
Left MB→
Right MB→
Material T1
T1CAI07 T1CAI08 T1CAI09
T1CAI010 T1CAI011 T1CAI012
C:\MIDAS\DATA\LIZ\ROB_B\PIR6T1B.DAT
0 - 7
8 - 15
16 - 23
24 - 31
32 - 39
40 - 47
48 - 55
56 - 63
64 - 71
72 - 79
80 - 87
88 - 95
96 - 103
104 - 111
112 - 119
120 - 124
789
10 11 12
T1
Origin:0114,0143 [R]
Cur:12,304=0[1]
Scale:2
Grid:1000 [none]
Overlap:0%
Cycle

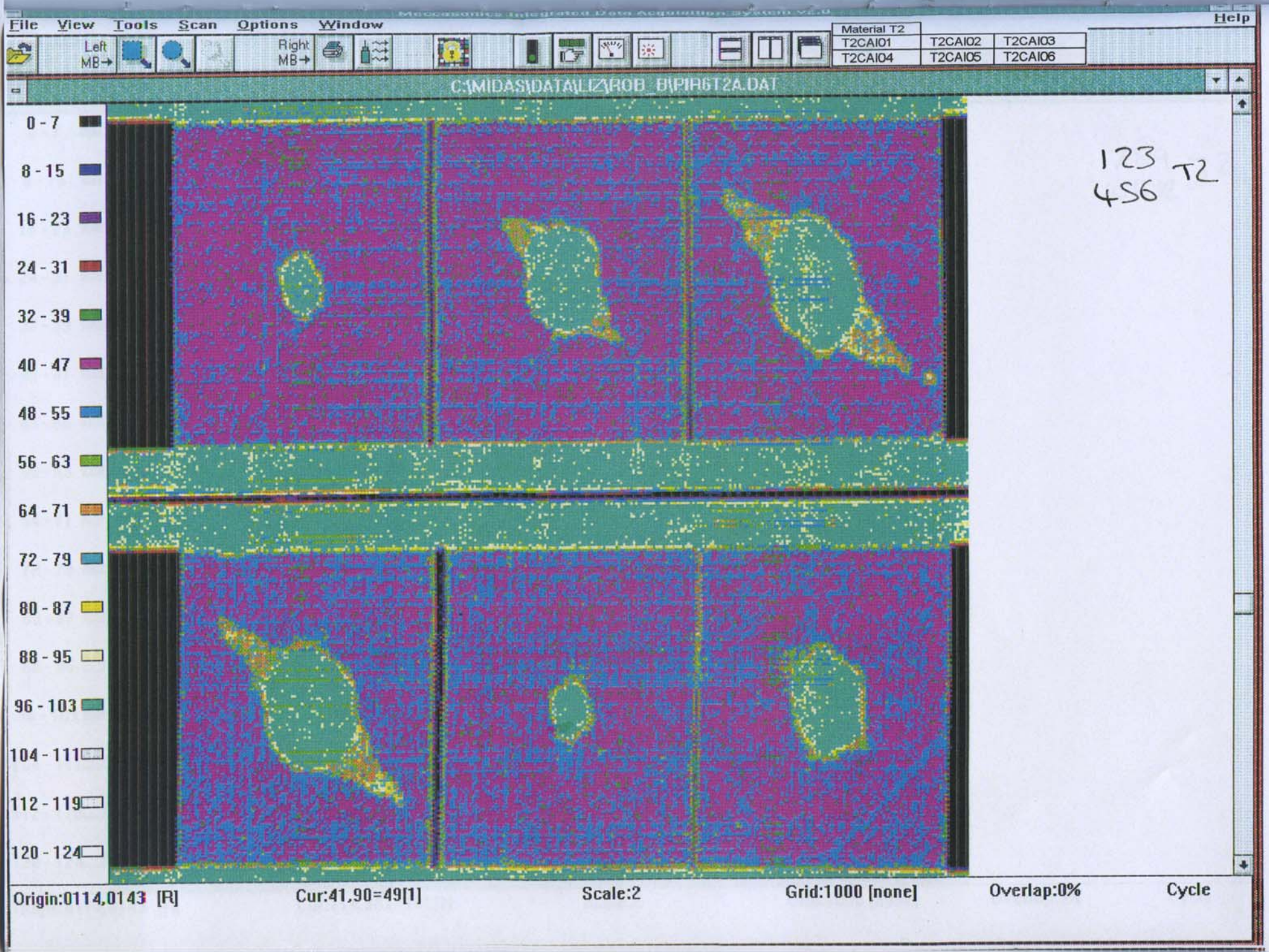
File View Tools Scan Options Window
Help
Left MB→
Right MB→
Material T2
T2CAI01 T2CAI02 T2CAI03
T2CAI04 T2CAI05 T2CAI06
C:\MIDAS\DATA\LIZ\ROB_B\PIR6T2A.DAT
0 - 7
8 - 15
16 - 23
24 - 31
32 - 39
40 - 47
48 - 55
56 - 63
64 - 71
72 - 79
80 - 87
88 - 95
96 - 103
104 - 111
112 - 119
120 - 124
123
456
T2
Origin:0114,0143 [R]
Cur:41,90=49[1]
Scale:2
Grid:1000 [none]
Overlap:0%
Cycle

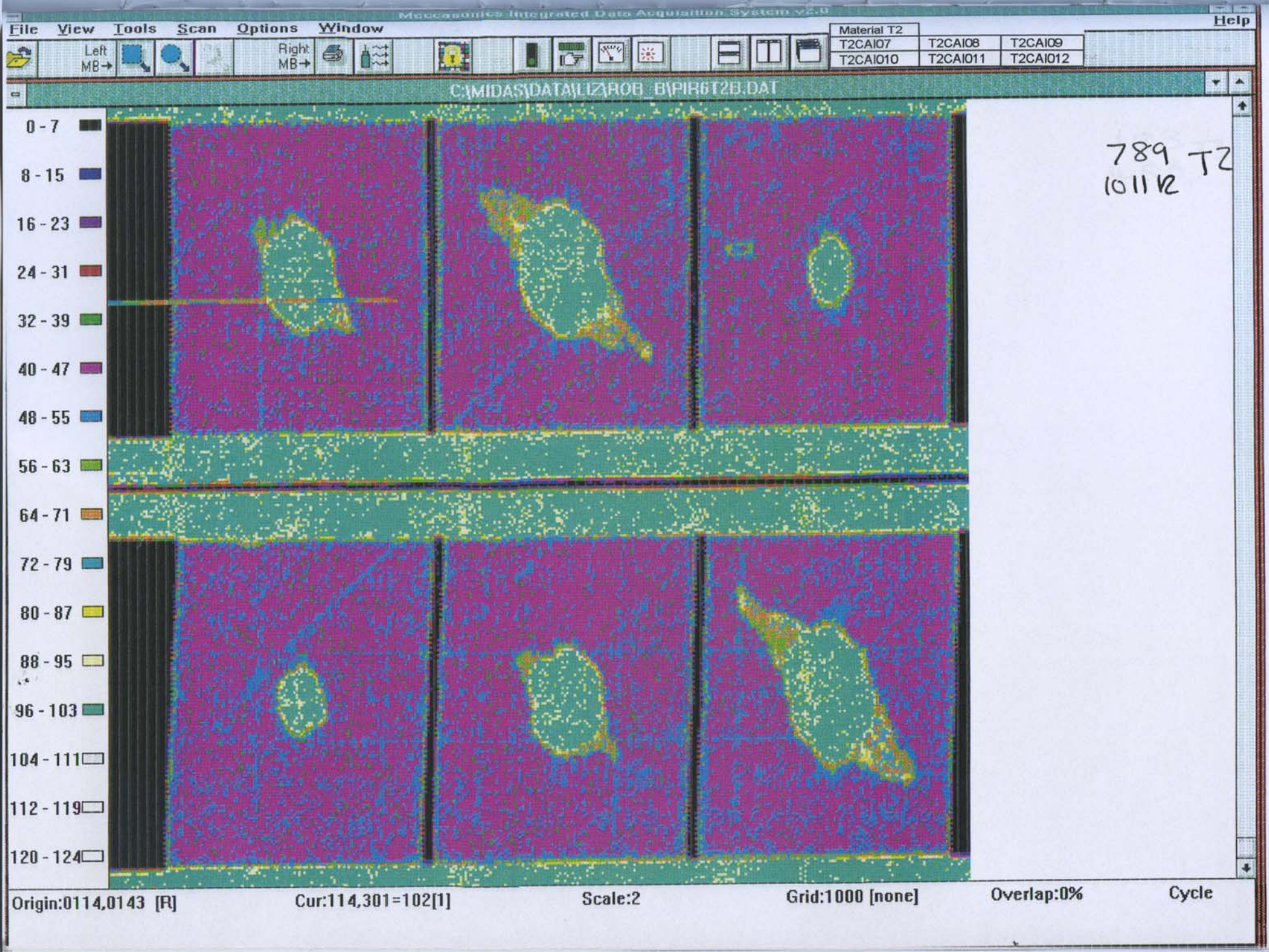
Meccasonics Integrated Data Acquisition System v2.0
File View Tools Scan Options Window
Help
Left MB→
Right MB→
Material T2
T2CAI07 T2CAI08 T2CAI09
T2CAI010 T2CAI011 T2CAI012
C:\MIDAS\DATA\LIZ\ROB_B\PIR6T2B.DAT
0 - 7
8 - 15
16 - 23
24 - 31
32 - 39
40 - 47
48 - 55
56 - 63
64 - 71
72 - 79
80 - 87
88 - 95
96 - 103
104 - 111
112 - 119
120 - 124
789 T2
1011 R
Origin:0114,0143 [R]
Cur:114,301=102[1]
Scale:2
Grid:1000 [none]
Overlap:0%
Cycle

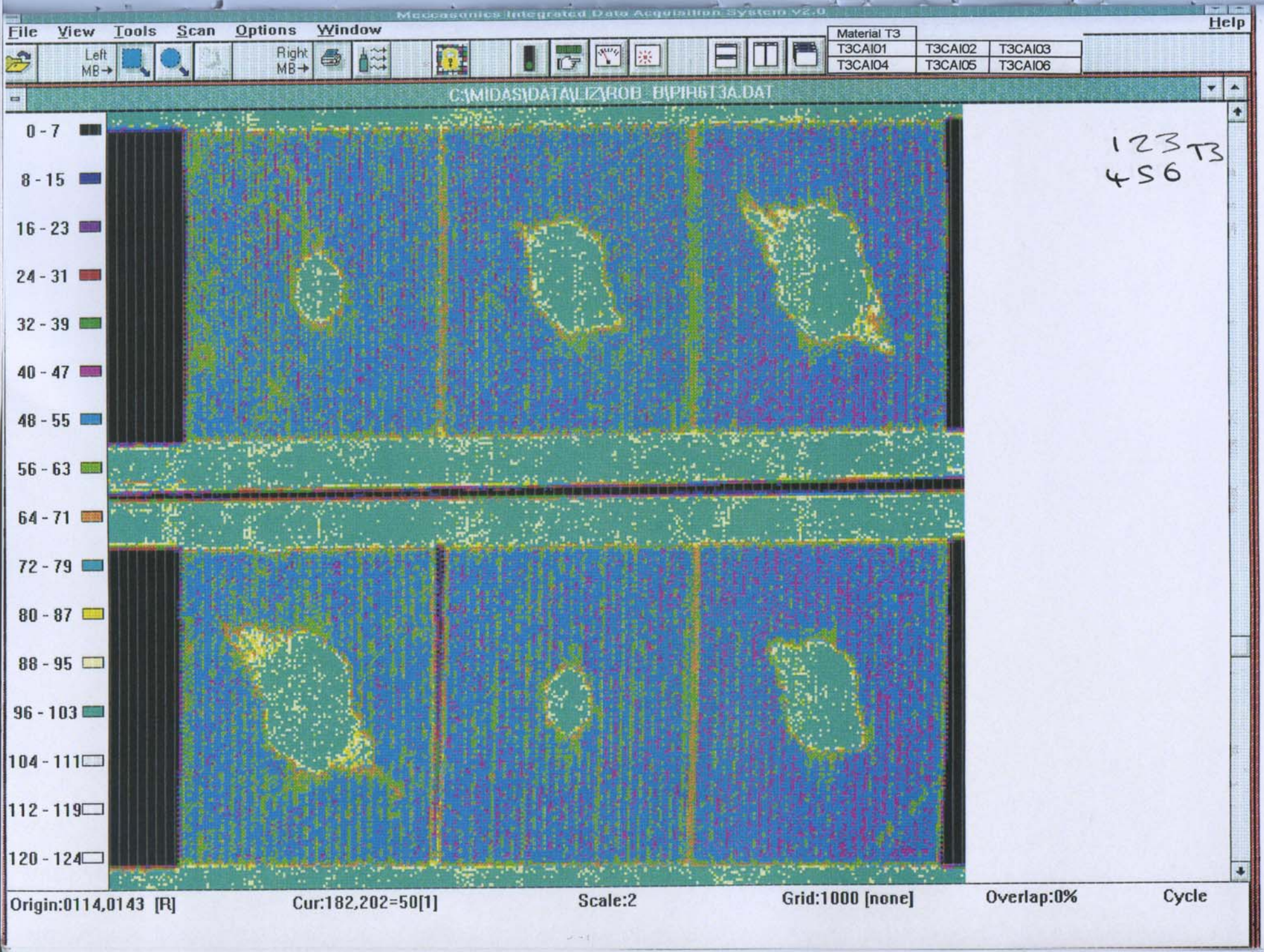
Meccasonics Integrated Data Acquisition System V2.0
File View Tools Scan Options Window
Help
Left MB→
Right MB→
Material T3
T3CAI01 T3CAI02 T3CAI03
T3CAI04 T3CAI05 T3CAI06
C:\MIDAS\DATA\LIZ\ROB B\PIP6T3A.DAT
0 - 7
8 - 15
16 - 23
24 - 31
32 - 39
40 - 47
48 - 55
56 - 63
64 - 71
72 - 79
80 - 87
88 - 95
96 - 103
104 - 111
112 - 119
120 - 124
1 2 3 T3
4 5 6
Origin:0114,0143 [R]
Cur:182,202=50[1]
Scale:2
Grid:1000 [none]
Overlap:0%
Cycle

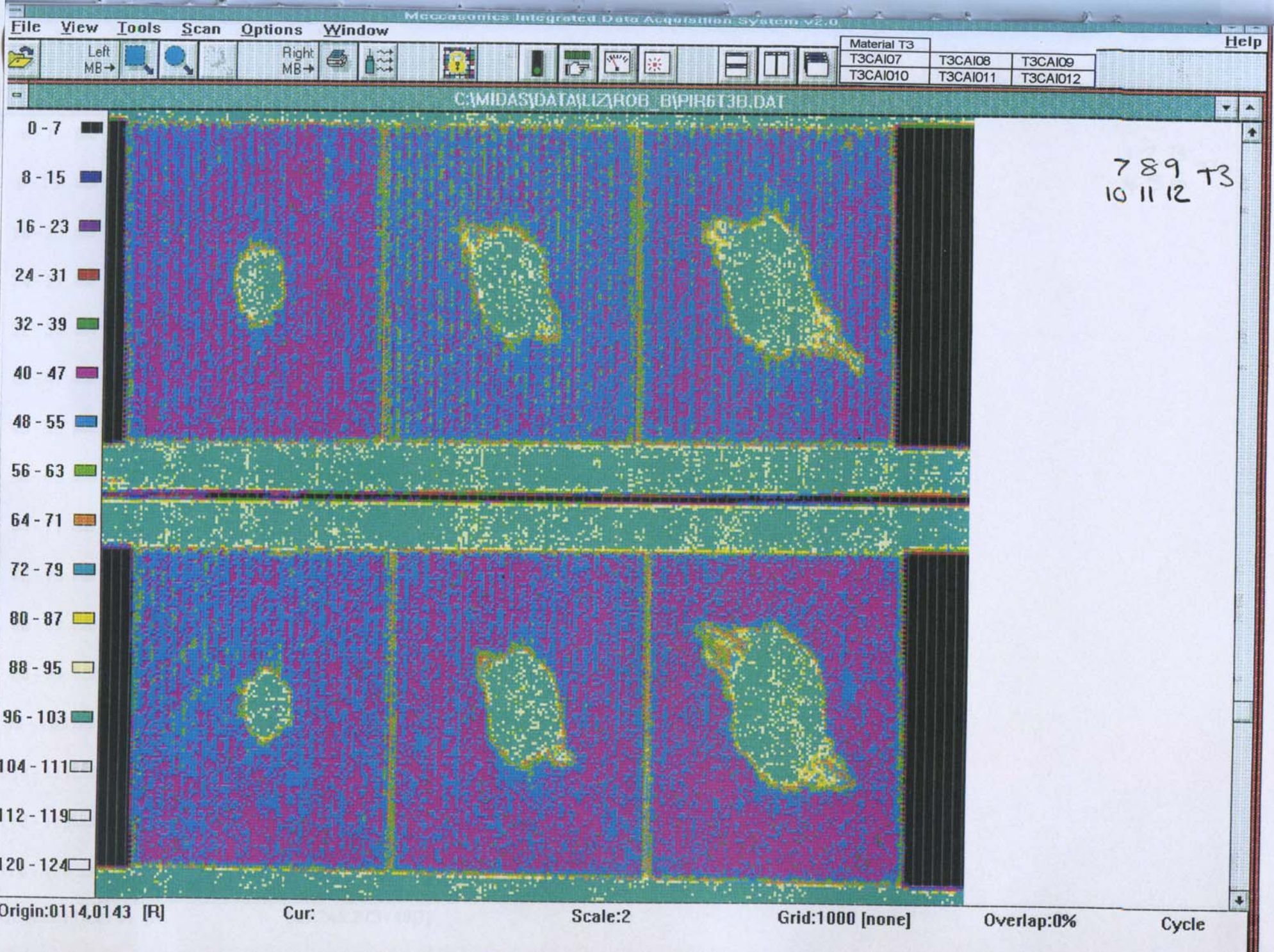
Meccasonics Integrated Data Acquisition System v2.0
File View Tools Scan Options Window
Help
Left MB→
Right MB→
Material T3
T3CAI07 T3CAI08 T3CAI09
T3CAI010 T3CAI011 T3CAI012
C:\MIDAS\DATA\LIZ\ROB_B\PIR6T3B.DAT
0 - 7
8 - 15
16 - 23
24 - 31
32 - 39
40 - 47
48 - 55
56 - 63
64 - 71
72 - 79
80 - 87
88 - 95
96 - 103
104 - 111
112 - 119
120 - 124
7 8 9 T3
10 11 12
Origin:0114,0143 [R]
Cur:
Scale:2
Grid:1000 [none]
Overlap:0%
Cycle

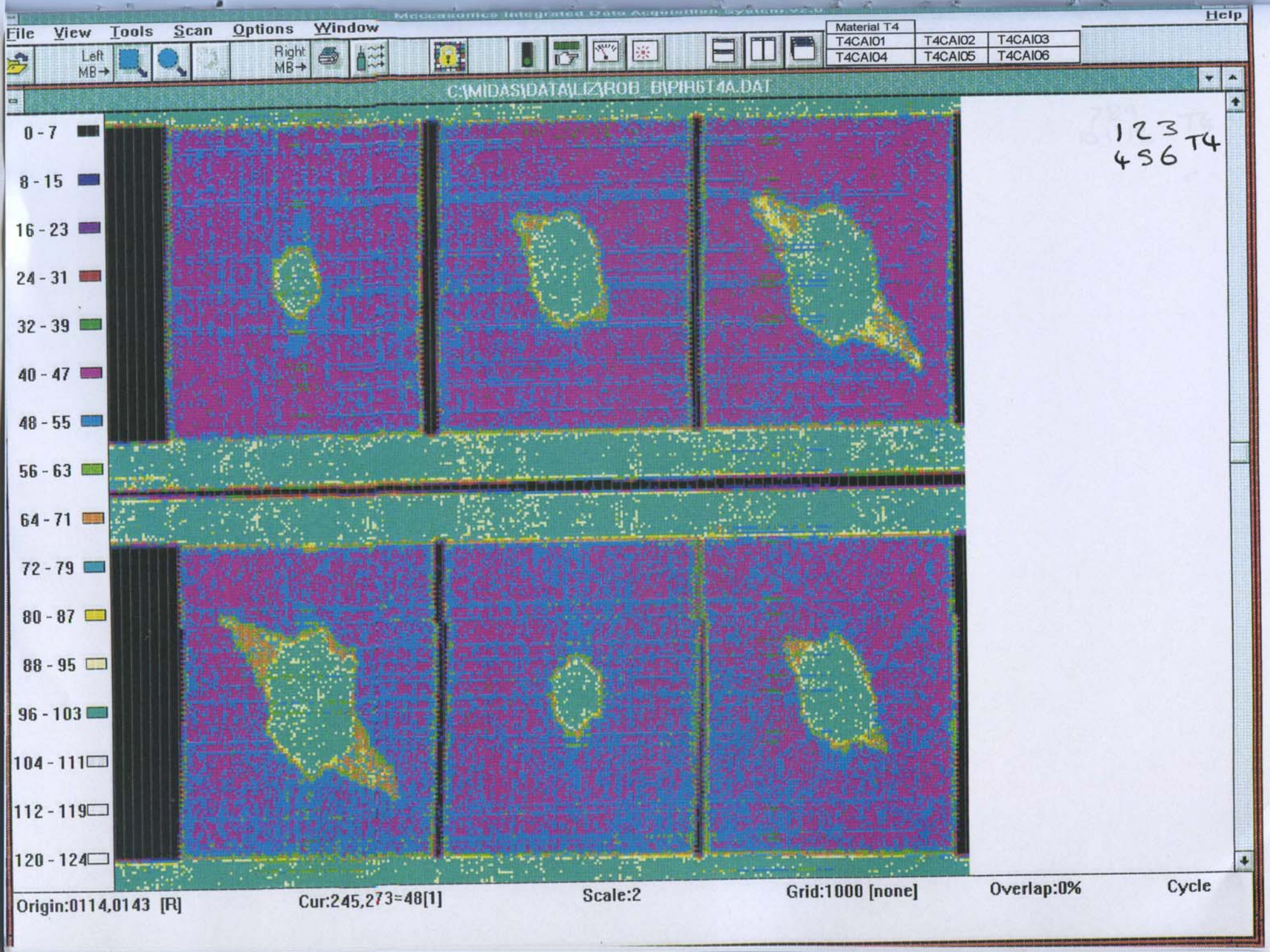
File View Tools Scan Options Window
Help
Left MB→
Right MB→
Material T4
T4CAI01 T4CAI02 T4CAI03
T4CAI04 T4CAI05 T4CAI06
C:\MIDAS\DATA\LIZ\ROB_B\PIR6T4A.DAT
0 - 7
8 - 15
16 - 23
24 - 31
32 - 39
40 - 47
48 - 55
56 - 63
64 - 71
72 - 79
80 - 87
88 - 95
96 - 103
104 - 111
112 - 119
120 - 124
1 2 3
4 5 6 T4
Origin:0114,0143 [R]
Cur:245,273=48[1]
Scale:2
Grid:1000 [none]
Overlap:0%
Cycle

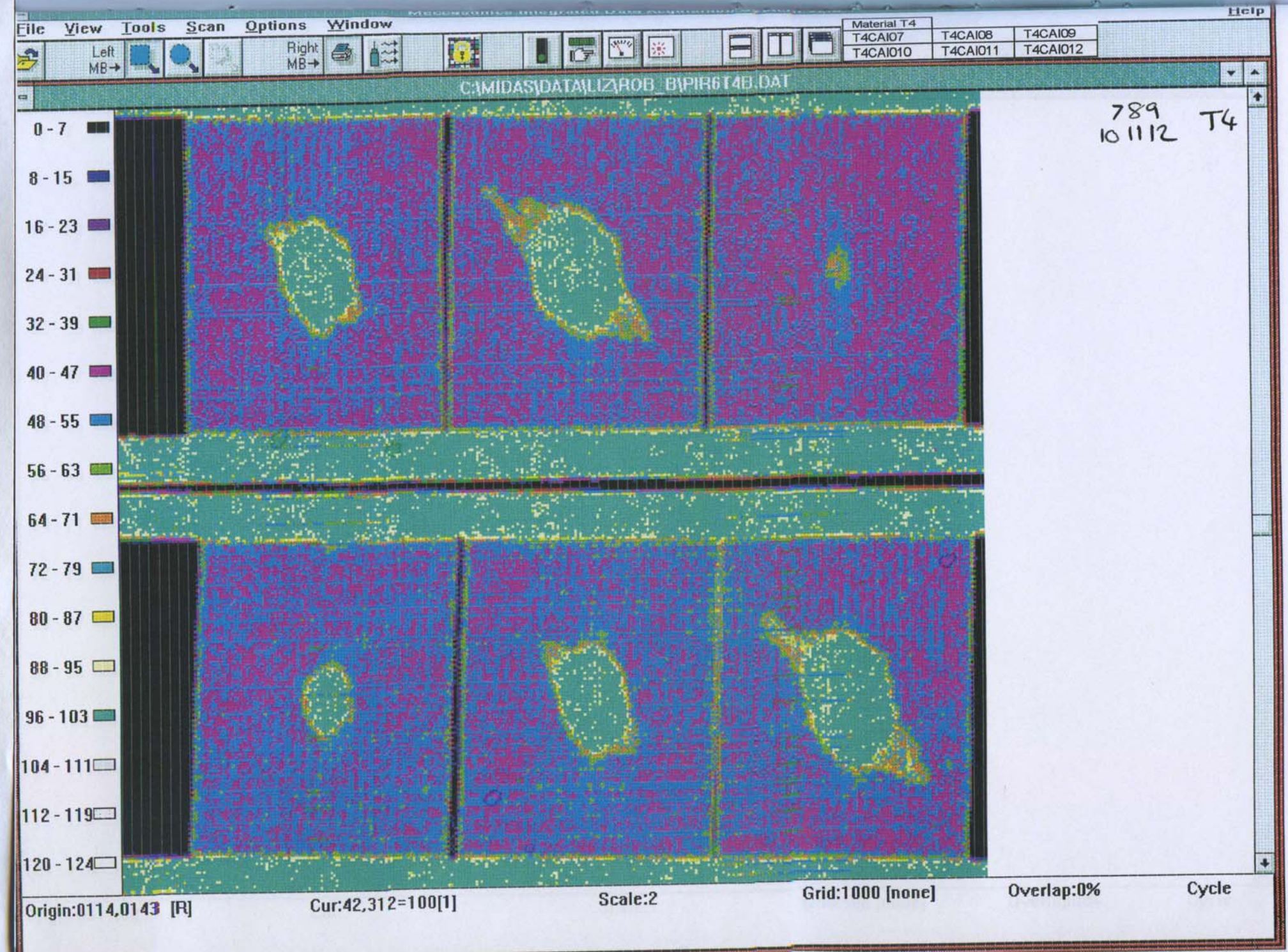
File View Tools Scan Options Window
Help
Left MB→
Right MB→
Material T4
T4CAI07
T4CAI08
T4CAI09
T4CAI010
T4CAI011
T4CAI012
C:\MIDAS\DATA\LIZ\ROB_B\PIR6T4B.DAT
789
10 11 12
T4
0 - 7
8 - 15
16 - 23
24 - 31
32 - 39
40 - 47
48 - 55
56 - 63
64 - 71
72 - 79
80 - 87
88 - 95
96 - 103
104 - 111
112 - 119
120 - 124
Origin:0114,0143 [R]
Cur:42,312=100[1]
Scale:2
Grid:1000 [none]
Overlap:0%
Cycle

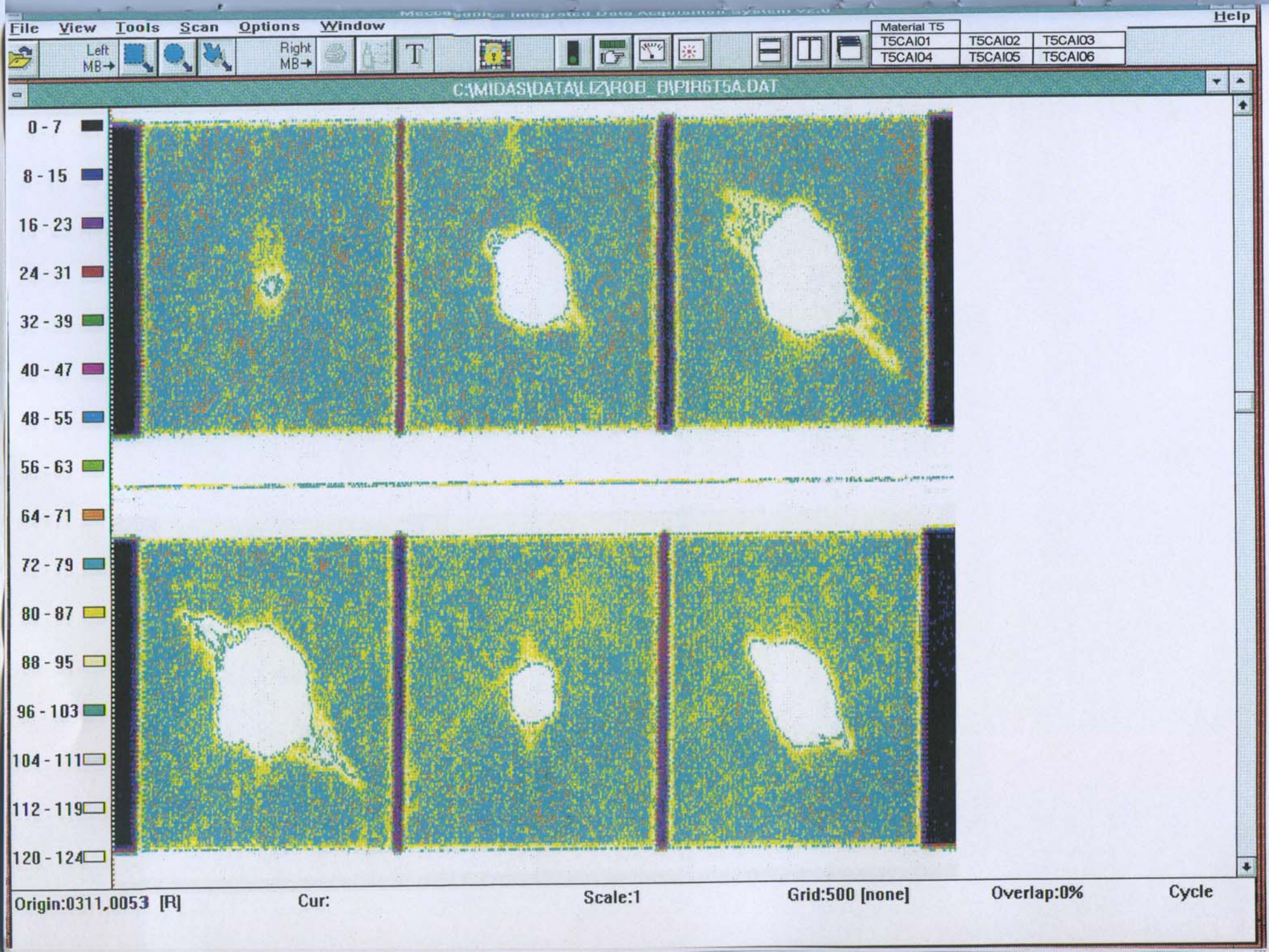
File View Tools Scan Options Window
Help
Left MB→
Right MB→
Material T5
T5CAI01 T5CAI02 T5CAI03
T5CAI04 T5CAI05 T5CAI06
C:\MIDAS\DATA\LIZ\ROB_B\PIR6T5A.DAT
0 - 7
8 - 15
16 - 23
24 - 31
32 - 39
40 - 47
48 - 55
56 - 63
64 - 71
72 - 79
80 - 87
88 - 95
96 - 103
104 - 111
112 - 119
120 - 124
Origin:0311,0053 [R]
Cur:
Scale:1
Grid:500 [none]
Overlap:0%
Cycle

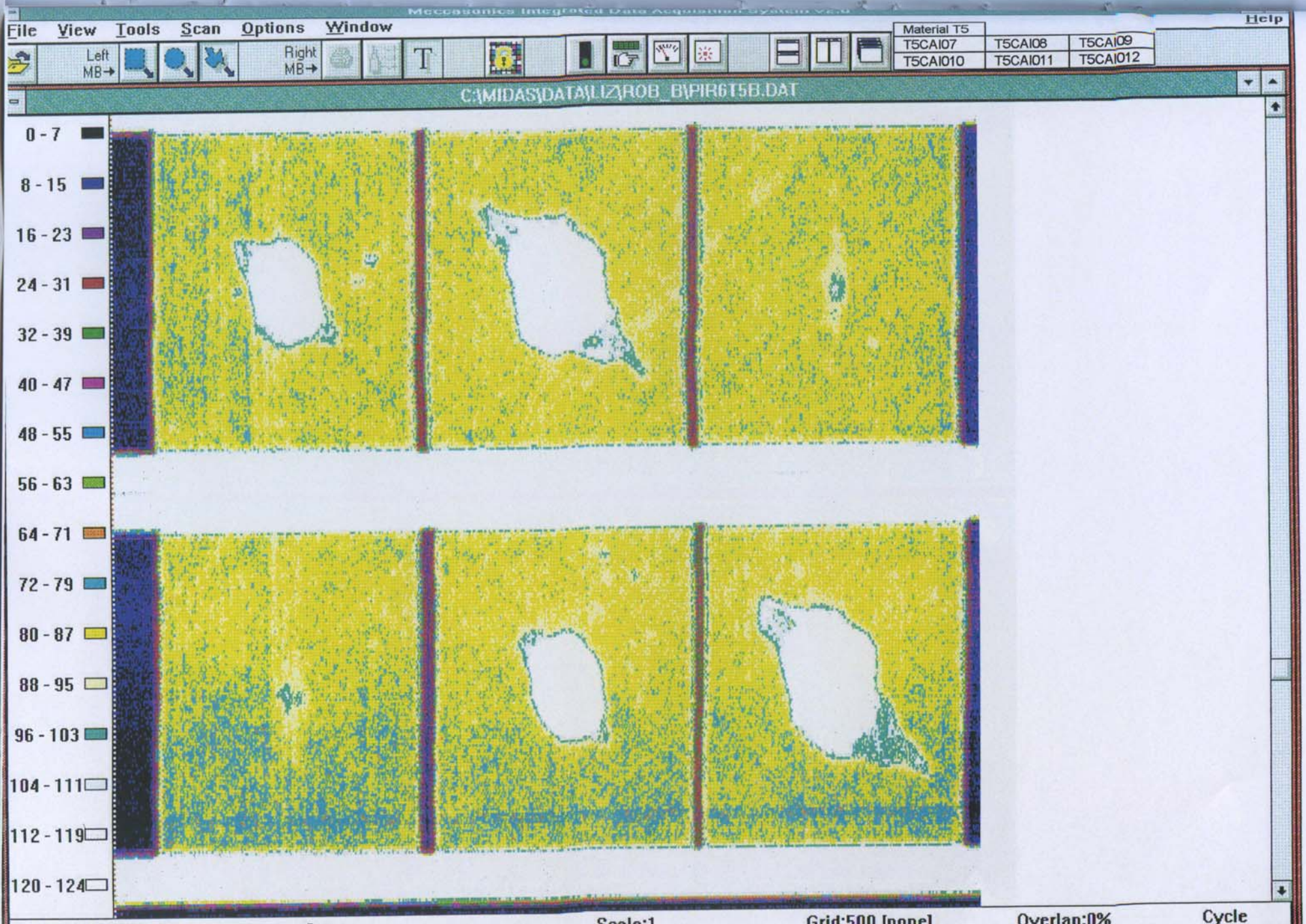
Meccasonics Integrated Data Acquisition System V2.0
File View Tools Scan Options Window
Help
Left MB→
Right MB→
Material T5
T5CAI07
T5CAI08
T5CAI09
T5CAI010
T5CAI011
T5CAI012
C:\MIDAS\DATA\LIZ\ROB_B\PIR6T5B.DAT
0 - 7
8 - 15
16 - 23
24 - 31
32 - 39
40 - 47
48 - 55
56 - 63
64 - 71
72 - 79
80 - 87
88 - 95
96 - 103
104 - 111
112 - 119
120 - 124
Origin:0311,0053 [R]
Cur:
Scale:1
Grid:500 [none]
Overlap:0%
Cycle

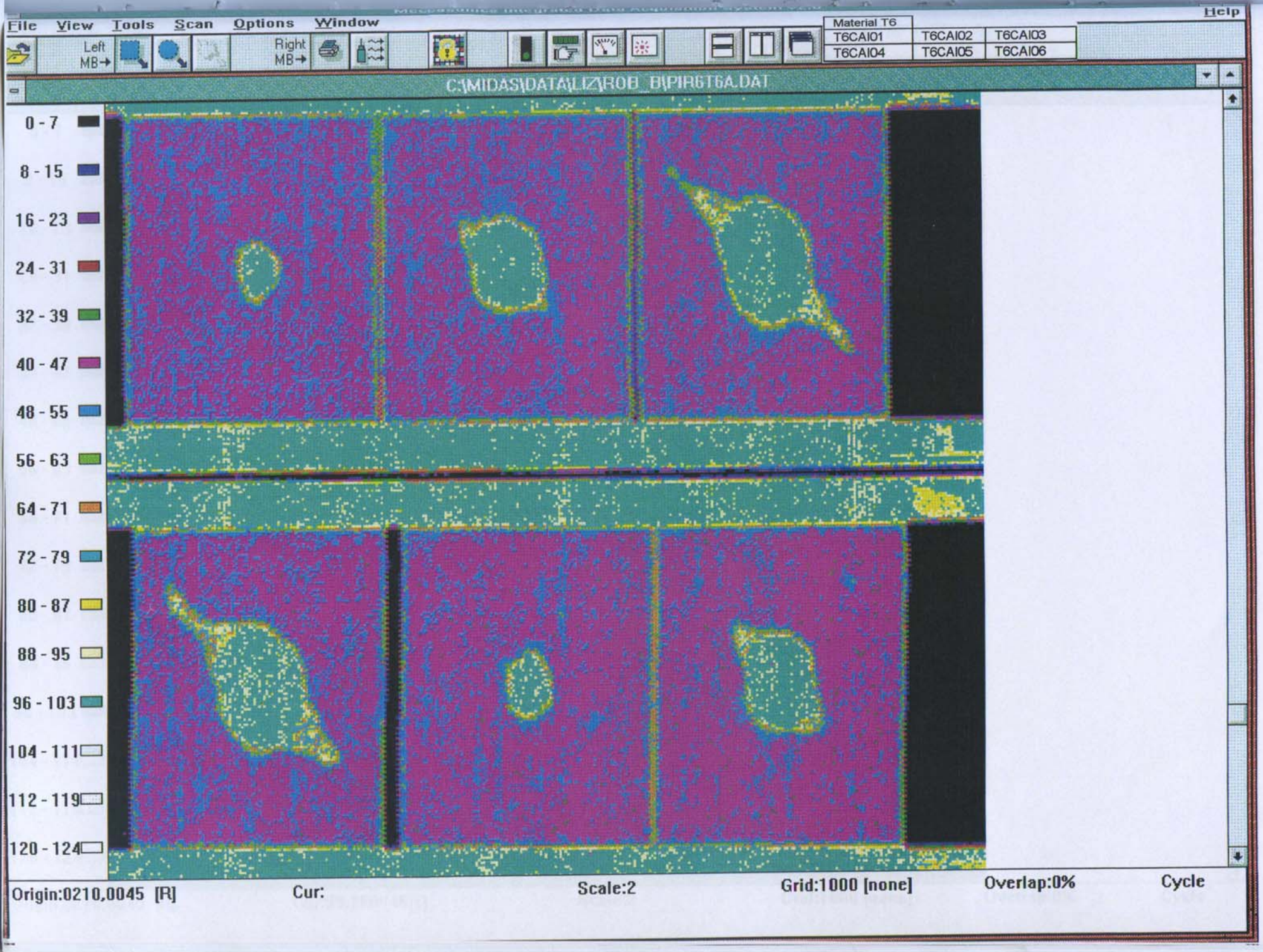
File View Tools Scan Options Window
Help
Left MB→
Right MB→
Material T6
T6CAI01 T6CAI02 T6CAI03
T6CAI04 T6CAI05 T6CAI06
C:\MIDAS\DATA\LIZ\ROB_B\PIR6T6A.DAT
0 - 7
8 - 15
16 - 23
24 - 31
32 - 39
40 - 47
48 - 55
56 - 63
64 - 71
72 - 79
80 - 87
88 - 95
96 - 103
104 - 111
112 - 119
120 - 124
Origin:0210,0045 [R]
Cur:
Scale:2
Grid:1000 [none]
Overlap:0%
Cycle

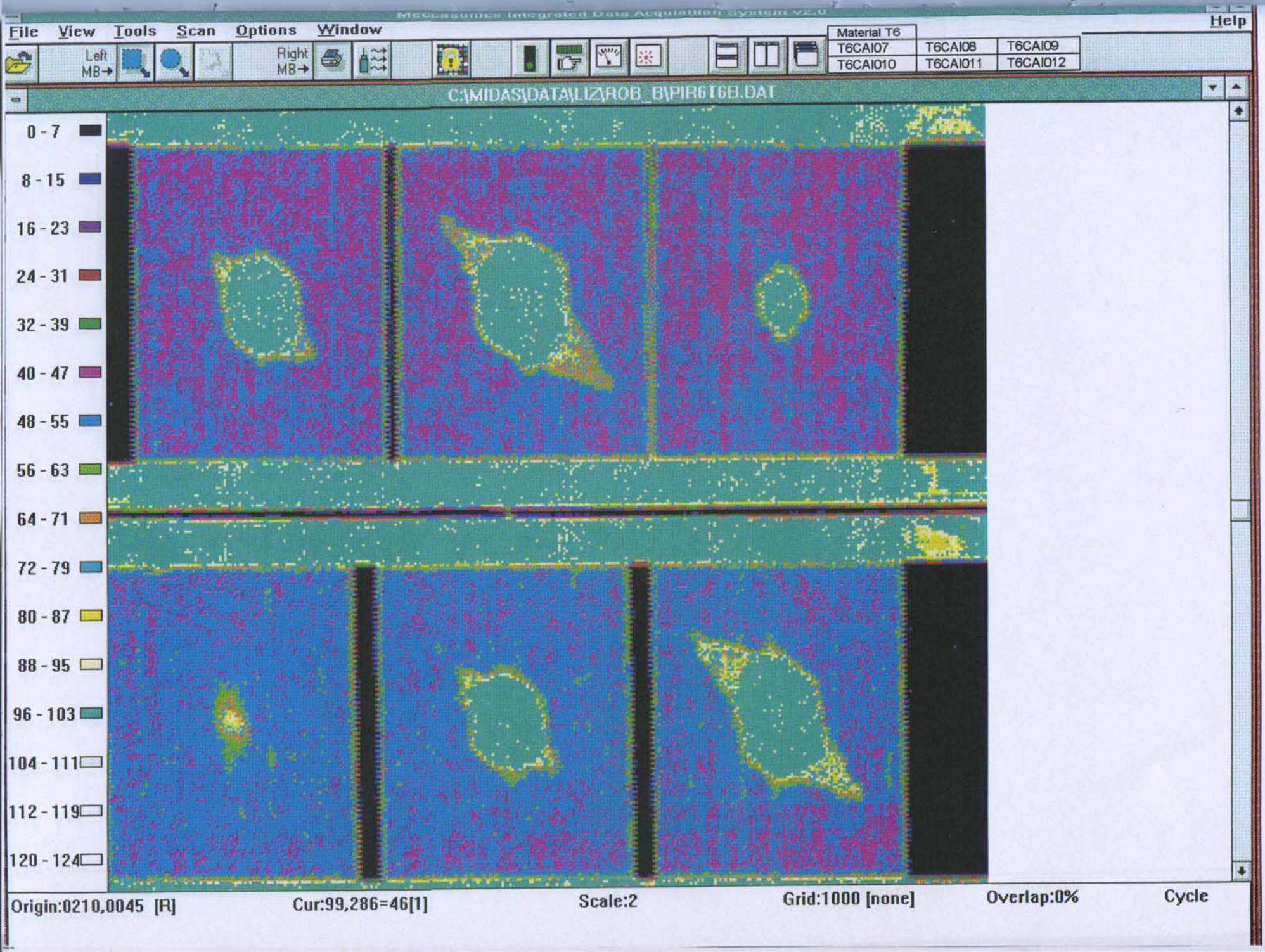
Meccanomics Integrated Data Acquisition System v2.0
File View Tools Scan Options Window
Help
Left MB→
Right MB→
Material T6
T6CAI07 T6CAI08 T6CAI09
T6CAI010 T6CAI011 T6CAI012
C:\MIDAS\DATA\LIZ\ROB_B\PIR6T6B.DAT
0 - 7
8 - 15
16 - 23
24 - 31
32 - 39
40 - 47
48 - 55
56 - 63
64 - 71
72 - 79
80 - 87
88 - 95
96 - 103
104 - 111
112 - 119
120 - 124
Origin:0210,0045 [R]
Cur:99,286=46[1]
Scale:2
Grid:1000 [none]
Overlap:0%
Cycle

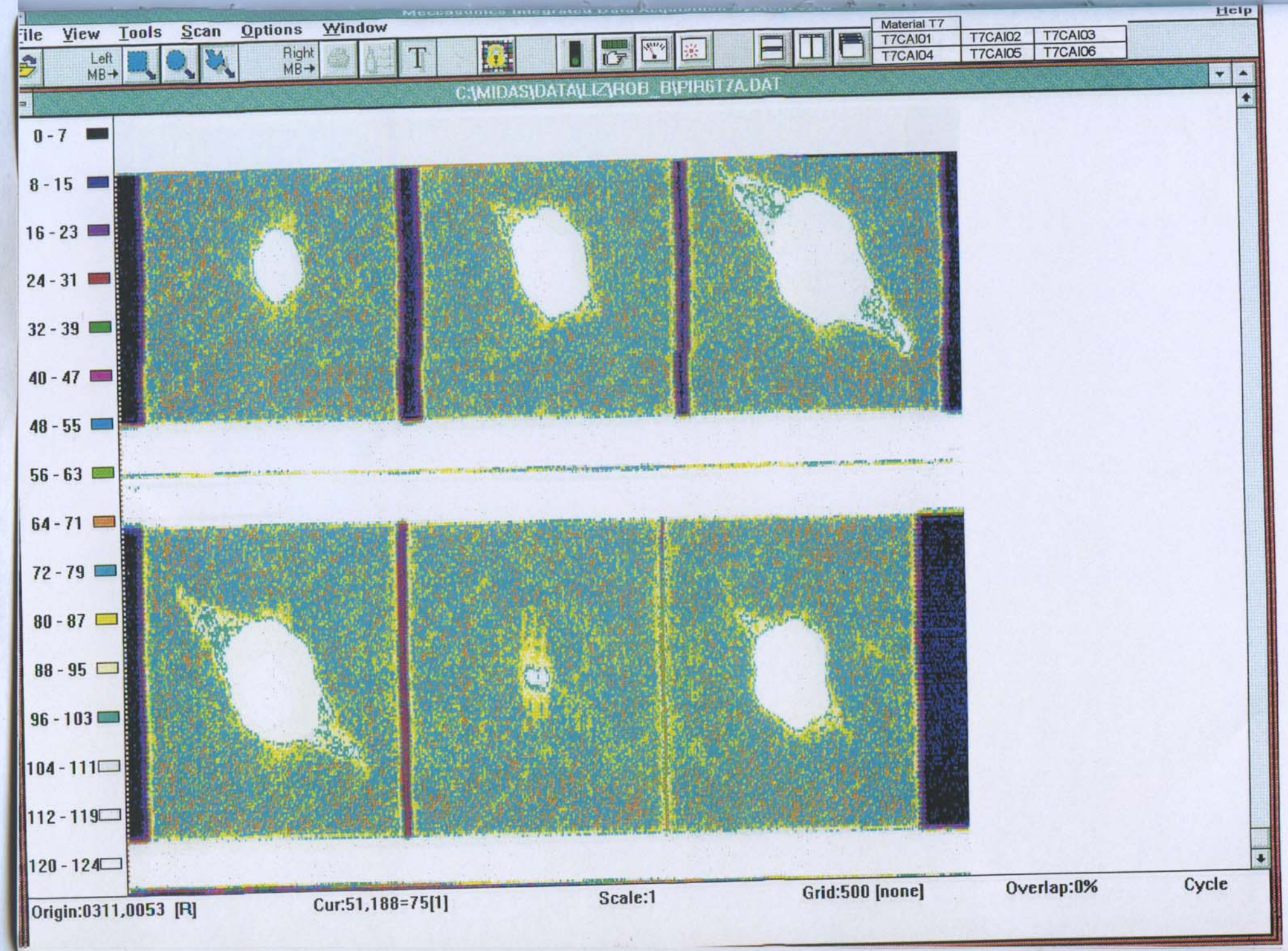
File View Tools Scan Options Window
Help
Left MB→
Right MB→
Material T7
T7CAI01
T7CAI02
T7CAI03
T7CAI04
T7CAI05
T7CAI06
C:\MIDAS\DATA\LIZ\ROB_B\PIR6T7A.DAT
0 - 7
8 - 15
16 - 23
24 - 31
32 - 39
40 - 47
48 - 55
56 - 63
64 - 71
72 - 79
80 - 87
88 - 95
96 - 103
104 - 111
112 - 119
120 - 124
Origin:0311,0053 [R]
Cur:51,188=75[1]
Scale:1
Grid:500 [none]
Overlap:0%
Cycle

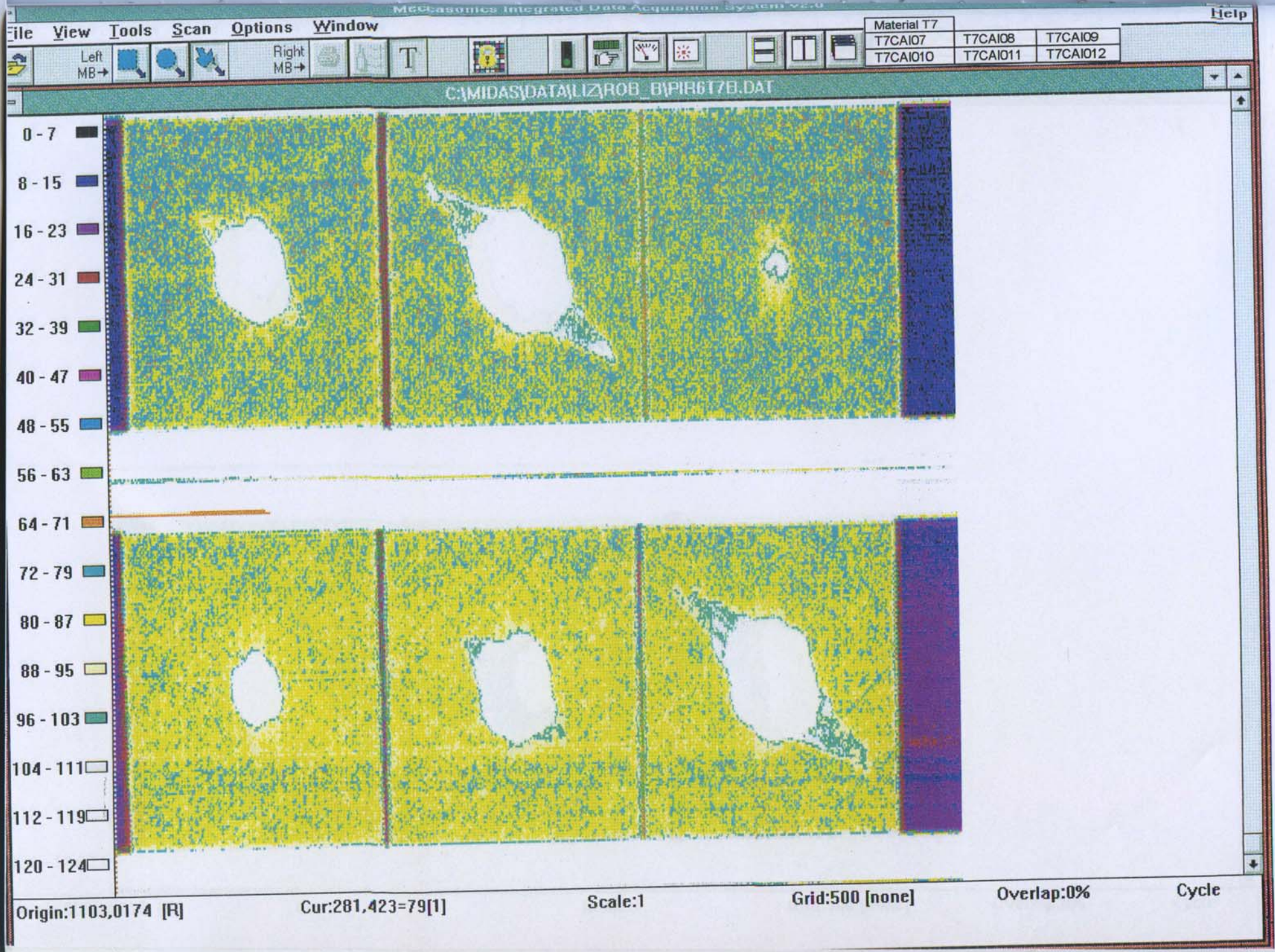
File View Tools Scan Options Window
Help
Left MB→
Right MB→
Material T7
T7CAI07
T7CAI08
T7CAI09
T7CAI010
T7CAI011
T7CAI012
C:\MIDAS\DATA\LIZ\ROB_B\PIR6T7B.DAT
0 - 7
8 - 15
16 - 23
24 - 31
32 - 39
40 - 47
48 - 55
56 - 63
64 - 71
72 - 79
80 - 87
88 - 95
96 - 103
104 - 111
112 - 119
120 - 124
Origin:1103,0174 [R]
Cur:281,423=79[1]
Scale:1
Grid:500 [none]
Overlap:0%
Cycle

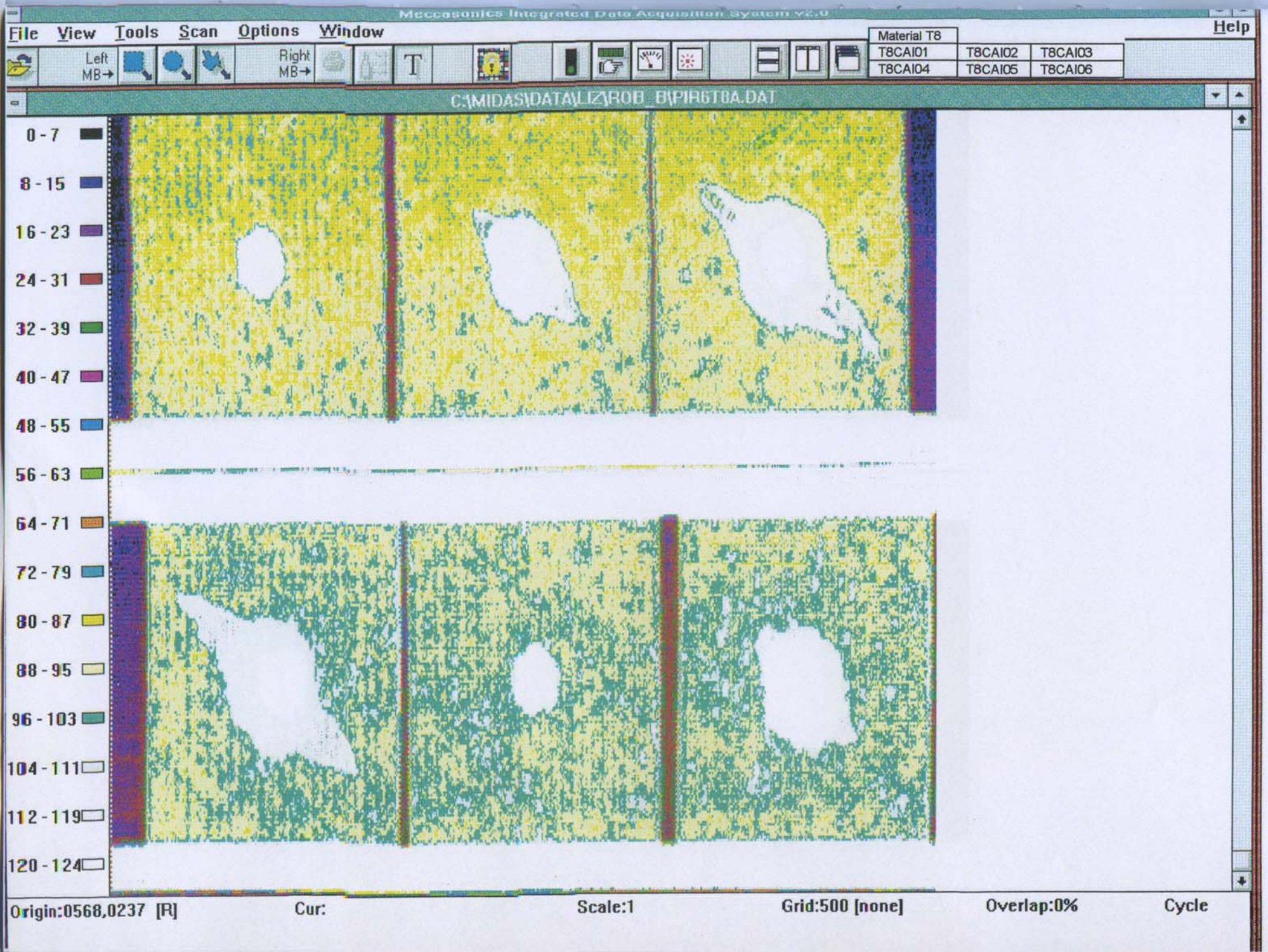
Meccasonics Integrated Data Acquisition System v2.0
File View Tools Scan Options Window
Help
Left MB→
Right MB→
Material T8
T8CAI01 T8CAI02 T8CAI03
T8CAI04 T8CAI05 T8CAI06
C:\MIDAS\DATA\LIZ\ROB_B\PIR6T8A.DAT
0 - 7
8 - 15
16 - 23
24 - 31
32 - 39
40 - 47
48 - 55
56 - 63
64 - 71
72 - 79
80 - 87
88 - 95
96 - 103
104 - 111
112 - 119
120 - 124
Origin:0568,0237 [R]
Cur:
Scale:1
Grid:500 [none]
Overlap:0%
Cycle

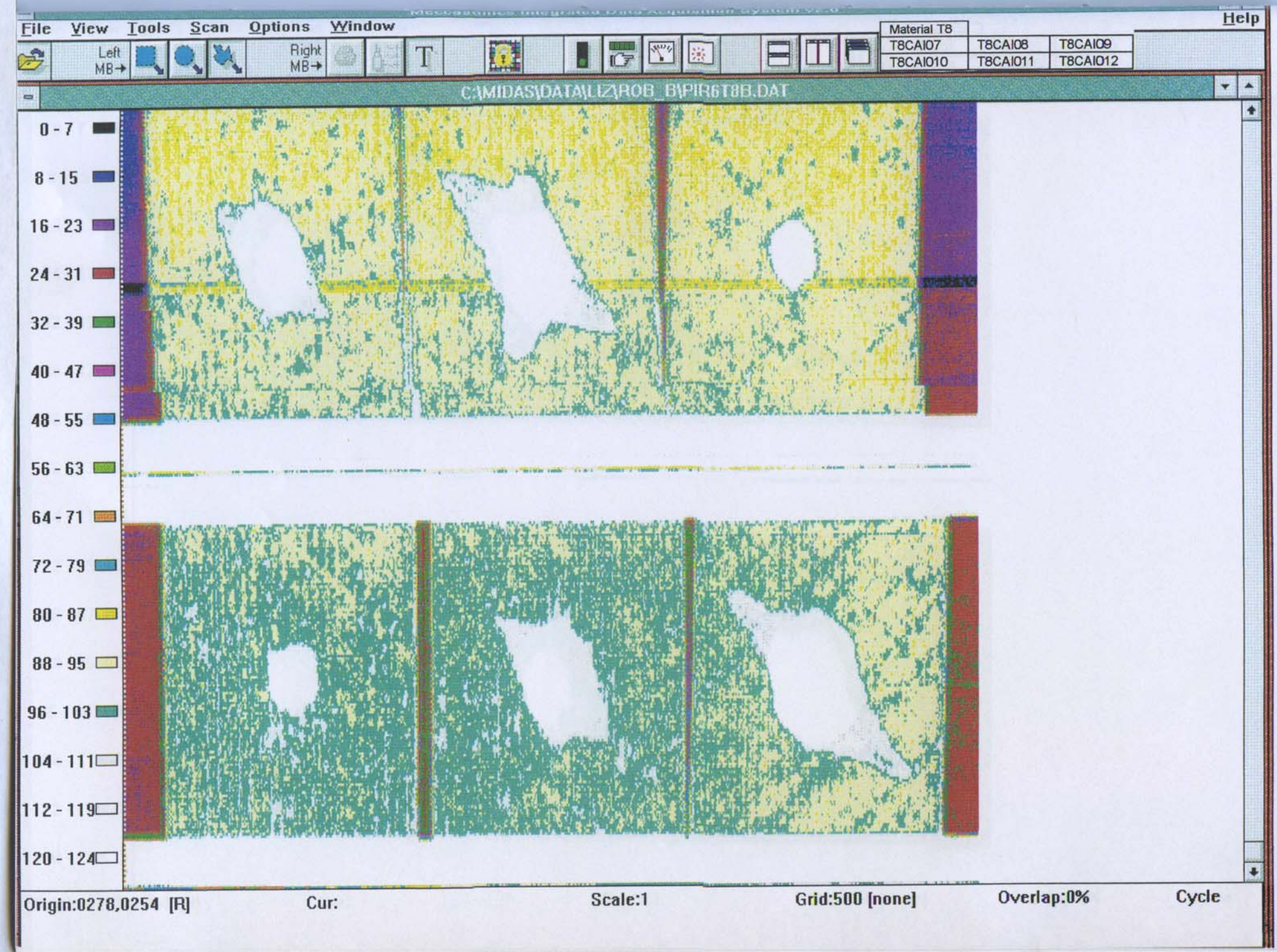
File View Tools Scan Options Window
Help
Left MB→
Right MB→
Material T8
T8CAI07 T8CAI08 T8CAI09
T8CAI010 T8CAI011 T8CAI012
C:\MIDAS\DATA\LIZ\ROB_B\PIR6T8B.DAT
0 - 7
8 - 15
16 - 23
24 - 31
32 - 39
40 - 47
48 - 55
56 - 63
64 - 71
72 - 79
80 - 87
88 - 95
96 - 103
104 - 111
112 - 119
120 - 124
Origin:0278,0254 [R]
Cur:
Scale:1
Grid:500 [none]
Overlap:0%
Cycle

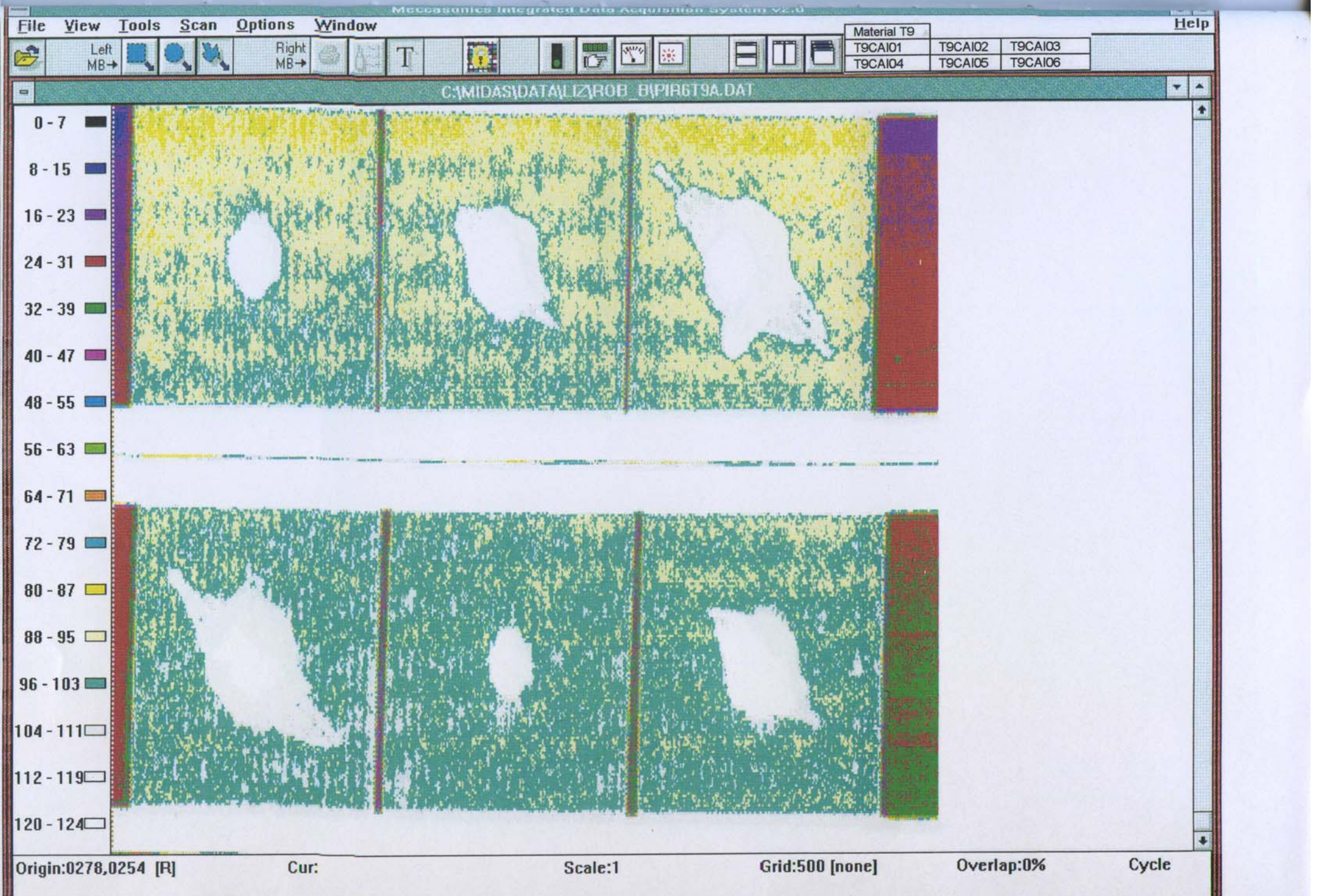
Meccasonics Integrated Data Acquisition System V2.0
File View Tools Scan Options Window
Help
Left MB→
Right MB→
Material T9
T9CAI01 T9CAI02 T9CAI03
T9CAI04 T9CAI05 T9CAI06
C:\MIDAS\DATA\LIZ\ROB_B\PIR6T9A.DAT
0 - 7
8 - 15
16 - 23
24 - 31
32 - 39
40 - 47
48 - 55
56 - 63
64 - 71
72 - 79
80 - 87
88 - 95
96 - 103
104 - 111
112 - 119
120 - 124
Origin:0278,0254 [R]
Cur:
Scale:1
Grid:500 [none]
Overlap:0%
Cycle

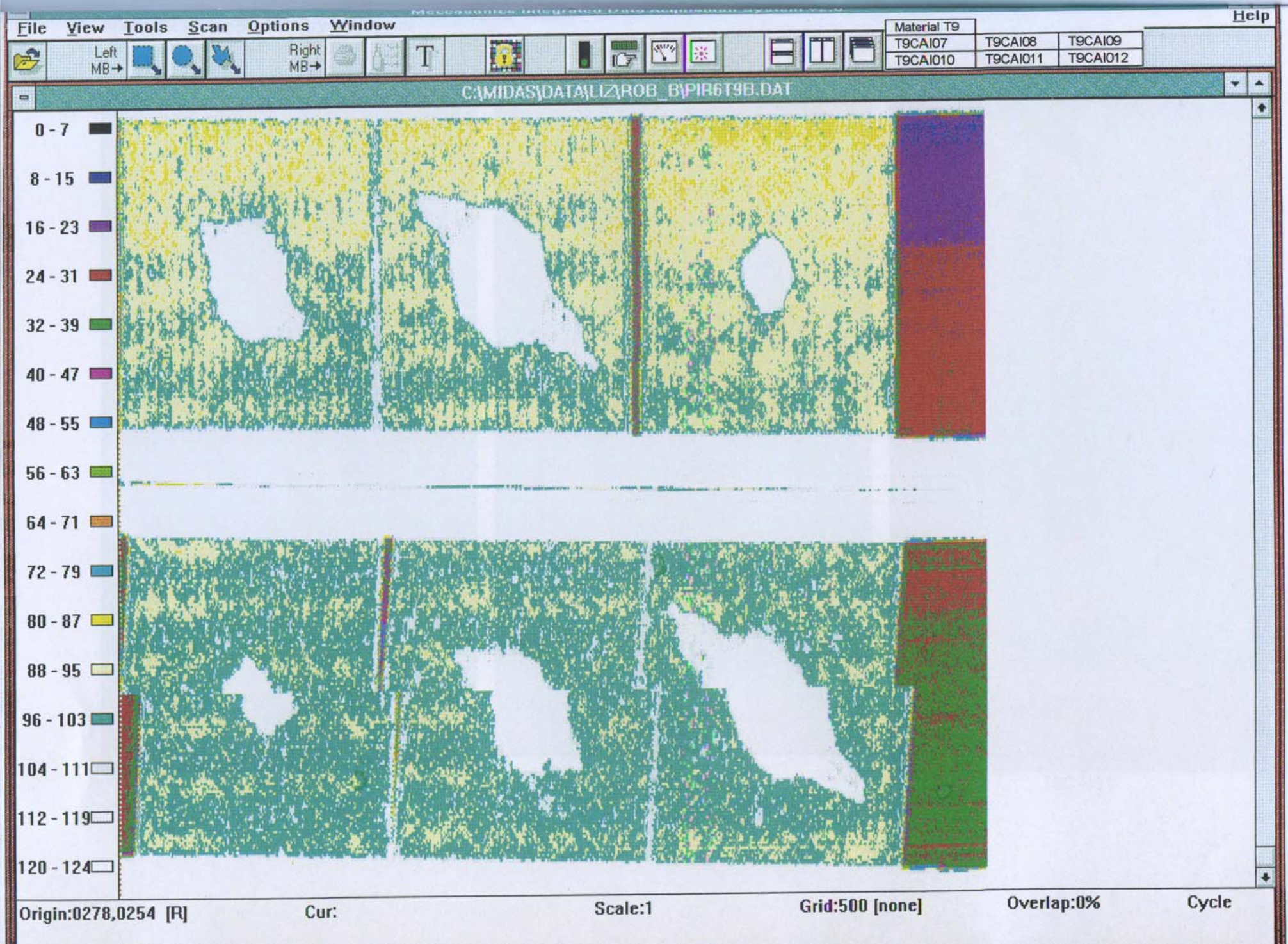
File View Tools Scan Options Window
Help
Left MB→
Right MB→
Material T9
T9CAI07
T9CAI08
T9CAI09
T9CAI010
T9CAI011
T9CAI012
C:\MIDAS\DATA\LIZ\ROB_B\PIR6T9B.DAT
0 - 7
8 - 15
16 - 23
24 - 31
32 - 39
40 - 47
48 - 55
56 - 63
64 - 71
72 - 79
80 - 87
88 - 95
96 - 103
104 - 111
112 - 119
120 - 124
Origin:0278,0254 [R]
Cur:
Scale:1
Grid:500 [none]
Overlap:0%
Cycle

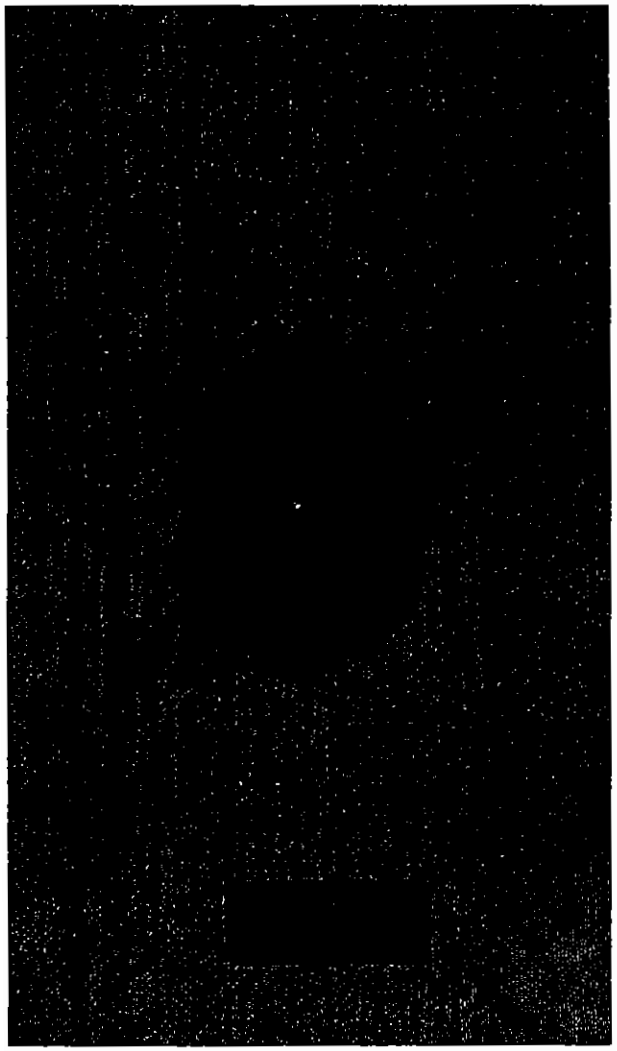

T1CAI11

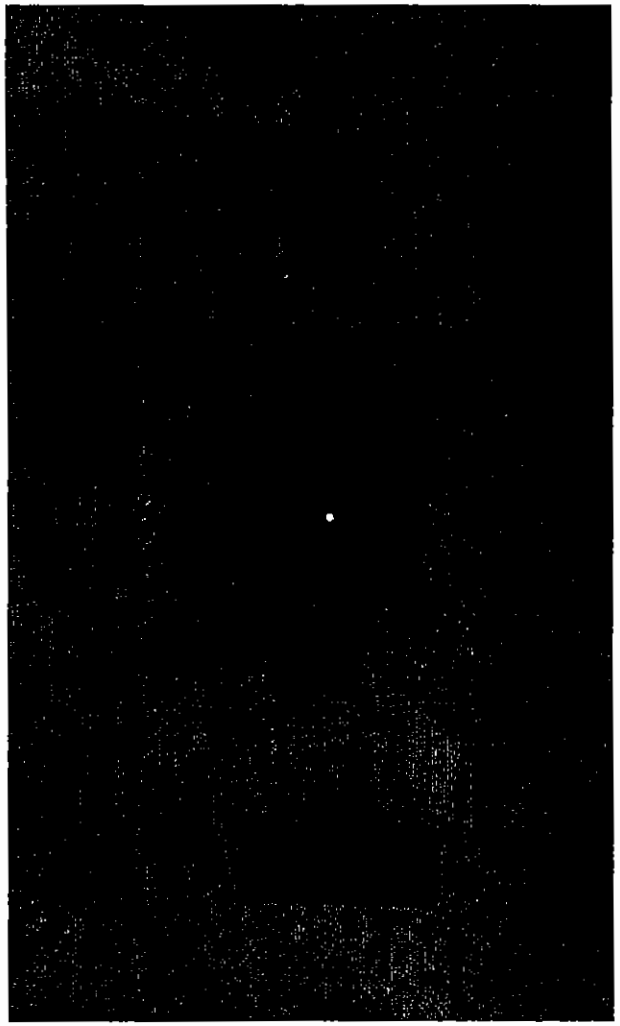

T2CAI06

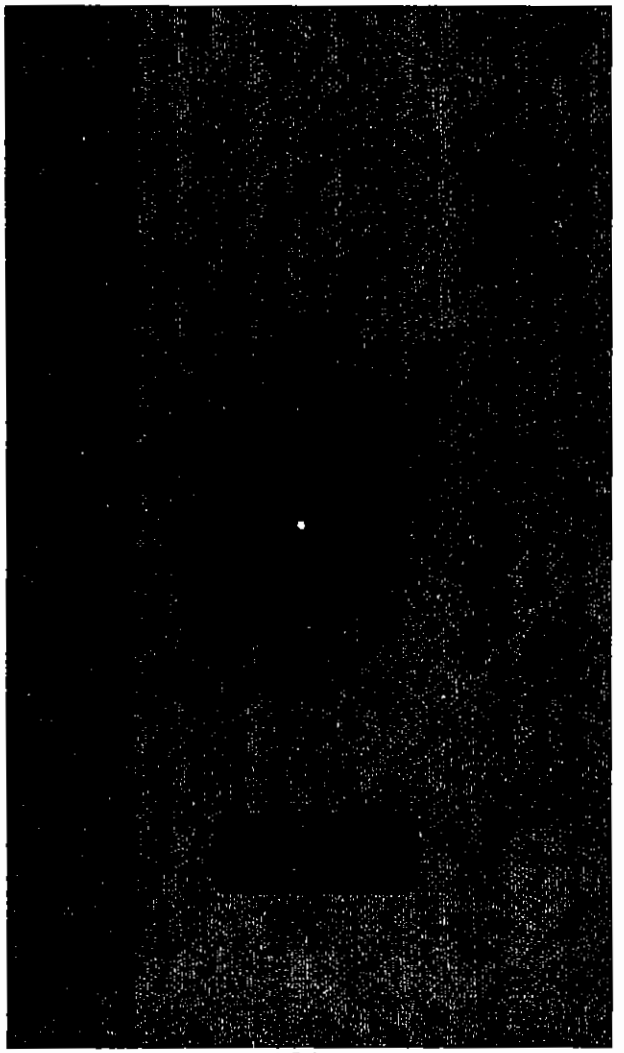

T3CAI11

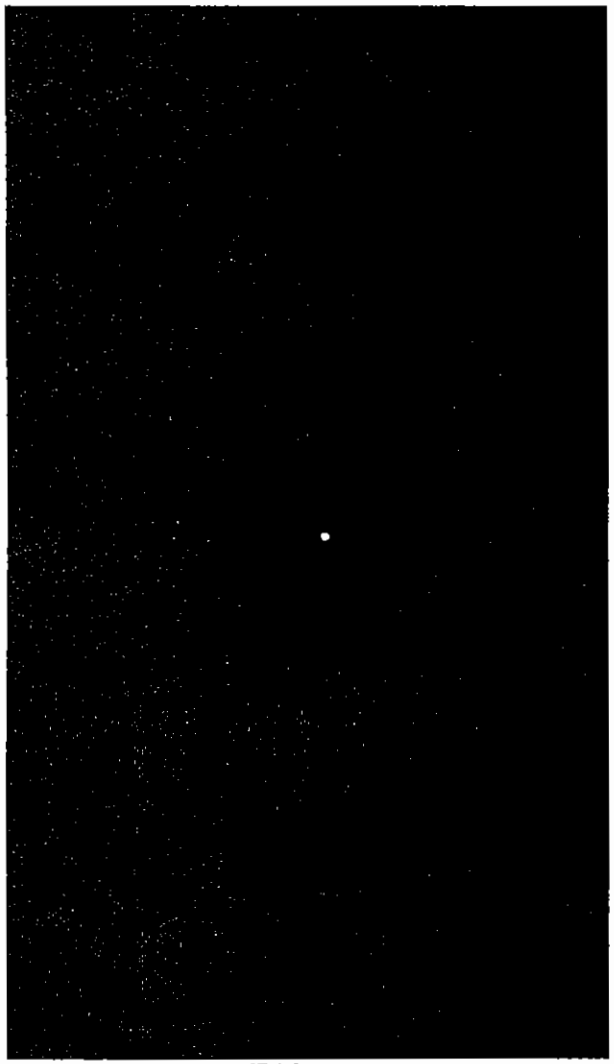

T4CAI06

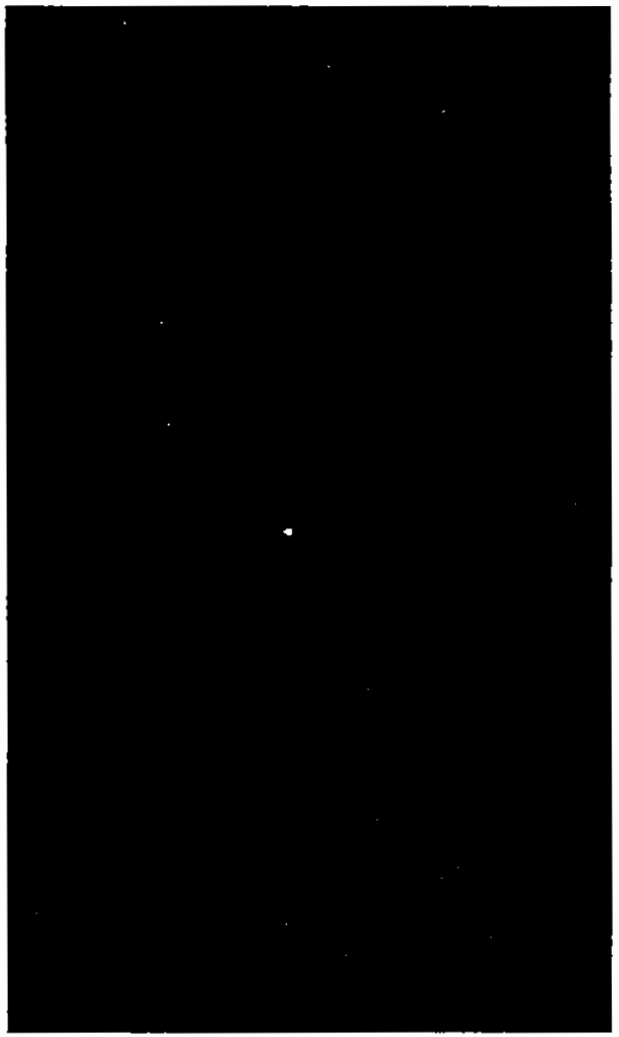

T5CAI11

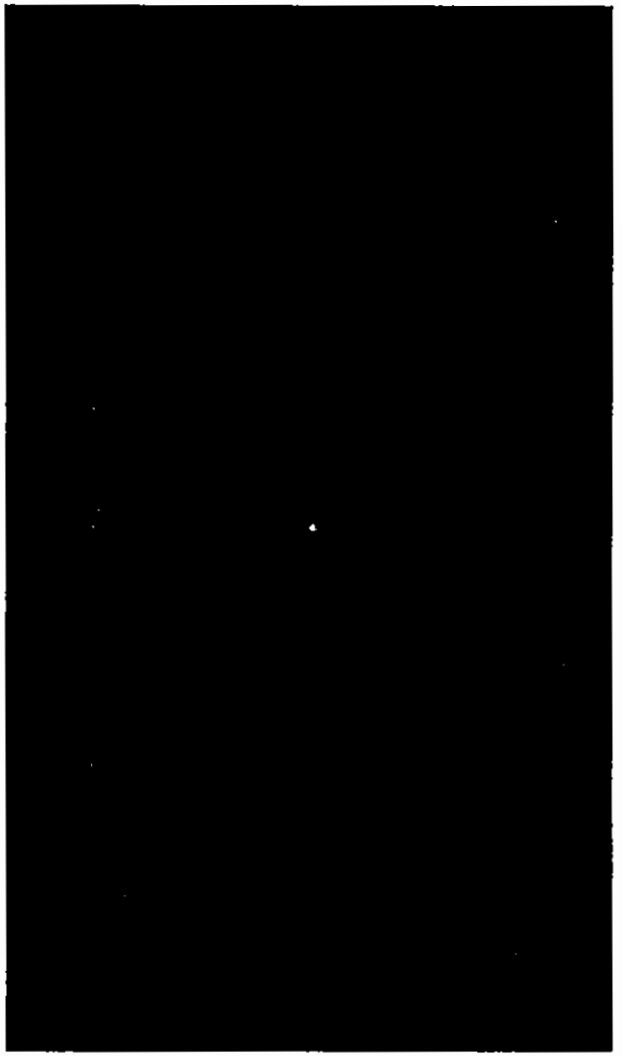

T6CAI02

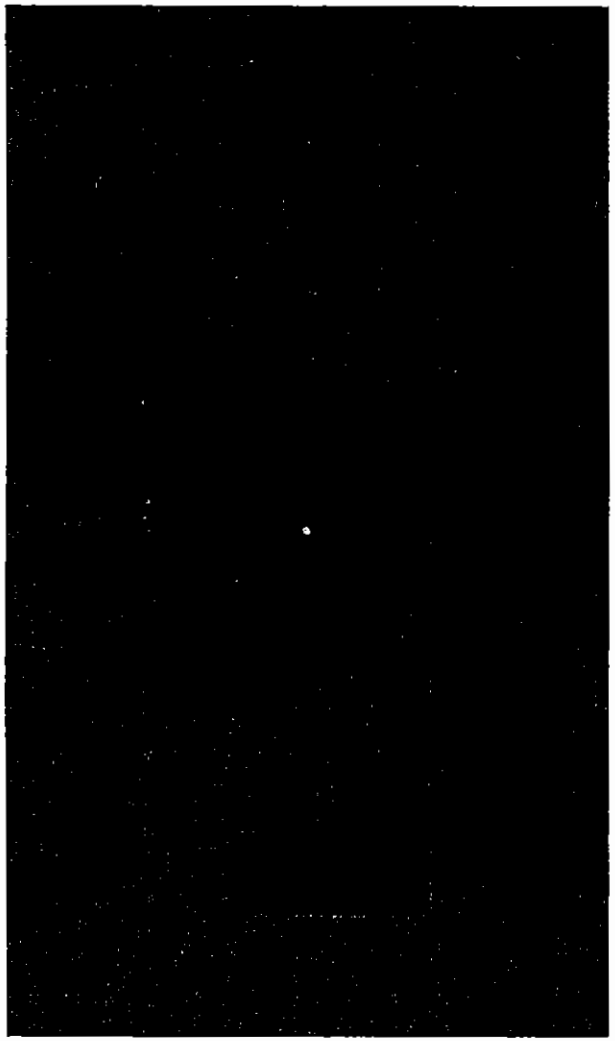

T7CAI11

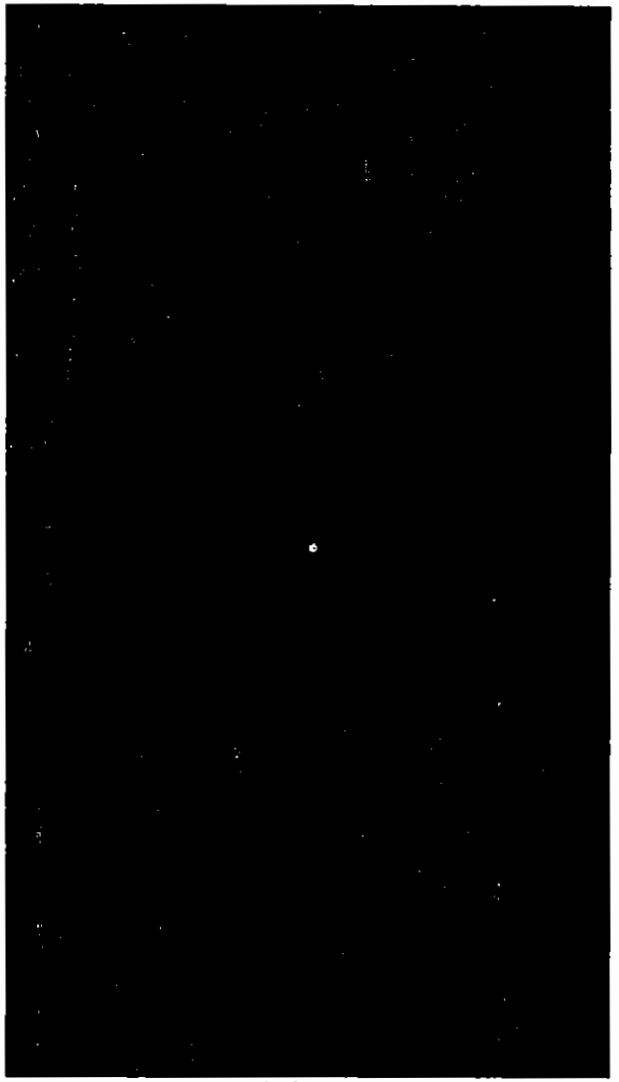

T8CAI02

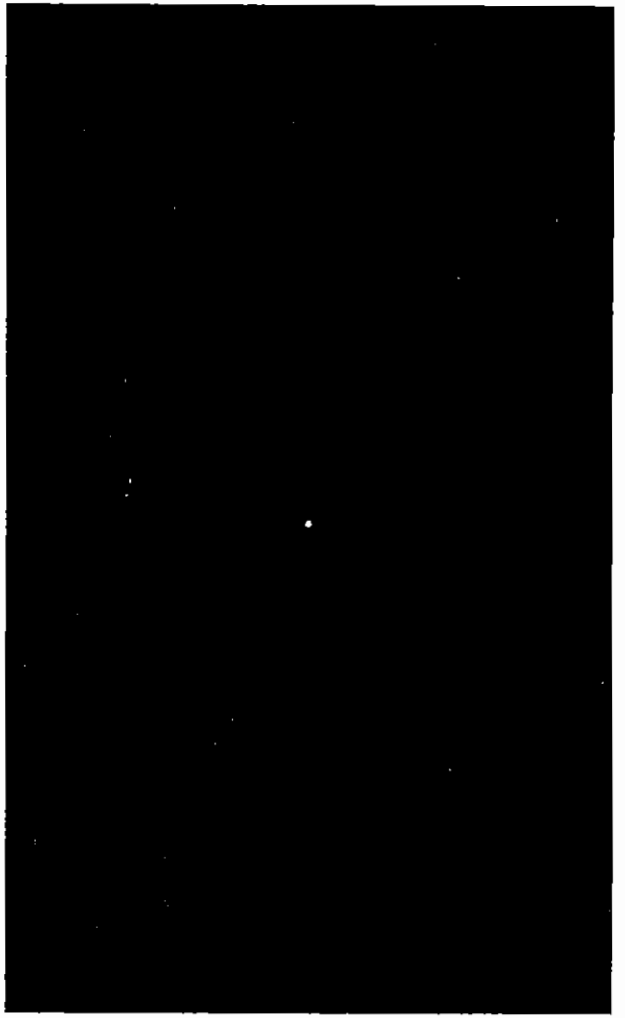

T9CAI07

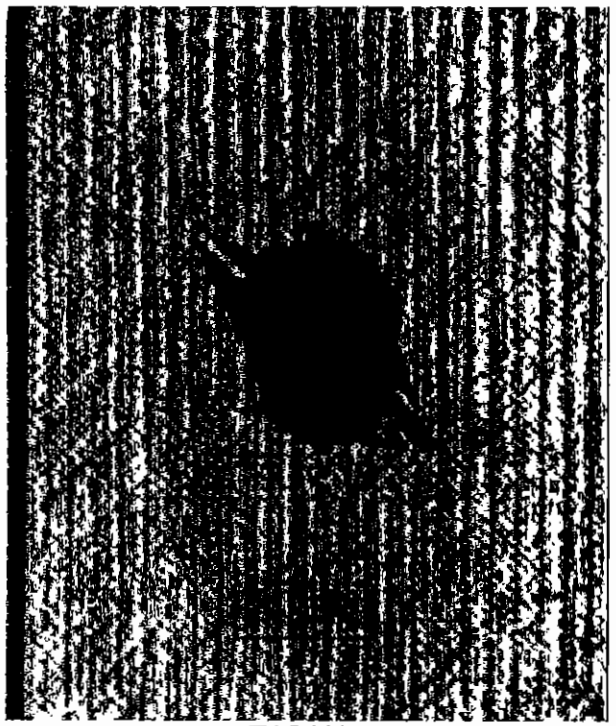

T1CAI11

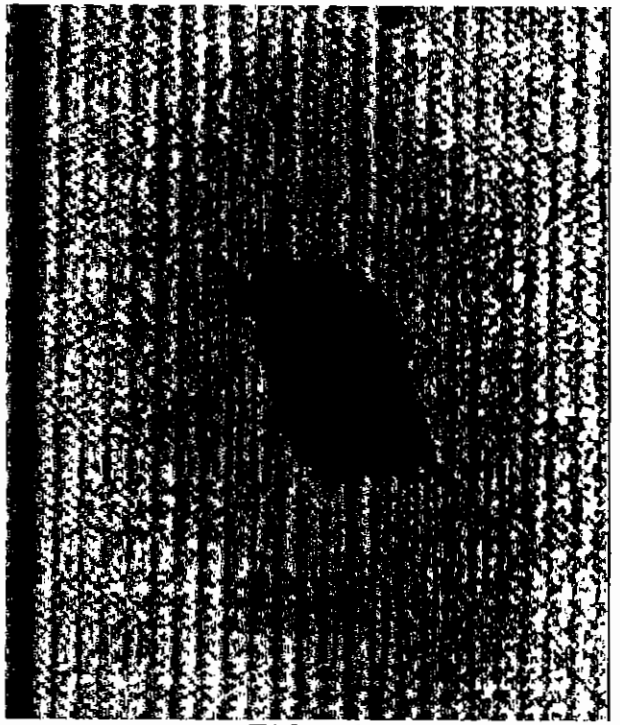

T2CAI06

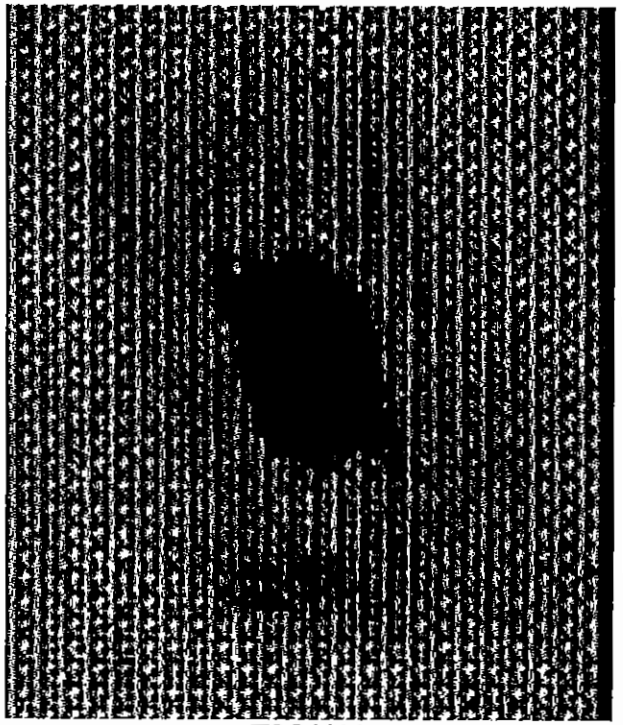

T3CAI11

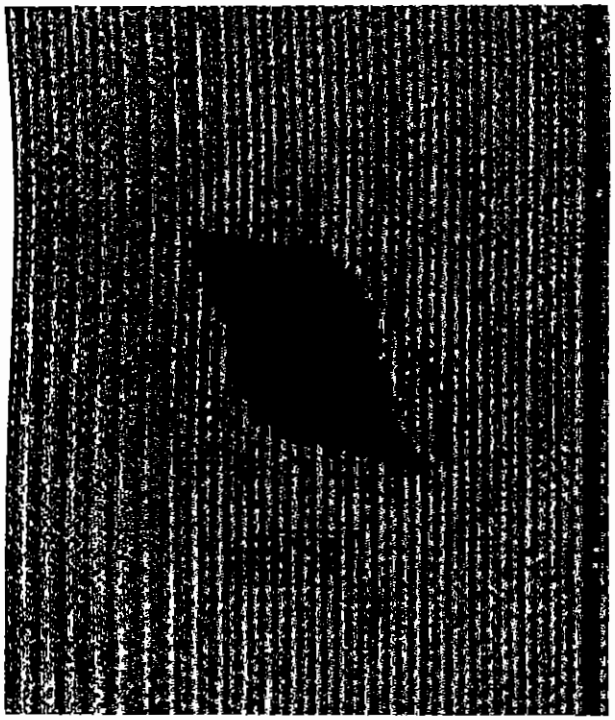

T4CAI06

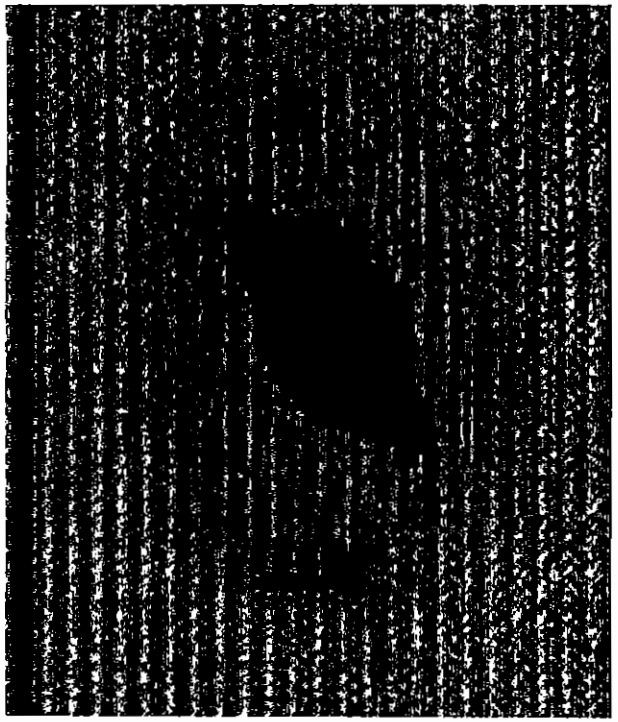

T5CAI11

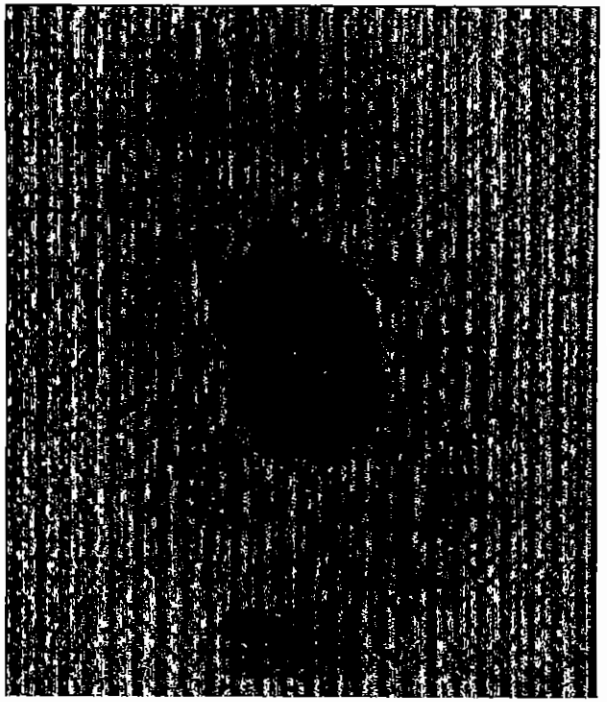

T6CAI02

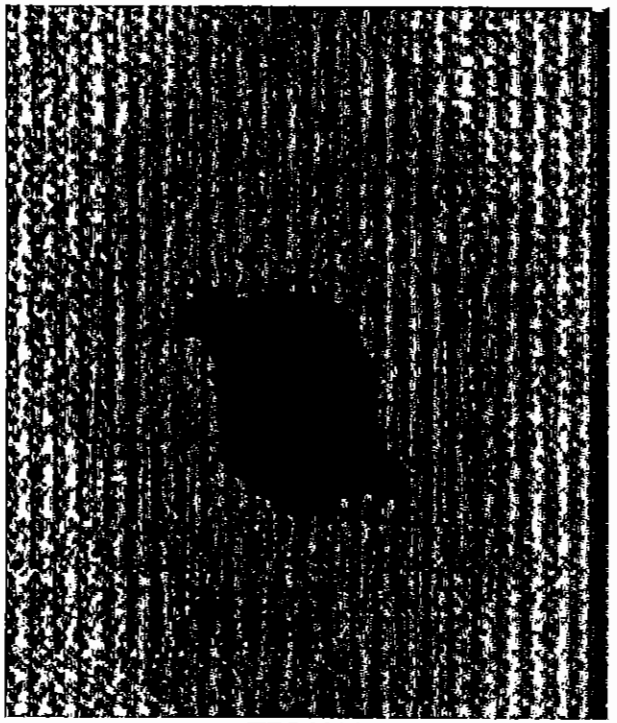

T7CAI11

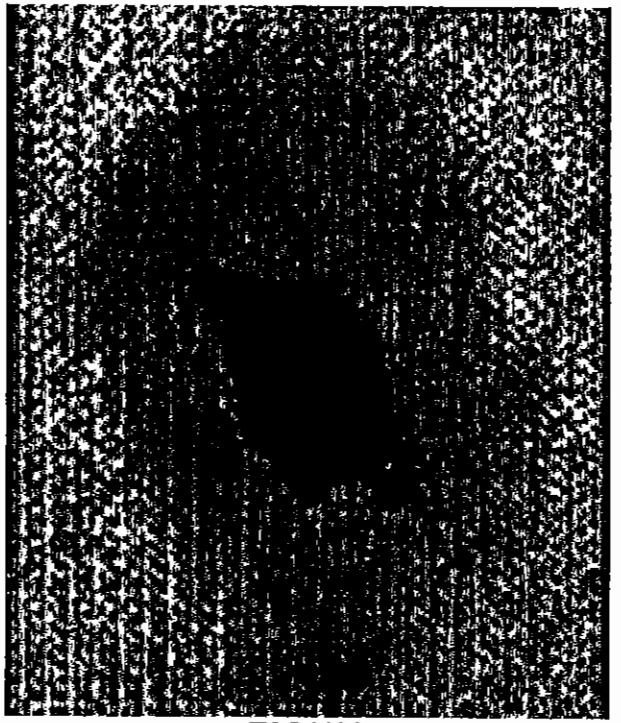

T8CAI02

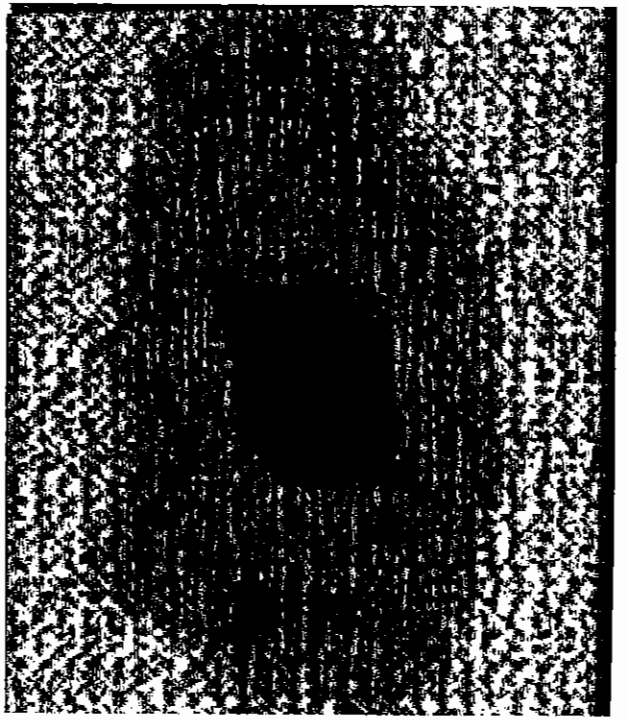

T9CAI07

Appendix B

Multiaxial Non-Crimp Fabric Manufacturers

Machine Manufacturers (Europe)

Karl Mayer Textilmaschinenfabrik GmbH
Bruhlstrasse 25
63179 Obertshausen
Germany
Tel. : 0049 6104/402-0
Fax : 0049 6104/43574

postal address:
Postfach 1120
63166 Obertshausen
Germany

PATENTS:
(US 5072602) Weft thread transporter
(US 4807450) Warp knitting machine with weft insertion arrangement
(US 4703631) Warp knitting machine
(US 4665719) Circulating thread guides
(US 4487039) Weft magazine arrangement for warp knitting machines
(US 4463580) Weft insertion magazine with continuous provision of weft thread for a warp knitting machine
(US 4449380) Warp knitted fabric and process for its production
(US 4442684) Control of weft thread insertion
(US 4437323) Warp knitting machine with weft insertion magazine and substrate provision arrangement
(US 4399670) Apparatus for transferring weft threads in a warp knitting machine
(US 4395888) Controlled thread guides for a weft thread magazine
(US 4385506) Weft thread laying arrangement with tension strip
(US 4380913) Weft thread laying apparatus with combing element
(US 4348876) Weft thread laying apparatus
(US 4255947) Warp knitting machine with weft insertion apparatus
(US 4220020) Warp knitting machine with weft inserters
(US 4192158) Weft thread tensioning device for warp knitting machines
(US 3967469) Warp knitting machine with improved thread feeding apparatus

Malimo Maschinenbau GmbH
Annaberger Strasse 97/99
09120 Chemintz
Germany
Tel. : 03 71/5 70 70
sales: 03 71/5707-220 or 215
Fax : 03 71/5707-221

postal address:
PO Box 713
09007 Chemintz
Germany

PATENTS (including the patents of VEB Kombinat Textima):
(US 5140841) Control system for warp yarns (steerable 0° system for Malimo)
(US 4893482) Warp-knitting fabric with oblique and diagonal filling threads

(US 4873844) Method and apparatus for the production of textile strip
(US 4852370) Warp-knitting machine, particularly stitch knitting machine
(US 4841747) Warp-knitting machine, especially sewing-knitting machine, and method for the production of warp-knit fabric with oblique and diagonal filling threads
(US 4638647) Method and flat warp-knitting machine for the production of a weft-and-warp-knit fabric
(US 4197723) Stitch bonded fabrics, method and apparatus for making the same
(US 3953989) Method and apparatus for warp knitting and resultant product

LIBA Maschinenfabrik GmbH
Postfach 1120
D-95112 Naila/Bayern
Germany
Tel. : 49/92 82/67-0

PATENTS:
(US 4723424) Process and device to operate a warp knitting machine, in particular a stitch-bonding machine
(US 4706475) Device for presenting weft yarns to the knitting needles of a warp knitting machine
(US 4677831) Apparatus for laying transverse weft threads for a warp knitting machine
(US 4411392) Speed-compensating device for the feeding of threads to a weaving or knitting machine
(US 4369639) Warp knitting machine apparatus
(US 4322956) Warp knitting machine arrangement
(US 4776185) Device for periodic offset displacement of the guide bar of a warp knitting machine
(US 4872323) Apparatus for laying transverse weft threads for a warp knitting machine
(US 4823564) Device for clamping weft threads in a warp knitting machine
(US 4706475) Device for presenting weft yarns to the knitting needles of a warp knitting machine

Fabric Manufacturers (Europe)

LIBA (multi-axial machines)

Ahlstrom
Ahlstrom 19
PO Box 18
Fin-48601
Karhula
Finland

Tel: 00358 (55) 3550 222
Fax: 00358 (55) 3550 290

Hexcel Composites
ZI Les Chartinieres
BP 27 Dagneux
F-01122 Montluel Cedex
France

Tel: 0033 72252627
Fax : 0033 78060292
PATENTS:
(US 5238728 Deformable textile structure)
(US 5176949 Textile reinforcements for composite materials and method of manufacturing thereof) - powder binder film for multi-axial non-woven fabrics
(US 4889063 Multi-layer textile material and method and apparatus for producing the same)

Devold (AMT) AS
N-6030 Langevag
Norway
Tel: 0047 70 19 35 55
Fax : 0047 70 19 32 08

Gamma Tensor
Plaza Emitlo Sala, 1
03800 Alcoy
Spain
Tel: 0034 6 5548870
Fax : 0034 6 5543484

Institut für Textiltechnik (ITA)
Der Rheinisch-Westfalischen Technischen Hochschule Aachen
Eilfschornsteinstrasse, 18
52062 Aachen
Germany
Tel: 0049 241 80 56 21
Fax : 0049 241 88 88 149

Saertex Wagener GmbH & Co KG
Industriestrasse, 9-11
D-48369 Saerbeck
Germany
Tel: 0049 2574 8051
Fax : 0049 2574 8231

(UK contact: Christex Ltd)
Tel: 01282 420924
Fax : 01282 437985

Selcom N.V.
Via del Torre 17
1-31010 Fregona (TV)
Italy
Tel: 0039 438 585188
Fax : 0039 438 585172

Syncoglas N.V
Industriepark B/1
Drukkarijstraat, 9
B-9240 ZELE

Belgium
Tel: 0052 44 76 11
Fax : 0052 44 95 02

Brunswick Technologies Europe
(formerly Tech Textiles International Ltd)
Unit 4/5 Crown Way
Walworth Road Industrial Estate
Andover
Hampshire
England
SP10 5LU
Tel: 01264 333400
Fax : 01264 359610
PATENTS:
(US 5442935) Apparatus for producing multi-axial non-woven fabric
(US 5445693) Method of producing a formable composite material - 'Thermo-preg'
(US 5055242) Process for continuously forming reinforcing articles

Flemings Industrial Fabrics (Biaxial LIBA only)
Belford Mills
Lawson Street
Kilmarnock
Ayrshire
KA1 3HZ
Tel: 01563 25203
Fax : 01563 22022

Fabric Manufacturers (Europe)

Karl Mayer

Saertex Wagener GmbH & Co
Industriestrasse, 9-11
D-48369 Saerbeck
Germany
Tel: 0049 2574 8051
Fax : 0049 2574 8231

(UK contact: Christex Ltd)
Tel: 01282 420924
Fax : 01282 437985

Welbeck UK Ltd. (Mayer RS3MSU)
9 College Street
Nottingham
NG1 5AT

Fabric Manufacturers (Europe)

Malimo

Brochier S.A. Ciba Composites
Moulin-Cassal

01122 Montluel Cedex
France
Tel: 0033 72257106
Fax : 0033 72257028
PATENTS:
(US 5238728 Deformable textile structure)
(US 5176949 Textile reinforcements for composite materials and method of manufacturing thereof) - powder binder film for multi-axial non-woven fabrics
(US 4889063 Multi-layer textile material and method and apparatus for producing the same)

Saertex Wagener GmbH & Co
Industriestrasse, 9-11
D-48369 Saerbeck
Germany
Tel: +49 2574 8051
Fax : +49 2574 8231

(UK contact: Christex Ltd)
Tel: 01282 420924
Fax : 01282 437985

Technical University of Dresden
Institut fur Textil und Bekleidungstechnik
Der Technischen Universitat Dresden
Mommsenstrasse, 13
01062 Dresden
Germany
Tel. : (0351) 4658-370
Fax : (0351) 4658-361

Fabric Manufacturers (Europe)

Unknown machine types

Duflot Industrie
31 rue du General de Gaulle
BP 68
42402 Saint Chamond Cedex
France
Tel. : +33 7731 2512
Fax : +33 7731 9959
Manufacturer of textiles for technical users and particularly for composite users. Braids, crotchet fabrics, felts, multi-axial fabrics 'Duftech' and '4Dir', in glass, carbon, aramid and ceramic.

Les Fils d'A Chomarat et Cie
7 rue Roy
75008 Paris
France
Tel. : +33 1 4293 1168
Fax : +33 1 4293 4853#
NOTES:

Multi-axial fabrics manufactured by superimposing layers of uni-directional fibres and bonding the sheets by perforating the layers and implanting fibres through the fabric by needling.

in UK:
Bamford House
South View
Rochdale
OL11 5LB
Tel. : (01706) 350994
Fax : (01706) 42543

Vorwerk Technotex
Kulmbach
Germany
Tel. : +49 9221 508 23
Fax : +49 9221 508 22
NOTES:
Manufactures multi-ply, multi-axial, and space (distance) fabrics for the composites industry

Fabric Manufacturers (USA)

Bay Mills Limited
201 Hugel Ave
Midland
Ontario, Canada
Tel. : +1 705 526 7867
Fax : +1 705 526 2801
also at (St. Catharines, CA)
PATENTS:
(US 5439726) Bituminous roofing membrane including a lightweight grid and over-under construction
(US 5399419) Reinforced film and method of manufacturing same
(US 5393559) Process for reinforcing paving
(US 5314556) Process for manufacturing reinforced roofing membranes
(US 5246306) Reinforcements for asphaltic paving processes for making such reinforcements and reinforced pavings
(US 5189769) Manufacture of a multiple biased fabric by folding
(US 5110627) Process for making reinforcements for asphaltic paving
(US 5057172) Method of manufacturing a reinforced film
(US 4989529) Manufacture of a multiple biased fabric by folding
(US 4957390) Reinforcements for asphaltic paving processes for making such reinforcements and reinforced pavings
(US 4905969) Electric fence wire construction
(US 4879163) Textiles containing interstices and processes for making such textiles
(US 4780350) Reinforcing composite for roofing membranes and process for making such composites
(US 4762744) Reinforcing composite for roofing membranes and process for making such composites
(US 4699542) Composition for reinforcing asphaltic roads and reinforced roads using the same

(US 4578141) Weft forming apparatus
NOTES:
Bitumen coated multi-axial warp knit fabrics for roofing membranes and paving systems. Also supply materials for aerospace, electronics and sporting goods.

Bean Fiber Glass Inc.
Union Street
Jaffrey, NH 03452
Tel. : (603) 532 7765
Fax : (603) 532 6505
Acquired by Johnson Industries, Alabama

Brunswick Technologies Inc.
One Maine Street
Brunswick, ME 04011
Tel. : (207) 729-7792
Fax : (207) 729-7877
Manufactures Bitex and Cofil glass fibre fabrics by a non-crimp stitch bonding process. Vetrotex Certain Teed are minority shareholders in the business. Recently acquired Advanced Textiles, Seguin, Texas and Tech Textiles International Ltd, Andover, UK

Burlington Industries Incorporated
Greensboro, NC 27420-1207 USA
Tel. : (910) 379-2000
PATENTS:
(US 519177) Weft Inserted, warp knit, woven-look fabric and apparatus and methods of making the fabric
(US 4724179) Weft insertion drapery fabrics
(US 4729860) Multiple, thick graphite fabric production

Du Pont de Nemours, E. I., & Co., Inc.
Wilmington, DE 19880-0010 USA
Tel. (free): (800) 441-7515
external affairs Tel. (free): (800) 298-7668
PATENTS:
(US 4189811) Method for producing non-woven webs of cross-laid strands

Hexcel Incorporated
Dublin CA
Trading as Knytex (and Hi-Tech Composites Inc.)
Use LIBA multi-axial machine technology to produce quadri-axial quasi-isotropic material for NASA ACT program

Hexcel - Hi-Tech Composites Inc.
Manufacture linear weft/bias multi-axial warp knit composites under 'Spanply' or 'Mass Spanply' name. Hexcel (Dublin CA) are known to have a division trading as Hexcel Hi-Tech, manufacturing 2.5 m wide 8 ply multi-axial warp knit fabrics using a LIBA type system, which it is claimed was developed by Hexcel. The machine is able to manufacture fabric at 50 linear yards/hour. Hexcel are unable to supply multi-axial warp knit non-crimp fabrics into Europe and LIBA are unable to sell

machines in USA, believed to be due to disputes over this machine. Hexcel also manufacture fabrics as 'Knytex' in joint venture with Owens-Corning

Hitco
Irvine CA
PATENTS:
(US 4325999) Bias fabric
NOTES:
Fabric having parallel spaced yarns at ±45° relative to the long axis if the fabric, formed by directing a plurality of yarns back and forth across the width of the fabric and securing the yarns around pins on the opposite conveyor using an adjustable roller arrangement on the shuttle or alternatively using a plurality of pin mounting rings which move to engage with the yarns, slotted guides may alternatively be used which travel with the rapier and engage with the conveyor mechanism. The fabric is stabilised prior to removal from the pins with stitching threads along the length, or deposition of a bead of molten plastic along the length, application of an adhesive coated film or impregnating with a partially cured resin.

J.B. Martin Company, Inc.
PO Box 607
Leesville SC 29070
Tel. : (803) 532 6277
Fax : (803) 532 3833
'4-DIR' fabric (non-linear multi-axial warp knit - believed to be Malimo system)
'Proform' fabric likely to be same as '4-Dir'.
PATENTS:
(US 4,854,352) Textile fabrics having a plurality of warp and filling layers and attendant method of making
NOTES:

J. B. Martin Ltee
445 rue St-Jacques
St-Jean-sur-Richelieu
Quebec J3B 2M1
Tel. : (514) 346-6853
Fax : (514) 347-4910
Manufacturer of non-linear (weft yarns not parallel) multi-axial warp knit fabrics.

J.B. Group Inc.
Greenwich CT
PATENTS:
(US 4877470) Method for the production of bias fabrics
(US 4556440) Method and apparatus for production of bias fabrics
(RE 33418) Method and apparatus for production of bias fabrics
(US 5047109) Apparatus for production of bias fabrics

NOTES:
May be part of J. B. Martin company and may also have traded as Proform Inc. Ron Krueger (inventor) is known to work/have worked for Hexcel Hi-Tech and Knytex

Knytex Corporation
201 Executive Office Park

PO Box 5293
Midland TX 79701
Tel. : (915) 694-8912

1913 N King Street
Seguin TX 78155
Tel. : (210) 379-1580
PATENTS:
(US 4550045) Biased multi-layer structural fabric composites stitched in a vertical direction
(US 4484459) Biased multi-layer structural fabric composites stitched in a vertical direction and process and apparatus for making same
(US 4664961) Structural fibre pre-forms and method of making
(US 4567738) Structural fabric and method of making
(US 4484459) Biased multi-layer structural fabric composites stitched in a vertical direction and process and apparatus for making same
NOTES:
50:50 joint venture between Hexcel (Dublin CA) and Owens-Corning (Toledo OH) to produce speciality fabrics already produced by Hexcel under its Knytex name. Marketed in USA as 'DBM' fabric, material has linear inlayed weft/bias yarns.

Milliken & Co.
New York, NY 10018 USA
212-819-4200
FAX: 212-819-4691
PATENTS:
(US 5017425) Tricot knitting machine improvement
(US 5060489) Tricot knitting machine improvement
(US 4388364) Heat set warp knit weft inserted fabric and coating thereof
(US 4304813) Pressure sensitive tape with a warp knit and weft insertion fabric
NOTES:
Home & Industrial Textiles, Greige Goods, Shop Towels, Apparel Fabrics.
Milliken Research Corporation (Spartanburg SC) - presumed part of same group manufactures multi-axial non-crimp fabrics using Mayer RS2DS weft insertion warp knitting machine (trialed in NASA ACT program) and only one in USA.

Peabody ABC Corporation
Warwaw IN
PATENTS:
(US 4615934) Warp knit weft insertion fabric and plastic sheet reinforced therewith
NOTES:
Weft inserted warp knit reinforcing sheet used for industrial applications including fabrication of mine ventilation tubing.

Proform Inc.
Minneapolis MN
PATENTS:
(US 4416929) Multi-layered stitched knitted fibre glass composite
(US 4444025) Carrier mechanism for weft insertion
NOTES:
Johnston Industries Composite Reinforcements Inc
(formerly Tech Textiles USA)

3503 Lakewood Drive
Phenix City AL 36867
Tel. : (334) 291-7704
Manufactures composite reinforcement fabrics and is a wholly owned subsidiary of Johnston Industries. Tech Textiles USA was established in December 1992 as a joint venture between Tech Textiles Ltd (Andover UK). and Johnston International (New York, USA). The company makes VECTORPLY (R) and other multi-axial non-crimp reinforcing fabrics from glass, carbon, and aramid fibres. Manufactures using Karl Mayer based knitting technology and LIBA type weft insertion systems. Some weft insertion technology development (patented) while joint venturing with Tech Textile Ltd.

Xerkon Inc.
Minneapolis MN
PATENTS:
(US 4774120) Method for multiple-end-close-set uniform density parallel weft insertion and products thereof
NOTES:
A multiple-end weft-insertion process which is capable of achieving extremely high yarn density which is uniform in plies of structural fabrics is disclosed, making use of conventional machinery and systems. Yarn is transferred from a shuttle to yarn transfer elements spaced a sufficient distance apart to avoid damage to the yarn, and then transferred to yarn holding elements. Each successive pass of the shuttle is adjusted by moving the yarn transfer element parallel to the holding elements, so as to overlap each band deposited by the shuttle. The amount of movement necessary to achieve any desired density is calculated according to established parameters.

Machine/Fabric Manufacturers (Japan)

Kurashiki Boseki Kabushiki Kaisha
Jurashiki, Japan
PATENTS:
(US 4460633 Non-Woven reinforcement for composite)
NOTES:
non-woven reinforcement for resin composite comprising warps of non-twist multi-filament yarns and wefts on one or both sides of similar materials but containing an adhesive agent. This allows warp and wefts to be bonded at their intersection resulting in a stable crimp free multi-axial fabric.

Teijin Limited/Gunze Limited
Osaka/Kyoto, Japan
PATENTS:
(US 5118569 Reinforcement Sheet)
NOTES:
Reinforcing sheet comprising reinforcing yarns arranged in parallel to and spaced from one another in a matrix knitting structure.

Toray Industries Inc.
Tokyo, Japan
PATENTS:
(US 4786541) Fiber material for reinforcing plastics
(US 4622254) Fiber material for reinforcing plastics
NOTES:
Longitudinal warp with ±25-65° weft inlay, integrated by stitching repeatedly in the direction of lamination.

Cranfield Campus Vision - a shared endeavour

- A distinctive, research intensive, global university
- A former RAF base

The airport of course is an unusual attribute for a university. It is a matter of considerable pride and distinction that it plays the vital part that it does in our work here. But beyond this, and notwithstanding significant investment in buildings/infrastructure, the physical origins of our campus are still very much in evidence in the character and juxtaposition many of the buildings.

Yet the campus is gradually, inexorably, changing – indeed, rather rapidly just recently!

As new capital investment opportunities come along the more pressing of the long list of 'crucial needs' are addressed, helping to ensure continuing vitality and relevance. Opportunities to do something substantive tend to come up serendipitously, so there is a risk to be avoided. The risk is that the 'journey' representing evolution of our campus is more akin to a random walk than measured progression along a well planned path; the risk that individual developments, each making eminent sense individually, do not add as much as they might to the coherence, ambience and effectiveness of the campus as a whole. Each of us will have our examples of fine developments that enhance - and perhaps of one or two that don't do so as much as we might have wished. And our views won't all be the same! For me, the very recent developments represent a great advance. The new residential blocks already in use have improved the average standard of the living accommodation we are able to offer to students. The 250 additional bedrooms that become available at the beginning of 2008 with the opening of another 5 new blocks, to be known collectively as Stringfellow Hall, will raise the standard yet again. (Named incidentally, for the avoidance of doubt, not for the infamous London club but the mid 19th century pioneer of heavier than air manned flight.) But not all of our accommodation is of the quality we would wish: as circumstances allow, further investment surely will be needed to secure an appropriate mix in terms of price/value and facilities for individuals, couples and families. This is an example of where we would benefit from having a well mapped out forward perspective of our aspirations for the University's estate.

Of course, it's not just about residential accommodation. Let's look at the academic buildings. Some, such as the purpose built Cranfield Management Development Centre and the Kings Norton Library, were designed from the outset for the role that they play. In my view they measure up well against the highest expectations for such purposes. Others have been imaginatively converted to very good effect. A former RAF H-building has just been remodelled and extended, at relatively modest cost by the scale of these things, to provide us with an outstanding building as the focus for our management research activities in the Cranfield Management Research Institute. A few years ago the former aircraft hanger known as B83 was transformed by the addition of an extension and a modern wrap-around section to give us an excellent home for, amongst other things, some important 'facilities of substantial scale' in the School of Engineering. Currently we have a major development programme centred on another former aircraft hanger, B52, that will provide a superb new home for Cranfield Health, some additional space for the School of Applied Sciences and a new 200-seat lecture theatre. Taken together the Library, B83, along with B52 when completed represent a group of buildings with very positive visual impact (although for me the car park at their centre rather takes the edge off it all!).

Lest all this talk of new buildings and developments should get you over excited, though, I must immediately emphasise that we have not discovered a previously untapped source of major capital financing! So it will be a case of continued incremental development; I do not envisage immediate, wholesale, major, developments around the campus of a scale previously not seen. But I am convinced that working together we could collectively share our thoughts and help formulate a forward-looking 'Vision for the Cranfield Campus'. I believe it now would be right for us to do so and thereby help inform the future of Cranfield University. This 'Campus Vision' should not be a straight-jacket but rather a flexible framework within which future development opportunities can be positioned and around which we could rally support. The aim is to ensure that investments both meet the immediate needs while at the same time contributing to the desired overall 'transformational development' of our campus. They should contribute to the full in helping to provide a truly fitting home for the postgraduate and research community that constitute this most distinctive university of global standing.